1995 Annual water column monitoring report

Massachusetts Water Resources Authority
Environmental Quality Department
Report ENQUAD 1996-07

Water Column Monitoring in Massachusetts and Cape Cod Bays: Annual Report for 1995

submitted to

Massachusetts Water Resources Authority
Environmental Quality Department
100 First Avenue
Charleston Navy Yard
Boston, MA 02129
(617) 242-6000

prepared by

Stephen J. Cibik
ENSR
35 Nagog Park
Acton, MA 01720

and

Brian L. Howes
Craig D. Taylor
Donald M. Anderson
Cabell S. Davis
Woods Hole Oceanographic Institution
Woods Hole, MA 02543

and

Theodore C. Loder, III
Robert D. Boudrow
University of New Hampshire
Durham, NH 03824

James D. Bowen
University of North Carolina
Charlotte, NC 28223

MWRA Environmental Quality Department
Technical Report Series 96-07

Massachusetts Water Resources Authority
Charlestown Navy Yard
100 First Avenue
Boston, MA 02129
(617) 242-6000

Citation:

Cibik SJ, Howes BL, Taylor CD, Anderson DM, Davis CS, Loder TC, III, Boudrow RD, Bowen JD. 1996. 1995 Annual water column monitoring report. Boston: Massachusetts Water Resources Authority. Report ENQUAD 96-07. 254 p.

Acknowledgements

The authors wish to acknowledge the innumerable people who contributed to the monitoring studies presented in this annual report. First and foremost, we recognize the scientific teams fielded by the many organizations who participated in the MWRA's monitoring program, both at sea and in the laboratory. It was their expertise and dedication which produced the high-quality data reported herein, despite working frequently under exceedingly difficult conditions. Special recognition is given to Mr. Steven Wolf, ENSR Operations Manager, for his logistical skills which made it all happen, and to Ms. Dale Goehringer of WHOI, Mr. Rob Boudrow of UNH, Mr. Richard Lacouture of the Academy of Natural Sciences' Estuarine Research Center, and Mr. Steve Mattingly of E3I for coordinating the various lab efforts, and to Ms. Becky Celluza and Ms. Kristyn Lemieux for their special contributions on data reduction, visualization, and interpretation. We also thank the masters and crews of the vessels *Isabel S* and *Christopher Andrew*, with special thanks to Mr. Frank Mirarchi and Mr. Chip Rhyther of CR Environmental for their capable support of our sea operations.

The authors also received generous technical support and information from numerous agencies outside of the program. We thank in particular Fran Hotchkiss, Bill Strahle, and Dr. Rich Signell of the USGS Woods Hole office for providing data and information on mooring deployments. We thank Tom Shepard, Russell Gadoury, and Jessica Stock-Alvarez of the USGS Marlborough, Massachusetts, Office for providing river discharge data. Thanks also to Douglas Hankins of WETLabs for providing timely data for continuous chlorophyll monitoring, and to Kathy Vreeland of the Northeast Regional Climate Center for meteorological data. Thanks also to Drs. Jeffrey Brown and Charles Yentsch of Bigelow Labs for providing satellite imagery and interpretation, and to Dr. Bernie Gardner of UMass Boston for his input on the interpretation of physical oceanography data.

Finally, we acknowledge that there are certainly several people we have overlooked who deserve specific mention, to whom we extend our thanks and our apologies for our momentary lapse in memory.

CONTENTS

CONTENTS
(Cont'd)

CONTENTS
(Cont'd)

LIST OF TABLES

LIST OF FIGURES

LIST OF FIGURES
(Cont'd)

LIST OF FIGURES
(Cont'd)

LIST OF FIGURES
(Cont'd)

LIST OF FIGURES
(Cont'd)

LIST OF FIGURES
(Cont'd)

LIST OF FIGURES
(Cont'd)

EXECUTIVE SUMMARY

The Massachusetts Water Resources Authority (MWRA) has implemented a long-term Harbor and Outfall Monitoring (HOM) Program in the Massachusetts Bay system. The objective of the HOM Program is to establish baseline conditions in the system prior to the relocation of the Deer Island wastewater discharge to its new site approximately 15km offshore. Once the relocation has been completed, data collected by the HOM Program will be used to assess the effects of the discharge by comparison with the baseline record.

This report presents the results of the 1995 water column monitoring program. Water column monitoring is performed 17 times per year within the nearfield region, a 10 x 10 km sampling grid encompassing the new outfall site. A broader farfield sampling program in Massachusetts Bay, Cape Cod Bay, and Boston Harbor is performed six times per year. Each survey includes physical, chemical, and biological measurements of the water column, providing data on water column structure, nutrient chemistry, chlorophyll, dissolved oxygen, primary productivity, respiration, and plankton taxonomy. An overview of the 1995 results is provided below, and a tabular summary provided in Section 9.

Physical Characterization of the Water Column. The Massachusetts Bay system undergoes a seasonal progression from a vertically mixed water column in winter to a stratified system in summer. Water column stratification in 1995 (defined as a surface-to-bottom change in sigma-t of less than 1.0 kg/m^3) lasted approximately four months, beginning in early June and terminating by mid-October with the onset of the fall turnover. During this time there were periodic mixing and upwelling events which often resulted in detectable changes in nutrient availability and biological activity. Other observable physical features included intrusions of water mass from the Gulf of Maine, which were identified through satellite imagery and reductions in surface salinity.

Nutrients and Chlorophyll Cycles. The system typically exhibits a progression of seasonal events which occur on an interannual basis and are closely related to the physical changes described above. These events typically include spring and fall phytoplankton blooms which are triggered by increasing sunlight and water temperatures (spring) and release of bottom water nutrients (fall turnover). In 1995 there was a modest late winter bloom event in the beginning of March, a spring bloom in late April, and a bloom initiated by the fall turnover. The observed bloom events were consistent with an annual nutrient cycle, which is characterized by partial depletion of nutrient concentrations throughout the water column during late winter and spring, nutrient depletion in surface water and nutrient increases in bottom water during the stratified summer period, and fall water column mixing. Average measured chlorophyll concentrations on a regional basis were the lowest for the four-year baseline period.

Dissolved Oxygen. The annual DO maximum in the vertically mixed water column occurred in late February, with saturated conditions maintained through May. After the onset of stratification there was a continuous decline in bottom concentrations, except for a short ventilation event which occurred in July. DO minima in stratified bottom waters occurred in all regions around the beginning of October, with regional average minimum values ranging from 6.6 mg/L in Cape Cod Bay to around 7.0 mg/L in areas of Massachusetts Bay. On an interannual basis, DO minima did not quite reach the baseline period lows which occurred during 1994.

Primary Production. Primary productivity was measured in the nearfield and outside Boston Harbor. The peak period of primary production in the nearfield occurred during late April, comprising 20 percent of total annual production. A secondary peak occurred during the late October bloom. However, productivity during the fall surveys was severely limited by low ambient sunlight. When comparisons were made of maximum potential production based on the theoretical light field for that time of year, the October period was the most productive, comprising 37 percent of potential production on an annual basis. Productivity in Boston Harbor reached its annual peak during late summer (August).

Photosynthetic parameters (α, P_{max}) were found to be sensitive indicators of changes in nutrient availability and the onset of phytoplankton blooms. Both coefficents dramatically highlighted an upwelling event in July that resulted in increased concentrations of nutrients within the euphotic zone. Photosynthesis efficiency increased to theoretical limits, indicating the onset of a phytoplankton bloom. Search for a proxy model of photosynthesis needs to continue. Evaluation of the BZpIo model indicated a 1.4-2 fold range of error in prediction based on 1995 data. Bio-optical models based upon active fluorescence should be considered.

Water Column and Sediment Respiration. Water column respiration was uniformly distributed during the pre-stratified period. During the stratified period bottom waters rates were an order of magnitude lower than the surface mixed layer rates due to lower temperature and lower quantity and quality of particulate carbon substrate. Carbon-specific respiration increased in late July, apparently due to the delivery of higher quality substrate availability from enhanced production from the early July upwelling event. Respiration in the sediments comprised a small fraction of the annual carbon remineralization, however during the stratified period the sediments accounted for about half of the total carbon remineralization below the pycnocline. The seasonal distribution of carbon mineralization suggested that the spring bloom and summer production periods were the key intervals related to sub-pycnocline oxygen uptake.

Plankton. The plankton communities showed a general trend of increasing abundance until mid-summer. For the most part, the blooms described above were driven by seasonal centric diatom assemblages. The exception was the fall bloom, which was dominated by the pennate diatom *Asterionellopsis glacialis*. This event was second only to 1993 in magnitude over the four-year baseline record. A substantial spring

grazing event was apparent during the third survey in late March. A four-fold increase in zooplankton abundance coincided with a substantial decrease in chlorophyll and productivity, and an order of magnitude decrease in phytoplankton densities. At the same time, water clarity and light penetration were at their annual maxima.

Carbon and Oxygen Budgets

Based on the results from the 1995 monitoring, oxygen and carbon balances were derived. From these, two conceptual models were developed:

- Bottom water oxygen depletion in the system is driven primarily by *in situ* respiration. This process is driven by temperature, duration of stratification, and substrate quantity and quality, and mediated by physical processes which control ventilation.

- Carbon fixation is sufficient to supply remineralization during the mixed period. During stratification, carbon production is in excess of respiration, suggesting that horizontal advection from the mixed layer is occurring. The fate of this advected carbon needs to be established.

1.0 INTRODUCTION

The Massachusetts Water Resources Authority (MWRA) has implemented a long term monitoring plan for the proposed MWRA wastewater outfall in Massachusetts Bay. The purpose of the Harbor and Outfall Monitoring (HOM) Program is to verify compliance with the discharge permit and to assess the potential effects of the relocated discharge of treated effluent into Massachusetts Bay. To help establish the present conditions, ENSR conducted the baseline water quality monitoring in 1995. This report represents the fourth continuous year of monitoring results since the program was established in February, 1992.

The objective of this report is to describe the 1995 seasonal baseline conditions of the water column in Boston Harbor and Massachusetts and Cape Cod Bays. Vertical profiles of the water column, along with discrete water samples obtained at predetermined depths, provide the basis to identify the predominant spatial scales of variability, the sources of the variability, and the general features of circulation and mixing at the time of the measurements. Analysis of seasonal fluctuations is performed to assess the temporal variability of each of the water properties, as well as the primary mechanisms responsible for the variability. Comparison to data collected in previous years is made to help establish interannual variability and to distinguish any trends.

The water quality data presented herein include the physical characteristics of temperature, salinity and density, annual nutrient cycling, chlorophyll, dissolved oxygen, productivity and respiration, and phytoplankton and zooplankton. Each are discussed in separate sections. A concluding section summarizes the principal events/observations noted within each section, and synthesizes results with a discussion of carbon cycling under existing and future discharge conditions. Consideration is given to the effectiveness of existing monitoring protocols, with recommendations provided where necessary.

2.0 DATA SOURCES AND 1995 PROGRAM OVERVIEW

This section identifies the various sources of information and data integrated in this annual report. The MWRA has a comprehensive bibliography of technical reports generated by the HOM Program. A general description of the documents associated with the 1995 water column monitoring tasks is provided below, along with an overview of the sampling program.

2.1 Data Sources

Full details of technical procedures, equipment, and quality controls are presented in the Combined Work/Quality Assurance Project Plan (CW/QAPP) for Water Quality Monitoring: 1995-1997 (Bowen *et al.*, 1995). This includes descriptions of standard survey methods, instrument specifications, laboratory support, and quality control procedures. Individual survey locations and descriptions, sampling methodologies, sequences of events, navigational and vessel information, and scientific crew are documented in individual survey plans prior to each survey and confirmed in survey reports. These reports also describe deviations in standard methods, detail any marine mammal observations, and present raw sensor data after each survey is completed.

Detailed summaries of water column survey data are available in three data reports (nutrient, plankton, and productivity/respiration) that are issued five times a year. Nutrient reports include sensor and chemistry data and plankton reports cover whole-water phytoplankton, screened phytoplankton, and zooplankton results. Finally, semiannual reports integrate results and provide initial interpretation of data. All quantitative data generated by the program are available in MWRA's HOM Program Database.

2.2 1995 Monitoring Program Overview

There were 17 water quality monitoring surveys conducted in Boston Harbor and Massachusetts and Cape Cod Bays during 1995. They were divided into two main types of surveys: nearfield/farfield combined surveys, which comprehensively samples all stations in the monitoring program (Figures 2-1) over several days, and nearfield surveys to sample the stations in the nearfield grid (Figure 2-2). Additional components were included within this framework to meet specific objectives. These included a Stellwagen Basin survey which was conducted in late fall to monitor dissolved oxygen levels at station F12 (located in Stellwagen Basin, see Figure 2-1), and a winter nutrients survey to determine the winter nutrient levels in the Massachusetts Bay area after the fall mixing event. Note however that inclement weather during the winter nutrients survey restricted data collection to the nearfield only.

The nearfield stations are located in a grid pattern over the future outfall site to provide a detailed picture of conditions in the water column in the vicinity of the discharge (Figure 2-2). The farfield stations are located throughout Boston Harbor, Cape Cod Bay and Massachusetts Bay in a strategic pattern that is intended to provide an overall characterization of the area. Stations are grouped into six regions in the Farfield area according to their location (Figure 2-1). These regions include Boston Harbor (stations F23, F30 and F31), the coastal region (stations F18, F24, F25, F14, F13, and F05), an offshore region (stations F22, F19, F16, F15, F10, F06 and F07, and F17), a boundary region (stations F26, F27, F28, F12, and F29), and Cape Cod Bay (stations F01, F02, and F03).

The nearfield/farfield combined surveys were conducted six times during the course of the year, intended to capture periods of peak activity in the Massachusetts coastal waters. Two surveys during February, and one each in April and June, encompass the potential range of the spring bloom and the onset of stratification. One took place in August during peak stratification of the water column, and the last survey was in October during the late summer dissolved oxygen minima and prior the onset of the fall water column turnover. The nearfield-only surveys were performed an additional eleven times throughout the year at intervals of every two to three weeks (Table 2-1), from February through early December.

Altogether there are 46 stations located in the nearfield and farfield survey areas, 21 in the nearfield and 25 in the farfield. N16 is sampled as both a nearfield and farfield station. Stations are assigned categories which signify the types of analyses conducted at that station, with each category represented by a letter (A, D, E, F, G, R, and P) (Table 2-2). These station categories are also depicted in the station maps (Figures 2-1 and 2-2).

At each station, five depths are typically sampled (surface, mid-surface, middle, mid-bottom, and bottom, designated A, B, C, D and E, respectively). Shallower inshore stations were only sampled at three depths (surface, middle, and bottom). Detailed descriptions of station coverages and individual analyses performed are available in each of the survey plans and in the CW/QAPP.

TABLE 2-1

1995 Schedule of Survey Events

Event Number	Type of Survey	Date
W9501	Nearfield/Farfield	February 6-14
W9502	Nearfield/Farfield	February 28-March 5
W9503	Nearfield	March 20-22
W9504	Nearfield/Farfield	April 3-10
W9505	Nearfield	April 24-27
W9506	Nearfield	May 15-17
W9507	Nearfield/Farfield	June 20-25
W9508	Nearfield	July 5-7
W9509	Nearfield	July 24-26
W9510	Nearfield	August 8-10
W9511	Nearfield/Farfield	August 21-26
W9512	Nearfield/Plume[1,2]	September 6-14
W9513	Nearfield/Plume[1]	September 25-29
W9514	Nearfield/Farfield	October 9-13
W9515	Nearfield	November 1-4
W9516	Nearfield/Stellwagen	November 27 & December 5
W9517	Nearfield/Winter Nutrients	December 17-19

[1] Additional in-situ measurements taken to develop methods for outfall plume tracking.
[2] See Proni *et al.*, 1996, for further studies conducted during this period using acoustical technologies.

TABLE 2-2

Station Types and Analyses (and Number of Depths Sampled)

Analysis	A	D	E	F	G	P	R
Dissolved Inorganic Nutrients (NH_4, NO_3, NO_2, PO_4, SiO_4)	5	5	5	5	3		
Other Nutrients (DOC, TDN, TDP, PC, PN, PP, Biogenic Si)	2	3			2		
Chlorophyll	5	5			3		
Total Suspended Solids	3	3			3		
Dissolved Oxygen	4	4		4	3		
Phytoplankton and Urea		2			2		
Zooplankton		1			1		
Respiration							3
Productivity						5	

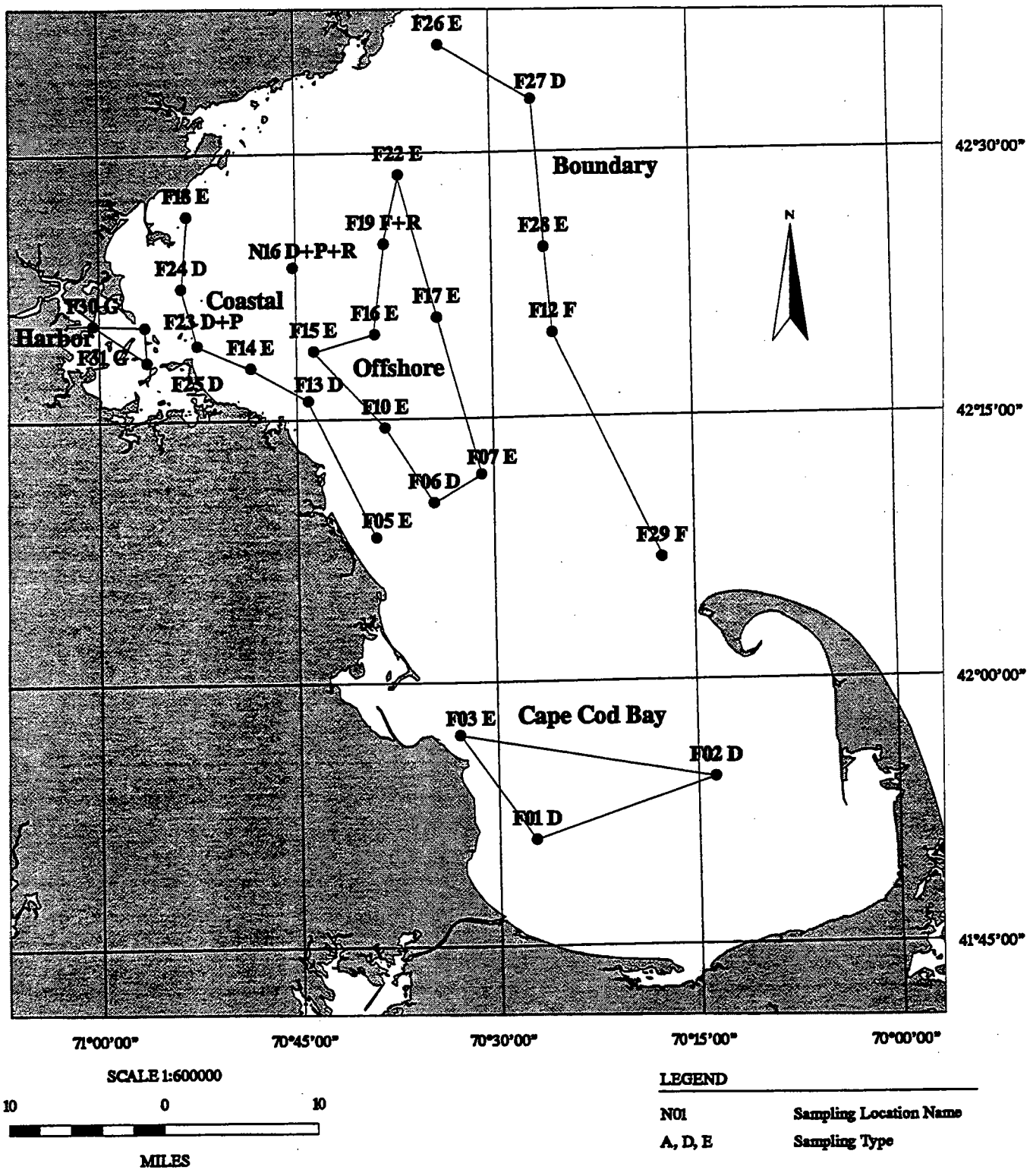

Figure 2-1

1995 Farfield Sampling Stations and Regional Classifications

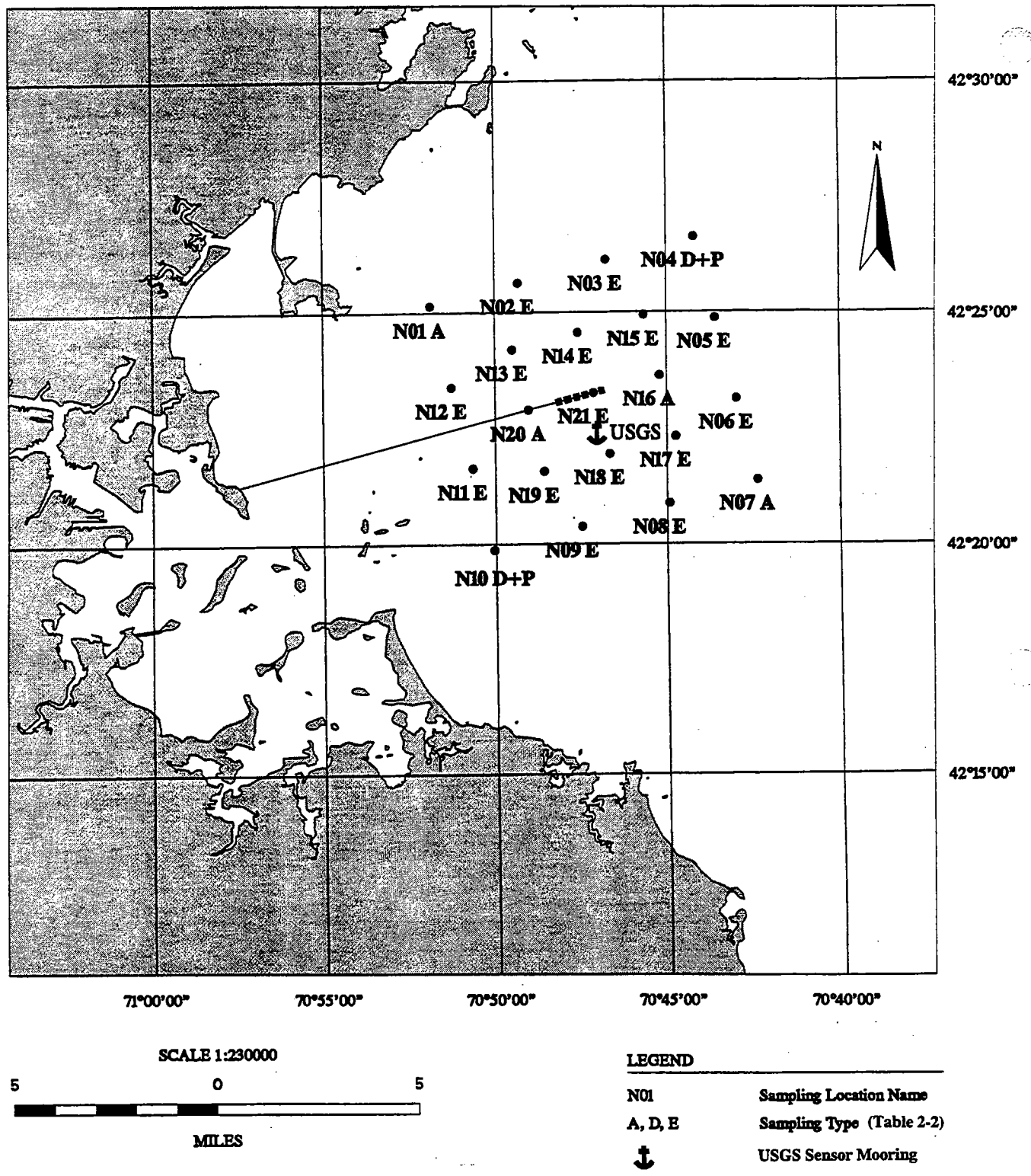

FIGURE 2-2

Nearfield Grid
Showing Location of USGS Mooring

3.0 PHYSICAL CHARACTERIZATION OF SYSTEM

This section provides a basic overview of the physical structure of the water column in the Massachusetts Bay system. Data from the 1995 monitoring period are illustrated to contrast conditions in the various regions of the monitoring area, and to provide the context in later sections for presentations of chemical and biological processes also sampled by the HOM program. For easy reference and to facilitate integration of results from the various sections, significant events throughout the year are summarized in Table 9-1. The 1995 record is also compared with 1992-1994 baseline monitoring data to support interannual comparisons of monitoring results.

3.1 Annual Temperature Cycle

3.1.1 Nearfield

The 21 monitoring stations in the nearfield were sampled with the greatest frequency (n=17), providing the best resolution for the annual temperature cycle in Massachusetts Bay based on shipboard measurements. Additional continuously-recorded temperature data were available from USGS arrays moored within the nearfield (USGS, 1996a). During the 1995 period, these sensors were located 5m below the surface, 10m above the bottom (ca. 20m depth) and 1m above the bottom.

Nearfield temperature data from the 1995 HOM sampling program are presented for three regions: inner nearfield stations which are influenced by the Harbor's strong tides (Stations 10 and 11; refer to Figure 2-2); Broad Sound (off of Winthrop and Nahant) as represented by Station N01; and outer nearfield as represented by offshore stations N04, N07, N16, and N20 (Figure 3-1a, b, and c).

February data indicated that water temperatures in the inner nearfield area were colder than was observed in the more offshore stations, which appeared to still be cooling during February. By late March, average water temperatures were uniform both horizontally and vertically across the nearfield (ca. 4°C), after which surface warming began. Maximum surface (typically <2.5m depth) temperatures had been reached by August, with inshore water averages somewhat warmer (ca. 21°C) than offshore waters (< 20°C). With surface waters beginning to cool after early August, bottom waters (typically >80 percent water column depth) continued toward their maxima around the beginning of October, with temperatures uniform around 13°C. The water column appeared to be vertically homogenous by early November.

Continuous data collected in 1995 from the USGS mooring located south of nearfield station N21 (Figure 2-2) were plotted along with the outer nearfield stations described above (Figure 3-2). These continuous measurements at the surface and bottom confirmed that the outer nearfield stations reached their annual

minima during March. Moored sensor and shipboard measurements were quite similar except for surface measurements during the summer, which is attributable to the difference in depth (5m for mooring, typically <2.5 m for shipboard measurements).

One notable feature evident in the moored temperature data occurred during early July when the array documented a substantial drop in surface water temperature. The onset of this event was captured by shipboard measurements from survey 9 (see ΔT line in Figure 3-1), but the majority of the event occurred during the subsequent two weeks prior to survey 9. In combination with salinity data (Section 3.2.1), these results indicate that an upwelling event occurred during the period. Upwelling involves an offshore transport of surface waters and onshore transport of water below the pycnocline. The primary evidence for its occurrence during this period was that the bottom temperature also decreased and the bottom salinity increased.

Other events evident in the mooring record included mixing (where surface and bottom characteristics converge from vertical exchange of water) in April and October, and horizontal advection (movement of water mass from one region to another) in late May and mid-August. Further discussion of advection follows in the next section.

3.1.2 Regional Comparisons

Regional comparisons were made using farfield survey data and thermal imagery from satellite data. Average surface and bottom temperature data were calculated from farfield survey data (n=6) for the regions defined in Section 2. The satellite imagery was particularly useful for the identification of potential upwelling events or other water mass movements which may have occurred during 1995.

In late winter, regionally averaged survey temperatures revealed colder waters inshore throughout the water column (Figure 3-3a through e). After April, surface temperatures were for the most part similar for the rest of the year. Bottom waters reflected the differences in regional depths, with harbor waters reaching maximum temperatures around 18°C in late August, while bottom waters in deeper offshore and boundary regions warmed more slowly and reached maxima of only around 10°C in October. With the exception of cooler bottom waters during August, Cape Cod Bay was similar to the coastal stations.

Thermal imagery from NOAA's advanced very high resolution radiometer (AVHRR) was examined to identify regional differences and apparent water mass movements in the bays ecosystem. The AVHRR is a scanning instrument with a swath width of 2700 km and ground resolution of 1 km. The radiometer has three bands in the infrared and two in the visible. In combination, the three bands in the infrared correct for the influence of the atmosphere and measure the sea surface temperature. The temperature scale is from 1°C to 30°C and has an accuracy of one degree. A total of 41 images were selected (Brown and Yentsch, 1995) as suitable from those available for 1995 from the CoastWatch Northeast Node. Of

those images, several included indications of either upwelling or intrusion from the Gulf of Maine (Table 3-1).

In January, coastal surface waters were around 4°C, apparently still cooling based on satellite and shipboard readings from February. Most of Massachusetts Bay was around 6°C. An intrusion of warmer (7°C) offshore water was noted from Wilkinson Basin (east of Stellwagen Bank), which extended to the eastern edge of the nearfield.

During February, surface waters had cooled to 2°C, with baywide temperatures around 4°-5°C. Intrusions from Wilkinson Basin were again evident through a thermal front running between Cape Ann and Cape Cod. One entered northern Massachusetts Bay, with a second intrusion entering Cape Cod Bay off Race Point.

March and early April had 2°C surface water near the coast and fairly uniform 4°C surface waters in more offshore regions. Southern and eastern Cape Cod Bay was slightly warmer. Imagery from late April showed several "hot spots" (9°-10°C relative to overall 8°-9°C) offshore, over Stellwagen Bank, a region northeast of Cape Ann, and in eastern Cape Cod Bay. Narrow bands of 7°-8°C were seen between Race Point and Duxbury and in southern Cape Cod Bay.

In the beginning of May, surface temperatures were between 9° and 10°C throughout most of Massachusetts Bay. A large area of 8°-9°C water was evident north of Cape Ann, with some intrusion into northern Massachusetts Bay. By mid-month, this water mass was displaced by colder water from the north and appeared to move entirely into Massachusetts Bay except for the western coast and Cape Cod Bay. Late in the month (5/23 and 5/28), the northern portion of Massachusetts Bay had warmed to 12°-13°C. However, cooler (10°-11°C) water dominated southern Mass Bay and northern Cape Cod Bay, either a result of the advection from the north or from offshore waters to the east around Race Point.

Images from June 1 indicated an upwelling event may have occurred along the coast. Cooler water (13°-14°C compared with overall temperatures of 14°-16°C) was evident off Scituate and in western Cape Cod Bay, along with a smaller area south of Cape Ann. Within one week there was a reduction in the area of cooler water in Cape Cod Bay, but an increase in area off Nahant and the coast north of Cape Ann. By late June, temperatures in Massachusetts and Cape Cod Bays were nearly uniform with the exception of a band of cool water along the south shore of Cape Cod Bay (12°-13° compared with 14°-16°C waters overall).

An area of 1°C cooler water along western Massachusetts Bay and north of Cape Ann in early July suggested upwelling may have occurred. In late July there was another band of cooler water (15°C vs. 18°C) along the southern shoreline of Cape Cod Bay.

In early August, a major intrusion of cool surface water (temperatures of 16°-17°C) entered the warmer waters (19°-20°C) of Massachusetts Bay in the region of Stellwagen Basin. August 28 imagery also revealed two major intrusions occurring in Massachusetts Bay, one apparently associated with the general cooling around Cape Ann while the other was evident around Stellwagen Bank. Both these intrusions were around 19°C while temperatures in the Bay were generally between 20° and 21°C.

September imagery indicated a gradual cooldown in Massachusetts Bay and offshore waters, with the warmest waters in southern Cape Cod Bay. Some intrusion of offshore waters was evident on September 11 in the outer regions of Massachusetts Bay. Following near uniform temperatures in early October, imagery from October 19 and 23 showed cooler water from the north intruding into the Massachusetts Bay and Boston Harbor area. By month's end (10/29), there was further evidence of northern coastal water being carried to the south and west, as well as the cooling influence from the Merrimack and other northern rivers along the coast north of Cape Ann. November and December imagery documented inshore cooling progressing toward uniform surface water temperatures regionwide.

3.1.3 1992-1995 Interannual Comparisons

The annual cycle for average nearfield surface and bottom water temperatures for the period 1992 to 1995 was plotted to examine interannual differences (Figure 3-4, top). Surface temperatures were similar for each year, although 1995 had a brief period approximately 2°C higher than that seen in previous years. The most pronounced feature of the four-year record is the relatively high bottom temperatures evident in the latter parts of 1994 and 1995. While bottom temperatures did not exceed 9°C during either 1992 or 1993, the maximum temperature during 1994 was around 12°C, and was just slightly higher during 1995.

More importantly, the bottom temperature in the outer nearfield during 1994 exceeded the 9°C 1992-1993 maxima for a duration of almost five months. Although peak bottom temperatures were slightly higher in 1995, the duration of temperatures above 9°C was only around two months. The potential for high metabolic activity and respiration was therefore greatest during 1994. This potential is discussed in greater detail in Sections 6 and 7.

A similar scenario was evident in Stellwagen Basin (Figure 3-4, bottom). Surface temperatures were similar in each of the four years except for the August 1994 survey which yielded cooler than usual temperatures (16°C). Average maximum bottom temperatures in Stellwagen Basin during 1992-1993 were only around 7°C. However, the maximum bottom temperature in 1994 was around 10°C, while maximum temperatures in 1995 were around 9°C. The frequency of farfield measurements did not permit a precise determination of how long temperatures in 1994 & 1995 remained above 1992-1993 maxima, but it appeared that this may have lasted for a minimum of two months.

3.2 Salinity

3.2.1 Nearfield

As with the temperature data, surface and bottom salinity profiles were plotted for the three regions of the nearfield (Figure 3-5). General trends showed surface salinities decreasing steadily through June, while bottom salinities continued to decrease through mid-August. Salinity then increased through the fall, with the notable exception of a decrease seen in both surface and bottom waters in late November.

A closer examination of the survey results indicated a large influx of fresher waters at the surface documented by the late March sampling event, followed by a rapid convergence of surface and bottom salinities by early April. In May, there was a noticeable reduction in surface and bottom salinities during the sixth survey. Surface water salinity reductions were also evident in data collected in late June and early August.

Continuously-recorded data from the USGS mooring documented the convergence of surface and bottom salinities in the nearfield during the early parts of April, May, and October (Figure 3-6). Coupled with the temperature data, these results would indicate that water column mixing occurred during these periods. Reductions in salinity at the surface during June and August were not evident in bottom water measurements, suggesting that these events were the result of surface advection of fresher waters into the nearfield.

3.2.2 Regional Comparisons

Harbor and coastal stations had the lowest regional salinity averages (Figure 3-7). Harbor surface waters were consistently lower in salinity than bottom waters through the April survey, after which only slight vertical differences were evident in both the harbor and coastal waters. Coastal stations did exhibit convergence of surface and bottom salinities in August.

Offshore and boundary stations were fairly homogenous through the April survey. The June survey documented more than a 1.0 PSU difference between surface and bottom, while subsequent surveys indicated much less vertical difference. Cape Cod Bay averages indicated that any vertical salinity differences were quite modest, and overall were quite similar to the coastal stations.

3.2.3 Influence of Precipitation and River Discharge on Salinity

Precipitation data from Logan Airport obtained from the Northeast Regional Climate Center (NRCC, 1996) documented two large precipitation events (> 1" rainfall) in January (Figure 3-8a). This rainfall combined with the meltdown of approximately two feet of snow on the ground and resulted in peak winter/spring discharges in the Merrimack River (ca. 25,000 cfs)[1] and the Charles River (ca. 850 cfs)[2] (Figure 3-8b and c). Additional periods of heavy rain in late February and early March resulted in a second pulse of riverine discharge, with the Merrimack peaking twice over 20,000 cfs and the Charles discharging over 500 cfs for approximately one month. Following smaller discharge peaks in April and May, median discharge rates were reached by June 1.

The periods of heavy discharge from the two rivers during January and March coincide with the precipitous drops in salinity seen in the moored data during these periods (refer to Figure 3-6). Precipitation events in May/June and again in late July to early August coincided with modest surface salinity drops. Autumn precipitation events starting in late September resulted in annual peak river discharges in November (37,800 cfs[1] in the Merrimack River and 1,070 cfs[2] in the Charles). There was a concurrent drop in salinity visible in the nearfield survey data and moored sensor data during late November and early December.

3.2.4 Wind Effects on Salinity and Temperature

Temperature fluctuations consistent with upwelling regimes have been shown to be significantly correlated with southwesterly wind patterns in Massachusetts Bay (Geyer *et al.*, 1992). During a sustained southwesterly wind event, sub-thermocline waters reach the surface in the coastal areas in western Massachusetts Bay. A typical characteristic of an upwelling event would be colder surface temperatures at coastal stations (e.g., F05, F13, N10, N01, etc.) than at the more seaward stations. This may well be accompanied by observable elevations in surface salinity at the inshore stations. The most intense occurrence is typically in the area of Broad Sound (Geyer *et al.*, 1992). Conversely, sustained northeasterly winds can produce downwelling along the coast, which can tend to erode the pycnocline.

Wind data from Logan International Airport were obtained to identify periods where wind patterns were favorable for upwelling or downwelling conditions. Wind data from May through September were plotted along with the continuously recorded surface (5m) temperature and salinity recorded by the USGS

[1] Merrimack R. data from gage 01100000 in Lowell, MA., multiplied by 1.08 to estimate discharge at mouth of river (USGS, 1996b)

[2] Charles R. data from gage 01104500 at Waltham, MA., multiplied by 1.27 to estimate discharge at mouth of river (USGS, 1996b)

moorings near station N21 (Figure 3-9). The data suggest that wind effects on water column integrity may have occurred during early June and July, and during the second week of August. On each occasion, several days of west-southwesterly winds were accompanied by decreasing surface temperatures and increasing surface salinities.

This evidence of upwelling during June and July is consistent with the interpretation of satellite imagery in Section 3.1.2. Interestingly, northeasterly winds occurred just before and after the August period, coinciding with the two Gulf of Maine intrusions documented in the satellite imagery. This sequence may have contributed to an enhanced degree of inshore mixing during August.

3.2.5 Interannual Comparisons

Interannual plots of surface and bottom salinities in the nearfield and Stellwagen Basin indicated that the highest salinities occurred in 1994, and the lowest in 1992 and 1993 (Figure 3-10). Conditions in 1995 were more similar to 1994, particularly in bottom waters. Surface waters in the nearfield in 1995 were similar to 1992 and 1993 but lacked a spring minimum.

3.3 Water Column Stratification

Massachusetts Bay is typically characterized by a seasonal cycle from cold, well-mixed waters during winter months to strong stratification during summer. Early stratification during spring is salinity-driven due to freshwater runoff from the major rivers to the north and from coastal runoff, while temperature dominates the density structure during summer and fall (Geyer *et al.,* 1992). In the following sections, the water column structure in the nearfield during 1995 is compared with other regions within the system, as well as with previous baseline monitoring years.

3.3.1 1995 Nearfield Stratification

The density data for the both the inshore and offshore nearfield stations indicated that stratification did not develop until after the May survey W9506 (Figure 3-11). Afterwards, water column stratification was characterized by $\Delta\sigma_t$ values of approximately -1.5 to -3.0 kg/m^3 between surface and bottom waters until late September. The stratification was most pronounced in the Outer Nearfield stations.

Perturbations in the water column were most evident at the Inner Nearfield and Broad Sound stations, which are subject to breakdown of stratification from upwelling and downwelling events and to tidal influences from Boston Harbor through Nantasket Roads. However, each of the nearfield regions showed evidence of mixing during April, May, and July. The inner nearfield stations indicated an event in early August during which both surface and bottom densities dropped about 1 kg/m^3 from the previous survey's

measurements, due to the drop in water temperature (primarily) and salinity. This is noticeable to a lesser extent at Broad Sound and the Outer Nearfield Stations.

In late September the waters at the Inner and Broad Sound stations appeared to converge somewhat earlier than the outer nearfield stations, which showed convergence by the next survey (early October). The water column in the entire nearfield grid was homogenous after mid-November.

3.3.2 Regional Comparisons

The winter months were characterized by a well mixed water column throughout the survey area (Figure 3-12). Harbor stations exhibited little seasonal vertical structure. Offshore and Boundary stations were most similar to outer nearfield stations, as they were the most highly stratified stations during the summer months. Coastal stations, like the inner nearfield stations, exhibited a drop in the density throughout the water column in the August survey.

The seasonal progression of stratification was plotted for several stations representing a transect from inshore to offshore (Figures 3-13 to 3-18). The stations selected for this illustration included five productivity/respiration stations (F23, N16, N04, N07, and F19), allowing later reference to water column structure in the discussions of data in Section 7. Station N10 was included in this transect to demonstrate the tidal influence from the harbor on water column structure in the inner nearfield.

Harbor station F23 showed little vertical structure other than slight thermal stratification during the summer (Figure 3-13, using Figures 3-3 and 3-7 for reference). Nearfield stations N10 and N16 each showed a salinity-driven stratification during survey 3 which had disappeared by the next survey (Figures 3-14 and 3-15). The salinity-driven stratification was also evident in results from N04, but appeared to persist through surveys 4 and 5 (Figure 3-16). Station N07 did not exhibit the same degree of early season structure (Figure 3-17), while station F19 in Stellwagen Basin appeared to be similar to N04 (Figure 3-18, note reduced frequency of survey coverage).

Beyond this early season influence from salinity, the water column remained fairly homogenous until the onset of thermally-driven stratification by survey 6. The stratified period lasted from early May until October when the water column began to turn over (survey 14). However, the extent of the July mixing event described in earlier sections is well-documented in the nearfield station results. Mixing to a depth of at least 15m was evident in profiles from survey 8 and 9, particularly at the more inshore stations N10 and N16. Stratification had re-established by survey 10 at the more offshore stations and by survey 11 inshore. By survey 14, the water column had mixed almost to the bottom at each station.

3.3.3 1992-1995 Interannual Comparisons

A comparison of the surface and bottom densities for the 1992-1995 data record indicated that the structure of the water column in the nearfield was most stable during 1994 (Figure 3-19a). Although bottom water densities were for the most part similar from year to year, surface densities were highest and had the least amount of variability. Results from 1995 were more similar to 1994 than previous years, with the greatest departure associated with the July upwelling event and the August intrusions of Gulf of Maine water described earlier. Results for the Stellwagen basin stations were much more comparable between the years, with the main difference being the more dense surface waters during 1994 (Figure 3-19b).

TABLE 3-1

Summary of 1995 Satellite Imagery for Massachusetts and Cape Cod Bays

Month	Date	Upwelling	G.O.M. Intrusion	Image Number	Location
January	1/30/95		X	E9503017.MD7	Wilkinson Basin to Nearfield
February	2/17/95		X	E9504817.MD7	Wilkinson Basin to Nearfield
March	3/29/95			E9508812.MD7	
April	4/3/95			E9509312.MD7	
	4/25/95			E9511517.MD7	
May	5/4/95		X	E9512412.MD7	Northern Mass Bay
	5/14/95		X	E9513412.MD7	Mass Bay except western coast
	5/23/95			E9514312.MD7	
	5/28/95			E9514812.MD7	
June	6/1/95	X		E9515212.MD7	Western Mass and Cape Cod Bays
	6/6/95	X		E9515712.MD7	Western Mass Bay, north of Cape Ann
	6/16/95			E9516717.MD7	
	6/20/95			E9517112.MD7	Southern Cape Cod Bay
	6/27/95	X		E9517817.MD7	
July	7/5/95	X		E9518611.MD7	Western Mass Bay, north of Cape Ann
	7/6/95	X		E9518717.MD7	
	7/22/95			E9520312.MD7	
	7/31/95	X		E9521212.MD7	Southern Cape Cod Bay
August	8/1/95	X		E9521312.MD7	Stellwagen Basin
	8/7/95	X		E9521917.MD7	Stellwagen Basin
	8/13/95			E9522517.MD7	
	8/22/95	X		E9523417.MD7	Cape Ann and Stellwagen Basin
	8/28/95	X		E9524012.MD7	Cape Ann and Stellwagen Basin
Septembe r	9/3/95	X		E9524617.MD7	
	9/11/95			E9525417.MD7	Eastern Mass Bay
	9/12/95			E9525517.MD7	
	9/30/95			E9527317.MD7	

TABLE 3-1 (Cont'd)

Summary of 1995 Satellite Imagery for Massachusetts and Cape Cod Bays

Month	Date	Upwelling	G.O.M. Intrusion	Image Number	Location
October	10/9/95			E9528212.MD7	
	10/12/95	X		E9528517.MD7	Northern Mass Bay and Boston Harbor
	10/19/95	X		E9529211.MD7	Northern Mass Bay and Boston Harbor
	10/23/95			E9529612.MD7	
	10/24/95	X		E9529711.MD7	Northern Mass Bay and Boston Harbor
	10/29/95			E9530211.MD7	
November	11/5/95			E9530912.MD7	
	11/6/95			E9531012.MD7	
	11/17/95			E9532117.MD7	
	11/22/95			E9532617.MD7	
December	12/2/95			E9533617.MD7	
	12/5/95			E9533907.MS7	
	12/8/95			E9534223.MS7	
	12/10/95			E9534417.MD7	
	12/17/95			E9535123.MS7	
	12/29/95			E9536306.MS7	

[1]G.O.M. = Gulf of Maine
Source: http://narwhal.gso.uri.edu/cwatch1.html

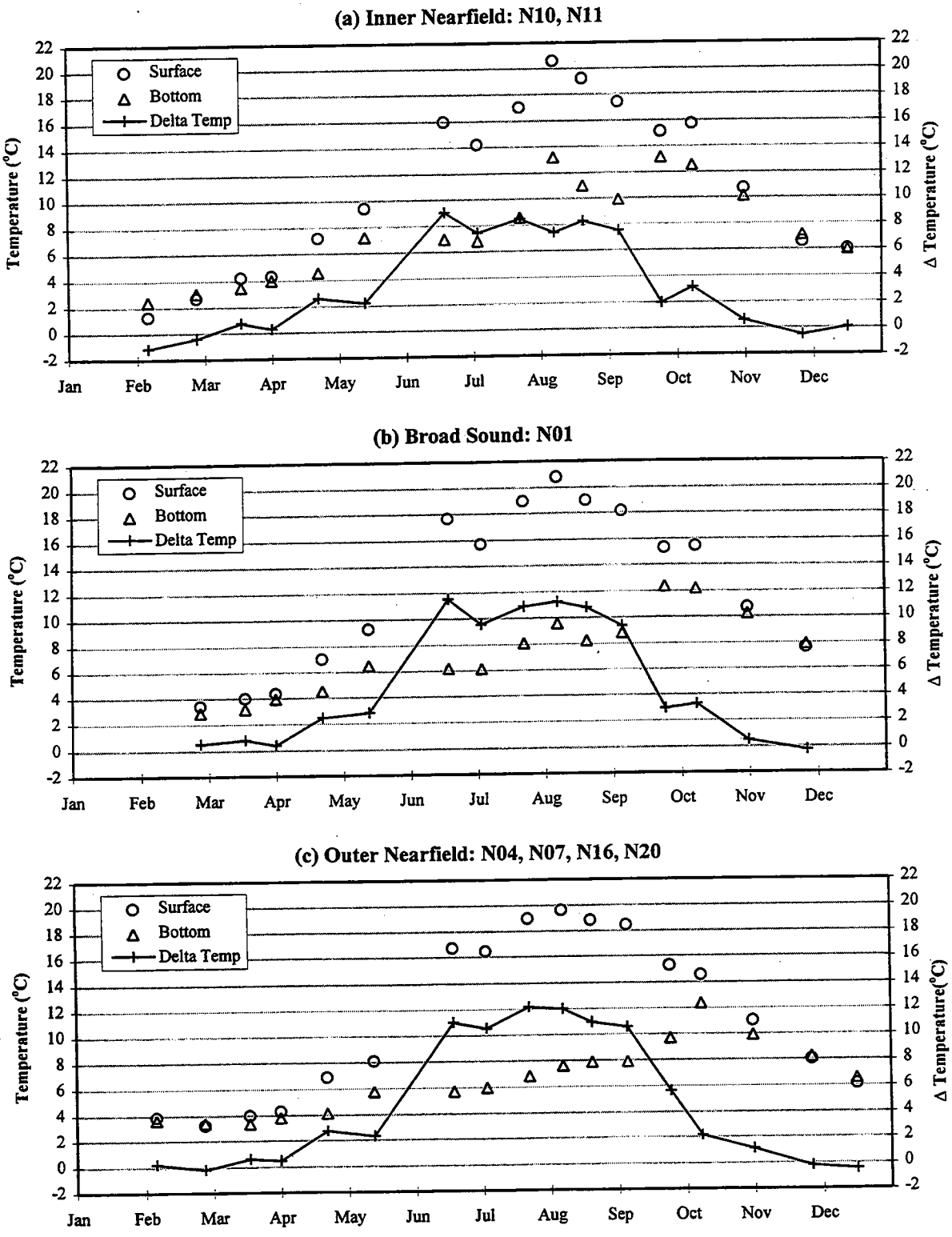

FIGURE 3-1

1995 Nearfield Temperature Cycle

Surface, Bottom, and Delta (Surface - Bottom) Survey Averages

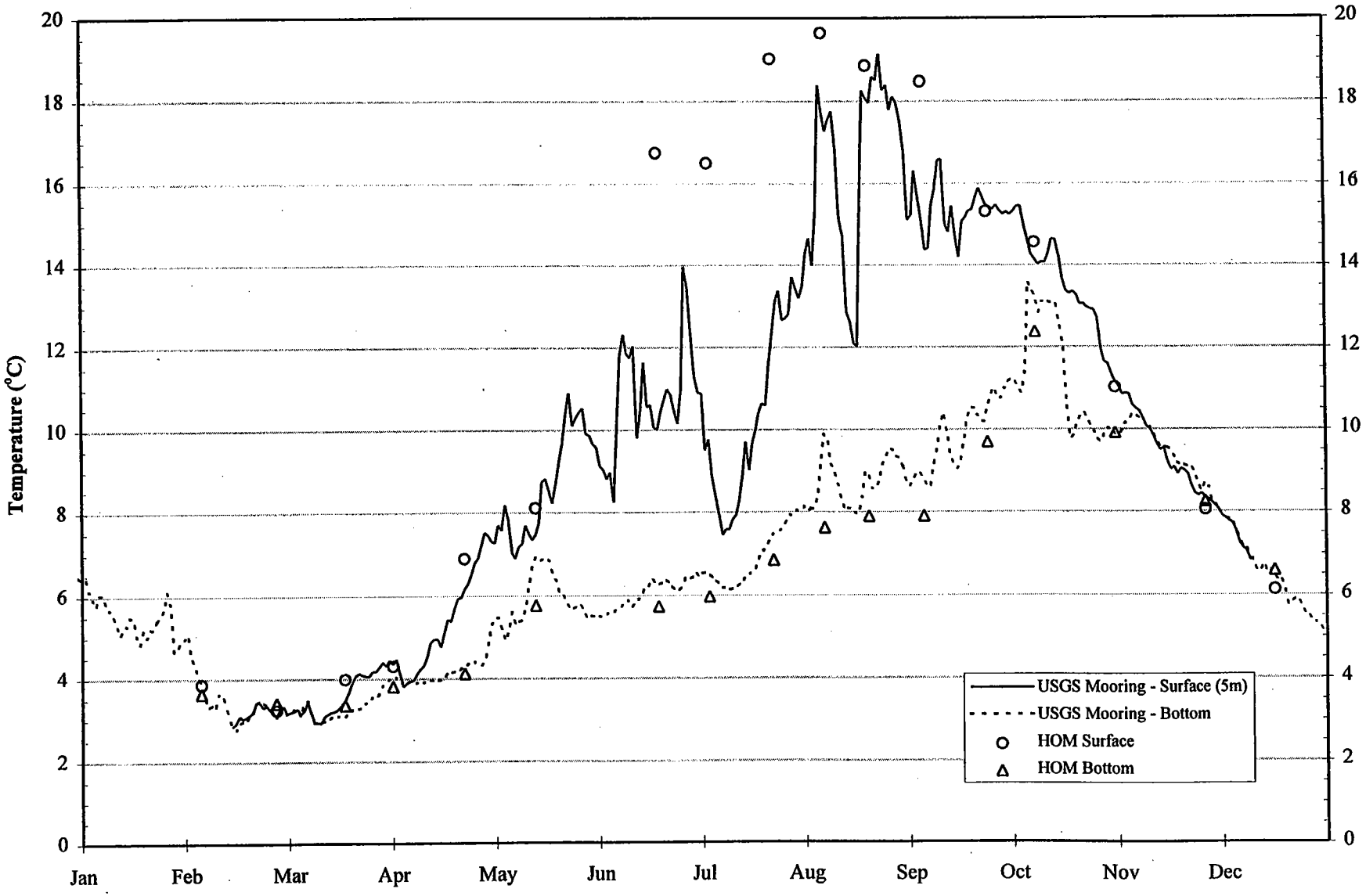

FIGURE 3-2

1995 Moored Temperature Sensor Data

with Outer Nearfield (N04, N07, N16, N20) Surface and Bottom Survey Data

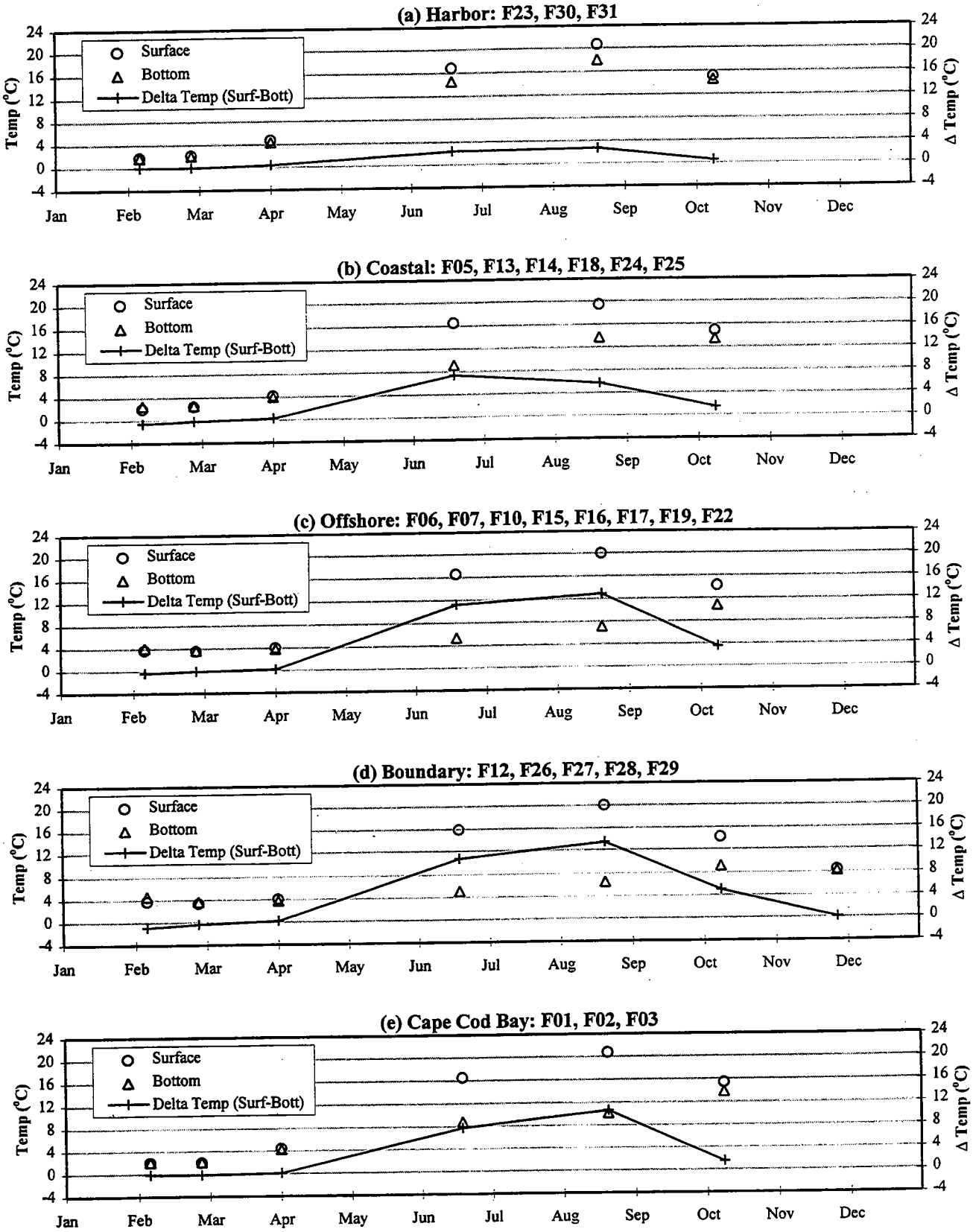

FIGURE 3-3

1995 Regional Temperature Averages

Surface, Bottom, and Delta (Surface - Bottom) Survey Averages

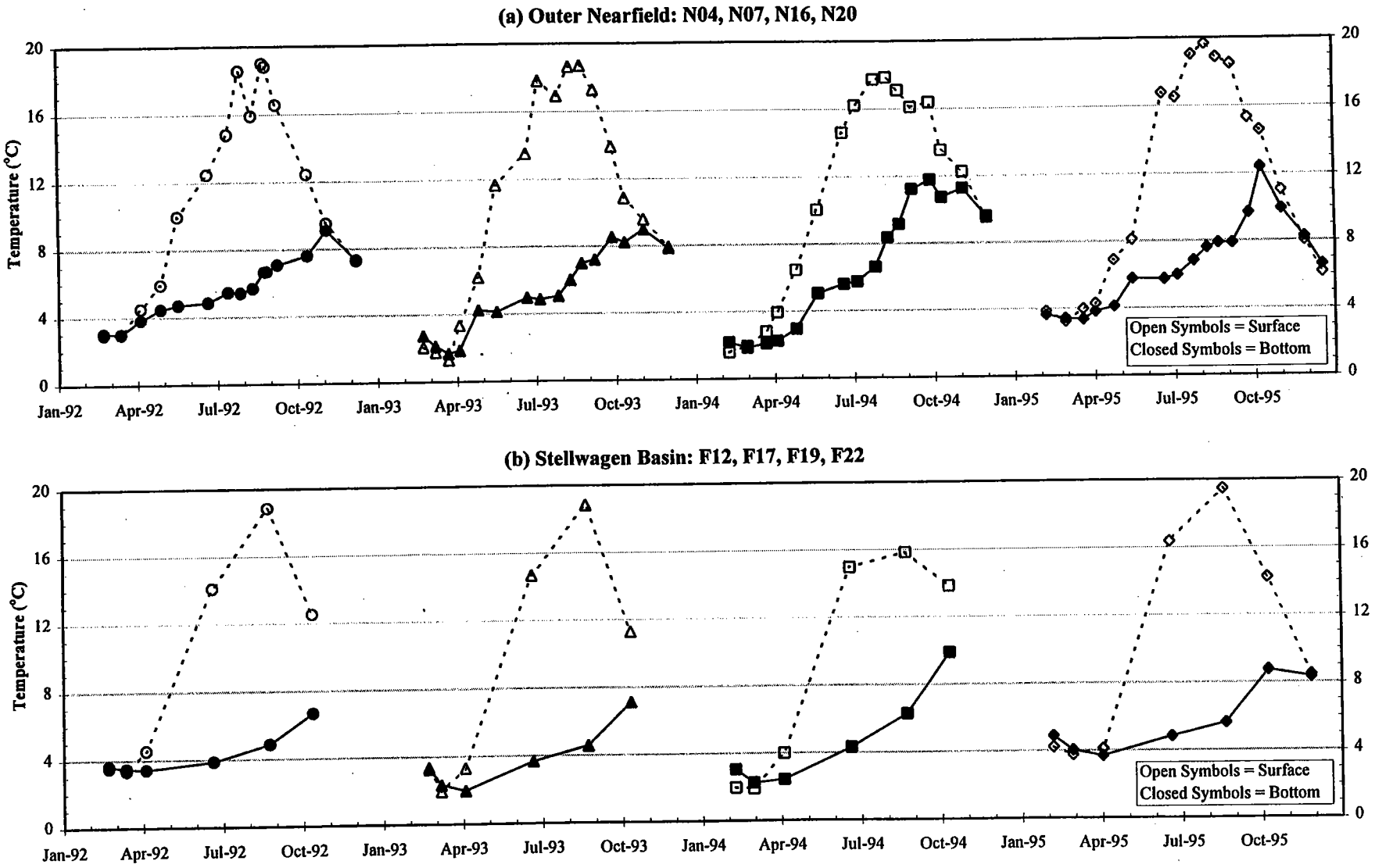

FIGURE 3-4

Interannual Comparison of Temperature in the Nearfield and Stellwagen Basin Regions

WC Casts, Surface (A) and Bottom (E) depths averaged over stations as indicated

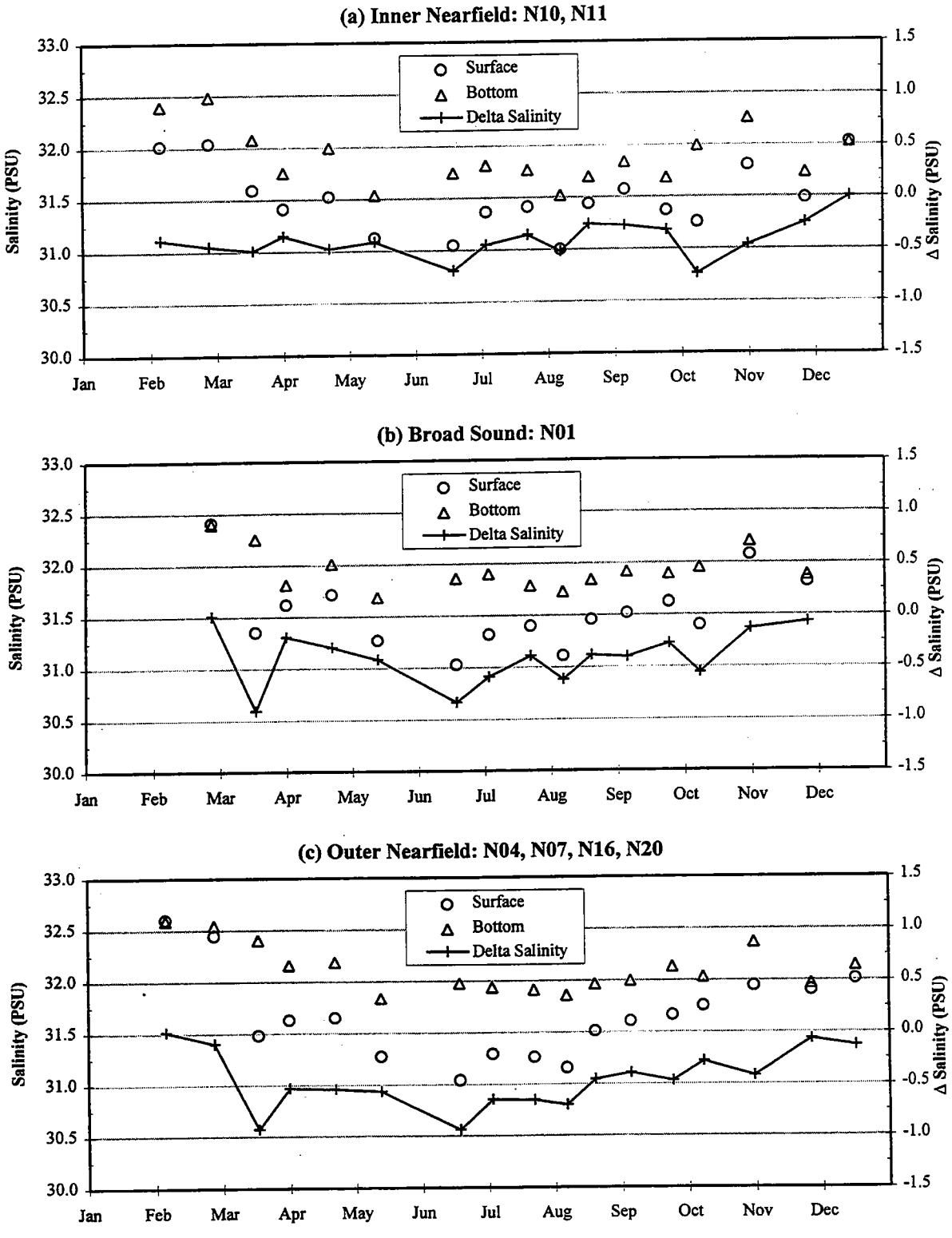

FIGURE 3-5

1995 Nearfield Salinity Cycle

Surface, Bottom, and Delta (Surface - Bottom) Survey Averages

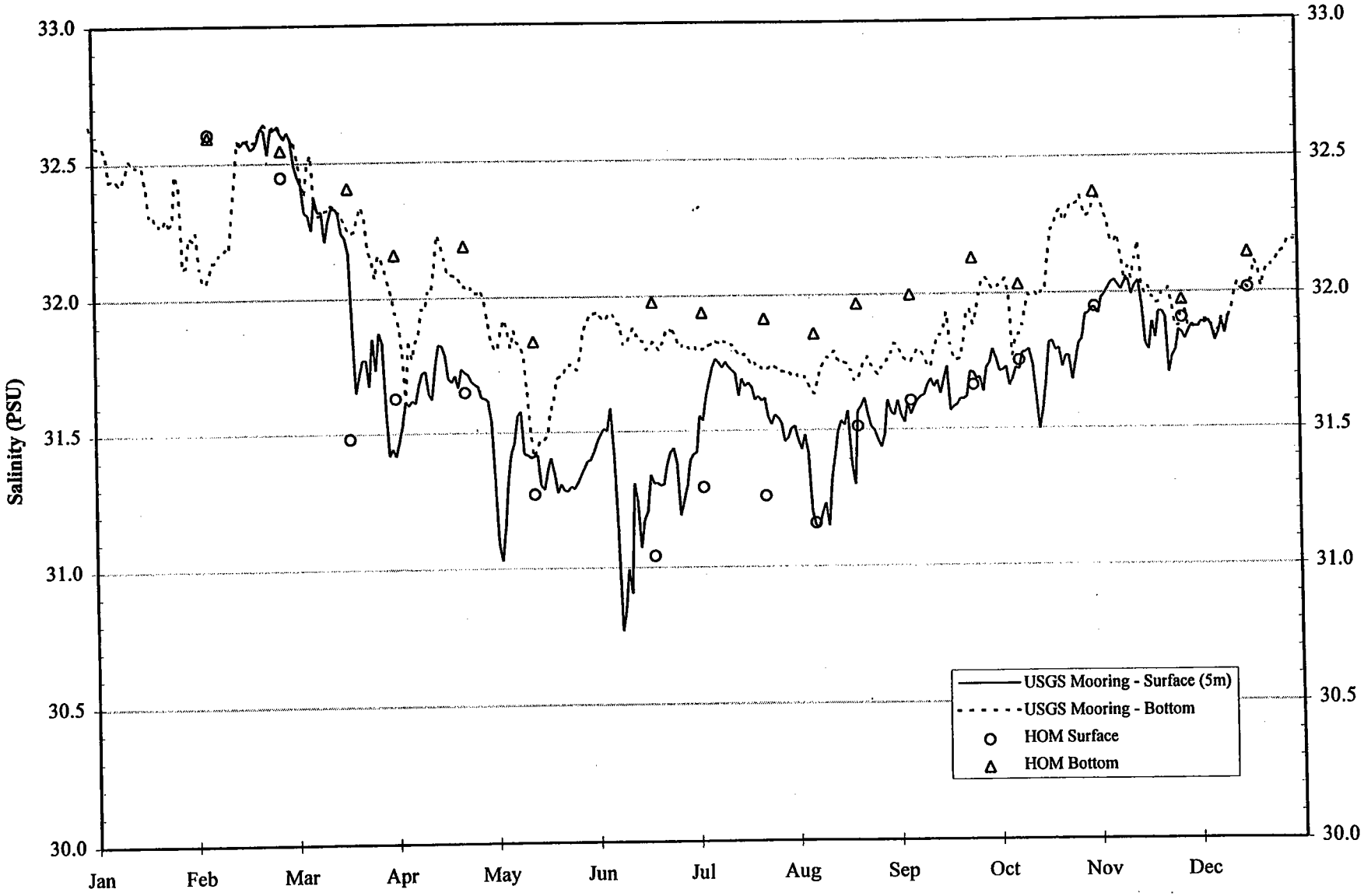

FIGURE 3-6

1995 Moored Salinity Sensor Data

with Outer Nearfield (N04, N07, N16, N20) Surface and Bottom Survey Data

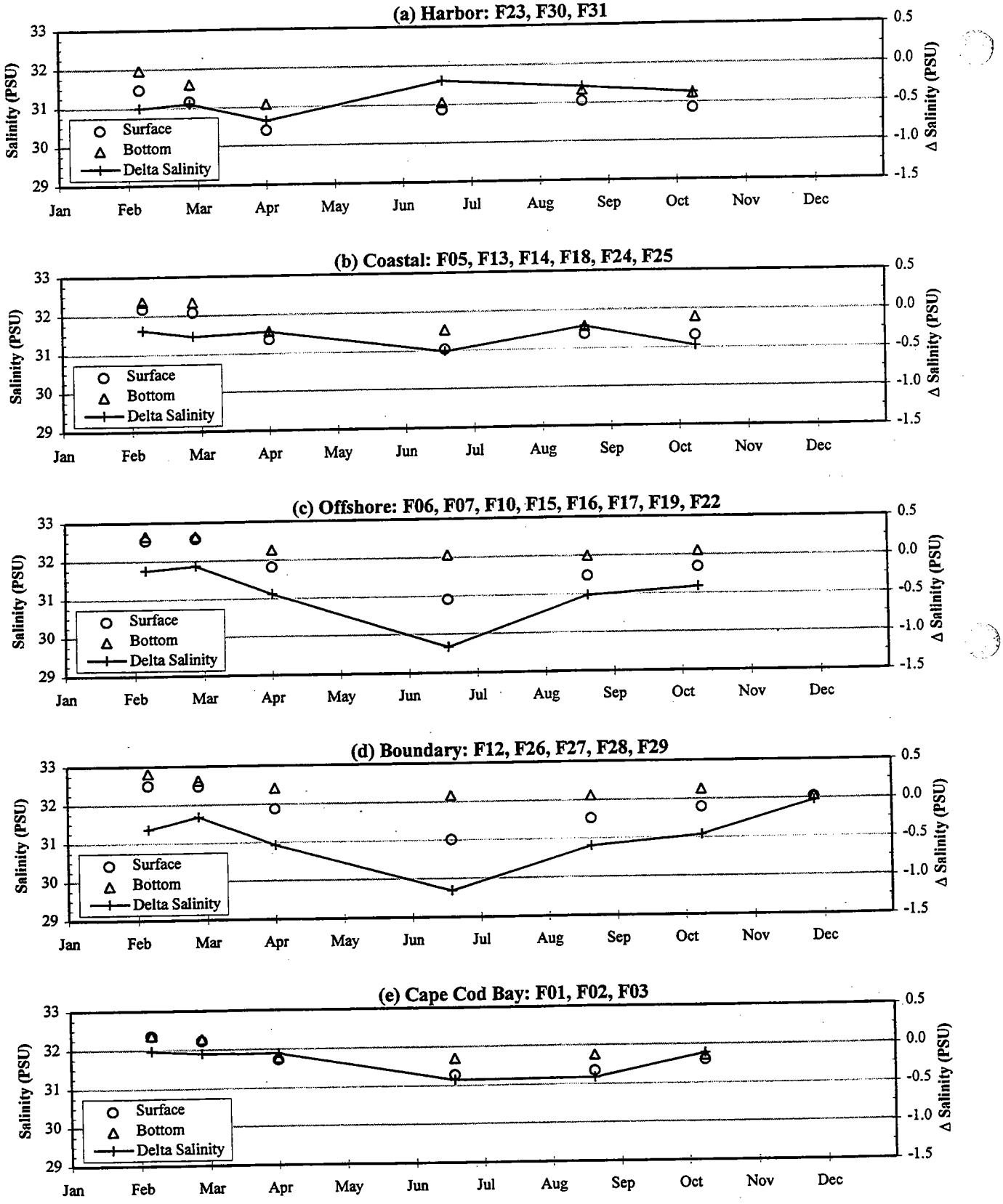

FIGURE 3-7

1995 Regional Salinity Averages

Surface, Bottom, and Delta (Surface - Bottom) Survey Averages

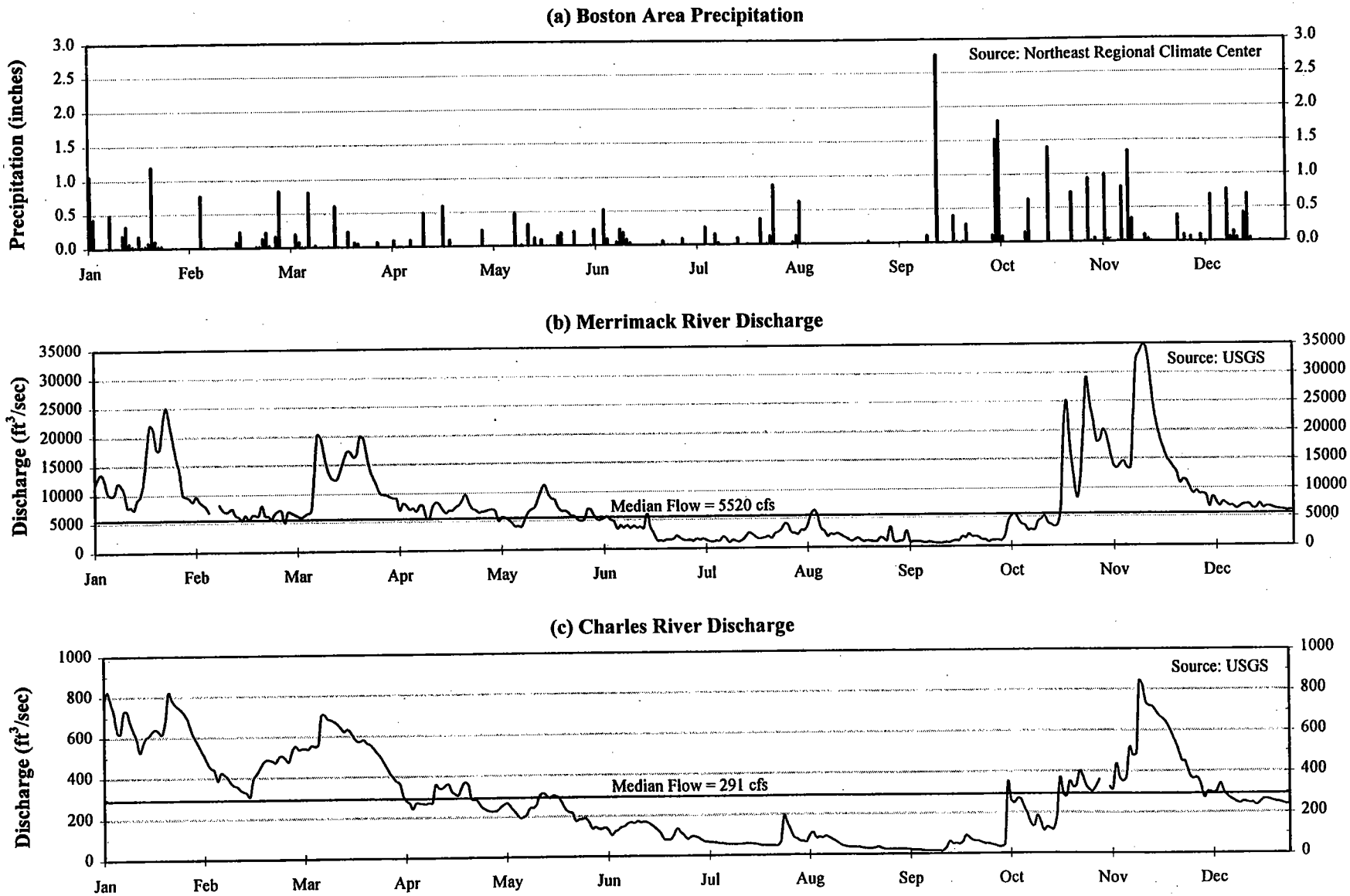

FIGURE 3-8

1995 Daily Precipitation (Logan International Airport) and River Discharge Data

Merrimack and Charles Rivers

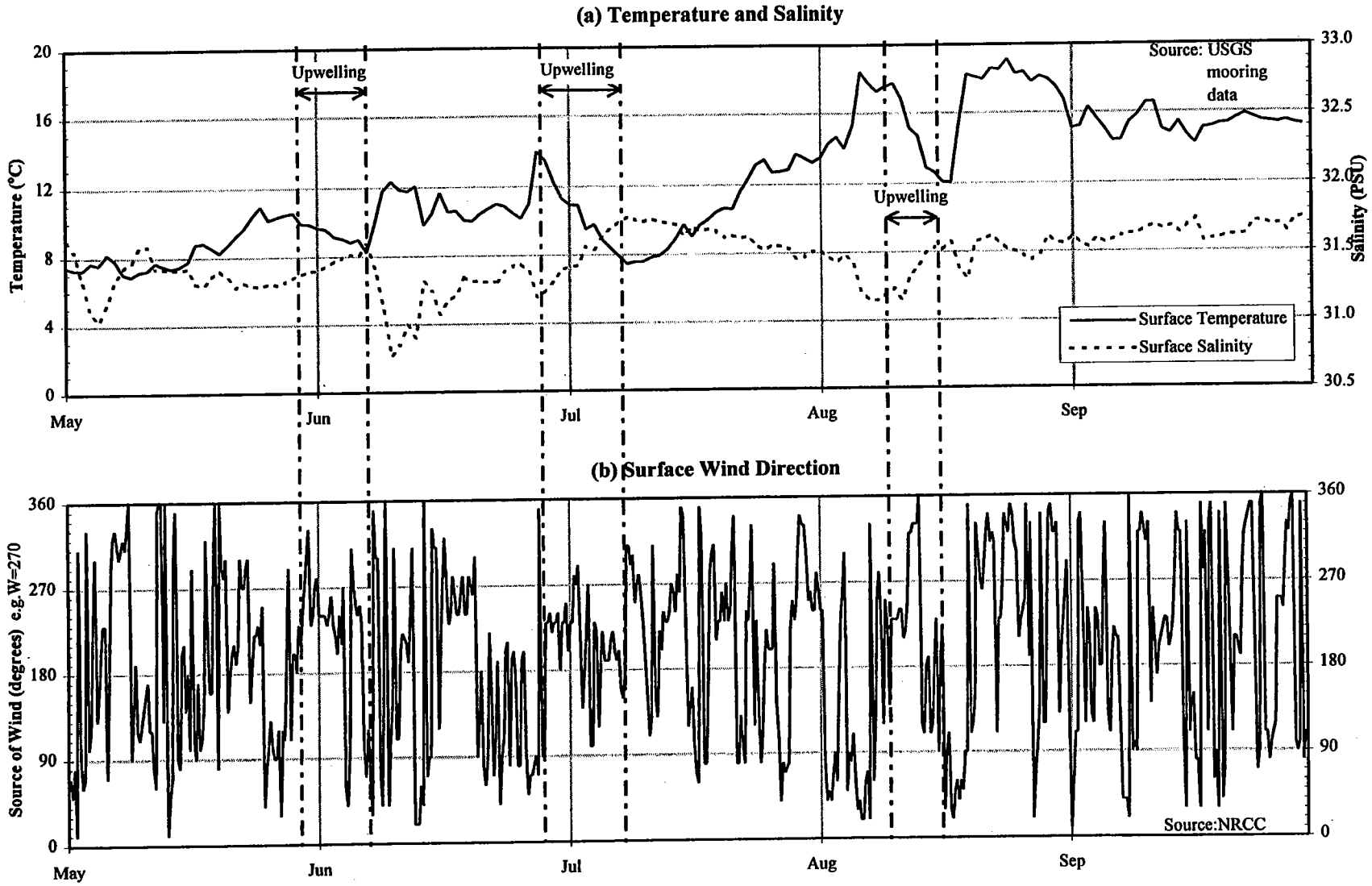

FIGURE 3-9
1995 Upwelling Events Based on Moored (5m) Temperature and Salinity Data,
and Surface Wind Data at Logan International Airport

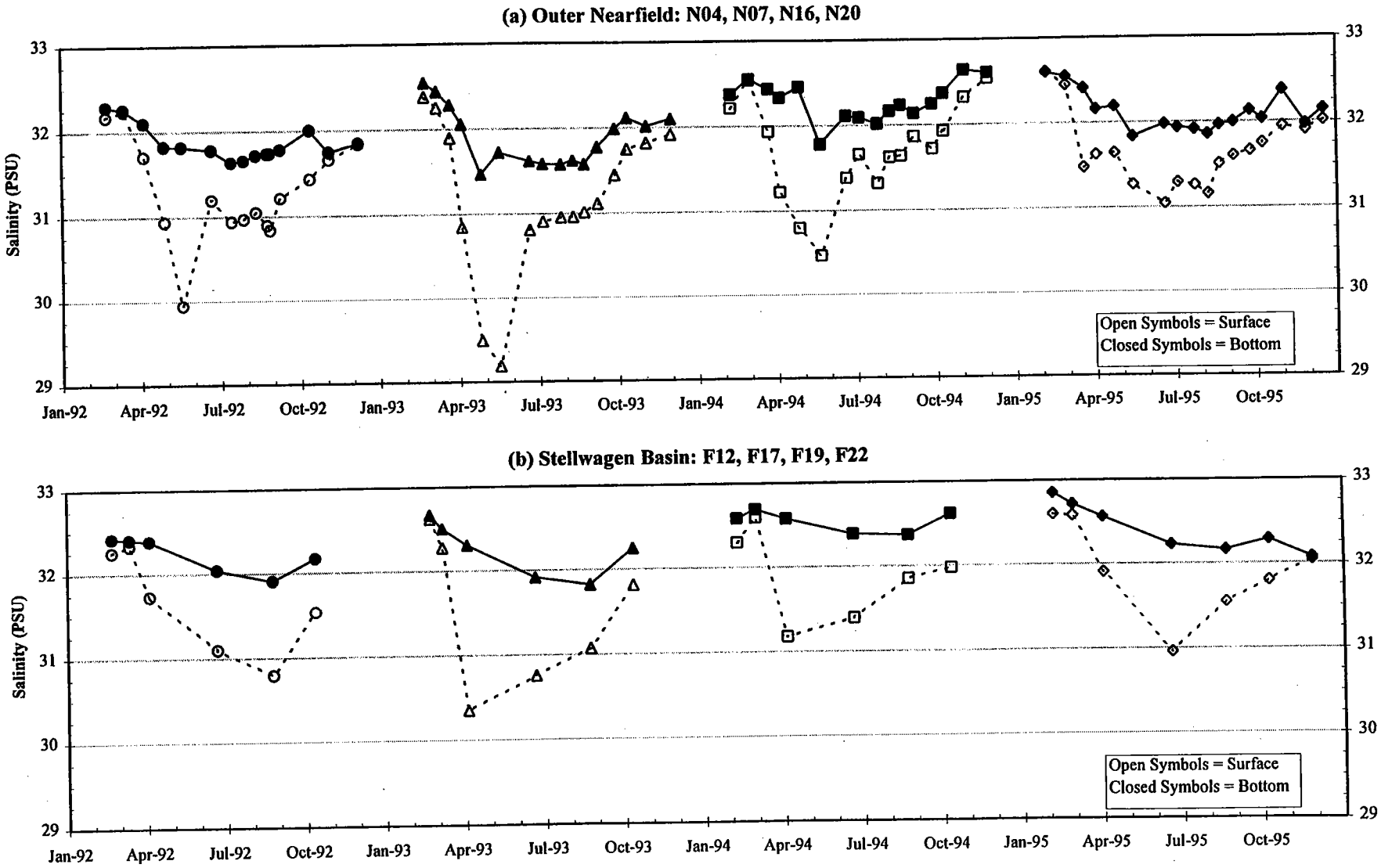

FIGURE 3-10

Interannual Comparison of Salinity in the Nearfield and Stellwagen Basin Regions

WC Casts, Surface (A) and Bottom (E) depths, Stations as indicated.

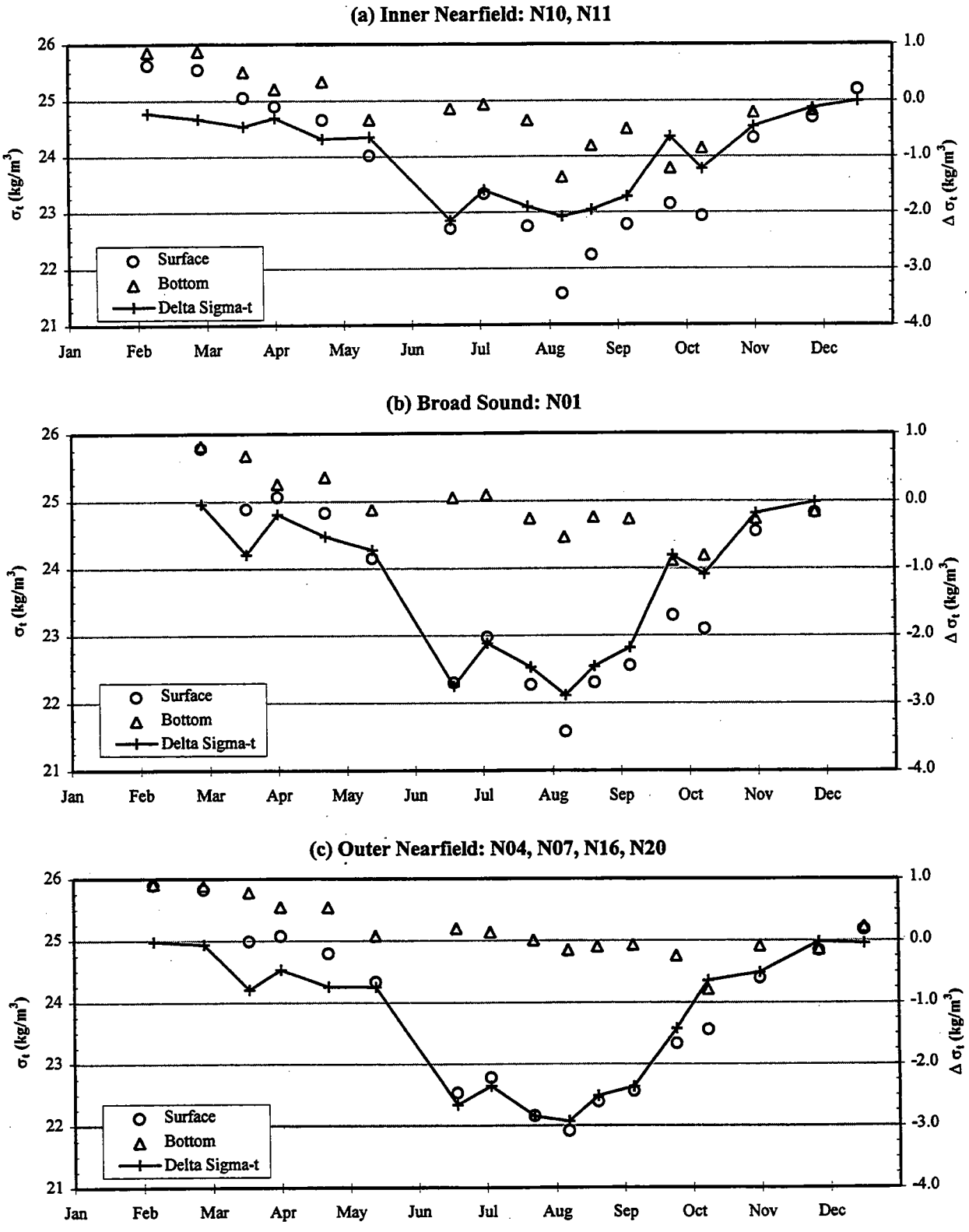

FIGURE 3-11

1995 Nearfield Density (σ_t) Cycle

Surface, Bottom, and Delta (Surface - Bottom) Survey Averages

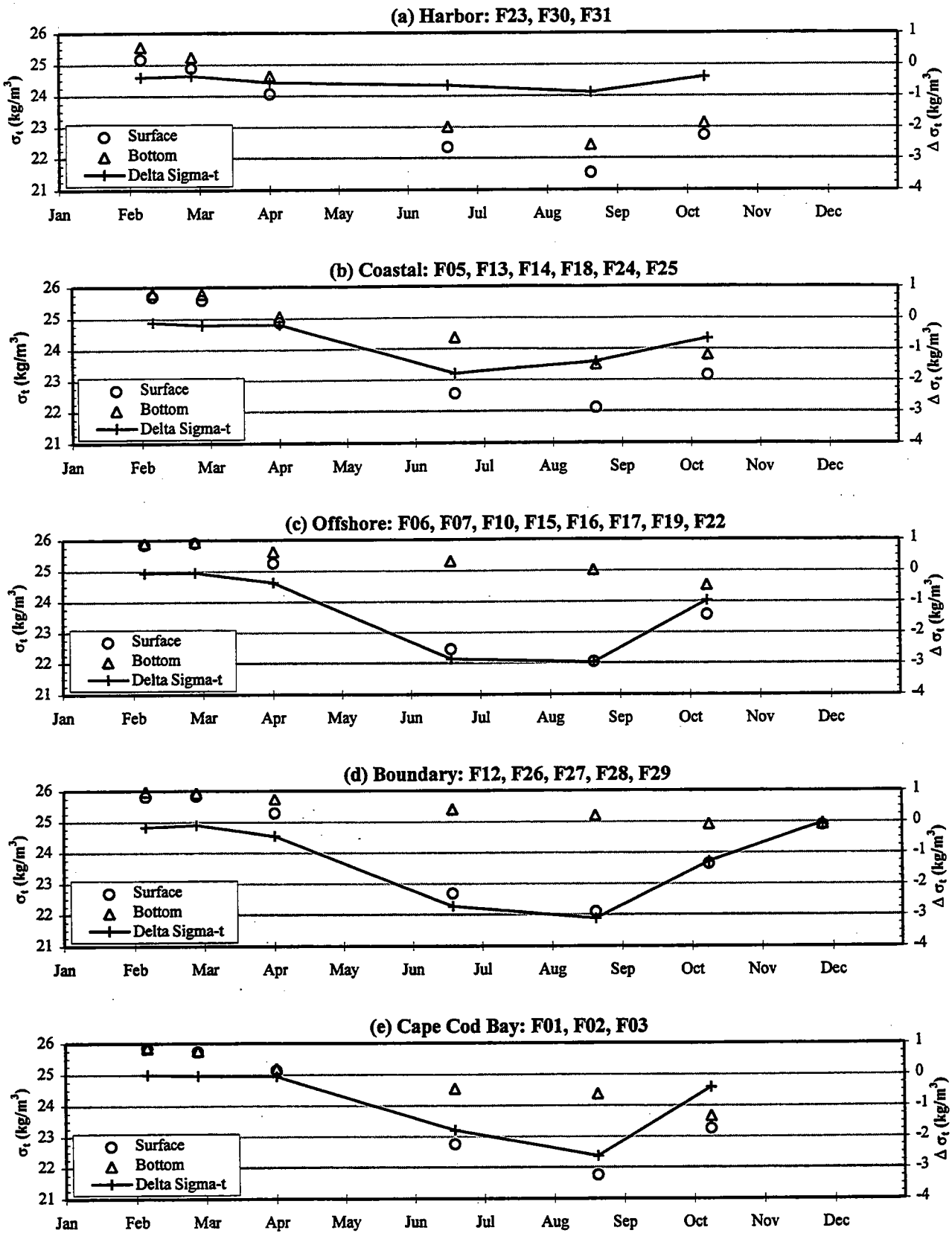

FIGURE 3-12

1995 Regional Density (σ_t) Averages

Surface, Bottom, and Delta (Surface - Bottom) Survey Averages

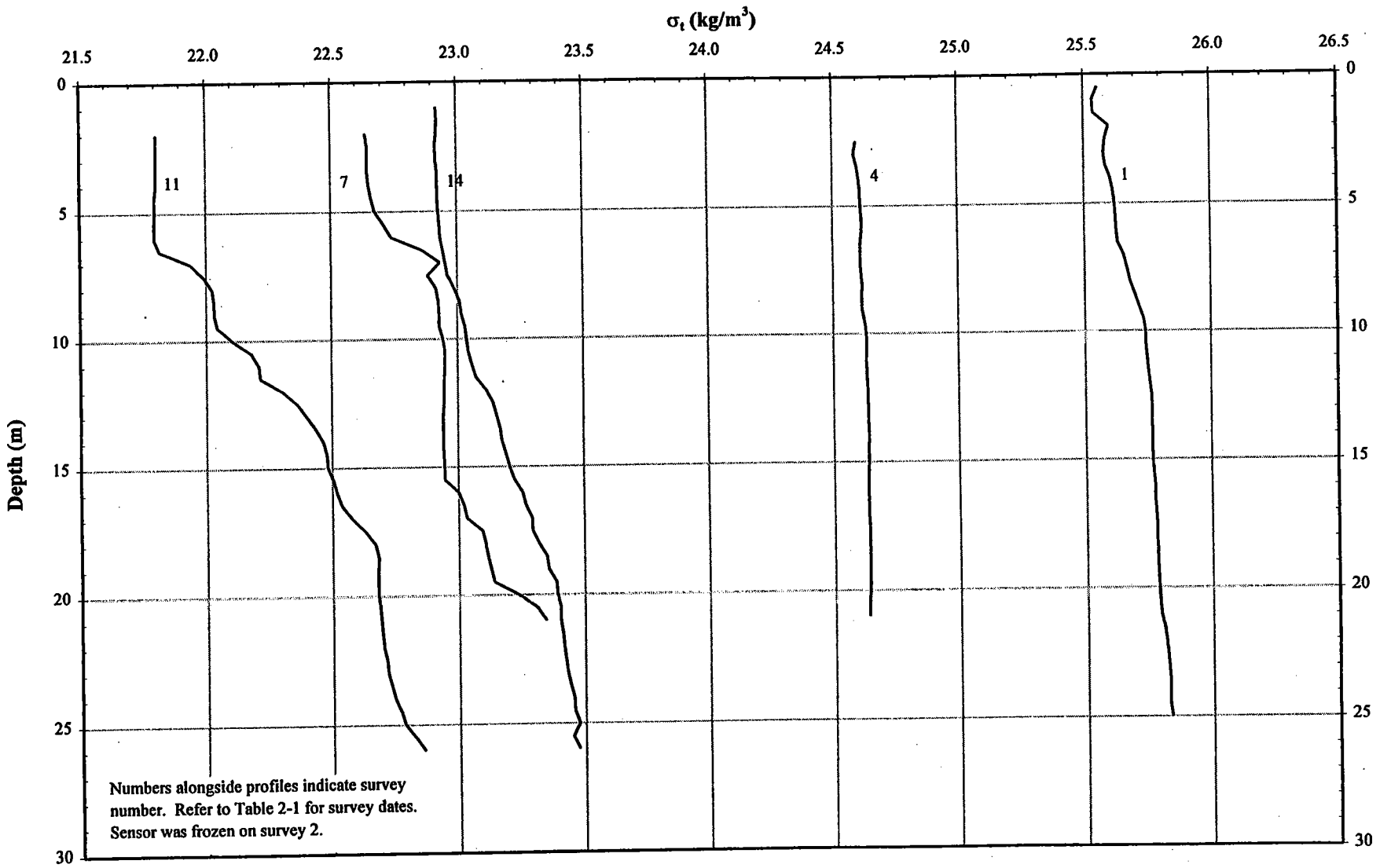

FIGURE 3-13

1995 Seasonal Density (σ_t) Cycle at Productivity/Respiration Station F23

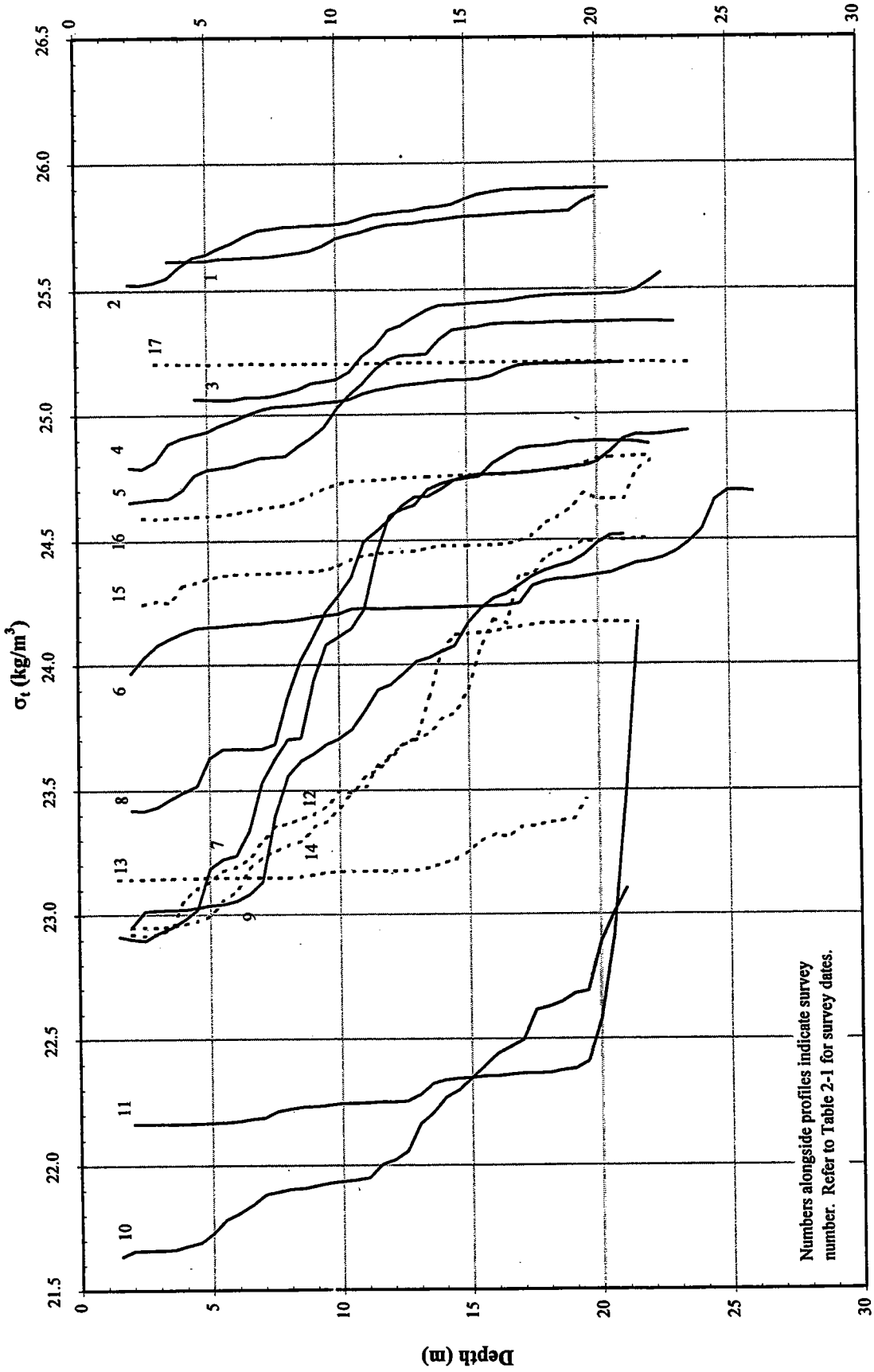

FIGURE 3-14
1995 Seasonal Density (σ_t) Cycle at Station N10

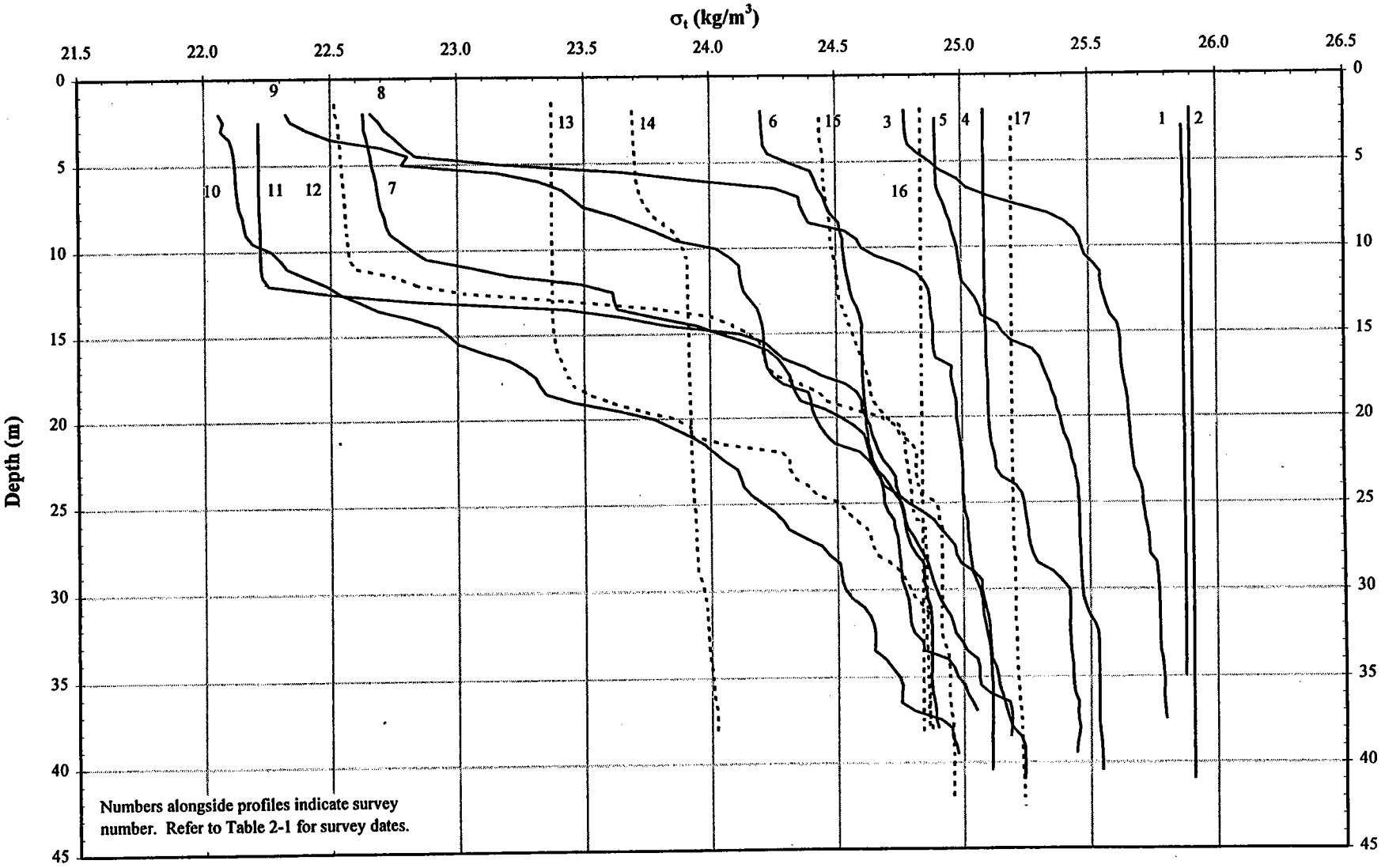

FIGURE 3-15

1995 Seasonal Density (σ_t) Cycle at Productivity/Respiration Station N16

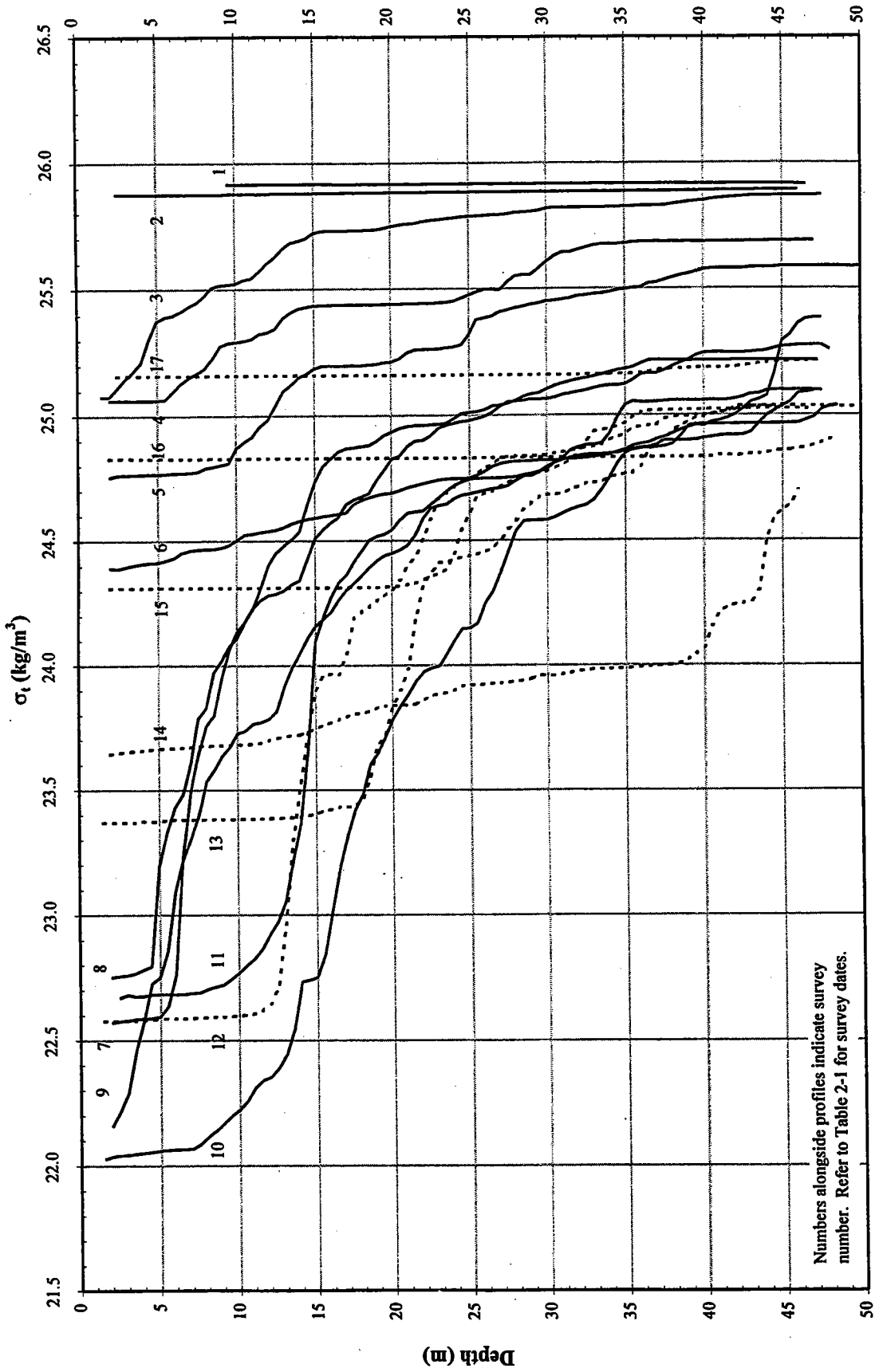

FIGURE 3-16
1995 Seasonal Density (σ_t) Cycle at Productivity/Respiration Station N04

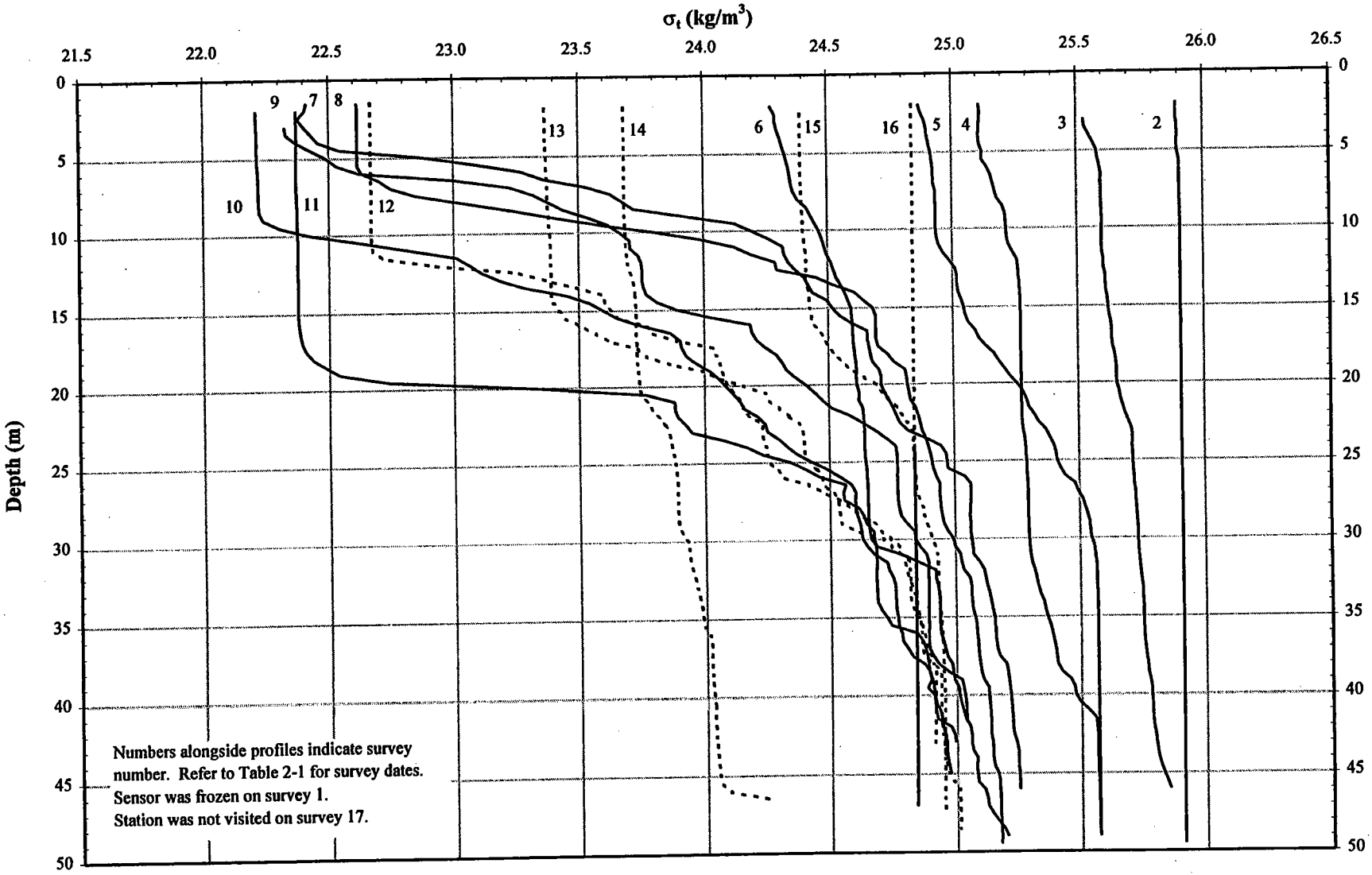

FIGURE 3-17

1995 Seasonal Density (σ_t) Cycle at Productivity/Respiration Station N07

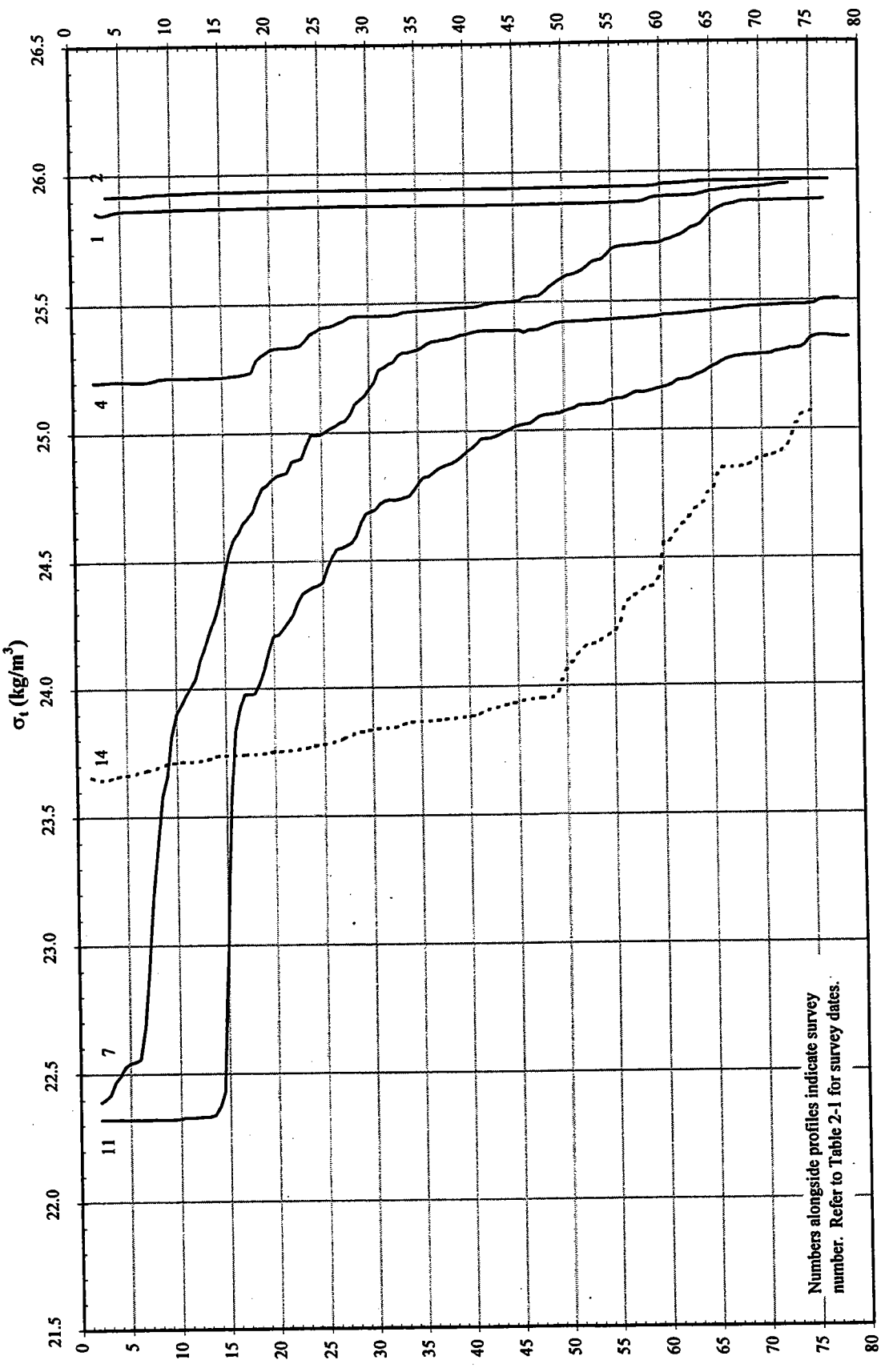

FIGURE 3-18
1995 Seasonal Density (σ_t) Cycle at Respiration Station F19

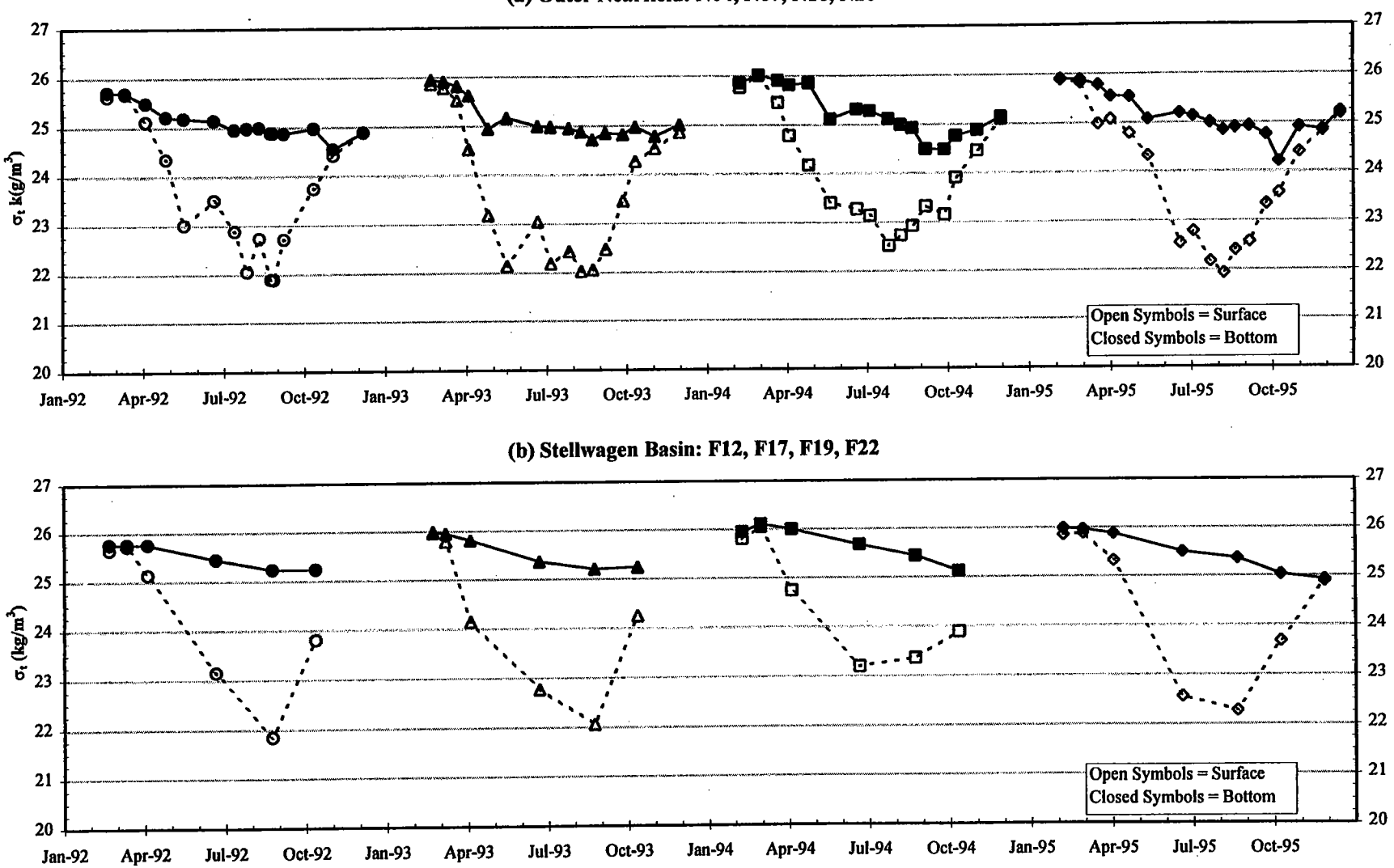

FIGURE 3-19

Interannual Comparison of Density (σ_t) in the Nearfield and Stellwagen Basin Regions

WC Casts, A and E depths, Stations as indicated

4.0 NUTRIENTS

This section provides an overview of the distribution of dissolved nutrients in the water column of the Massachusetts Bay system from February to December for the nearfield area and for February to October for the farfield regions. Selected data from the 1995 sampling period are presented and discussed both with regards to seasonal changes and to contrast nutrient conditions in various regions of the Bays. The 1995 nutrient record for the new outfall site in the nearfield is compared with similar data from the 1992-1994 sampling periods to illustrate interannual variability in this location. The nutrient data presented here include water column concentrations for nitrate + nitrite, ammonium, phosphate, and silicate and some combined data such as DIN (nitrate + nitrite + ammonium) and DIN/phosphate ratios. Some fluorescence data are also included in a similar plot style for reference.

4.1 Annual Nutrient Cycle in the Nearfield

Some of the nearfield stations were sampled for nutrients more consistently throughout this study than others, due to planned sampling schedules or unplanned weather problems. Thus subsets of the station data, representing the most consistent sampling during the year, were chosen to provide insights on temporal and spatial changes that occurred in this region during 1995. Some of these trends are summarized in Table 9-1 where they can be compared to other parameters. The stations chosen and their rationale are presented in each sub-section below.

4.1.1 Vertical Distribution of Nutrients in Nearfield

In order to show nutrient trends in the surface and bottom waters of the nearfield region, nutrient concentrations were plotted vs. time (Figures 4-1 to 4-7). All nearfield stations were included to show variability within the nearfield region. All data, as well as the average lines were plotted. Individual surface data (represented by the symbol "o") were samples from the A and B depths in the water column. Both of these depths were typically above the thermocline in the mixed surface layer. Bottom data (using the symbol "Δ") were samples from the D and E depths in the water column. Both of these depths were typically below the thermocline and at or near the bottom. Only the average line is shown for the mid-depth (C depth), which was typically centered on the thermocline. The average data lines show the seasonal differences and trends between the surface and bottom water concentrations. These differences reflect the effects of vertical mixing, stratification, and the different rates of phytoplankton uptake and nutrient regeneration in the surface and bottom layers.

All nutrients showed vertically uniform concentrations for surface to bottom samples from February until mid-March when the water column began to stabilize and again later in November and December after

the fall cooling and overturn (Figures 4-1 to 4-7). By mid-May, the bottom waters were well-depleted in nitrate + nitrite (Figure 4-1), and partially depleted in phosphate (Figure 4-4) and silicate (Figure 4-5). Ammonium had an opposite trend to the rest of the nutrients (Figure 4-2), showing slight increases from the late winter period.

During summer months, surface layers remained nutrient depleted, especially nitrate + nitrite (average values < 0.5 μM, Figure 4-1) while average phosphate values remained above 0.2 μM (Figure 4-4). After the spring blooms depleted silicate values to below 1.0 μM by June, the values increased slightly during the summer months (Figure 4-5). There was significantly more scatter in the bottom values for all nutrients during late summer. The minimum values in the bottom waters occurred in late February for silicate, mid-May for nitrate + nitrite and phosphate, and in both September and December for ammonium. The September low ammonium values coincide with some of the highest chlorophyll values during 1995 in the inner nearfield area of stations N10 and N11. This area normally exhibits some of the highest ammonium values due to nutrient loading from Boston Harbor. The bottom-water nitrate + nitrite, phosphate, and silicate concentrations all increased during the summer months, with only a temporary decrease during a fall bloom in early October.

The early winter (early November) average nutrient concentrations were higher for nitrate + nitrite, about the same for phosphate, and lower for silicate than the late summer (September) values. These differences may be due to differential rates of nutrient regeneration or some other processes not yet understood. Dissolved inorganic nitrogen (DIN = nitrate + nitrite + ammonium) to phosphorus ratios (DIN/P) in both surface and bottom waters were typically much lower than the Redfield ratio of 16:1, ranging on average from around 9-11:1 during the winter months down to around 2-5:1 during the summer months (Figure 4-6). These values slowly increased during the fall in the bottom waters as a result of regeneration. Overall, these waters were depleted in nitrogen relative to phosphorus throughout the whole year, especially in the surface waters during the summer months. A few of the surface samples did exhibit higher ratios of DIN:P, most likely due to both the harbor plume and coastal upwelling influence.

Diatoms, which frequently dominate phytoplankton assemblages in Massachusetts Bays, utilize DIN to silicate in a ratio close to 1 (ranging between 0.5 and 2), as can be seen by the slope of the DIN to silicate curves during the spring period for 1995 (Appendix D, pages 1C-5C in Murray et al. 1997). DIN to silicate ratios (DIN:Si) remained between 0.2 to 2 throughout almost the entire year, with higher values during the winter and lower values during the late spring and summer. These ratios demonstrate the impact of the early spring diatom bloom and the slow simultaneous return of the dissolved silicate and DIN to the water column (Figure 4-7). The observed ratios are typically within the range of diatom requirements.

With the exception of mid-June and September, there was always well more than 1 μM silicate in the water column, even in the surface layers. It is interesting to note that the ratios remain relatively constant

in the bottom waters (0.5 to 0.8 from May to October even though the actual concentrations increased dramatically during this time period. This suggests that nitrogen and silicate were being remineralized at similar rates.

4.1.2 Inner/Outer Nearfield Nutrient Gradient

In order to characterize the differences between nearfield stations located close to the present plume and those representing the future receiving waters, average station data for both the western and eastern portions of the nearfield were calculated. Stations N10 and N11, from the southwestern corner of the nearfield (Figure 2-2) were chosen to represent the inner nearfield. Due to tidal influence with harbor waters, these two stations often showed elevated concentrations of nutrients associated with the harbor and present outfall plume. Stations N04, N05, N06, and N07 on the eastern edge of the nearfield station grid were chosen to represent the outer nearfield transect. In order to make plots, data from each of the 5 depths (A-E) were separately averaged across the chosen stations and then plotted at the average depth for each of the depths and each of the 17 sampling periods (Figures 4-8 to 4-13). The average depth of the inner stations was about 20-25 m, while the average depth for the outer stations was nearly 50 m.

In general, concentrations of most nutrients were vertically uniform for the first 3 surveys and the last two surveys of 1995 (Figures 4-8 to 4-12). During the remainder of the spring, summer, and fall seasons, nutrient concentrations were higher in the bottom waters than at the surface. The exceptions to this were ammonium and phosphate in the inner nearfield where surface concentrations were sometimes higher than the bottom concentrations (Figures 4-9 and 4-11). This is due to the influence of the harbor and present outfall, whose fresher waters mix into the surface waters raising the ammonium and phosphate levels. This surface enrichment of phosphate and ammonium is also seen for the last five surveys during the fall and early winter when the highest concentrations for the year were observed.

Although the outer-nearfield transect water column remained vertically mixed during the first three surveys, the late winter/early spring plankton bloom (during survey W9502) significantly reduced all nutrient concentrations, from surface to bottom, by a factor of two to four. They were also reduced at the inner nearfield stations, especially in the deeper waters. All nutrients except ammonium then increased in concentration for the next two to three surveys. By survey W9505 in late April, the water column had begun to thermally stratify (Figure 3-1) and a second bloom, as indicated by increased fluorescence, was in progress (Figure 4-13). By survey W9506 in mid-May, the nitrate + nitrite concentrations were reduced to their summer low values (< 0.5 μM) and remained low until after survey W9515 in November. Silicate and phosphate concentrations were also reduced, though they did not reach their lowest surface-water concentrations until late June. Surface ammonium values were also low (< 1 μM) and remained low for the rest of the year (Figure 4-9).

It was during this late spring-early summer period that the nutrients reached their lowest concentrations in the bottom layers, well below the pycnocline as was discussed in section 4.1.1. For example, by survey W9506 (mid-May), the nitrate + nitrite values were below 1 μM at 35 m and only 3-4 μM (about one third of the winter values) at the bottom depth. Both phosphate and silicate were also well depleted in the deeper waters. The late June/early July upwelling, described in section 3.2.4, did not show a strong effect in the nutrient distributions, though the average concentrations of nutrients at the surface (A+B) and mid-depth (C) showed slight increases, especially for phosphate and silicate. The average DIN in the surface layers and at mid-depth showed only a few tenths of a μM increase during that time. However, nutrient concentrations may have continued to increase given the mooring data's indication that the upwelling event continued beyond survey W9508.

In the outer nearfield, surface concentrations of nitrate + nitrite remained very low during the summer and early fall months, while concentrations at the bottom two depths (D and E) continued to increase, so that by late September and October they had returned to close to normal winter concentrations. Ammonium, on the other hand, reached its bottom water maximum (> 3 μM) by survey W9508 (early July) in the outer nearfield. Phosphate and silicate also exhibited this deep water concentration increase. By September ammonium concentrations were uniformly low (< 1.0 μM) throughout the water column. There was a mid-fall bloom, as indicated by increased fluorescence (Figure 4-13), which depressed all nutrient concentrations (except ammonium) in the surface and deeper waters. In early November, by Survey W9515, the water column was again nearly vertically mixed (based on temperature data, Figure 3-1), though the nutrient concentrations did not become vertically uniform until December (Surveys W9516 and W9517) after vertical mixing was nearly complete. This mixing caused a reduction in the scatter of the observed concentrations. However, only phosphate had reached its early February concentrations by Survey W9517 (mid-December). Nutrient concentration trends in the inner nearfield were similar to those in the outer nearfield, except for the previously mentioned increases in ammonium and phosphate in the surface waters in the inner nearfield.

4.1.3 Interannual Nutrient Variability in the Nearfield

In order to illustrate interannual variability in the area of the future effluent discharge in the nearfield, four stations which had the most complete data coverage during the four years of monitoring were chosen to represent this area. These stations (N16, N04, N07, N20) form a triangle with station N16 in the center (Figure 2-2). Data from these stations for five depths (A-E) were averaged over stations for each depth and then plotted at each average depth for the 17 sampling surveys, producing time/depth contour plots of concentration (Figures 4-14 to 4-20). The average depth of the bottom samples at these stations was about 38-42 m.

The plots for a given nutrient suggest that there were significant changes in concentration patterns over the four years presented. However, it is important when examining these plots that the viewer be aware

that the sampling season was longer (started earlier and ended later) in 1995 than in the previous years, especially 1993. For example, it appears that there were much higher DIN concentrations in the water column in 1995 than in 1992. Indeed this is true, but the inclusion of the mid-February and late December data in an average calculation would tend to prejudice the 1995 data toward the high end. To avoid such bias, the whole year average values given in Table 4-1 do not include survey 1 and 17 for 1995 and survey 1 for 1994. All of the nutrients continually increased in average concentration (except ammonium) over the four years that are presented. Nitrate + nitrite showed the largest percentage increase from 1992 to 1995 (234%) while silicate, phosphate and DIN all showed increases of 133% to 216%. Although ammonium also increased over the four years, it decreased slightly from 1994 to 1995. The cause of these increases is difficult to pinpoint since nutrient concentrations are affected both by source terms as well as phytoplankton removal and mixing of different water masses.

Other trends are evident between the years in the time/depth contour plots. The late winter bloom or initial spring diatom bloom, as indicated by relatively low silicate concentrations throughout the water column, occurred anytime from the beginning of February to the beginning of March during the different years sampled (Figure 4-18). After the relatively early blooms in 1992 and 1995, silicate concentrations increased until the water column stratified completely and surface water production could remove all nutrients for the summer stratified period. It appears that during years of an early diatom bloom, silicate concentrations are only reduced to about 3-4 μM. They then increase until late spring or early summer, after which they are reduced to very low concentrations. During years of a late spring bloom, there does not appear to be a major recovery of silicate concentrations and they continue to decrease until they reach summer surface water concentrations of below 1 μM.

The initial occurrence of nutrient depleted surface water typical of summer conditions also varied between years. Using nitrate + nitrite concentrations of < 1 μM as a criterion, these conditions occurred as early as late March (1994) and early April (1992 and 1993) to as late as mid-May (1995). During years of early depletion, low concentrations were found throughout the water column, whereas when it happened later (1995), the lowest values were only found to mid-depths. During all years, surface nitrate + nitrite concentrations remained below 0.5 μM throughout the summer and early fall months. During this same time period ammonium, phosphate and silicate were also very low in the surface waters. However, in the bottom waters, all of the nutrients slowly increased due to regeneration as discussed in section 4.1.1 and 4.1.2.

In all years sampled, there was a fall bloom, as evidenced by the increased fluorescence values (Figure 4-20) which occurred during October and early November. This helped keep the surface values of all the nutrients low until the fall overturn which generally occurs in early November. This process mixes high nutrient concentration deep water with low nutrient concentration surface water so that the resultant water mass has intermediate concentrations, which then slowly increase to winter values.

The ammonium trends for the different years were generally similar to each other, but different than the other nutrients. The highest values were found during the summer months in the bottom waters while the lowest values (< 0.5 μM) were found in surface waters during most of the year and throughout the water column during some late winter and fall periods. The DIN/P ratio plots show that the nearfield region has ratios that are characteristically lower than the Redfield ratio throughout the year (Figure 4-19).

Although the general distribution of nutrient concentrations remains the same throughout the year, there are significant variations from year to year in these concentrations at different depths over times scales of several months. The effect of the relocated outfall on the nutrient concentration trends in this region is easy to predict in a general sense (it will probably smooth out the variations in the bottom waters) but hard to predict in a biological effects sense. Since the outfall diffusers will discharge to the bottom layer, it is expected that DIN (mostly due to increased ammonium) and phosphate concentrations will be higher than the present bottom water values throughout most of the year. The DIN/phosphate ratios may also change, although not appreciably, since for most of the year present bottom values range from about 3-10 and the ratio for projected secondary treatment sewage will be about 9 (Hydroqual and Normandeau, 1995).

4.2 Annual Nutrient Cycle in Massachusetts and Cape Cod Bays

The annual nutrient cycle in the Massachusetts Bays was examined using both nutrient vs. depth plots and nutrient vs. nutrient plots for all near and farfield stations. On all plots, the data were plotted using different symbols for each of the six areas of Massachusetts Bays as shown in Figures 2-1 and 2-2 in order to distinguish regional concentration differences and processes. The data were not averaged because of the large differences between stations within areas.

4.2.1 Regional Nutrient Variability With Depth

In order to examine both the horizontal and vertical distribution of nutrient concentrations throughout the Massachusetts Bays system, concentration vs. depth plots were made that included all data (Figures 4-21 to 4-27). Only a few of the nutrient vs. depth plots (which are comprehensively available in Murray *et al.*, 1997a; 1997b) are presented here to make specific points about regional processes.

During 1995, as in previous years, several trends were apparent. Within the Massachusetts Bay system, nutrient levels changed due to different biological regimes and different nutrient sources. Boston Harbor, Cape Cod Bay, and to some extent, greater Massachusetts Bay sometimes act as independent systems with regards to temporal and spatial variability of nutrients, as well as other parameters. Greater Massachusetts Bays can be further divided into boundary, offshore, nearfield, and coastal regions as shown in Figure 2-1. It is important to note that the sampling of the entire system occurred only six times per year and that

these survey data are "snapshots" at these points in time. To help in interpretation of the trends, nearfield data were included on the plots as well.

In mid February (survey W9501), nutrient concentrations were relatively high in all regions of Massachusetts Bay, with slightly lower values in Cape Cod Bay and much higher values evident in Boston Harbor (Figures 4-21 to 4-23). Water in the harbor region, as well as some harbor-affected coastal and nearfield stations, showed elevated concentrations for all nutrients. The higher concentrations of ammonium and phosphate typically can be used as markers to track plumes of harbor water. The presence of elevated silicate and nitrate levels at the surface was associated with lower salinity water from riverine input. This was confirmed by large rain events and snowmelts recorded in late January (Section 3) and in DIN vs. salinity plots (refer to 1995 Semi-annual Water Column Reports).

By early March (survey W9502), a diatom bloom had occurred in lower Cape Cod Bay as evidenced by the over 85 percent reduction of nitrate and silicate levels there. Smaller planktonic blooms on different time scales were also evident throughout Massachusetts Bay by the notable decrease and scatter in nutrient concentrations (i.e. DIN and silicate, Figure 4-24).

By early April (survey W9504), nutrient concentrations throughout the water column began to increase again after the spring blooms in March (i.e. DIN and silicate, Figure 4-25). This could be due to a combination of local nutrient regeneration and the influx of higher nutrient coastal waters. As is usual for Boston Harbor and its associated plume, ammonium and phosphate concentrations were elevated while nitrate and silicate remained comparable with the rest of Massachusetts Bays. Cape Cod Bay remained a distinct system with all nutrient concentrations being lower than the rest of the system (Figure 4-25).

In late June (survey W9507), the water column had become well stratified (Figure 3-3). Nutrients in all regions appeared to have been depleted to a large extent in the surface layers (i.e. DIN, Figure 4-26, W9507), including Boston Harbor and its associated plume. While some residual phosphate and silicate did remain in the surface layers, the system was probably nitrogen limited and remained so throughout the summer (with the usual exception of Boston Harbor). A nutricline was established at 15-20m depth for most of Massachusetts Bay and remained until the fall.

By late August (survey W9511), water column stratification was very strong with nutrient remineralization occurring in the deeper waters of the offshore and boundary region. The harbor region and some plume-affected nearfield and coastal stations all exhibited higher DIN concentrations (Figure 4-26, W9511), as well as ammonium and phosphate concentrations. The silicate and nitrate concentrations were only slightly elevated. Surface concentrations of all nutrients appeared to be increasing on different time scales.

By October (Survey W9514), phosphate and silicate concentrations had increased slightly, but the surface layers still remained somewhat nitrogen depleted for most of Massachusetts Bays (Figure 4-27). However,

Boston Harbor and its associated coastal area plume exhibited higher concentrations of DIN (due to ammonium) and phosphate than previously observed during the year (Figure 4-27).

4.2.2 Nutrient-Nutrient Relationships

Nutrient relationships were investigated through the use of nutrient-nutrient plots (Figures 28 through 4-32). Nutrient ratios relating nitrogen to phosphorus (N:P) and nitrogen to silicate (N:Si) are useful in determining nutrient limitation of phytoplankton growth. Plots of these nutrient relationships can also be used to identify water masses with unique nutrient signatures and provide insights into nutrient sources and removal processes. Using these plots, three distinct systems, Boston Harbor-Coastal, Massachusetts Bays (Nearfield, Offshore, and Boundary), and Cape Cod Bay become evident during certain times of the year.

Mid-February, early March, and early April (surveys W9501-W9504) all showed similar trends with respect to dissolved inorganic nitrogen (DIN) and phosphate, though the overall concentrations decreased during this period. In mid-February, DIN to phosphorus ratios (DIN:P) were ~10-14:1 for most of Massachusetts Bays, while the Harbor region exhibited values of around 14-16:1 due to enrichment from the harbor and existing outfall (Figure 4-28). Cape Cod Bay data were just slightly set off from the rest of Massachusetts Bays, indicating earlier uptake activity by the phytoplankton community.

In March, the overall concentrations had decreased from February. The DIN:P ratios also decreased to around 10:1, while DIN:Si ratios diverged indicating two separate water masses with different characteristics (Figure 4-29). During this period, the higher DIN:Si waters of the harbor and harbor-influenced stations, and the lower DIN:Si waters of the Boundary area both mixed with the waters in the nearfield region creating the bifurcated distribution of these properties. Most of the harbor and harbor-influenced coastal and nearfield stations had ratios of around 2:1, while most of the deeper offshore and boundary stations exhibited ratios that ranged from between 2:1 to 1:1.5 with a trend slope of around 1:2. Cape Cod Bay concentrations were all much lower then the rest of the system due to the near completion of the late winter diatom bloom, with the DIN:Si removed at about a 1:1 ratio.

In early April, the DIN:P ratios returned to the previously cited values while conforming more to the 16:1 trend line. Mixing and regeneration narrowed the concentration ranges of data, and the bifurcation seen earlier in the DIN:Si ratios slowly began to disappear as DIN:Si centered on a ratio of about 1:1 throughout the Bays.

During the summer months, the concentration data became significantly more scattered, though still showing a 16:1 trend for DIN:P and around 1:1-2 for DIN:Si (i.e. late June, Figure 4-30). The actual DIN:P ratios in the nearfield were low since most of the DIN values in the surface waters were below 2 μM. The trend line intercepts the zero DIN value at a phosphate concentration of about 0.4 μM, indicating

that as the nitrogen is used up there is still a residual amount of phosphate in the water column. This situation continued throughout the summer and into the fall.

In October (Survey W9514), the DIN and phosphate concentrations were tightly covariant and fell on a trend line of 16:1 throughout all of Massachusetts Bay (Figure 4-31). The zero DIN intercept was about 0.4 μM phosphate as observed earlier in the summer. However, the DIN to silicate plot shows divergent trends with the harbor and coastal waters indicating a DIN:Si of about 2:1 (enriched in nitrogen) while the same ratio for the nearfield, boundary and offshore regions is about 1:2 (Figure 4-31).

Although the DIN and phosphate plot does not show this divergent trend, nitrate and phosphate, and ammonium and phosphate do show this divergence. The nitrate:phosphate trend line is about 16:1 for nearshore/offshore samples, while only 4:1 for the harbor/coastal samples (Figure 4-32). The ammonium:phosphate trend line is nearly the opposite, so for harbor/coastal samples it was about 16:1, while for the nearfield, boundary and offshore regions it was less than 4:1 (Figure 4-32). The high covariance between DIN and phosphate results from these similar, but opposite, nitrate:phosphate and ammonium:phosphate ratios in the two different major regions.

Year	Number of Samples	Depth (m)	DIN* (µM)	N+N (µM)	NH4 (µM)	PO4 (µM)	SiO4 (µM)	DIN/P
1995	292-300	19.6	4.44	3.53	0.91	0.64	5.52	6.07
1994	288-300	19.0	3.81	2.83	0.97	0.60	4.12	5.76
1993	316-320	17.8	3.44	2.61	0.79	0.50	4.85	5.63
1992	280-300	18.2	2.32	1.78	0.55	0.46	4.66	4.13

* The average values shown for each nutrient were calculated by first averaging concentrations at each of the 5 depths (A-E) for stations N04, N07, N16, N20 for each cruise, and then averaging all of the averages.

TABLE 4-1

1992 to 1995 Whole Year Outer Nearfield Average Nutrient Values

Late February/Early March to Early/Mid December

Outer Nearfield: N16, N04, N07, and N20

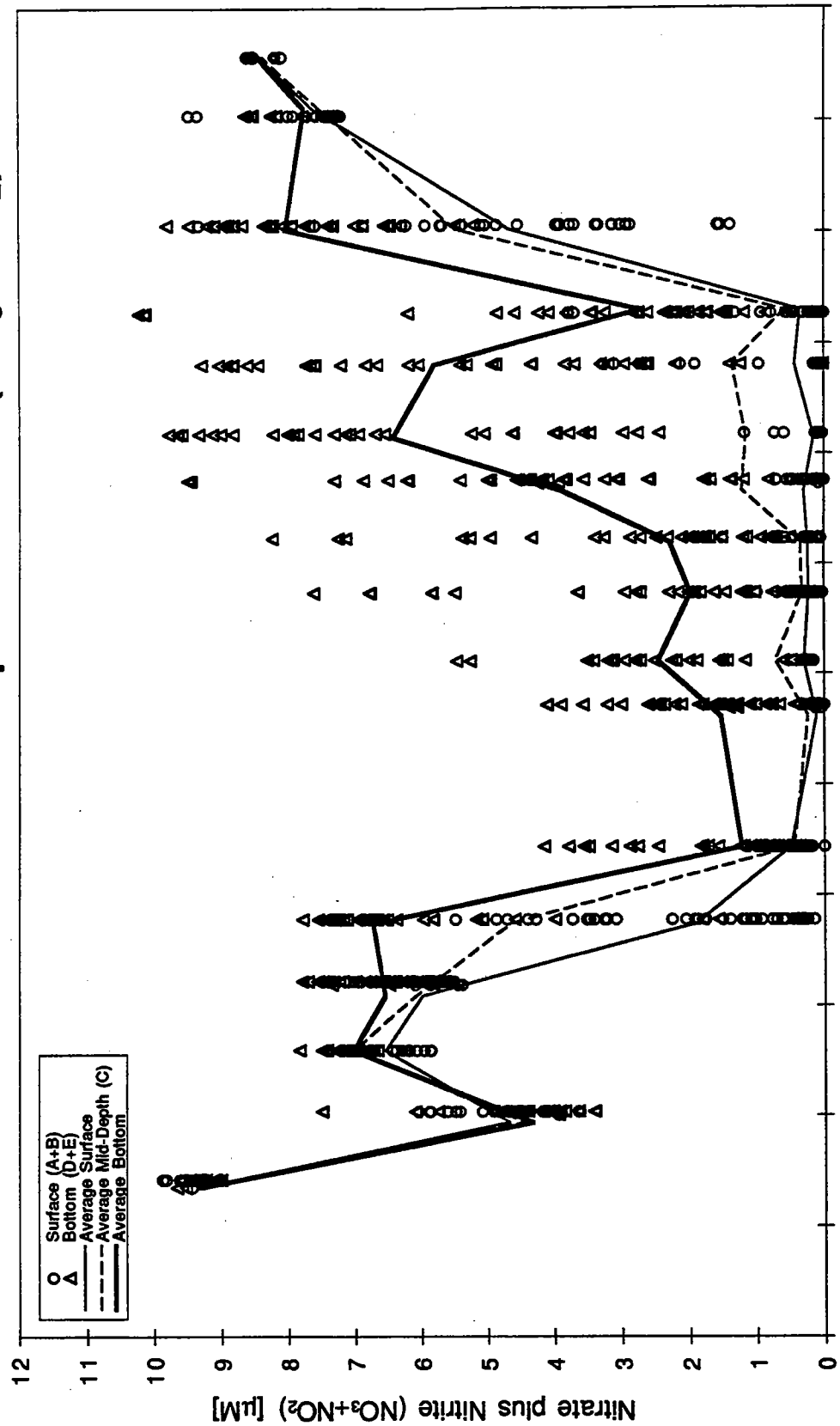

Figure 4-1. Nitrate plus nitrite concentrations for all nearfield stations for 1995. Symbols and trendlines show average values for surface (A and B), mid (C), and bottom (D and E) depths.

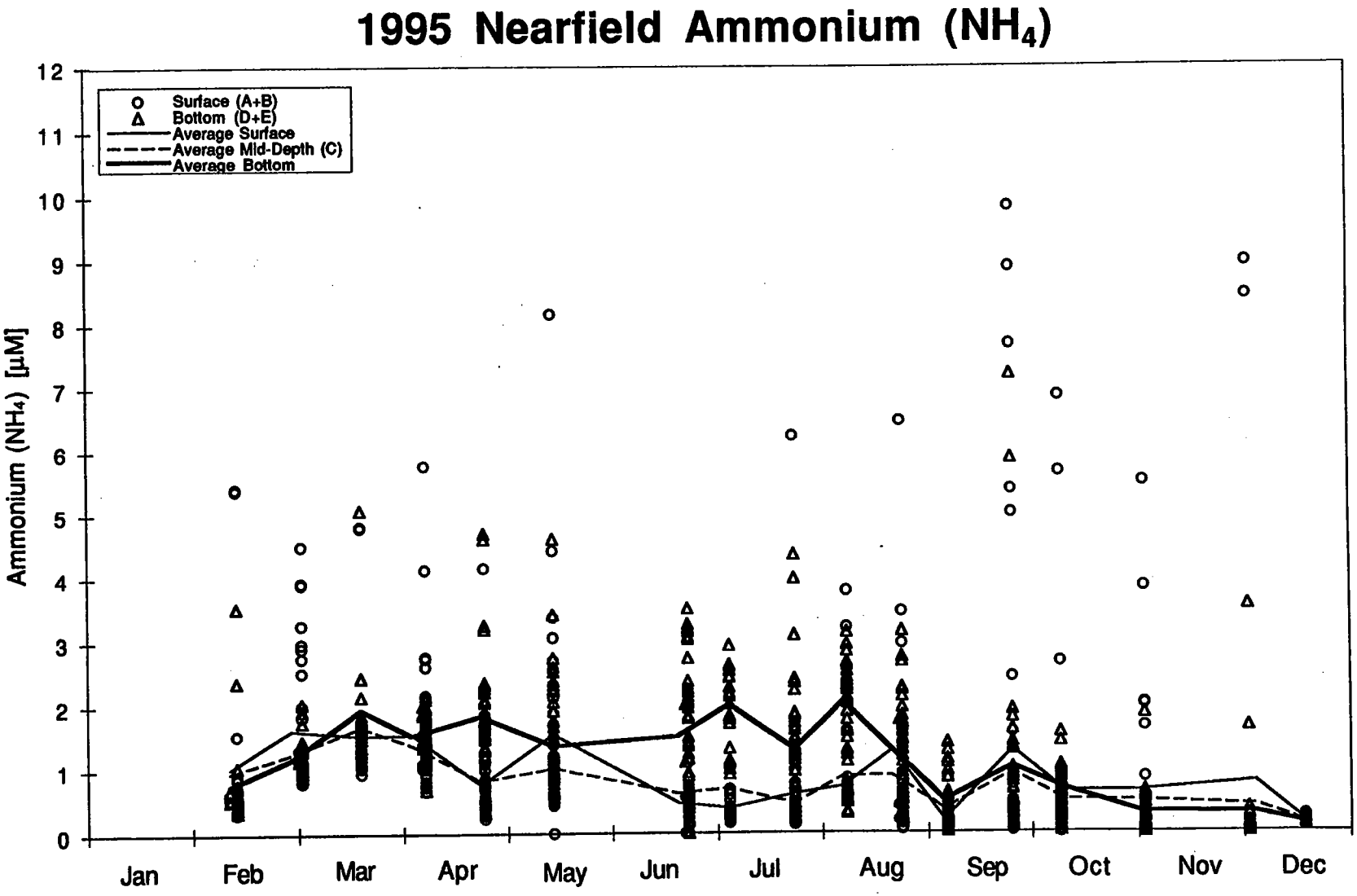

Figure 4-2. Ammonium concentrations for all nearfield stations for 1995. Symbols and trendlines show average values for surface (A and B), mid (C), and bottom (D and E) depths.

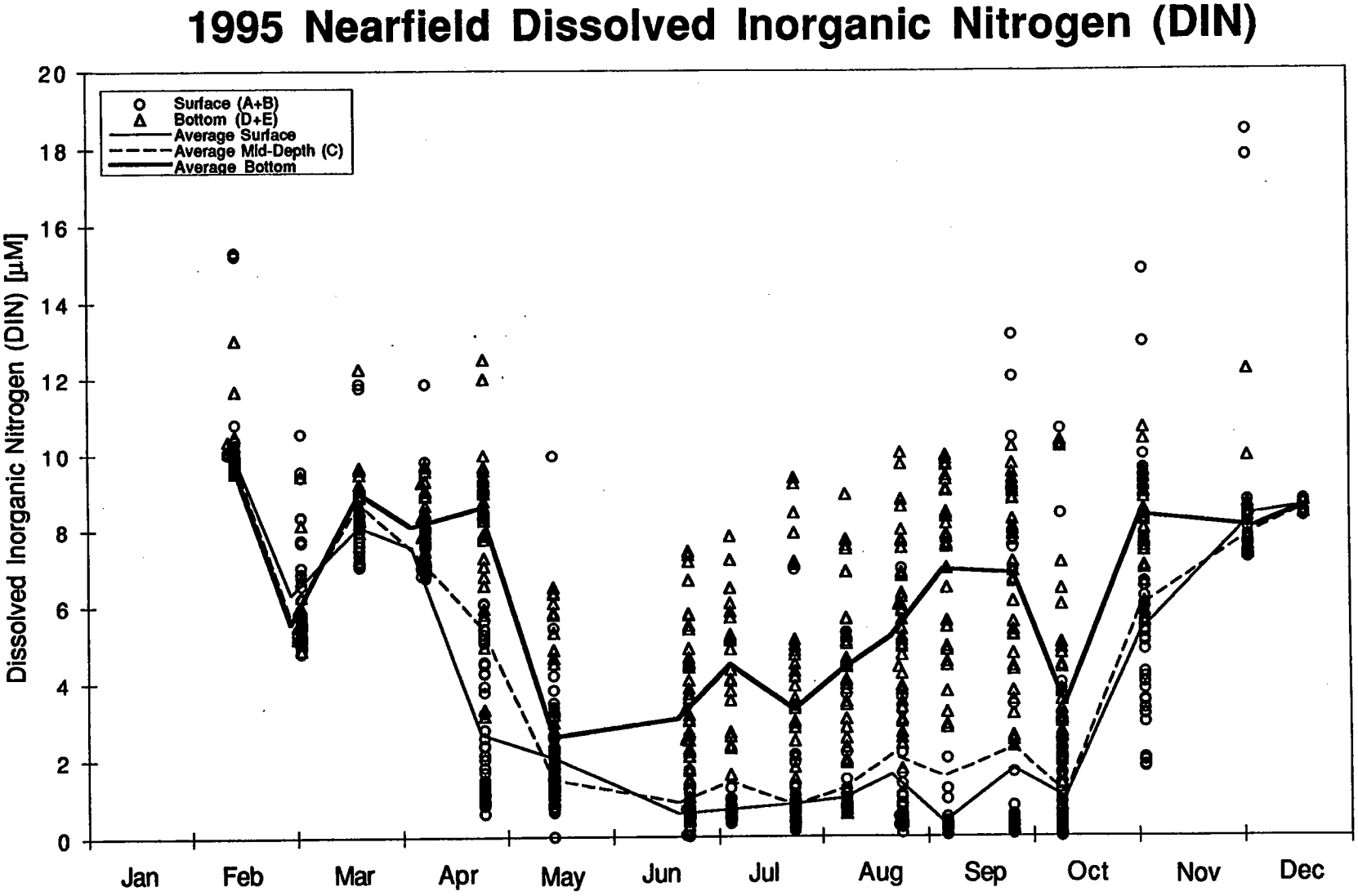

Figure 4-3. Dissolved inorganic nitrogen concentrations for all nearfield stations for 1995. Symbols and trendlines show average values for surface (A and B), mid (C), and bottom (D and E) depths.

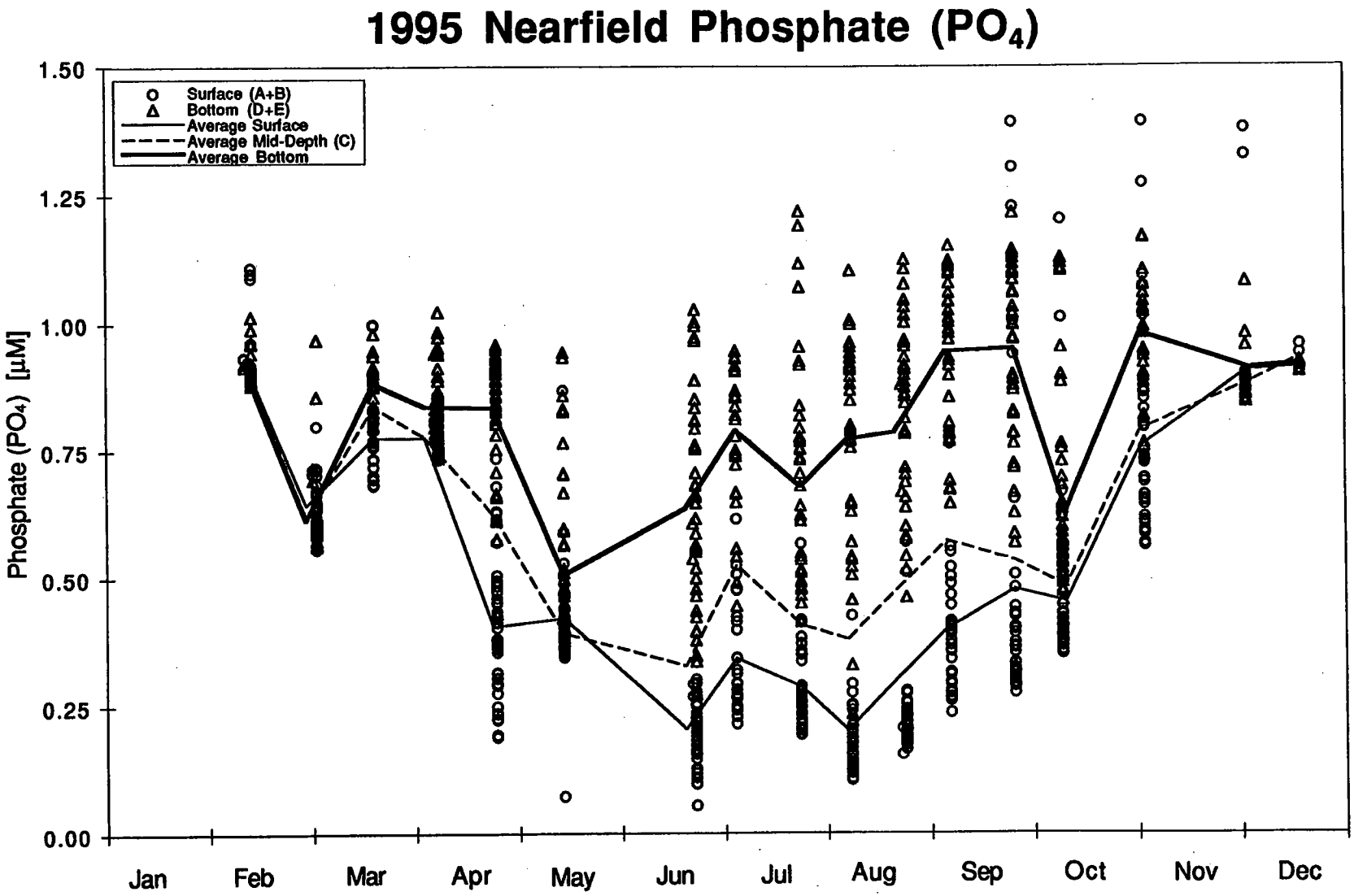

Figure 4-4. Phosphate concentrations for all nearfield stations for 1995. Symbols and trendlines show average values for surface (A and B), mid (C), and bottom (D and E) depths.

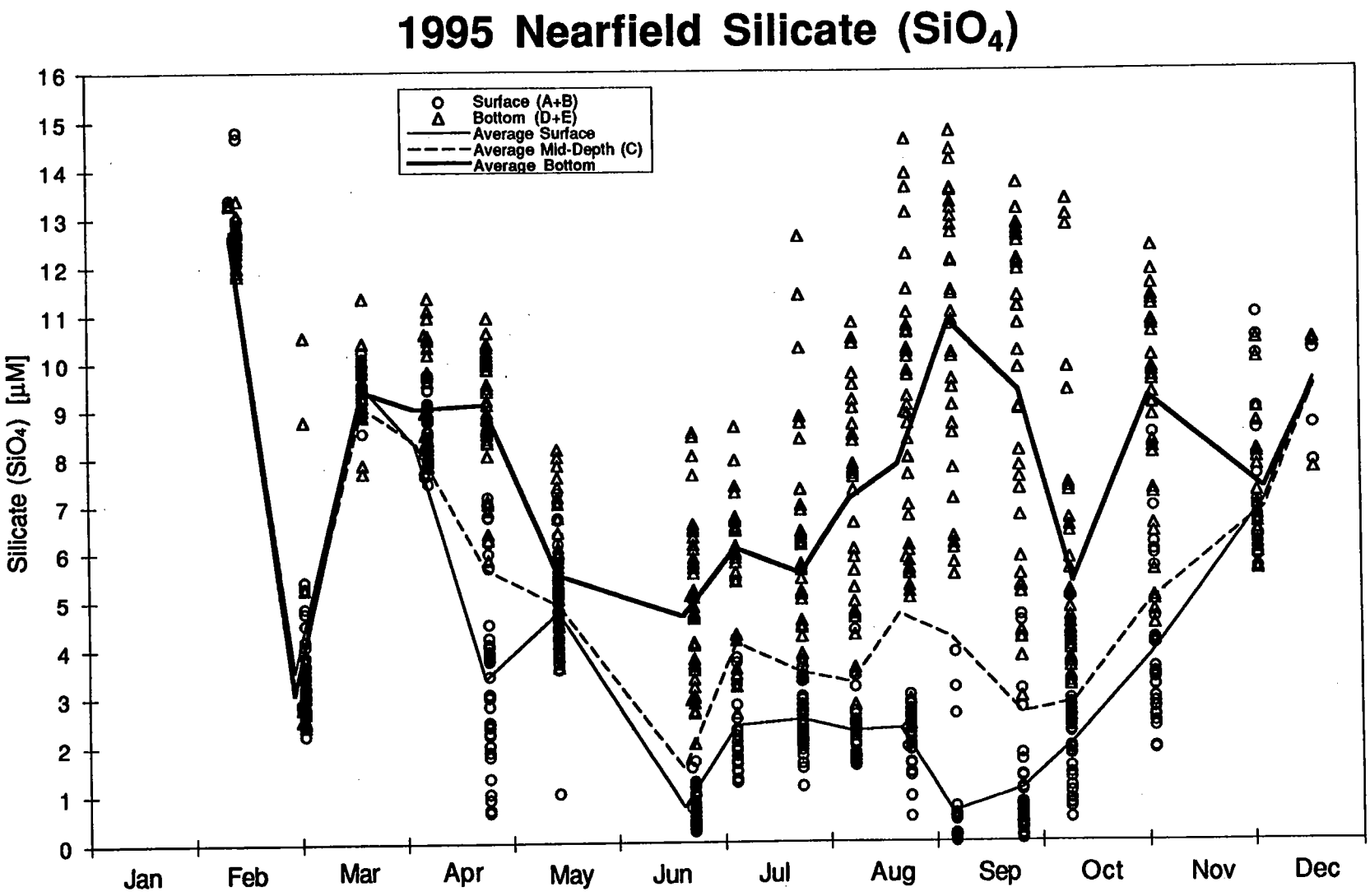

Figure 4-5. Silicate concentrations for all nearfield stations for 1995. Symbols and trendlines show average values for surface (A and B), mid (C), and bottom (D and E) depths.

1995 Nearfield Dissolved Inorganic Nitrogen to Phosphate Ratios (DIN:P)

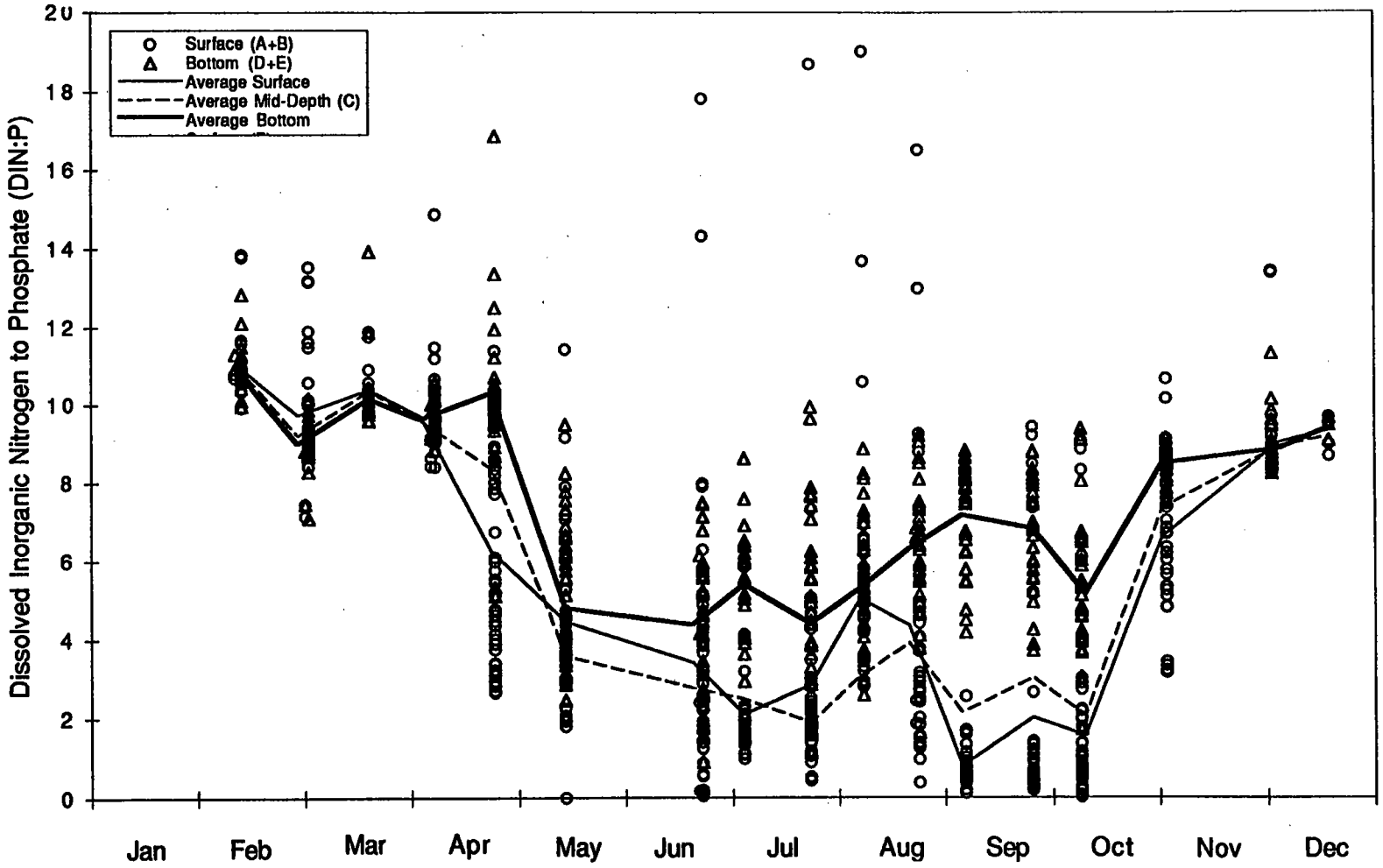

Figure 4-6. Dissolved inorganic nitrogen to phosphate ratios for all nearfield stations for 1995. Symbols and trendlines show average values for surface (A and B), mid (C), and bottom (D and E) depths. Note that nearly all data points fall below the Redfield ratio of 16:1.

1995 Nearfield Dissolved Inorganic Nitrogen to Silicate Ratios (DIN:Si)

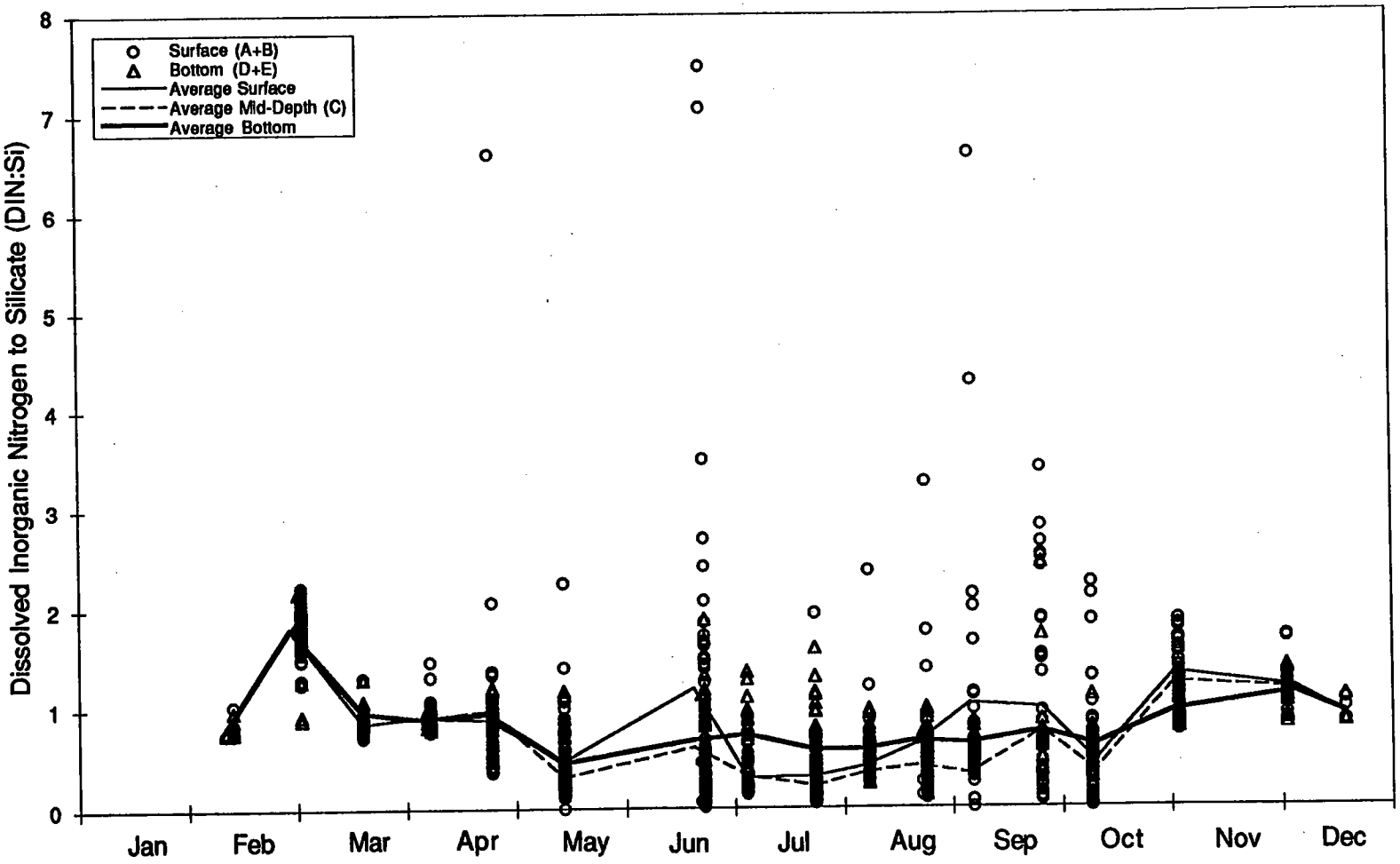

Figure 4-7. Dissolved inorganic nitrogen to silicate ratios for all nearfield stations for 1995. Symbols and trendlines show average values for surface (A and B), mid (C), and bottom (D and E) depths.

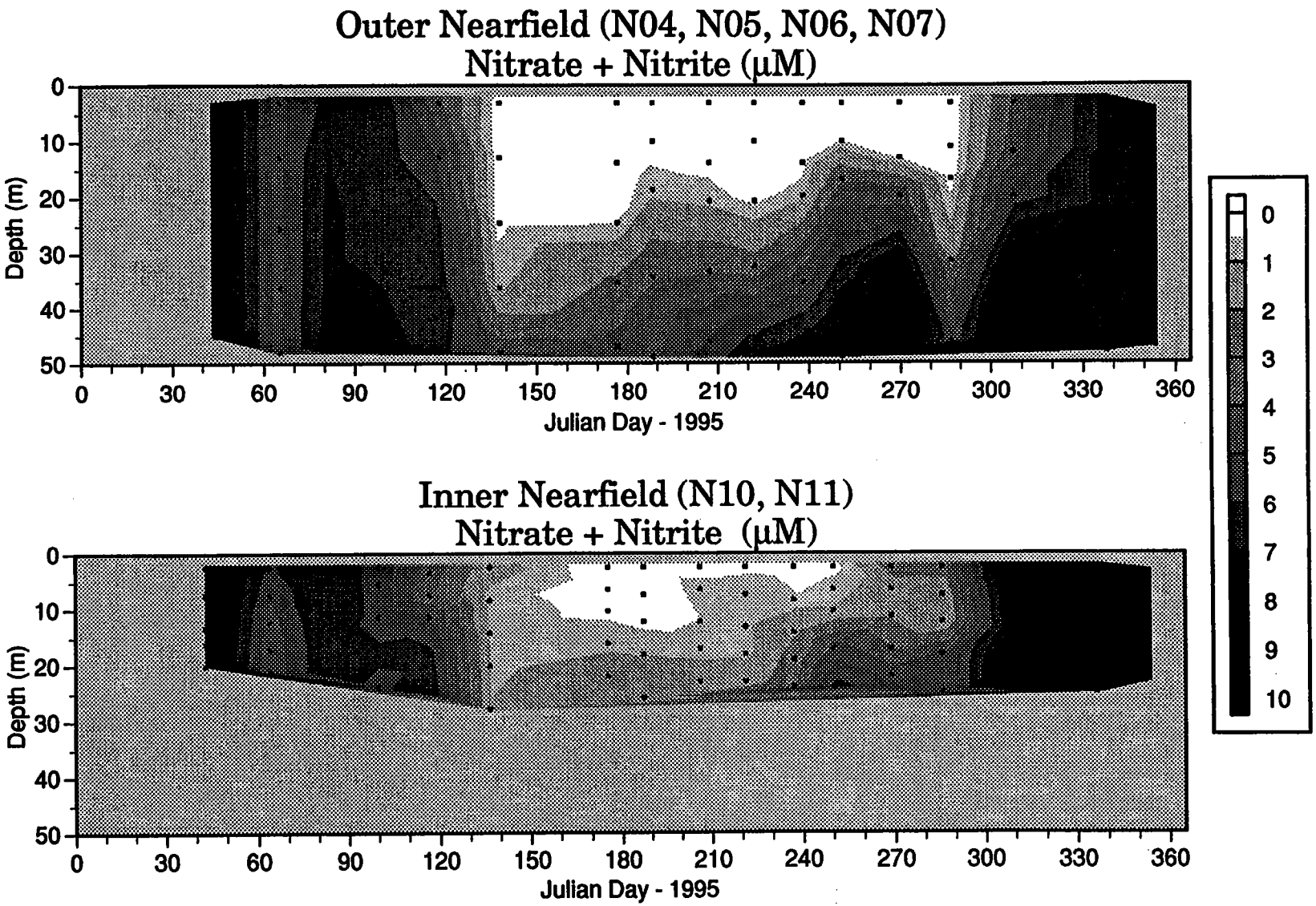

Figure 4-8. Depth-averaged nitrate plus nitrite concentrations for inner (N10 and N11) and outer (N04, N07, N16, and N20) nearfield stations for 1995.

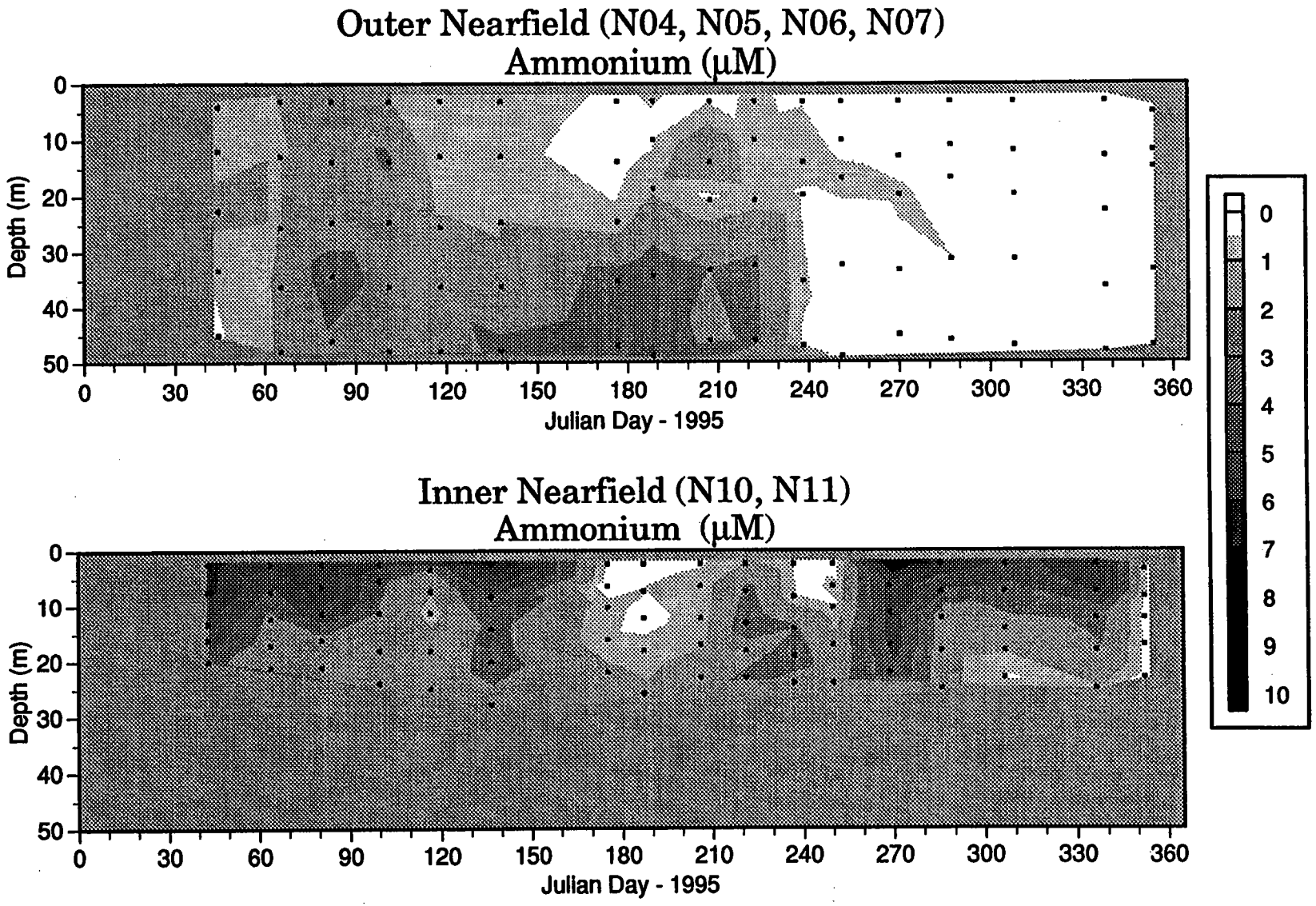

Figure 4-9. Depth-averaged ammonium concentrations for inner (N10 and N11) and outer (N04, N07, N16, and N20) nearfield stations for 1995.

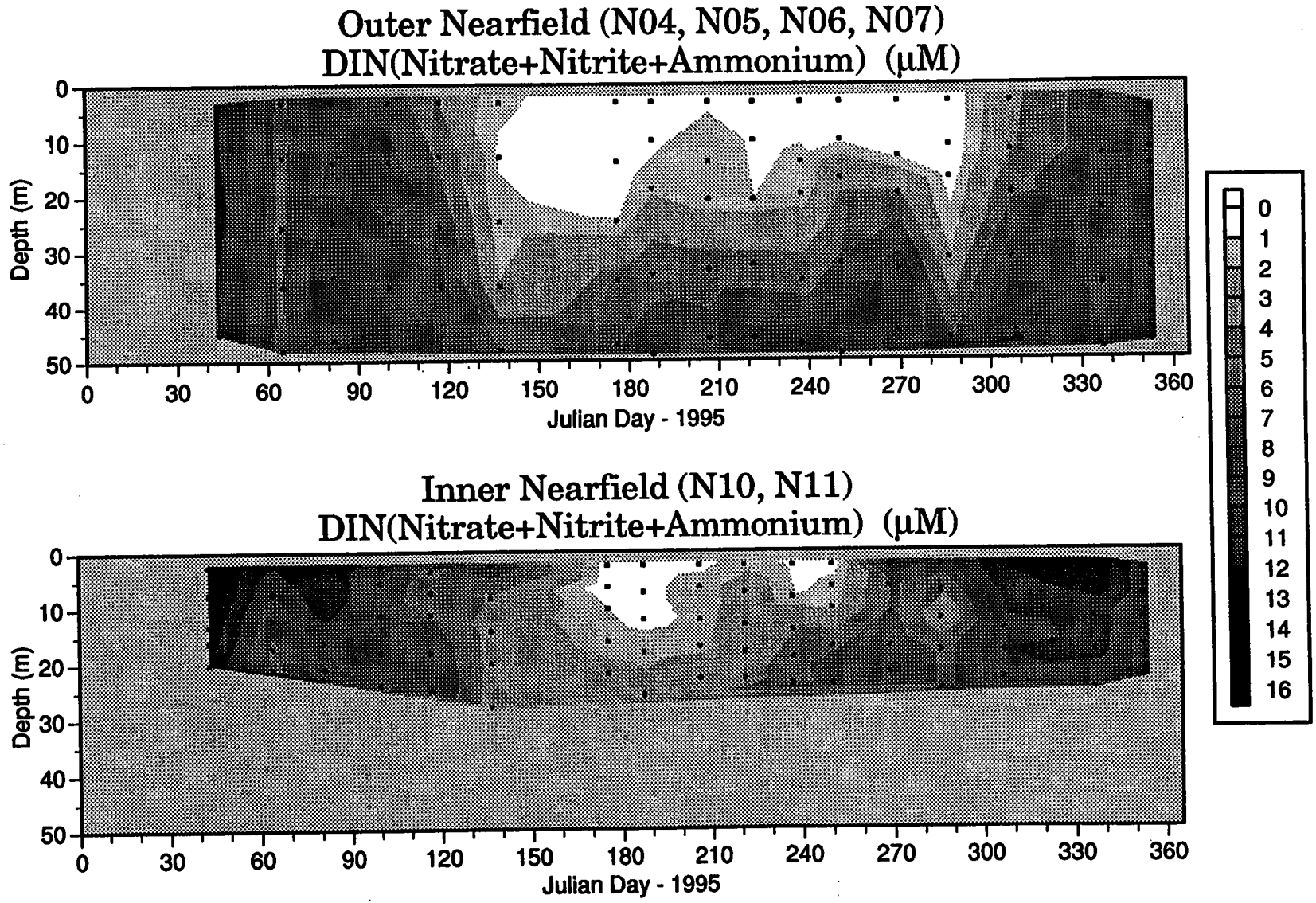

Figure 4-10. Depth-averaged DIN concentrations for inner (N10 and N11) and outer (N04, N07, N16, and N20) nearfield stations for 1995.

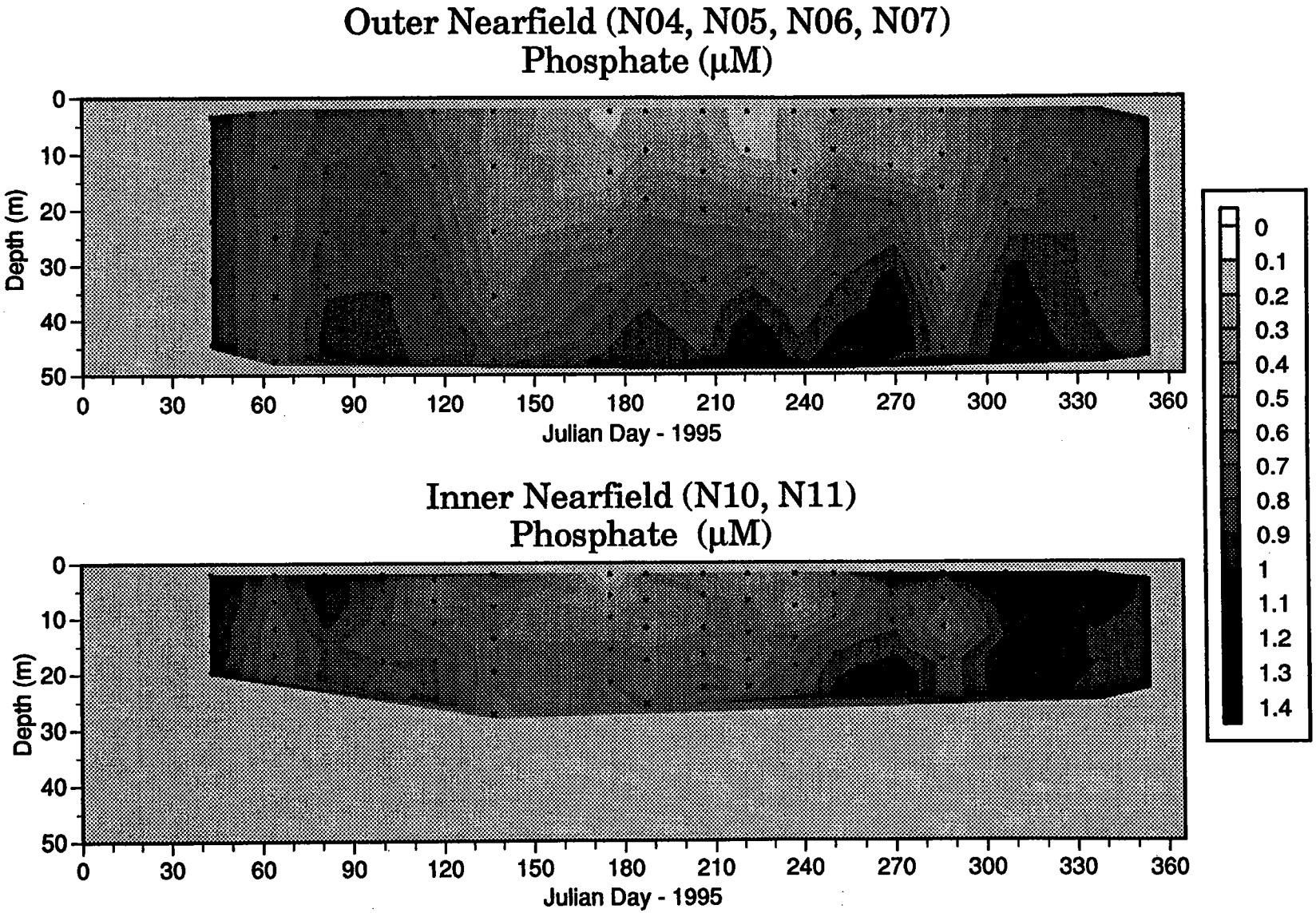

Figure 4-11. Depth-averaged phosphate concentrations for inner (N10 and N11) and outer (N04, N07, N16, and N20) nearfield stations for 1995.

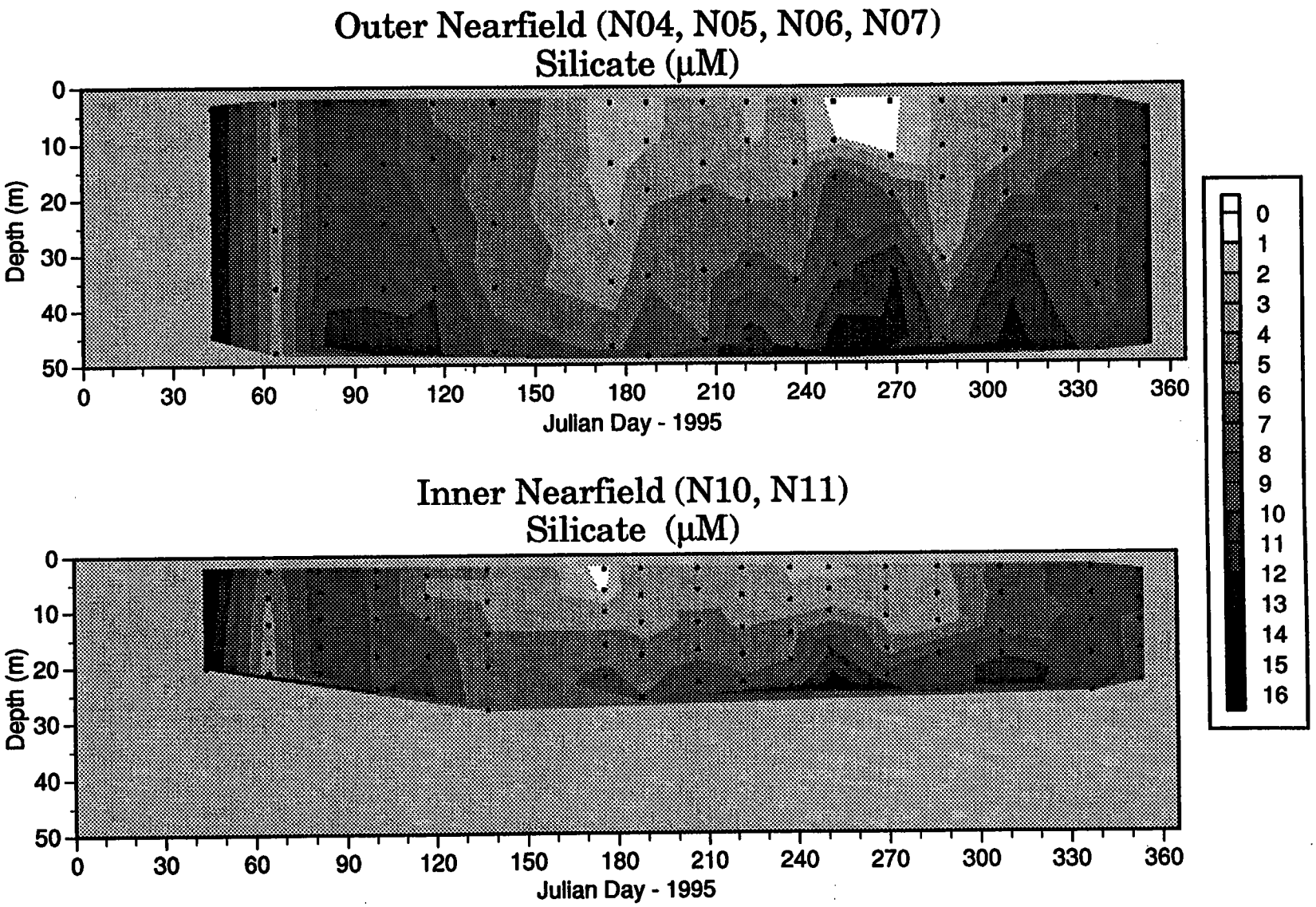

Figure 4-12. Depth-averaged silicate concentrations for inner (N10 and N11) and outer (N04, N07, N16, and N20) nearfield stations for 1995.

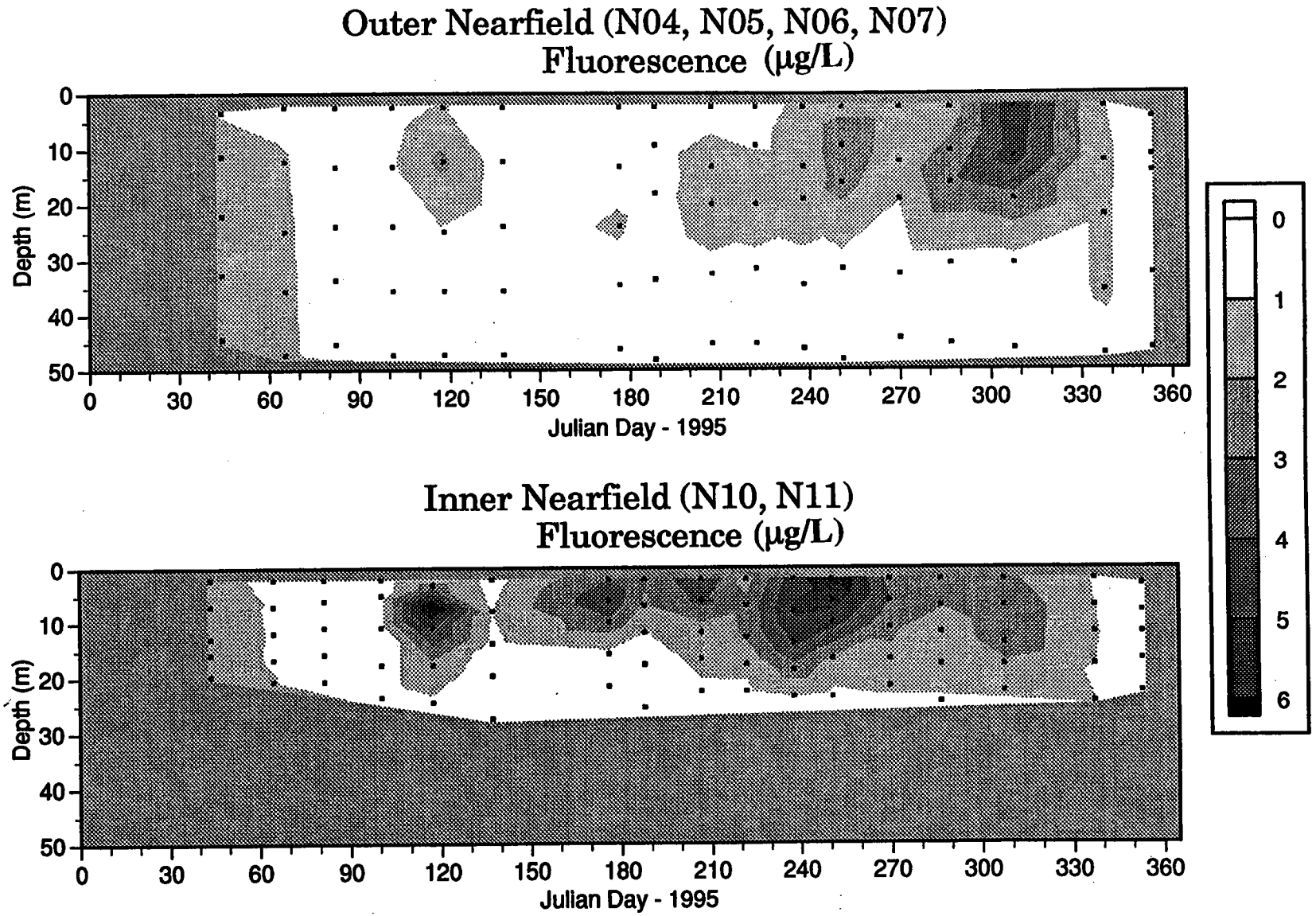

Figure 4-13. Depth-averaged fluorescence data for inner (N10 and N11) and outer (N04, N07, N16, and N20) nearfield stations for 1995.

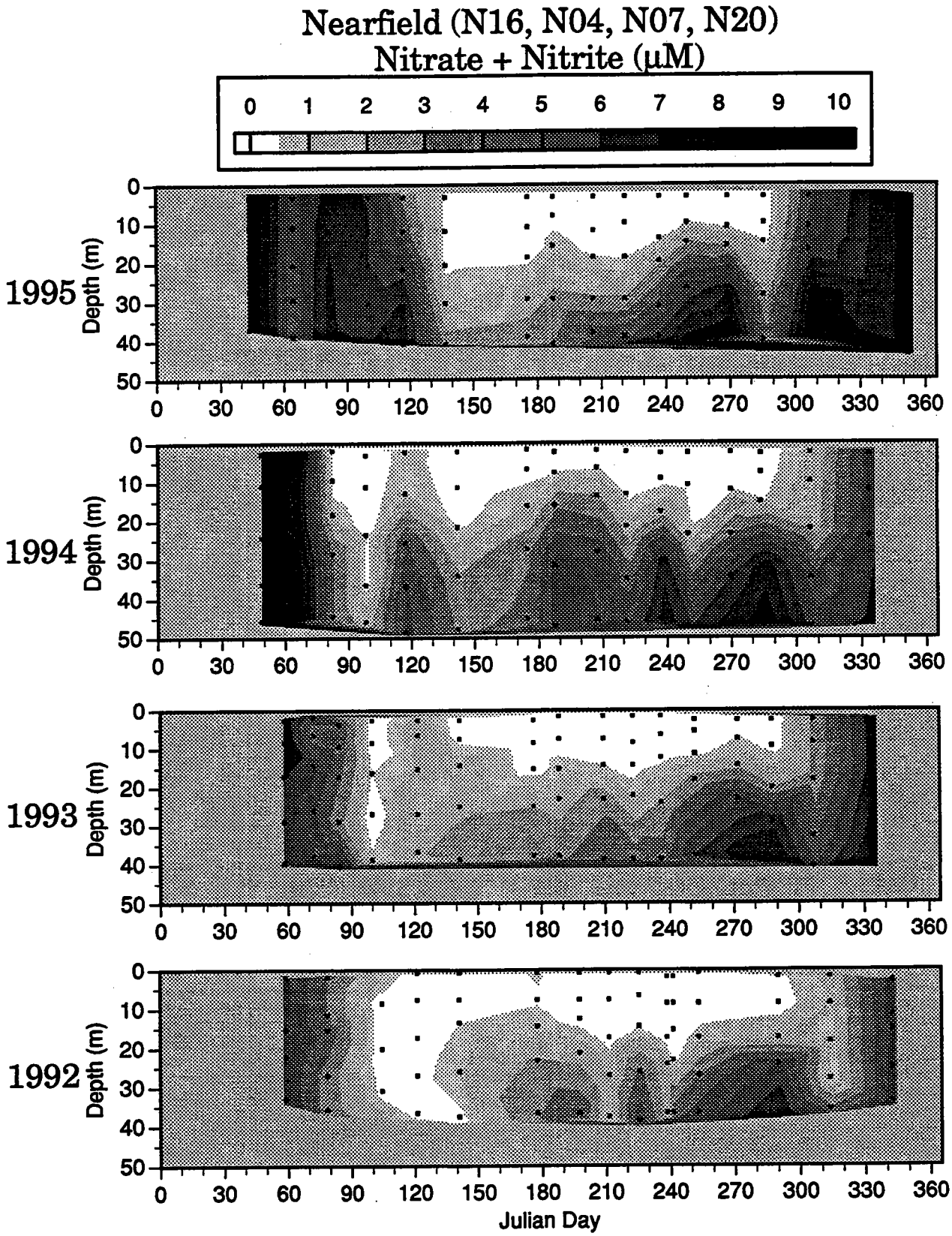

Figure 4-14. Nearfield nitrate plus nitrite concentrations for 1992-1995.

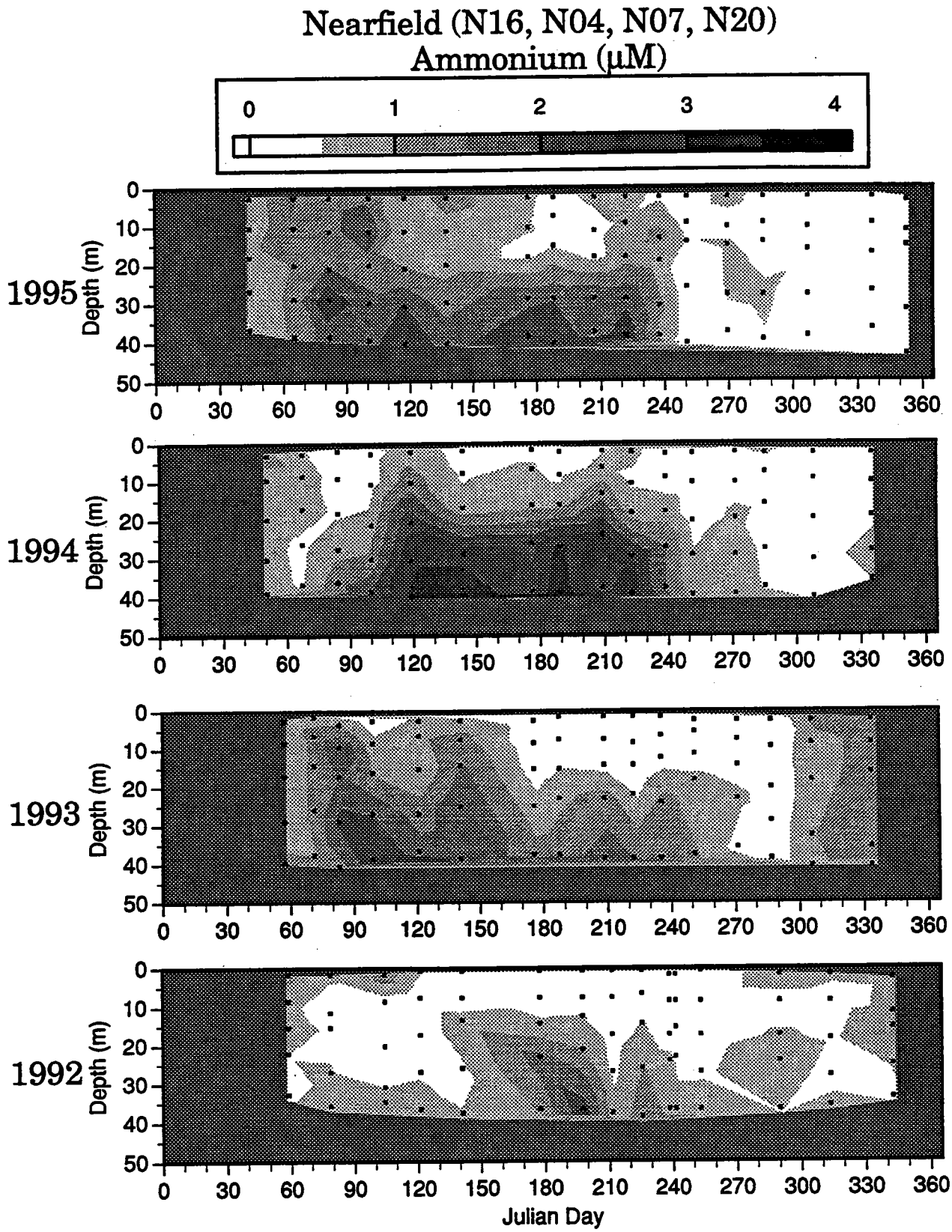

Figure 4-15. Nearfield ammonium concentrations for 1992-1995.

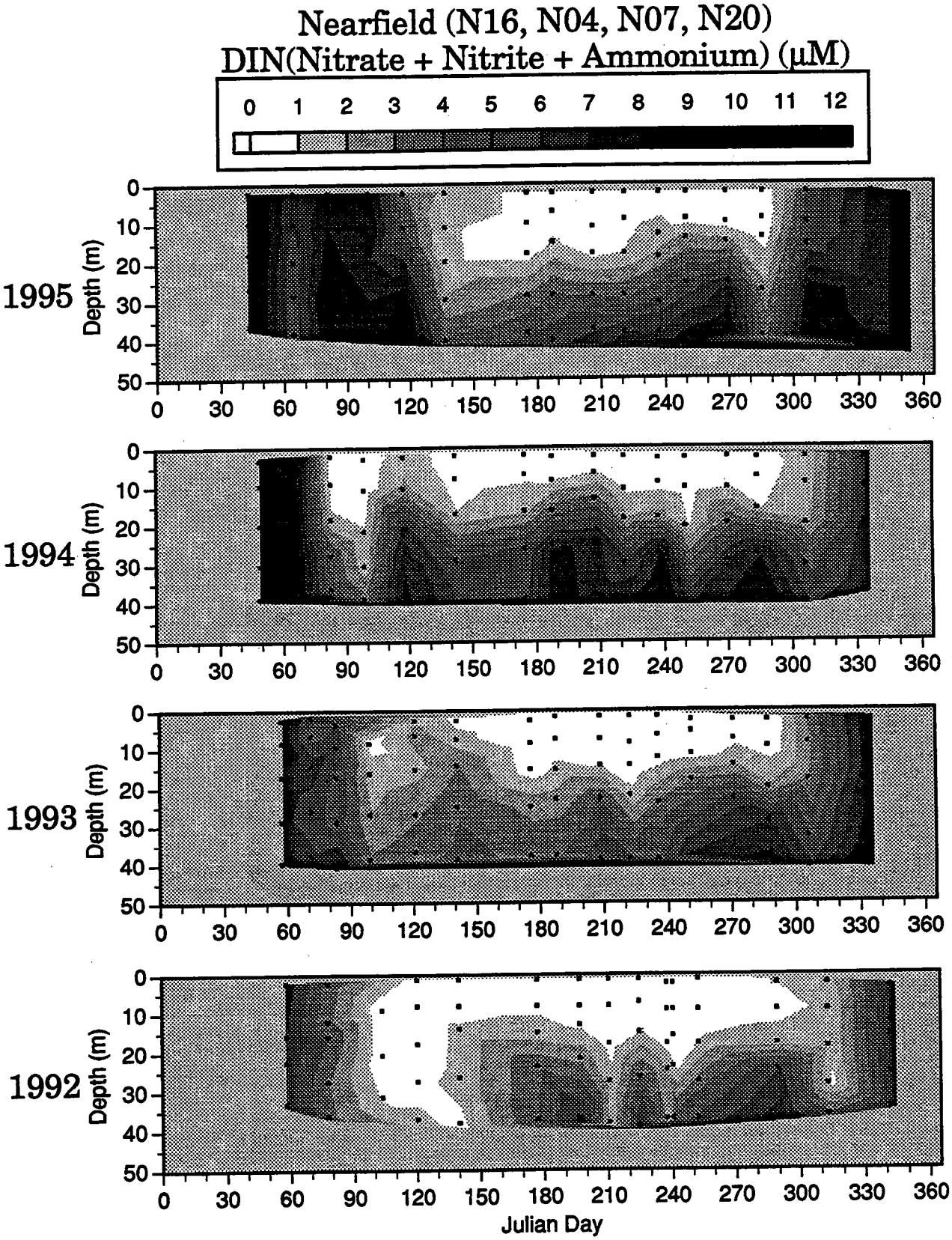

Figure 4-16. Nearfield DIN concentrations for 1992-1995.

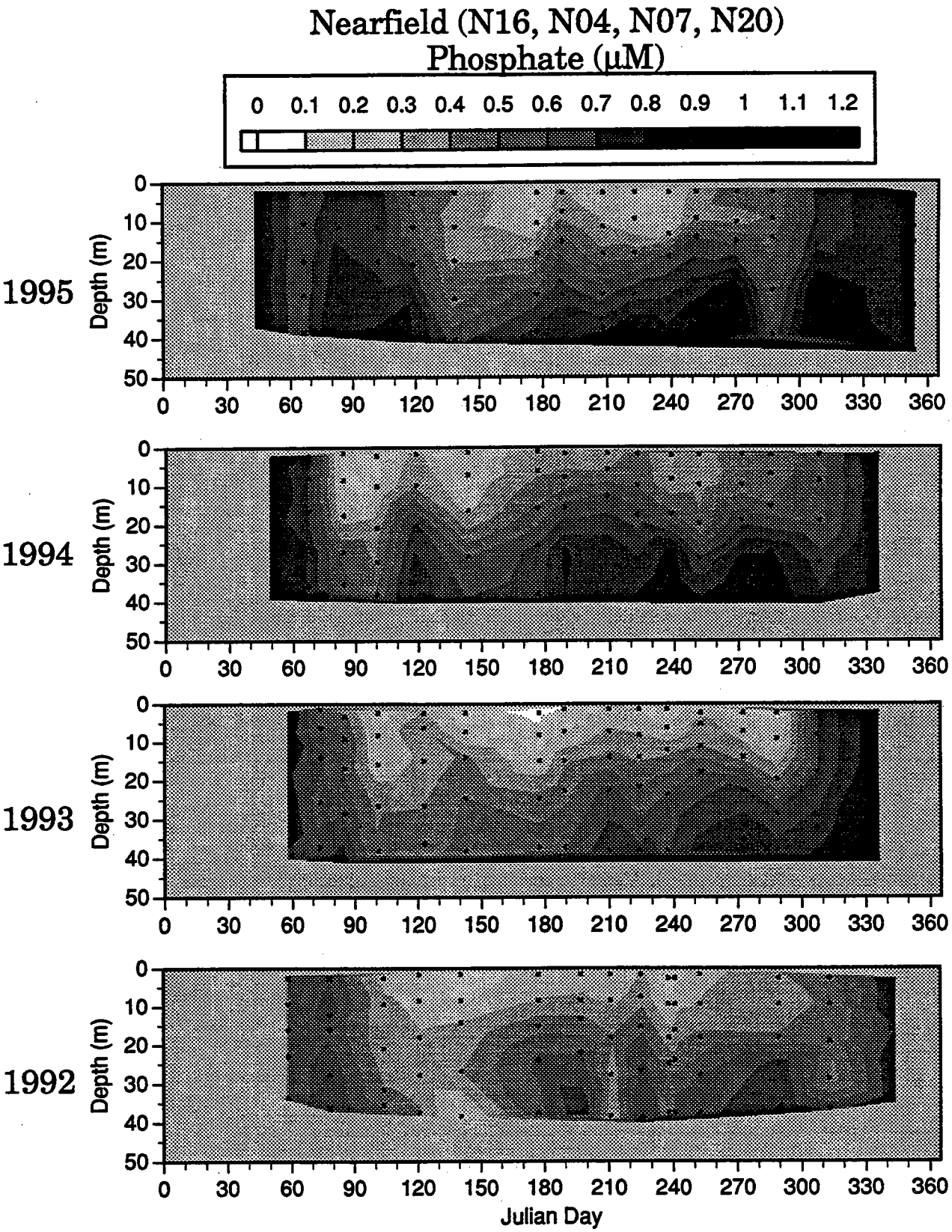

Figure 4-17. Nearfield phosphate concentrations for 1992-1995.

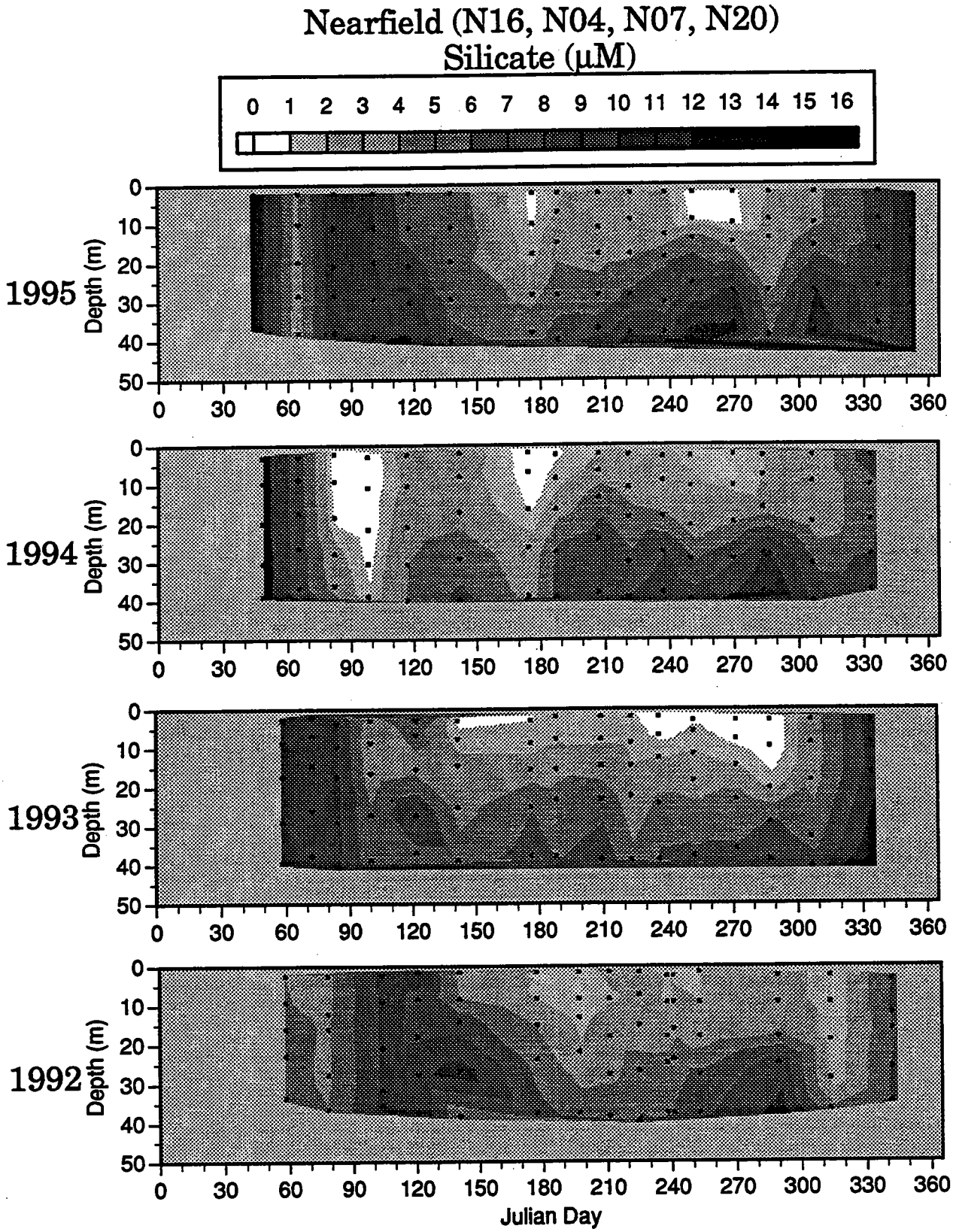

Figure 4-18. Nearfield silicate concentrations for 1992-1995.

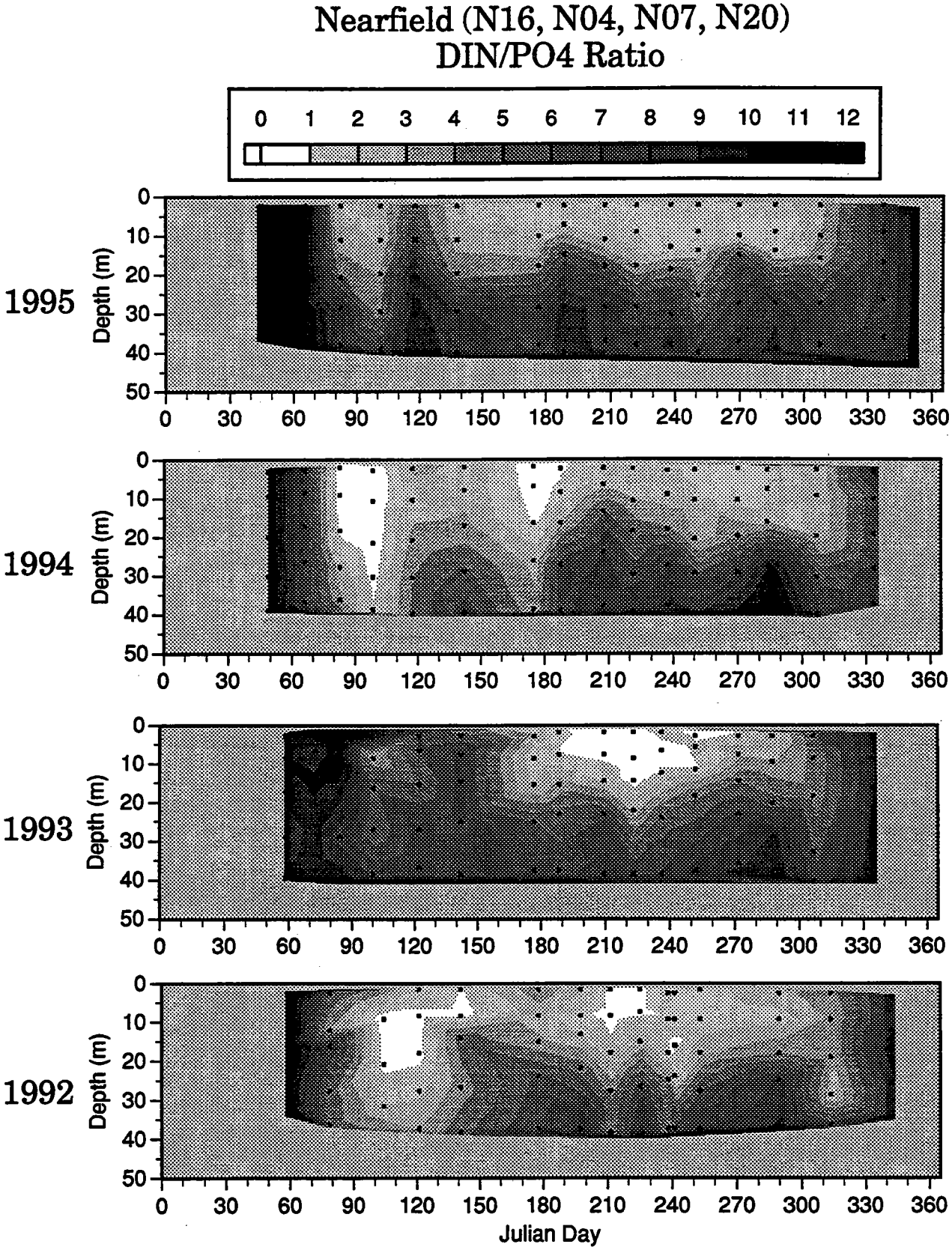

Figure 4-19. Nearfield DIN/PO4 ratios for 1992-1995.

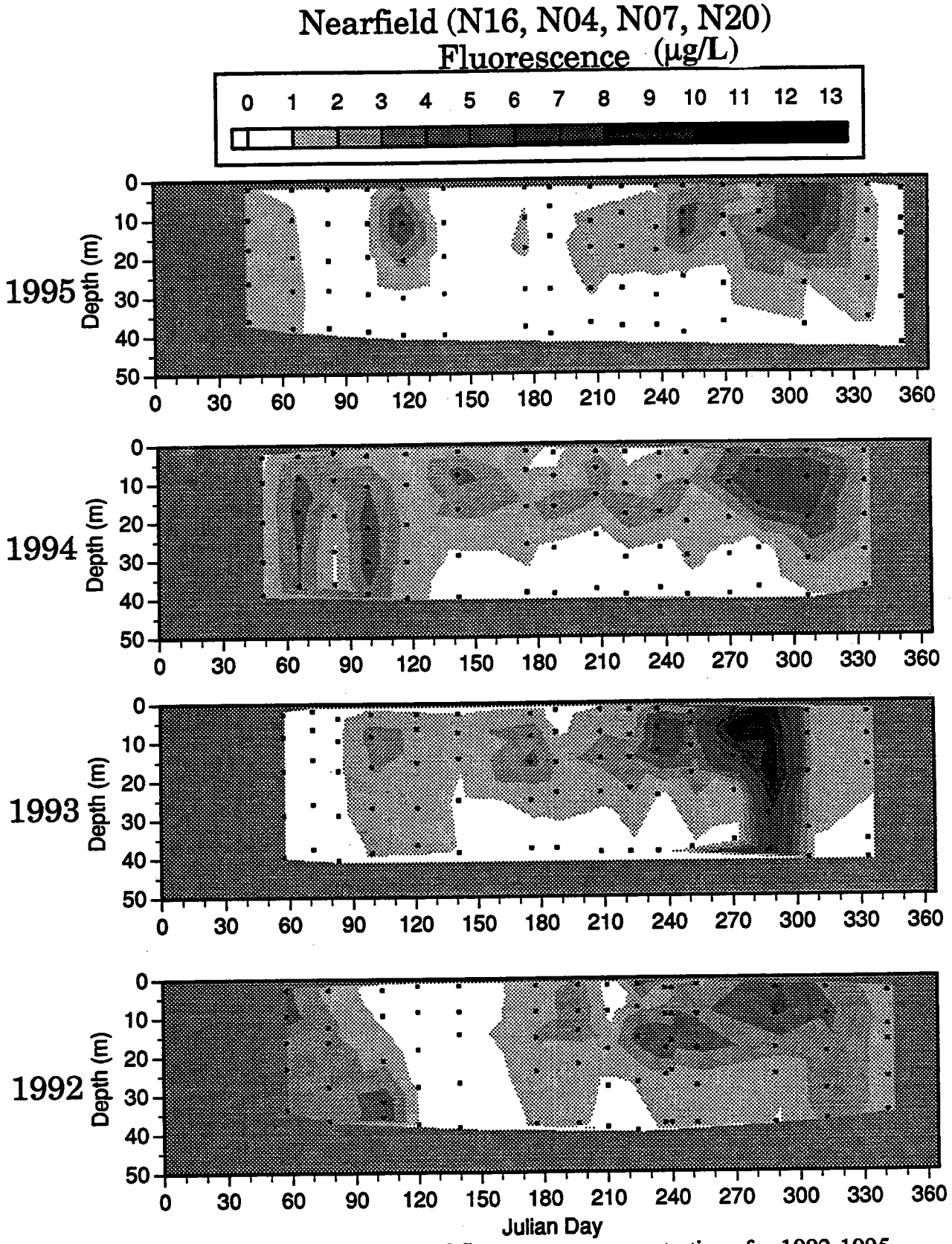

Figure 4-20. Depth-averaged fluorescence concentrations for 1992-1995.

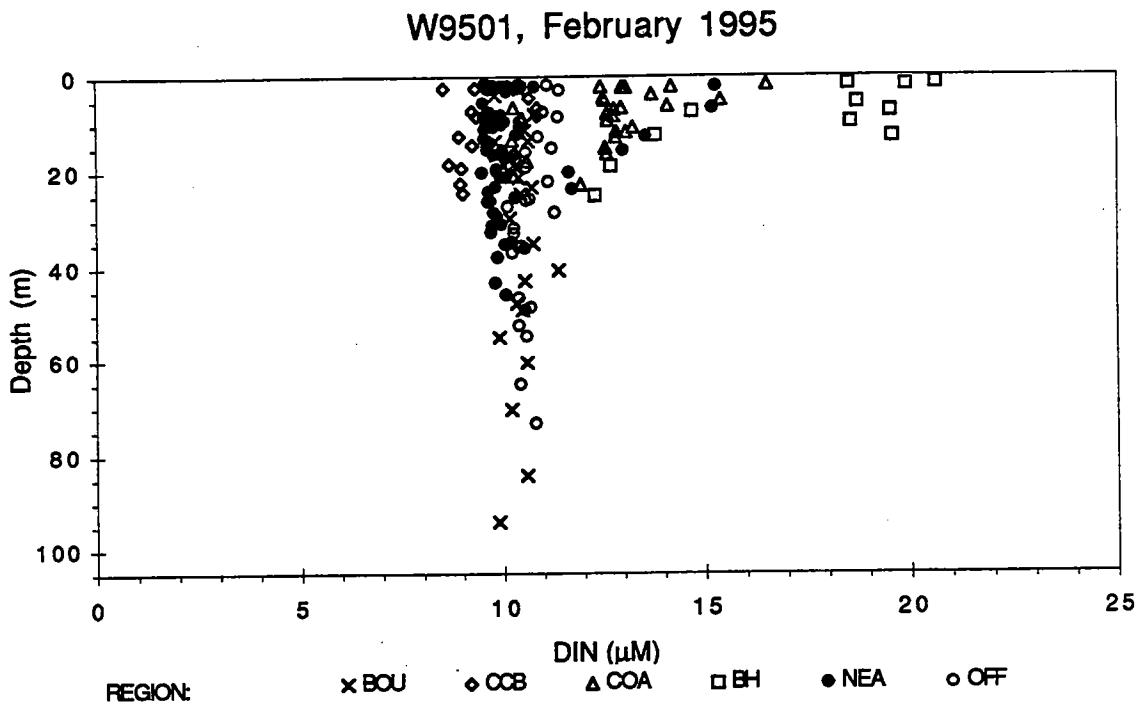

Figure 4-21. Dissolved inorganic nitrogen concentration vs. depth for survey W9501, (February, 1995).

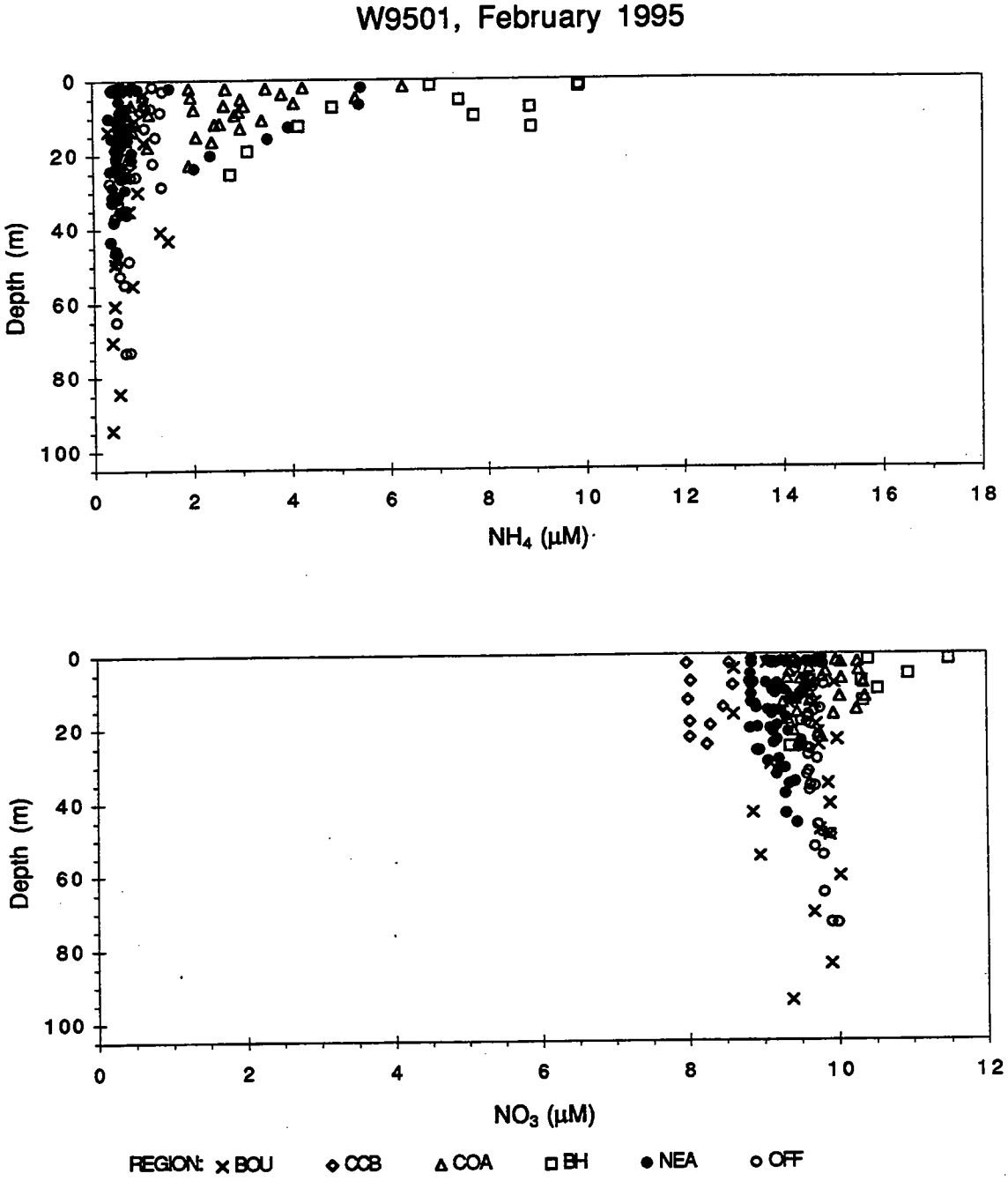

Figure 4-22. Ammonium and nitrate concentrations vs. depth for survey W9501, (February, 1995).

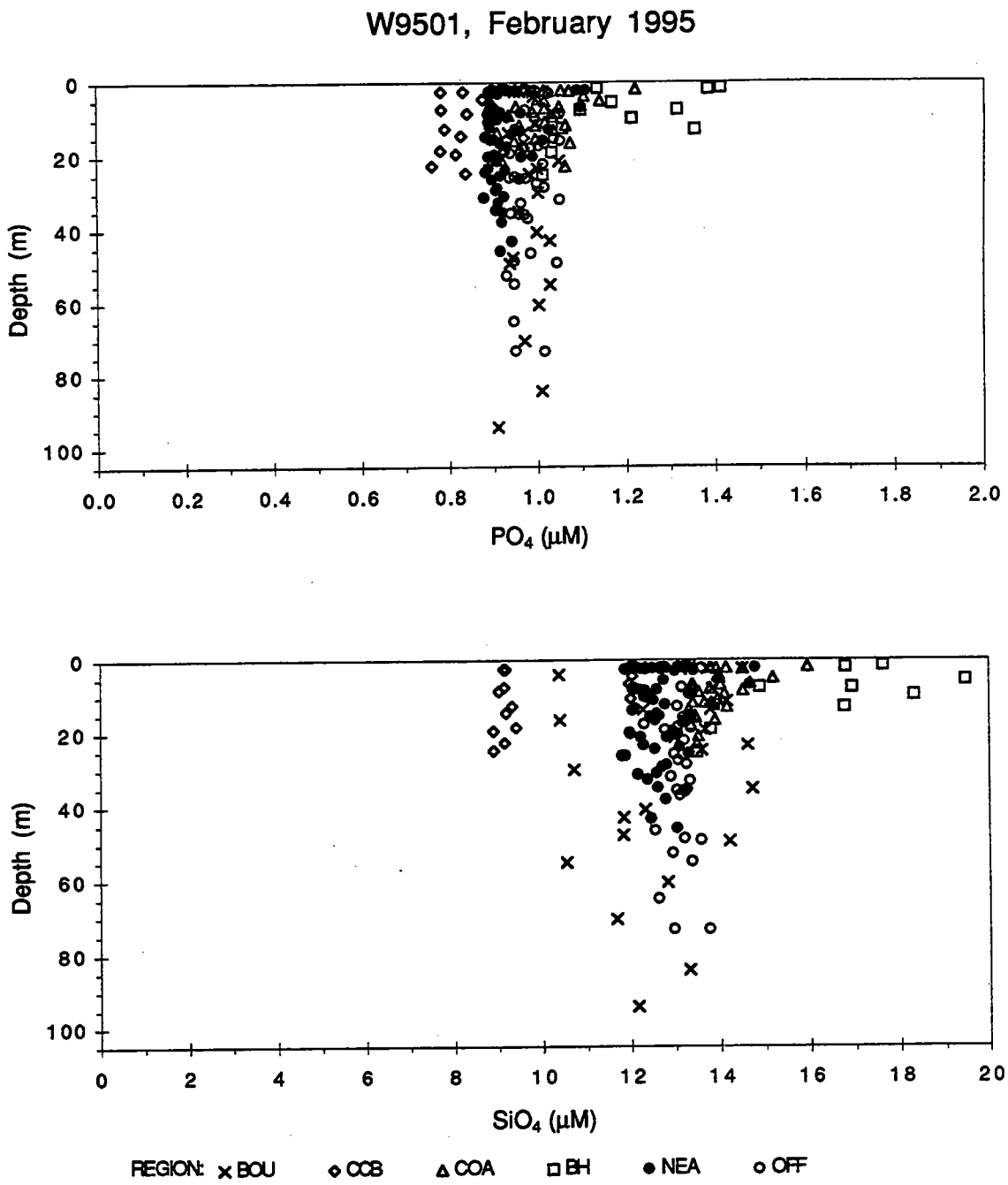

Figure 4-23. Phosphate and silicate concentrations vs. depth for survey W9501, (February, 1995).

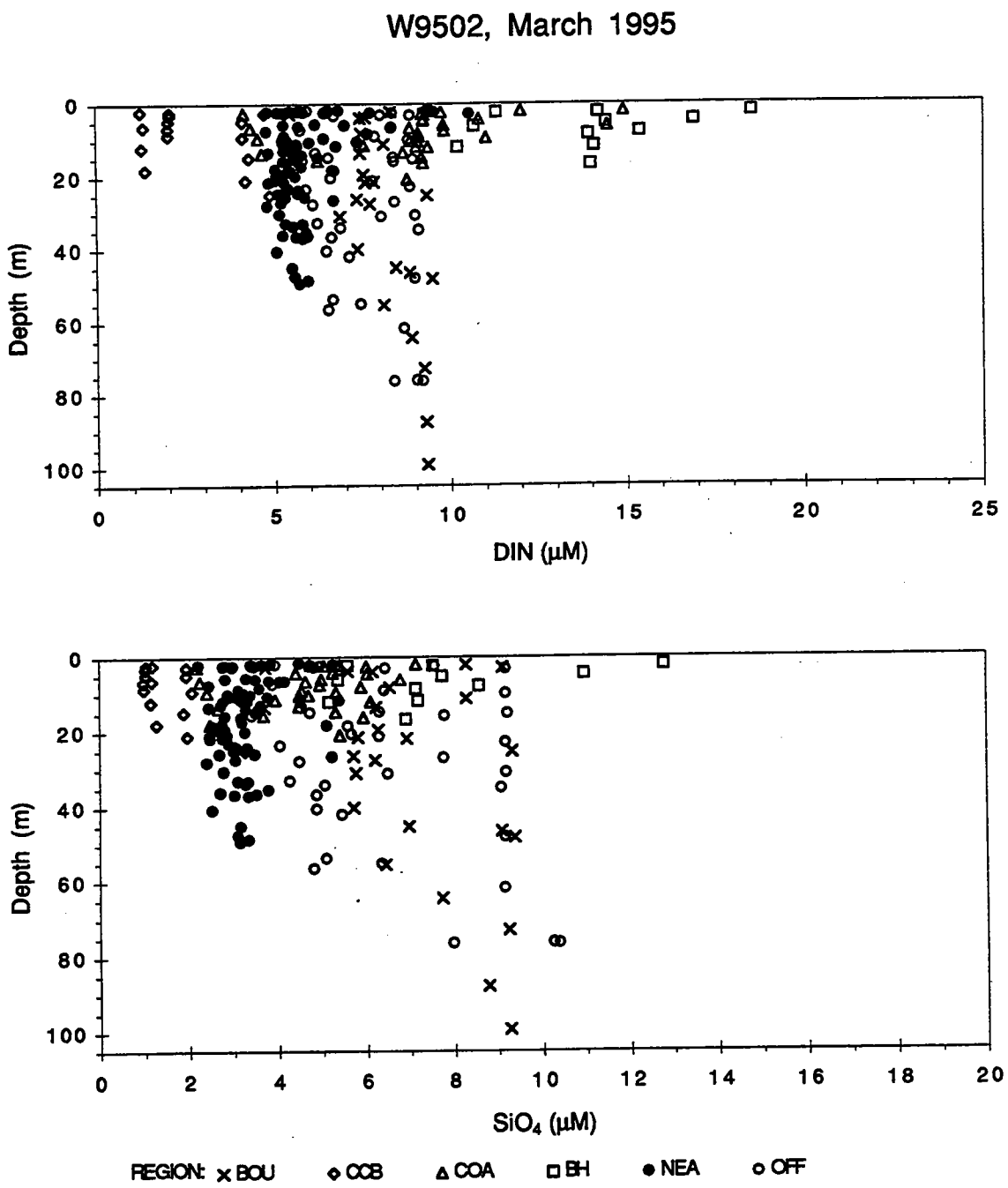

Figure 4-24. Dissolved inorganic nitrogen and silicate concentrations vs. depth for survey W9502, (March, 1995).

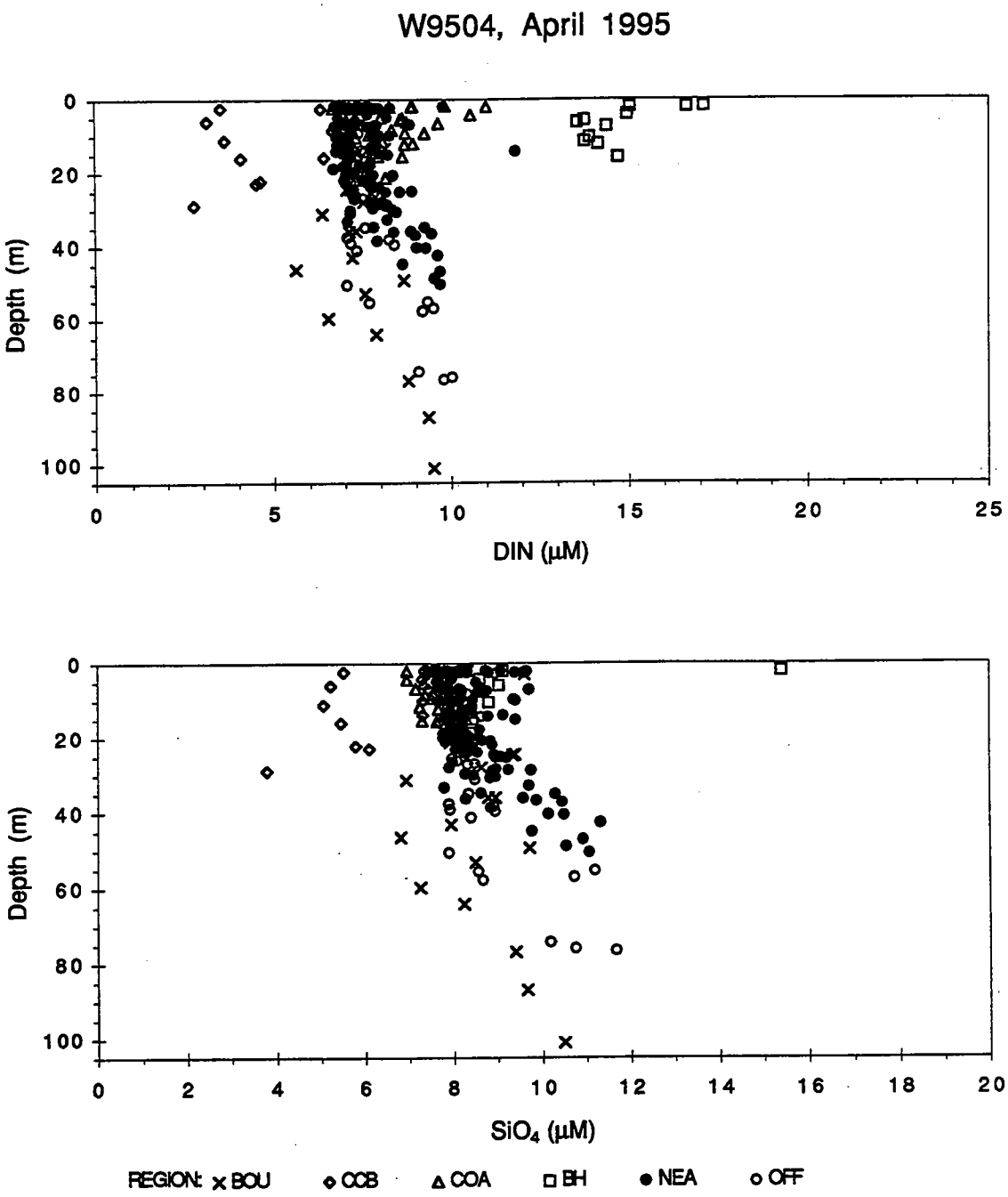

Figure 4-25. Dissolved inorganic nitrogen and silicate concentrations vs. depth for survey W9504, (April, 1995).

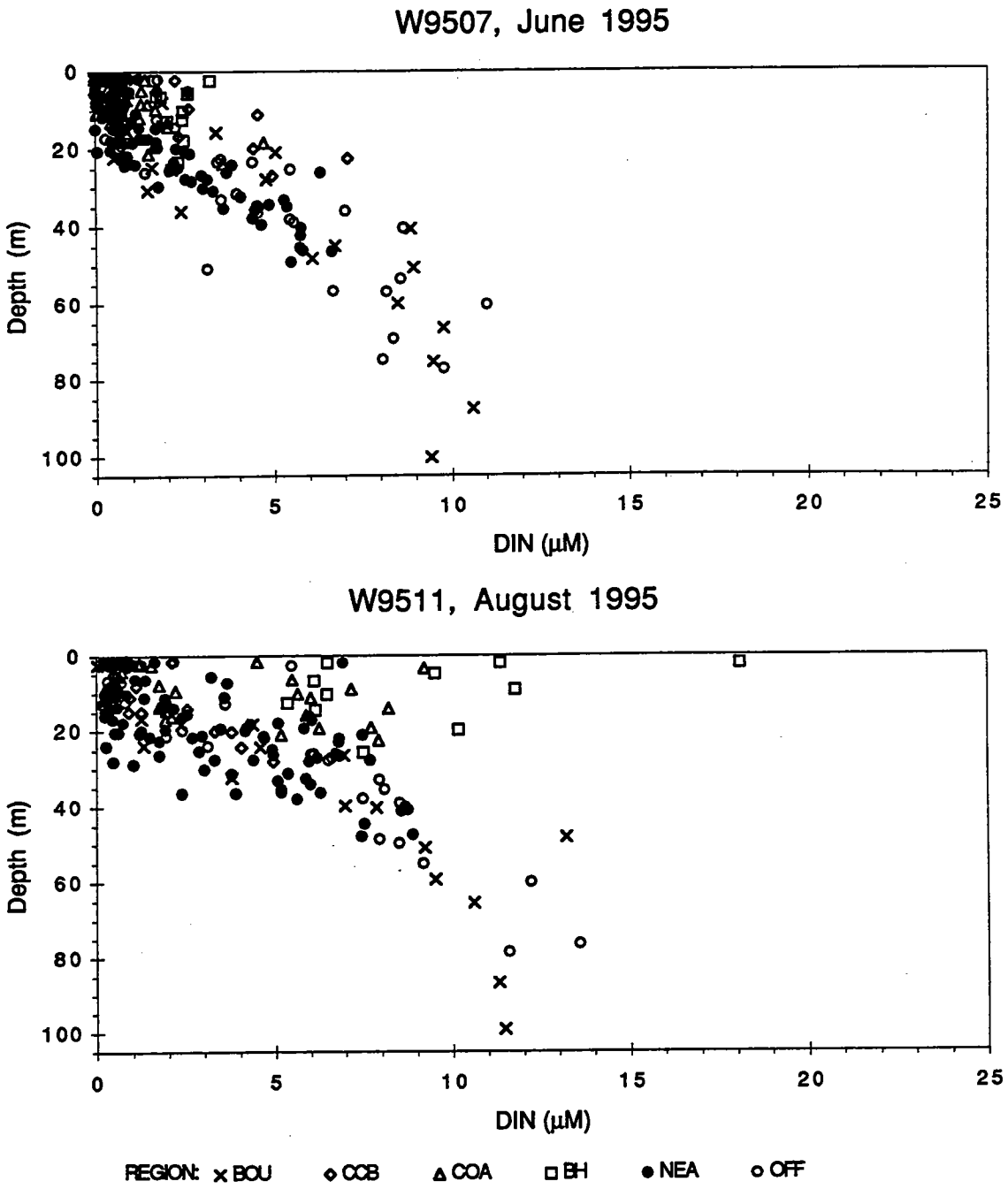

Figure 4-26. Dissolved inorganic nitrogen concentrations vs. depth for surveys W9507, (June, 1995) and W9511, (August, 1995).

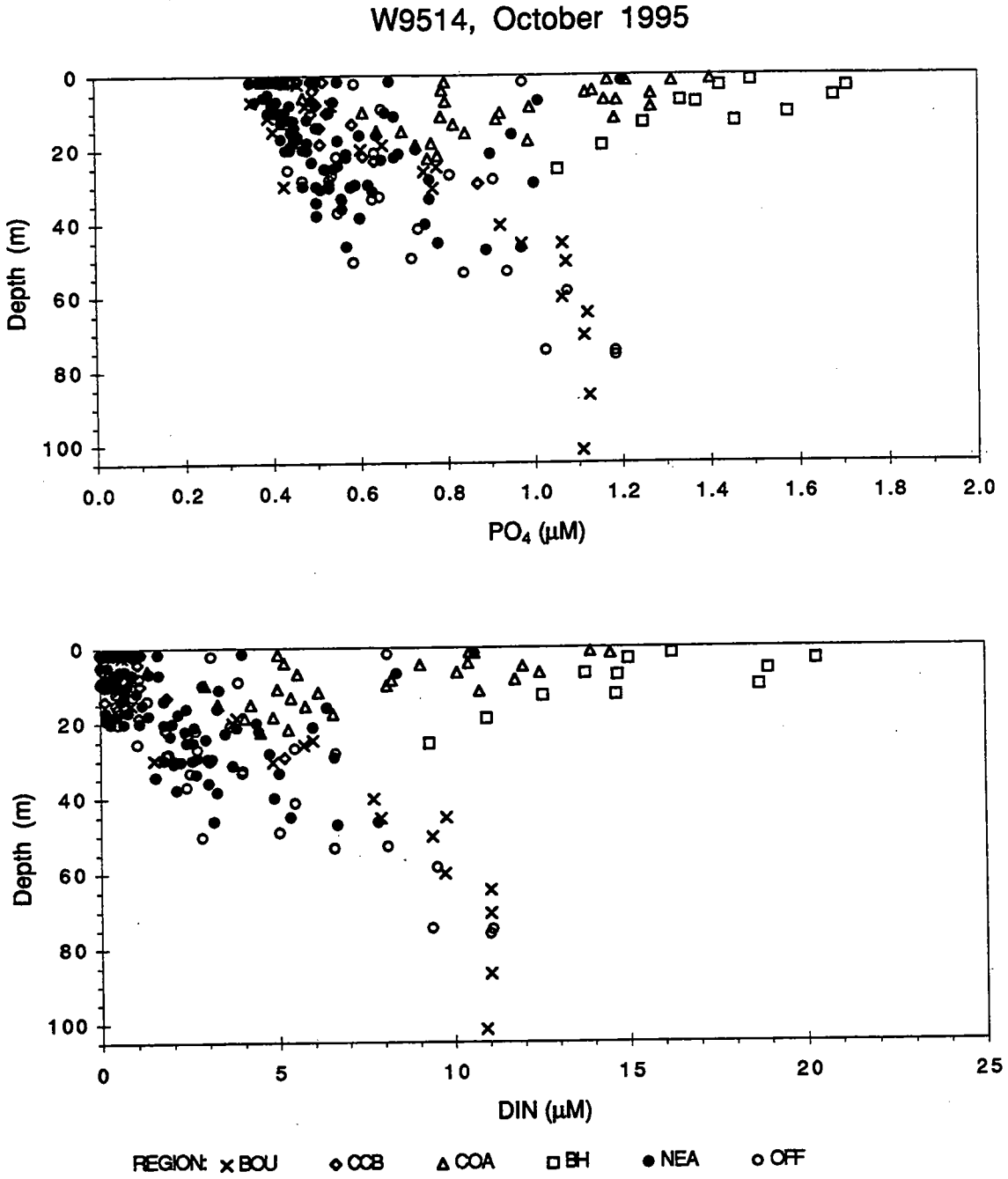

Figure 4-27. Phosphate and dissolved inorganic nitrogen concentrations vs. depth for survey W9514, (October, 1995).

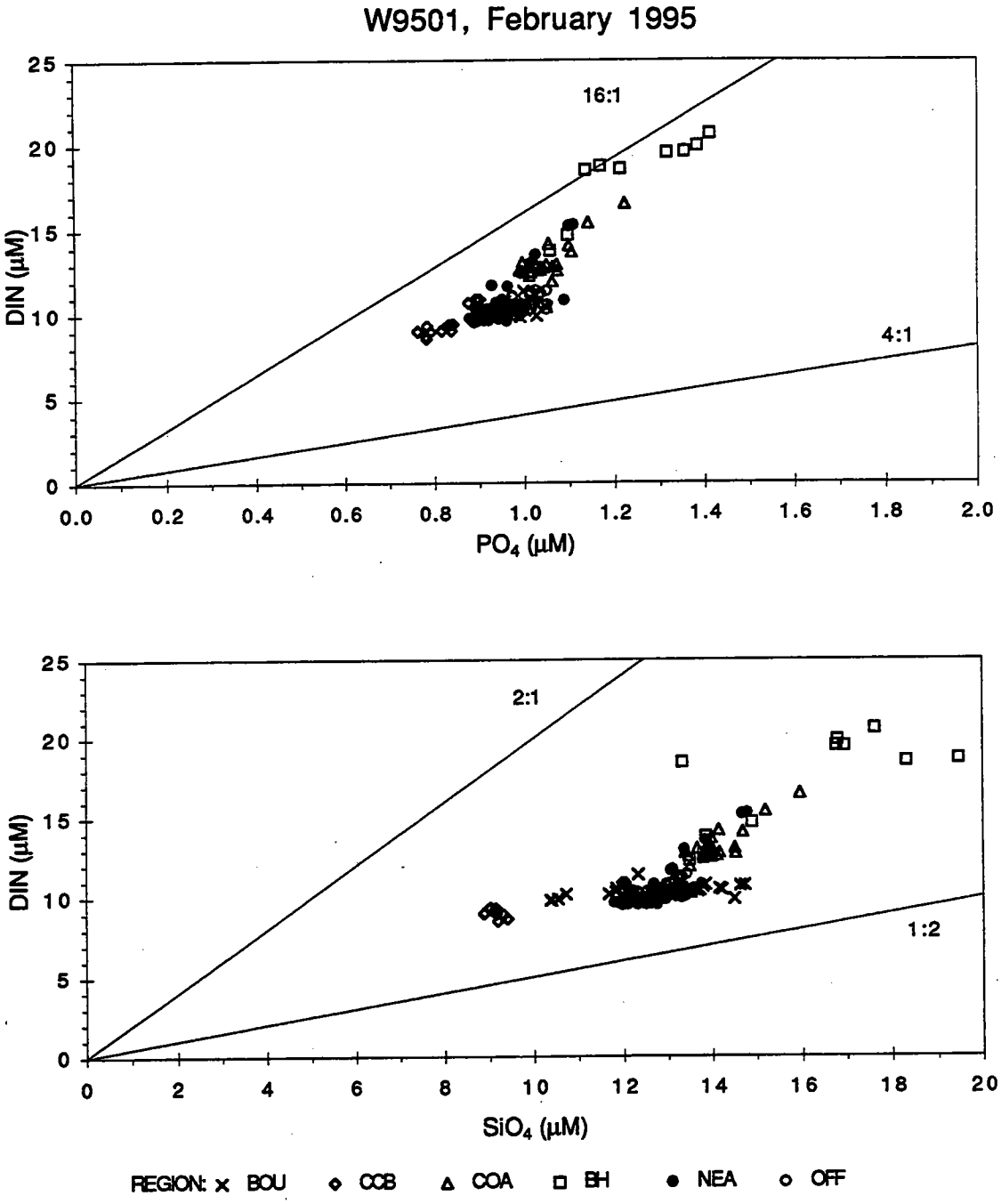

Figure 4-28. DIN vs. phosphate and silicate concentrations for survey W9501, (February, 1995).

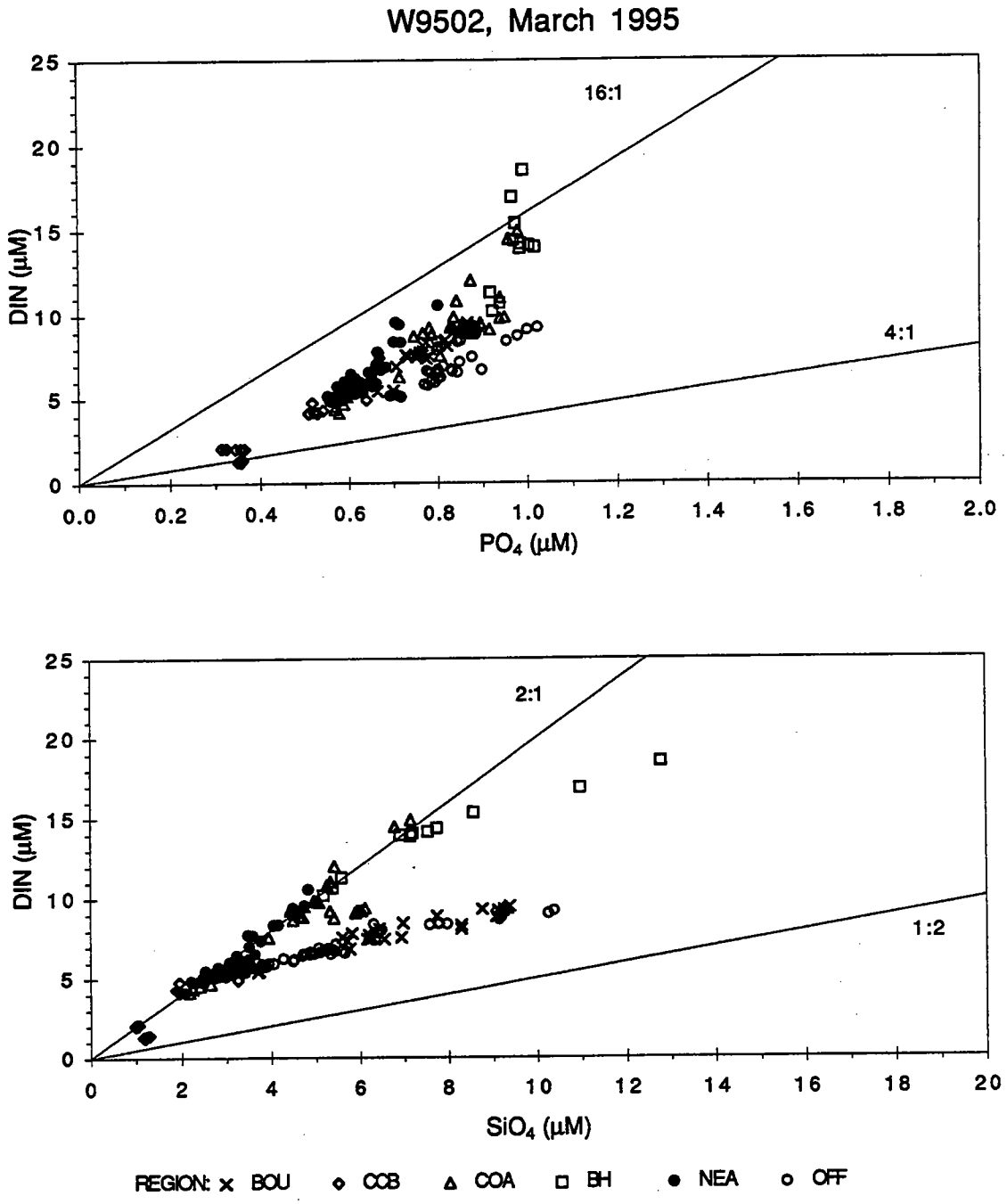

Figure 4-29. DIN vs. phosphate and silicate concentrations for survey W9502, (March, 1995).

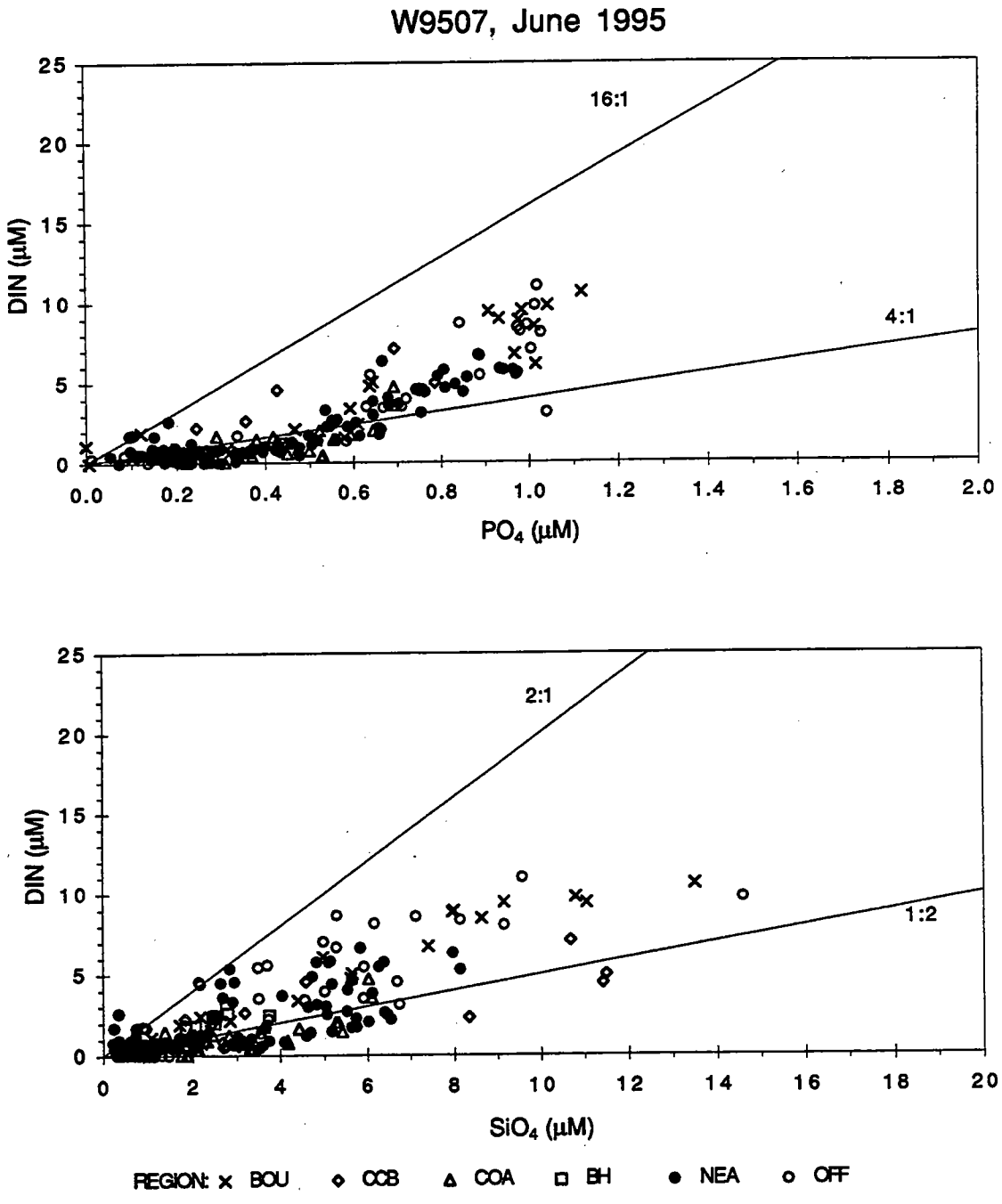

Figure 4-30. DIN vs. phosphate and silicate concentrations for survey W9507, (June, 1995).

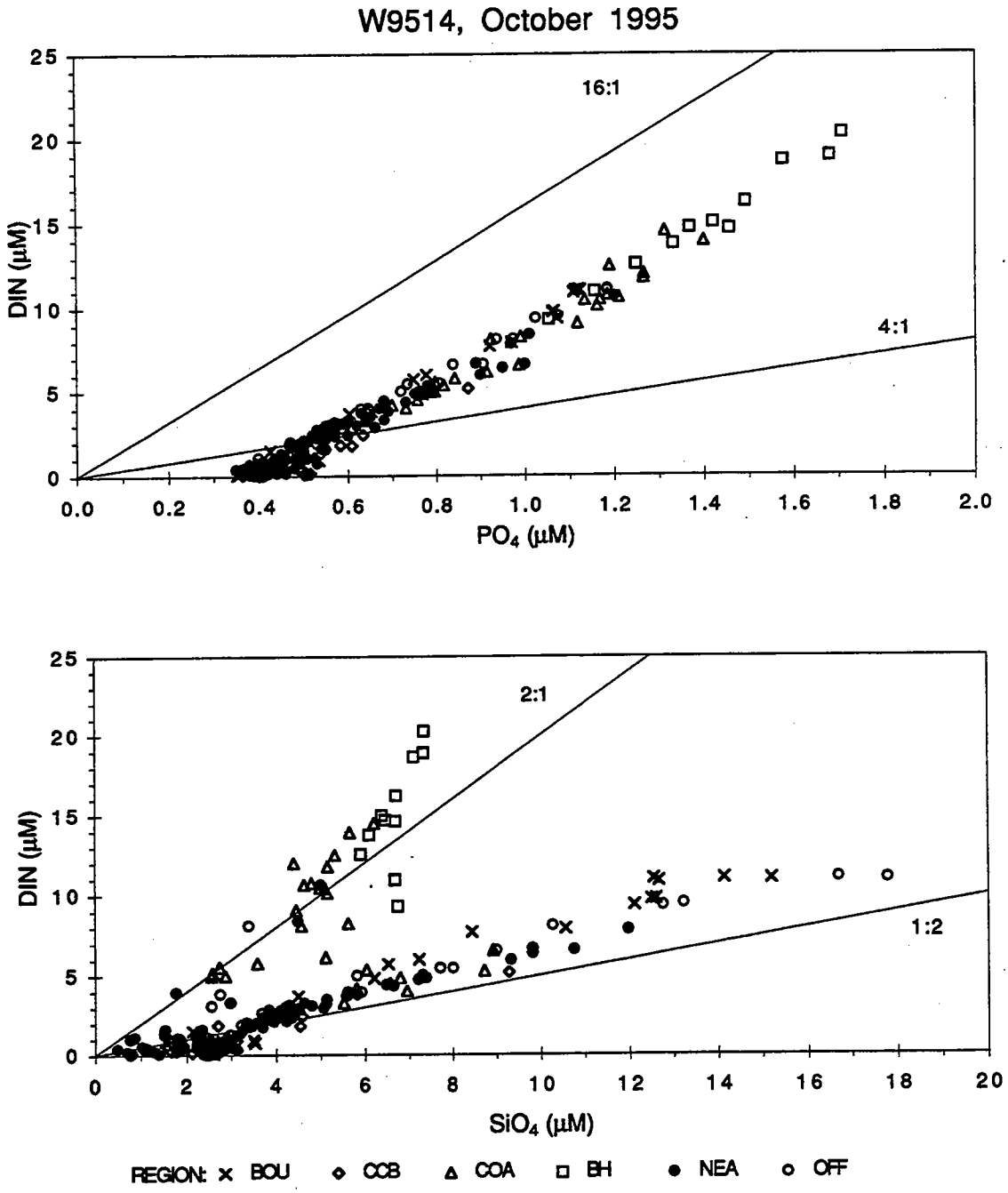

Figure 4-31. DIN vs. phosphate and silicate concentrations for survey W9514, (October, 1995).

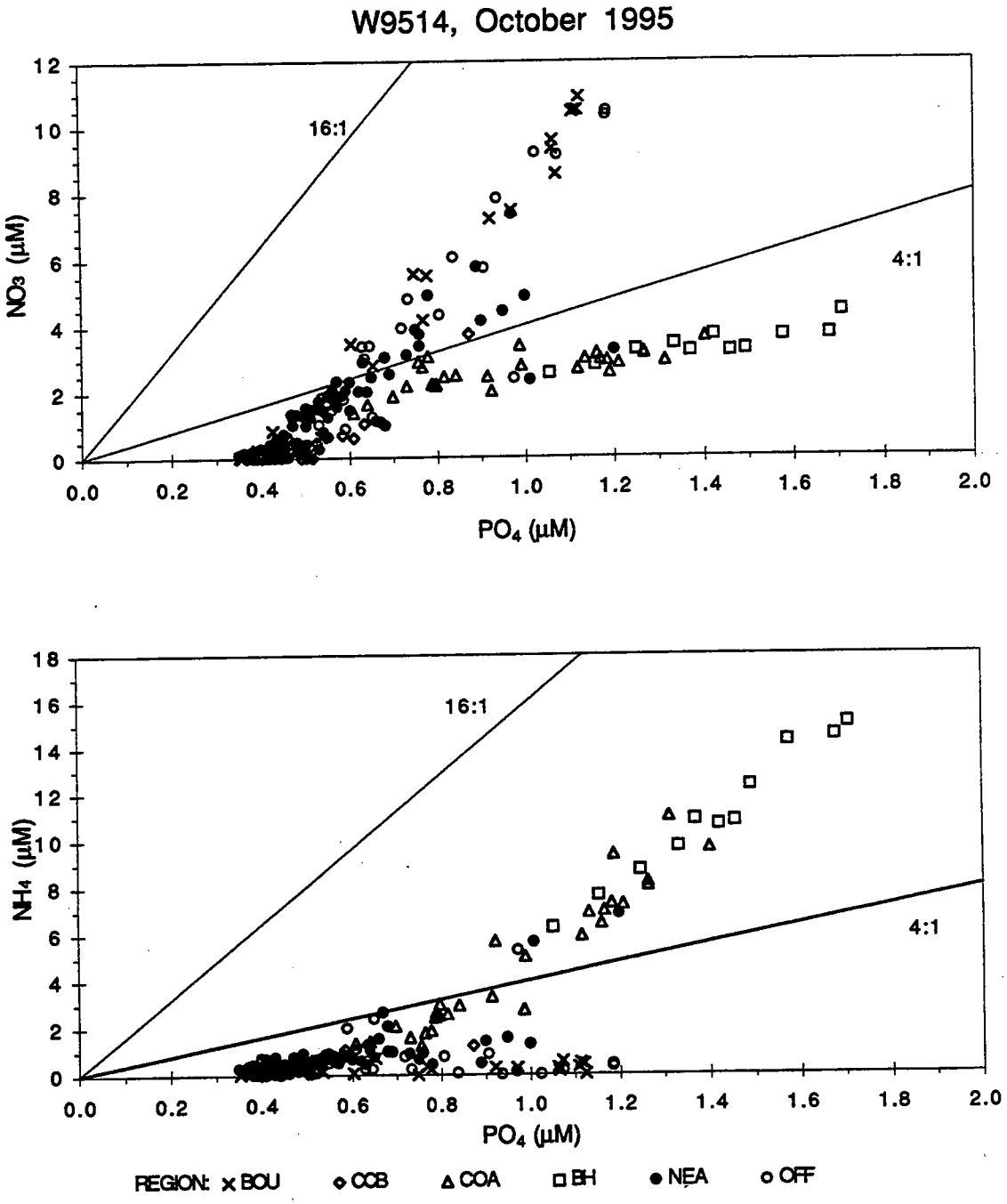

Figure 4-32. Nitrate and ammonium vs. phosphate concentrations for survey W9514, (October, 1995).

5.0 CHLOROPHYLL

Chlorophyll concentration is an indicator of phytoplankton biomass and thus used in the HOM Program as a surrogate for biomass and standing stock of phytoplankton, to normalize productivity measurements, and to ultimately assess the potential for eutrophic effects from the outfall relocation. Chlorophyll was measured on a comprehensive scale by *in-situ* fluorometry during continuous downcasts at each sampling station, and during upcasts when discrete Niskin bottle samples were taken to allow comparisons with nutrients, DO, and other parameters.

The *in-situ* fluorometric sensor was calibrated to analytical determinations of chlorophyll *a* from a subset of the discrete samples. Discrete chlorophyll analyses also included determination of the concentration of phaeopigments, which are degradation products of chlorophyll *a*. These results can be used to assess the physiological status of the phytoplankton community, and can be an indicator of zooplankton grazing when productivity is high (breakdown of chlorophyll *a* by digestion leading to proportionally high phaeopigment concentrations).

In this section, chlorophyll results from the 1995 monitoring activities are presented for the nearfield stations and on a regional basis, and are compared with the 1992-1994 data set. Unless otherwise stated, the results presented consist of calibrated *in situ* fluorescence readings taken at the upcast sampling depths. Included is an evaluation of results taken from the surface and at the chlorophyll maximum (chl_{max}) which relates these results to total phytoplankton densities determined from concurrent samples, with complete presentation of phytoplankton monitoring results presented in Section 8.1. Further detail on chlorophyll concentrations at individual stations within the nearfield grid is included with the discussion of primary productivity in Section 7.1. As with previous sections, significant events in the chlorophyll data are summarized in Table 9-1.

5.1 1995 Nearfield Results

The frequency distribution of chlorophyll results for all stations and all depths (Figure 5-1) indicated that the majority of samples had relatively low concentrations. Approximately 64 percent of results were less than 1 µg/L, and around 90 percent were less than 3 µg/L. The average concentration for the year was 1.39 µg/L (n=1682, with a standard deviation of 2.32; Table 5-1). The maximum concentration was 18.1 µg/L. Less than two percent of results exceeded 10 µg/L, while only 6.2 percent exceeded 5 µg/L. Five percent of results were categorized as zero, which indicated that the fluorescence recorded by the sensor was predominantly due to the presence of phaeopigments. For comparative purposes, the average

analytical result for chlorophyll *a* was 1.26 µg/L (n=904, with a standard deviation of 1.82), and the maximum was 13.4 µg/L (Table 5-2).

The temporal and spatial distributions of chlorophyll for subregions within the nearfield grid were plotted for several subsets of stations within the nearfield grid to illustrate the temporal response of phytoplankton to the horizontal inshore-offshore nutrient gradient (see Section 4). Surface, mid-depth, and bottom concentrations were plotted to evaluate vertical differences (Figure 5-2). The inshore station N10, which is influenced by tidal exchange with Boston Harbor and also subject to a lesser degree of stratification (refer to Figure 3-11; also see Townsend *et al.*, 1991; Kelly and Turner, 1995), exhibited a different pattern from other nearfield areas after June (Figure 5-2b). It had higher concentrations from June through August, especially in surface waters and at mid-depth. It also exhibited a late summer peak of much greater intensity than seen at N01 (off Nahant) or in the more offshore stations. This peak can be attributed to station N10's tidal linkage to the harbor, which based on concurrent data from station F31 (inside the harbor, see Figure 2-1), was also exhibiting bloom conditions during this period (Figure 5-2a).

In addition, station N10 did not develop the type of bloom during the fall turnover which was evident at the other nearfield areas (Figures 5-2c and 5-2d). During this fall bloom, Station N01 had the greatest chlorophyll concentrations. It is also noteworthy that station N01 had the highest chlorophyll concentrations during the spring bloom. Despite these temporal differences in concentration between N10 and N01, they still yielded almost identical annual averages when all depths are included (1.74 µg/L at N10 compared with 1.73 µg/L at N01). The outer nearfield stations had a much lower annual average of 1.18 µg/L.

One other notable feature of the plots in Figure 5-2 is the slightly elevated chlorophyll concentrations noted during the first survey in early February (Figure 5-2b and 5-2d). Concentrations were in decline by the second survey and were quite low by the third survey. Nutrient results presented in Section 4 all documented a substantial reduction in the concentrations of DIN, PO_4, and dissolved silicate by the second survey. These results, particularly the reduction in silicate, suggested that a brief but significant diatom bloom had occurred prior to the second survey (and perhaps prior to the first survey). In such a case, the chlorophyll concentrations reported from survey W9501 may have actually been in decline from an earlier event.

Continuously recorded optical transmission chlorophyll readings (WETLabs ac-3) from the USGS mooring south of N21 were obtained for the two periods during 1995 when data were available (February/March and September/October) to compare with the shipboard survey measurements. These results were plotted with the chl_{max} depth results from the outer nearfield stations (Figure 5-3). Beyond the daily variability which might arise from both physical and biological factors, these data indicated short-term maxima of varying intensity (approximately 1 µg/L in February, Figure 5-3a; up to 3 µg/L in October, Figure 5-3b) which often occurred at almost weekly intervals. Based on these periods, the results suggest that

shipboard measurements may have underestimated biomass during the latter part of February, and to a degree, a slight potential to overestimate biomass during October prior to the fall bloom.

To further evaluate the vertical distribution of chlorophyll in the nearfield, ratios were calculated to compare chlorophyll concentrations from the chl_{max} sample depth with the surface samples for several stations (Figure 5-4). The ratio at the two depths at inshore station N10 did not diverge greatly over the year (Figure 5-4b), even during stratified periods (refer to Figure 3-11). This observation was similar to that seen at the adjacent harbor station (Figure 5-4a). The more offshore stations developed more pronounced maxima at depth, reaching ratios of 4:1 or greater during peak stratification in late July (Figure 5-4c through 5-4e). These chlorophyll results were reflected in ratios calculated for phytoplankton densities for these depths at N10 and N16 (Figure 5-5). Surface phytoplankton densities were typically slightly higher inshore (Figure 5-5a) and during non-stratified periods offshore (Figure 5-5b), while peak phytoplankton densities for the chl_{max} offshore were approximately twice that reported for the surface depth during the stratified period (Figure 5-5b).

The relative proportion of chlorophyll *a* to total pigments in the nearfield was plotted to examine seasonal patterns in the pigment ratios (Figure 5-6). The active chlorophyll *a* concentration at the surface in most regions was typically between 60 and 80 percent of the total pigment concentration. There were notable variations from this, the first being the decline in active chlorophyll at all depths during the third survey. Coupled with the decline in phytoplankton densities and increased abundance of zooplankton during this survey (refer to Section 8), it may be concluded that a collapse of the late winter diatom bloom and/or zooplankton grazing may have been responsible for this decline.

A second noteworthy event depicted in Figure 5-6 occurred during survey W9508 (early July), when the surface and bottom ratios converged at the nearfield stations. These observations coincide with the July mixing event described in Section 3 (refer to Figures 3-2, 3-7, and Figures 3-14 through 3-17). At each station, the percent chlorophyll *a* increased in the bottom sample. These increases were accompanied by concurrent decreases in surface ratios at N16 and N07, but not at N04.

5.2 1995 Regional Comparisons

A frequency distribution for chlorophyll *a* results was also calculated for all stations and all depths in Massachusetts and Cape Cod Bays sampled during the combined nearfield/farfield events (Figure 5-7). These results indicated that the distribution of chlorophyll concentrations were similar baywide as that seen in the nearfield (refer to Figure 5-1). The average concentration for the year was 1.20 µg/L (n=1102, with a standard deviation of 1.74). The maximum concentration was 15.0 µg/L (Table 5-1). The average analytical result for chlorophyll *a* was 1.39 µg/L (n=1278, with a standard deviation of 1.91), and the maximum was 14.5 µg/L (Table 5-2).

Regional plots of fluorescence data indicated highest chlorophyll concentrations during late summer in the harbor and coastal waters (Figure 5-8). These summer results showed highest concentrations in surface samples in the harbor, whereas at the more stratified coastal and offshore stations they were highest at the chl_{max} depth. While most regions exhibited a modest late winter/spring event followed by a trend toward increasing concentrations through the summer, Cape Cod Bay showed maximum concentrations in the late winter and spring and low chlorophyll concentrations during the summer. Along with the offshore and boundary stations, Cape Cod Bay appeared to be increasing in chlorophyll concentration during the October survey (W9514), suggesting the fall bloom evident in the nearfield stations by the end of the month may have also occurred in these regions but between surveys.

5.3 Interannual Comparisons of Chlorophyll Concentration

5.3.1 Nearfield Comparisons

The annual seasonal cycles for chlorophyll (surface and bottom) in the nearfield for the period 1992 to 1995 are plotted in Figure 5-9. These results show a substantial amount of short-term temporal variability, as well as small-scale spatial patchiness within each year's data record. However, annual events are easily identifiable, most pronounced of which is the overwhelming magnitude of the fall bloom event relative to spring and summer. In all cases, the area of Broad Sound represented by station N01 exhibited the highest peaks (Figure 5-9b). Also evident was the relatively small fall maxima in 1992 and 1994 in most regions, particularly in 1992.

The late summer peak seen in the inner nearfield in 1995 was quite similar to that observed in 1992 (Figure 5-9a). The two years also provide confirmation of the potential for late winter bloom activity in the nearfield. Inner nearfield data from both years had bimodal peaks (although quite subtle in 1995), leading to the speculation that the late winter and early springs blooms may be two separate events with different phytoplankton assemblages. Alternatively, this scenario might result from varying grazing pressure. Further discussion with respect to the two biological communities in Section 8.

The extent of spatial and temporal variability for nearfield stations as a whole is depicted in Figure 5-10. Again, the most notable difference between the four years is the magnitude of the fall event, particularly in 1993 and 1995. The size of the error bars (standard deviations) indicate the degree of horizontal and vertical variability encountered during one survey. Large interannual differences can also be seen during the early part of the year. Late winter blooms were more evident in 1992 and 1994, whereas in 1993 and 1995 there were more pronounced peaks during the spring. This graphical representation of the data also demonstrates that both the spring and fall events may reach peak densities over a period of a month or more.

Despite the differences observed in the magnitude of bloom events from year to year, annual nearfield averages only differed by around 1 µg/L, ranging from 1.39 µg/L in 1995 to 2.36 µg/L in 1993 (Table 5-1). The overall average calculated for the 1992-1995 baseline period was 1.95 µg/L. This relative insensitivity in annual averages to year-to-year variability would tend to argue for interannual differences to be evaluated on a seasonal basis. Even though recurring bloom events may shift by a month or more, these seasonal patterns are easily identifiable.

5.3.2 Regional Comparisons

Table 5-1 also provides annual averages for results from the regional stations sampled during the six combined surveys (1992 through 1995). Average results ranged from 1.2 µg/L to 2.84 µg/L, with results from 1995 again the lowest of the four years. The lower annual average concentration seen in 1995 may be in part due to monitoring program changes (instituted in 1994) which changed the station coverage used in previous years. For instance, four oligotrophic stations were added in the boundary region starting in 1994. As such, the 1995 and 1994 averages are the most comparable to each other.

In order to more closely examine these interannual differences on a regional and temporal basis, averaged calibrated sensor results for each sampling region were plotted for 1992 through 1995 (Figures 5-11 and 5-12). Average results from the harbor stations were most similar (Figure 5-11a), as was the seasonal pattern produced by the data from the six surveys. Results from the coastal stations (Figure 5-11b) indicated that the fall bloom was much more extensive in 1993 than any other period. This was also evident in average results throughout the other regions during 1993 (Figures 5-12a, b, and c). The greater fall bloom seen in the high frequency sampling of the nearfield (Figure 5-11c) supports the contention that difference in the farfield stations in 1993 is "real" rather than due to interannual differences in the timing of sampling.

The four-year record also documented a large early season bloom event (mid-February) in 1992 in the boundary region (station F12) and Cape Cod Bay (Figure 5-12a and c). This was also evident to some degree in the nearfield and coastal stations (Figure 5-11b and c). In later years, this early-season event seemed to be captured in the second survey (late February) and was most pronounced in Cape Cod Bay (Figure 5-12).

Year	Mean (µg/L)	Standard Deviation	N	Maximum (µg/L)
Nearfield				
1992	2.08	1.69	1465	17
1993	2.36	3.11	1850	20.5
1994	1.96	1.48	1863	13.7
1995	1.39	2.32	1682	18.1
1992-1995 Baseline	**1.95**	**2.29**	**6861**	**20.5**
Massachusetts Bay				
1992	2.24	1.75	2200	
1993	2.84	3.85	1103	21.1
1994	2.27	2	1132	16.9
1995	1.20	1.74	1102	15.0

TABLE 5-1

Comparison of Annual and Regional In-situ Chlorophyll a Characteristics

Nearfield = N*, all depths, Mass Bay = F* + 6 NF, all depths

Year	Mean (µg/L)	Standard Deviation	N	Maximum (µg/L)
Nearfield				
1992	2.67	2.44	215	13.2
1993	2.44	3.72	527	31.6
1994	1.84	1.46	614	8.7
1995	1.26	1.82	904	13.4
1992-1995 Baseline	**1.83**	**2.44**	**2260**	**31.6**
Massachusetts Bay				
1992	2.90	2.34	333	12.6
1993	2.51	3.55	645	31.6
1994	2.06	1.93	922	18.1
1995	1.39	1.91	1278	14.5

TABLE 5-2
Comparison of Annual and Regional Analytical Results for Chlorophyll *a* Characteristics
Nearfield = N*, all depths; Mass Bay = F* + 6 NF, all depths

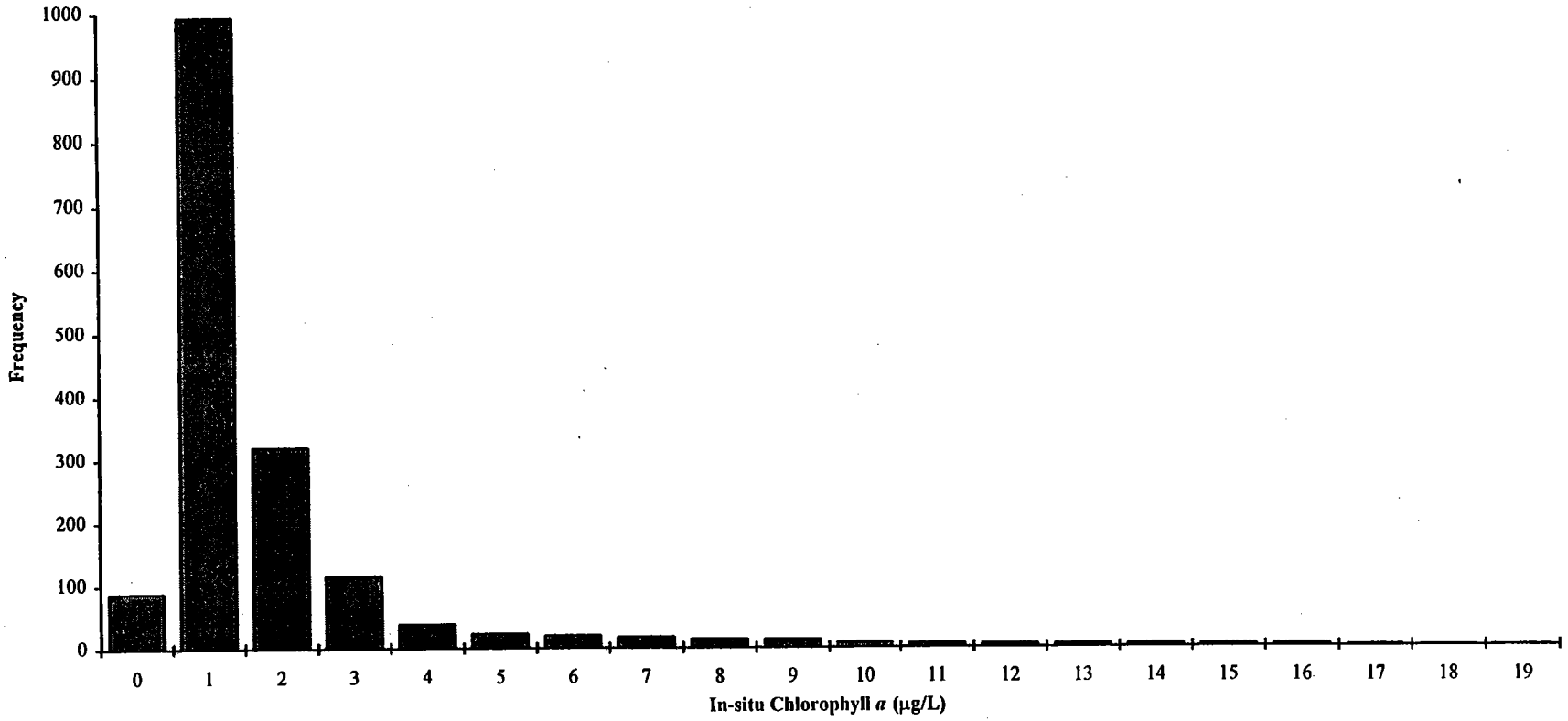

																					Total
Nearfield	88	993	320	115	38	23	20	17	14	13	8	6	5	5	5	4	4	2	1	1	1681
Percent	5.2%	59.1%	19.0%	6.8%	2.3%	1.4%	1.2%	1.0%	0.8%	0.8%	0.5%	0.4%	0.3%	0.3%	0.3%	0.2%	0.2%	0.1%	0.1%	0.1%	100%
Cumulative #	88	1081	1401	1516	1554	1577	1597	1614	1628	1641	1649	1655	1660	1665	1670	1674	1678	1680	1681	1682	
Cumulative %	5.2%	64.3%	83.3%	90.2%	92.4%	93.8%	95.0%	96.0%	96.8%	97.6%	98.1%	98.5%	98.8%	99.0%	99.3%	99.6%	99.8%	99.9%	100%	100%	

Note: Bin number denotes upper limit of bin.

FIGURE 5-1

Frequency Distribution of 1995 Nearfield In-situ Chlorophyll *a* Results

All depths at all nearfield stations on all nearfield surveys.

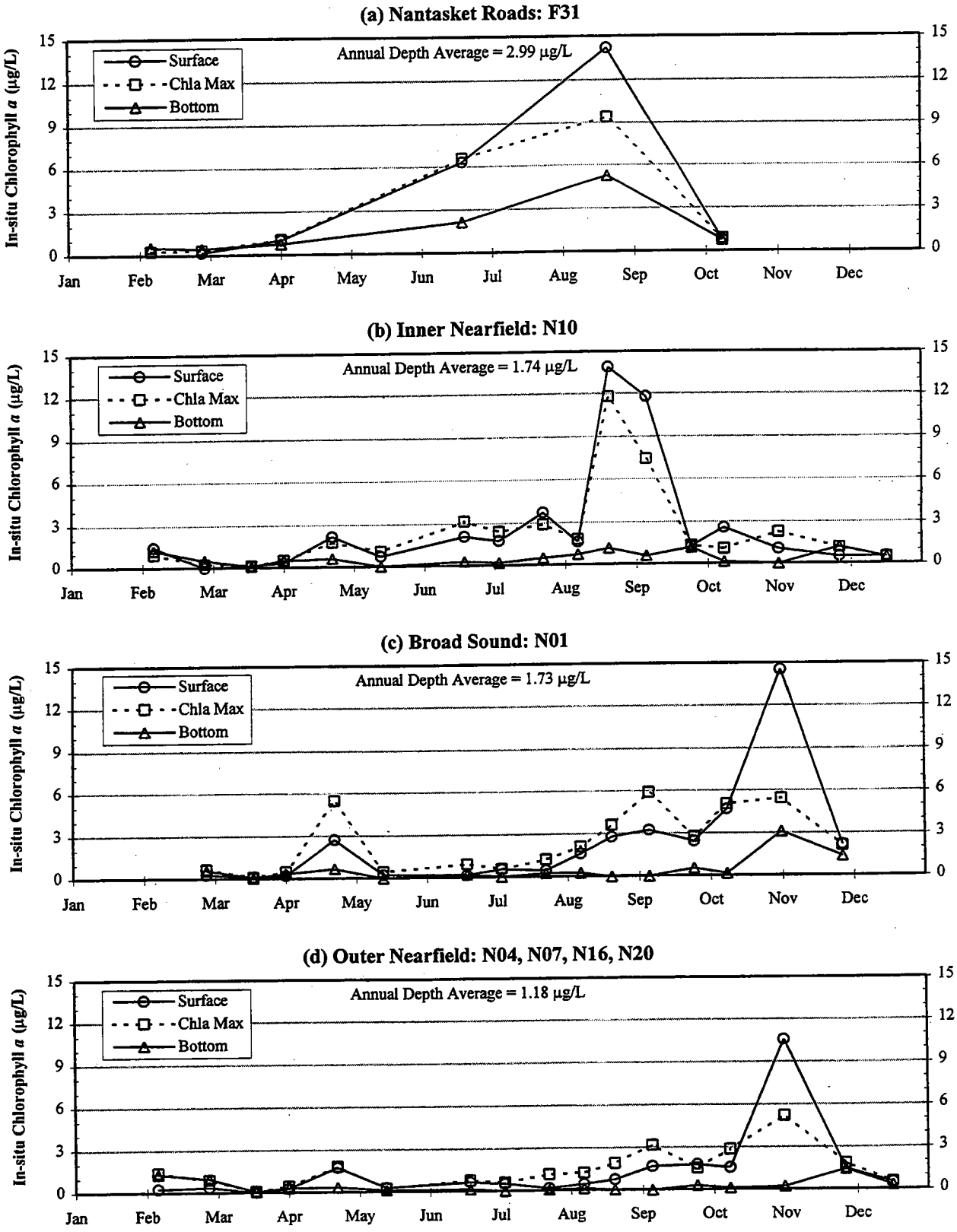

FIGURE 5-2

1995 In-situ Chlorophyll *a* Patterns for Selected Areas in Nearfield

Symbols indicate surface, chla max, and bottom depth survey averages.

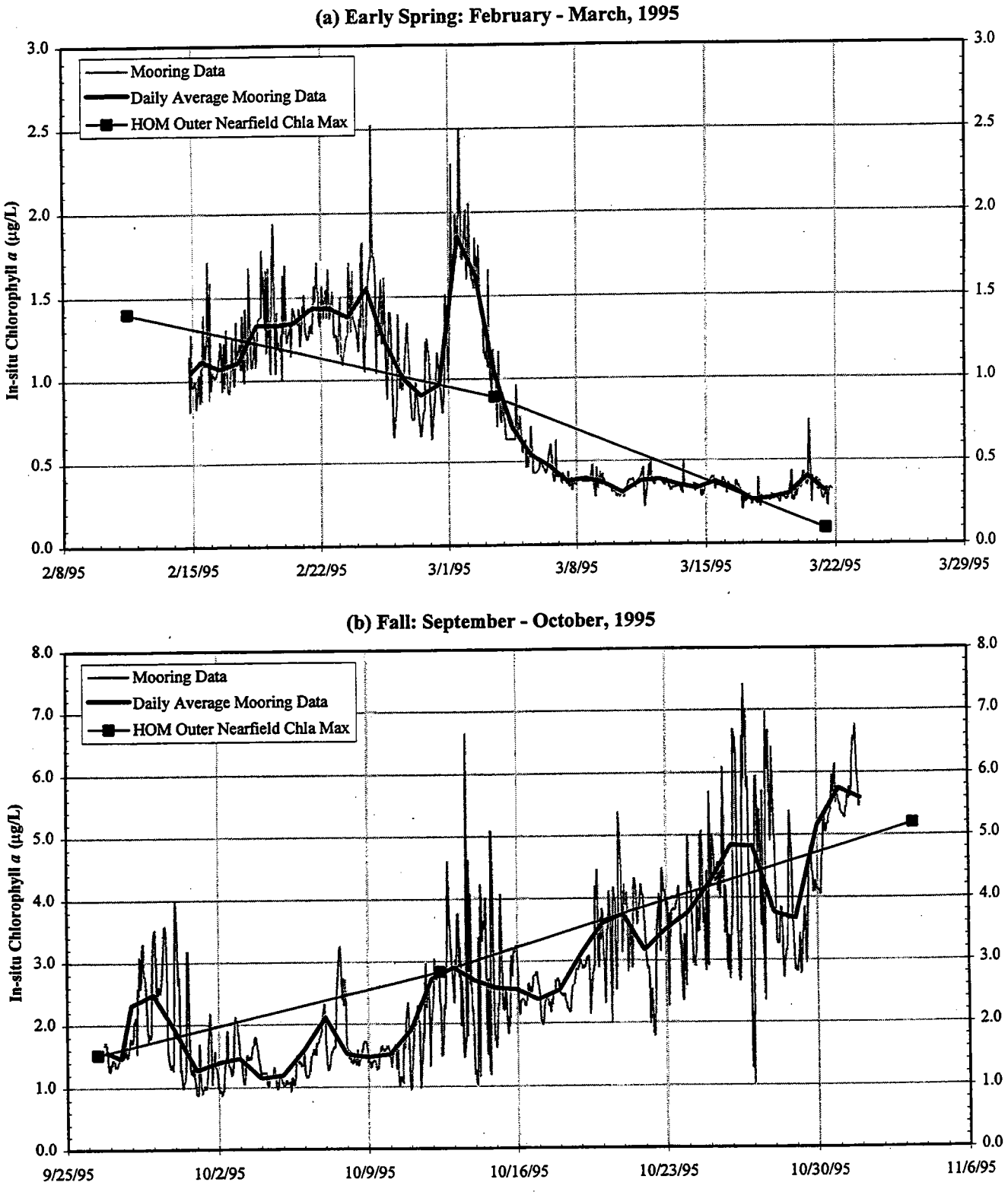

FIGURE 5-3

1995 Moored In-situ Optical Transmission Chlorophyll Data

with Outer Nearfield In-situ Chlorophyll *a* Results from Chla Max Depth

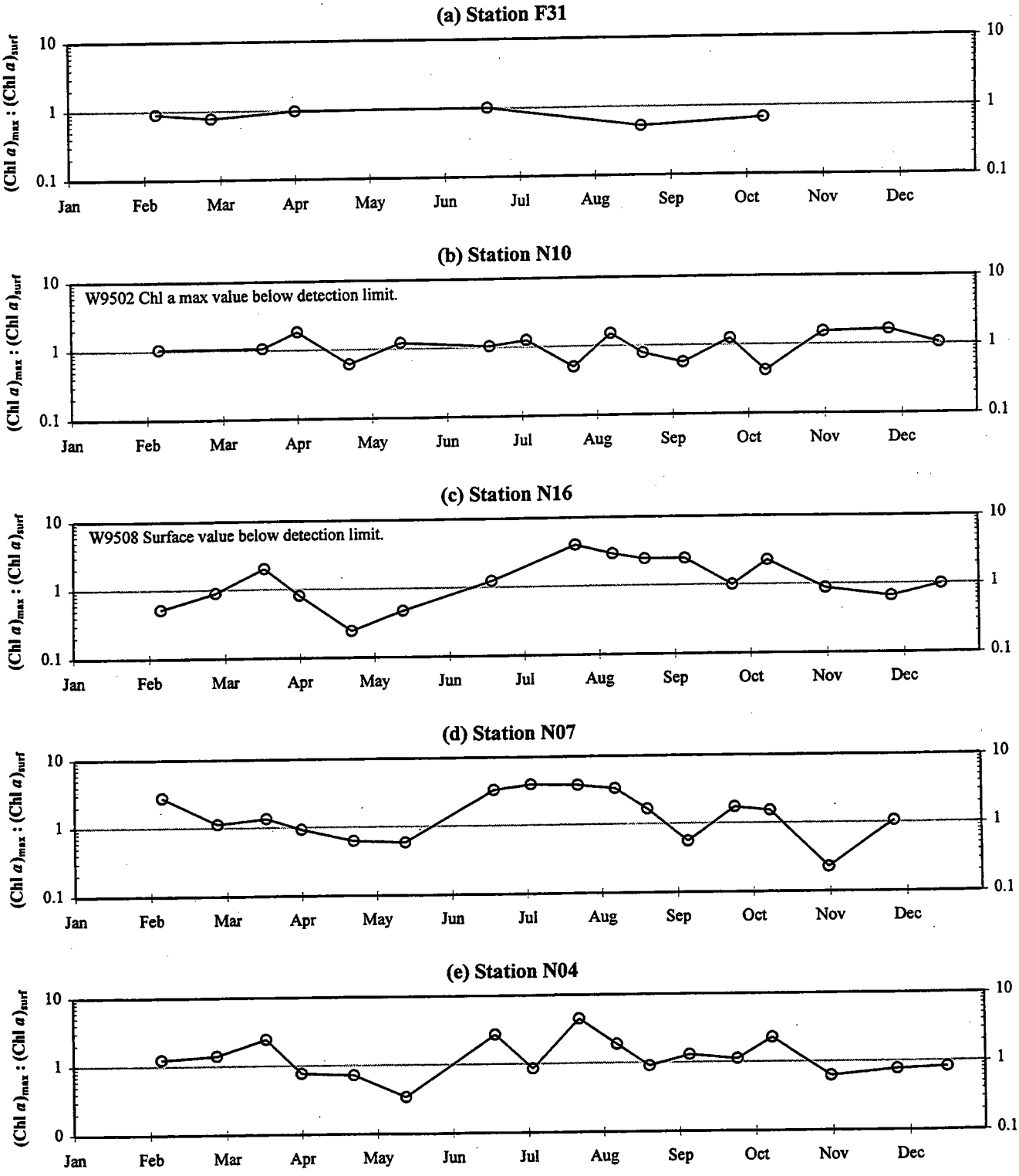

FIGURE 5-4

1995 Ratio of Chlorophyll Maximum : Surface Sample Concentrations

In-situ chlorophyll *a* results.

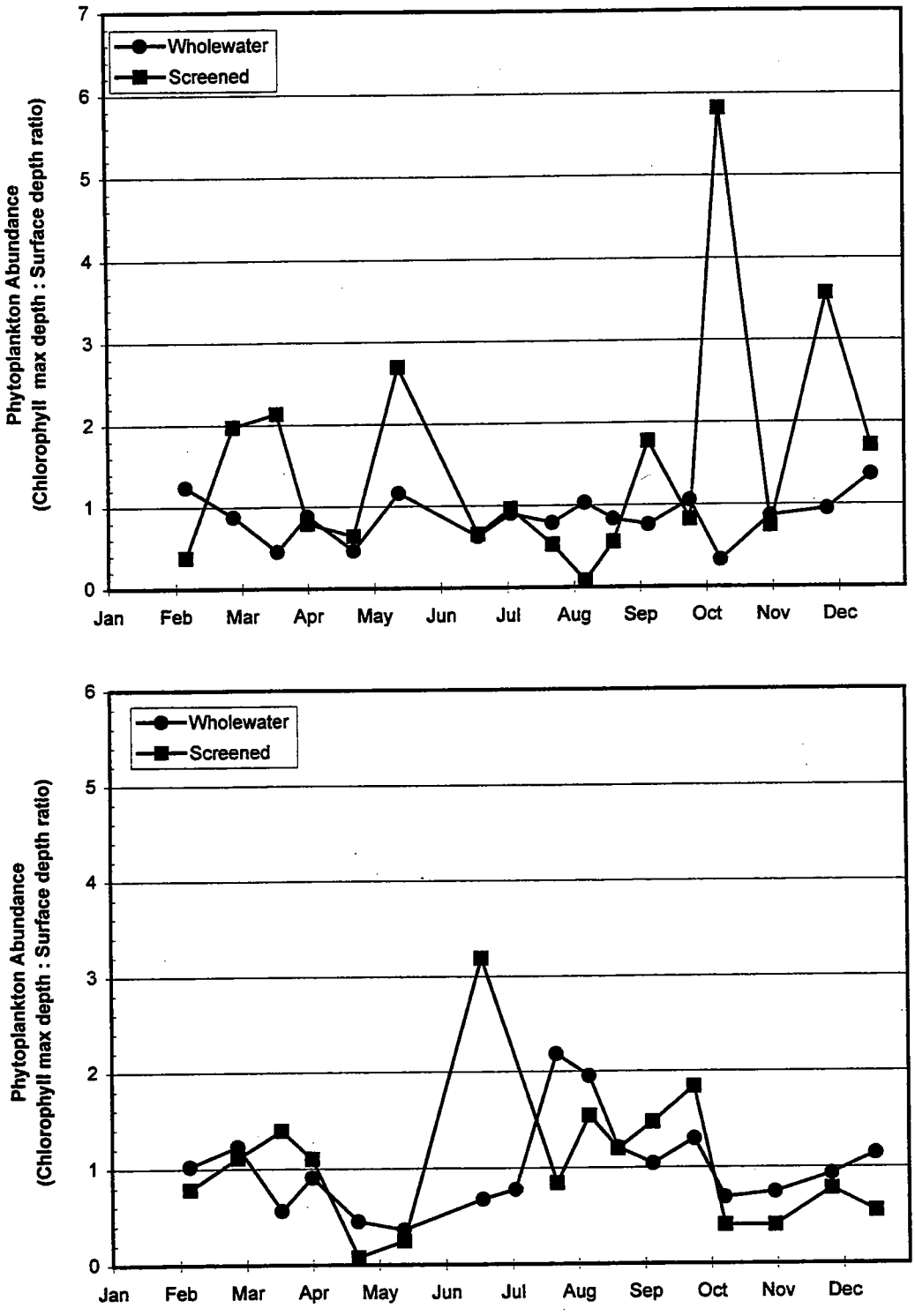

FIGURE 5-5

Ratio of Total Phytoplankton Densities at Chlorophyll a Maximum depth : Surface depth
Top: N10, Bottom: N16

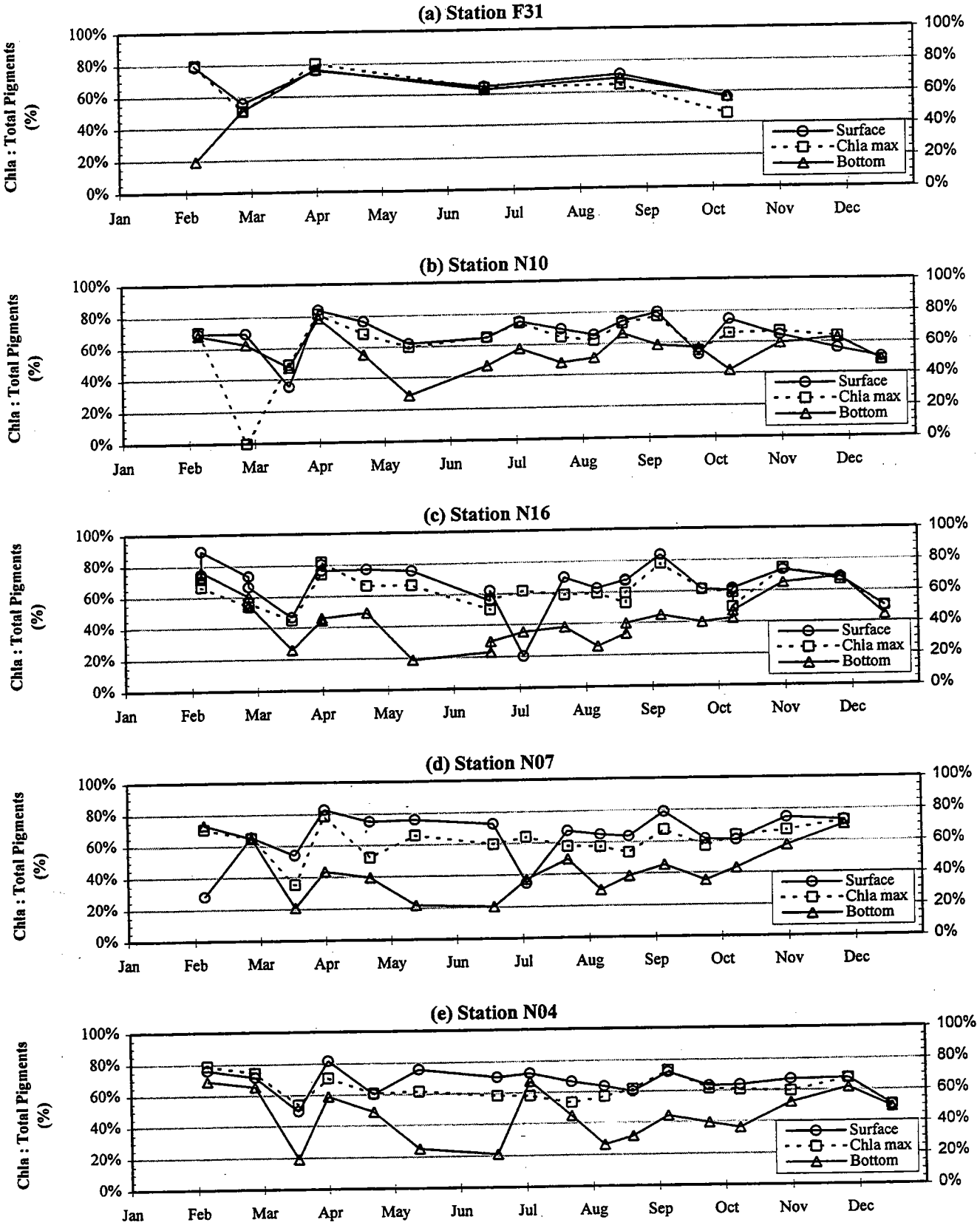

FIGURE 5-6

1995 Ratio of Chlorophyll *a* to Total Pigments in Nearfield

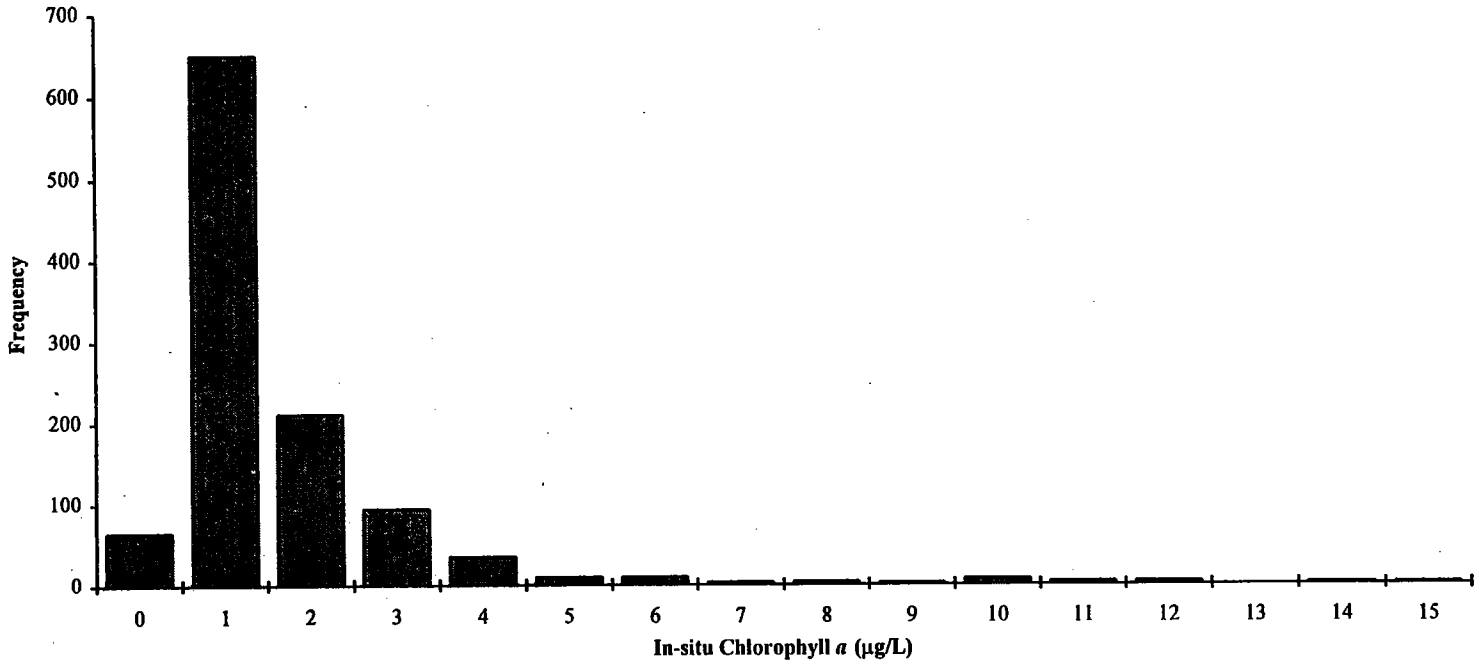

																	Total
Boundary	23	82	31	12	1	1	0	0	0	0	0	0	0	0	0	0	150
Cape Cod Bay	5	28	17	18	12	5	5	0	0	0	0	0	0	0	0	0	90
Coastal	0	103	47	8	10	1	2	0	1	2	2	2	2	0	0	0	180
Harbor	2	61	16	9	2	1	2	3	1	0	5	2	1	0	1	1	107
Nearfield	12	210	58	35	7	1	1	0	1	0	0	0	1	0	1	1	328
Offshore	23	165	42	12	3	1	0	0	1	0	0	0	0	0	0	0	247
Total Number	65	649	211	94	35	10	10	3	4	2	7	4	4	0	2	2	1102
Percent	5.9%	58.9%	19.1%	8.5%	3.2%	0.9%	0.9%	0.3%	0.4%	0.2%	0.6%	0.4%	0.4%	0.0%	0.2%	0.2%	100%
Cumulative Number	65	714	925	1019	1054	1064	1074	1077	1081	1083	1090	1094	1098	1098	1100	1102	
Cumulative Percent	5.9%	64.8%	83.9%	92.5%	95.6%	96.6%	97.5%	97.7%	98.1%	98.3%	98.9%	99.3%	99.6%	99.6%	99.8%	100%	

Note: Bin number denotes upper limit of bin.

FIGURE 5-7

Frequency Distribution of 1995 Massachusetts Bay In-situ Chlorophyll *a* Results

All depths, all FF and 6 NF stations, all combined surveys.

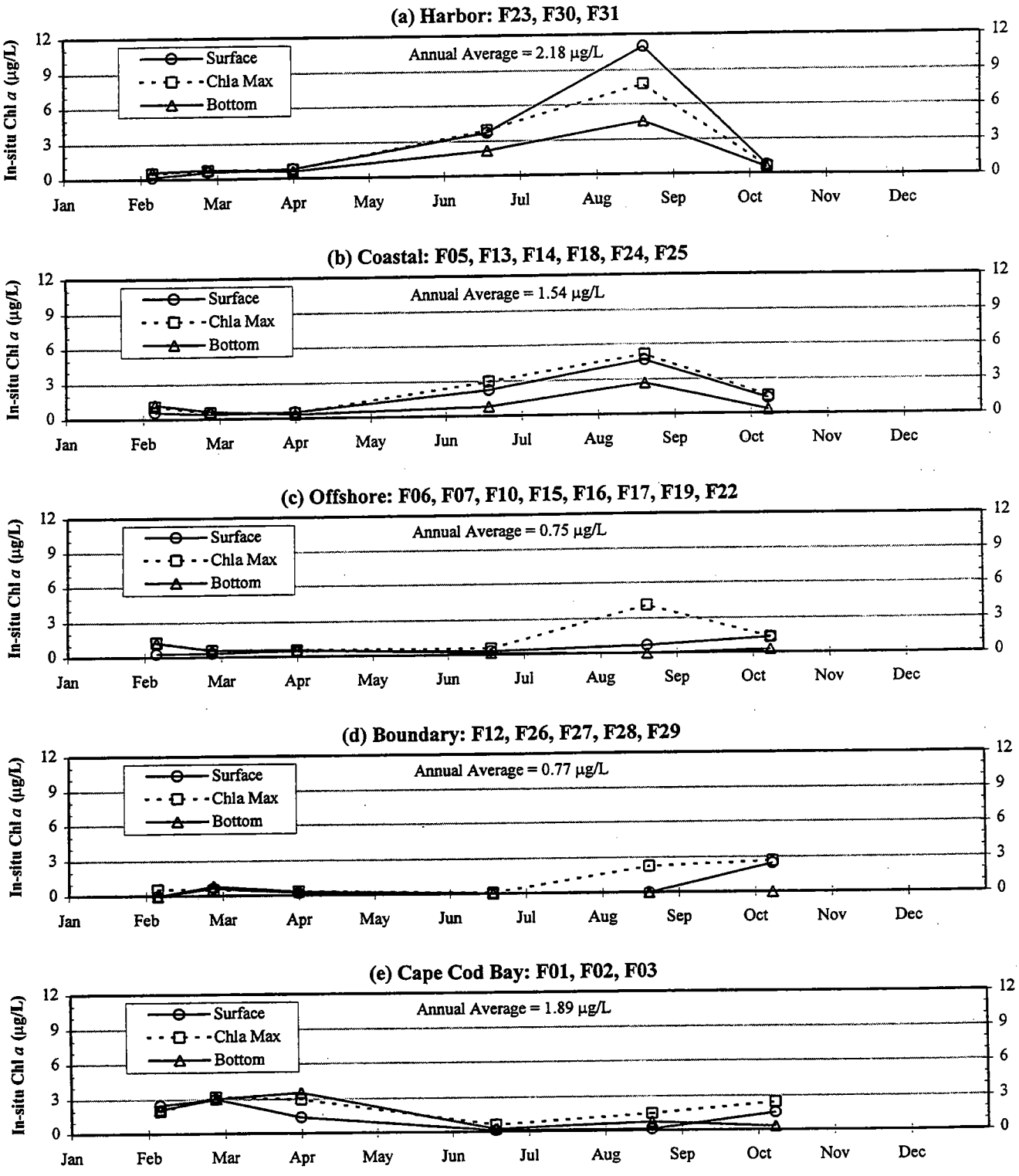

FIGURE 5-8

1995 In-situ Chlorophyll *a* Patterns for Massachusetts Bay

Symbols indicate surface, chla max, and bottom depth survey averages.

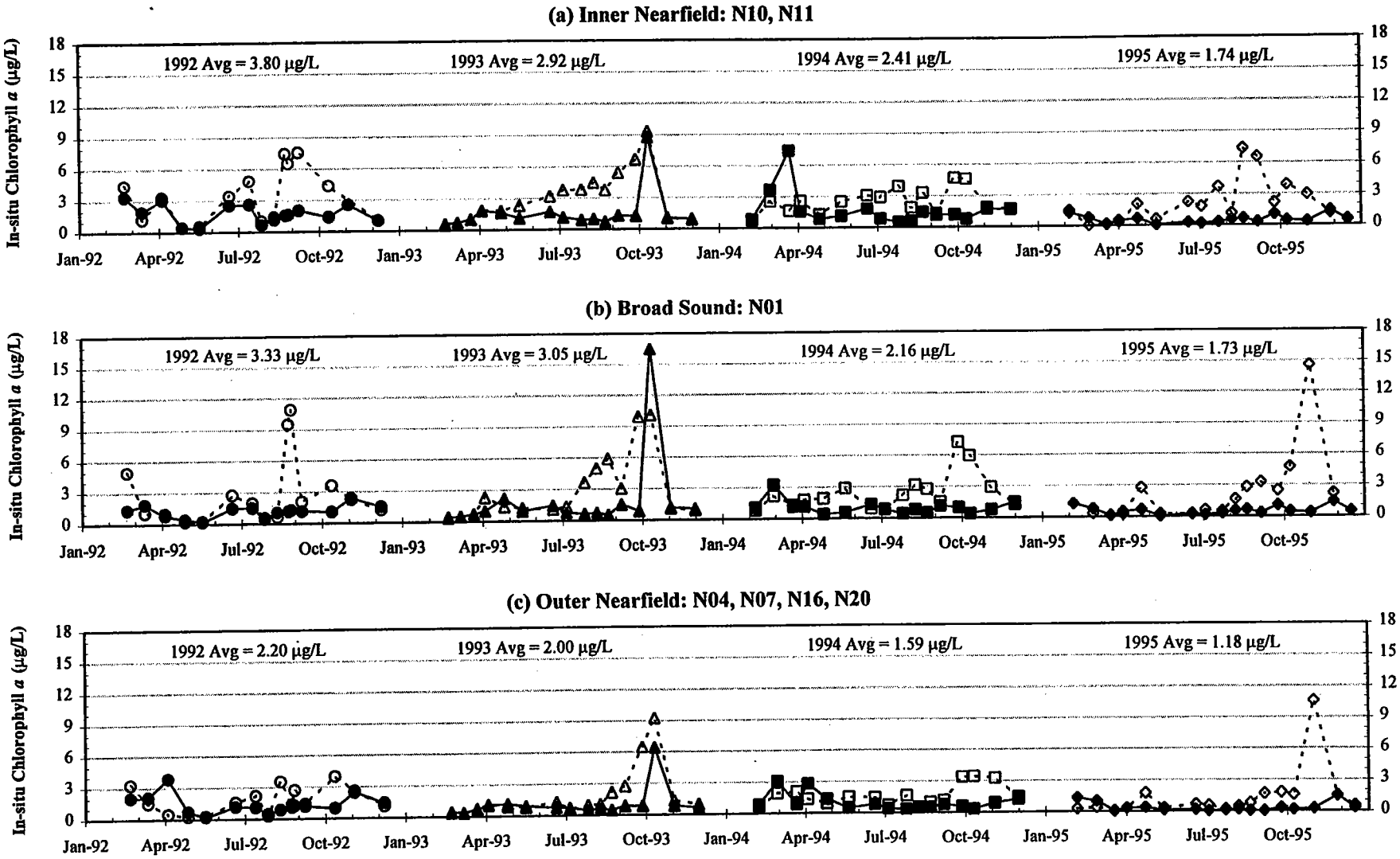

FIGURE 5-9

Interannual In-situ Chlorophyll a Patterns for Selected Areas in Nearfield

Open symbols indicate surface (A depth) average.

Closed symbols indicate bottom (E depth) average.

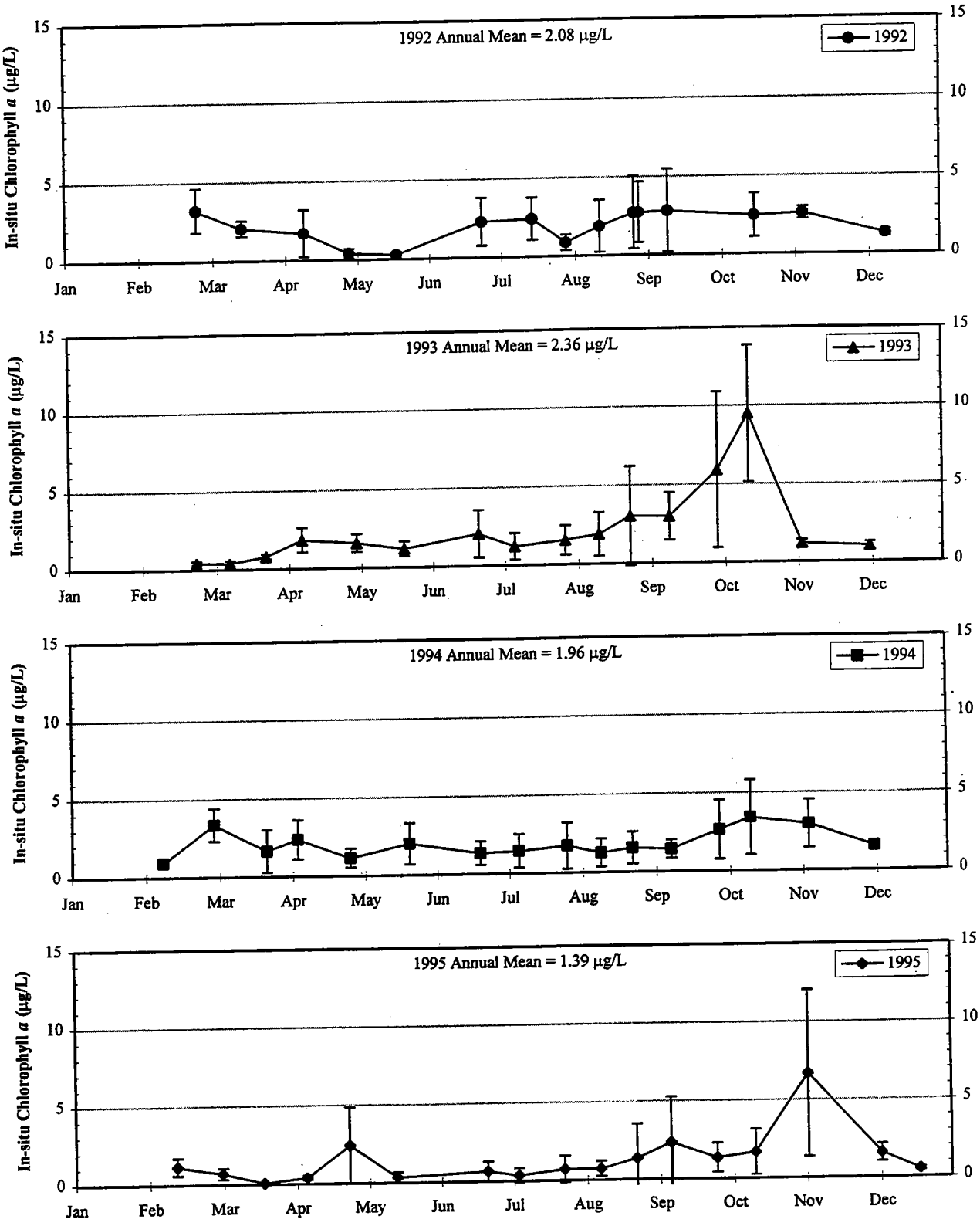

FIGURE 5-10

Interannual Nearfield Survey In-situ Chlorophyll a Averages

All depths at all nearfield stations included.

Error bars represent +/- one standard deviation.

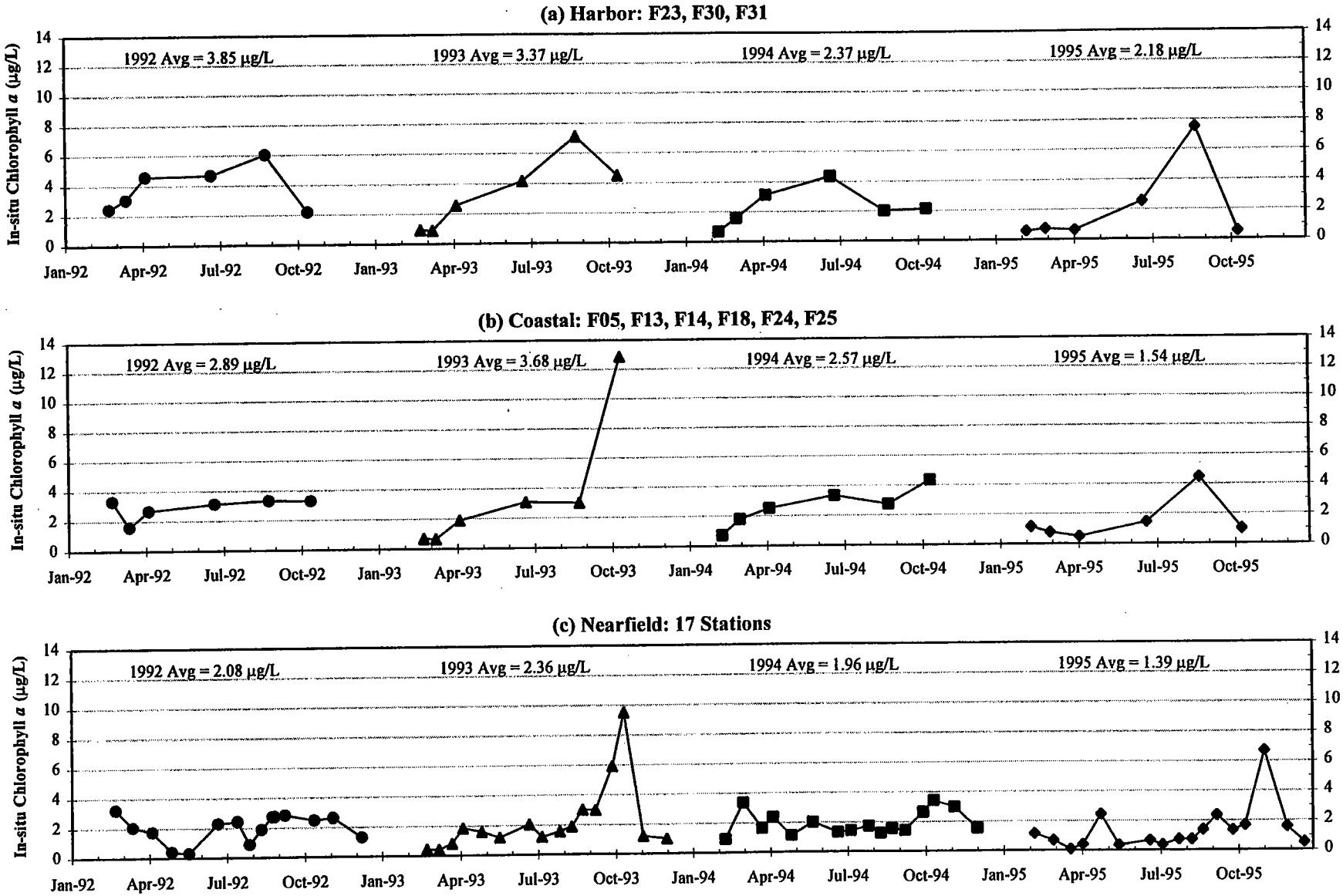

FIGURE 5-11

Interannual Regional In-situ Chlorophyll *a* Averages

Harbor, Coastal and Nearfield. All depths.

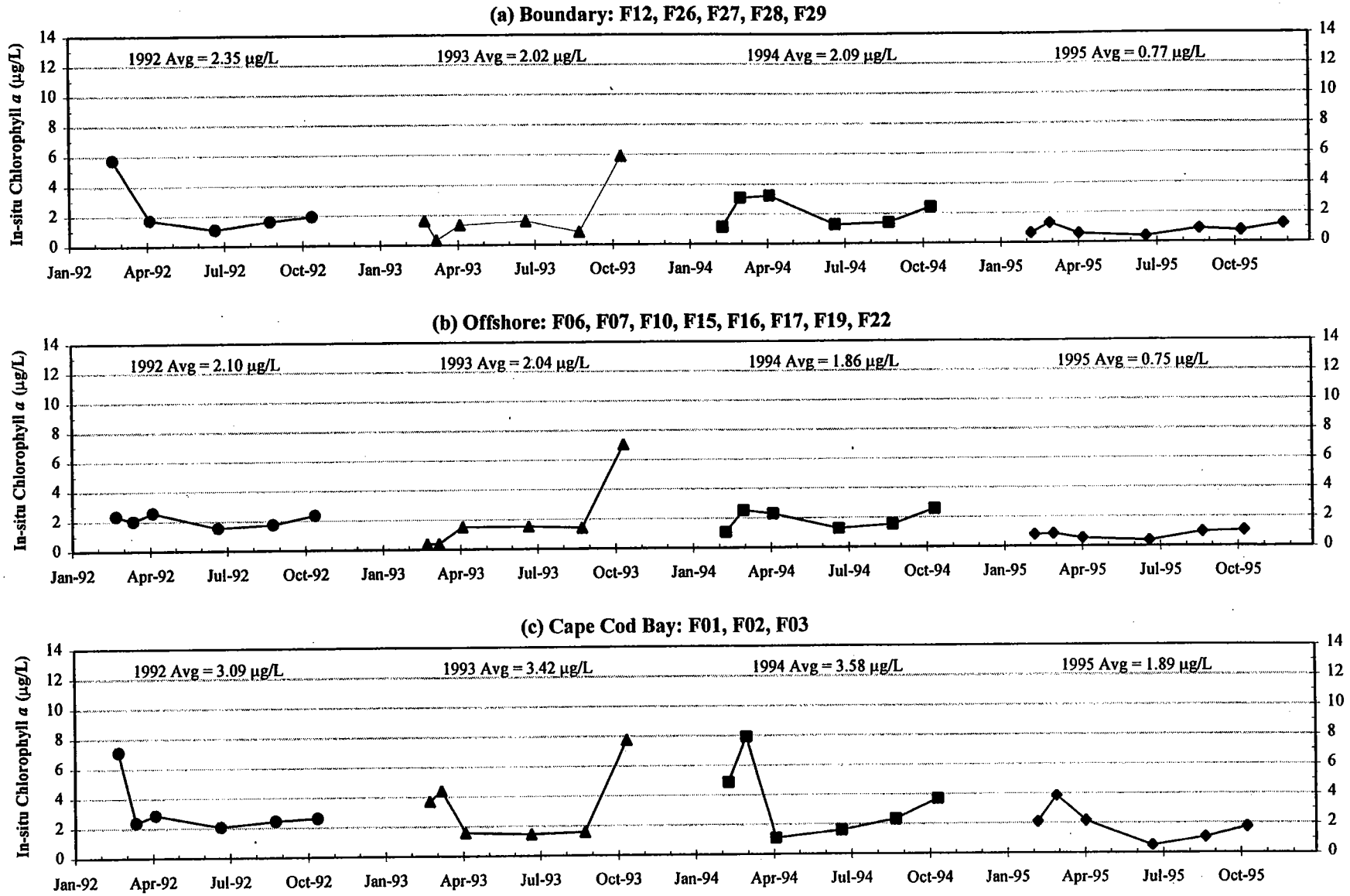

FIGURE 5-12

Interannual Regional In-situ Chlorophyll *a* Averages

Boundary, Offshore, and Cape Cod Bay. All depths.

6.0 DISSOLVED OXYGEN

Dissolved oxygen (DO) concentrations in the water column and the sediments are important from both a regulatory and an ecological perspective. The Commonwealth of Massachusetts has established water quality standards for minimum water column DO concentrations. The state standard for Class SA waters, which include all of the study area outside of Boston Harbor, is 6 mg/L. From an ecological perspective, DO in the water column and sediments is of interest not only because it a requisite for the life of aquatic animals, but because it is an integrator of the physical and biological process in the aquatic food web. Accordingly, DO depletion is seen as an indicator of the changes that may result from the introduction of municipal wastewater into the aquatic environment.

This section reports the results of DO monitoring in Massachusetts and Cape Cod Bays. The focus is on the results for 1995, but monitoring results for previous years are also presented for comparative purposes. Due to the stratified nature of the system, the focus is also on DO depletion in the bottom waters of the nearfield and Stellwagen Basin after prolonged periods of stratification. The data indicate that DO in Massachusetts and Cape Cod Bays follows a predictable seasonal pattern that determines the timing, but not the magnitude, of the annual DO minimum.

DO results presented in this section consist of calibrated upcast sensor data for the upper most (surface) and lower most (bottom) sample depths. Downcast vertical profiles of DO and other parameters measured during the 1995 surveys have been reported earlier in periodic nutrient data reports. Additional information on sampling can be found in Section 2 and in the CW/QAPP (Bowen *et al.*, 1995).

6.1 Annual DO Cycle in Nearfield

6.1.1 1995 Results

During 1995, DO concentrations in the nearfield region followed a seasonal pattern that is typical of coastal waters at temperate latitudes. The highest DO concentrations occurred during winter and early spring (Figure 6-1a), when the water column was unstratified, the water temperature was at or near the annual minimum, and respiration in the water column was low. During this time, DO in the nearfield, expressed as a percentage of the saturation concentration, ranged from 92% to 115% (Figure 6-1b). Until late April there was only a slight difference between DO concentrations in the surface and bottom waters.

Surface and bottom waters were frequently different in DO concentration from late April through early November. During this time, surface waters were usually oversaturated with DO, while DO in the bottom waters declined to a minimum nearfield average concentration which occurred in late September, 6.6 mg/L

and 74% saturation (Figure 6-1) with the single station minima at F02, 5.7 mg/L. By mid-November, when the water column was again thoroughly mixed (see Figure 3-11), the difference in surface and bottom water concentrations had disappeared. Surface water DO concentrations were undersaturated, on average, during the final three surveys of 1995 (Figure 6-1b). Bottom water DO concentrations increased during this time from 7.2 mg/L to 9.2 mg/L (Figure 6-1a).

At several times during 1995 it appeared that the bottom waters in the nearfield region were ventilated through mixing with the oxygenated surface waters. Between the late April and mid May survey, the water column remixed just as stratification was beginning to set up. During this period the bottom water DO increased by approximately 0.5 mg/L (Figure 6-1a). A smaller increase during the summer stratified period, which temporarily reversed the decline of DO, occurred between the two July surveys (Figure 6-1a). During both of these periods, the temperature data collected from continuous sensors (Figure 3-2) showed either a temporary increase in bottom water temperature (in May), or a temporary decrease in surface water temperature (in July). In both cases, mixing events decreased vertical stratification and infused the bottom waters with DO. The prolonged mixing in the fall results in the ventilation of bottom waters and ends the seasonal decline in bottom water DO in late September (Figure 3-2 and 6-1a).

6.1.2 Interannual Comparison of DO Concentrations

All years showed similar trends in bottom water DO and timing of DO minima. Compared to previous years, nearfield average DO concentrations in 1995 were most similar to 1994. Like the previous year, but unlike 1992 or 1993, the average bottom water DO concentration dipped below 7.0 mg/L during September (Figure 6-2; note that in 1994 the average bottom water DO concentration nearly dropped below 6.0 mg/L). DO concentrations early in 1995 were approximately 1.0 mg/L lower than 1993 or 1994, and more than 2.0 mg/L less than 1992. During the period of density stratification, the surface to bottom differences in DO concentrations were greater in 1995 than either 1992 or 1993, but not so great as 1994. With the exception of 1993, the top-to-bottom difference in DO had disappeared by mid-November in all years.

6.1.3 Interannual Comparison of DO Decline Rate

A summer and early fall decline in nearfield region bottom water DO occurred in each of the four years of monitoring. The rate of the decline was relatively uniform during each year, ranging from a low of 0.024 mg/L/d in 1992 to a high of 0.031 mg/L/d in 1994 (Figure 6-3). The rates of decline were comparable in all four years, however, the starting points in 1992 and 1993 were higher (by approximately 1 mg/L). By the end of stratification, 1994 and 1995 DO concentrations were approximately 1.5 mg/L lower than 1992 or 1993.

Similar relationships were seen in plots of percent saturation (Figure 6-4). The data indicate that the phenomenon which causes the higher initial mass of oxygen at the onset of stratification does not result in higher rates of oxygen decline, but merely a shift in the final concentration of bottom water oxygen in the fall. While the underlying mechanism is not yet clear, it is likely to be physically, not biologically, linked as the observed temporal shifts in bottom water oxygen concentration can be very rapid and large (Fig 6-2).

6.2 Annual DO Cycle in Stellwagen Basin and Other Areas

6.2.1 1995 Results

DO dynamics in Stellwagen Basin and other parts of Massachusetts and Cape Cod Bays were generally similar to that observed in the nearfield region. The average DO concentration in the four Stellwagen Basin stations (F12, F17, F19, and F22) had a maximum value of 10.0 mg/L that occurred early in the year, before the water column became vertically stratified (Figure 6-5a). As was seen for the nearfield region, surface concentrations during this time were slightly undersaturated (Figure 6-5b). From April to October, surface and bottom DO concentrations differed, with the surface waters oversaturated and the bottom waters undersaturated. DO in the bottom water declined steadily through the summer and early fall, reaching a minimum concentration of 6.7 mg/L (71% saturation) during mid-October (Figure 6-5). As with the nearfield region, by late November the surface to bottom difference in the mean Stellwagen Basin DO concentration had disappeared. The water column was undersaturated with DO at this time.

Not surprisingly, the range of DO concentrations measured at individual stations was larger than that of the mean values presented above. In 1995, the minimum DO concentration in the upcast data (5.6 mg/L) occurred in mid-October (W9514) at station F02 in eastern Cape Cod Bay (Table 6-1). The survey average DO concentration at this time was 7.1 mg/L (Figure 6-6). During the previous nearfield-only survey, which occurred in late September, a slightly higher survey minimum value of 5.7 mg/L was measured at station N11, on the southwestern border of the nearfield region. During 1995 the range of bottom water DO concentrations during a survey was approximately 2 mg/L (Figure 6-6).

Differences in regional patterns in DO concentrations were relatively minor in 1995. The temporal pattern was similar to that of the nearfield region, such that the maximum DO concentration, which ranged from 9.8 to 10.8 mg/L (Figure 6-7), occurred in late February. However, the minimum DO concentration showed some regional differences. The minimum observed Boston Harbor concentration of 6.5 mg/L (84% of saturation) occurred during the mid-August survey (Figure 6-7). The measured DO concentrations reached minima in all the other regions in October, and ranged from 6.6 mg/L in Cape Cod Bay to approximately 7.0 mg/L in the coastal, offshore, and boundary regions (Figure 6-7). These concentrations correspond to saturation percentages of 75% to 81% (Figure 6-7). A late November nearfield survey included Stellwagen Basin station F12, which is considered to be a boundary station. The

DO concentration at this station had recovered to 8.7 mg/L or 92% of the saturation concentration by late November (Figure 6-7).

6.2.2 Interannual Comparisons

In all four years of sampling, the minimum dissolved concentration in the bottom water occurred in early October (Figure 6-6). For the four years of sampling, the annual minimum concentration, and the station where the minimum concentration was measured was as follows:

- 1992 - DO minimum = 7.10 mg/L at nearfield station N10,
- 1993 - DO minimum = 6.68 mg/L at Cape Cod Bay station F02,
- 1994 - DO minimum = 4.82 mg/L at nearfield station N01,
- 1995 - DO minimum = 5.60 mg/L at Cape Cod Bay station F02.

Both nearfield stations N01 and N10 are on the western boundary of the sampling grid, nearest to Boston Harbor. The Cape Cod Bay station F02 is in eastern half of the Bay. The range of bottom water DO concentrations during a survey has been fairly constant over the four years. The range has been occasionally over 3 mg/L, but is generally around 2 mg/L (Figure 6-6).

DO dynamics in Stellwagen Basin appear to be very similar over the four years of monitoring. The mean DO concentration in the four stations achieved a maximum in late February and declined to a minimum concentration in early October (Figure 6-8). The Stellwagen Basin mean concentration was approximately 1 mg/L lower in 1994 and 1995 compared with 1992 and 1993. In the latest two years the mean DO concentration in Stellwagen Basin stations during the mid-October survey was approximately 6.5 mg/L (Figure 6-8).

6.2.3 DO Decline in the Bottom Waters

Like the nearfield stations, the DO declined steadily in the Stellwagen Basin stations during summer and early fall. The rate of decline in Stellwagen Basin is generally lower than the nearfield region, ranging from 0.017 mg/L/d in 1995 to 0.023 mg/L/d in 1992 and 1993 (Figure 6-9). The highest rate of decline the nearfield region, as well as the lowest DO concentration at the end of the decline period, occurred in 1994. While 1995 began with significantly lower DO concentrations in the first two surveys as compared to all three previous years (Figure 6-8), the mean DO concentration by the end of the decline period was very similar to that measured in 1994.

6.3 Discussion

Both the nearfield and Stellwagen Basin exhibit similar seasonal DO dynamics. From the four year data record, it is apparent that there are several components critical to the magnitude of DO depression by the end of the season. First and foremost, the initial water temperature and DO concentration early in the season determine the "setup" conditions for the year. The timing of the onset of stratification is integral to this setup. Second, the duration of the stratified period, particularly the initiation of fall turnovers, determines how long respiration below the pycnocline will affect DO concentration. The temperature throughout the period, as well as the quantity and quality of labile carbon available for respiration, determine the rate of DO decline during the stratified period.

The frequency and magnitude of mixing events that disturb the water column structure also affect the magnitude of oxygen depression. Similarities can be seen between the interannual DO concentrations in Figure 6-6 and the interannual temperature and salinity profiles shown in Figures 3-4 and 3-10. For example, in each of 1992 and 1993, there were two potential upwelling events between June and August. The smallest of these was in August of 1993. These deviations coincide with increases in bottom DO concentration, with the August 1993 period again the smallest in magnitude. Smaller events occurred in late June of 1994 and 1995, which are also apparent in the DO data from the period. A small deviation in the stratification pattern of August 1995 may have prevented the bottom DO from reaching the minimum concentrations seen in 1994.

These apparent physical influences on the degree of bottom water DO depression may have a significant role in modifying annual cycles, but the key processes involve the quantity and quality of labile substrate and the associated metabolic processes. These are discussed in detail in Section 7.2.

TABLE 6-1

Magnitude and Location of DO Maxima and Minima in the Bottom Waters

Event ID	Survey Minima		Survey Maxima	
	Value (mg/l)	Location	Value (mg/l)	Location
W9501	9.31	N04	10.65	F01
W9502	9.54	F12	11.20	N12
W9503	9.50	N06	10.19	N20
W9504	9.03	F16	10.37	N09
W9505	9.33	N13	10.33	N16
W9506	9.93	N10	10.86	N08
W9507	7.95	F02	9.67	N08
W9508	8.63	N05	9.22	N10
W9509	8.21	N16	9.94	N12
W9510	7.94	N06	8.63	N19
W9511	6.31	F23	8.78	N17
W9512	6.69	N10	7.70	N13
W9513	5.67	N11	7.11	N04
W9514	5.60	F02	7.91	N16
W9515	6.38	N10	7.88	N18
W9516	7.97	N06	9.02	N10
W9517	9.20	N04	9.49	N10

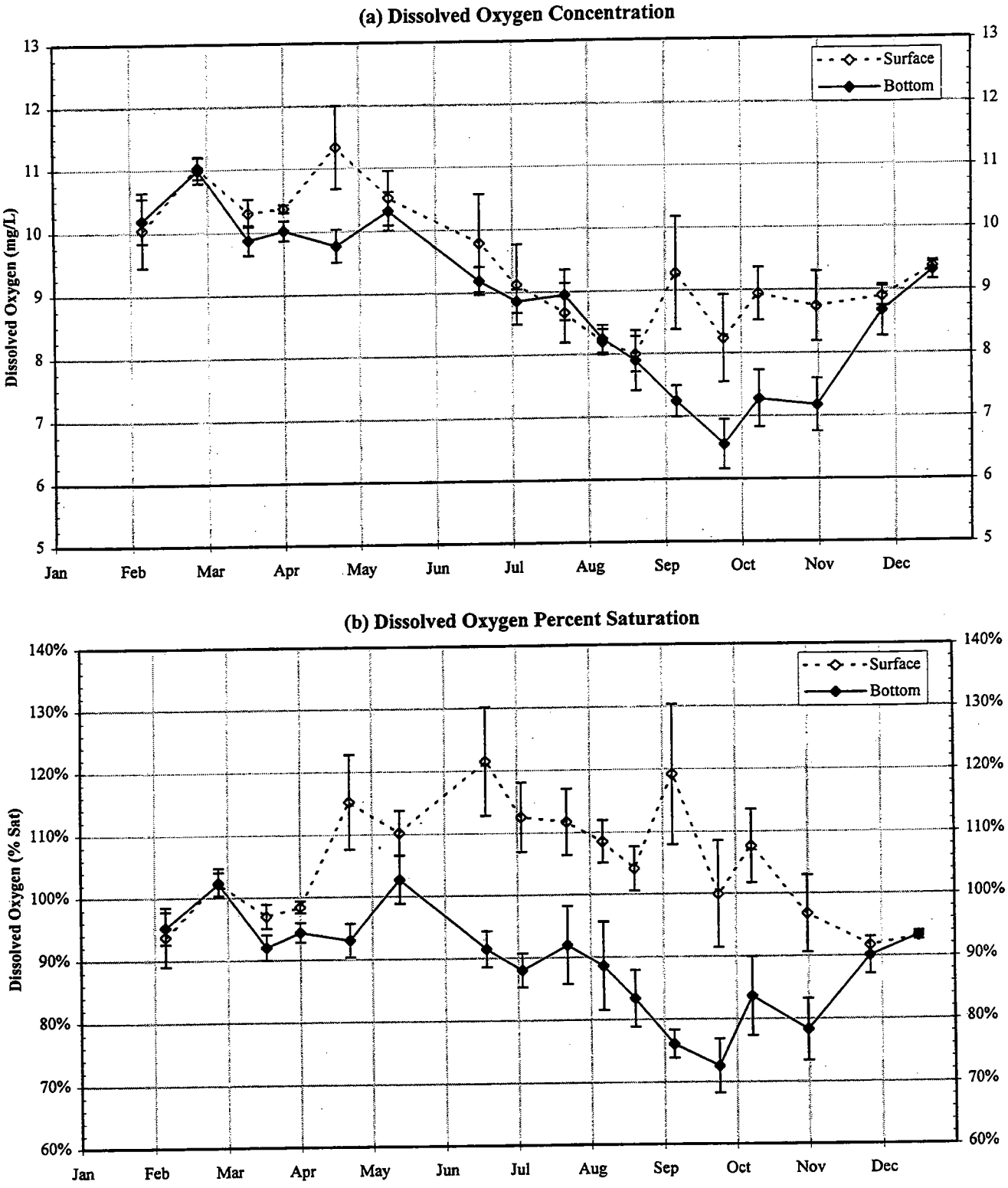

FIGURE 6-1

1995 Nearfield Dissolved Oxygen in Surface and Bottom Waters

Symbols indicate the mean of 17 nearfield stations; error bars represent +/- one standard deviation.

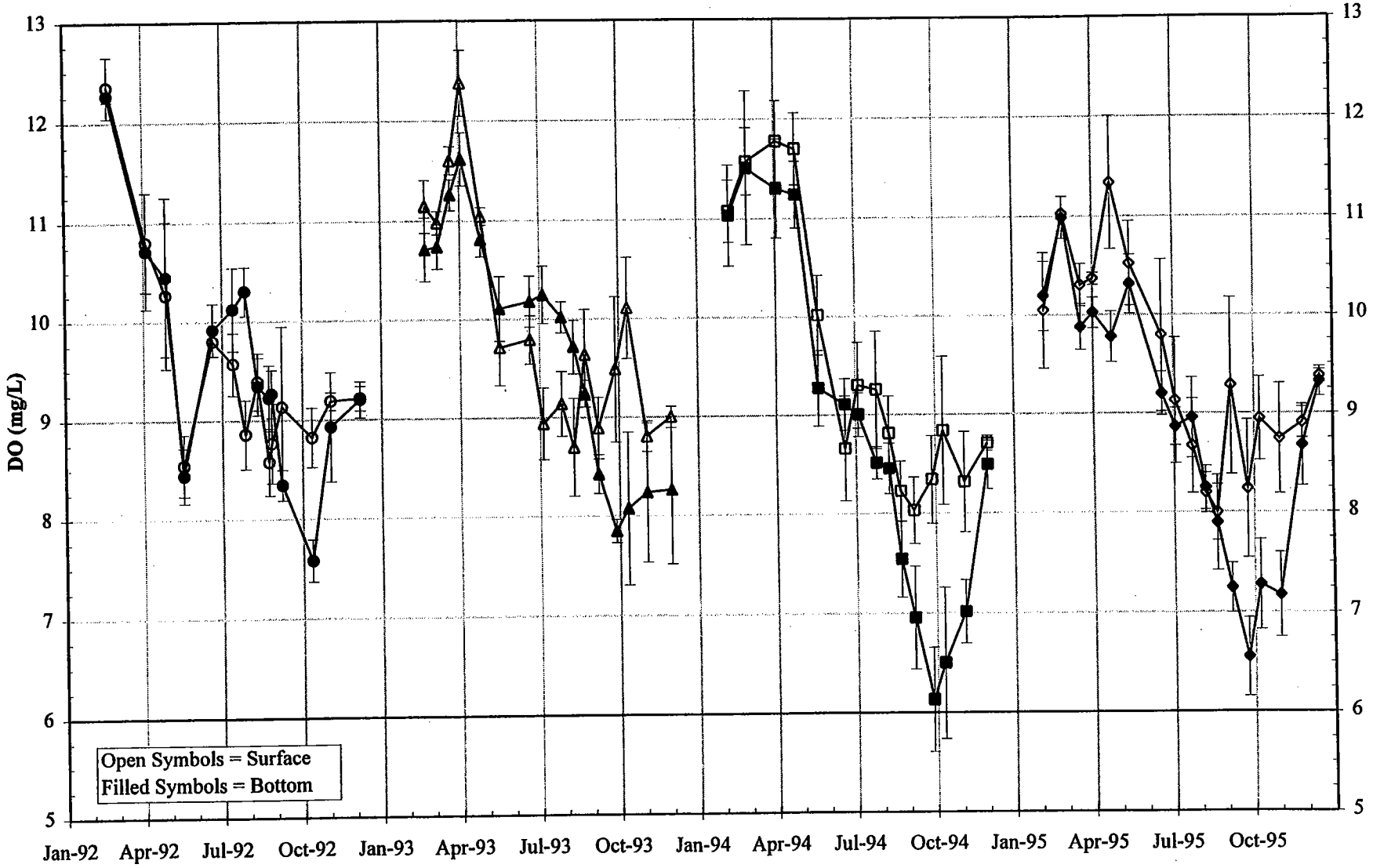

FIGURE 6-2

Interannual Nearfield Dissolved Oxygen Cycle in Surface and Bottom Waters

Symbols indicate the mean of 17 nearfield stations; error bars represent +/- one standard deviation.

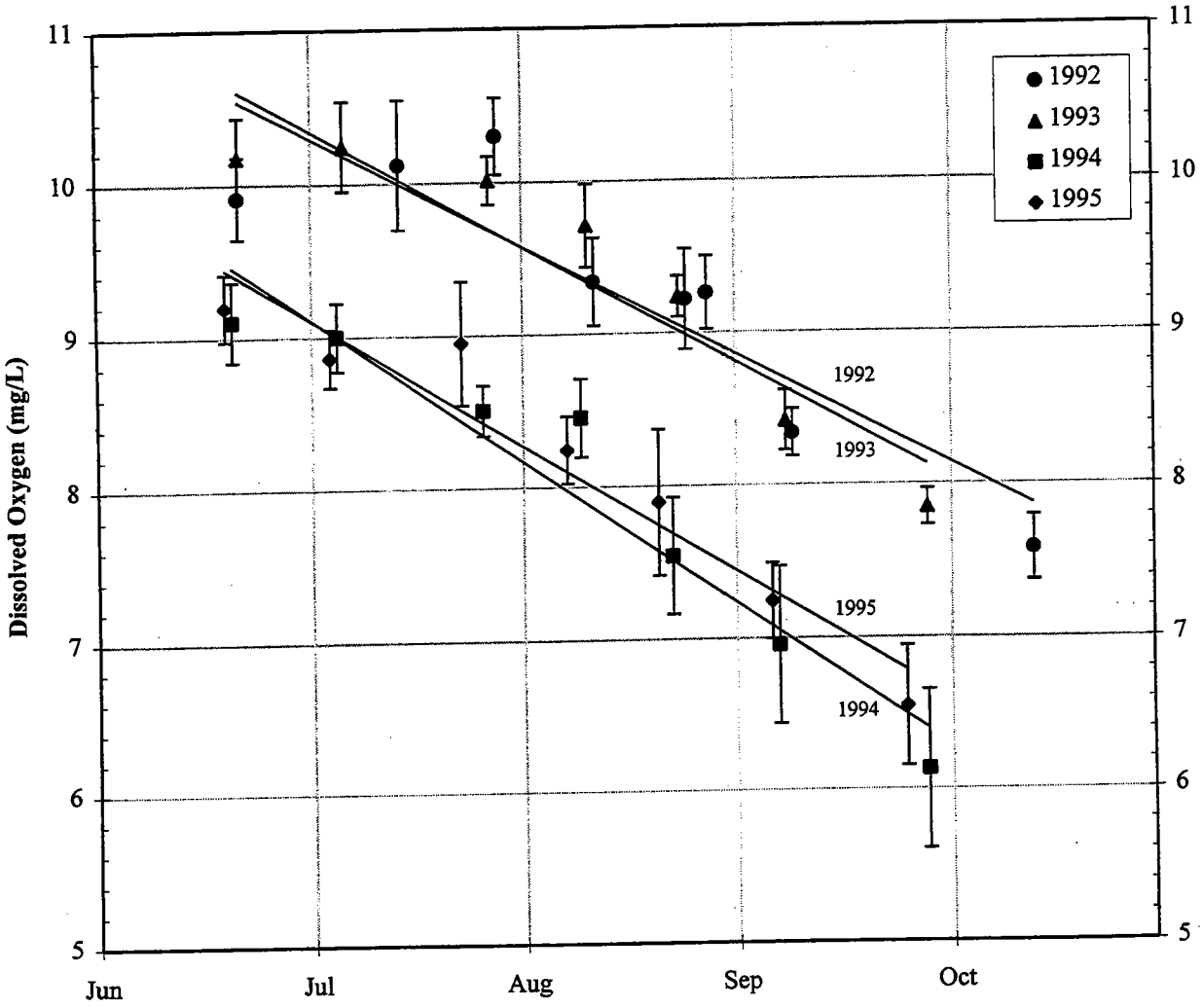

Year	Slope (mg/L/day)	Intercept* (mg/L)	R^2
1992	-0.024	11.0	0.808
1993	-0.025	11.1	0.885
1994	-0.031	10.1	0.929
1995	-0.027	9.9	0.932

* Predicted DO on June 1st based on:

DO = Slope * Date + Intercept

FIGURE 6-3

Nearfield Dissolved Oxygen Concentrations in Bottom Waters

Symbols indicate the mean of 17 nearfield stations; error bars represent +/- one standard deviation.

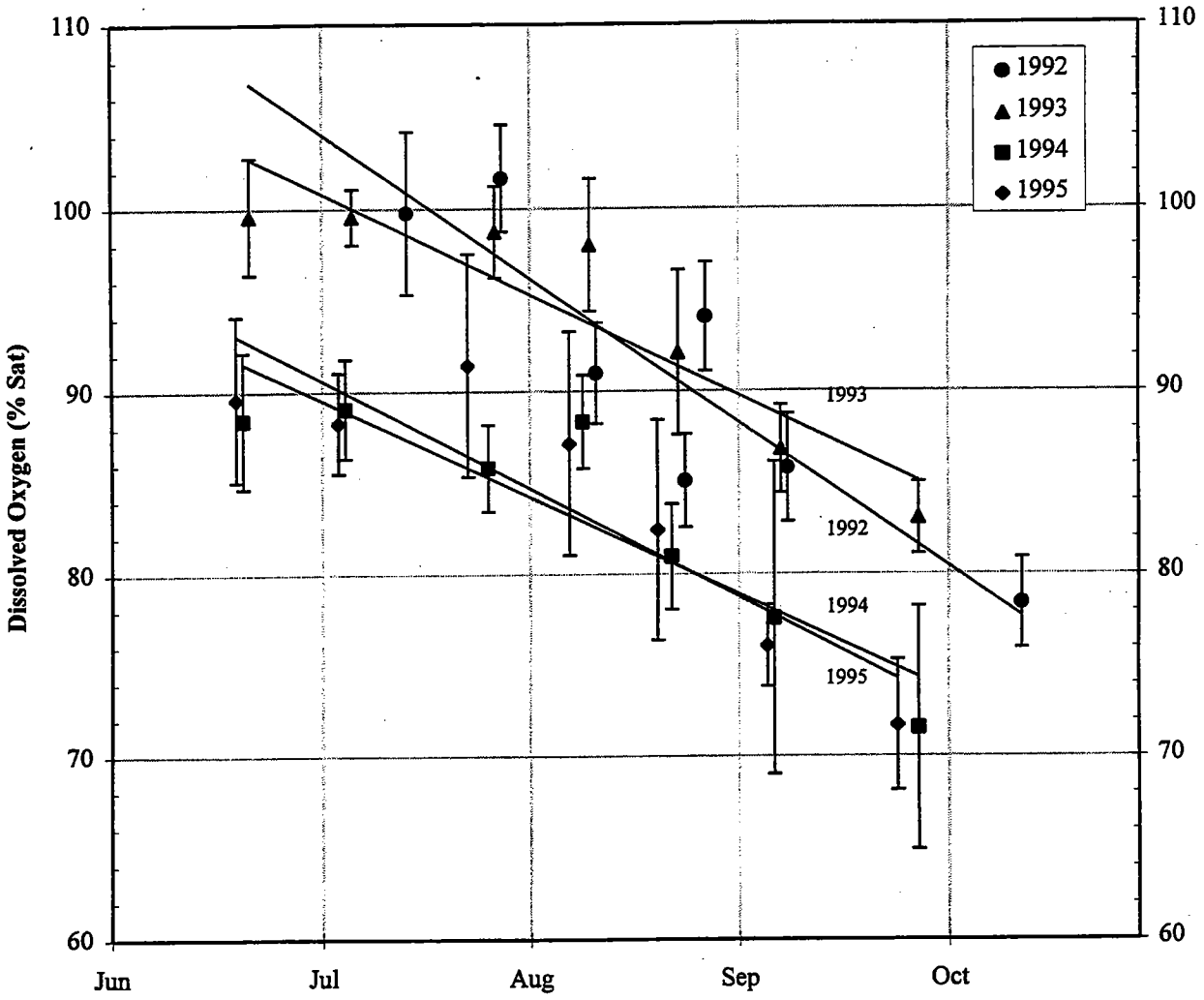

Year	Slope (%/day)	Intercept* (% Sat)	R^2
1992	-0.258	112.0	0.818
1993	-0.181	106.4	0.845
1994	-0.174	94.9	0.821
1995	-0.194	96.6	0.805

*Predicted DO Saturation on June 1st based on:

% Saturation = Slope * Date + Intercept

FIGURE 6-4

Nearfield Dissolved Oxygen Percent Saturation in Bottom Waters

Symbols indicate the mean of 17 nearfield stations; error bars represent +/- one standard deviation.

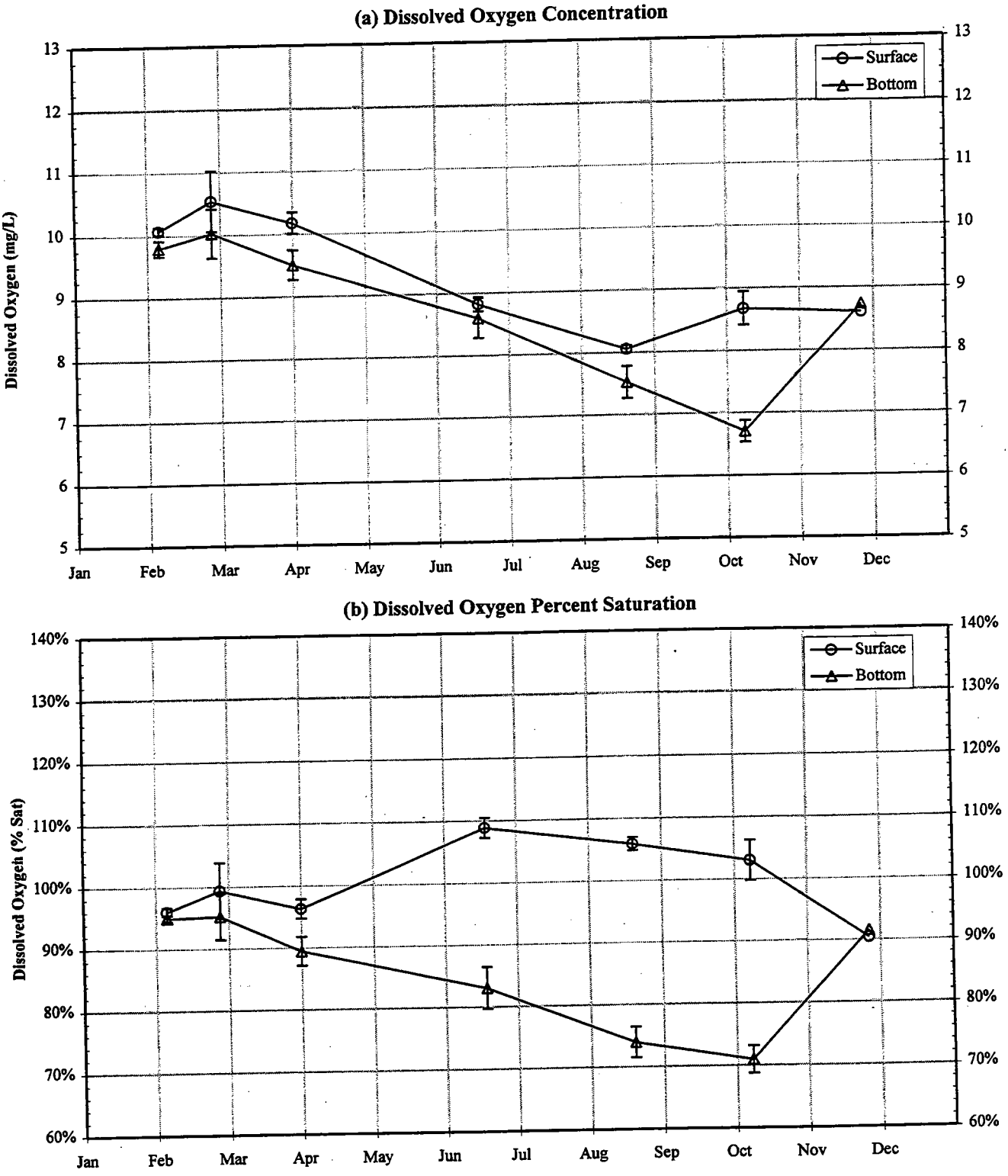

FIGURE 6-5

1995 Stellwagen Basin Dissolved Oxygen in Surface and Bottom Waters

Symbols indicate the mean of 4 Stellwagen Basin stations; error bars represent +/- one standard deviation.

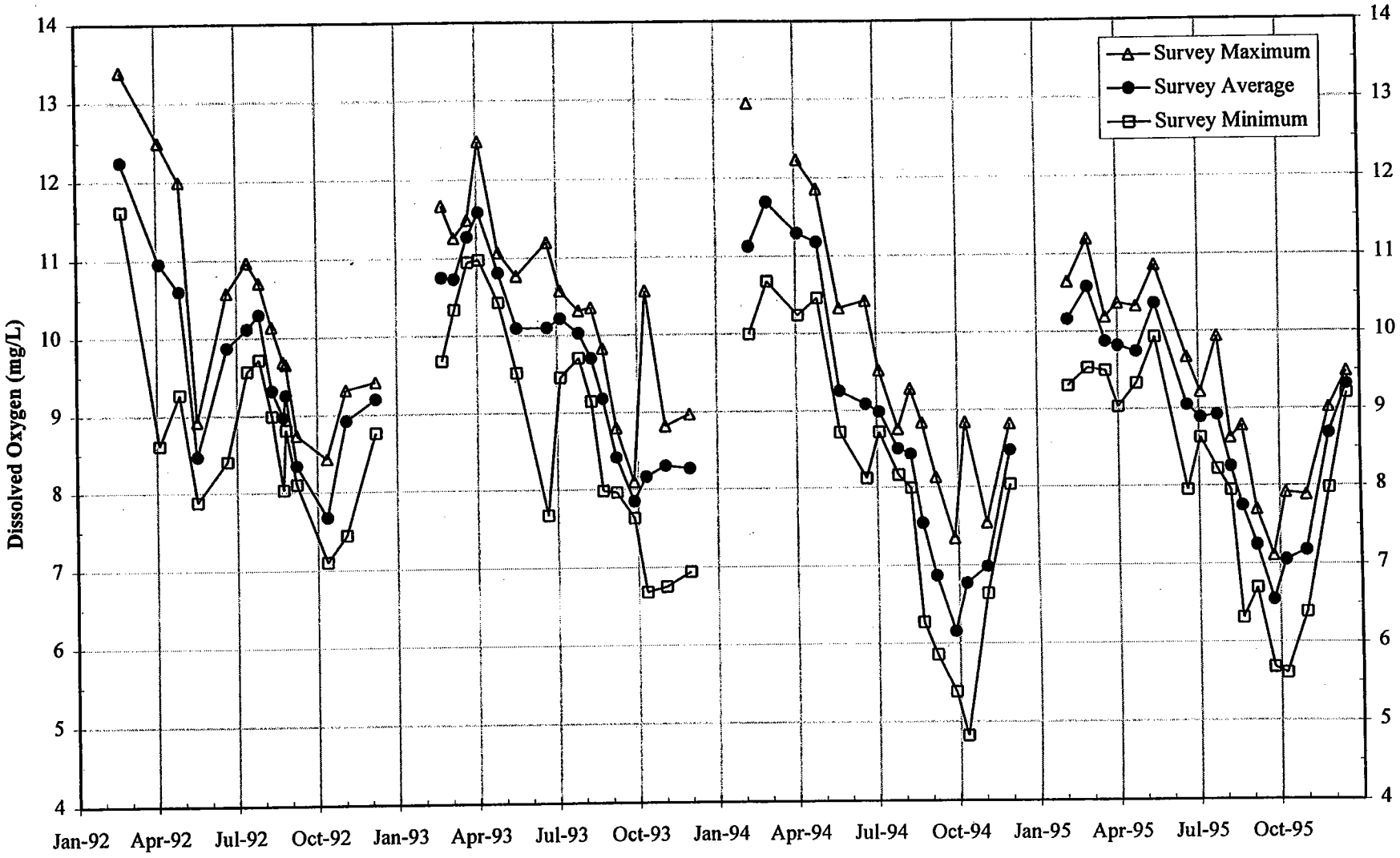

FIGURE 6-6

Interannual Dissolved Oxygen Cycle in Bottom Waters

All nearfield and farfield stations. Symbols indicate maximum, average and minimum value for each survey.

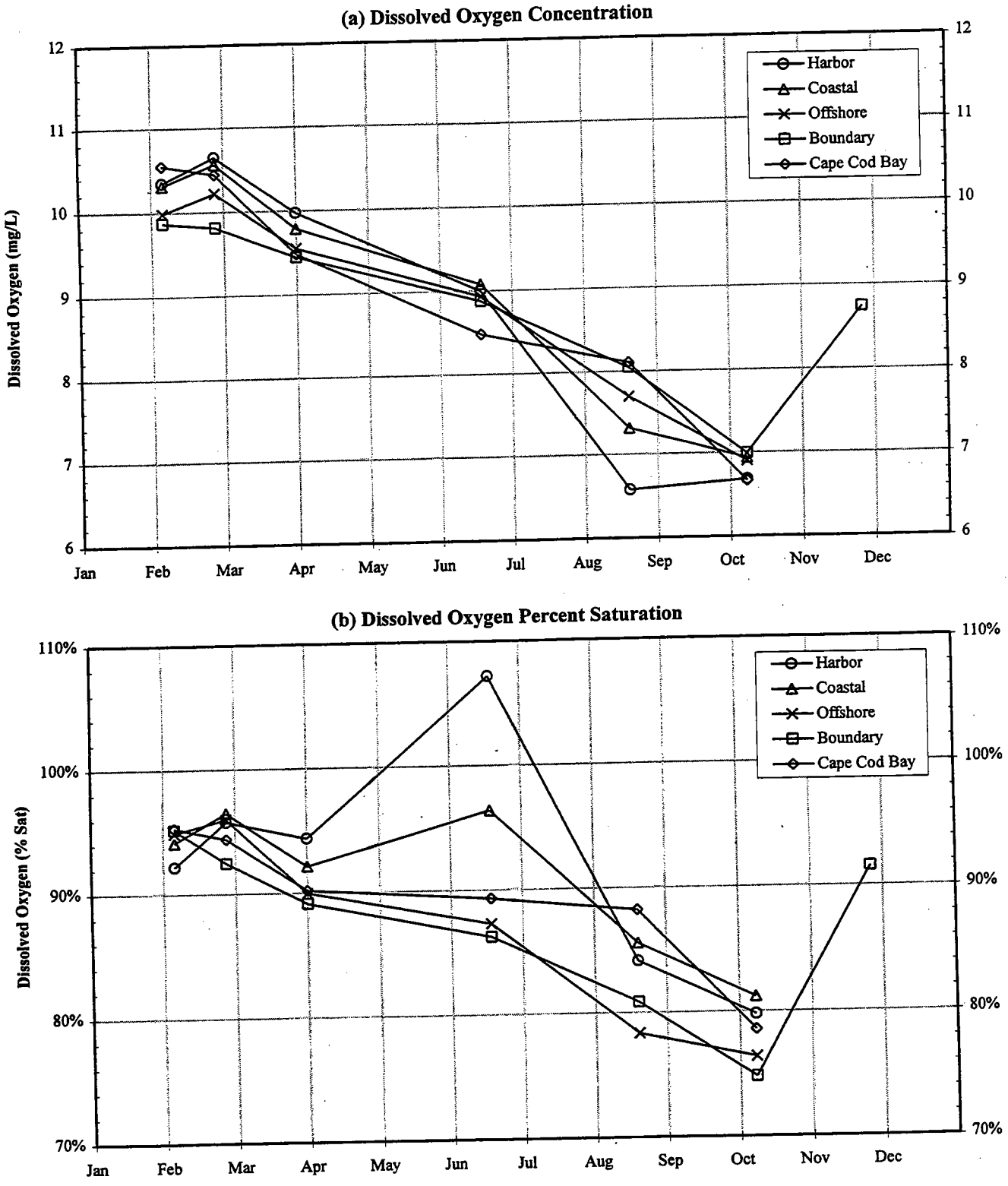

FIGURE 6-7

1995 Spatially Averaged Dissolved Oxygen in the Bottom Waters of Massachusetts and Cape Cod Bays

Symbols represent the average of all stations within each region.

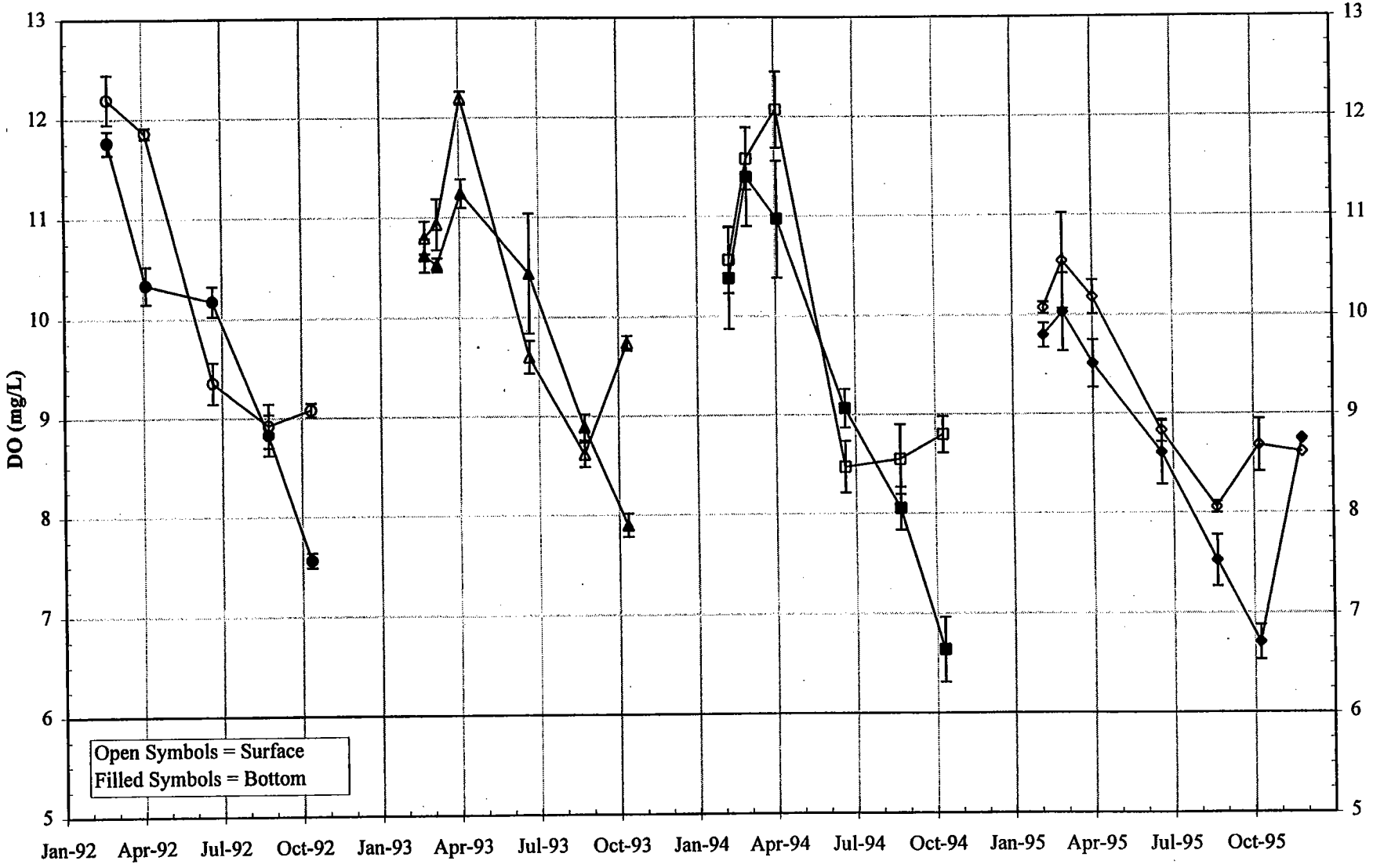

FIGURE 6-8

Interannual Stellwagen Basin Dissolved Oxygen Cycle in Surface and Bottom Waters

Symbols indicate the mean of 4 Stellwagen stations; error bars represent +/- one standard deviation.

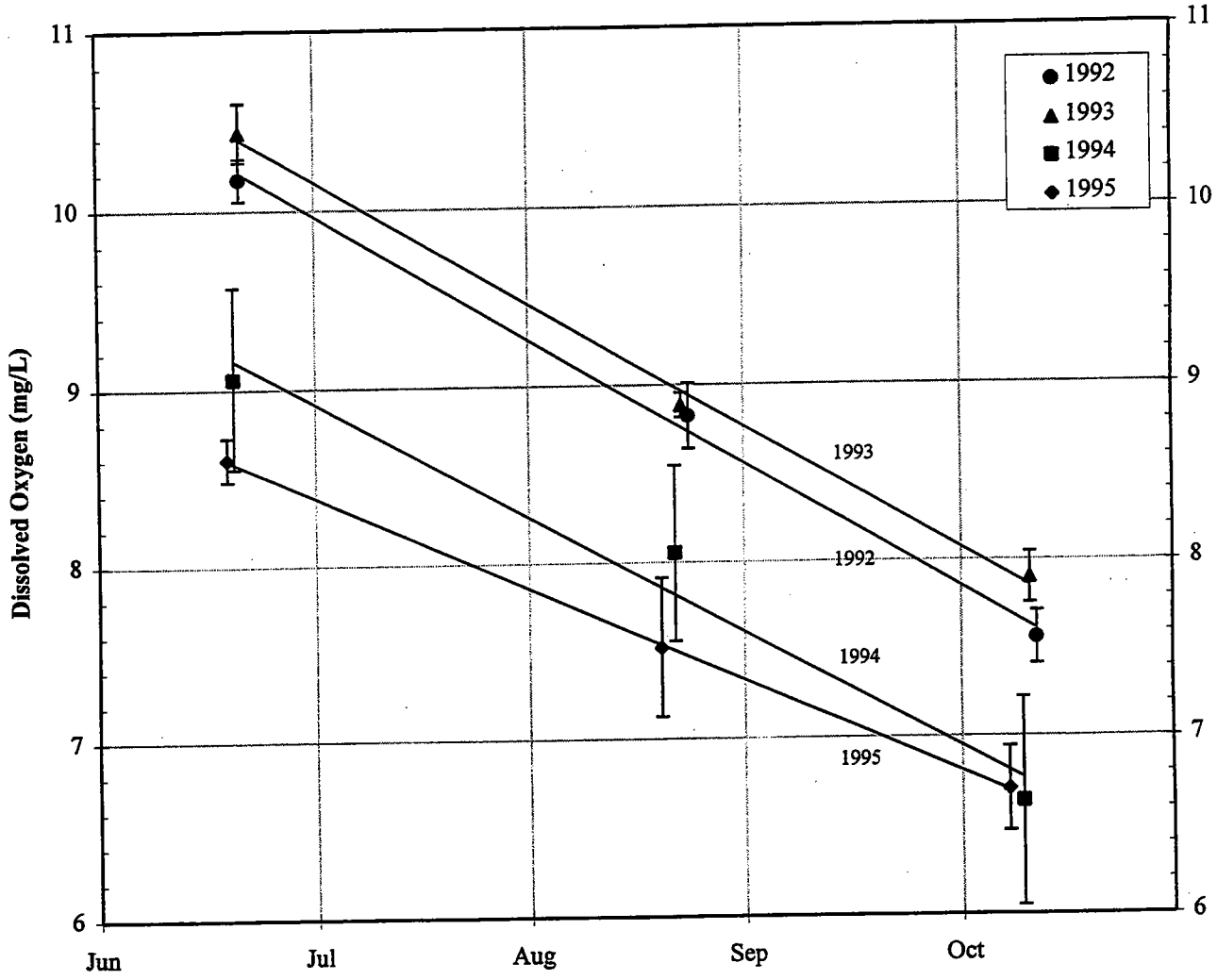

Year	Slope (mg/L/day)	Intercept* (mg/L)
1992	-0.023	10.7
1993	-0.023	10.9
1994	-0.021	9.6
1995	-0.017	8.9
* Predicted DO on June 1st based on: DO = Slope * Date + Intercept		

FIGURE 6-9

Stellwagen Basin Dissolved Oxygen Concentrations in Bottom Waters

Symbols indicate the mean of 4 Stellwagen stations; error bars represent +/- one standard deviation.

7.0 PRODUCTIVITY/RESPIRATION

Oxygen depletion in the bottom waters of Massachusetts Bay, Stellwagen Basin and Cape Cod Bay results from the integration of organic matter inputs from inshore sources (allochthonous) and *in situ* production and organic matter remineralization via respiration within Bay waters and sediments. Oxygen levels are maintained within the surface mixed layer of the water column during remineralization of autochthonous carbon, since the oxygen produced during photosynthesis is sufficient to support the subsequent remineralization of that carbon. Oxygen depletion can occur only when there is a physical separation of the oxygen and fixed carbon produced during photosynthesis or if there are independent outside sources of carbon (e.g., allochthonous inputs). Within the surface mixed layer, physical loss of the oxygen (e.g., to atmosphere during super-saturation) or differential transport of the fixed carbon (e.g., sinking particles) creates such a separation. However, due to contact with the "infinite" oxygen pool of the overlying atmosphere, oxygen concentrations within the mixed layer are generally at or above saturation (Fig. 6-1a) throughout the year.

In contrast to the mixed layer, bottom waters generally receive organic matter in excess of that derived from photosynthesis below the pycnocline, typically via sinking of senescent phytoplankton or fecal pellets. In addition, during stratification inputs of oxygen to bottom waters through ventilation is inhibited so that respiration draws primarily from the initial oxygen pool. In fact, it appears that the physical processes of the timing and duration of stratification and the initial oxygen levels at stratification are the proximate controls on the extent of bottom water oxygen depletion (Section 6). The ultimate control, however, is the rate of oxygen consumption related to biological respiratory processes.

Preliminary estimates of oxygen balance within the nearfield (Kelly and Doering, 1995) suggested that allochthonous inputs of organic matter to the nearfield may be significant and that respiration rates during stratification were higher than the observed rates of bottom water oxygen depletion. This latter finding would require significant ventilation of the bottom waters during stratification, either through horizontal advection of oxygen-rich deep water or inputs from above the pycnocline via eddy diffusion. It appeared that physical processes may so overwhelm *in situ* biological processes in the determination of the oxygen balance that changes in rates of respiration and productivity might not be good indicators of potential oxygen deficits.

In contrast, if the oxygen balance of the bottom waters is determined primarily through *in situ* processes of phytoplankton production and remineralization, then these biological processes would provide essential indicators from which to predict potential future oxygen declines. Measurements of primary production may be useful in detecting nitrogen stimulation which is not manifest in biomass increases (e.g., due to

high grazing pressure). Such stimulation of production would result in higher delivery of organic matter to the bottom water, where resultant oxygen reductions may occur.

Clearly, it is critical to determine both the physical and biological processes which control the extent of annual oxygen depletion in bottom waters. The approach taken here to address this problem has been to perform detailed measurements of primary productivity and organic matter remineralization within the nearfield study area. Vertical profiles of these biological rates were determined during each of the 17 surveys of 1995. Sampling of production and respiration were coupled to allow direct comparisons of the resulting rates. The ultimate goal of this effort is to determine (1) the importance of phytoplankton production to system oxygen uptake, (2) the role of carbon remineralization within the bottom waters and sediments relative to bottom water oxygen depletion, (3) the role of physical processes in mediating biological effects on oxygen deficits, and (4) the coupling of nutrient inputs to carbon fixation and respiration. Biological rate data are presented within this Section with integration into oxygen and carbon balances in Section 9.

7.1 Primary Production

7.1.1 Approach to Production Measurement

Phytoplankton production was measured at three outer nearfield stations (N04, N07, N16) and one station at the outer edge of Boston Harbor (F23) during 1995. Stations were visited six (F23, N07) or seventeen (N04, N16) times throughout 1995.

^{14}C production was determined using standard procedures (e.g., Parsons *et al.*, 1984; see Bowen *et al.*, 1997 for details) at various light intensities ranging between approximately 5 - 1200 $\mu Em^{-2}s^{-1}$. Samples were obtained at five depths throughout the euphotic zone and incubated in a temperature controlled incubator. The resulting photosynthesis vs. light intensity (P-I) relationships (Figure 7-1; comprehensively available in Murray *et al.*, 1997a; 1997b) measurements of light attenuation with depth (CTD-mounted 4π sensor) and incident light time series measurements (on-deck 2π scalar irradiance sensor; e.g., Figure 7-2A) were used to determine hourly production ($\mu gCL^{-1}h^{-1}$ or $mgCm^{-3}h^{-1}$; Figure 7-2B) at intervals throughout the day for each sampling depth.

Hourly production over the course of the day was often invariant ("flattened") at high light intensities due to effects of light saturation (compare incident light curves at upper depths, Figure 7-2A with upper 2-3 production curves, Figure 7-2B; e.g., Interface, Surface, Mid-surface curves). Daily depth-dependent production ($\mu gCL^{-1}d^{-1}$ or $mgCm^{-3}d^{-1}$; Figure 7-2C) was determined by integration of hourly production over the course of the photoperiod. Areal production ($mgCm^{-2}d^{-1}$; Figure 7-2C Inset) was determined by integration of measured activity over the depth interval of the measurements. Calibrated chlorophyll *a*

profiles (e.g., Figure 7-2D; Figure 7-3) were used to determine chlorophyll-specific photosynthetic parameters.

An advantage of this approach is that the effects of cloud-mediated fluctuations in light intensity (e.g., Figure 7-2a) over the course of the day, and gradual variations in light due to changes of season, are automatically incorporated into production computations. Additionally, it is possible to experimentally manipulate the incident light field for the purpose of assessing potential phytoplankton response to an alternative light field. It may be of interest, for example, to assess the photosynthetic capabilities of a population during full sun, if by chance the actual production measurements were made on an overcast day.

7.1.2 Non-Chlorophyll-Specific P-I Curves

P-I curves for deriving α^* [$mgCm^{-3}h^{-1}(\mu Em^{-2}s^{-1})$] and P_{max}^* ($mgCm^{-3}h^{-1}$) used in the computation of ^{14}C production are shown in Figure 7-1. Of 230 incubations only one (Survey W9511, F23, mid-bottom sampling depth) showed evidence of photoinhibition. There is no obvious explanation for this one observation. All other samples from this station showed no evidence for photoinhibition and there were no remarkable changes in the trends of the chlorophyll or temperature profiles to suggest any particular uniqueness for this sample. Except for this one instance the model described by Webb *et al.*, 1974 (see Murray *et al.*, 1997a; 1997b) was used to find best fit estimates of P_{max}^* and α^*. Chlorophyll-specific P-I relationships will be covered in Section 7.1.4.2.

7.1.3 Seasonal Phytoplankton Production

7.1.3.1 Nearfield Production

Spring Bloom. Areal production over the annual cycle (Figure 7-4) in the outer nearfield (stations N04, N07, N16) was generally characterized by an increasing trend in production from 300 - 500 $mgCm^{-2}d^{-1}$ in February - April to between 1000 - 2500 $mgCm^{-2}d^{-1}$ in the summer period. Production then decreased back into the 300 - 500 $mgCm^{-2}d^{-1}$ range by the fall/winter months. At the future outfall station (N16) this general trend was punctuated by an intense short duration bloom in late April (survey 5) that constituted 20% of total annual production. The 7.1-fold increase in production was not, however, observed at the northeastern corner station N04, which suggested that fairly short range (3 km) spatial differences in production rates existed in the region at this time.

Average photic zone chlorophyll for stations N16 and N04 (Figure 7-5) and the vertical distribution of chlorophyll (Figure 7-6) at this time of year demonstrated a pattern similar to that observed for production. In the spring, station N16 also exhibited a similar increase in chlorophyll biomass over levels found on either side of the bloom (surveys 4 and 6), while increases at station N04 also paralleled the measured

increase in activity. Chlorophyll at station N07 was similar to or slightly higher than that found at station N04, but associated phytoplankton production was missed by the low temporal resolution time series conducted for that station.

A clearer picture of the spatial distribution of chlorophyll biomass is illustrated in Figure 7-7, which presents a contour map of the average water column chlorophyll (note the relative differences in average photic zone chlorophyll and average water column chlorophyll, squares and crosses, respectively in Figure 7-5). The outer nearfield was clearly on the steep outer edge gradient of a chlorophyll biomass dome or plateau that was present in the central region of the nearfield box (see E-W sections in Figure 7-7). The reasonable correspondence of photic zone chlorophyll with phytoplankton production rates at N16 and N04 suggests that the gradient in phytoplankton production will be similar to the observed chlorophyll pattern. To the extent that the chlorophyll-specific properties of the phytoplankton at station N16 is representative of those in the central nearfield, Figure 7-7 also suggests that this region may have exhibited more intense production than was measured in the outer reaches of the nearfield grid, perhaps up to 1.5-2 fold greater.

Spring Grazing Event. Also evident in the outer nearfield region in early spring (late March - early April, surveys 3 and 4) was a period of very low phytoplankton production that was paralleled by similarly low average chlorophyll (Figures 7-5 and 7-6). The pattern was also reflected by an abrupt order of magnitude drop in phytoplankton total abundance, a corresponding four-fold increase in zooplankton total abundance (Figure 8-22), and significantly enhanced water clarity (Figure 7-8) that translated into the maximum depth of the photic zone for the year. It was also at this time of year that the photic zone reached or approached the sediment surface. As will be discussed in more detail in Sections 8.1 and 8.2, evidence suggests that a grazing event may have been responsible for the dramatic decreases in water column particle content and phytoplankton production.

Summer-Fall Blooms. Continued inspection of average photic zone chlorophyll over the remainder of the year suggested an intense, short duration fall bloom in early November (Figures 7-5 and 7-6) that, in contrast to the spring bloom, was strongly evident in each of the eastern nearfield stations (N04, N16 and N07). Light attenuation was greatest during this time of year (Figure 7-8), reflecting the heavy particulate loading in the water column associated with the bloom. Similar to the pattern in spring, the central nearfield region contained substantially greater chlorophyll biomass than the eastern outer edge (Figure 7-9) and may be a focus of higher production, perhaps up to 1.5 times higher. A short duration subsurface bloom also occurred in early September (Figure 7-6). This bloom was located at the base of the thermocline (15 m, Figure 3-1) where the chlorophyll maximum was sharply focused (Figure 7-3, W9512).

Potential Production. It is interesting to note that during the fall when all biomass indicators suggested the presence of a large bloom, parallel measures of phytoplankton production did not reflect similarly enhanced activity. Cloudiness on the day of sampling caused this apparent lack of production. However,

because of the approach taken for production rate computations it is possible to experimentally manipulate the daily incident light field to assess the photosynthetic potential of the phytoplankton population. When a cloudless daily light field typical of that time of year (Figure 7-10) is substituted for the light field of the day of sampling, a measure of the maximum or "potential" areal production is obtained. Note that measured productivity may be slightly higher than the predicted potential production due to the application of a "best-fit" regression to site-specific measurements.

When this was performed on the data (Figure 7-11), the fall bloom became the dominant feature of annual production. It is of interest to note that for station N16, 16% and 37% of "potential" annual production are encompassed by the spring and fall blooms, respectively, based on integration of production data. That is, potentially 53% of the year's production can result from bloom events occurring over time periods encompassing less than 16% of the annual cycle. Though somewhat of an exaggeration because not all days are sunny, the example does illustrate that in the Massachusetts Bay environment major portions of annual production can occur during abrupt and spatially varying blooms. An advantage of the potential production computation is that it can provide an upper limit estimate of production which can be useful in carbon balance computations.

Effects of Temporal Sampling on Estimates of Annual Production. Low temporal resolution sampling programs can result in significant errors in annual production estimates due to the potential to miss or exaggerate effects of sporadic events (Taylor and Howes, 1994). Based on the chlorophyll results (Figure 7-5), it appears that in 1995 two significant nearfield blooms could have been missed by the sampling regime for station N07. Depending upon the extent to which the spring and fall blooms were expressed at N07, the annual production estimate could be biased low.

To provide an example of the possible effects of the 1995 low resolution sampling scheme on annual production estimates, data from the two nearfield stations that were sampled more frequently (17 times per year) were mathematically down-sampled to simulate the results of the 1995 lower frequency sampling program. Shown in Figure 7-12 and Table 7-1 both the spring and fall bloom events were potentially misrepresented by the 6 point time series study. The spring bloom would have been completely missed and depending upon light conditions the fall bloom may have been significantly under-represented. If sampled at low frequency, estimates of nearfield production would have hovered near 300 $gCm^{-2}y^{-1}$ and the stations would have looked fairly similar. Annual production for both N04 and N16 would have been underestimated (Table 7-1), particularly the latter because of the missed spring bloom.

In reality, production based on the full set of measurements at N16 was significantly higher (about 37% vs. 11% determined by low frequency sampling) than N04, likely because of its closer proximity to higher chlorophyll biomass in the central nearfield (Figures 7-7, 7-9). If viewed from the perspective of potential production at full sun, annual production at N04 and N16 would have been dramatically underestimated at both stations, primarily because of under-representation of the fall bloom. Inclusion of the missed

blooms resulted in a 37% and 78% increase in estimated annual production at N04 and N16, respectively, compared to low frequency estimates (Table 7-1). These numbers represent an upper limit because, as mentioned above, not all days are sunny. However, it is clear that sampling of critical stations at frequencies less than about 17 times per year can miss important stochastic and seasonal events, and introduce errors in determined annual production that are of a magnitude (60-70%, depending upon the ratio of sunny to cloudy days) sufficient to affect the accuracy of carbon balance computations and resultant predictors of water quality.

Because of the low temporal resolution of directly measured annual production in previous years (Figure 7-13) comparison of year to year estimates of production is subject to the possible errors suggested above. Interannual trends do not exceed the between station variability that was observed in high temporal resolution studies conducted in 1995.

7.1.3.2 Harbor Edge Phytoplankton Production

Harbor edge station F23 exhibited the highest phytoplankton production of the study (Figure 7-4). The 0.5% euphotic zone rarely penetrated deeper into the water column than 15 m (Figure 7-8) relegating the majority of production to the upper 10 m of the water column. Nevertheless, given a high chlorophyll biomass (Figure 7-5) that was rivaled only by the fall bloom in the nearfield, maximum seasonal harbor edge areal production (about 7,500 $mgCm^{-2}d^{-1}$) was twice the highest nearfield bloom production rates (approximately 4,000 $mgCm^{-2}d^{-1}$) and nearly four times greater than maximum nearfield production during non-bloom periods (about 2,000 $mgCm^{-2}d^{-1}$). Total annual production at the harbor edge (763 $gCm^{-2}y^{-1}$) was between 1.8 and 2.5 times higher than annual production measured at any of the nearfield stations (310, 330, and 424 $gCm^{-2}y^{-1}$ for stations N04, N07, and N16, respectively). Even from the perspective of potential production (Figure 7-11) the harbor edge was still 1.4 - 2.3 times more productive than any of the nearfield stations.

This shallow harbor station was replete with nutrients throughout the year and, compared with the nearfield, is in a poorly stratified, tidally active region (Figures 3-11, 3-12). Production rates paralleled average photic zone biomass (Figures 7-4, 7-5, and 7-6), with the summer production maximum in late August occurring at the seasonal temperature maximum (Figure 3-3). Because of the poor temporal resolution it is not possible to assess if any of the bloom events observed in the nearfield occurred at the harbor edge. However, based on the apparent linkage between Harbor Station F31 and N10 (Figure 5-2), the November bloom may not have occurred to any extent in the harbor or adjacent waters.

7.1.4 Chlorophyll-Specific Measures of Production

7.1.4.1 Seasonal Production vs. Seasonal Chlorophyll-Specific Production

Nearfield phytoplankton production resided essentially in the upper 15 m of the water column, and was often restricted to the surface mixed layer during periods of intense summer stratification (Figures 7-14 through 7-18). The major common features in the pattern of nearfield production paralleled the temporal and depth-dependent distribution of photic zone chlorophyll (Figure 7-6). The two major events were a dominant fall bloom in mid October-early November (Julian days 280-310), and a late summer event in early September (around Julian day 250).

To varying degrees the late summer event was associated with a subsurface chlorophyll maximum. The dominance of the fall bloom is clearly manifest in the surface waters when production potential was expressed in terms of maximum available light for that period of the season (Figures 7-17 and 7-18). The intense spring bloom in early April (Julian days 100-140) was present in the mixed layer waters of station N16 and to a much lesser extent in the outer nearfield, again paralleling the chlorophyll distribution for those stations (Figures 7-6, 7-7).

An early summer episode of production (late June/early July) also occurred in the nearfield (approximately Julian days 175-190) particularly on the eastern edge. A unique feature of this event was that, in contrast to photosynthesis at other times of the year, it appeared to occur when photic zone chlorophyll was low (Figure 7-6). Also, because production was predominantly restricted to the upper 5 m of the water column this period of photosynthesis was less manifest when expressed on an areal basis (see Figure 7-4).

Expression of phytoplankton production on a chlorophyll-specific basis provides a means for visualizing relative efficiency of production over the course of the season. Shown in Figures 7-15 through 7-18, photic zone chlorophyll-specific production exhibited a pattern very different from the dominant features in production. A feature common to all of the nearfield stations was an intense maximum of chlorophyll-specific production in early summer, centering on survey W9508 and W9509 (Julian days 188, 207). This episode of relatively higher photosynthetic efficiency overlapped with, and perhaps extended slightly beyond, the above-described low chlorophyll, surficial water production that occurred in early summer at the outer edge of the nearfield.

Two other major chlorophyll-specific photosynthesis maxima occurred in the nearfield in 1995. The most intense event, which was most evident at N16 but was also seen at N04, occurred in mid March (W9503, centering on Julian day 81). This was the period when both production and chlorophyll were low (Figures 7-4 and 7-5, respectively) and zooplankton abundance high (Section 8.2). The remaining maxima occurred in the fall and was associated with the beginning (Julian days 280-290) of the fall bloom which peaked

at the beginning of November (approx. Julian day 308). All high chlorophyll-specific events appeared to have been associated with periods of lower biomass and conditions conducive to higher phytoplankton activity. These conditions included:

- active populations that appeared to be controlled by grazing rather than nutrients (W9503);
- populations responding physiologically to a physical perturbation that distributed nutrients into the euphotic zone (W9508, W9509); and
- stimulation of phytoplankton by the fall overturn (W9514) which ultimately lead to a bloom (W9515).

The majority of production at the harbor edge was restricted to the upper 6-7 m of the water column because of the large chlorophyll biomass and sharp light attenuation. The production peak, as discussed above, occurred in summer rather than the fall (compare low temporal resolution contour plots for stations F23 and N07 in Figure 7-14). Chlorophyll-specific production was high (>200 $mgC(mgChl\textit{a})^{-1}d^{-1}$) in the upper 5 m of the water column over the majority of the summer period (Figure 7-15). The temporal breadth of this activity may reflect the effects of continually available nutrients and tidal flushing of phytoplankton from the harbor area. This tidal flushing would leave a more actively photosynthetic population than would occur if the system were less dynamic. Discussion of possible high chlorophyll-specific production that appeared at the very beginning of the study will be reserved until 1996 data are included.

7.1.4.2 Chlorophyll-Specific P-I Relationships

Frequency Distributions. Values for chlorophyll-specific initial slope of light-dependent production, α, expressed in units of $gC(gChl\textit{a})^{-1}h^{-1}(\mu Em^{-2}s^{-1})^{-1}$ and P_{max}, expressed in $gC(gChl\textit{a})^{-1}h^{-1}$, were calculated by dividing α" and P_{max}* by chlorophyll *a* measurements made at each of the 5 depths for stations N04, N07, N16 and F23 (see Appendix A).

The frequency distributions of these parameters are shown in Figures 7-19 and 7-20. Inspection of the frequency distribution of α among the four stations did not reveal a discernible difference between the outer nearfield stations (N04, N07, N16) or between the nearfield and harbor edge (F23). When all data were pooled (n=230), a positively skewed distribution (skewness, 4.49) was observed with a median α of 0.0432 $gC(gChl\textit{a})^{-1}hr^{-1}(\mu Em^{-2}s^{-1})^{-1}$. Nearly all (96%) of the determined values of α fell below the theoretical maximum of approximately 0.11 $gC(gChl\textit{a})^{-1}h^{-1}(\mu Em^{-2}s^{-1})^{-1}$ established by a number of investigators (e.g., Cleveland *et al.*, 1989; Scofield *et al.*, 1991; Lohrenz *et al.*, 1994). Only nine values (3.9%) exceeded an α value of 0.12 (an occurrence which has also been observed by others, e.g., Lohrenz *et al.*, 1994); three were greater than 0.18 and are probably faulty measurements. If the nine high values

are omitted, the geometric mean for α was determined to be 0.044 (median, 0.043; normally distributed mean and standard deviation, 0.048 ± 0.022). These values are somewhat lower than the mean determined for 1994 by Kelly and Doering, 1995 (0.06 from a data set where poor P-I curve fits were omitted), but not statistically different.

As with α, the outer nearfield and harbor edge P_{max} distributions were not discernibly different from one another. A slight drift of the distribution towards higher values of P_{max} is apparent for station F23, but given the relatively low numbers involved the difference is not statistically significant. Pooled data (n=230) revealed a positively skewed (skewness, 1.50) and possibly bimodal distribution with a median P_{max} of 7.34 $gC(gChl\textit{a})^{-1}h^{-1}$. The large majority (95%) of the determined values of P_{max} were less than the theoretical maximum of approximately 25 $gC(gChl\textit{a})^{-1}h^{-1}$ (e.g., Lohrenz, 1994). Only four values within the data set (1.7%) were above 30. If these values are omitted the geometric mean for the data set was 7.40 (median, 7.28; normally distributed mean and standard deviation, 9.2 ± 6.2) and essentially the same as the values determined for 1994 by Kelly and Doering (1995) [7-8 $gC(gChl\textit{a})^{-1}h^{-1}$].

Seasonal variation in α. Examination of α over the 1995 season (Figures 7-21 and 7-22) revealed a very interesting pattern. Shown particularly by the more highly resolved data for nearfield stations N04 and N16 (Figure 7-21), α was essentially invariant over most of the year, hovering at a value of about 0.04 (Figure 7-19). In general, there also appeared to be a significant depth-dependent decrease in α with depth throughout most of the year, a property more easily viewed in Figure 7-22. The most striking feature of the data set was an abrupt increase (by two-fold or more) in α during mid-summer, from an average of about 0.05 to a range of 0.10-0.12 (the theoretical maximum). In addition, the phenomenon extended throughout the entire water column, which is in sharp contrast to the usual trend of higher α nearer the surface.

The large excursion of α to its theoretical limits began with survey W9508 (6 July), extended into survey W9509 (25 July) and abruptly returned to average conditions by survey W9510 (09 August). It is likely that a similar occurrence happened at station N07 and perhaps F23, but the three-week event would have been completely missed by the low temporal resolution sampling regime used for monitoring those stations.

When data for α were pooled seasonally and presented as a function of depth (Figure 7-23), values typically fell within an envelope that was broadest at the surface and tapered with depth. The envelope ranged from 0.03 $gC(gChl\textit{a})^{-1}h^{-1}(\mu Em^{-2}s^{-1})^{-1}$ to slightly above the theoretical maximum (shaded bar) at the surface, and was confined to a narrow band around 0.03 $gC(gChl\textit{a})^{-1}h^{-1}(\mu Em^{-2}s^{-1})^{-1}$ at 50 m. There were no significant differences in the distributions among the four stations (compare upper panels, un-circled data). Data from surveys W9508 and W9509 (circled values), however, were distinct in that all values hovered at the theoretical maximum independent of depth until below 30 m, where values dropped back

into the envelope (outlying datum from 40m at N16 greatly exceeded theoretical maximum and thus excluded as an errant point).

Though the potential for a broad range in α exists in the surface water, the actual frequency distribution of this parameter in surface samples (median = 0.050) was not markedly different from the entire data set (Figure 7-24, upper panel, median = 0.0432). As was observed in earlier figures, samples from the July surveys were distributed to the high end of the spectrum near the theoretical limit (lower panel, median = 0.102).

The general pattern for α that we have observed in the 1995 study was similar to observations made by Kelly and Doering (1995) for the 1994 season. They found α to be invariant between harbor edge and nearfield stations, and observed a trend of decreasing values with depth in the water column. In partial contrast to our study, they also observed no trends with season. The result, however, may have been a consequence of the lower temporal resolution study conducted in 1994. As was evidenced in our study, the stations with lower temporal resolution, F23 and N07, did not exhibit the large perturbation of α that was seen at the stations with higher temporal resolution N04 and N16.

Seasonal variation in P_{max}. P_{max} values varied significantly over the season, and there was a marked decrease in this parameter with depth (Figures 7-25 and 7-26). As with α, the July phenomenon was the dominant feature in P_{max} variability (an increase of approximately two-fold), though higher values of P_{max} were spread over a broad portion of the summer season. July was the only time of year when the water column average P_{max} approached the theoretical maximum, and when higher values of P_{max} reached deep into the water column. Other major increases in P_{max} occurred in early Spring (approximately centered on Julian day 80) and early Fall (approximately centered on Julian day 285), which correspond with the timing of the possible grazing event and the beginning of the fall bloom, respectively. In fact, when compared with Figures 7-15 through 7-18, the annual pattern for P_{max} parallels the annual pattern observed for chlorophyll-specific production. The primary difference is that the capacity for higher P_{max} penetrates further into the water column than is actually realized due to the abrupt attenuation of light in the water column.

When seasonal P_{max} data were presented as a function of depth (Figure 7-27) values typically fell within a broad nearfield envelope that ranged from approximately 4 $gC(gChla)^{-1}h^{-1}$ to somewhat above the theoretical maximum (25-35 $gC(gChla)^{-1}h^{-1}$, shaded bar) at the surface. The upper boundary of the envelope decreased non-linearly with depth down to a minimum of about 4-5 $gC(gChla)^{-1}h^{-1}$ near the bottom. The top of the P_{max} envelope was populated by data from the July transient event and a few upper water column samples from station F23. As was the trend for α, the frequency distribution of P_{max} (median = 7.35, Figure 7-28) was influenced towards higher values by samples from the July surveys (surface samples, median = 11.6, compared with July surveys, median = 19.2).

7.1.5 Events Correlated with Observed Changes in α and P_{max}

The single most obvious event affecting photosynthesis occurred during the month of July when the water column was strongly stratified. The onset of major changes in α and P_{max} occurred on 6 July (Julian day 188, survey W9508), coincident with the upwelling event described in Section 3.1.1. Evidence from this perturbation persisted throughout most of July (into survey W9509), with the phytoplankton apparently responding to bottom water nutrients (DIN, phosphate, silicate) being lifted into the lower portion of the euphotic zone (Figures 4-8 through 4-18). Increased phosphate and silicate concentrations were more evident than nitrogenous compounds, possibly due to rapid biological utilization of the nitrogen.

While elevated chlorophyll biomass was not reported from either surveys W9508 or W9509, it appeared that the changes noted in algal physiology during W9508 foreshadowed an intermediate event, and data from the subsequent survey provide further evidence. The α and P_{max} terms computed from the photosynthesis data presented in Figures 7-22 and 7-26 indicated that phytoplankton of relatively constant physiological state (i.e., high α and P_{max}) were distributed deep within the water column, perhaps down to 35 m. Note, for example, that values of α during surveys W9508 and W9509 clearly lay outside the envelope expected for deeper water (Figure 7-23). Additional evidence included observed increases in carbon specific respiration in bottom water during survey W9509 (see Section 7.2.1.1), indicating inputs of "high quality" organic matter from the upper waters.

It is interesting that α and P_{max} also "flagged" the onset of the fall bloom (see Figures 7-22, 7-26 for station N16). Both parameters increased at the time of the breakdown of stratification which allowed a "persistent" exposure of the euphotic zone to higher nutrients and resulted in the fall bloom. We intend to further explore the cause-effect relationships between α and P_{max} and changes in environmental physical and chemical properties via multivariate analysis to substantiate the preliminary conclusions presented here. We will also explore the physiological bases for nutrient related changes in α and P_{max} in order to establish the robustness of these parameters as indicators of important environmental change.

7.1.6 Productivity Assessments

Results of the 1995 studies in Massachusetts Bay have demonstrated that the MWRA's photosynthesis program provided insight into the complexities of this ecosystem, and even documented events which the routine monitoring may have missed. The additional data provided by the methodology (i.e., estimates of potential production, indicators of photosynthetic efficiency) provided predictive capability and information regarding changes in which resulted from altered nutrient status (e.g. Lohrenz *et al.*, 1994). This information will serve to strengthen the numerical modeling efforts being undertaken to evaluate the outfall relocation. The July upwelling event, for example, was analogous to "effluent breakthrough" during stratified conditions, which might occur if physical events were to bring nutrient-rich effluent into the nutrient-depleted euphotic zone. Analysis of the subtle effects of such events on the bottom water will further our understanding of carbon and oxygen dynamics in the system.

Photosynthesis, however, is subject to variability on both temporal and spatial scales, and sufficiently intensive data collection is cost-prohibitive for long-term monitoring purposes. Therefore, it is necessary to seek potential proxy measures of photosynthesis based on variables that are easily attainable on highly resolved temporal and spatial scales. In the meantime, it is necessary to maintain the appropriate direct measurements from which to develop and evaluate new proxy measures.

A proxy model of carbon fixation must ultimately possess two capabilities. First, it must have the ability to accurately provide a measure of areal organic matter production, translatable into an accurate estimate of annual production. This parameter is important in carbon cycling studies and annual predictions of oxygen status (e.g., Section 7-2). Second, the proxy measure should also possess an ability to express changes in photosynthesis efficiency, since it appears that it is these parameters that hold the greatest value in being able to predict changes in physiological state that can "potentially" lead to bloom events (i.e., alert the investigator to physical/chemical conditions that should be more closely monitored, both spatially and temporally).

One such proxy measure which has been explored for the HOM (Kelly and Doering, 1995) uses a model based upon correlating a composite parameter BZpIo to measured ^{14}C production, where:

B = average photic zone chlorophyll *a* concentration;
Zp = photic zone depth (thus BZp = chlorophyll content of the photic zone); and
Io = incident daily light striking the sea surface.

Using this model for the 1995 (Figure 7-29) yields a regression for the nearfield: P=0.398[+/-0.093]*BZpIo+522[+/-618] (not forced through origin); P=0.638[+/-0.03]*BZpIo+0[+/-690] (forced through origin). Our latter equation forced through the origin agreed reasonably with Kelly and Doering (1995): P=0.61*BZpIo-94; 0.56*BZpIo+20. However, the 1995 data yielded a significant difference from earlier data in the fitted parameter for the harbor edge station (P=1.67[+/-0.15]+0[+/-723].

While there are a variety of theoretical and physiological factors which need to be evaluated in the use of this model, the variability in the BZpIo to carbon fixation relationship alone diminishes the utility of the model for actually computing an accurate estimate of production. For example, production and propagated error computed at BZpIo values of 1000, 2000, and 3000 were 638 [+/-691, c.v.=108%], 1276 [+/-694, c.v.=54%], 1914 [+/-700, c.v.=37%]. That is, in the observed range of production the error ranges on the order of 1.4 to 2 fold. This translates into an uncertainty in annual production that is unacceptable for carbon balance studies (Section 7-2).

Part of the variability is attributed to the fact that the model inherently assumes that, on average, the photosynthetic efficiency throughout the water column is the same and that exposure of chlorophyll to light will result in a proportional amount of production. Photosynthetic efficiency changes significantly,

particularly during perturbing events (Figure 7-30) and when photosynthesis in the upper portion of the water column is in varying stages of light saturation (Figure 7-31; Murray *et al.*, 1997a; 1997b). We attempted to apply this model in depth-sections throughout the water column, corresponding to production measurements made at the five depths (Figure 7-32), but were unable to improve the correlation. We began to see differences among the nearfield stations, in addition to the harbor edge station, and surface samples tended to be biased low (open circles) due to effects of light saturation.

Since proxy measures of photosynthesis are needed, bio-optical models should be evaluated which employ measures of active fluorescence and which are mechanistically more aligned with photosynthesis activity. These bio-optical models also permit determination of parameters related to photosynthetic efficiency (i.e., related to α). Proper application of these models should more closely align to the predictive and quantitative needs described above. We also intend to explore the utility of an approach to "fill in the gaps" of photosynthesis by using daily measures of the incident light field and gridded estimators of water column light attenuation, photic zone chlorophyll, and P-I parameter distributions. Success will depend upon the accuracy of the gridding operation compared to variability in the real world. Where possible, we will compare gridded parameters with measurements made at the USGS mooring. The exercise will be used in part to provide an estimate of the variability associated with a fluctuating light field and how that variability translates into errors in estimating annual production.

7.2 Water column and Sediment Respiration

Water column and sediment respiration are the dominant sinks of oxygen within the water column of the Bays. In systems like Massachusetts and Cape Cod Bays, water column respiration typically accounts for the majority of carbon mineralization (on an areal basis, m^{-2}). In order to understand the carbon and oxygen dynamics of Massachusetts Bay and the factors which control bottom water oxygen depletion, detailed water column respiration measurements were conducted. Sediment respiration measurements focussed on depositional environments to determine the upper limit of sediment oxygen uptake through this pathway. Measurements focused on (1) vertical distribution of water column uptake rates and sediment uptake during mixed and stratified water column periods, relating the fate of photosynthetically derived organic matter and the draw-down of bottom water oxygen levels (Section 7.2), (2) developing a carbon balance (see Section 9.3) to ascertain the potential importance of allochthonous carbon inputs; and (3) developing an oxygen balance from which to assess the potential for increases in oxygen deficits under changing organic matter inputs (see Section 9.2).

Both water column and sediment respiration are controlled by the availability of labile organic matter and the environmental temperature. These two regions of oxygen uptake differ primarily in their ability to "store" organic matter while it is being remineralized. Organic particles typically have a relatively short life-time (days-weeks) within the water column as they are freely advected or sink to the bottom sediments. In contrast, organic particles reaching the sediments remain available for decomposition for

months to years, with refractory compounds permanently accumulating in depositional areas. The result is that water column rates of respiration at fixed locations typically show large temporal variations compared to sediment rates which are buffered by their more constant organic matter pool. The following sections detail the major results of the water column (7.2.1) and sediment (7.2.2) respiration measurements within Massachusetts Bay through 1995.

7.2.1 Water column Respiration

Water column oxygen uptake is dominated by the respiration of phytoplankton, zooplankton, and heterotrophic micro-organisms. Within the bottom waters of Massachusetts Bay, heterotrophic forms predominate. Our measurements represent the combined oxygen uptake by all of these forms.

Rates of water column respiration were determined in the same time series as the primary production measurements (Section 7.1). Measurements were made at three depths (surface, mid and bottom). During stratification the upper two depths were generally within the mixed layer, at the surface and near the pycnocline. Triplicate samples were collected for determination of initial conditions and for incubation to determine oxygen uptake at each depth. Samples were kept at *in situ* temperatures in the dark. Since in open water rates of oxygen consumption are typically low due to carbon availability, care must be taken to maintain "clean" incubation bottles. Bottles were HCl washed between surveys and periodically "digested" with potassium persulfate to remove organic films. As a result triplicate incubations typically had a C.V. of ca. 10%. Analysis was by Winkler reaction and potentiometric titration (Oudot *et al.* 1988). Carbon-specific respiration was calculated by dividing the measured respiration rate by the particulate carbon concentration in order to evaluate the bio-reactivity (lability) of the available carbon substrate.

7.2.1.1 Vertical Distribution of Water column Respiration

Respiration ranged from showing a weak (<2 fold) vertical gradient within the water column to a very strong gradient (<10 fold) from surface to bottom waters in both the nearfield (Figure 7-33) and Stellwagen Basin (Figure 7-34). Not surprisingly, the steepness of the vertical gradient appears to be controlled primarily by the degree of vertical mixing of the water column (see Figures 3-2, 3-6).

During winter and early spring when the water column was unstratified, only a slight trend of decreasing respiration rate with increasing depth was observed. Since respiration is controlled primarily by temperature and the availability of labile organic matter, mixing of the water column serves to generate isothermal conditions (see Figure 3-1, surveys 1-6 and 14-16) and speed the delivery of organic matter to bottom waters resulting in the more uniform profiles of respiration. However, respiration was not completely uniform from surface to bottom during the mixed interval. Surface water respiration rates showed higher rates of oxygen uptake throughout the year. The higher respiration rates are consistent with the vertical distribution of primary production (Figure 7-6 and 7-15) and POC.

It is notable that even during the mixed period, particulate organic matter levels, most likely photosynthetically derived, remain significantly higher within the surface than bottom waters. This is most clearly seen in the detailed POC data from the Nearfield region (Figure 7-35 and 7-36). It is clear that during the mixed interval, the POC distribution is the predominant factor generating the vertical gradient in water column respiration. However, the generally low absolute rate of respiration is likely the result of the low environmental temperatures during this interval.

In contrast to the mixed period, water column respiration rates during stratification were strongly depth-dependent, with mixed layer rates more than an order of magnitude higher than bottom waters. The higher rates within the upper versus bottom waters appears to be the result of the higher POC levels and more than 10°C higher temperatures. In addition to the quantity, the quality of the organic matter also favors higher respiration within the surface waters. By correcting the *in situ* rates for the variable POC levels (i.e., the carbon specific respiration rate), it is possible to gain insight into variations in organic matter quality (i.e., lability) with depth (Figures 7-37 and 7-38). During the mixed period the water column is generally isothermal so that similarity in carbon specific rates over depth can only be the result of similar substrate quality. At these times it appears that accelerated delivery of POC to bottom waters results in similar substrate quality throughout the water column. However, during the stratified period, differences in substrate quality, in addition to temperature, appear to be a primary factor supporting higher surface versus bottom water rates.

Additional support for the importance of organic matter quality/delivery, is suggested by the spike in carbon-specific respiration during the July mixing event (Section 3, Figures 3-2 and 3-6). While it is not certain that the mixing event extended to Stellwagen Basin, the July sampling at that site also showed a spike in carbon specific respiration similar to that in the nearfield. However, the limited water column data from Stellwagen Basin does not allow a certain conclusion at this time.

During the July upwelling event, the lifting of the pycnocline appeared to enhance delivery of high-quality POC to bottom waters. The ratio of chlorophyll *a* to chlorophyll *a* + phaeopigments was also an indicator of the availability of "fresh" phytoplankton material in bottom waters. During the July event (W9508), the ratio increased within the bottom waters at each of the nearfield respiration stations (Figures 5-6 and 7-29). Due to the relatively low quality typical of bottom water POC during the stratified period (rate = 0.05 $\mu MO_2[\mu MC]^{-1}d^{-1}$), the increase (rate = 0.08 $\mu MO_2[\mu MC]^{-1}d^{-1}$) during the July event requires delivery of only a small mass of labile POC from the surface waters. Therefore the spike in carbon-specific respiration during the subsequent survey is consistent with the lack of observable change in bottom water POC concentration. It should be stressed that under constant conditions POC may be a useful indicator, but that variations in delivery alter the POC/respiration relationship.

It is possible to determine the relative importance of temperature versus organic matter quantity and quality effects on water column respiration by evaluating the relationship of carbon specific respiration

to environmental temperature. Since it is clear from pre-stratification data that vertical distribution of respiration is dependant primarily upon organic matter quantity and quality (see above), our analysis focused upon the later surveys. Nearfield and offshore stations exhibited a direct relationship between the rate of oxygen uptake per unit carbon and the environmental temperature (Figure 7-39). Based upon a linear regression of the data, carbon specific respiration increases by 2.5 fold for each 10°C increase in temperature (Q_{10}= 2.5). This temperature effect is smaller than the observed 4-5 fold difference carbon specific respiration and ca. 10 fold difference in gross respiration (Figure 7-35) between surface and bottom waters during stratification. It appears that during stratification, the higher rates of oxygen uptake in the surface versus bottom waters are most strongly influenced by the 3-4 fold higher POC concentrations (Figure 7-36), with the combined effect of ca. 10°C higher temperatures (Q_{10}= 2.5 fold increase, Figure 3.1.1) and organic matter quality (possibly 1.5-2.5 fold) accounting for the remaining difference. From this analysis, all three factors have a similar order of magnitude of impact in generating the ca. 10 fold higher rates of gross respiration in surface versus bottom waters, but with a rank order of: [POC] > Temp > POC quality. Therefore, during this interval when input of oxygen from surface waters is restricted, factors which increase either the delivery of labile organic matter to bottom waters or their temperature should serve to increase respiratory oxygen demands.

7.2.1.2 Seasonal Cycles of carbon fixation and remineralization

While water column mixing and stratification play the major role in mediating the vertical distribution of respiration rates through temperature and organic matter delivery, the ultimate factor controlling respiration is the mass of labile organic matter input from photosynthesis and from allochthonous sources. While the role of allochthonous sources requires further examination (see Section 9.3), it is clear that respiration within the euphotic zone generally parallels the measured rate of carbon fixation (Figure 7-40, 7-41). Major photosynthetic events generally exhibited proportional increases in respiration rates. This proportionality is particularly evident in the spring and fall blooms. Given the variability in daily photosynthesis with light field versus the greater temporal averaging which occurs in the factors controlling respiration rates, the photosynthesis/respiration relationship observed within the euphotic zone is reasonable (Figure 7-42, 7-43). Although variable, it appears that carbon fixation exceeds respiration within the euphotic zone throughout the year, but also that in-situ respiration remineralizes an amount nearly equivalent to fixation (see Section 9.2). As noted in the previous section, since almost all of the carbon fixed by photosynthesis occurs within the mixed layer, both organic matter quantity and quality are always highest within this zone (Section 7.1).

The near equivalence in organic matter production and remineralization within the euphotic zone (predominantly within the mixed layer), serves as a "biofilter" reducing organic matter transport to bottom waters during stratification. The lower bottom water respiration rates found throughout the nearfield and offshore stations during stratification are consistent with a low delivery of organic matter (Figure 7-44). However, as stated above, factors which increase organic matter delivery can increase oxygen uptake from

bottom waters. One such event may have been associated with the centric diatom bloom during September 1995, surveys 12 and 13. The spike in bottom water respiration during survey 13 (Figure 7-39, 7-40, 7-44) may have been related to delivery of bloom material to bottom waters as the bloom underwent senescence (see Figure 8.4). The die-off of the centric diatom bloom coincided with the initial breakdown of stratification which provides a mechanism for increased vertical transport. However, it is also possible that the high zooplankton populations during this bloom also facilitated vertical transport through fecal pellet formation (Figure 8-23).

Under existing conditions, seasonal variations in bottom water oxygen uptake appear to be dominated by the availability of organic matter (with secondary temperature effects). High rates of bottom water respiration occur during the unstratified intervals when vertical transport of POC is uninhibited and carbon fixation from the winter high production period and spring and fall blooms is greatest. In contrast, during the stratified period, bottom water respiration remains low, consistent with the generally small pool of chlorophyll *a* and low rates of photosynthesis within the mixed layer (see Section 7.1). During stratification, the vertical transport of organic matter to deeper water is restricted both by the strong pycnocline and by the significantly increased respiratory capacity of the surface waters, due to the warmer summer temperatures (Q_{10}=2.5). These data are discussed relative to annual carbon balance in Chapter 9.

7.2.1.3 1992 - 1995 Interannual comparison

Water column respiration rates were not a focus of study during the 1992-1994 monitoring effort. As a result interannual comparisons are limited. In addition, since respiration was measured on only six surveys interannual seasonal comparisons are not supported. However, sufficient data exist from 1994 (Kelly and Doering, 1995) from which to make some general observations. However, no bottom water respiration data were collected during 1994.

While the data are variable, surface water respiration rates in 1994 and 1995 within the nearfield were generally higher than offshore, consistent with the lower levels of chlorophyll *a* at the offshore stations (Figure 5-11, 5-12). In addition, the general trend of significantly higher respiration rates in surface versus deeper waters was observed in both years. However, the vertical distribution of respiration rates was not as obvious in 1994 between nearfield and offshore stations (e.g., Figure 19 in Kelly and Doering, 1995). Unfortunately, the limited sampling does not allow a rigorous comparison of rates in mixed versus stratified water column. However, the magnitude of the model-projected bottom water respiration in 1994 was higher than that measured in 1995 (Kelly and Doering, 1995). The lowest nearfield projected rate in 1994 was ca. 0.05 mg O_2/L/d, while the average bottom water measured rate during stratification in 1995 was 0.016-0.017 mg O_2/L/d. Due to the lack of correlation between surface and bottom water respiration rates evident in the 1995 data (Figure 7-34), it is unlikely that the modeled 1994 bottom water rates (based on surface water measurements) are sufficiently robust to allow inter-annual comparisons.

If the projected bottom water respiration rates in 1994 were accurate, the cause for the higher rates is unknown. It does not appear to be related to concentrations of POC (Figures 7-45) which were higher in 1995 when measured rates were lower. Nor does the difference in respiration relate to differences in temperature during sampling (Figure 3-4). It is most likely that the rate differences result from the limited data set in 1994 which did not capture the sharp decrease in respiration from surface to bottom waters, and the fact that consideration was not given to seasonal differences (all data were pooled). Modeling vertical changes in rates requires that the temperature and organic matter quality and quantity show constant differences year-round. It is now clear that these factors controlling respirations rates show significant differences between stratified versus vertically mixed periods.

7.2.2 Sediment Respiration

Annual oxygen uptake by benthic sediments is a measure of total community metabolism, the total organic matter turnover within the benthos. Total community metabolism includes the respiration of benthic animals and plants, as well as carbon remineralization by heterotrophic micro-organisms. Sediment respiration is similar to water column respiration in that it is controlled primarily by the availability of decomposable organic matter and *in situ* temperature. However, it differs in three major aspects. First, sediments can accumulate organic matter inputs over relatively long periods and therefore allow cumulative increases in oxygen uptake as organic matter is deposited over periods of weeks to months. Organic particles within the water column typically have relatively short residence times, especially in the non-turbulent waters below the pycnocline. Therefore, deposition into sediments represents the mechanism for potential carry-over of Fall or Spring bloom material into the stratified period. Second, the water column throughout the nearfield and Stellwagen Basin appears to be fully oxygenated, whereas, oxygen penetration into the sediments of these systems is relatively shallow (centimeters). The result is that in the sediments unlike the water column, a fraction of the organic matter decay is through anaerobic microbial processes, such as denitrification and sulfate reduction. Denitrification, although at present not a major pathway for carbon mineralization, represents an important potential sink for fixed nitrogen, particularly if concentrations of nitrate in the overlying water increase (Section 4).

Within deeper sediments, sulfate reduction produces sulfide as an end-product, some of which is permanently stored within the sediments as metal sulfides but most of which is re-oxidized to sulfate on an annual basis. However, due to the time-lag between sulfide formation in the deeper anoxic layer and oxidation of sulfide by surface exchanged oxygen, single time-point estimates of the rate of surface oxygen uptake can either over or underestimate the rate of carbon mineralization taking place. In most systems, an amount equivalent to the mass of sulfide produced over the course of a year is oxidized each year (except for the amount buried), the annual oxygen uptake rate reflects the annual carbon remineralization rate.

Furthermore, in systems like present Massachusetts Bay, carbon flow through sulfate reduction is almost certainly small relative to aerobic processes and therefore errors due to the sulfide oxidation time-lag are likely very small even on single time-point samples. Increases in the mass of total reduced sulfur and/or non-pyritic reduced sulfur over several years has been suggested as an indicator of an increase in the rate of organic matter loading to sediments. While reduced sulfur pools can reflect loading rates, they represent the residue of the much larger reduction-oxidation cycle. In contrast, annual sediment oxygen uptake rates represent the total carbon remineralization rate which should be a direct indicator of the annual loading of decomposable organic matter to the benthos.

Third, while both water column and sediment oxygen uptake affect bottom water oxygen levels, water column uptake is distributed throughout the hypolimnion, whereas sediment uptake is concentrated at the sediment-water interface. Only through mixing, diffusion etc. does sediment oxygen uptake interact with the full hypolimnion. The result is that the deepest waters of a system typically contain the lowest concentrations of oxygen on an annual basis. This increased oxygen depletion with depth (where it occurs) is also influenced by the increasing distance from the oxygen "source" in the overlying mixed layer. In addition, sediment oxygen dynamics are important on an ecological basis in that where low oxygen or high sulfide levels occur, infaunal populations, hence food chain dynamics, are affected.

For all of the above reasons and that sediments can be reliably re-sampled over a prolonged interval, sediment oxygen and nutrient dynamics have been measured over several years, and in 1995 at 4 stations on 5 occasions. Current issues involve the role of sediments (with water column respiration) in system carbon/nutrient mineralization and bottom water oxygen depletion and their sensitivity as an indicator of organic matter loading rates.

7.2.2.1 Harbor versus Massachusetts Bay

Rates of sediment oxygen uptake reflect the level of organic matter loading. Within the marine system, increasing water depth is generally associated with decreasing organic loading and sediment respiration as a higher and higher percentage of the organic matter is degraded during transport through the water column. Similarly, within the coastal zone, organic matter loading to sediments tends to decrease with increasing horizontal distance from shore, creating a parallel trend in sediment respiration. Both vertical and horizontal effects on sediment oxygen uptake reflect linkages between carbon fixation-transport-decay.

Within Massachusetts Bay, water column respiration accounts for more than two times the carbon mineralization of the sediments. This results from the higher temperatures and more labile carbon within the water column (see above, Figure 7-46). The importance of water column respiration within Massachusetts Bay, also, includes the mixed layer where turbulence maintains particles in suspension, which coupled with summer temperatures, helps to degrade organic matter before it can reach the bottom waters and finally the sediments. In contrast, while water column respiration in Boston Harbor is higher

than Massachusetts Bay (reflecting the higher POC levels and higher temperatures), the shallower water column promotes rapid delivery to the sediments which results in proportionally higher sediment respiration rates. This is also supported by the lack of a temperature gradient from surface waters to sediments. The apportioning of respiration is seen both in areas with amphipod mats, which are likely cycling some of the older sediment accumulation in addition to freshly deposited organic matter, and in areas where infaunal activity is minimal (QB).

Since Boston Harbor has shallower water (about 10m) than the stations of Massachusetts Bay (about 33m), the rate of water column respiration per unit volume is lower within the Bay. The lower per volume water column rate and sediment rate reflects both the lower temperatures and lower organic matter production within the Bay versus the Harbor. Increasing production within the mixed layer of Massachusetts Bay is likely to produce at least proportional increases in water column and sediment respiration. However, to the extent that increased deposition occurs just prior to stratification or that vertical transport during stratification is enhanced, bottom water oxygen deficits will be affected by both respiratory processes.

7.2.2.2 Seasonal cycle

Sediment oxygen uptake within the sediments of the western nearfield and Stellwagen Basin show a seasonal cycle linked to temperature and organic matter availability. All sites showed increasing oxygen uptake with increasing bottom temperatures. However, the major increase in respiration appeared to occur between late-May and July, which may reflect deposition of the Spring bloom as little temperature increase occurred during this interval. The temperature cycle was very different from that of the surface waters (see Section 3). Temperature was highest on the last survey in early October near the time of overturn (Figure 3-1C).

The effect of the temperature cycle is to produce the highest rates of respiration during the stratified period and fall bloom. The effect of the colder pre-stratification waters should be to help to "preserve" freshly deposited spring bloom material until waters warm. This warming occurs post-stratification. The effect of the warmer sediments during the fall bloom should be to promote the degradation of freshly deposited bloom material. Given the temporal sequence, much of the fall bloom should be degraded prior to the onset of stratification the following spring and summer. Since mixing occurs at the fall bloom (and appears to be related to it, cf. section 7.1), the effect of the fall bloom on bottom water oxygen deficit is unclear. Given the significance of benthic respiration to the overall bottom water oxygen balance during stratification and the seasonal distribution of rates, it is likely that the spring bloom plays a more important role in oxygen deficits than the fall bloom. As stated for water column respiration (section 7.2.1.2), factors which increase delivery of organic matter through the pycnocline during stratification should result in increases in the level of annual oxygen depletion in bottom waters of both the nearfield and Stellwagen Basin. Without further analysis of the potential lability of the organic matter thus delivered, it is not possible to determine the proportional increase in oxygen deficit per unit carbon deposited.

7.2.2.3 1993-1995 interannual comparison

Sediment oxygen uptake has been assayed within Massachusetts Bay and Stellwagen Basin as part of the pre-discharge monitoring program for the past few years. In 1995 the sampling program focussed upon fewer sites than previous years, but larger numbers of replicate assays (four vs. two or three) per station for each of the five sampling events. In addition to using measured sediment fluxes as a sensitive indicator of potential changes in future organic matter loading rates, we intensified the focus upon the role of sediment oxygen uptake in bottom water oxygen balance (Chapter 9).

Sediment oxygen uptake is highest from July to October within the western nearfield and Stellwagen Basin (flux stations F19-MB05; Figure 7-47). As indicated above, the elevated rates are due not just to the temperature but also organic matter availability. These late season rates are those most critical to bottom water oxygen deficit as they occur during the interval of water column stratification. Unlike bottom water column respiration (Figure 7-35) which is lowest during stratification, sediment respiration is highest when ventilation of bottom waters is lowest and the rate of bottom water oxygen decline is highest (Section 6).

It appears that there is little interannual variation in sediment oxygen uptake during the critical stratified period within the western nearfield (Figure 7-48). Comparing the mean July-August rates for 1993 and 1994 showed only a slight enhancement (<15%) over 1995 values. The relative constancy of these interannual measurements suggests that metabolic rate measurements within the sediments should provide a sensitive indicator of increases or decreases in organic matter loading rates. Samples from Stellwagen Basin (MB05) showed greater variation. MB05 was measured in August, but not July in 1993 and 1994. Given the difference in 1995 rates at MB05 from July (10.5 $mMm^{-2}d^{-1}$) to August (6.8 $mMm^{-2}d^{-1}$), the higher (July) rates in 1995 agreed well with the previously measured August rates. The cause of the lower rate at this site in August 1995 is presently unclear, and underscores the need for multiple samples during the stratified period for making interannual comparisons.

Given the apparently low quality organic matter generally reaching the bottom (Figures 7-37 and 7-38), a small enhancement (about 20%) in the quality or quantity of organic matter should be detectable. Additional sediment indicators (such as Eh, nutrient regeneration, infauna etc.) should also be used. However, the oxygen uptake results confirm the need for seasonal sampling, especially within Stellwagen Basin.

Station	Measured Annual Production			Potential Annual Production		
	Sampling Rate		Percent Increase	Sampling Rate		Percent Increase
	6x per yr	17x per yr		6 x per yr	17x per yr	
N04	279	310	11	285	390	37
N07	330	?	?	330	?	?
N16	311	424	36	305	544	78

Table 7-1

Effect of sampling frequency of measures of annual primary production. Production is expressed in $gCm^{-2}y^{-1}$. Percent increase is computed from high resolution production rate/low resolution production rate x 100.

W9515 Station N04

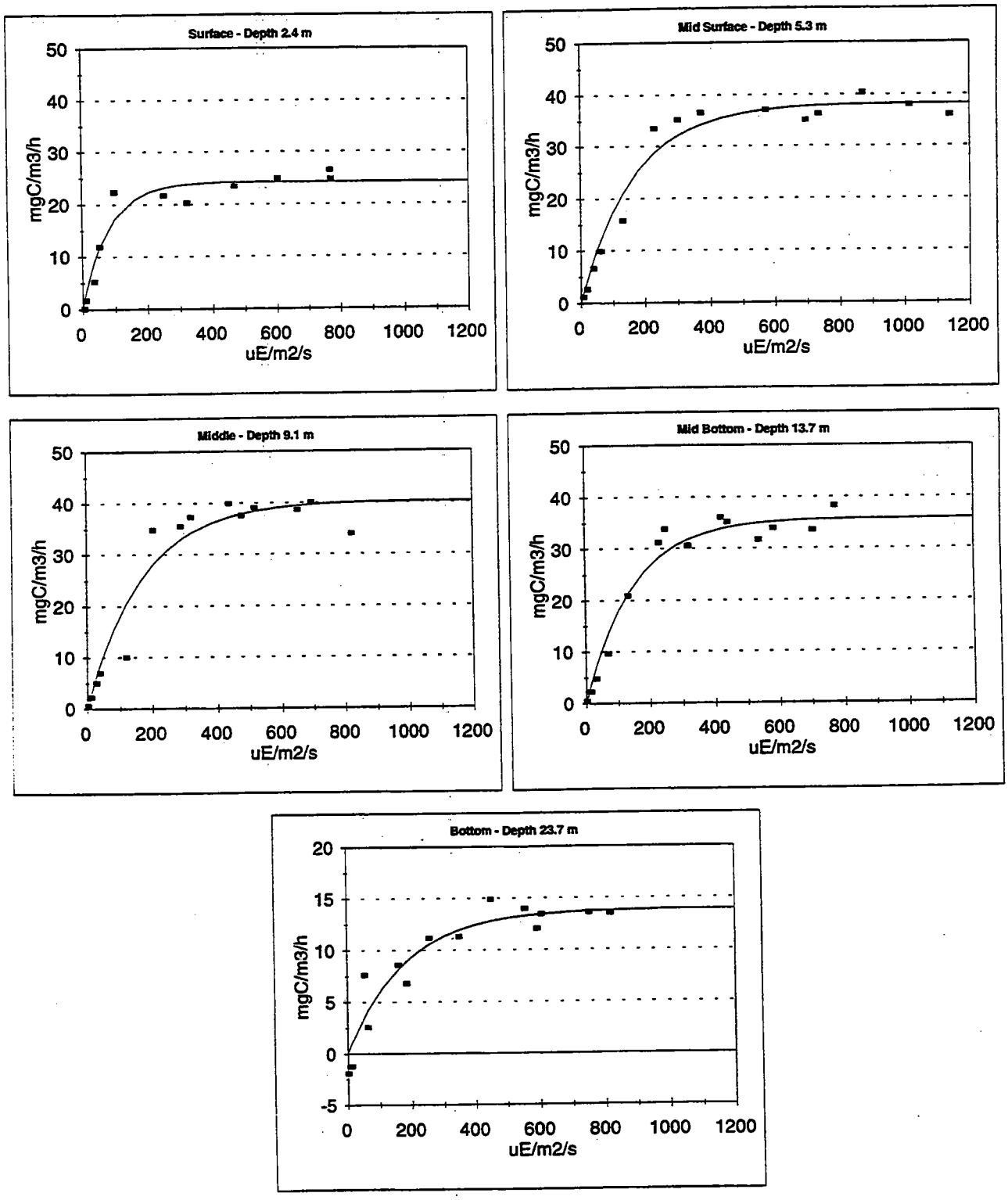

Figure 7-1

P-I curves of hourly production. These curves were used to obtain best fit estimates of α" [$mgCm^{-3}h^{-1}(mEm^{-2}s^{-1})^{-1}$] and Pmax" ($mgCm^{-3}h^{-1}$).

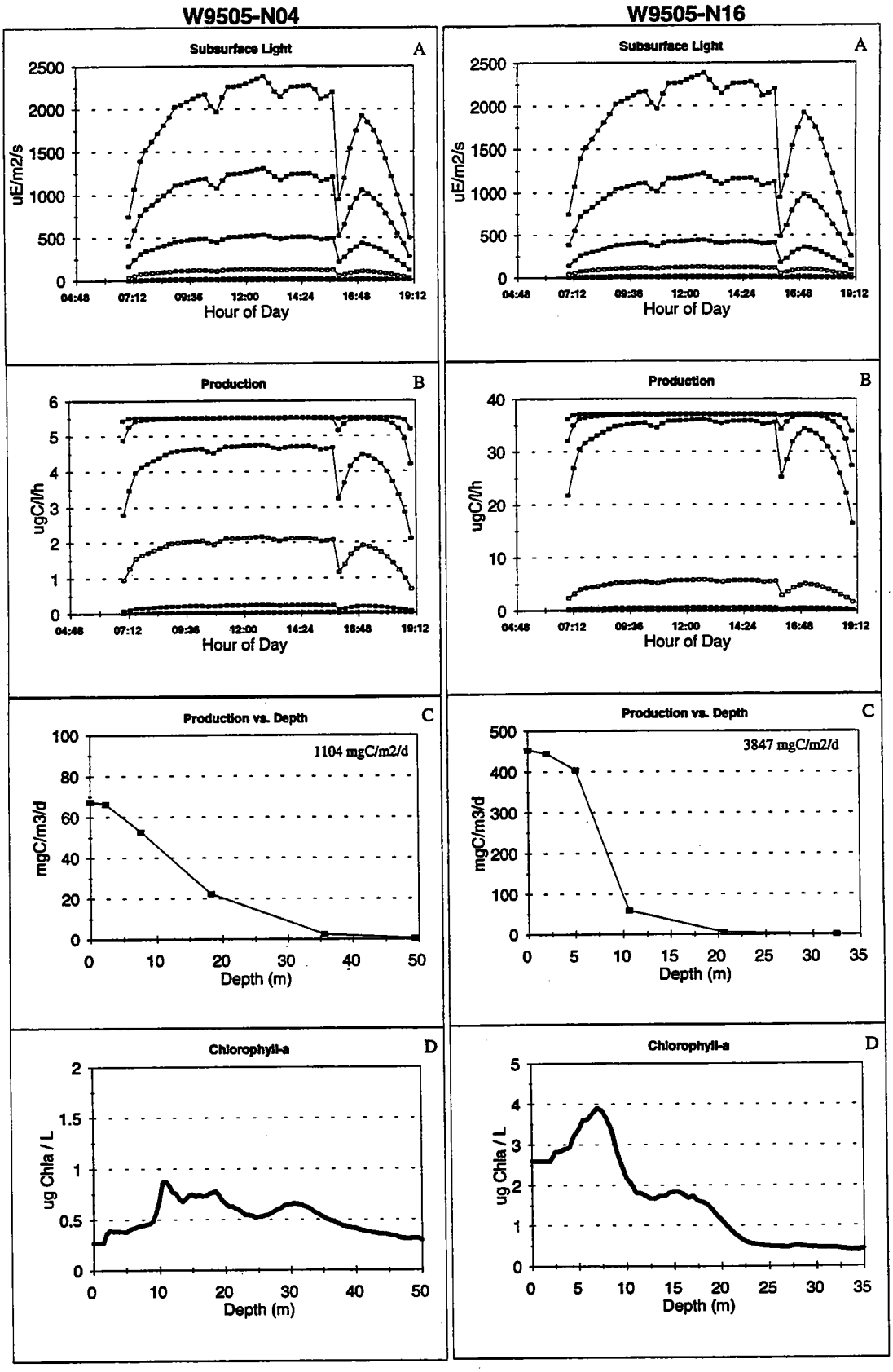

Figure 7-2

Example of typical 14-C phytoplankton results. Panel A, scalar irradiance over the course of the day. Panel B, hourly production determined from P-I relationships and in situ light intensity at 15 minute intervals throughout the day (includes model-derived 0 m depth rate). Panel C, daily production at each sampling depth determined by integration of hourly production from 0700 – 1900 (EDT). Inset, areal production determined by integration of depth-dependent daily production curve. Panel D, calibrated chlorophyll-*a* curve used to compute chl-specific P-I relationships and chl-specific production.

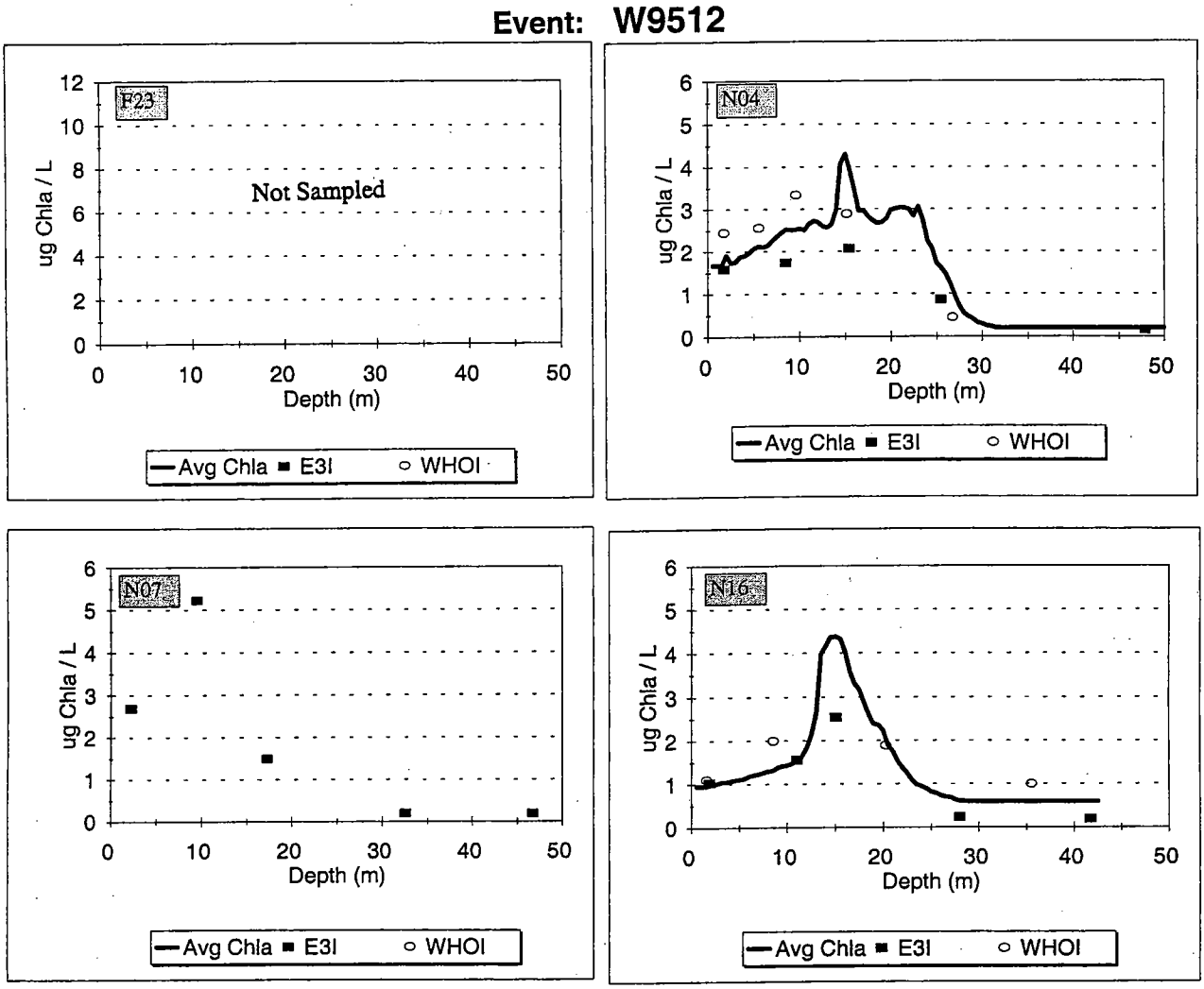

Figure 7-3

Chlorophyll-a profiles for Stations F23, N04, N07, N16. The continuous fluorometer profiles were averages of least 2 and sometimes 3 CTD downcasts and calibrated against Niskin samples that were obtained during the hydrocast, filtered aboard ship, extracted and analyzed in the laboratory (symbols). Results of analyses of two laboratories (E3I, fluorometric analysis; W.H.O.I., spectrophotometric analysis) are presented (see Methods for details).

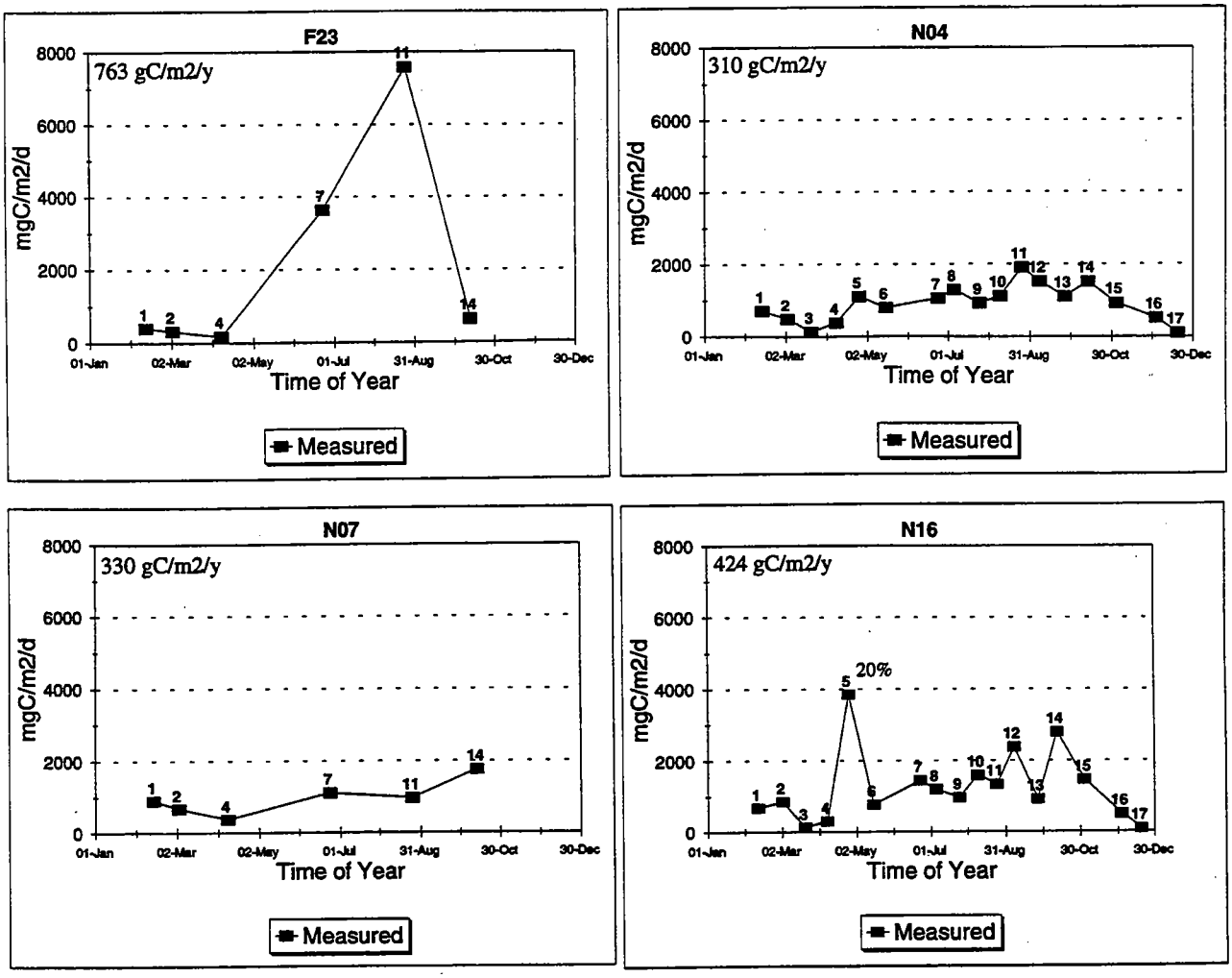

Figure 7-4

Areal production over the 1995 season. Production was computed using the incident light regime on the day of the cruise. Cruise numbers are indicated by the numbers above each datum point. Annual production for indicated station is shown in the inset of each panel.

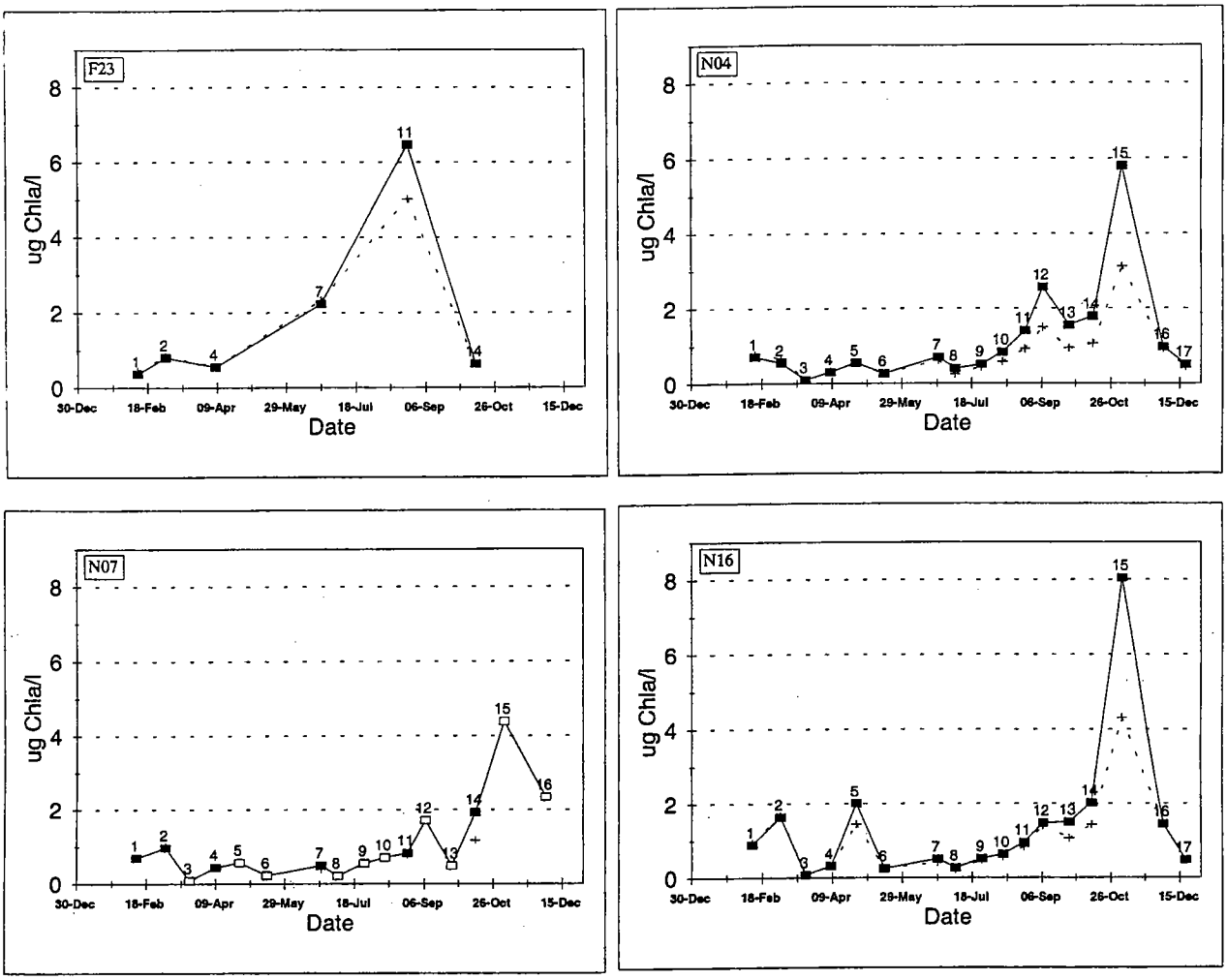

Figure 7-5

Chlorophyll distribution in 1995 at the harbor edge and outer nearfield. Squares, average chlorophyll-a concentration in the photic zone above the 0.5% light level. Closed squares, averages computed from calibrated CTD profiles. Open squares, averages computed from data interpolated at 2 m intervals from discrete chlorophyll-a analyses (see N07 data in Figure 7-3). Crosses, average chlorophyll-a concentration in the entire water column.

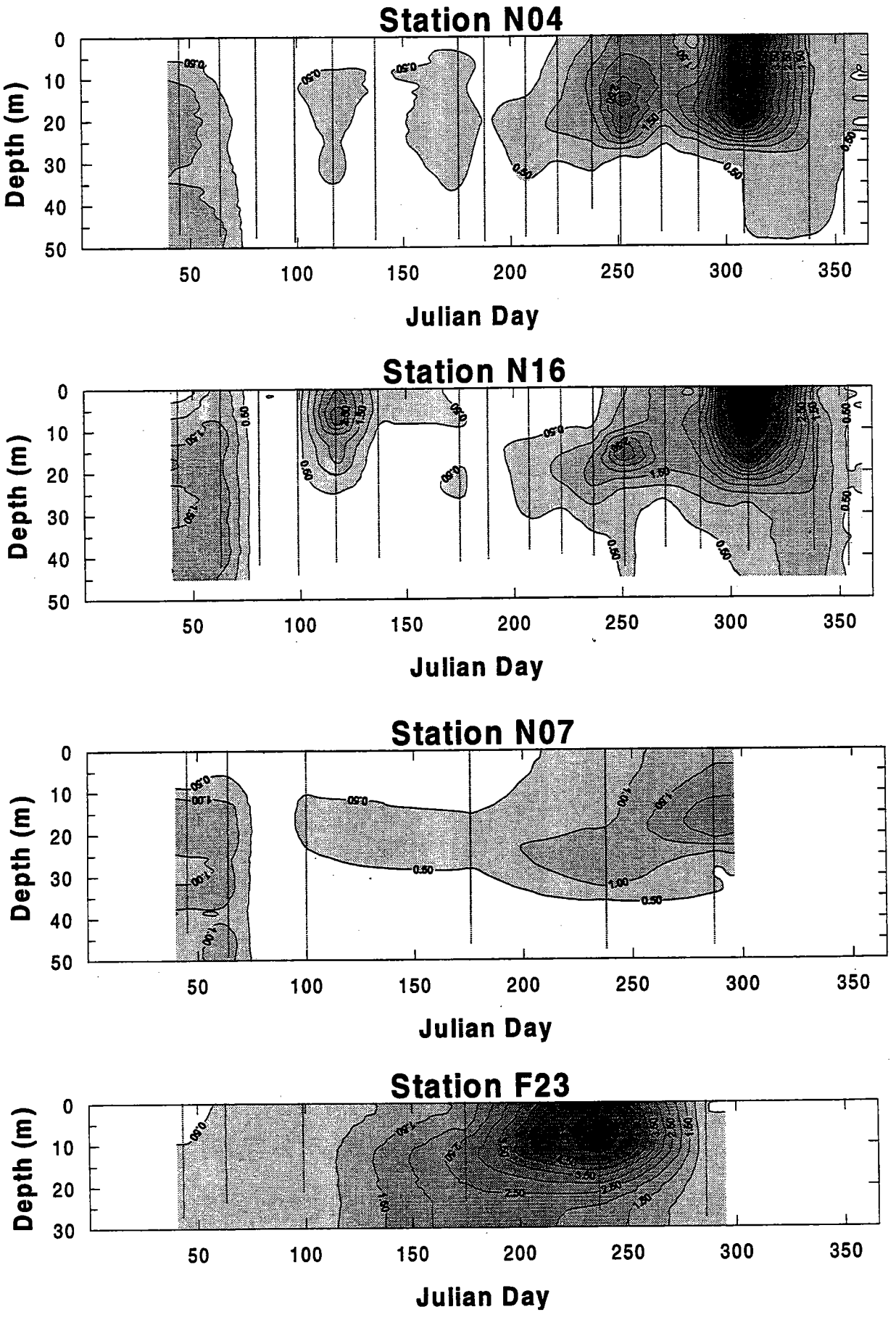

Figure 7-6

Chlorophyll-a distribution in the water column of the harbor edge and outer nearfield region. Dotted vertical lines represent date and depth of fluorescence measurement.

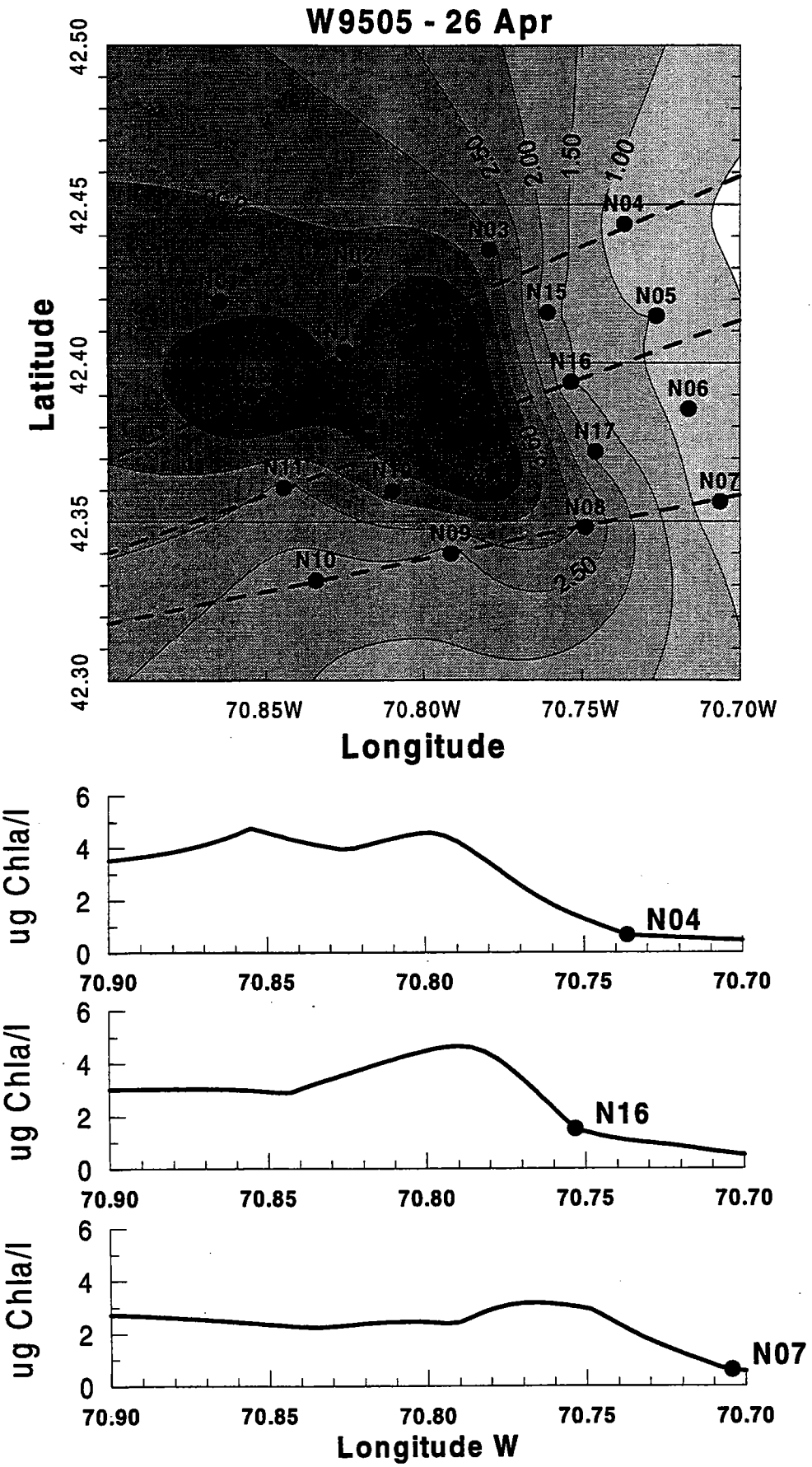

Figure 7-7

Distribution of average water column chlorophyll-a in the Nearfield. Lower panels are longitudinal projections of the sections indicated by the dashed lines in upper panel. To the left transects point toward the mouth of Boston Harbor.

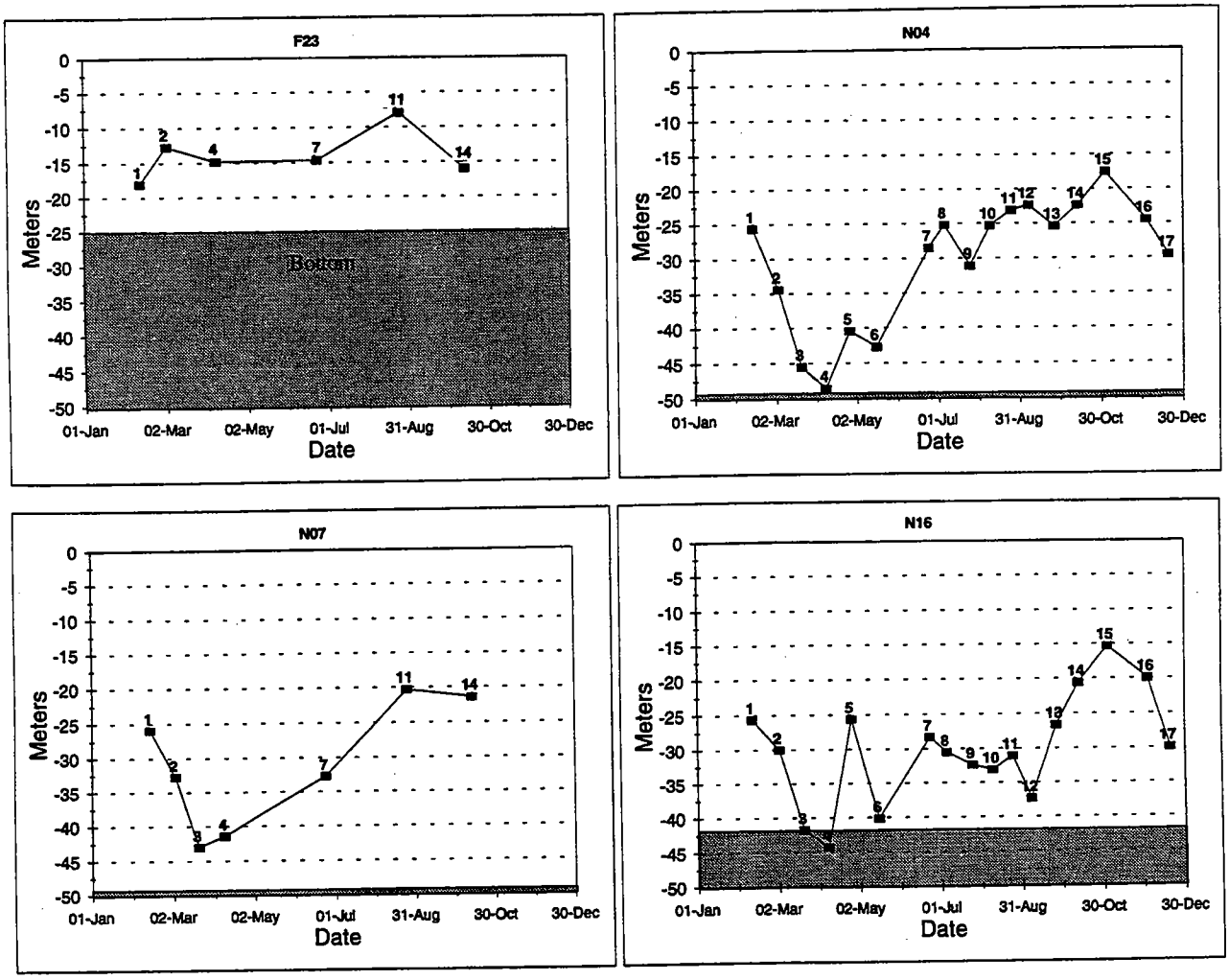

Figure 7-8

Depth of the photic zone as defined by the 0.5% light level. Cruise numbers indicated above each datum point. Data extending below the sediment surface is extrapolated from water column properties. In reality the photic zone extends to the sediment surface.

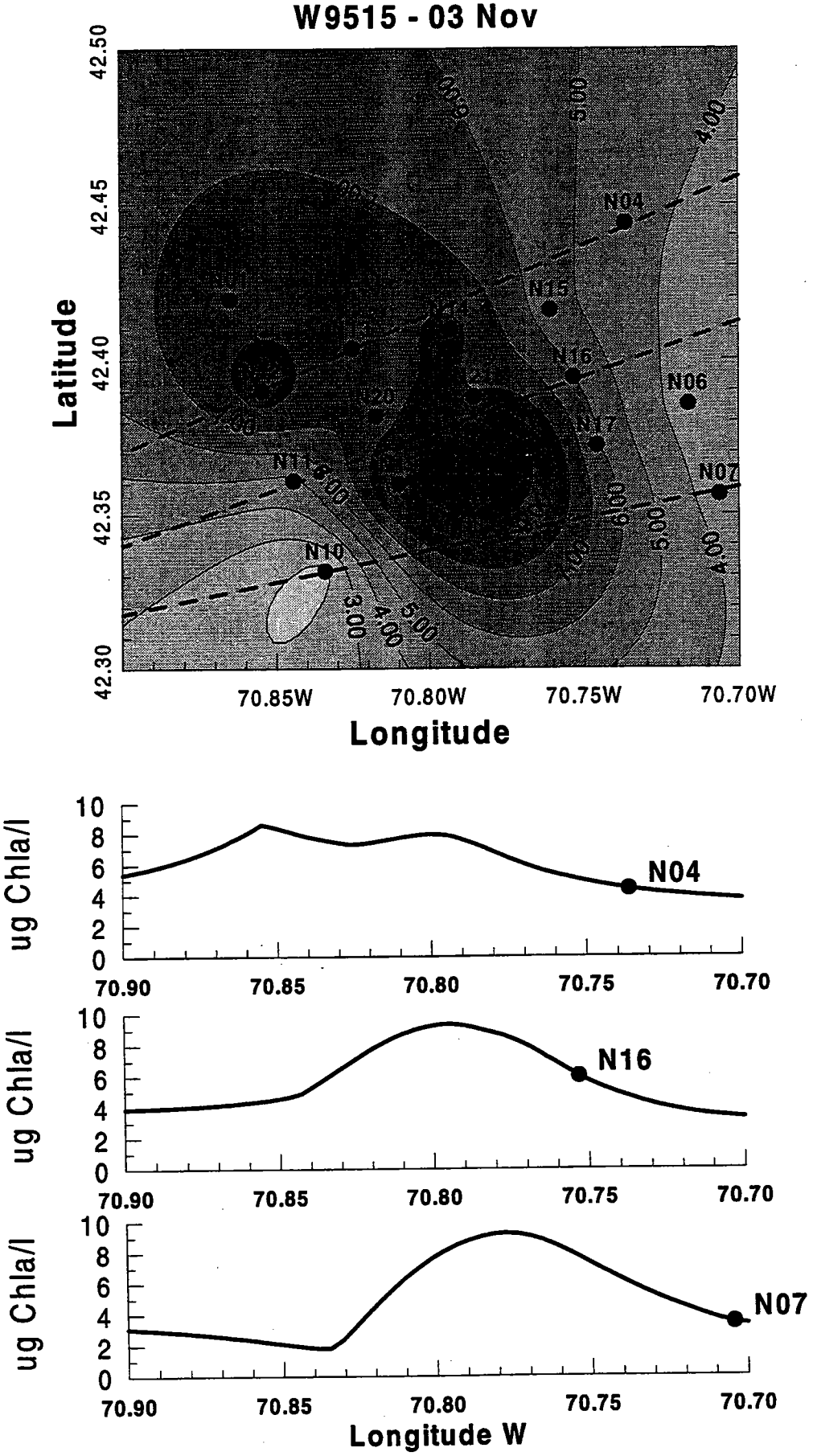

Figure 7-9

Distribution of average water column chlorophyll-a in the Nearfield. Lower panels are longitudinal projections of the sections indicated by the dashed lines in uper panel. To the left the transects point toward the mouth of Boston Harbor.

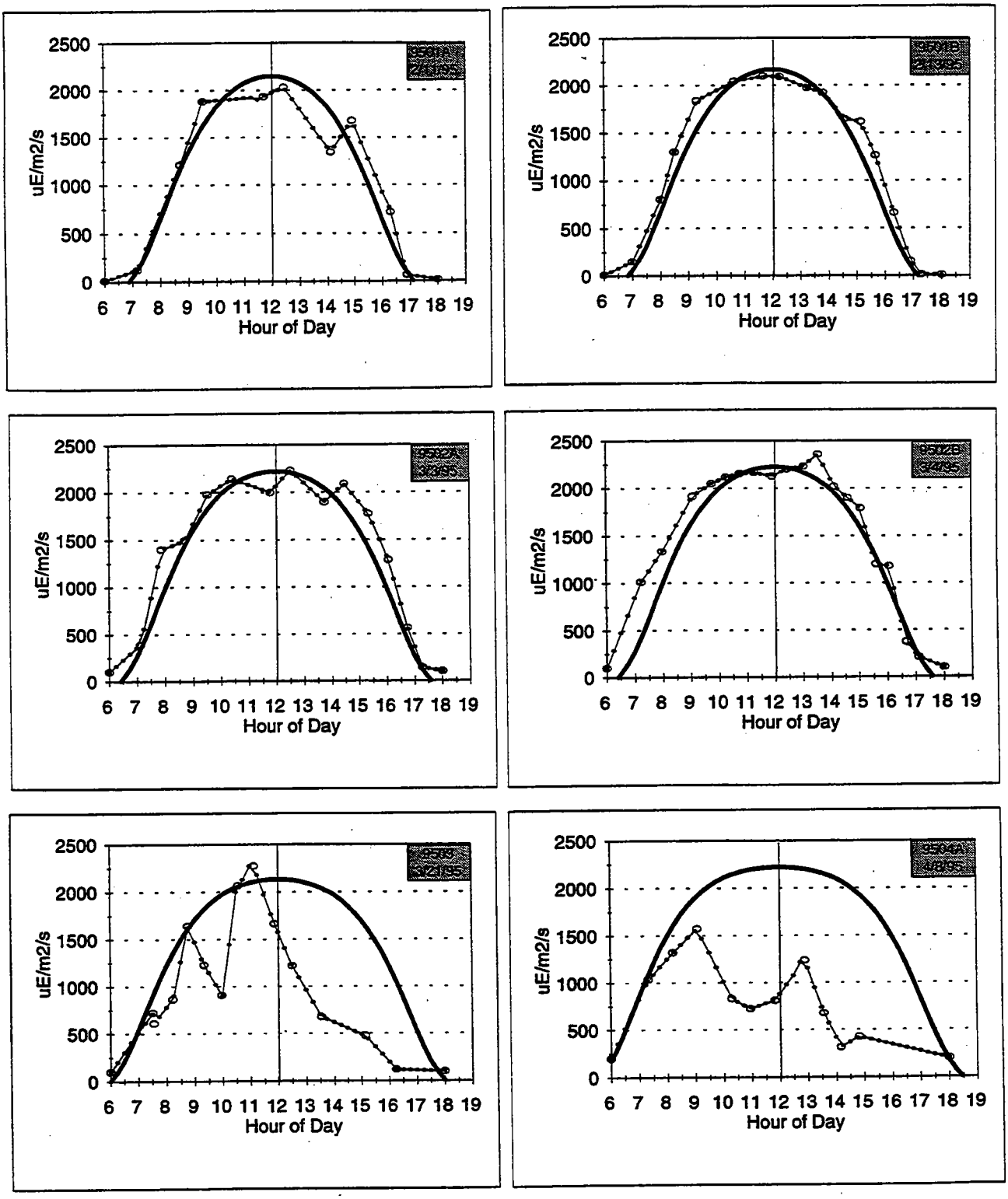

FIGURE 7-10A

Photoperiod light field over the course of the day on the dates of phytoplankton production measurements. Open circles, ship-based measurements of scalar irradiance. Heavy lines, theoretical cloudless day scalar irradiance. Cloudless day irradiance (PAR, 400-700 nm) was estimated using a BASIC program to effect the computations of the model described by Gregg and Carder, 1990, followed by transformation to scalar irradiance.

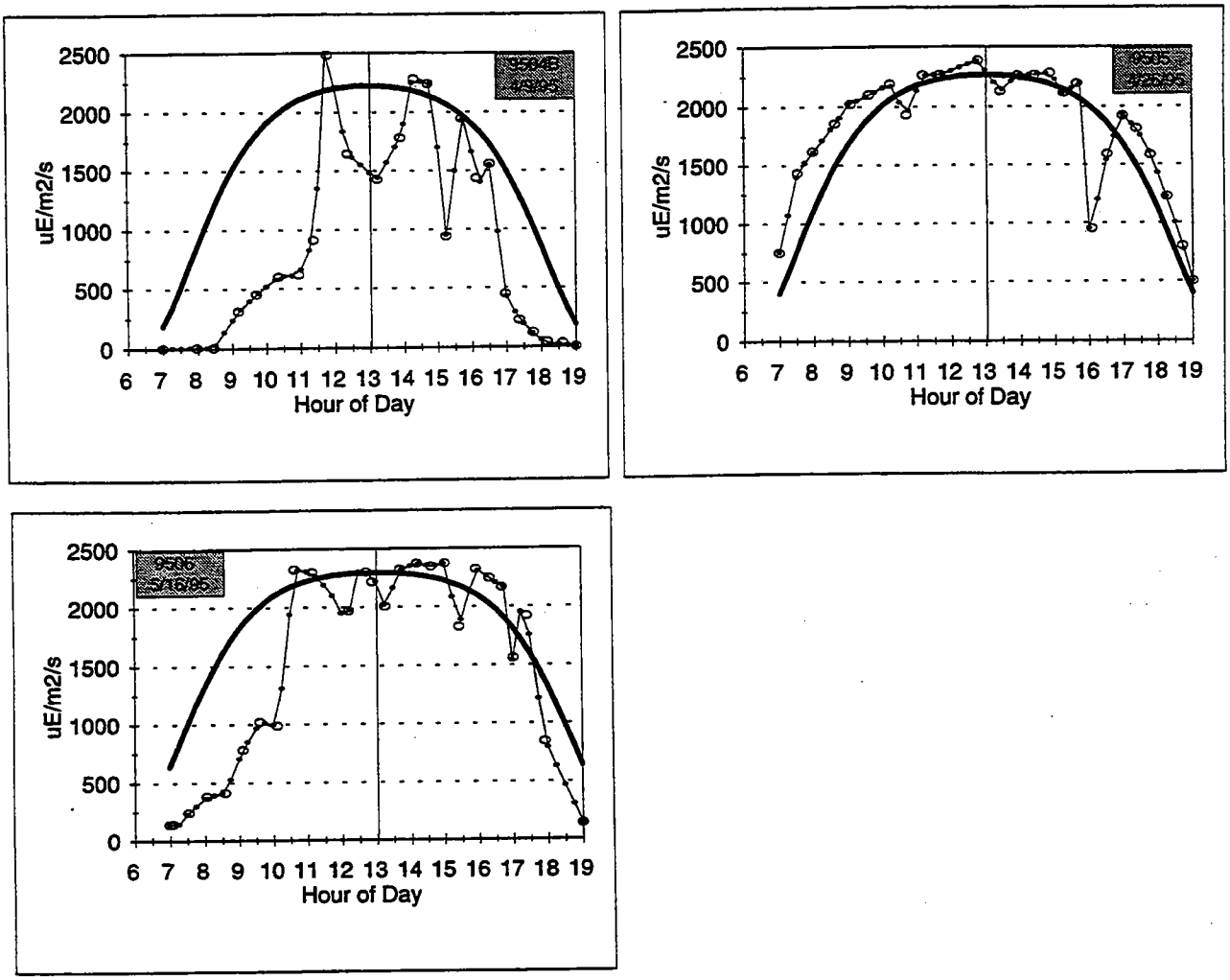

FIGURE 7-10B

Photoperiod light field over the course of the day on the dates of phytoplankton production measurements. Open circles, ship-based measurements of scalar irradiance. Heavy lines, theoretical cloudless day scalar irradiance. Cloudless day irradiance (PAR, 400-700 nm) was estimated using a BASIC program to effect the computations of the model described by Gregg and Carder, 1990, followed by transformation to scalar irradiance.

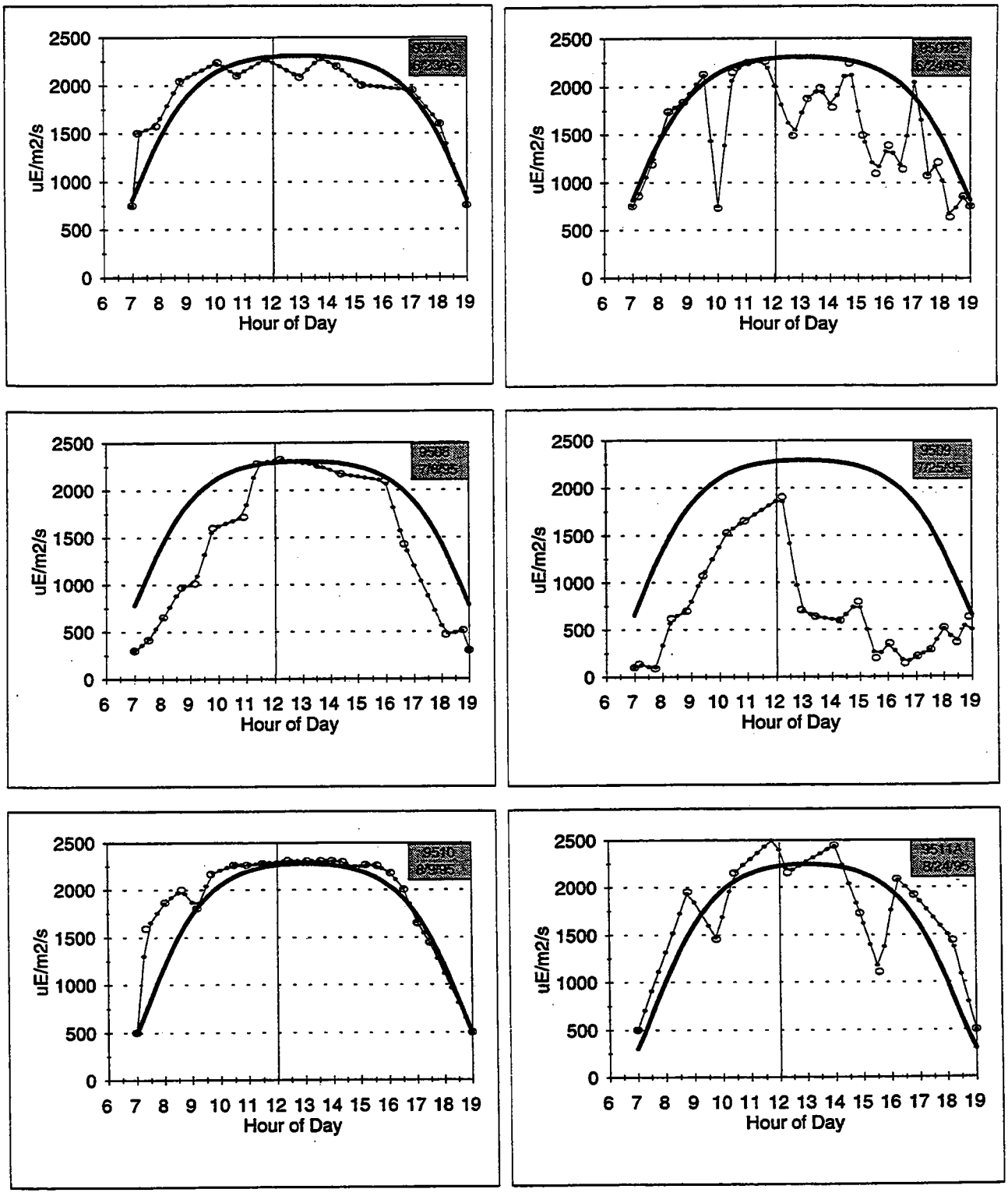

FIGURE 7-10C

Photoperiod light field over the course of the day on the dates of phytoplankton production measurements. Open circles, ship-based measurements of scalar irradiance. Heavy lines, theoretical cloudless day scalar irradiance. Cloudless day irradiance (PAR, 400-700 nm) was estimated using a BASIC program to effect the computations of the model described by Gregg and Carder, 1990, followed by transformation to scalar irradiance.

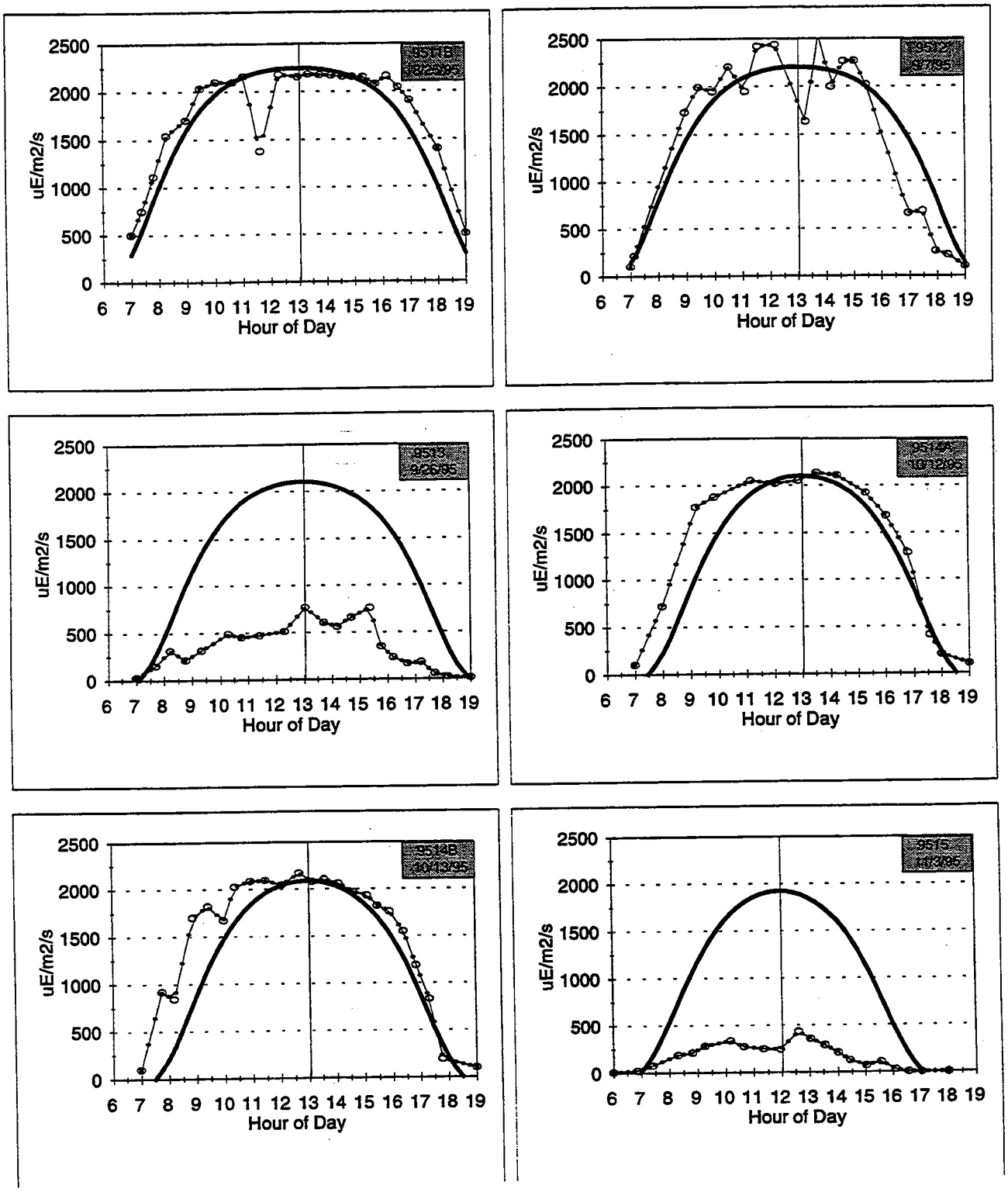

FIGURE 7-10D

Photoperiod light field over the course of the day on the dates of phytoplankton production measurements. Open circles, ship-based measurements of scalar irradiance. Heavy lines, theoretical cloudless day scalar irradiance. Cloudless day irradiance (PAR, 400-700 nm) was estimated using a BASIC program to effect the computations of the model described by Gregg and Carder, 1990, followed by transformation to scalar irradiance.

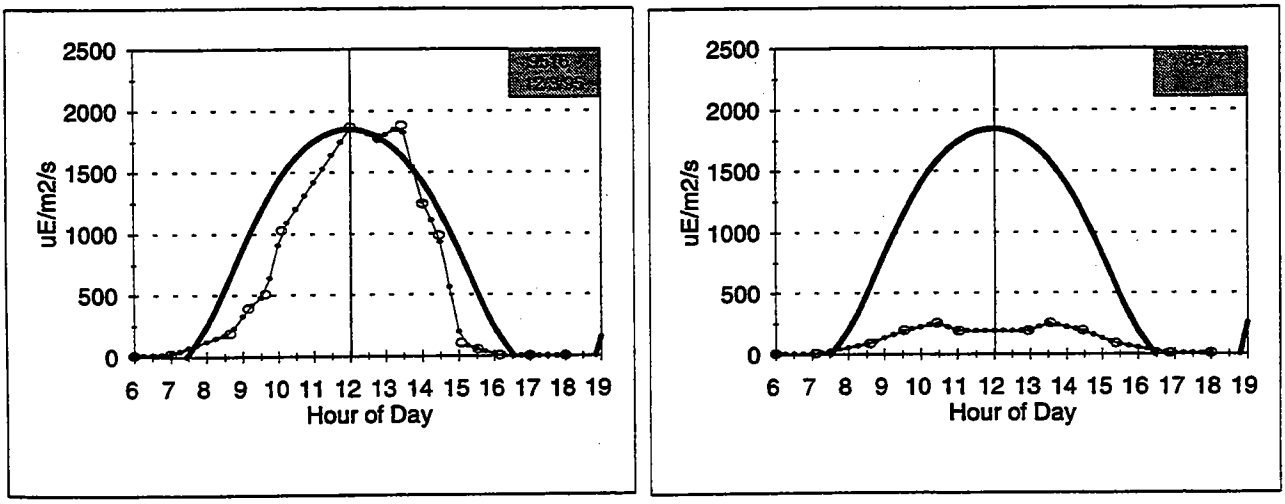

FIGURE 7-10E

Photoperiod light field over the course of the day on the dates of phytoplankton production measurements. Open circles, ship-based measurements of scalar irradiance. Heavy lines, theoretical cloudless day scalar irradiance. Cloudless day irradiance (PAR, 400-700 nm) was estimated using a BASIC program to effect the computations of the model described by Gregg and Carder, 1990, followed by transformation to scalar irradiance.

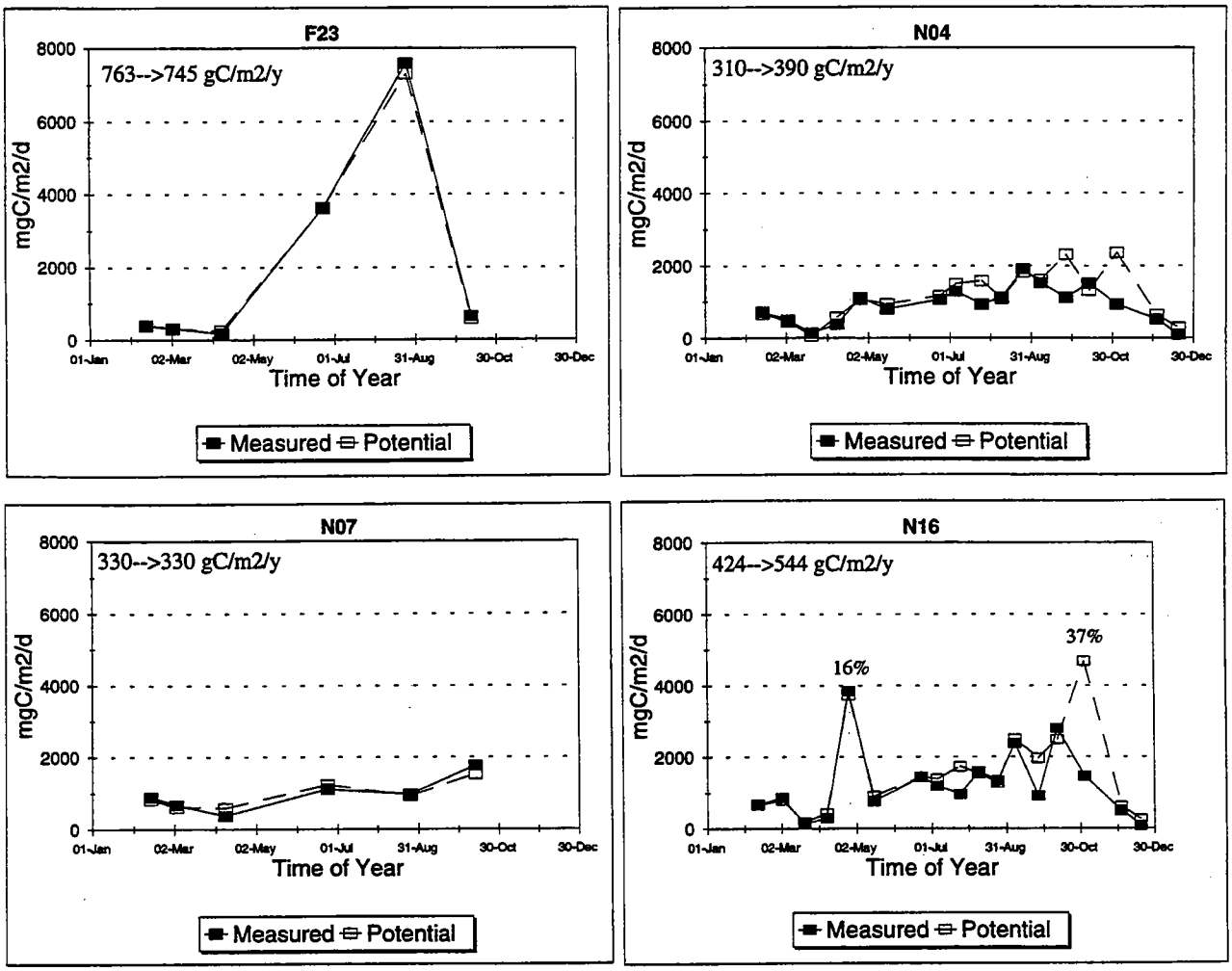

FIGURE 7-11

Areal production and potential production for the 1995 season. Areal production is as presented in Figure 7-7. Areal potential production was computed using a theoretical incident light regime that is equivalent to a cloudless day at the indicated time of the year. Annual production and potential annual production is indicated by the range respectively depicted in the inset of each panel.

Production

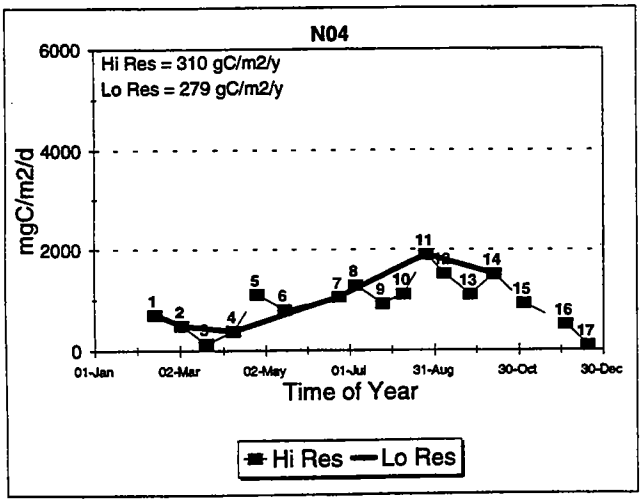

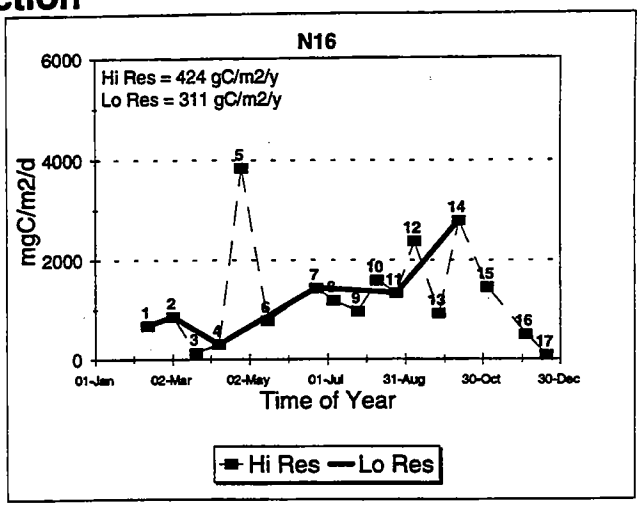

Potential Production

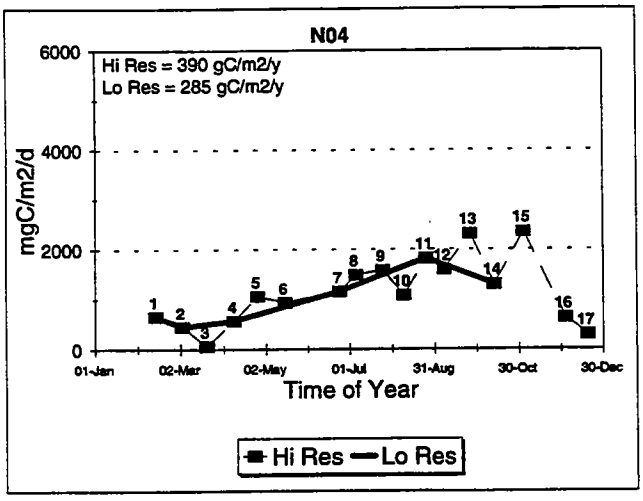

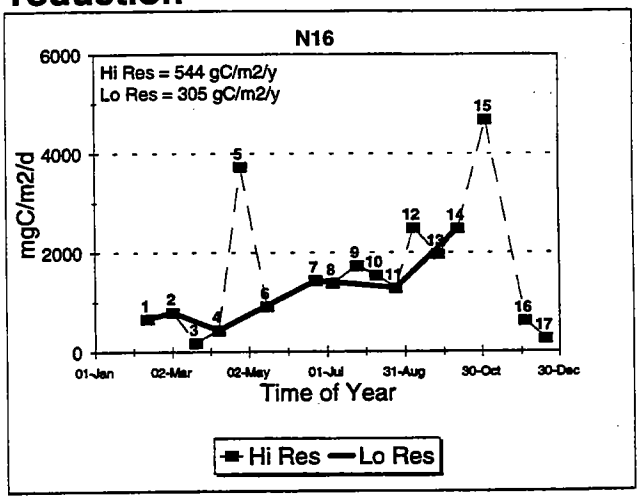

FIGURE 7-12

Comparison of Areal production over the 1995 season when sampled 6 times per year vs. 17 times per year. Production was computed using the incident light regime on the day of the cruise. Potential production was computed using a theoretical incident light regime that is equivalent to a cloudless day at the indicated time of the year. Annual production and potential annual are indicated in the inset. Cruise numbers are indicated by the numbers above each datum point.

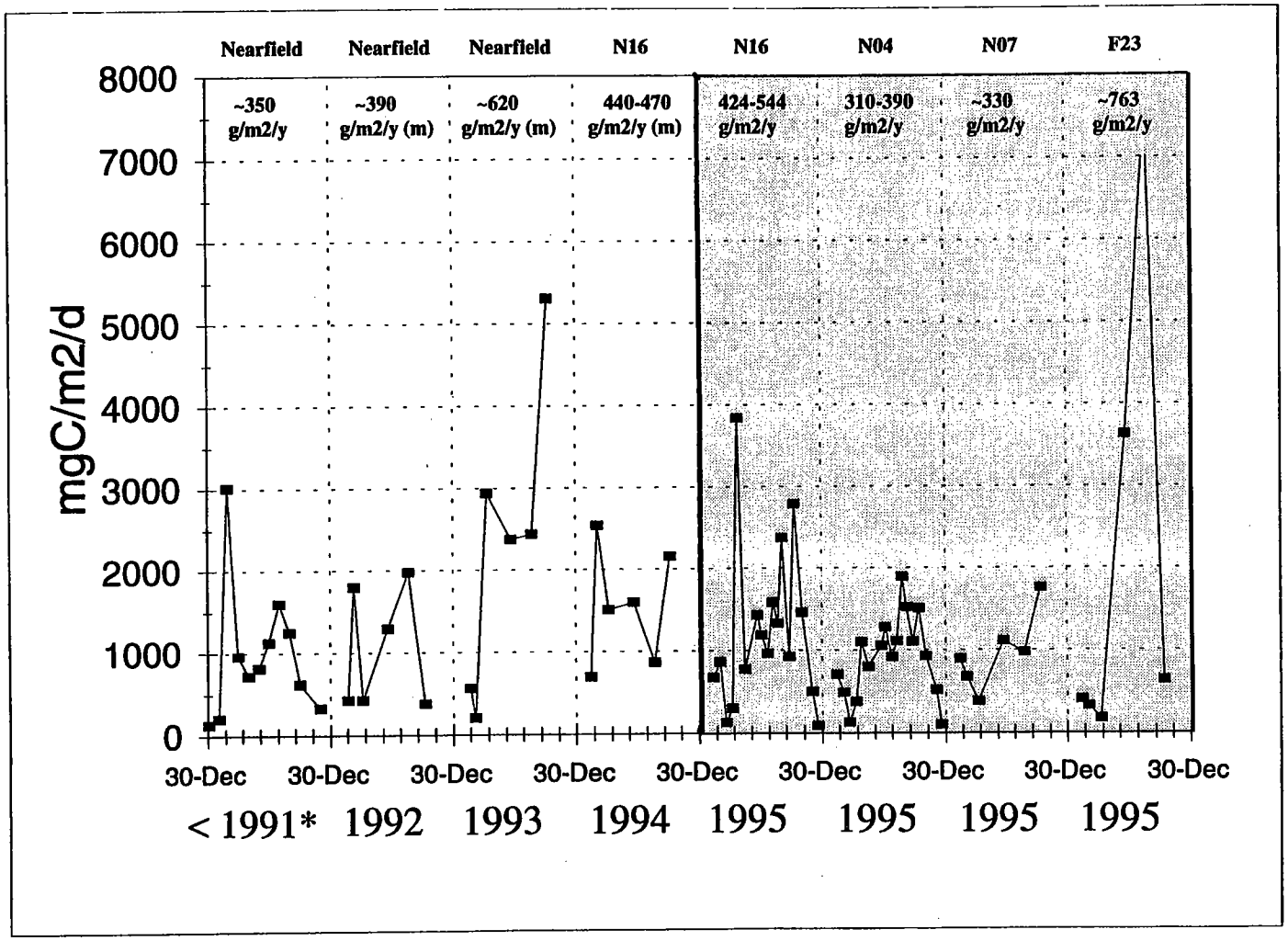

Figure 7-13

Measured phytoplankton production from 1991–1995. Data for 1995, present study. Data for 1992-1994 from Kelly and Doering, 1995. *Data prior to 1991 are composite of studies, taken from Cura, 1991.

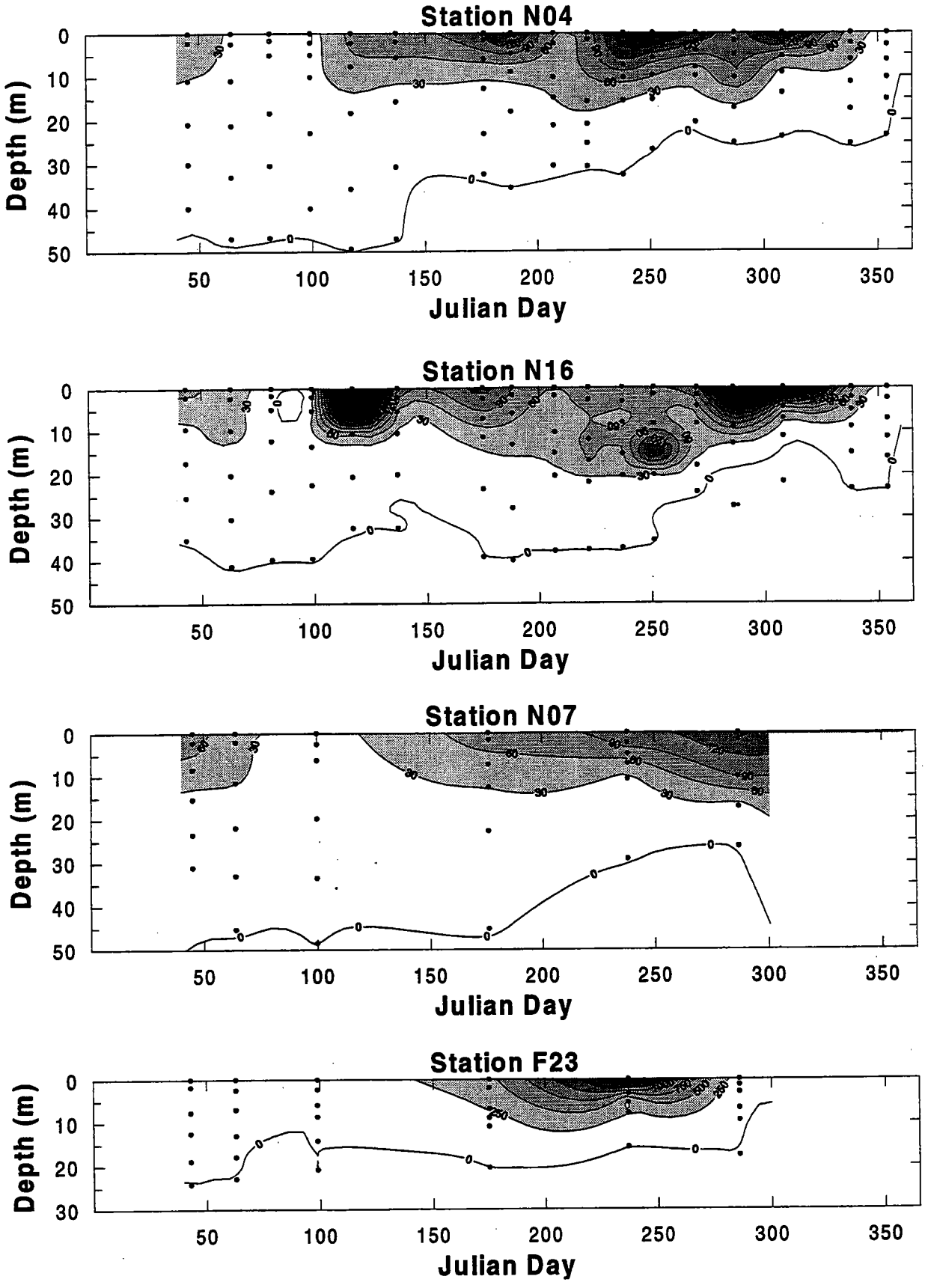

FIGURE 7-14

Daily Production. Contour values expressed in mgC/m3/d.

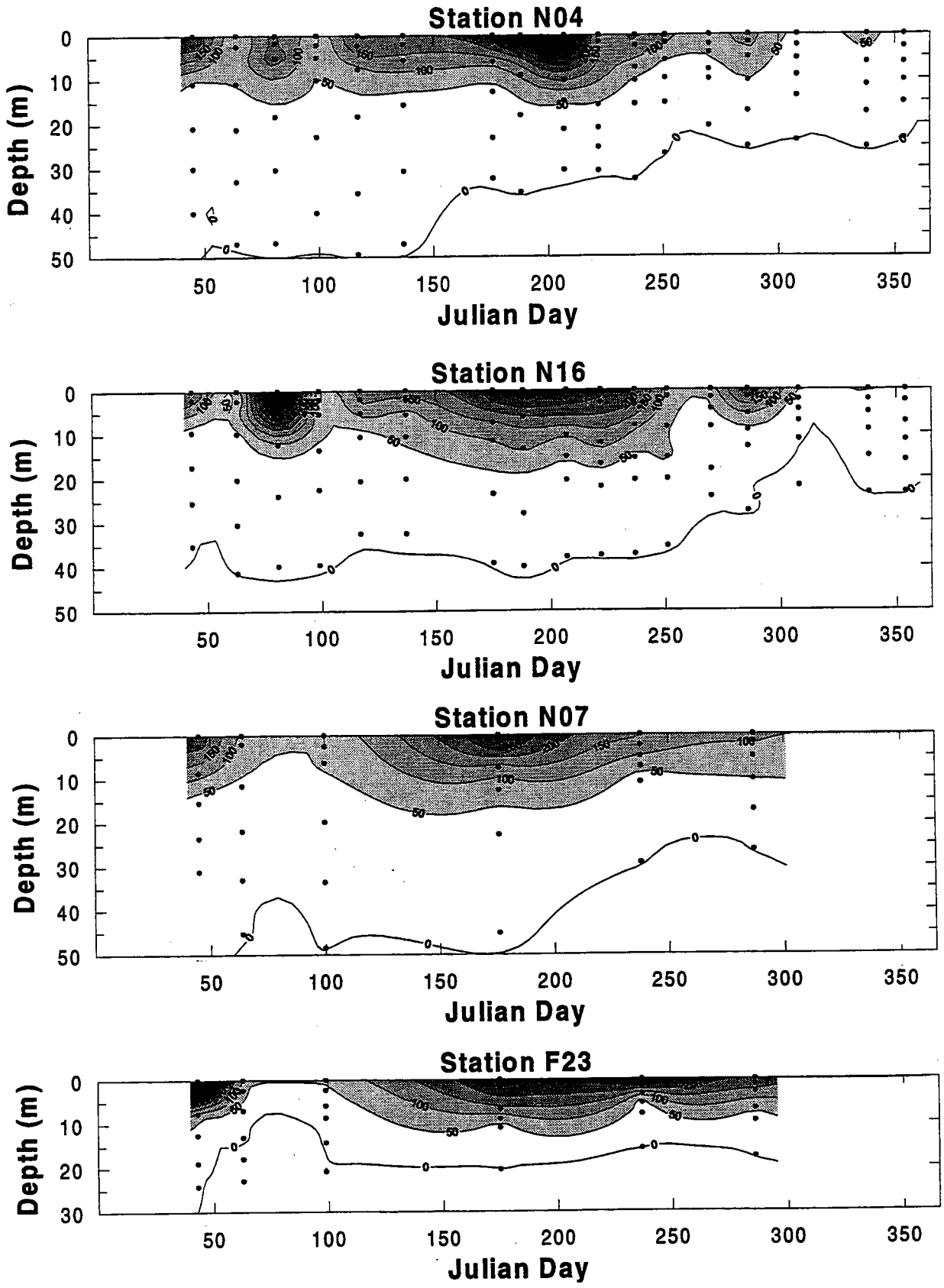

FIGURE 7-15

Chlorophyll-Specific Production. Contour values expressed in mgC/mgChla/d.

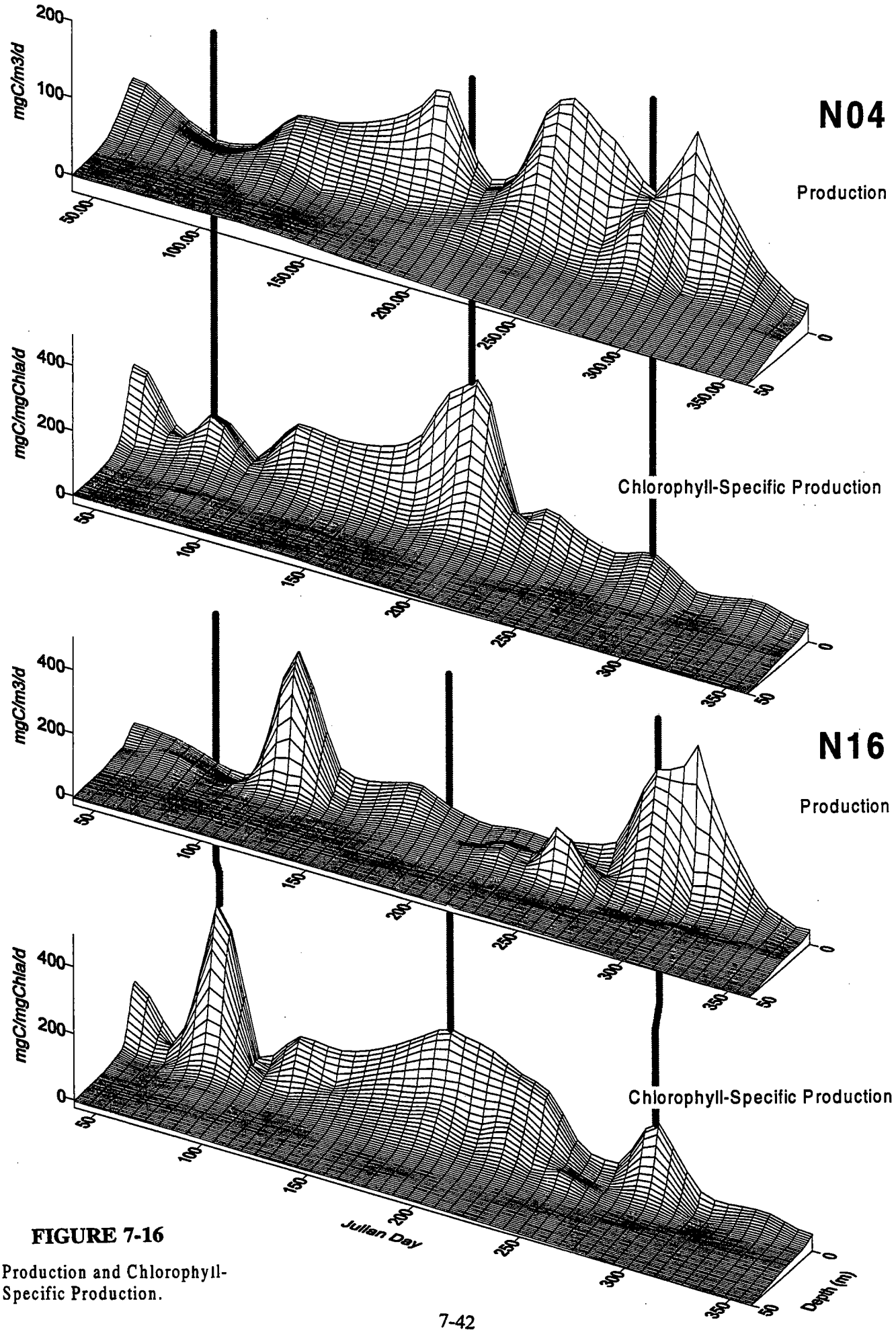

FIGURE 7-16

Production and Chlorophyll-Specific Production.

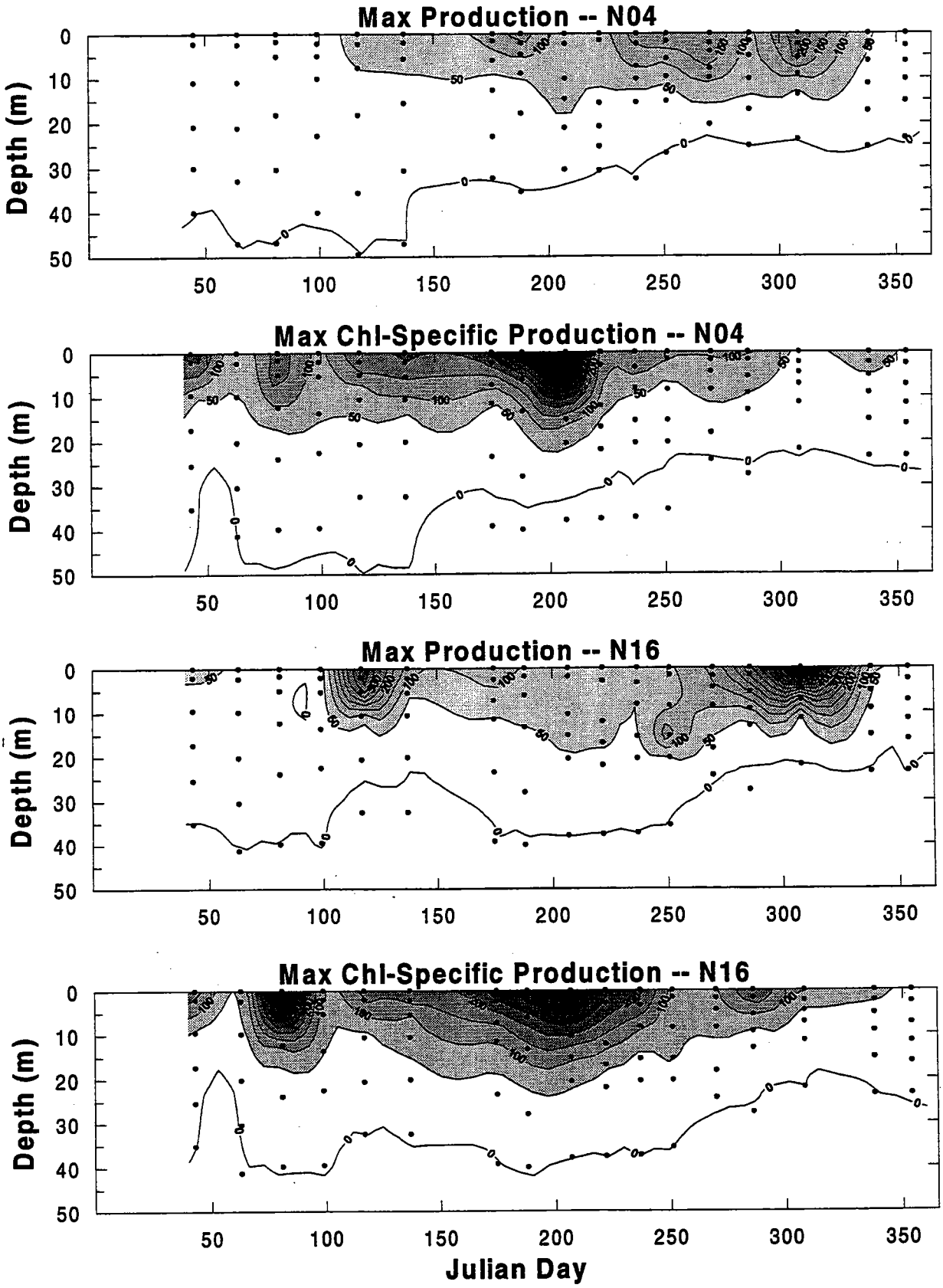

FIGURE 7-17

Potential Production and Potential Chlorophyll-Specific Production. Contour values expressed in mgC/m3/d and mgC/mgChla/d, respectively.

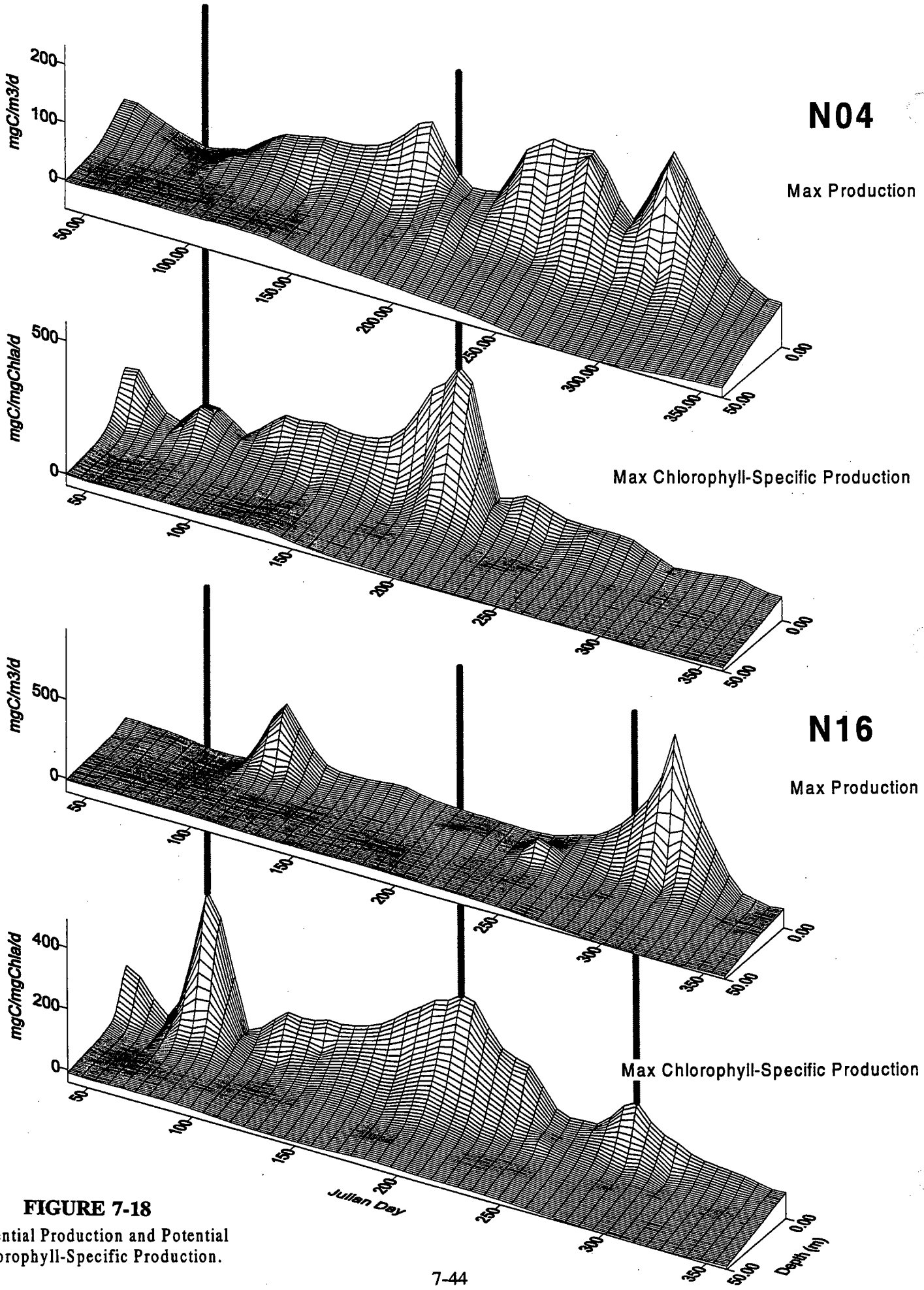

FIGURE 7-18

Potential Production and Potential Chlorophyll-Specific Production.

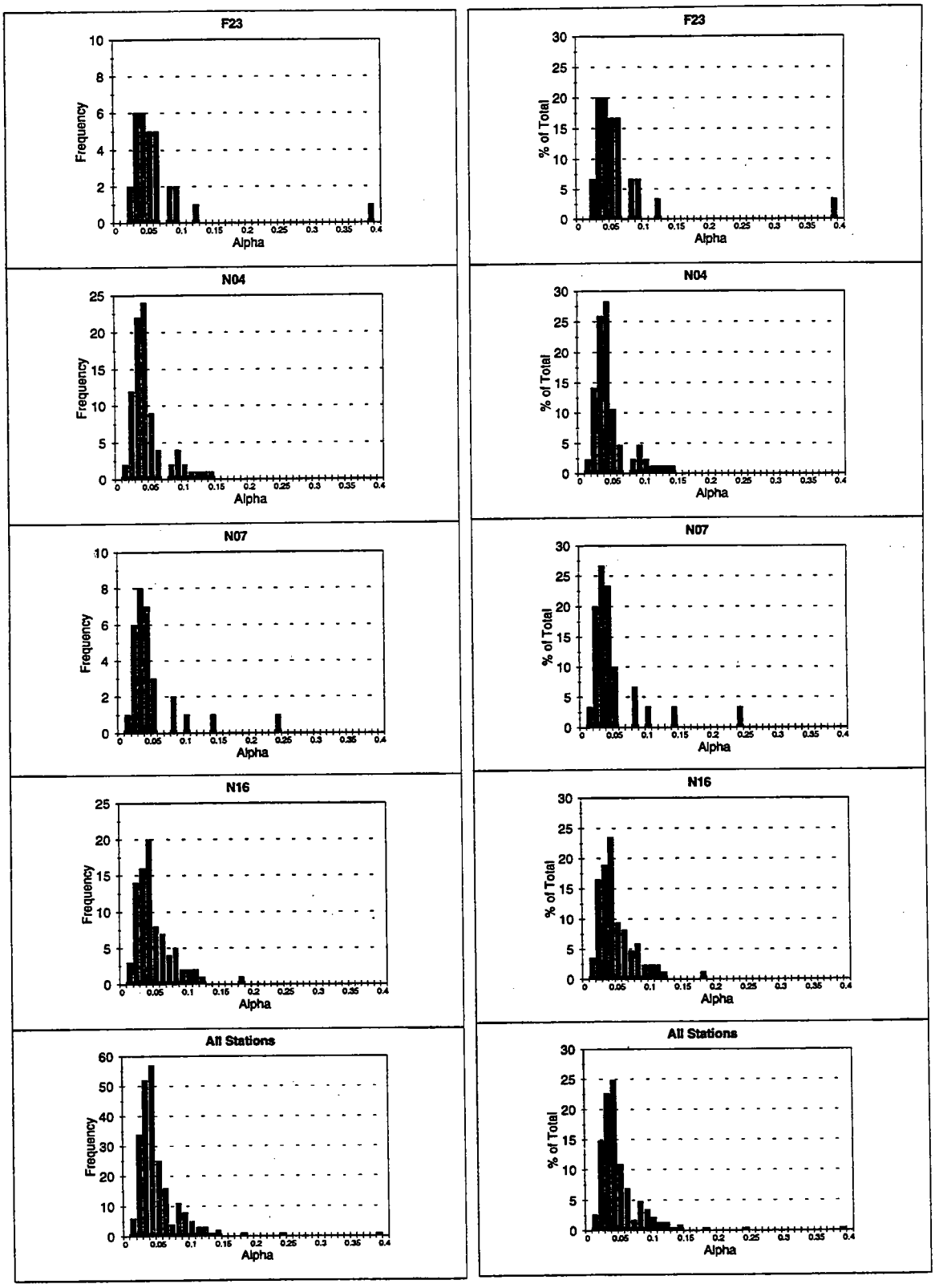

FIGURE 7-19

Frequency distribution for chlorophyll-specific alpha for stations F23, N04, N07 and N16 during 1995.

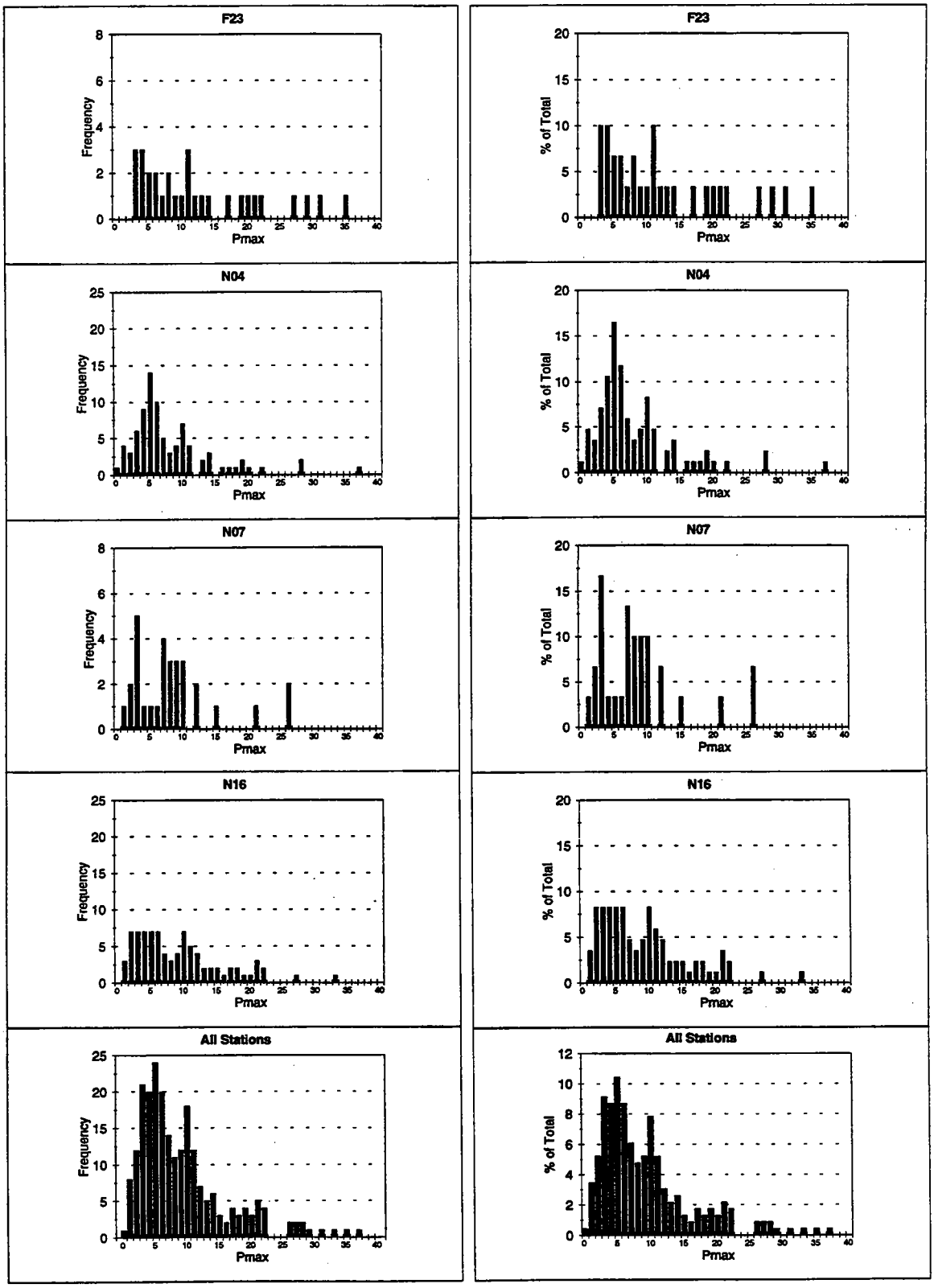

FIGURE 7-20

Frequency distribution for chlorophyll-specific Pmax for stations F23, N04, N07 and N16 during 1995.

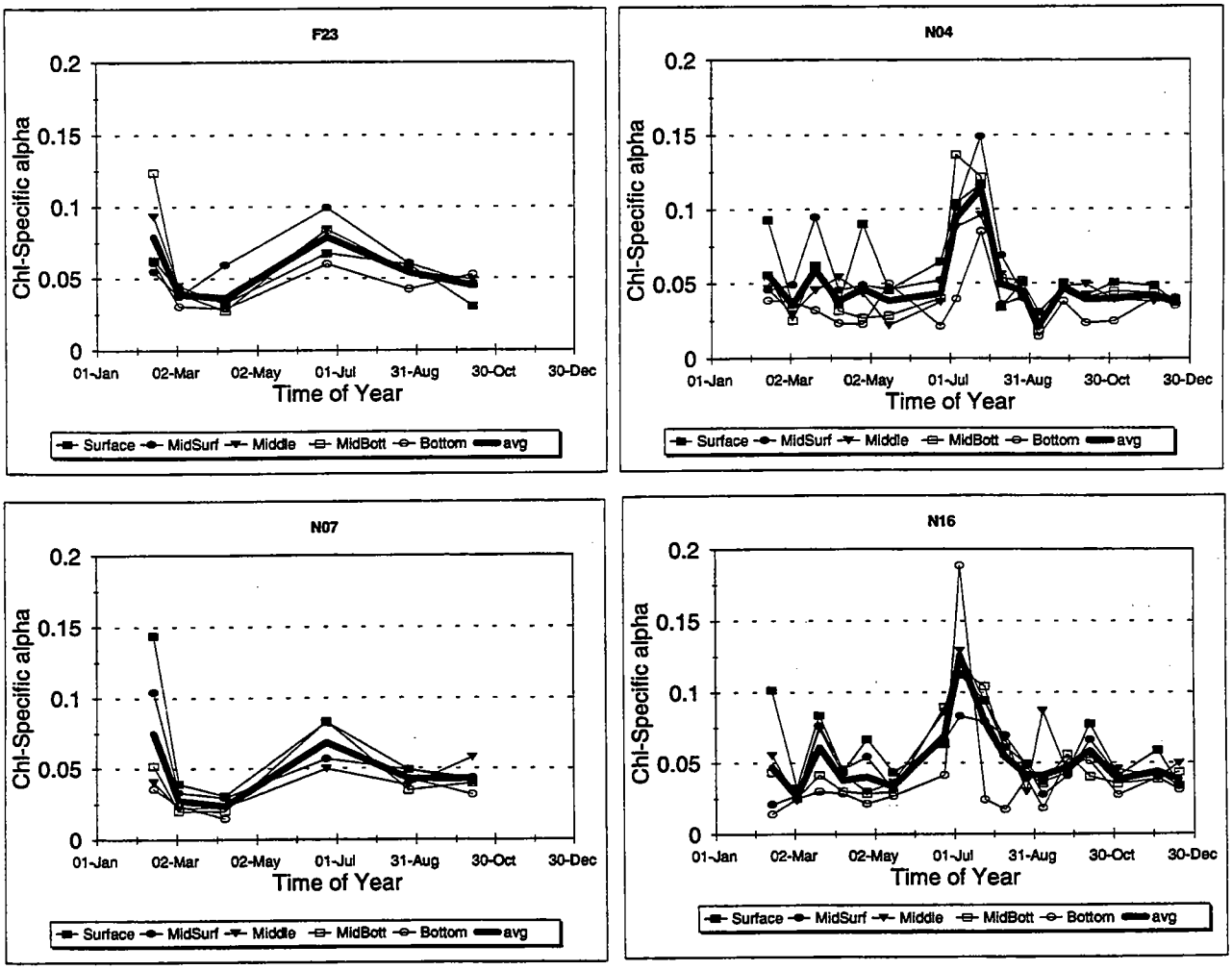

Note: Outlying datum excluded for N07, survey W9507

FIGURE 7-21

Chlorophyll-specific Alpha in 1995 at 5 depths.

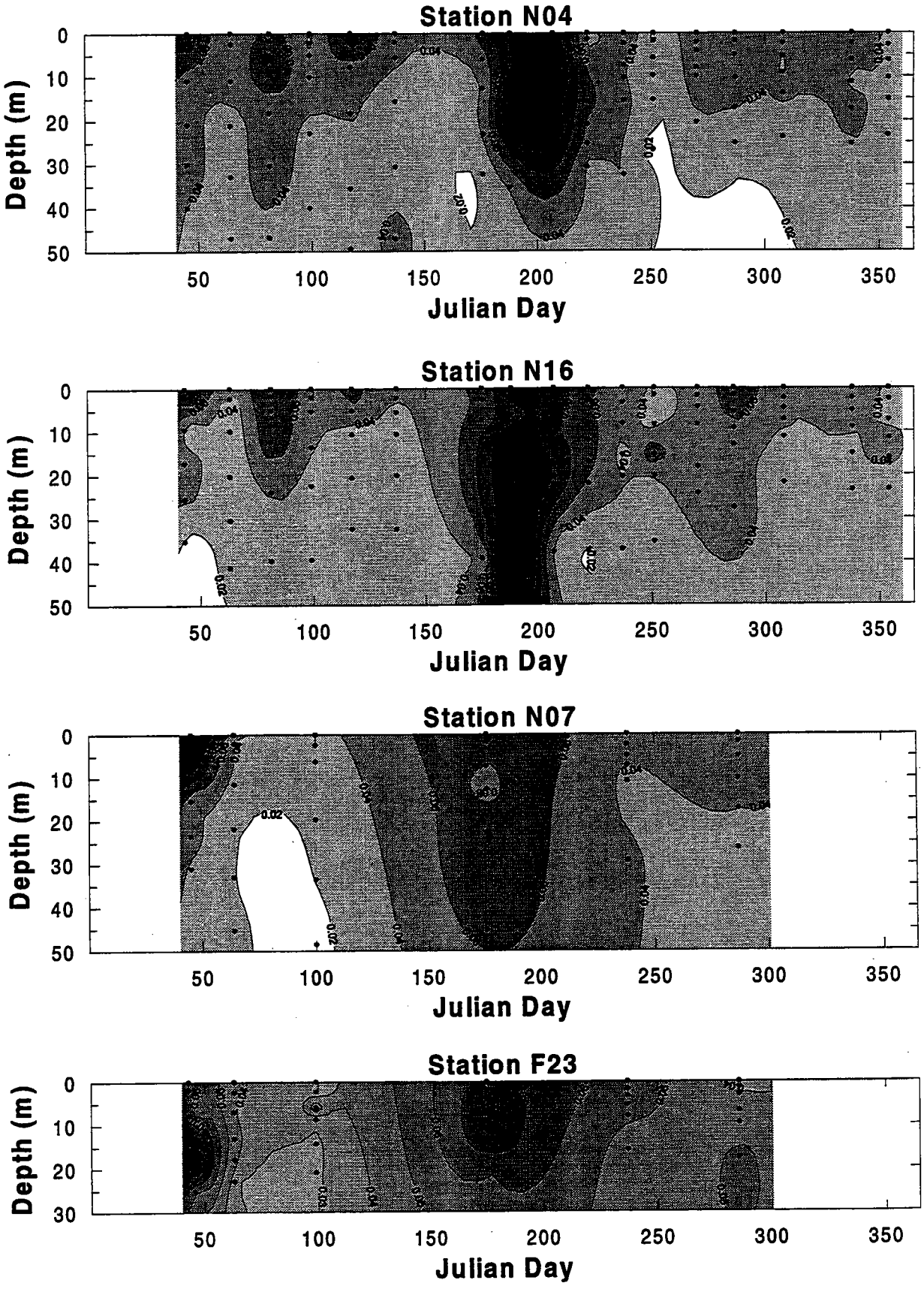

FIGURE 7-22

Contour plot of chlorophyll-specific alpha for 1995.

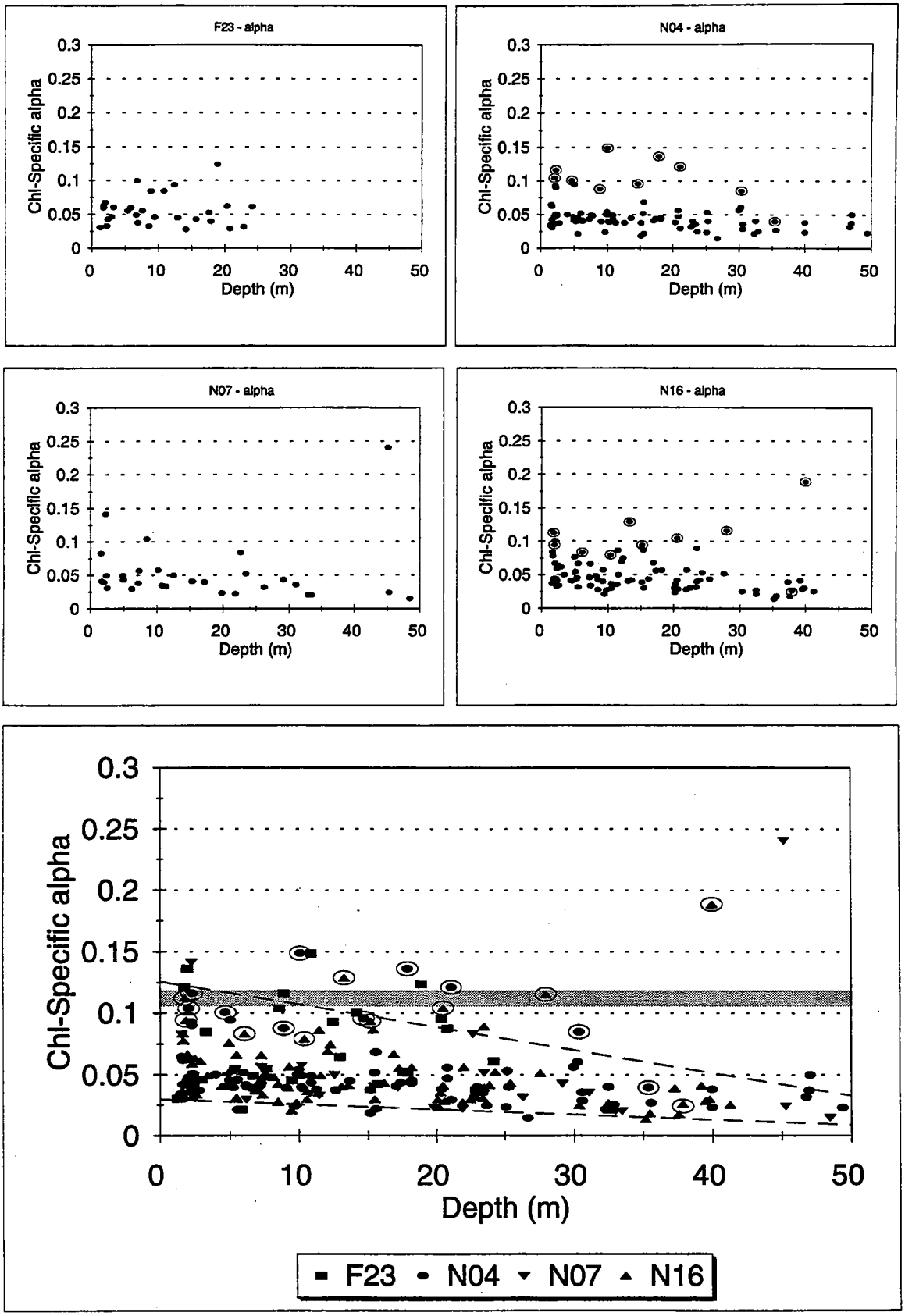

FIGURE 7-23

Depth distribution for chlorophyll-specific Alpha for stations F23, N04, N07 and N16 during 1995. Open circles identify samples for all depths of cruise W9508, W9509. Theoretical maximum Alpha shown by shaded bar.

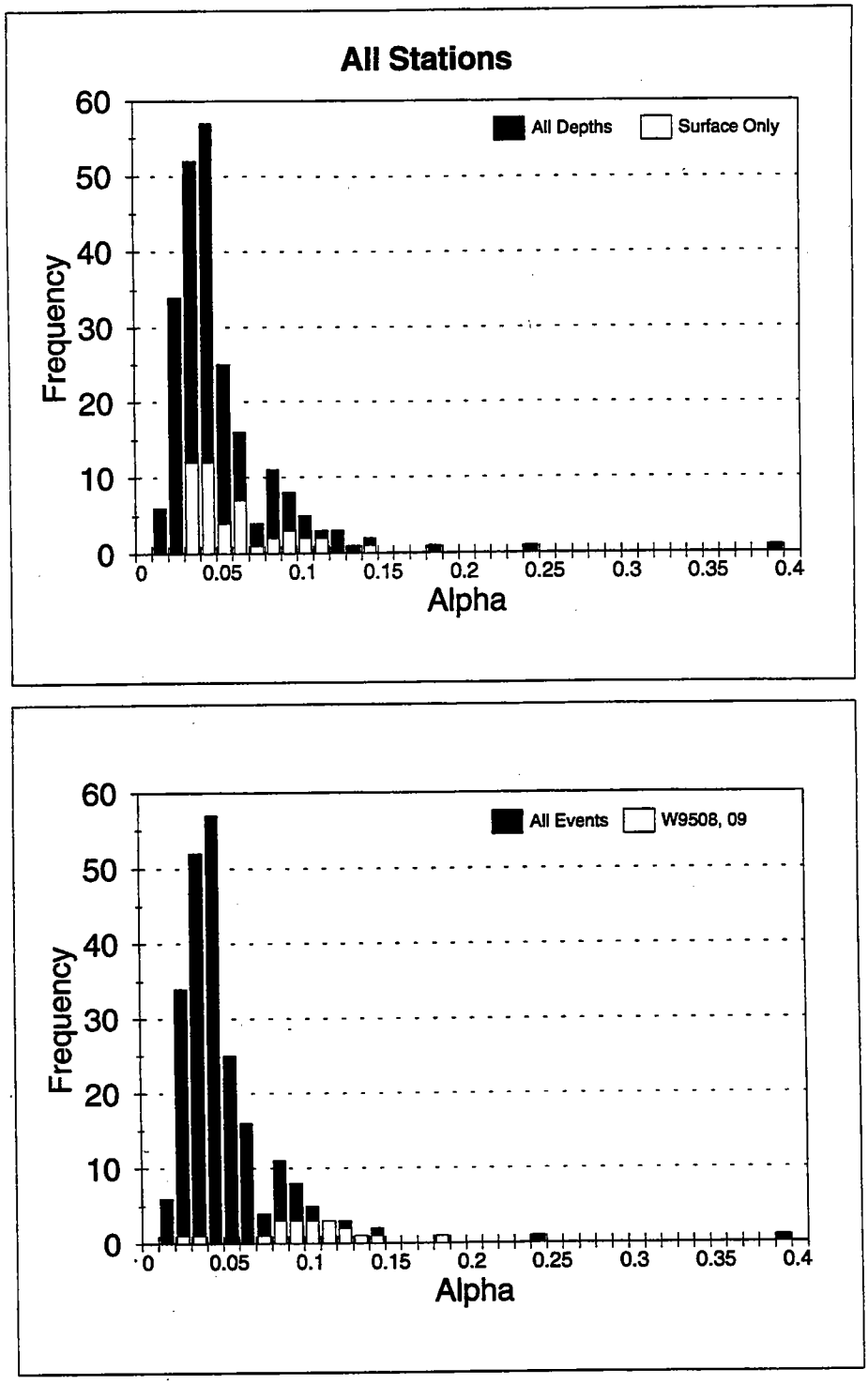

FIGURE 7-24

Frequency distribution for chlorophyll-specific alpha for stations F23, N04, N07 and N16 during 1995. White bars in upper and lower panels represent frequency distributions for surface samples only and for all depths of cruises W9508 and W9509.

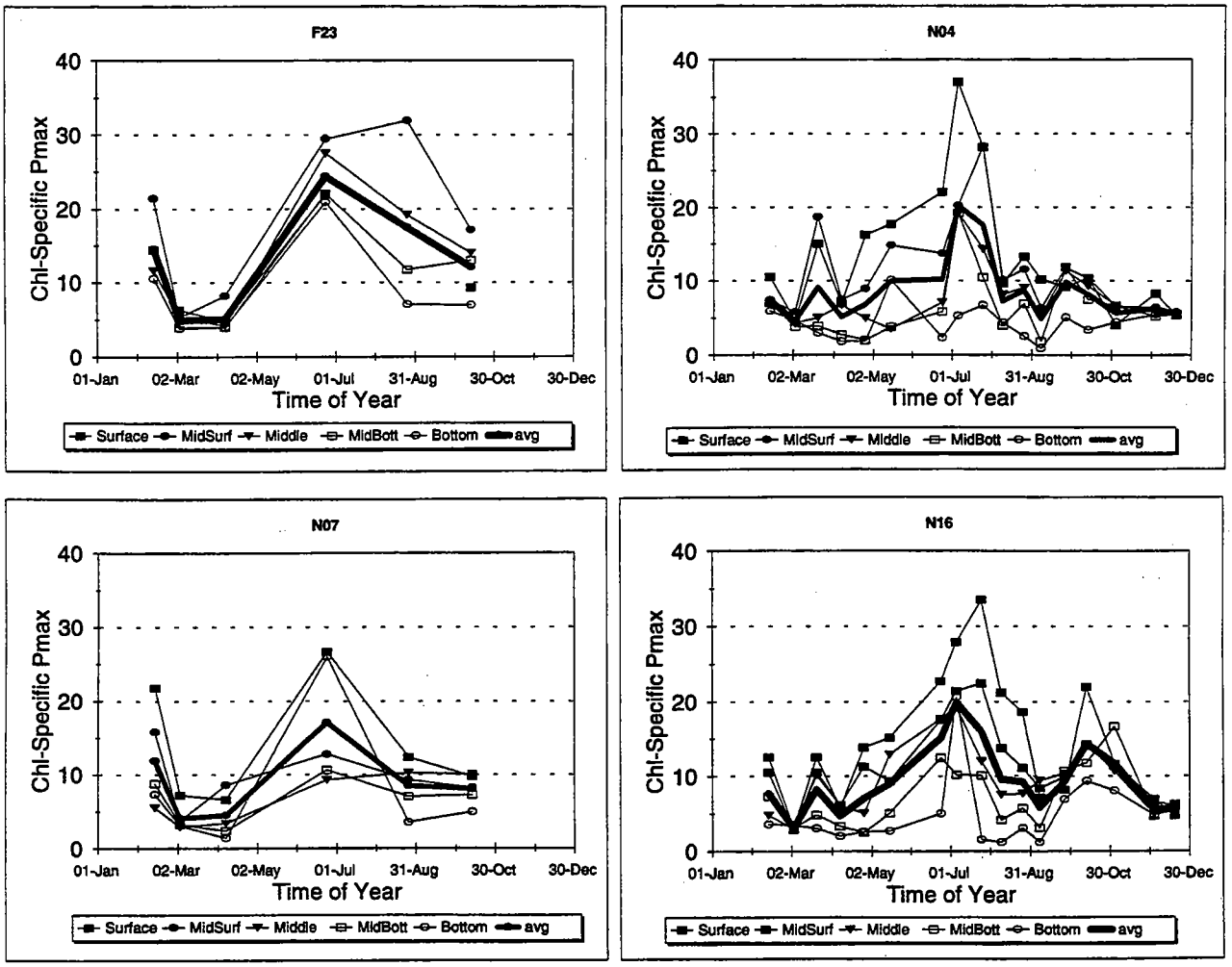

FIGURE 7-25

Chlorophyll-specific Pmax in 1995 at 5 depths.

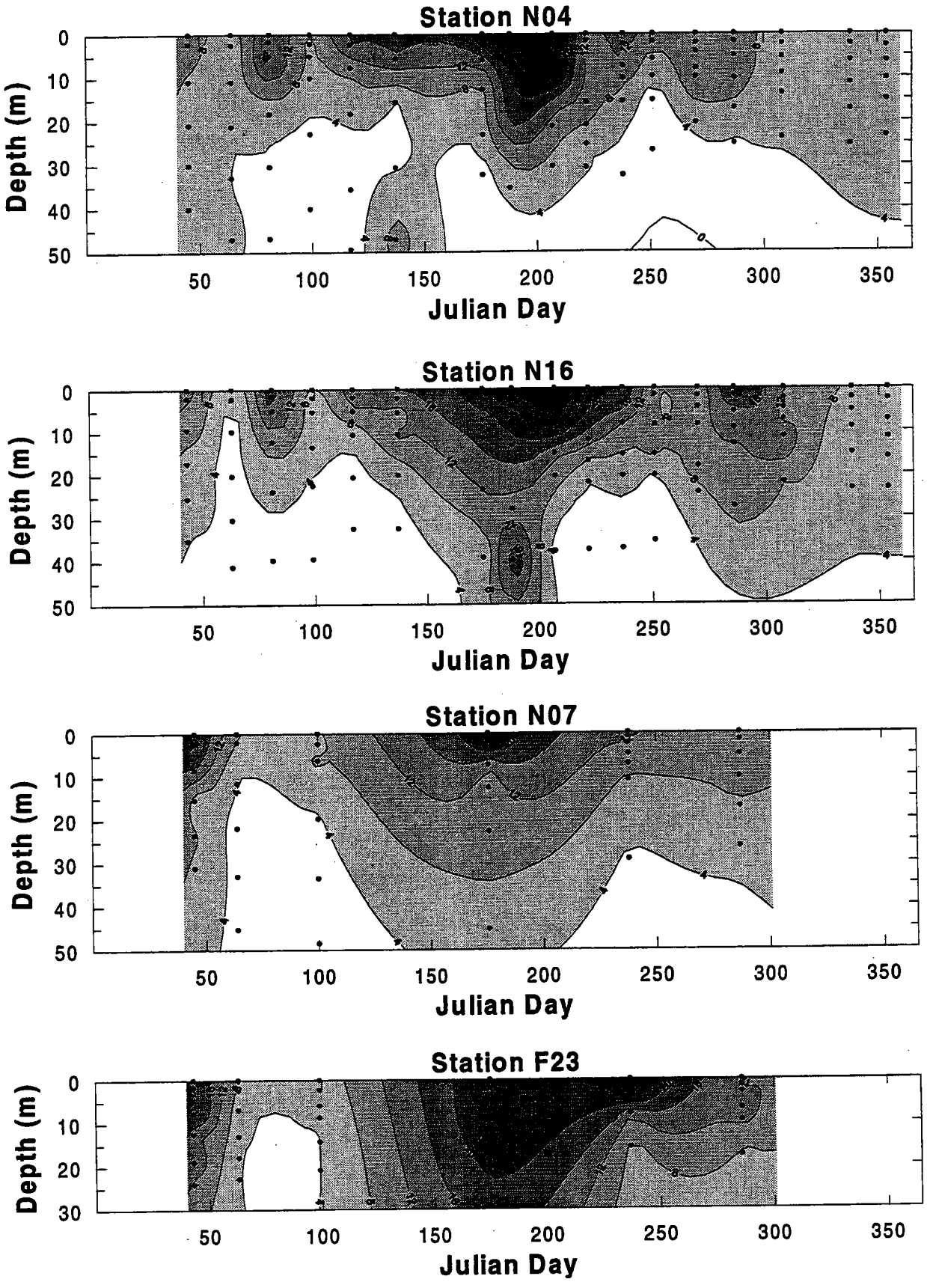

FIGURE 7-26

Contour plot of chlorophyll-specific Pmax for 1995.

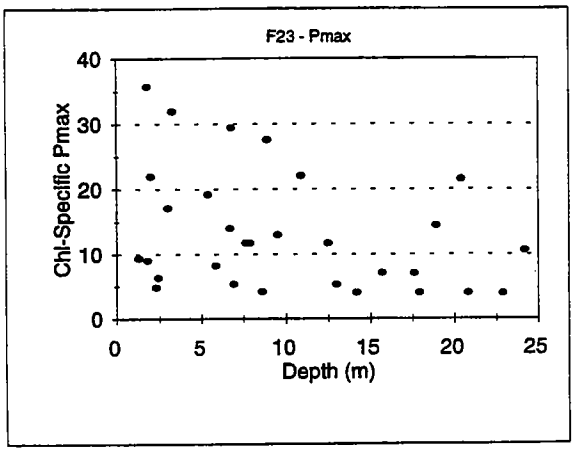

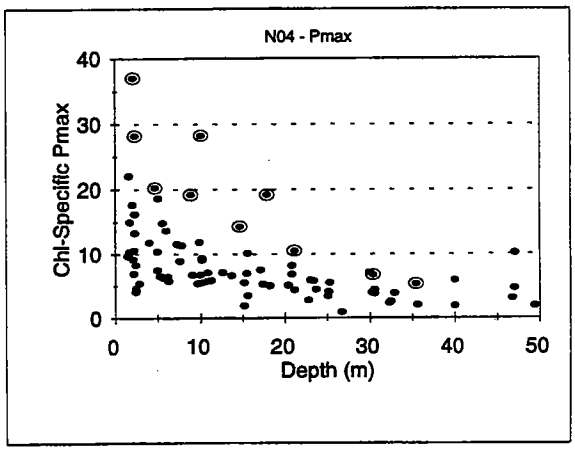

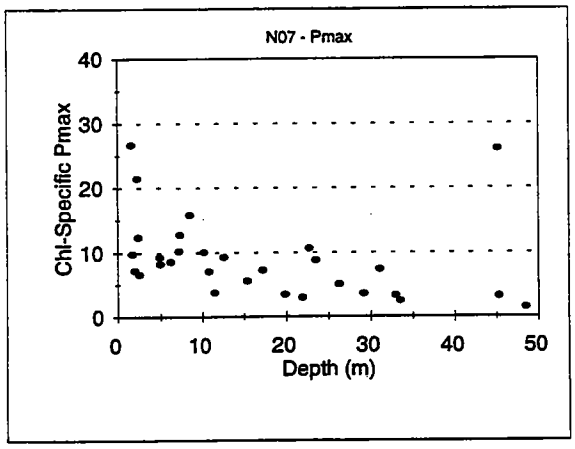

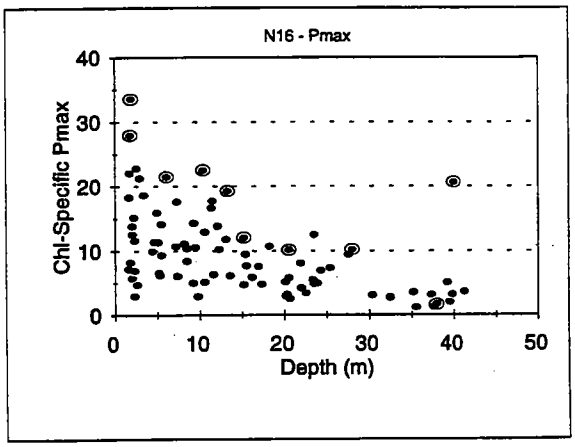

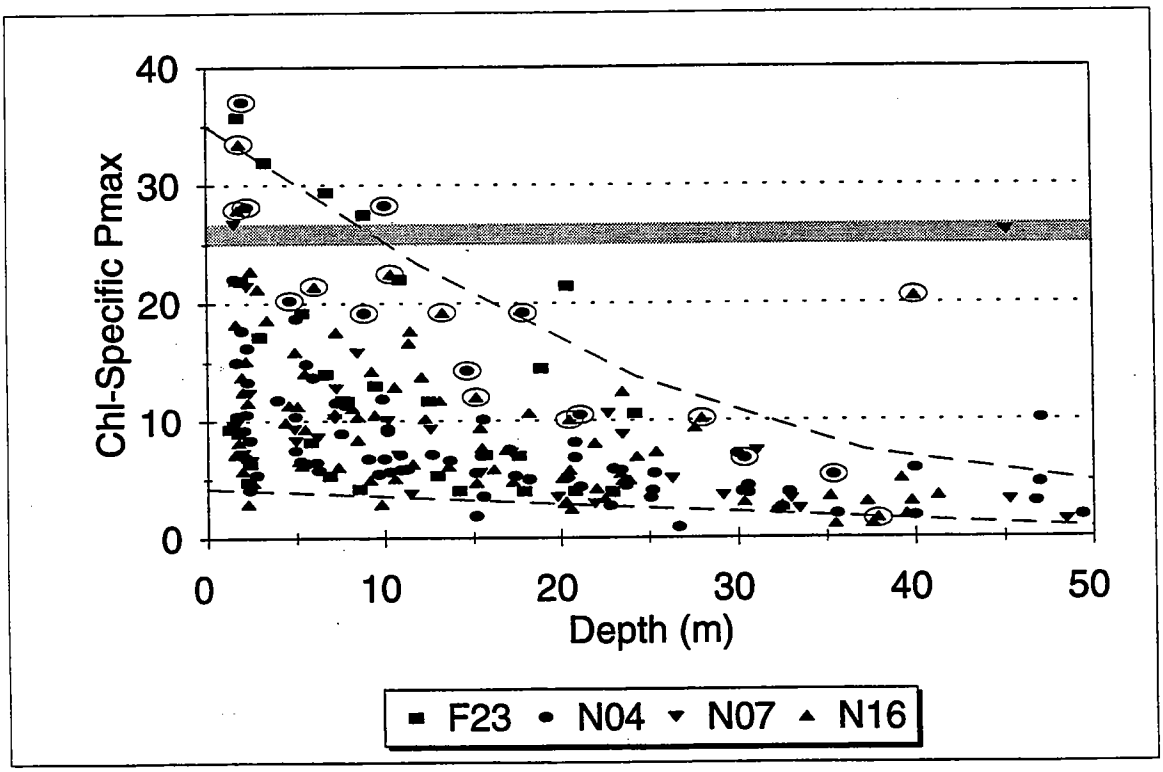

Note x-scale difference

FIGURE 7-27

Depth distribution for chlorophyll-specific Pmax for stations F23, N04, N07 and N16 during 1995. Open circles identify samples for all depths of cruise W9508, W9509. Theoretical maximum Pmax shown by shaded bar.

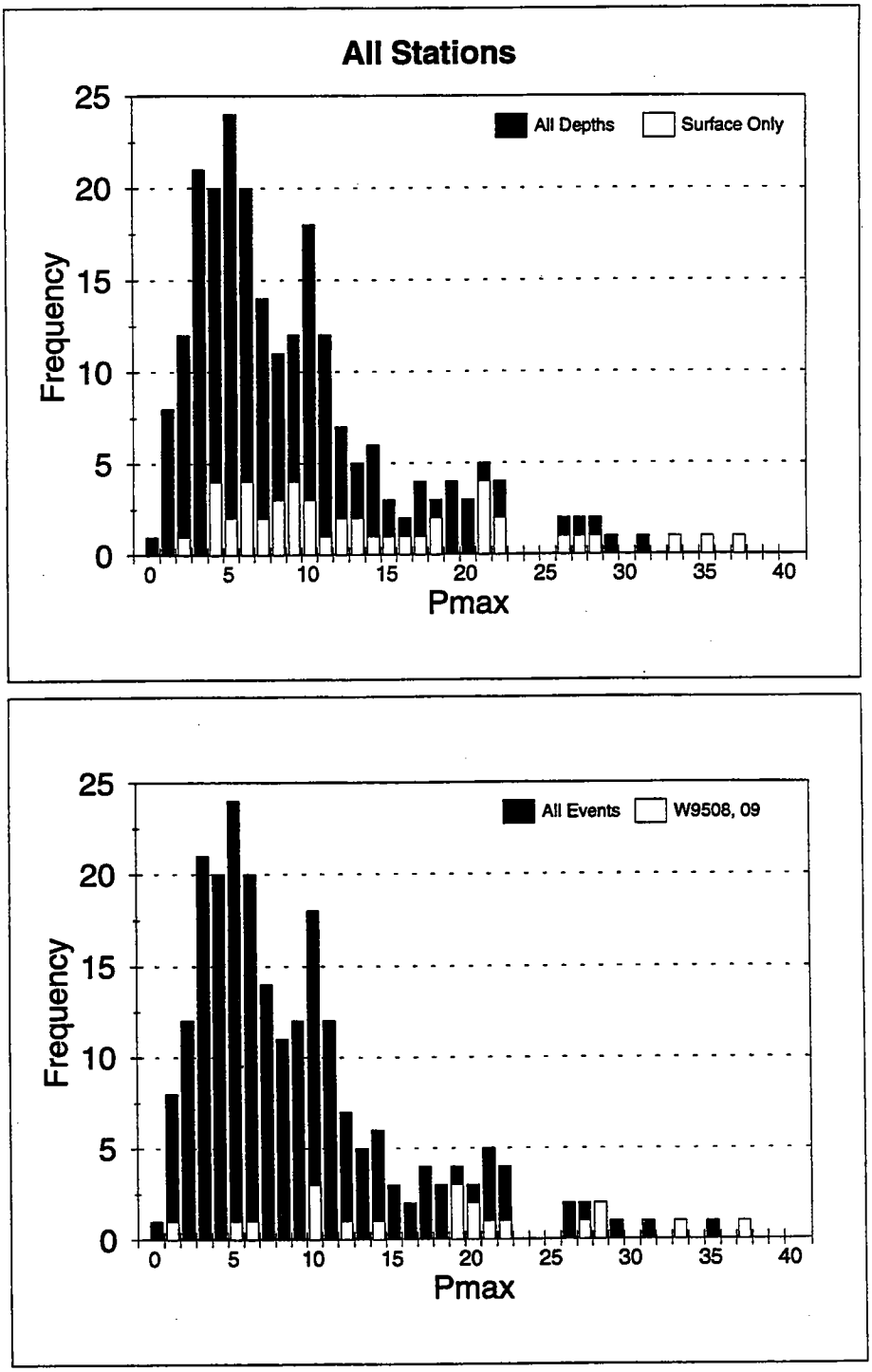

FIGURE 7-28

Frequency distribution for chlorophyll-specific Pmax for stations F23, N04, N07 and N16 during 1995. White bars in upper and lower panels represent frequency distributions for surface samples only and for all depths of cruises W9508 and W9509.

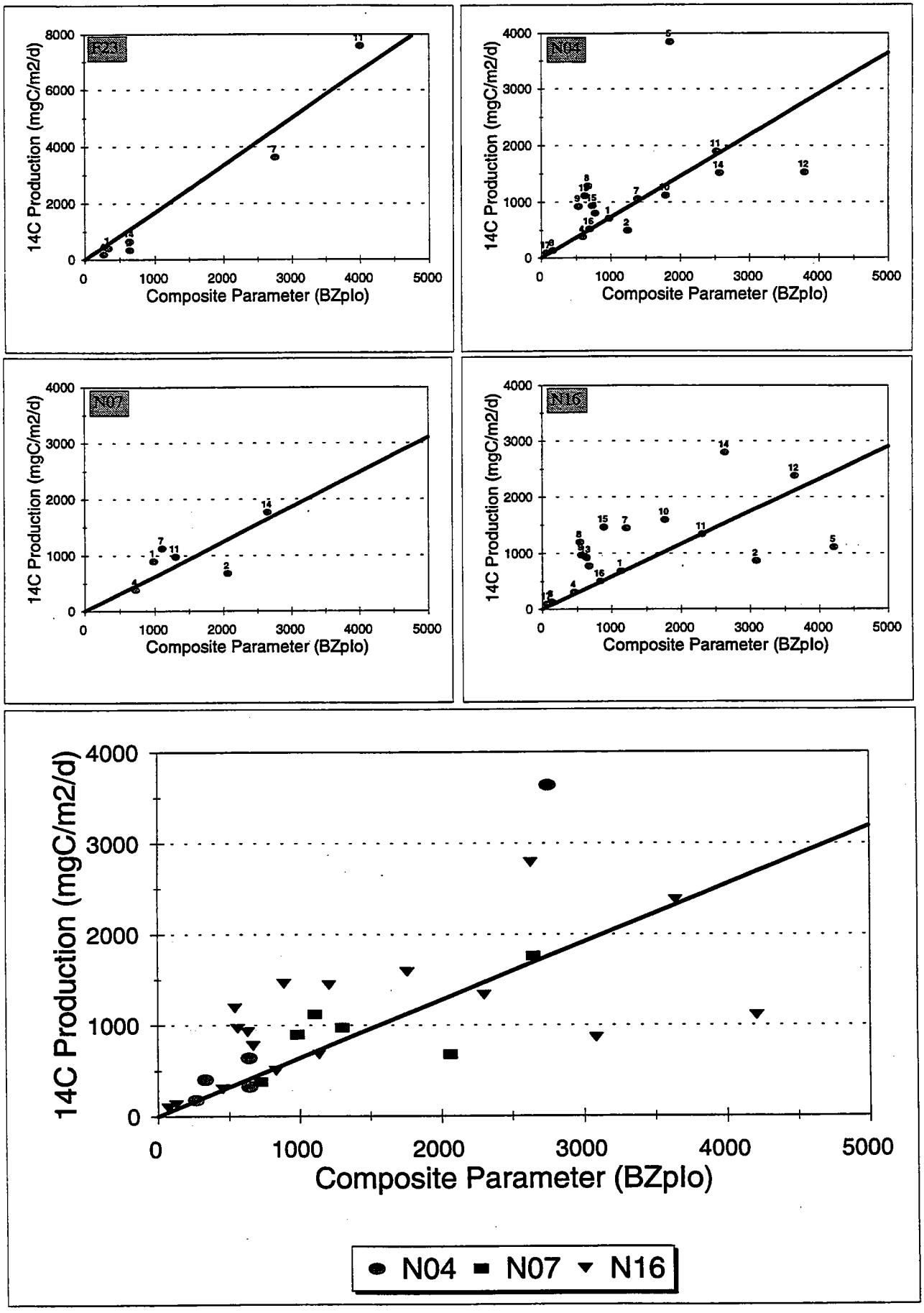

FIGURE 7-29

Note y-scale difference

BzpIo empirical model for Depth-Integrated Production in 1995

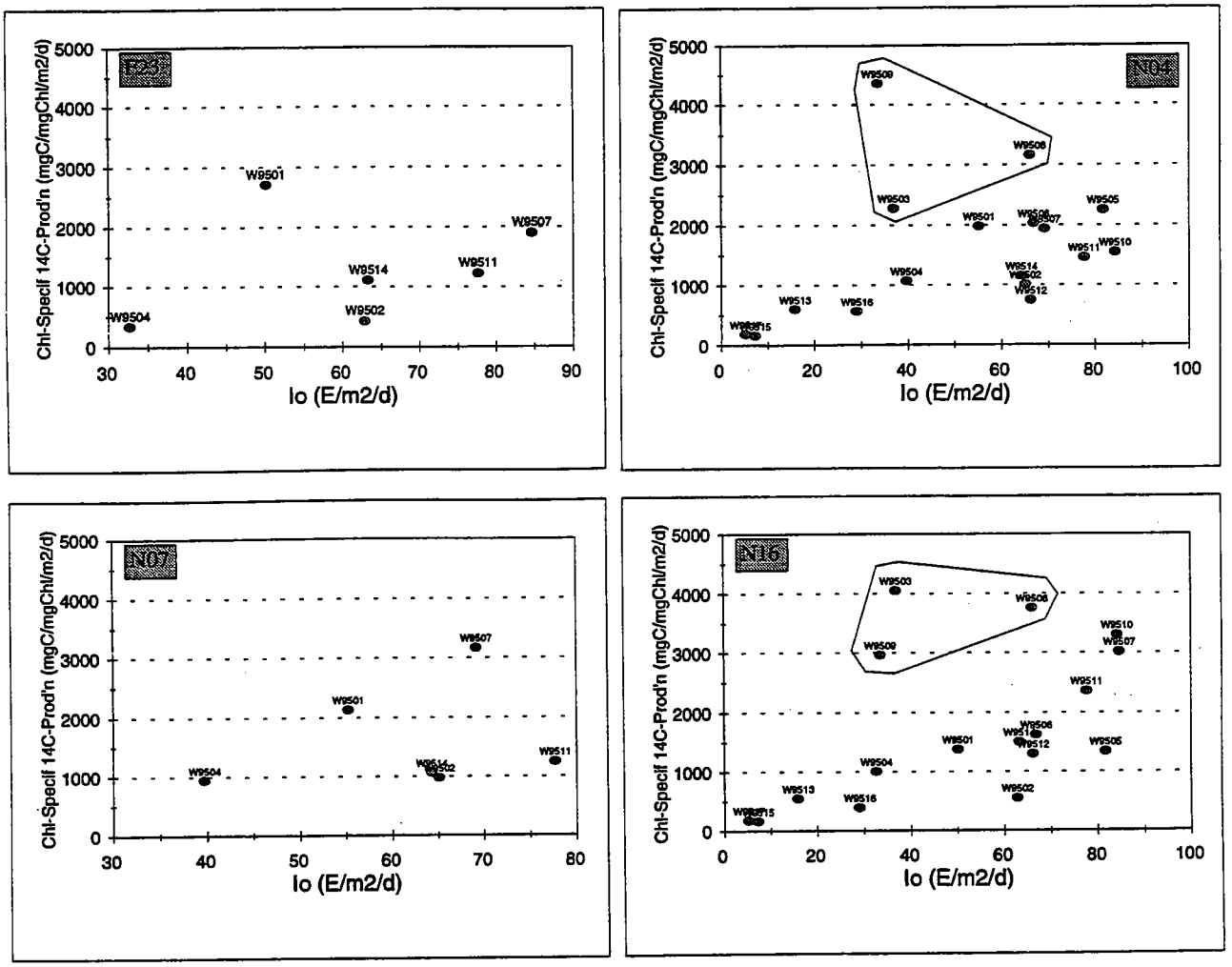

FIGURE 7-30

Chlorophyll-Specific Production vs. Incident Light (Note x-scale difference)

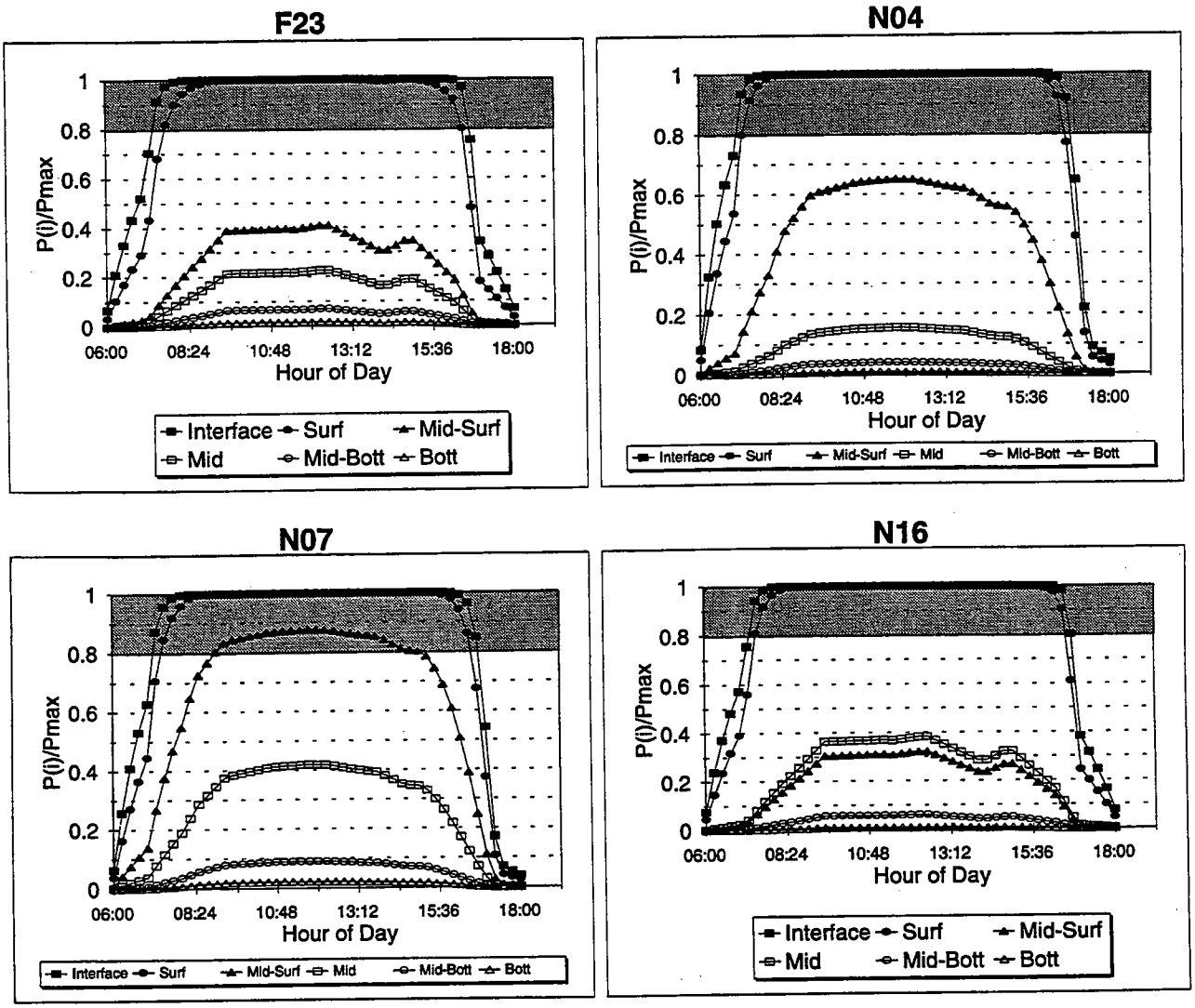

FIGURE 7-31

Degree of light saturation the phytoplankton population experienced at depth over the course of the photoperiod.

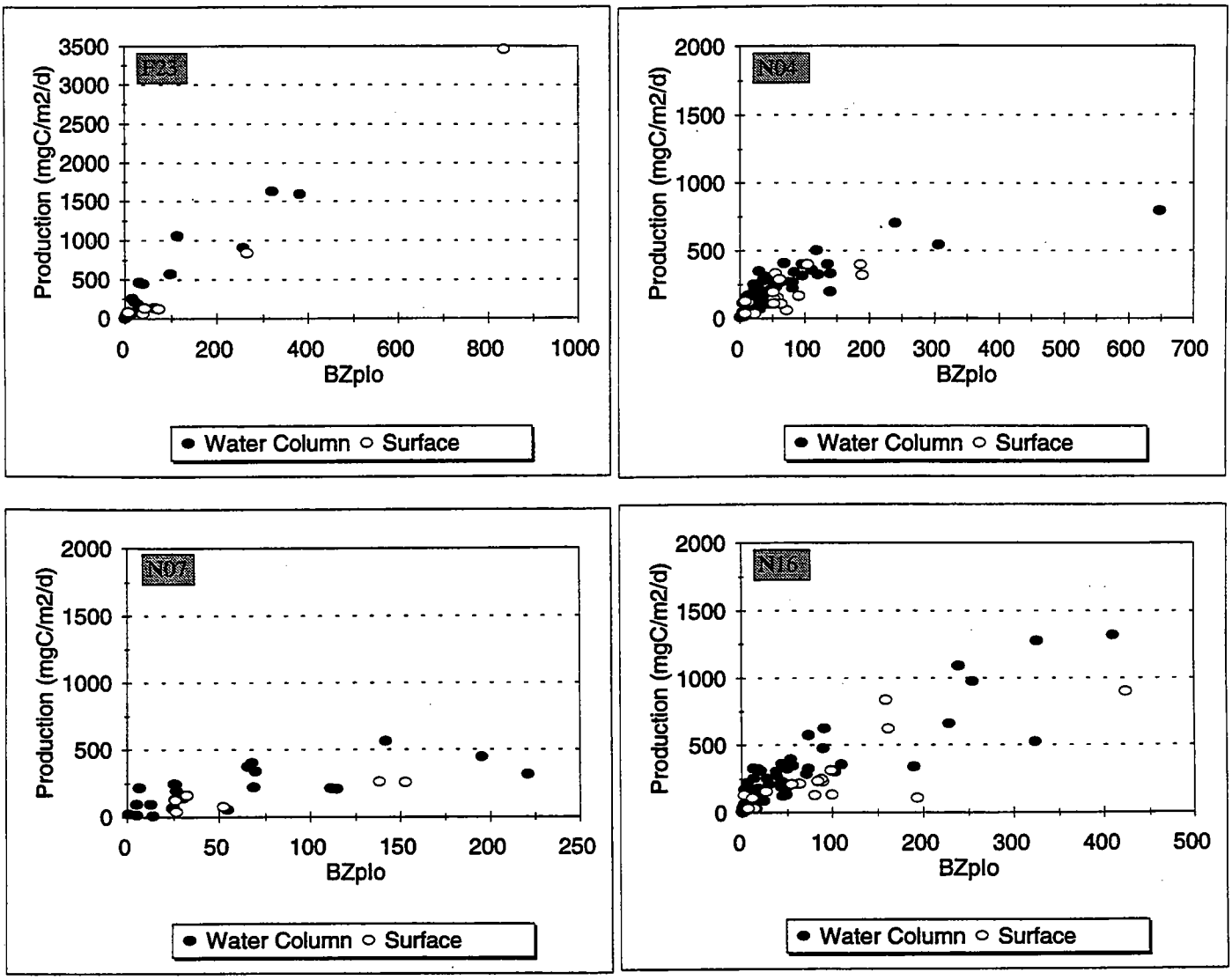

FIGURE 7-32

BzpIo empirical model for production from individual depth-sections within the water column (Note scale difference). BzpIo computed where B and Zp = depth interval of section and Io = incident light at top of section.

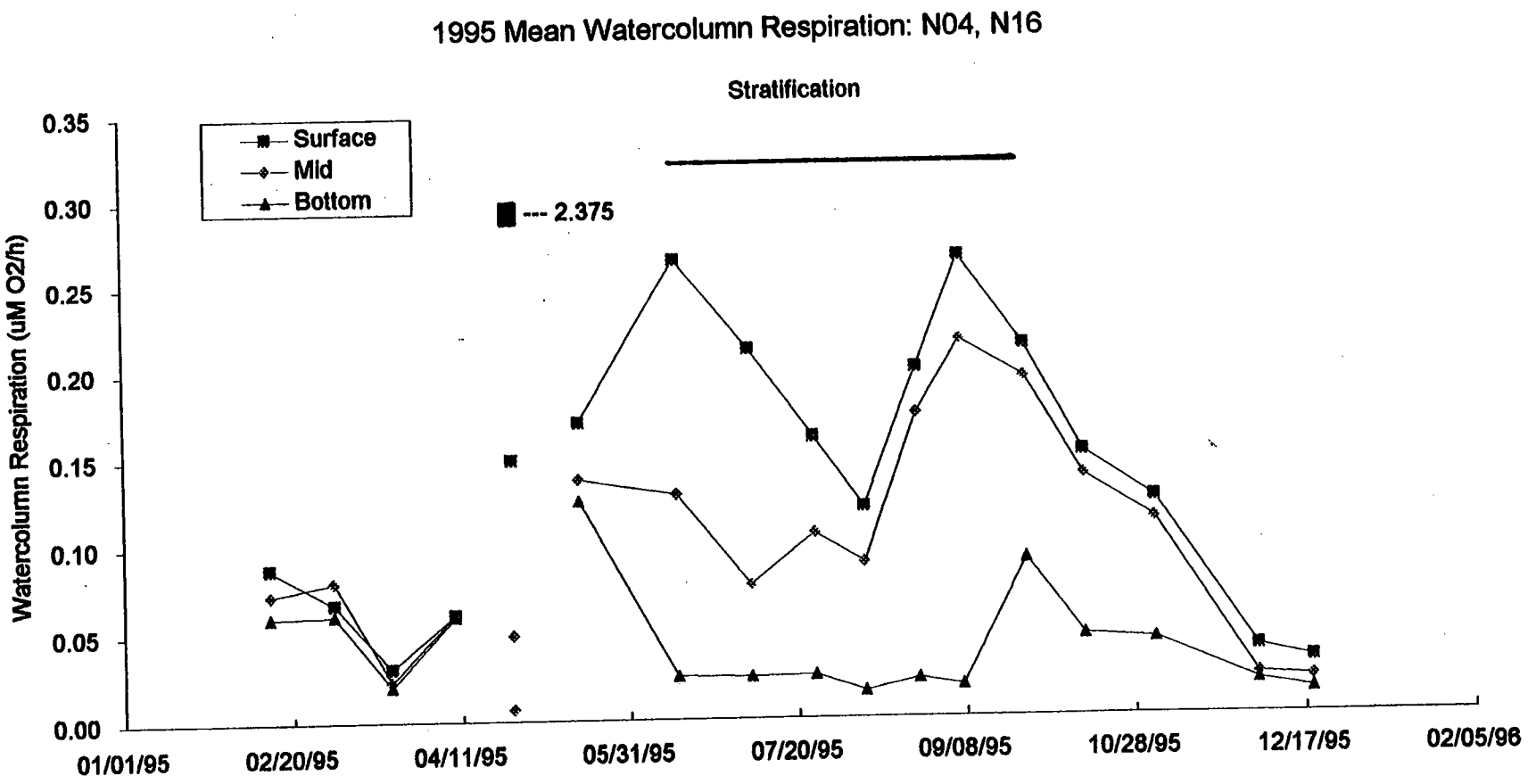

FIGURE 7-33

Vertical distribution of watercolumn respiration at the two high frequency sampling productivity/respiration stations (N04, N16) during 1995. Higher rates were consistently observed within the upper watercolumn (surface-boxes and mid/bottom of mixed layer-diamonds) with the lowest rates at depth (bottom-triangles.

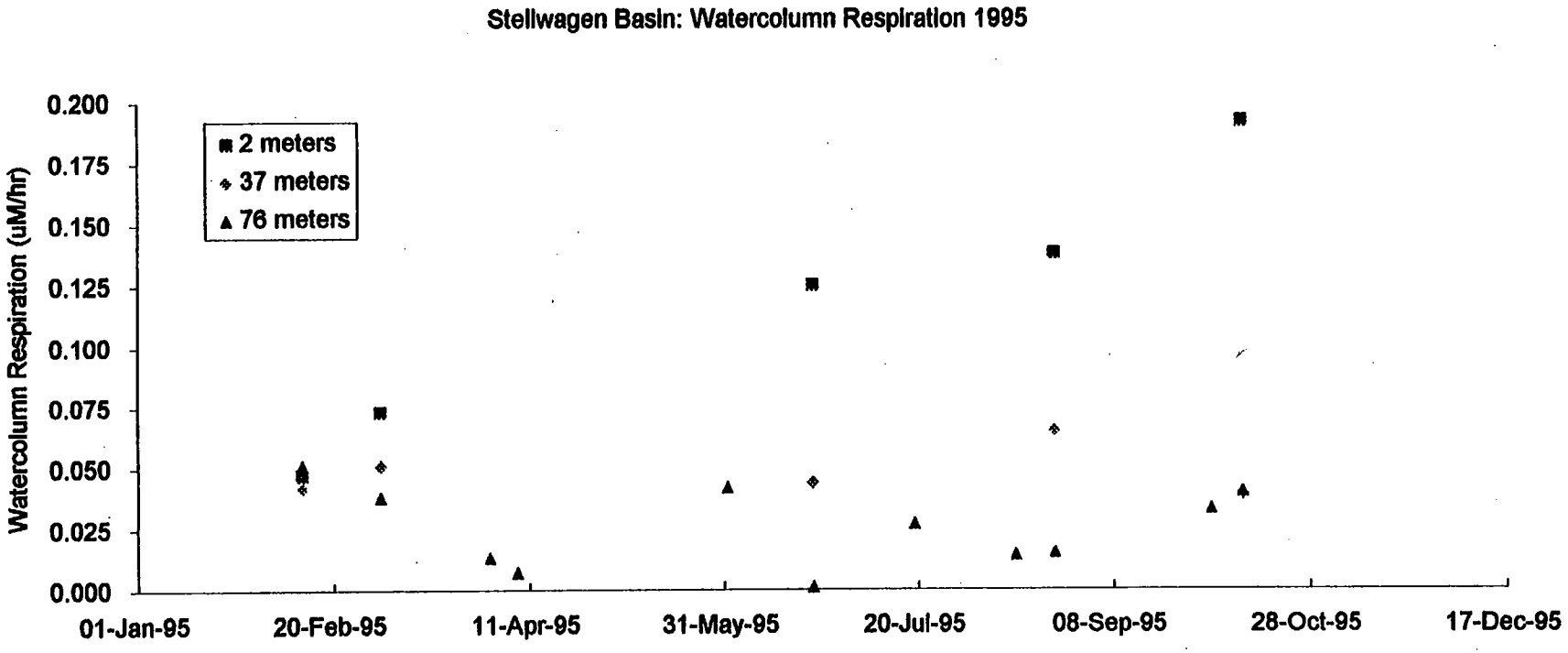

Note no surface data for W9504 due to sample loss

FIGURE 7-34

Vertical distribution of watercolumn respiration within Stellwagen Basin. Data are from station F19 (6X/year) and MB05 (5X/year, bottomwater only, in the benthic flux program). Note expanded scale from the nearfield.

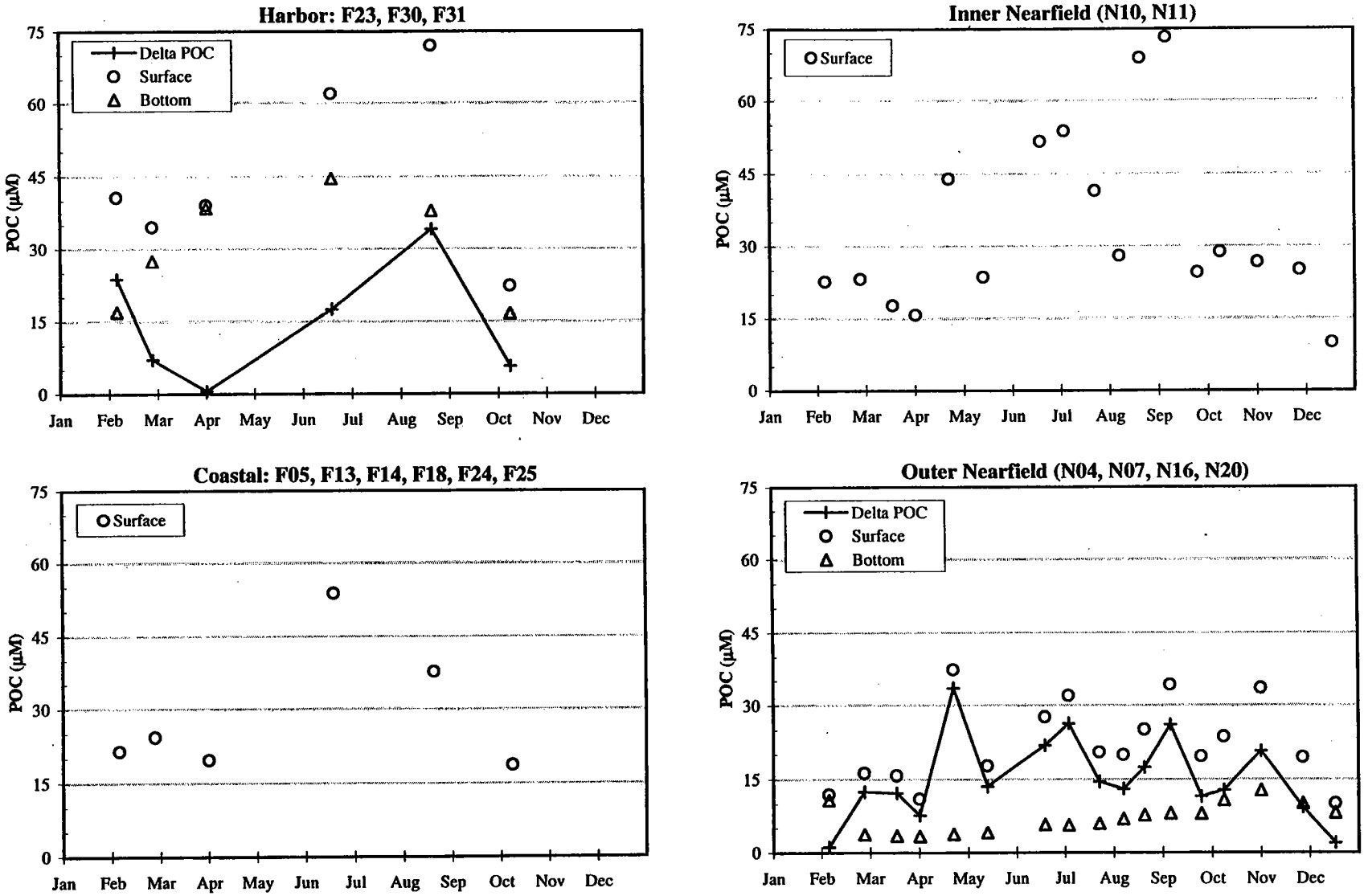

FIGURE 7-35

1995 Regional Particulate Organic Carbon (POC) Concentration Averages

Surface, Bottom, and Delta (Surface - Bottom) Survey Averages

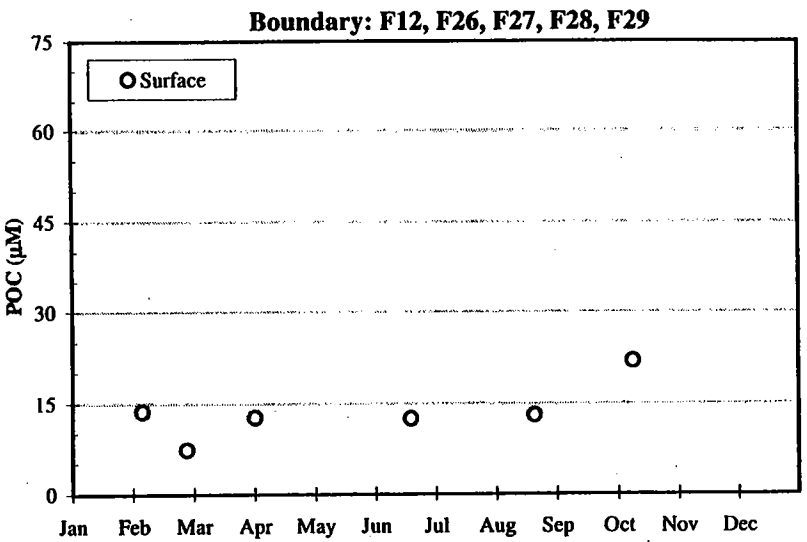

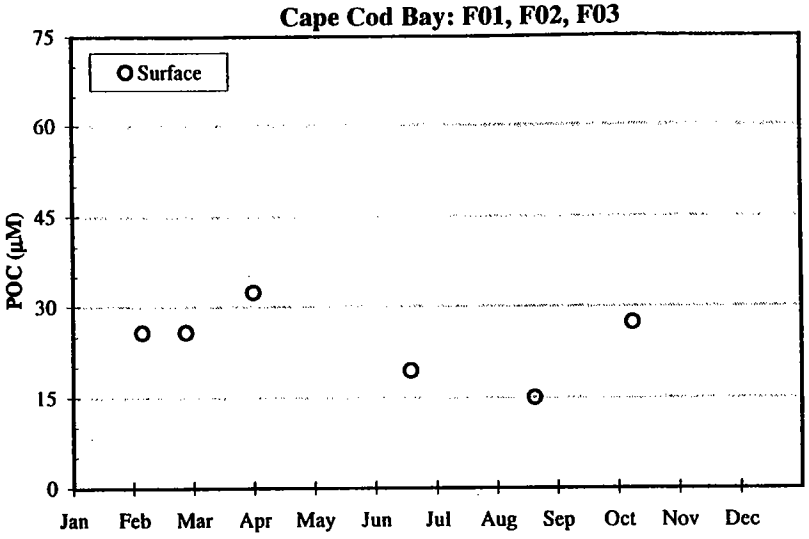

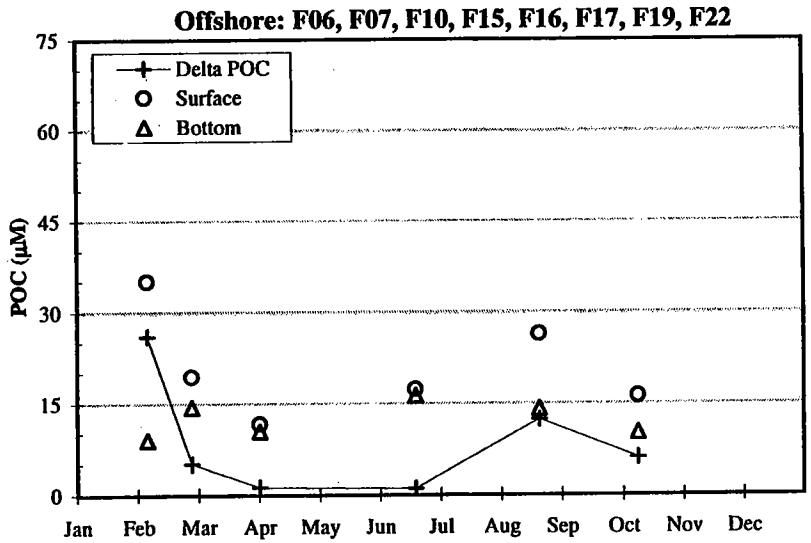

FIGURE 7-36

1995 Regional Particulate Organic Carbon (POC) Concentration Averages

Surface, Bottom, and Delta (Surface - Bottom) Survey Averages

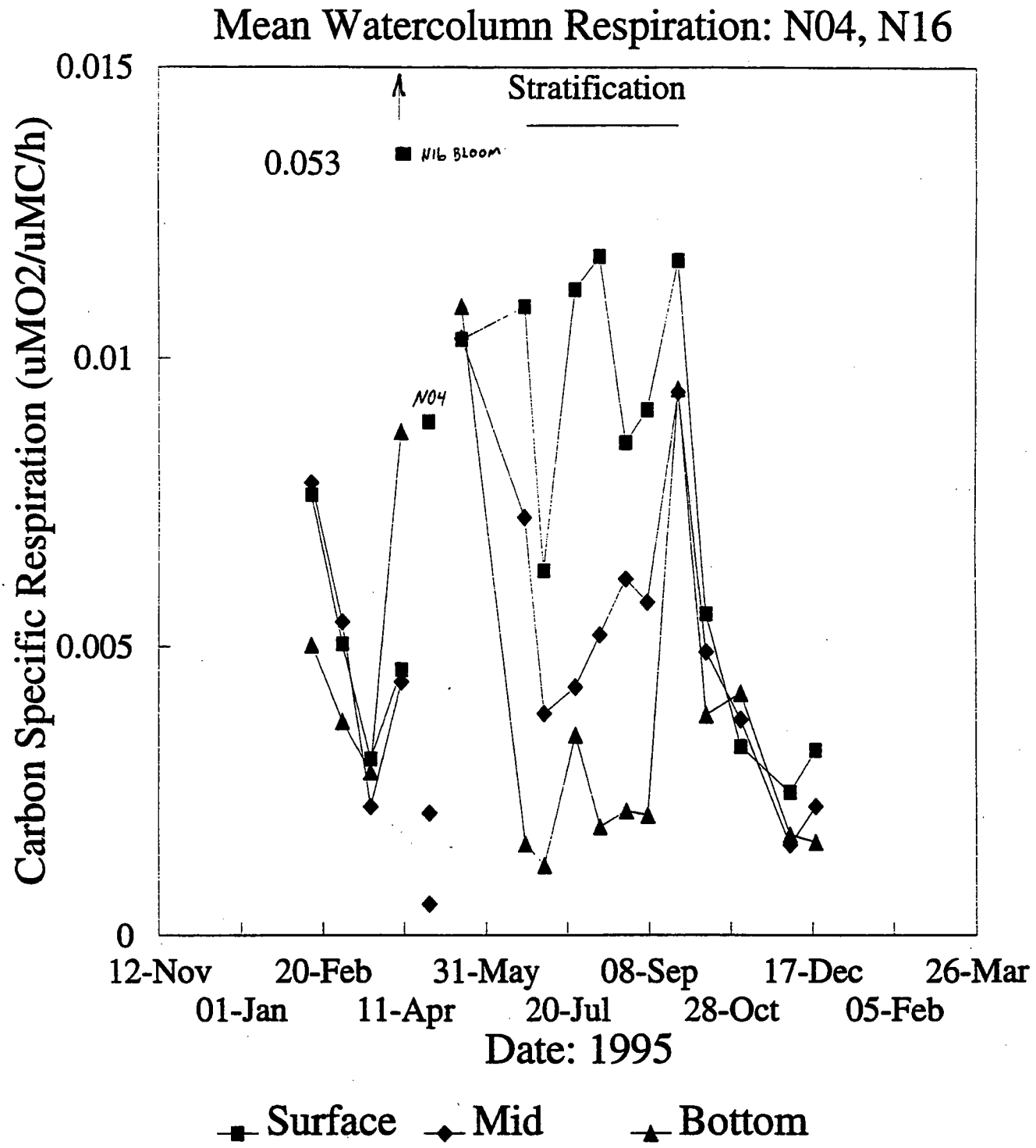

Note: Vertical distribution controlled primarily by temperature.

FIGURE 7-37

Vertical distribution of carbon specific respiration within the nearfield through 1995. Note point offscale during spring bloom at N16.

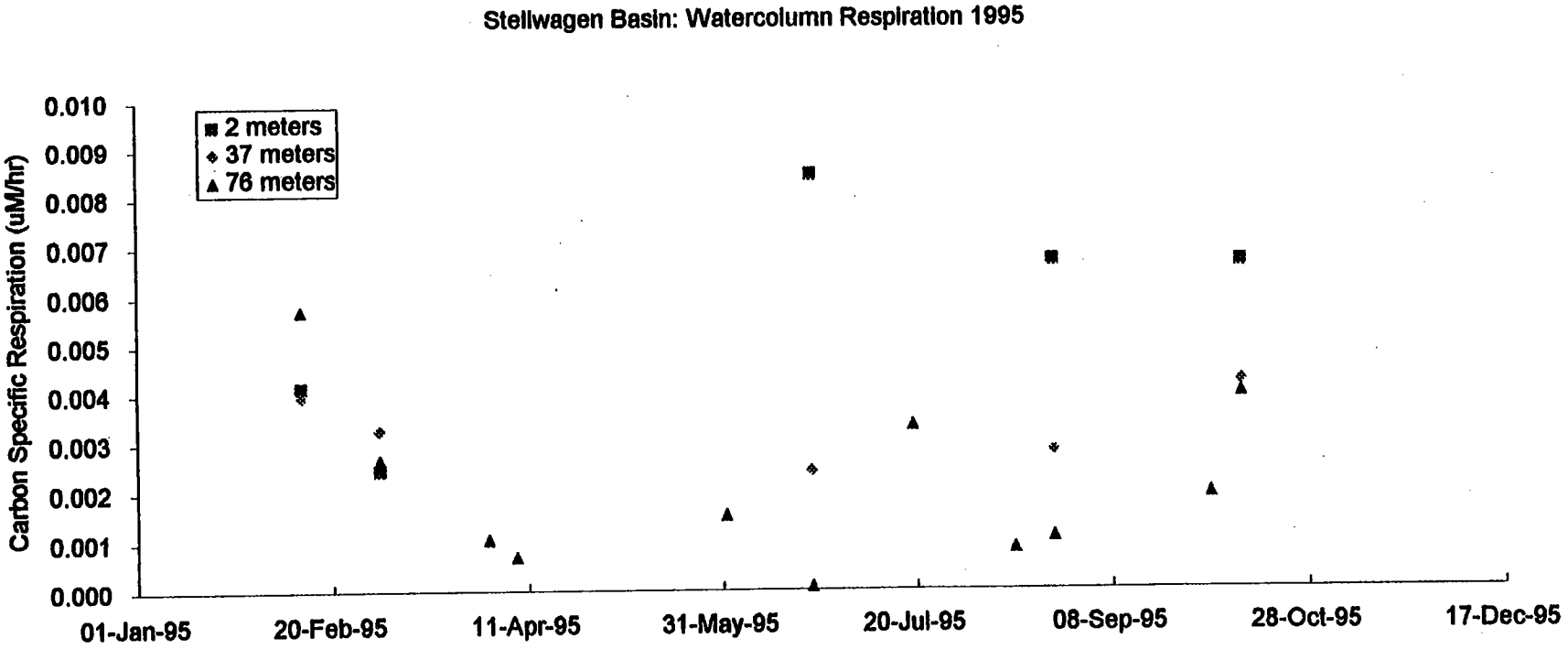

FIGURE 7-38

Vertical distribution of carbon specific watercolumn respiration within Stellwagen Basin through 1995. Data are from station F19 (6X/year) and MB05 (5X/year, bottomwater only, in the benthic flux program). Note expanded scale from the nearfield.

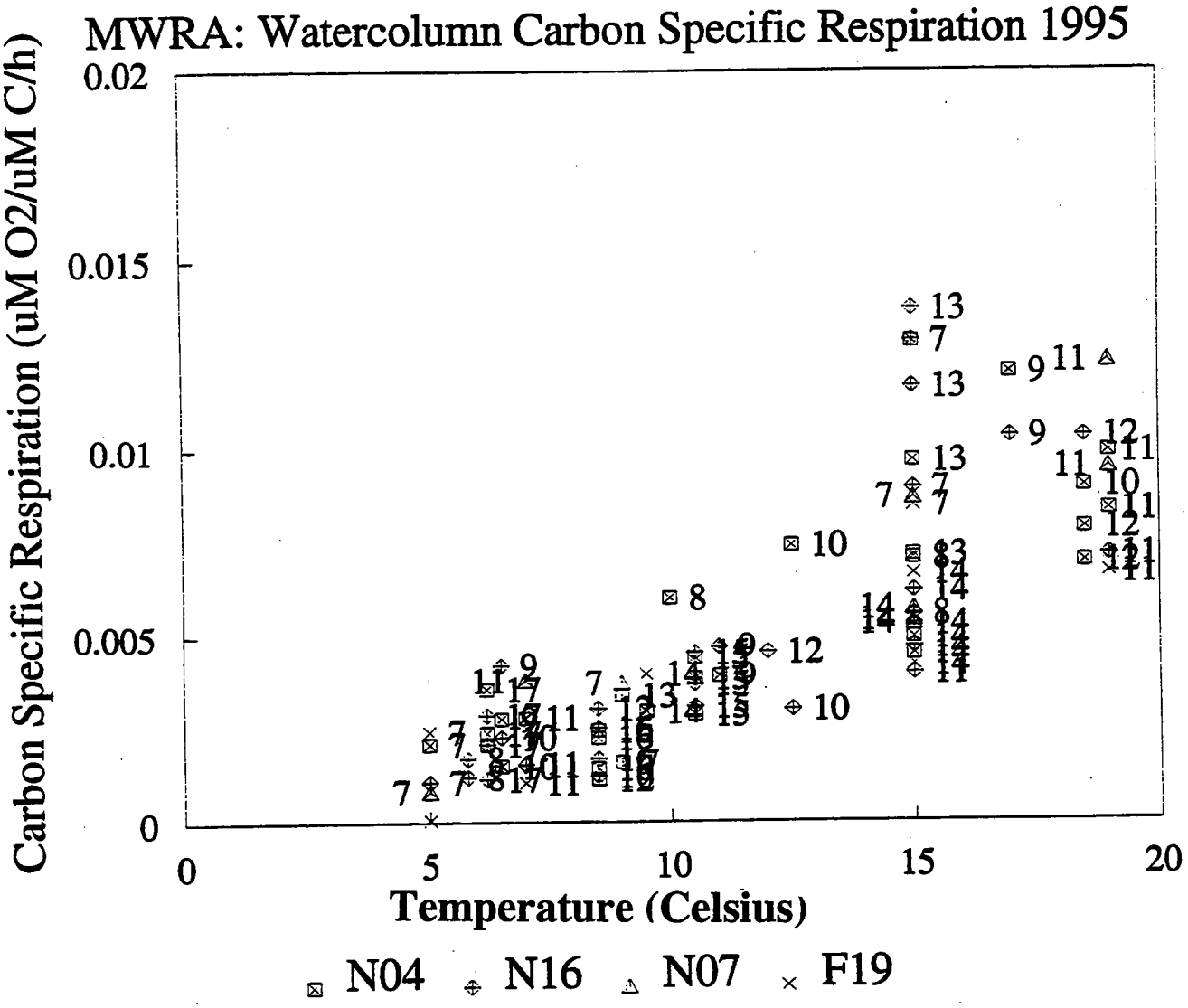

FIGURE 7-39

Carbon specific respiration versus temperature at the nearfield (N04, N16, N07) and offshore (F19) stations sampled in summer and fall of 1995. Numbers indicate sampling cruises.

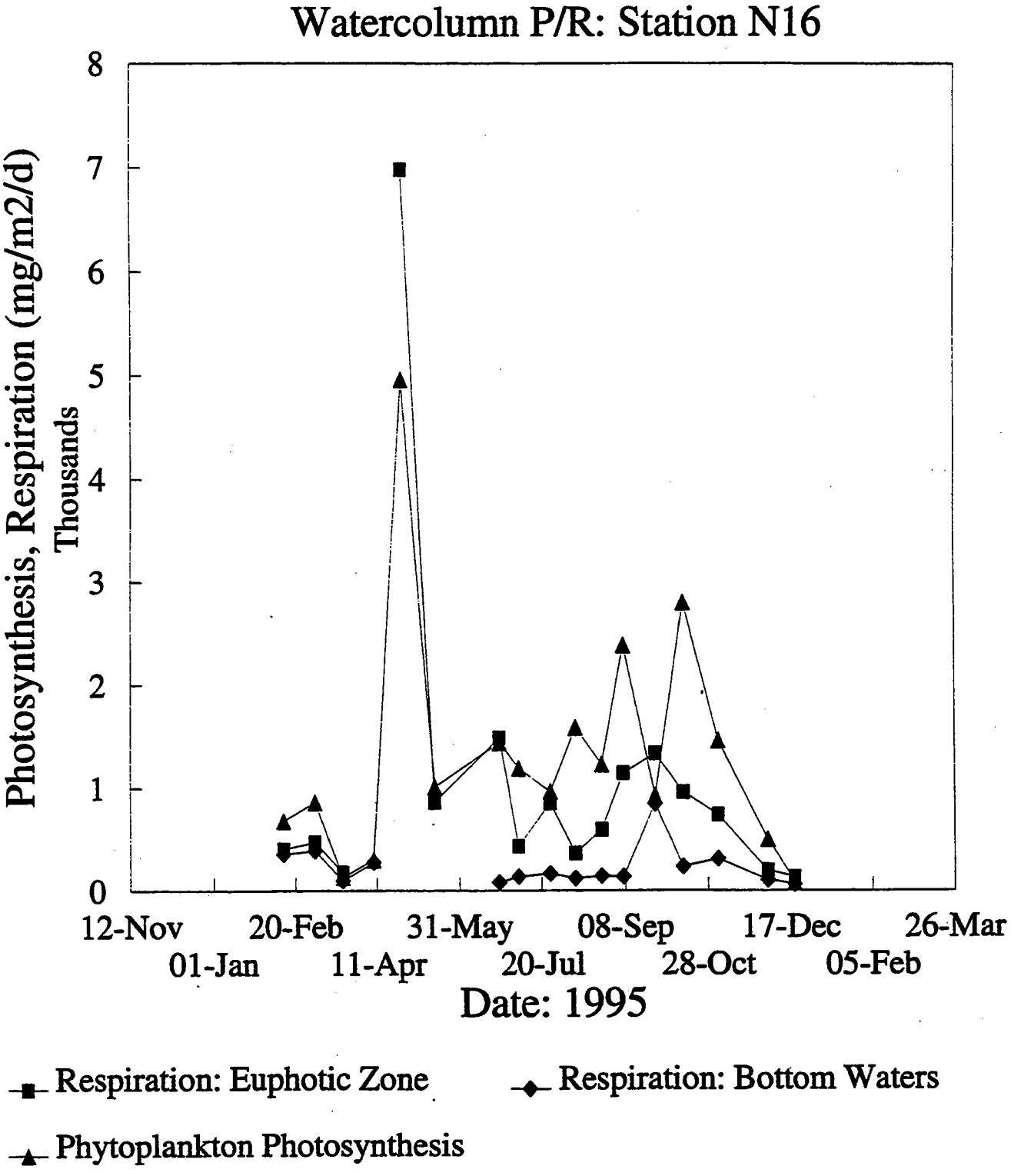

FIGURE 7-40

Photosynthesis and respiration within the euphotic zone and bottom water respiration at nearfield station N16 throughout 1995. Rates are integrated through the appropriate water depths on an areal basis.

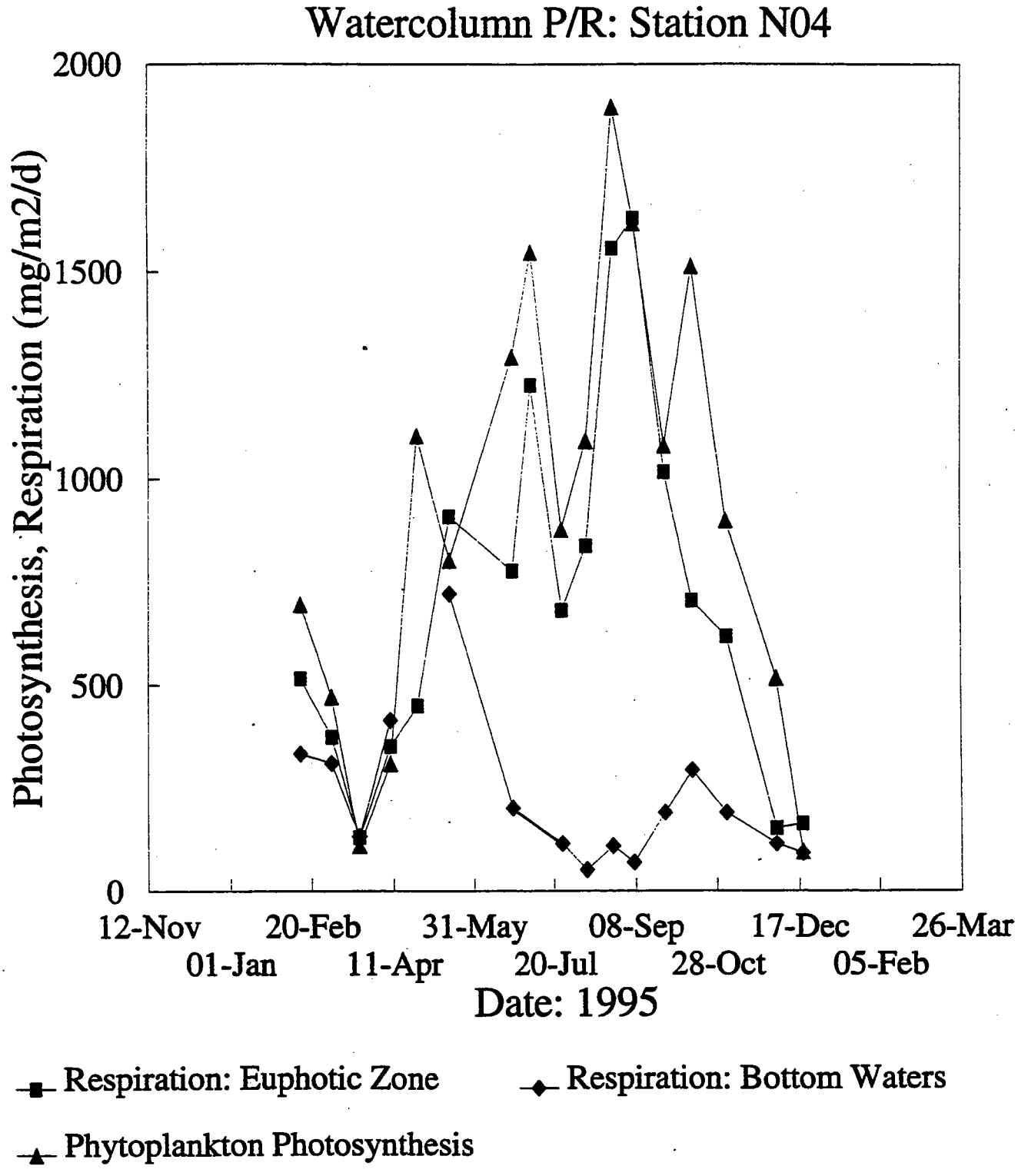

FIGURE 7-41

Photosynthesis and respiration within the euphotic zone and bottom water respiration at nearfield station N04 throughout 1995. Rates are integrated through the appropriate water depths on an areal basis.

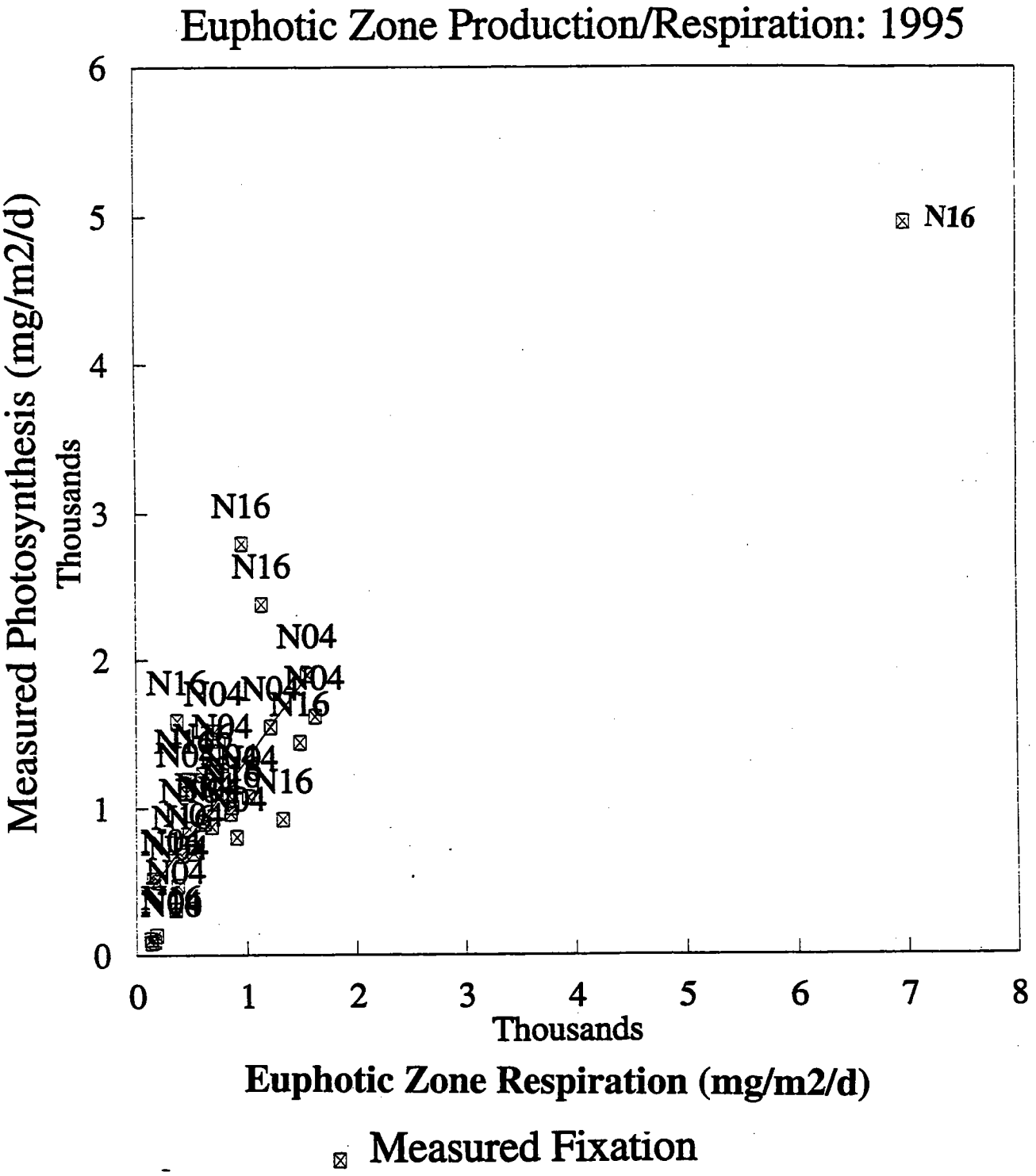

FIGURE 7-42

Relationship of watercolumn respiration and photosynthesis within the euphotic zone of nearfield stations N04 and N16 measured in 1995. The highest value was during the spring *Chaetoceros* and *Thalassiosira* bloom at station N16 (see Section 8.1.1). Values represent the total euphotic zone rate per m^{-2}, symbols indicated station.

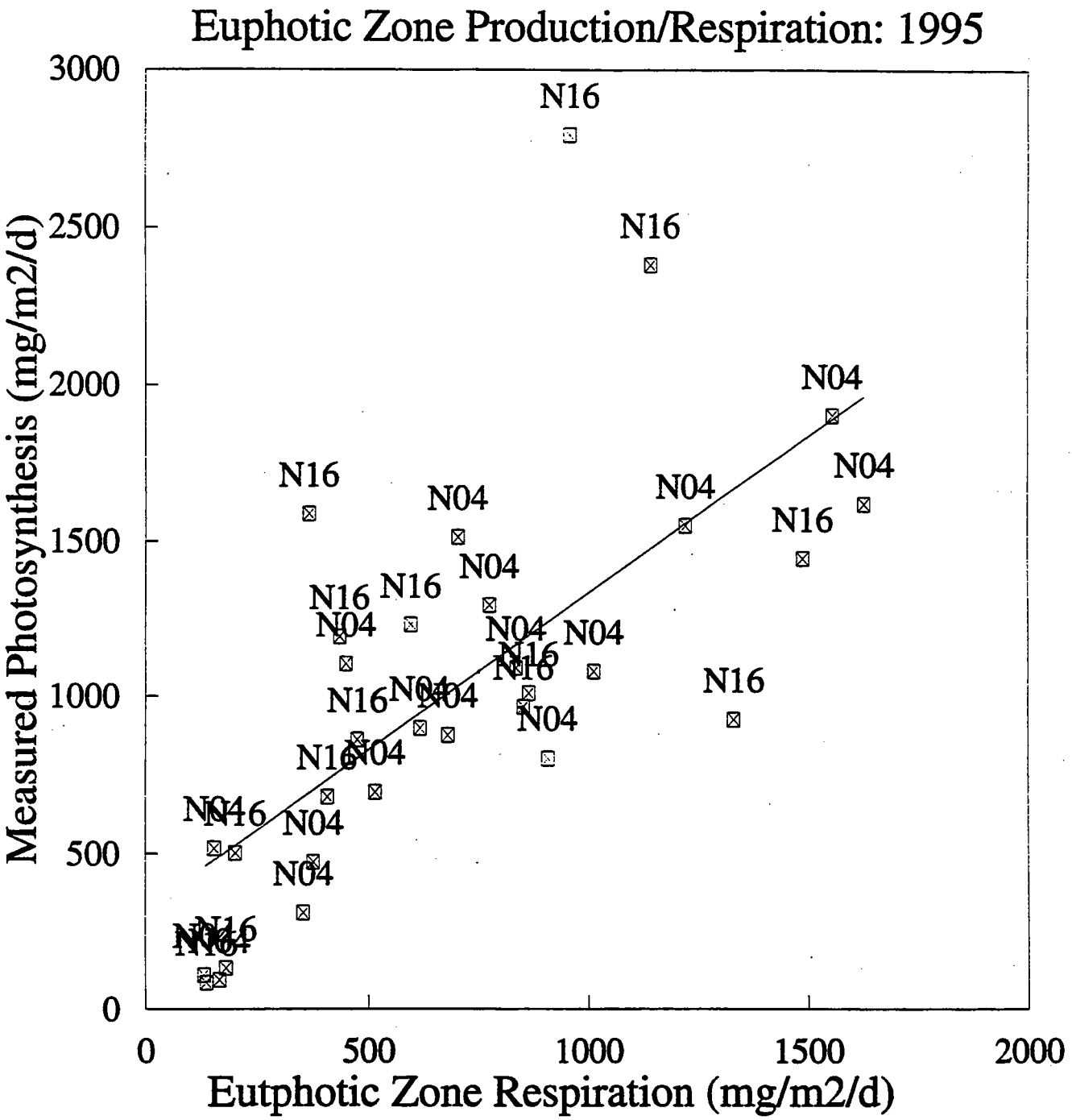

FIGURE 7-43

Relationship of watercolumn respiration and photosynthesis within the euphotic zone of nearfield stations N04 and N16 measured in 1995. The highest value was during the spring *Chaetoceros* and *Thalassiosira* bloom at station N16 (see Section 8.1.1). Values represent the total euphotic zone rate per m^{-2}, symbols indicated station.

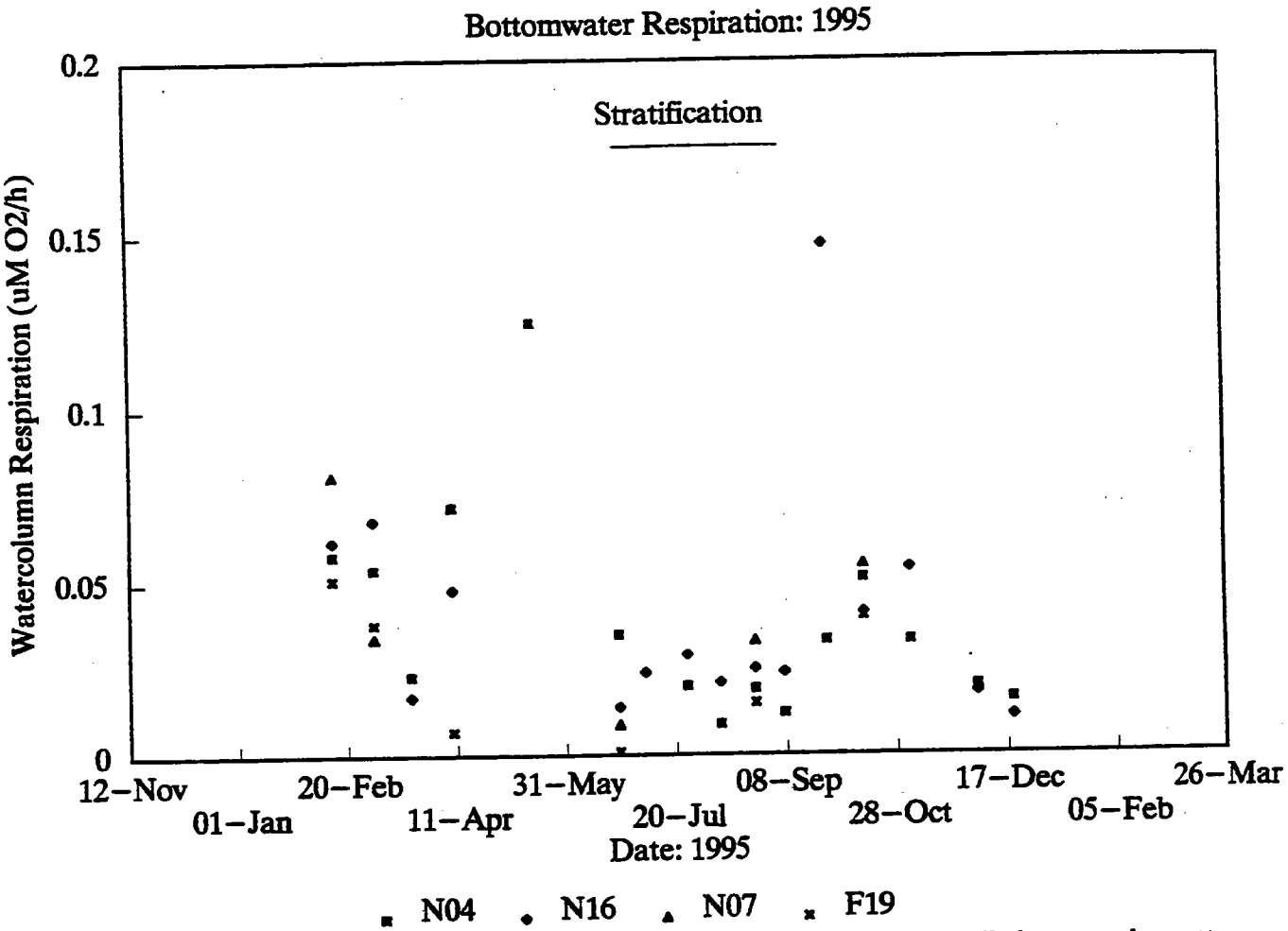

Note: Vertical distribution of respiraNote: Respiration is controlled primarily by organic matter.

FIGURE 7-44

Relationship of watercolumn respiration and photosynthesis within the euphotic zone of nearfield stations N04 and N16 during 1995 excluding the spring bloom sampling. Values represent the total euphotic zone rate per m^{-2}, symbols indicated station.

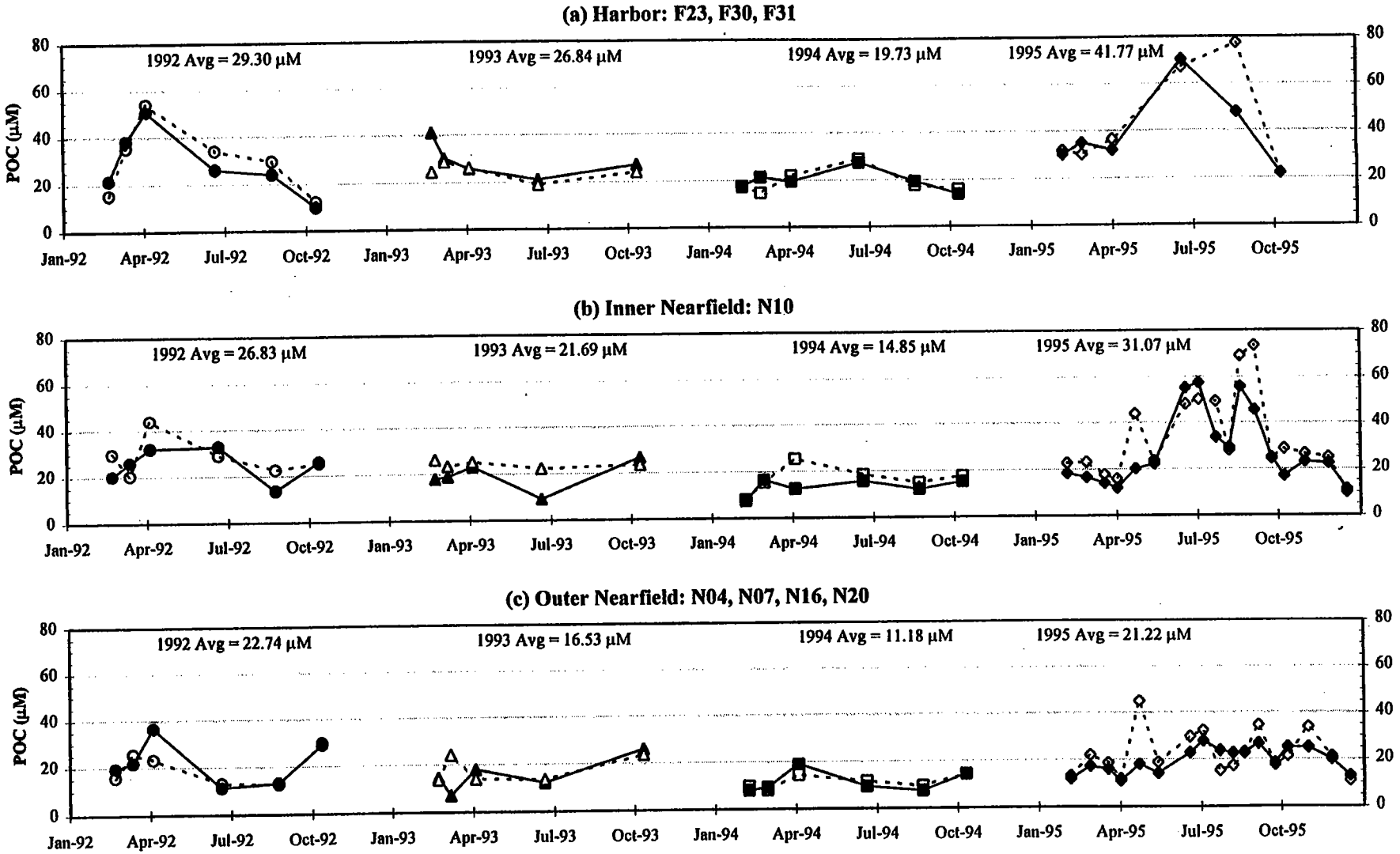

FIGURE 7-45

Interannual POC Concentration Survey Averages for Selected Areas in the Harbor and Nearfield Regions

Open symbols indicate surface average. Closed symbols indicate chla max average.

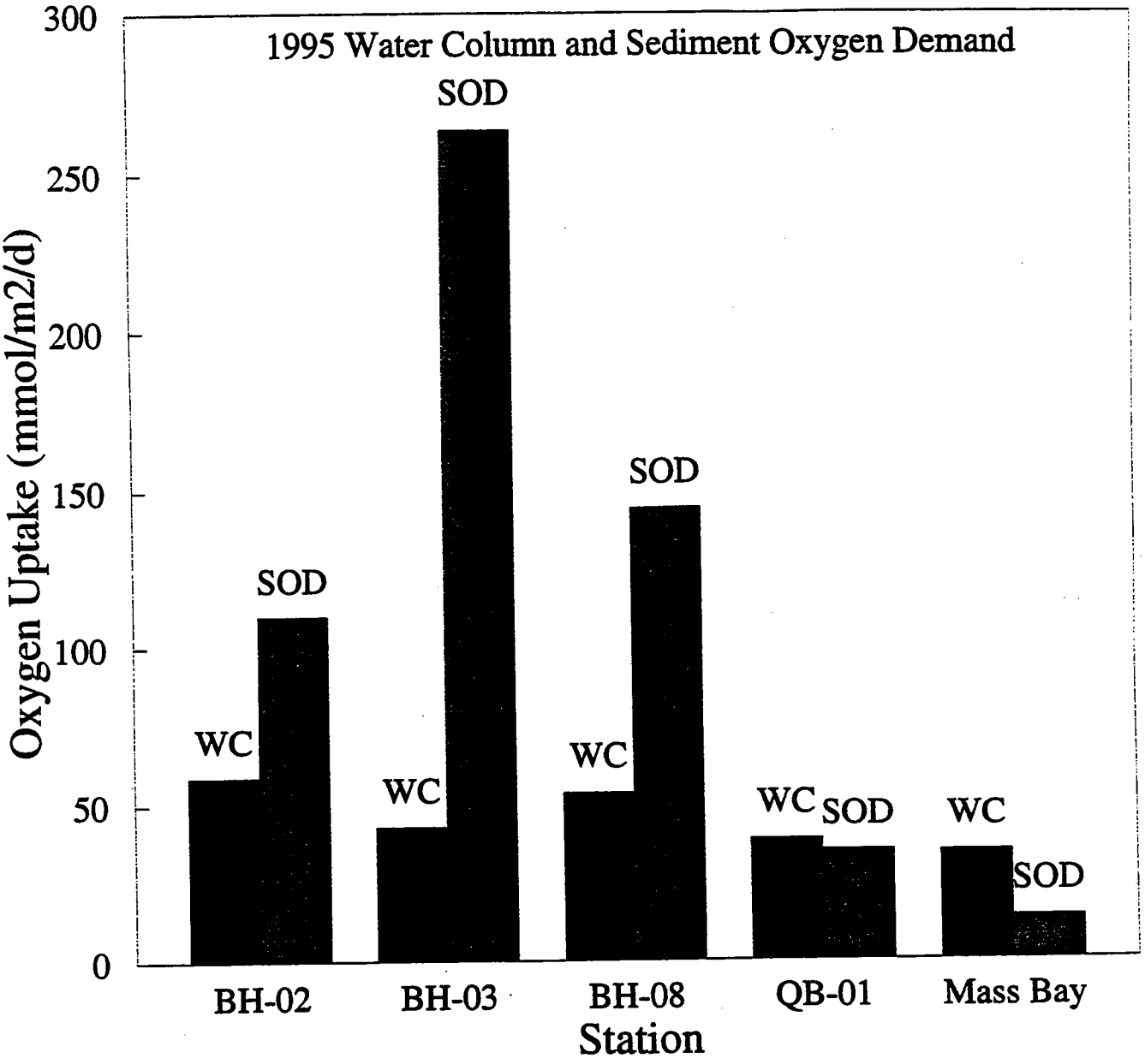

FIGURE 7-46

Rates of sediment and integrated watercolumn respiration within Boston Harbor (BH02, BH03A, BH08A, QB01) and Massachusetts Bay stations. Massachusetts Bay stations are about three times the depth (ca. 33m) of those in the Harbor.

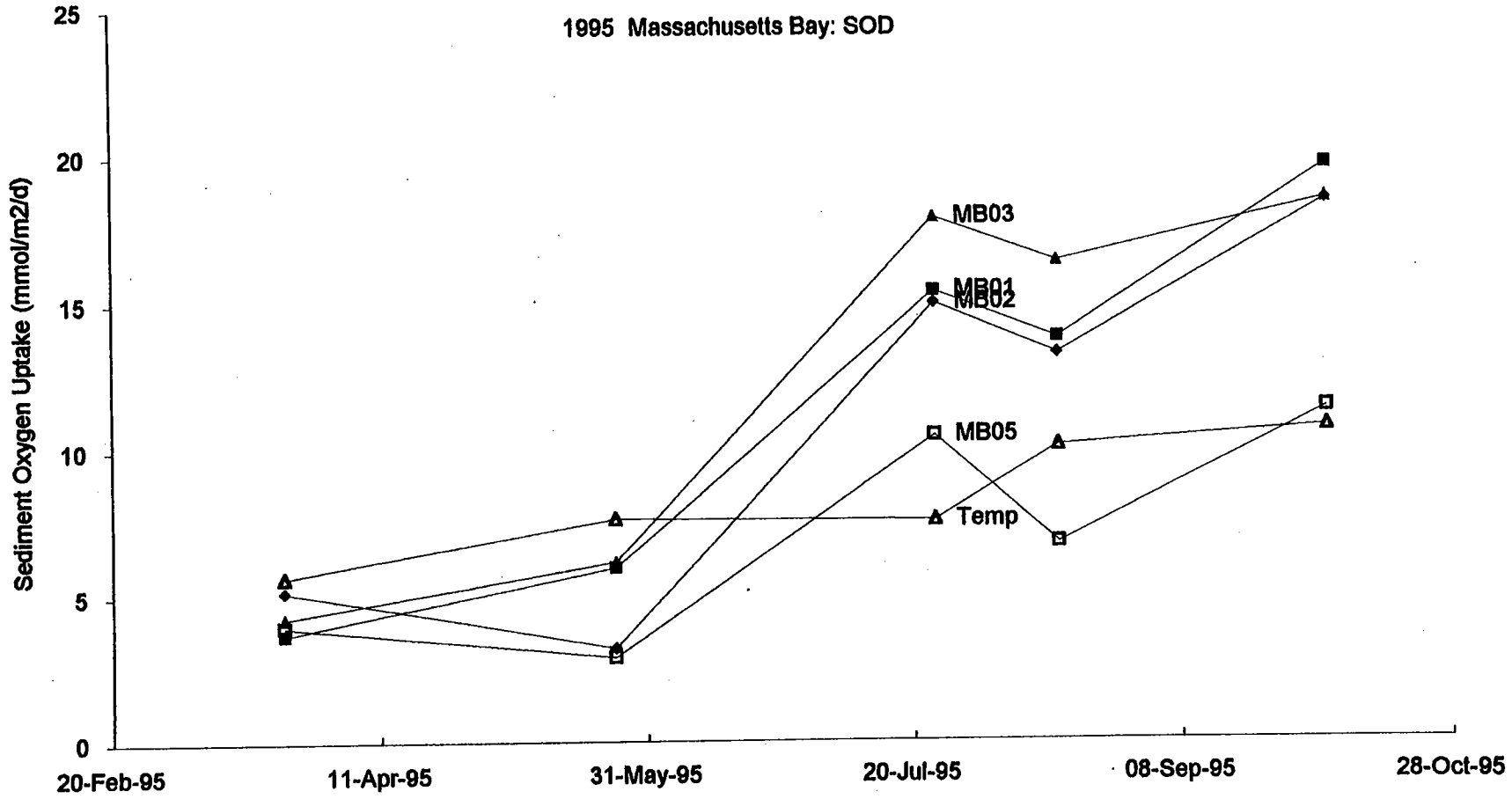

FIGURE 7-47

Sediment Respiration within the eastern nearfield (MB01, MB02, MB03) and western Stellwagen Basin (MB05) throughout 1995 and mean temperature (°C) of water ca. 1 meter above sediment surface.

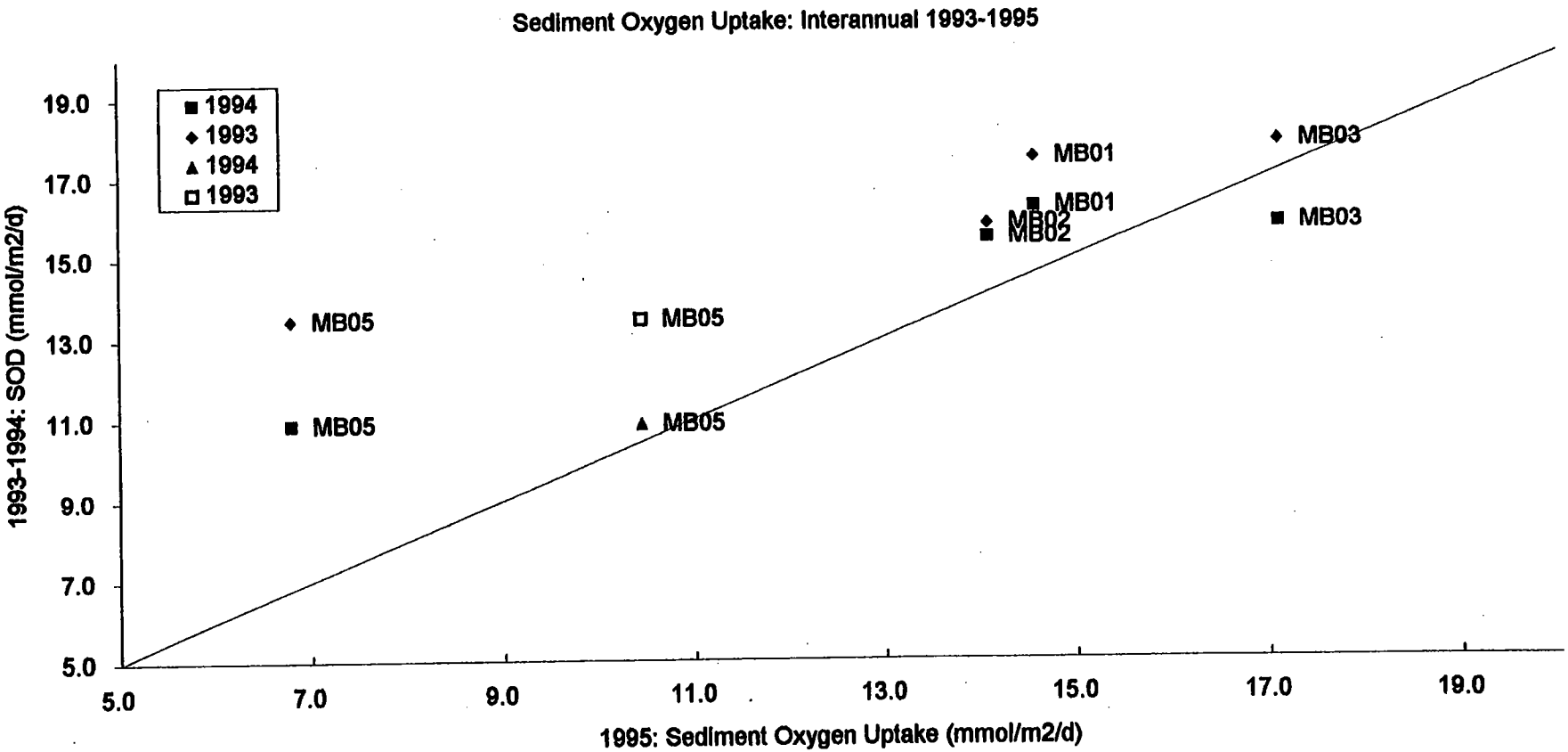

FIGURE 7-48

Interannual comparison for sediment oxygen uptake from the eastern nearfield (MB01, MB02, MB03) and western Stellwagen Basin (MB05) monitored from 1992-1995. Data from 1993 and 1994 represent average July and August values except MB05, which is August only (Giblin et al. 1995) and plotted against July and August 1995 values separately. Values above the line represent measurements that are greater than those of 1995.

8.0 PLANKTON

The 1995 HOM Program included analysis of the plankton community in Boston Harbor, Massachusetts Bay, and Cape Cod Bay during 11 nearfield and six combined nearfield/farfield surveys conducted from February to December. Two stations were occupied in the nearfield surveys, while an additional ten locations were sampled during the combined events (Figure 8-1).

Sampling included whole-water phytoplankton collections at the surface (<2.5m) and at the water column chlorophyll maximum (chl_{max}), as determined from in-situ fluorescence hydrocasts. Additional samples were taken at these two depths and screened through 20μm Nitex mesh to retain and concentrate larger dinoflagellate species. Oblique zooplankton tows were performed at each of the stations. Details regarding sampling and analysis can be found in the Combined Work Plan/QAPP for water column monitoring (Bowen *et al.*, 1995).

Quantitative taxonomic analyses were performed during 1995, continuing the monitoring record begun in 1992. For 1995, carbon equivalence estimates were made for both phytoplankton and zooplankton communities using species-specific carbon data from the literature. The objective of these analyses is to provide the baseline from which to evaluate the potential effects of the relocation of the Deer Island discharge to its 1998 discharge site in Massachusetts Bay. This evaluation focuses on the potential alteration in biomass or community structure that may result from the stimulatory effects of nutrient enrichment, or alternatively from inhibitory effects due to effluent toxicity. Additionally, these data can support assessments of the phytoplankton community's effect on water clarity or color.

In this section, the 1995 plankton record is presented with a discussion of spatial and temporal trends. Comparisons are made with previous baseline data collected from 1992 to 1994.

8.1 Phytoplankton

8.1.1 Abundance and Species Succession in the Nearfield

Whole-water phytoplankton results from 1995 nearfield sampling showed an annual cycle which included a spring bloom in April, several summer maxima, and a fall bloom (Figure 8-2a and b). Cell densities were highest during the summer maxima. Results from the inshore station N10 were similar to the more offshore station N16 early in the year (through May), but cell densities were typically higher inshore from June through September. The fall bloom appeared to be more pronounced at station N16. There was evidence of a late winter event as well, which was characterized by declining densities during the first two

surveys. There was also evidence of this in the nutrient concentrations (e.g. Figures 4-1 through 4-5) and in the chlorophyll results (Figures 5-2b and 5-2d).

During most surveys (particularly in summer months), the phytoplankton assemblage was numerically dominated by small (<10 μm) flagellated species (Figures 8-3 a and b). However, carbon equivalence estimates for the individual taxa present during the surveys indicated diatom species, particularly during frequent bloom events (e.g. late April, late June/early July, late August/September, and late October/early November), often were dominant (Figures 8-4 a and b). In some cases, this contribution was as high as 97 percent (September 6). Dominant diatom taxa during these peaks included *Chaetoceros* and *Thalassiosira* spp. (spring); *Thalassiosira* spp., *Skeletonema costatum*, *Rhizosolenia fragilissima*, and *Leptocylindrus danicus* (summer periods), and *Asterionellopsis glacialis* (fall).

Other groups contributed large percentages to the overall biomass during some periods. Dinoflagellate species occasionally (e.g., late winter/spring and fall) comprised from 40 to 60 percent of estimated biomass, particularly at nearfield station N16 (Figures 8-4 a and b). An unidentified species of *Gymondinium* was responsible for this biomass in the early spring period, while the presence of *Ceratium longipes* contributed to the dinoflagellate biomass in late spring. Cryptophytes also contributed a large fraction during the spring at station N10. The late summer dinoflagellate primarily responsible for the relatively high biomass contribution was *Ceratium tripos*, with additional contribution by *Gymnodinium* spp. and *Prorocentrum micans*.

8.1.2 Regional Comparisons for 1995

8.1.2.1 Whole-Water Samples

Phytoplankton data from the six combined sampling events in 1995 were reviewed to examine spatial and temporal trends in other regions relative to the two nearfield stations. To facilitate this review, individual survey results were averaged for the regions depicted in Figure 2-1. Survey results were then plotted for total densities and for major taxonomic groups (Figures 8-5 through 8-10). Note that only one station was sampled within the each of the offshore and boundary regions (Figure 8-1; Table 8-1).

Highest overall total phytoplankton and microflagellate densities were evident in the harbor and coastal waters (Figures 8-5 and 8-6), with a continuing gradient toward lower densities with distance from shore. Based on total abundance results from the six farfield surveys, annual maxima in the harbor, coastal, and nearfield waters occurred in the summer, whereas the more offshore waters exhibited a slower trend toward late summer maxima. Cape Cod Bay had the highest relative total cell densities in late winter/early spring, but had offshore, low density conditions during the summer.

Chlorophyll data indicated that the spring bloom in Cape Cod Bay occurred earlier than other regions (Figure 5-8). Densities of centric diatoms were higher in Cape Cod Bay relative to the other regions throughout this period (Figure 8-7). The nearfield reached its spring maximum three weeks later (documented during a nearfield only sampling event). Peak abundances of centric diatoms were reached in the summer in the inshore waters and nearfield, whereas Cape Cod Bay and the Boundary waters had much lower densities, similar to the offshore region. Centric diatoms appeared to contribute to some extent to the fall bloom event around the end of October.

Pennate diatoms appeared to increase gradually through the year at most stations, although the more intensive sampling at the nearfield stations gave some indication of the substantial variability which can occur. The most notable event was the bloom of *Asterionellopsis glacialis* during the fall turnover in the nearfield (Figure 8-8). The extent of this species' regional distribution could not be ascertained, as this nearfield bloom occurred after the last combined sampling event.

Flagellated groups such as cryptophytes (Figure 8-9) and dinoflagellates (Figure 8-10) appeared consistent with the other groups, with summer maxima and higher densities inshore. The nearfield cryptophyte assemblage was more similar to harbor and coastal waters than was the case with the dinoflagellates, for which summer maxima were highest in the inshore waters. These regional averaging schemes will not reveal localized blooms of individual species or genera, however. These blooms are currently being investigated for a number of dinoflagellate species, and will be reported elsewhere.

8.1.2.2 Toxic and Nuisance Species

The HOM program includes monitoring for toxic and nuisance species, particularly *Alexandrium tamarense*, *Phaeocystis pouchetii*, and *Pseudo-nitzschia multiseries*. *Alexandrium tamarense* is a dinoflagellate which can cause paralytic shellfish poisoning (PSP) when shellfish which have concentrated the toxin are consumed. Screened phytoplankton samples were employed at each sampling location to concentrate these relatively rare organisms, as well as other dinoflagellate species.

Alexandrium in the Massachusetts Bay region may arise from two sources: locally from benthic cysts and from advective transport of cells arising from riverine discharges in southern Maine, usually during the period April to June (Anderson and Keafer, 1992; Franks and Anderson, 1992). Once established, abundance and distribution are governed by nutrient availability, wind patterns and coastal currents. These physical controlling factors may alternatively disperse the population offshore or lead to conditions of increased residence time which allow localized blooms (Anderson and Keafer, 1995).

During 1995 there were three surveys in the nearfield during the period when *Alexandrium* might be encountered, and only one (mid-June) in the farfield. There was no evidence of *Alexandrium* in the nearfield or other Massachusetts Bay regions in the 1995 HOM plankton data. However, separate surveys

by D.M. Anderson under a joint Sea Grant/MWRA contract did document the distribution and abundance of toxic *Alexandrium tamarense* cells in the bay in the late-spring/early summer period of 1995. Those surveys were conducted on April 26, 27, May 10, May 26, June 6, and June 20, 1995. *Alexandrium* was detected during all surveys, but the highest levels were found on May 10, when there were several stations with up to 56 cells/L (Figure 8-11). In general, 56 cells/L is well below densities that would cause toxin to reach detectable levels in shellfish. These plankton data are consistent with results from the Massachusetts Division of Marine Fisheries, which detected no toxicity anywhere within the Bays during weekly shellfish sampling in 1995 (Figure 8-12). Thus 1995 was a "non-bloom" year for *Alexandrium* within Massachusetts and Cape Cod bays.

The fact that *Alexandrium* was detected within the bays during the Anderson surveys but was not detected in any of the HOM surveys (several of which were during May and June) is explained by two factors. First, *Alexandrium* cells were in very low abundance, such that the normal procedures use by the HOM Program to concentrate and count cells might miss such rare cells, even in the screened samples. Second, *Alexandrium* cells were not uniform in concentration throughout the bay, but were patchy and typically in higher densities offshore, toward Stellwagen Bank. It would have been easy to miss the patch of cells during sampling, especially at the nearfield stations. At higher, bloom concentrations, the methods used in the HOM program would detect this species, but would probably not be able to provide very much detail on overall cell distribution and abundance since the frequency of sampling is not designed to document patchy and short-lived blooms, such as those typical for *Alexandrium*.

Phaeocystis may occur as individual flagellated cells which are typically in the 5μm to 8 μm diameter range (smaller than the 20μm Nitex screening used for the screened phytoplankton samples), or as gelatinous colonies which can be from 500μm to 2,000μm in diameter which would be captured on the Nitex screening. Similarly, the diameter (< 8μm) of the rod-shaped *Pseudo-nitzschia* cells could permit their passage through the screen, although their longitudinal colony formation and long length (70-160μm) would likely result in retention of most cells. Both whole-water analyses and screened samples were therefore examined for the presence of these two species.

Phaeocystis was not reported in the 1995 HOM plankton monitoring. *Phaeocystis* is a cold-water form that would typically be present in the late fall or winter surveys. In the absence of large conspicuous colonies, individual cells of this species may have been included in the unidentified microflagellate count. It can therefore only be concluded that bloom densities or colonial stages were not evident during the periods covered by the sampling events.

The toxin-producing strains of *Pseudo-nitzschia* cannot be differentiated from non-toxic species under the light microscope. The potential distribution of *Pseudo-nitzschia multiseries* in the nearfield was examined by plotting all reported results for the morphologically similar species *Pseudo-nitzschia pungens* (Figure 8-13). This approach should be viewed as a conservative indicator of whether a toxic species may be

present. The 1995 record indicated that *P. pungens* occurred primarily in the summer and fall, with similar distribution in the surface and chlorophyll maximum samples. Concentrations never exceeded 100,000 cells/L, a density threshold above which the toxic form can cause accumulations of toxin in shellfish (Bates, 1997). Its sporadic presence did not indicate any regional trends.

8.1.3 1992-1995 Interannual Comparisons

While the previous (1992 to 1994) HOM sampling included six sampling stations within the nearfield, comparisons were restricted to stations N10 and N16 to examine the interannual trends without confounding averaging schemes. This approach also allowed examination of the gradient across the nearfield represented by these two stations.

For whole-water samples, the general trend toward multiple peaks and increasing densities through the summer which was evident in the 1995 record was also seen in previous years, both in total cell densities (Figure 8-14) and the seasonal succession of taxa within major groups (Figures 8-15 through 8-19). In Figures 8-14 (total abundance) and 8-15 (microflagellate abundance), the magnitude of the peaks during 1995, particularly in summer, was higher than previous years due to the use of higher magnification during the 1995 counting procedures. This resulted in higher abundance of smaller taxa (microflagellates and unidentified monads which are typically in the 2-5μm size range), and may have led to reduced precision in the estimated densities of larger taxa.

Also evident in all years of the interannual record is the elevated abundance of phytoplankton at the inshore station N10, particularly in the summer months. There appears to be enhanced abundances for taxa in most of the major groups (Figures 8-15 through 8-19), suggesting that this is a function of the higher nutrient availability inshore.

The plankton data demonstrate the considerable interannual variability which characterizes the nearfield. As was seen in the nearfield chlorophyll data (Figures 5-10), the 1995 spring diatom maxima (Figure 8-16) was a month later in 1995 than in the other three baseline years. As an example of interannual differences in seasonal abundance, the 1994 results for centric diatoms were an order of magnitude lower than for the other years. Similarly, the fall 1995 pennate bloom of *Asterionellopsis* (Figure 8-17) was a month later than in previous years, and was comparatively subdued in 1992 and 1994 relative to the other two years.

The distributions of *Alexandrium*, *Phaeocystis*, and *Pseudo-nitzschia* also show a high degree of interannual variability (Figures 8-20, 8-21, and 8-22). *Alexandrium* was detected by the HOM program in 1992, 1993, and 1994, but not in 1995 (Figure 8-20). Concentrations were low (<100 cells/L in all but one sample) in all three years according to these data. However, these concentrations are not indicative of the true nature of the *Alexandrium* blooms in any of those years, for the reasons given earlier.

More importantly, 1993 was a year with extensive shellfish toxicity in Massachusetts and Cape Cod Bays, with high cell concentrations (100 to 900 cells/L) and paralytic shellfish poisoning (PSP) toxicity persisting for two months from first detection (Anderson and Keafer, 1995). These results again highlight the inability of the HOM program to document short-lived and patchy blooms of key species such as *Alexandrium*. They also make it difficult to assess the interannual variability in *Alexandrium* abundance.

Perhaps a better way to accomplish this is to examine shellfish toxicity levels, which provide an integrated record of the presence and abundance of toxic *A. tamarense* cells. Figure 8-12 shows 10 years of data from the Massachusetts Division of Marine Fisheries, presented in the form of the maximum annual toxicity at three stations within Massachusetts Bay. It is immediately apparent from these data that toxicity varies significantly between years, from undetectable to dangerous levels of nearly 400 micrograms per 100 grams of shellfish meat. The large differences between 1993, 1994 and 1995 are clear. Given this natural interannual variability, it will be a challenge to define "natural" levels of toxicity against which future measurements can be compared to demonstrate whether the outfall has enhanced *Alexandrium* abundance. Methods to accomplish this will be discussed elsewhere.

Phaeocystis colonies were detected in 1992, 1993, and 1994, but not in 1995 (Figure 8-21). Concentrations of this species varied by four orders of magnitude in these years, with 1992 and 1994 having the highest concentrations. *Pseudo-nitzschia pungens* was generally observed in the fall, with densities relatively constant from year to year (Figure 8-22).

8.2 Zooplankton

8.2.1 Abundance and Species Succession in the Nearfield

Zooplankton abundance in the nearfield exhibited a strong seasonal cycle (Figures 8-23). Densities generally increased from February through the summer at both stations. Peak densities during the summer at N16 appeared to be more variable than those seen at the inshore station.

Total abundance was lowest during early February (around 8,000/m^3), and had begun to increase by month's end (Figure 8-24). The assemblage was typically dominated by copepods and copepod nauplii. By late March, average abundance was near 15,000/m^3 inshore, and over 20,000/m^3 offshore at N16. The transitional nature of the nearfield region was evident in the higher proportion of barnacle nauplii at the near-shore station in late winter and spring (abundances of around 3,000/m^3) relative to the very low densities at N16.

With the exception of a drop in early July at both stations, zooplankton densities continued to increase throughout the spring and summer. Maximum densities were reached inshore by late July (over $1.0x10^5/m^3$; Figure 8-24, top panel), and mid-August offshore at N16 (Figure 8-24, bottom panel). From

August to December there was an consistent decrease in abundance at N10, but at N16 there was an additional peak in late October. This second maximum preceded the fall productivity peak seen at station N16 (Figure 7-4).

Copepods were the most abundant group throughout the year, and the dominant species of copepods had characteristic seasonal patterns. Seasonal abundance and succession in the nearfield was investigated for the top ten dominant species (Figure 8-25, left panel). Samples taken early in the year were dominated by *Oithona similis*, *Pseudocalanus newmani*, and *Calanus finmarchicus*, with the emergence of *Temora longicornus* by June as a co-dominant. Later, *Acartia tonsa* and *Centropages typicus* joined *Oithona* as co-dominants as *Calanus*, *Temora*, and *Pseudocalanus* declined. Other late season forms included *Centropages hamatus*, *Microsetella norvegica*, *Acartia hudsonica* and *Paracalanus parvus*.

To investigate the contribution of these dominant taxa to overall community biomass, carbon content for these species was approximated by multiplying the numerical abundance by literature values of body carbon weight of adults. While this overestimates total biomass, it provides a reasonable weighting for examining the relative proportion of biomass among species. Body weights used for the 10 species plotted (*Oithona similis* to *Paracalanus parvus*) were 1, 10, 10, 15, 10, 125, 10, 10, 1, and 5 µgC, respectively. For species where body weight was unknown, weights of similar sized species were used.

Although Oithona was clearly the most important copepod in the nearfield in terms of numerical abundance, *Calanus finmarchicus* is by far most important in terms of total biomass (Figure 8-25, right panel). Subdominants in terms of biomass included *Pseudocalanus newmani* and *Centropages typicus*. In terms of productivity, given that *Calanus finmarchicus* is dominant during the cold season, the turnover of its biomass is probably slow due to its long generation time (ca. 60 days at 5°C). During late summer and fall, the total biomass is lower due to the decreased *Calanus finmarchicus* abundance, but this lower mass is undoubtedly turning over much faster owing to the much higher temperatures of (ca. 20°C). Although a detailed analysis of copepod production is necessary, it is likely that the late summer period is the most productive for the copepods as a whole.

8.2.2 Regional Comparisons for 1995

The spatial distributions of zooplankton taxa revealed two distinct groups with affinities for nearshore or offshore regions. The near shore assemblage is characterized by the two *Acartia* species (*A. tonsa* and *A. hudsonica*), *Centropages hamatus*, *Eurytemora herdmani*, the cladoceron *Podon* spp., and polychaete larvae (Figure 8-26). Note that the seasonality of the data are represented in the figure by their relative position on the horizontal line, and that the higher frequency of sampling in the nearfield is depicted by smaller, more numerous bars. These taxa all are known to be tied to the sea-floor to some degree. In addition, *Podon* and the polychaete larvae may be restricted to nearshore regions because of salinity intolerance.

The four copepod species in the inshore assemblage produce bottom resting eggs and are restricted to shallow regions (<60m). It is also well known that *Acartia* requires extremely high concentrations of food in order to achieve maximal growth and reproduction (Paffenhofer and Stearns, 1988; Durbin *et al.*, 1983, 1992; Durbin and Durbin 1992; Peterson and Belatoni, 1987). It is therefore thought that this genus is restricted to eutrophic nearshore habitats due to food limitation offshore (Fulton, 1984; Sullivan and Banzon, 1990).

The offshore assemblage (Figure 8-27) comprises the open ocean copepods *Centropages typicus, Paracalanus parvus, Calanus finmarchicus, Oithona similis, Pseudocalanus newmanii,* and *Microsetella norvegica,* as well as the larvacean *Oikopleura dioica* (not shown). As evident from the species data in Figures 8-26 and 8-27, the nearfield region represents a transition zone between the nearshore and offshore zooplankton assemblages. Several studies have documented similar trends along sewage-derived nutrient gradients (Arfi *et al.*, 1981; Champalbert and Patriti, 1982; Fulton, 1984; Theodorou *et al.*, 1994).

As with the nearfield, copepods were the most abundant group in the other regions throughout the year, and the dominant species of copepods had characteristic seasonal patterns. The seasonal cycles of the ten most abundant copepod species were plotted for each region (Figures 8-28 through 8-32). Continuing the contrast between numerical abundance and biomass performed for the nearfield (Section 8.2.1), each plot is accompanied by a depiction of the estimated biomass for each taxon.

Oithona similis was the numerically dominant copepod species at all stations throughout the year except in Boston Harbor. The harbor was dominated numerically by *Acartia tonsa* and *A. hudsonica* (Figure 8-28, left panel), followed by *Oithona similis* and *Centropages hamatus*. Peak densities in the harbor were reached during late summer. The two *Acartia* species also dominated the harbor in terms of estimated biomass (Figure 8-28, right panel), peaking in during the September - October period. *Centropages hamatus* was also a dominant in terms of biomass during this period. *Calanus finmarchicus* contributed the largest fraction of biomass during the winter spring period.

The coastal region (Fig 8-29) shared characteristics of the harbor and nearfield, though it was more closely aligned with the latter (refer to Fig 8-25). The coastal region was similar to the nearfield in its numerical dominance by *Oithona*, and was transitional with respect to the other copepod species. Peak estimated carbon biomass was similar in magnitude to that in the harbor (ca. 1.5 $x10^5$ $\mu gC/m^3$), however peak biomass occurred earlier in the year due to the dominant contribution from *Calanus finmarchicus*.

Beyond the nearfield, the offshore and boundary regions continued to be dominated by *Oithona similis,* with increasing abundance of *Centropages typicus* and *Temora longicornus* (Figures 8-30 and 8-31). There was a decrease in contribution to the copepod assemblage from the two *Acartia* species, and to a lesser extent from *Pseudocalanus newmani.* Biomass was dominated by *Calanus finmarchicus, Centropages typicus, Temora longicornus,* and *Pseudocalanus newmani.*

The zooplankton population in Cape Cod Bay appeared to be transitional between the nearfield and offshore assemblages (Figure 8-32). It was numerically dominated by *Oithona similis*, *Centropages typicus*, and *Pseudocalanus newmani*. Biomass dominants included *Calanus finmarchicus* in spring, *Pseudocalanus newmani* in summer, and *Centropages typicus* in the fall.

8.2.3 1992-1995 Interannual Comparisons

Plots of dominant taxa for the 1992-1995 baseline record (Figures8-33 to 8-36) revealed substantial interannual variability. For example, survey results for adult *Oithona similis* typically varied by two orders of magnitude (Figure 8-33). Note the higher frequency of sampling in the nearfield which began during 1995. Additional years of high-intensive sampling will further strengthen interannual comparisons. It appeared that 1992 and 1993 yielded higher peak abundance of *Oithona* in regions other than the nearfield, which was comparable to previous years.

Adults of *Calanus finmarchicus* appeared to be more abundant during 1995 in the nearfield, whereas densities in Cape Cod Bay were lower compared with results from 1992 (Figure 8-34). Further in-depth analysis of potential relationships between these biological data and the physical characteristics (e.g. temperature differences, Figure 3-4) is needed to help understand these apparent differences.

Two apparent discrepancies were noted in the 1992-1995 zooplankton database. In one case, 1992-1994 results indicated no overlap between the seasonal occurrence of the two dominant *Acartia* species, *A. hudsonica* and *A. tonsa*, with a sharp transition evident in mid-year (Figure 8-35). Results reported from sampling during 1995 indicated substantial overlap, with the winter-spring form, *A hudsonica*, continuing to proliferate in Massachusetts and Cape Cod Bays through the summer period.

In the second case, *Paracalanus parvus* was reported as a dominant copepod in late winter and spring from 1992-1994, whereas *Pseudocalanus newmani* was reported as the early season form in 1995 (Figure 8-36). It is possible that the similar body morphology could cause these genera to be confused with one another. However, *Paracalanus* is a warm water species and is unlikely to occur in the Bays region until water temperatures are above 10°C, i.e., until late summer and early fall. In both instances, further analysis of these samples is recommended to reconcile these differences.

These issues described above will be examined further in the upcoming Plankton Issues Report.

8.3 Plankton Discussion

The nearfield currently represents a transition between coastal and offshore assemblages, which is particularly evident in the zooplankton data. The existing nutrient gradient from the harbor to offshore waters likely dictates much of this transitional nature, although other physical and chemical factors also exert controls which vary temporally and spatially.

The change in the loading and distribution of nutrients associated with the outfall relocation may result in changes in plankton abundance and community composition. The phytoplankton may respond with increased biomass and/or altered community structure. Potential changes in zooplankton may be attributable to these changes in phytoplankton community structure (bottom-up effects) due to the close relationship between the two communities (Figure 8-37). These general changes will be subject to seasonal differences, and in particular, to the differences in water column physics and chemistry under non-stratified and stratified conditions.

One possible manifestation of a eutrophic response by the zooplankton community is that the assemblage character in the nearfield may lose its transitional character and become more similar to the inshore assemblage. The nearshore species would become dominant in the nearfield region, potentially displacing the offshore species assemblage. Since most of the dominant inshore zooplankton species are warm-water species, this displacement would likely be most pronounced in summer and fall.

Another scenario which has been postulated is a decrease in the surface loading of nutrients to the nearfield due to the elimination of the surface loading from the harbor (Kelly, 1993). While increased flux across the pycnocline was predicted during stratified periods, it was calculated to be less than 20 percent of the existing horizontal surface flux. Based on such mass loading calculations and water quality model projections (Hunt and Steinhauer, 1994), a net reduction in chlorophyll biomass in nearfield surface waters was predicted. Given the seasonal stratification pattern in the nearfield, this scenario would have the most pronounced effect during the summer.

These two scenarios suggest the possibility that the nearfield zooplankton assemblage may shift in either direction (toward a coastal or offshore assemblage) depending on the degree of eutrophication. Further, the physical dynamics of the system will undoubtedly influence the basic seasonal trends. Most influential among these will be large-scale upwelling or mixing events during stratified periods, advection of large nutrient-rich or nutrient-poor water masses into the nearfield, and interannual variability in temperature and salinity.

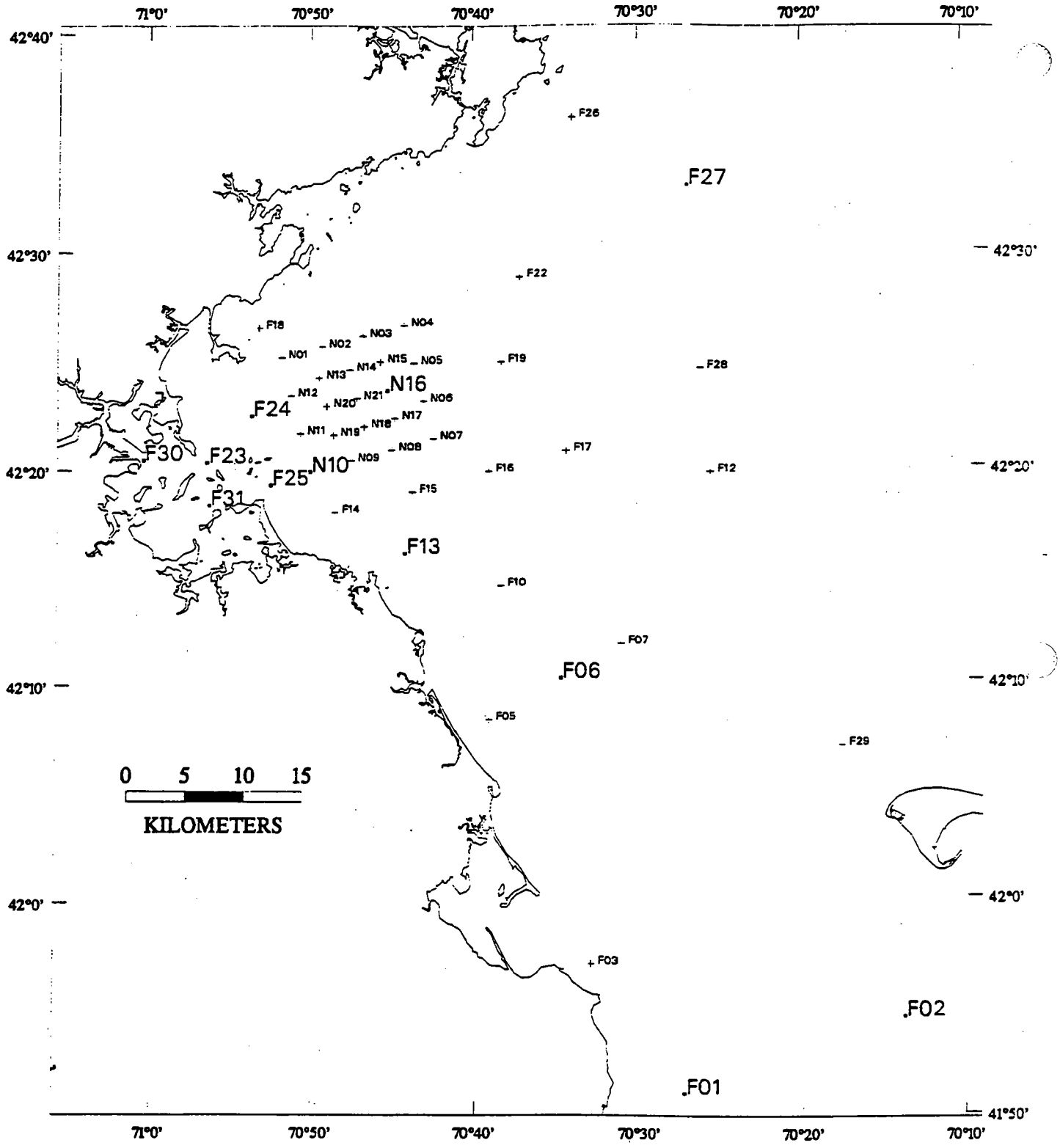

FIGURE 8-1
1995 HOM Plankton Stations Locations
(shown in enlarged text)

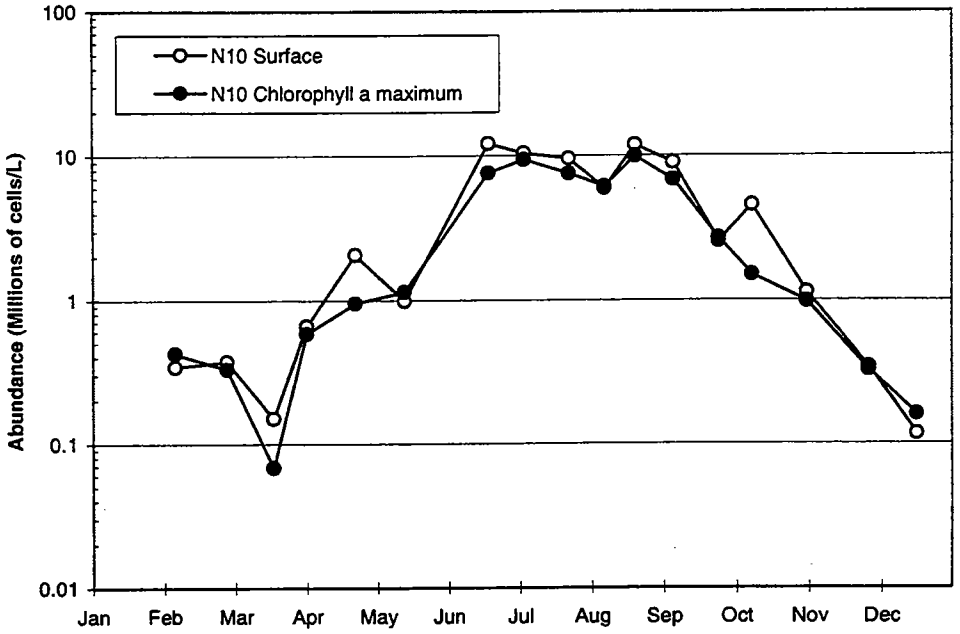

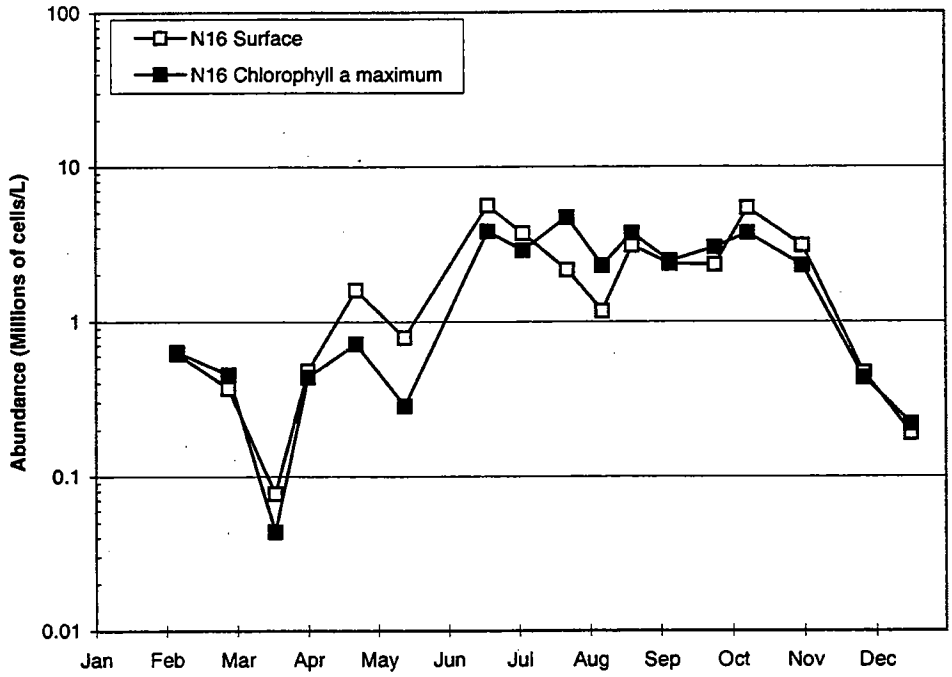

FIGURE 8-2
1995 Total Phytoplankton Abundance in Nearfield at Surface and Chlorophyll a maximum depths
(a) Top: N10, (b) Bottom: N16

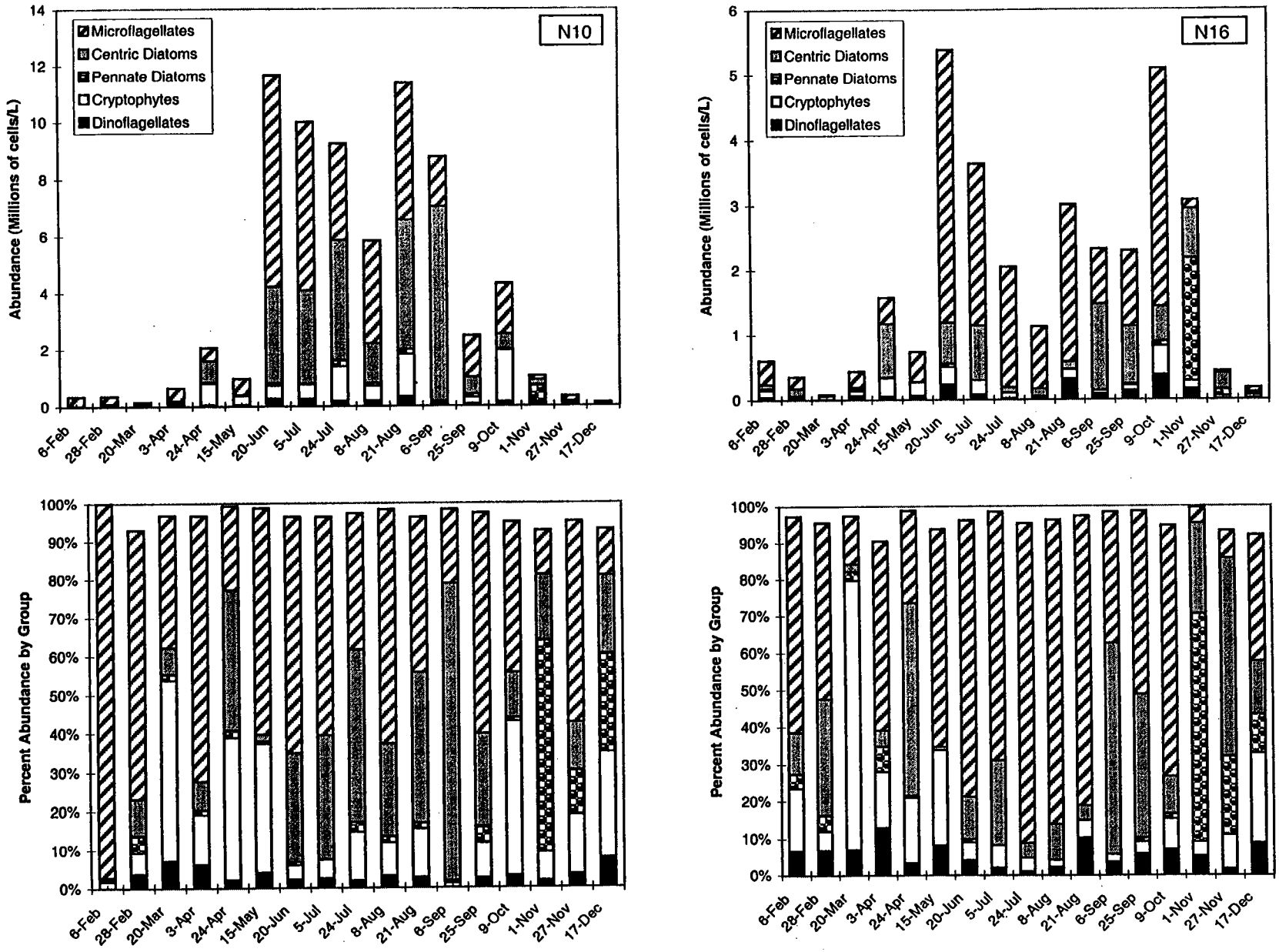

FIGURE 8-3a
Distribution of Major Taxonomic Groups and Relative Percent Abundance in 1995 Surface Samples
Nearfield Stations
Left:N10, Right: N16

*Note difference in y-scale axis

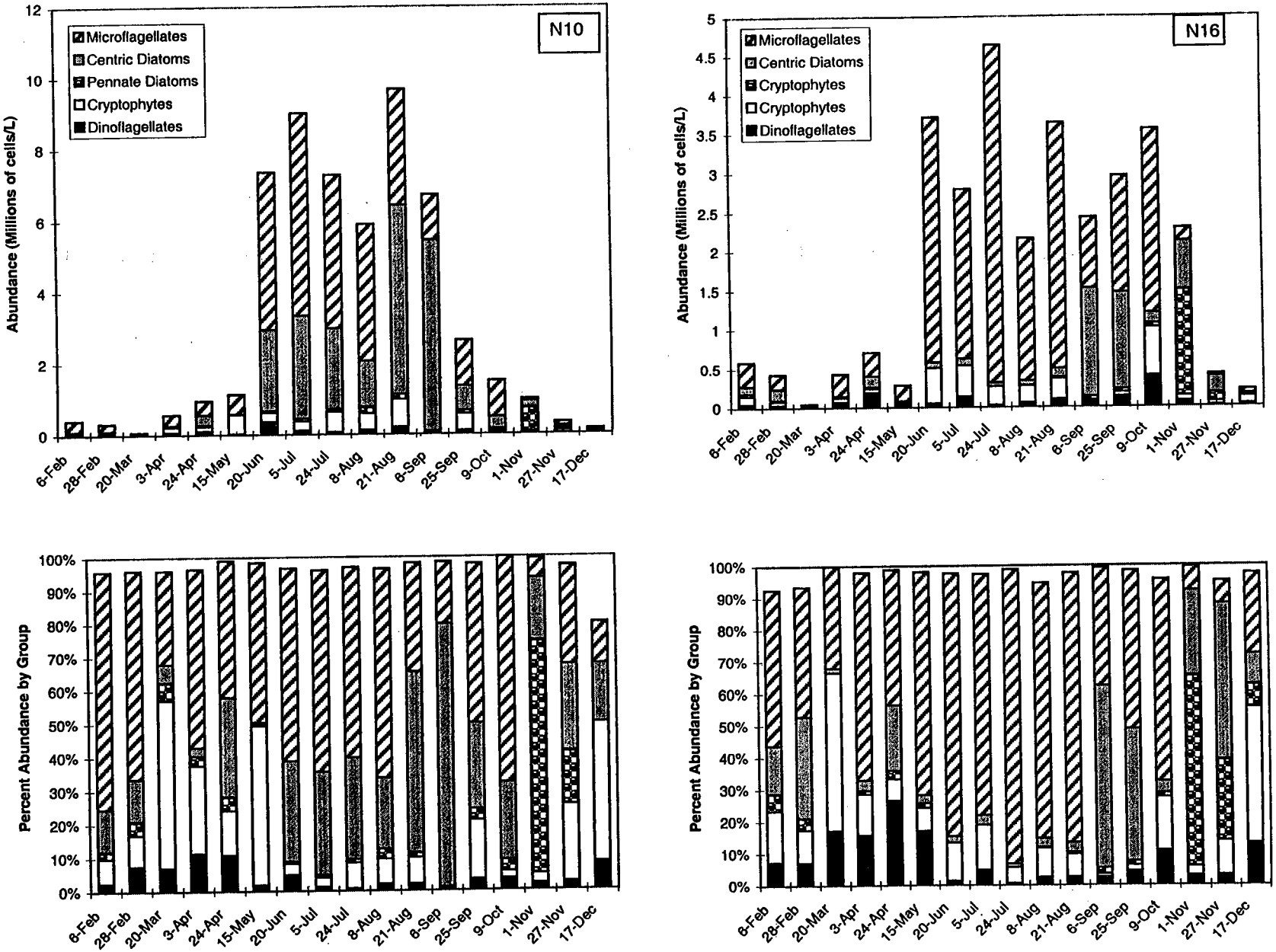

FIGURE 8-3b
Distribution of Major Taxonomic Groups and Relative Percent Abundance in 1995 Chlorophyll a Maximum Samples
Nearfield Stations
Left: N10, Right: N16

*Note difference in y-scale axis

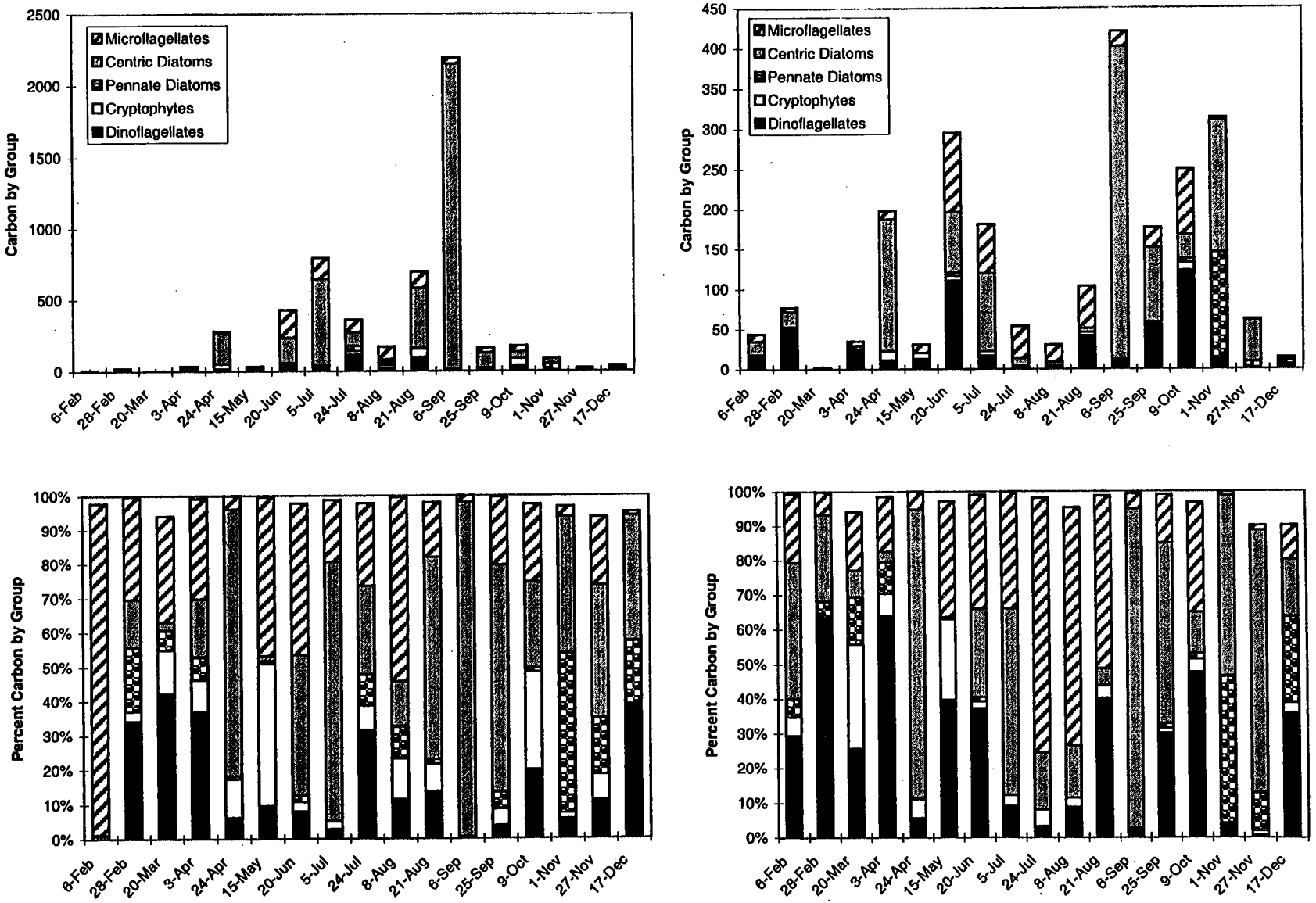

FIGURE 8-4a

Distribution of Carbon by Major Taxonomic Groups and Relative Percent Carbon in 1995 Surface Samples
Nearfield Stations
Left: N10, Right:N16

*Note difference in y-scale axis

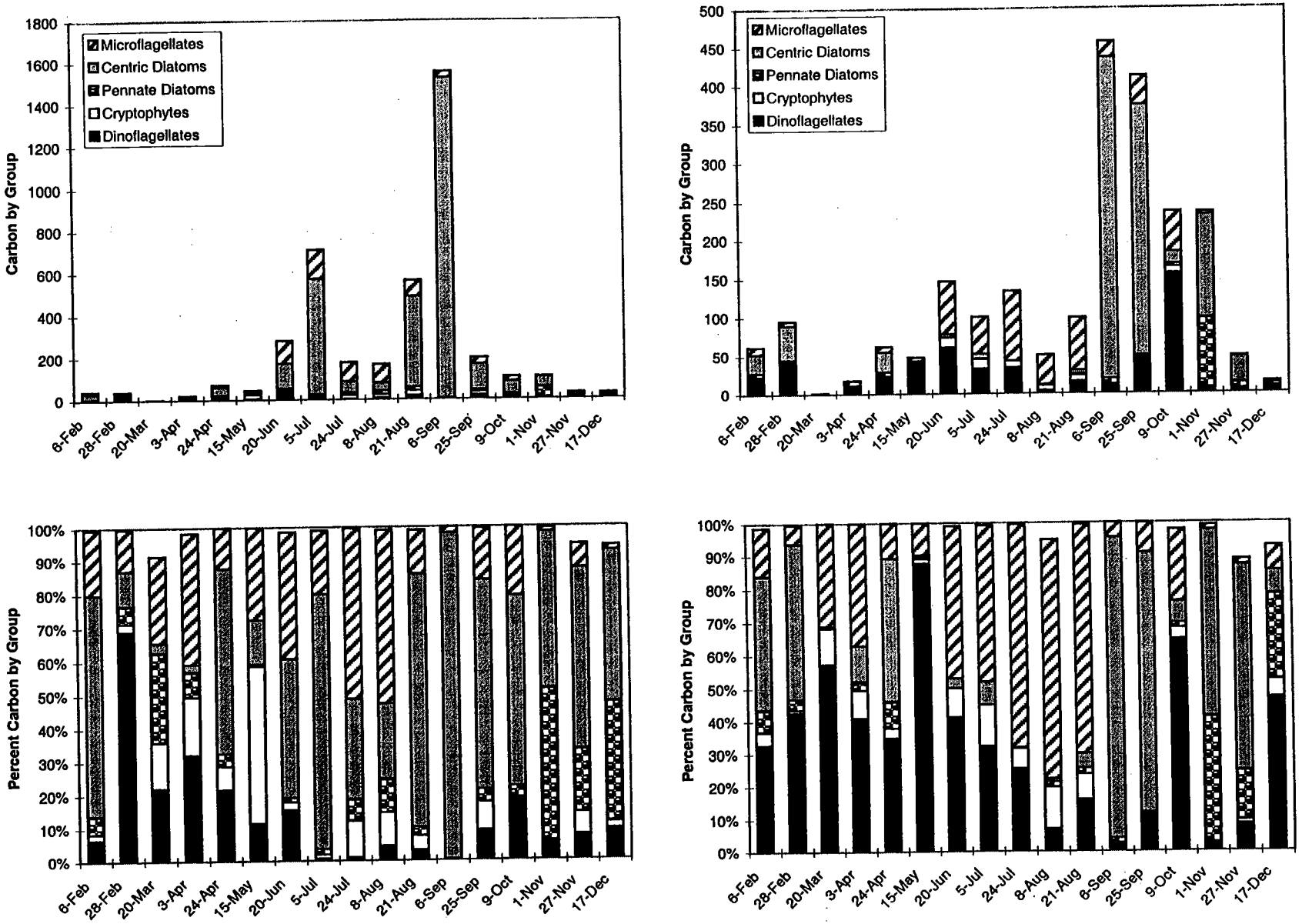

FIGURE 8-4b

Distribution of Carbon by Major Taxonomic Groups and Relative Percent Carbon in 1995 Chlorophyll a Maximum Samples
Nearfield Stations
Left: N10, Right: N16

*Note difference in y-scale axis

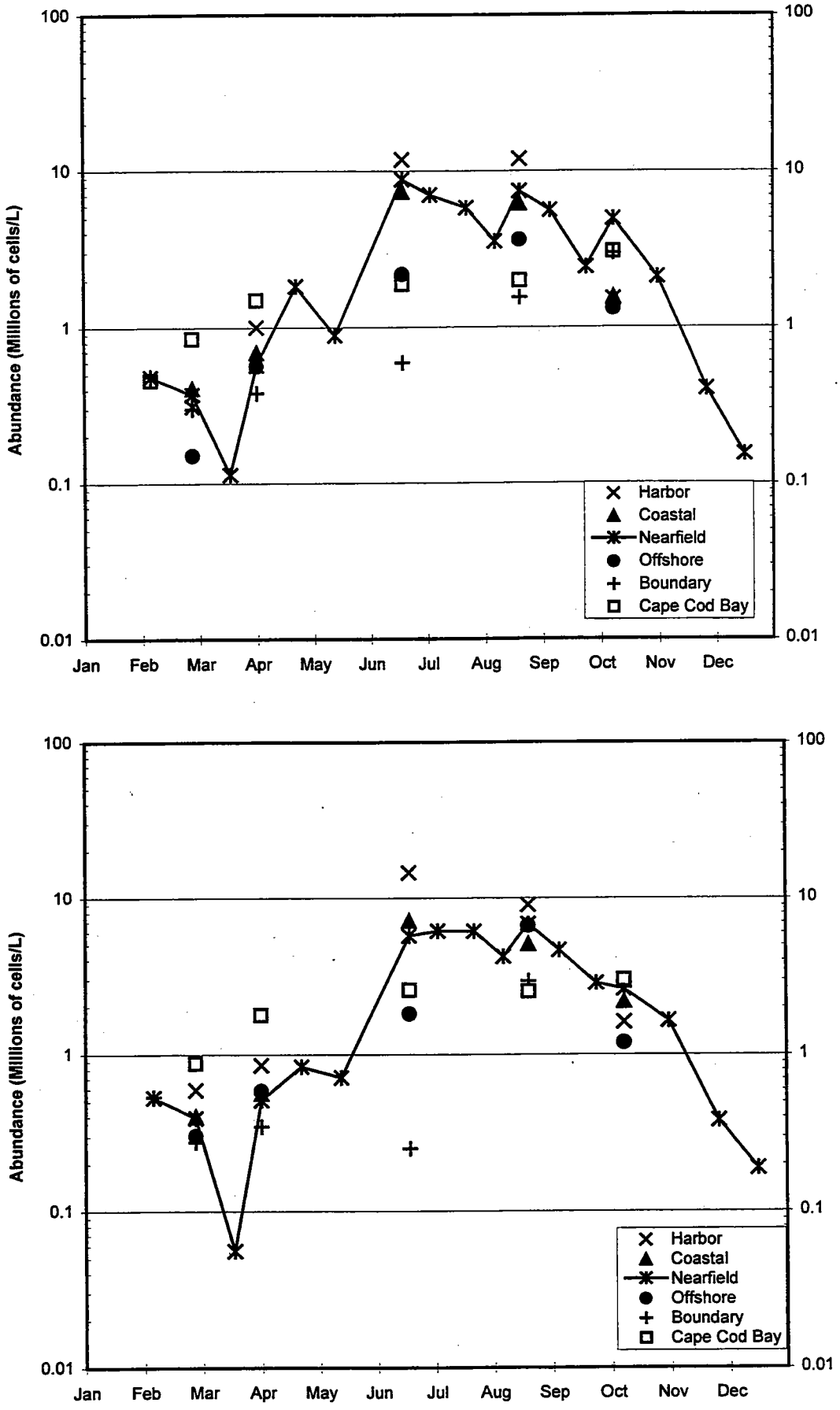

FIGURE 8-5
1995 Regional Total Phytoplankton Abundance
Top: Surface Data, Bottom: Chlorophyll a Maximum Data

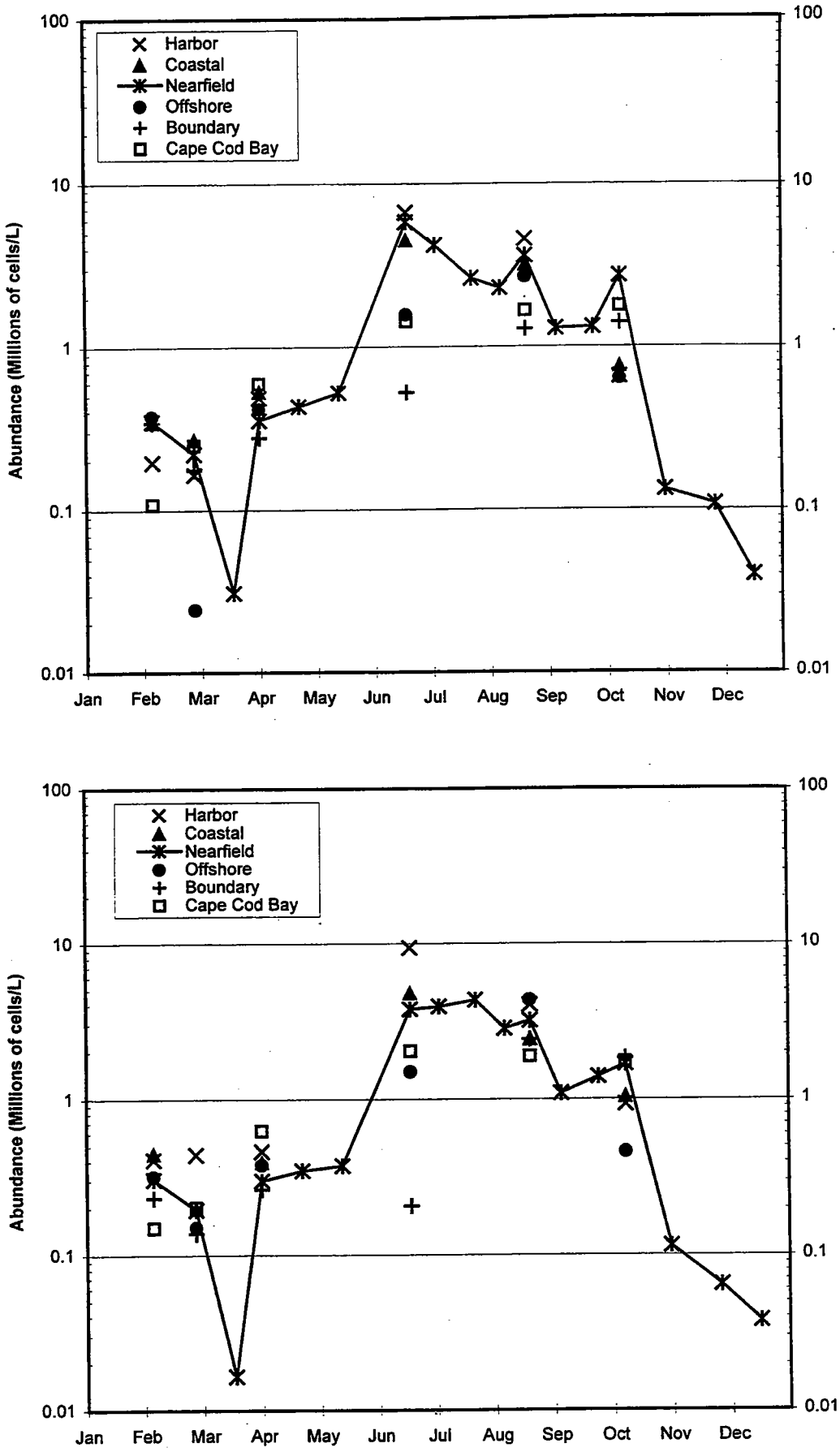

FIGURE 8-6

1995 Regional Abundances for Microflagellates

Top: Surface Data, Bottom: Chlorophyll a Maximum Data

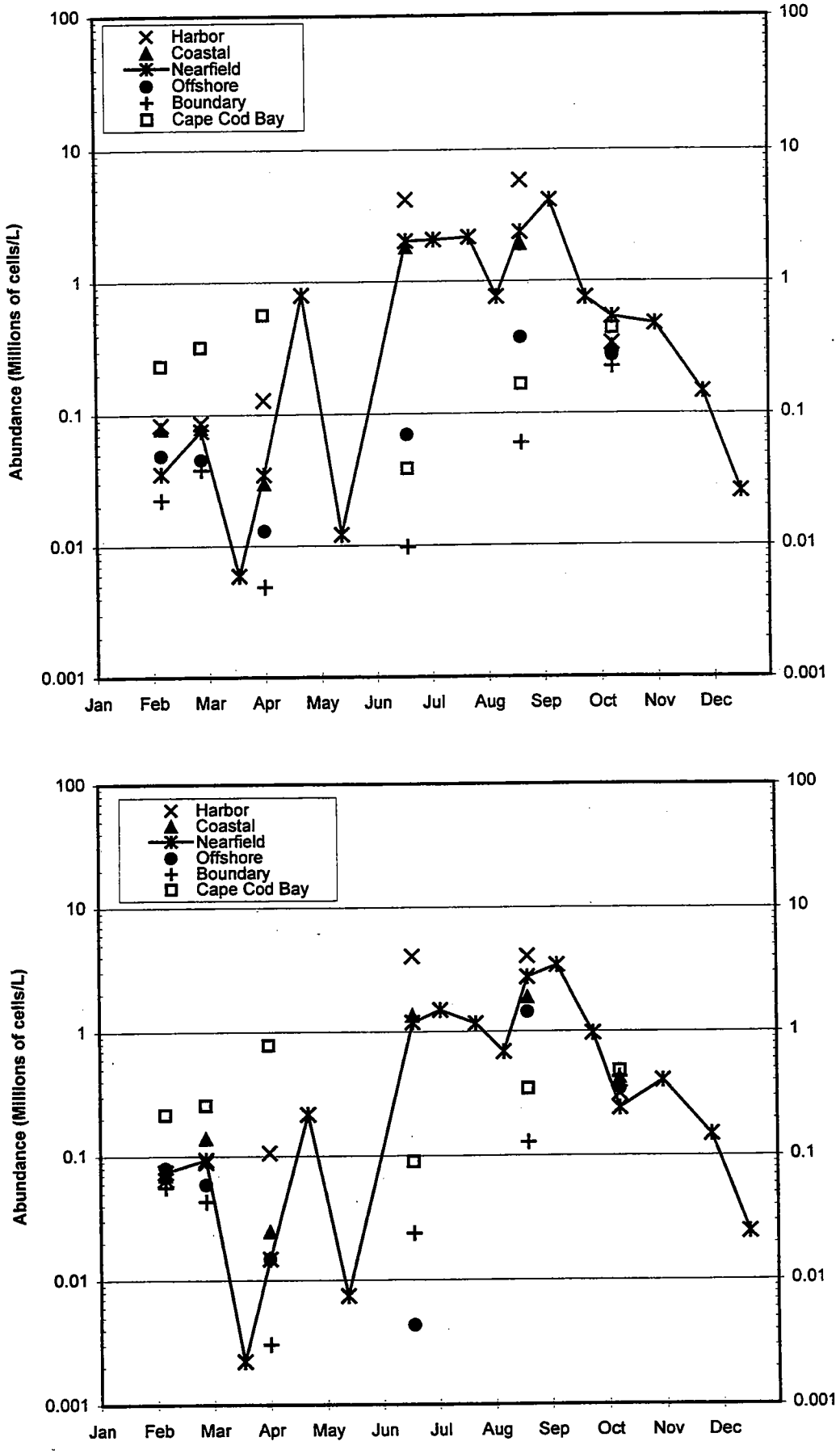

FIGURE 8-7

1995 Regional Abundances for Centric Diatoms

Top: Surface Data, Bottom: Chlorophyll a Maximum Data

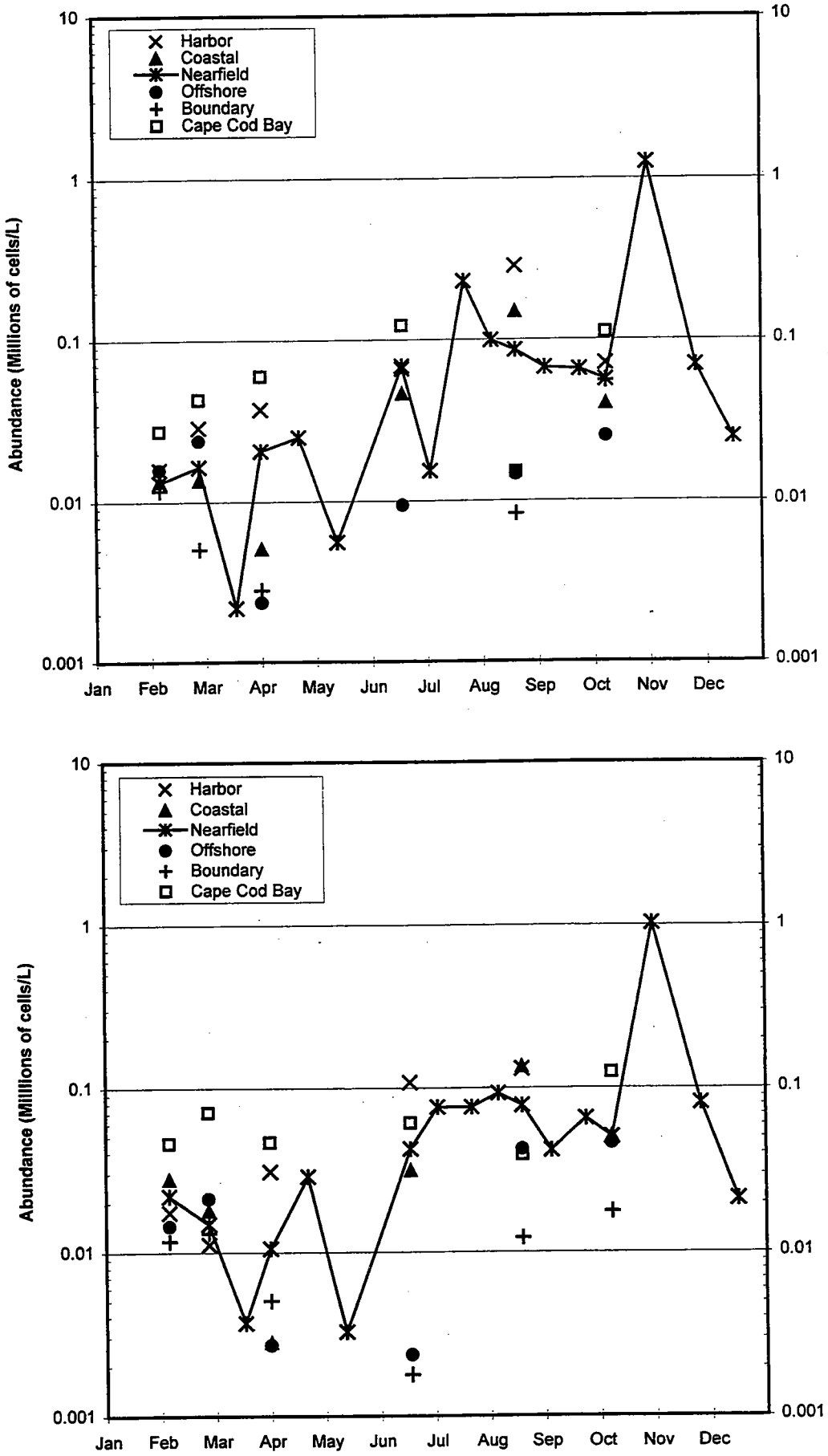

FIGURE 8-8

1995 Regional Abundances for Pennate Diatoms

Top: Surface Data, Bottom: Chlorophyll a Maximum Data

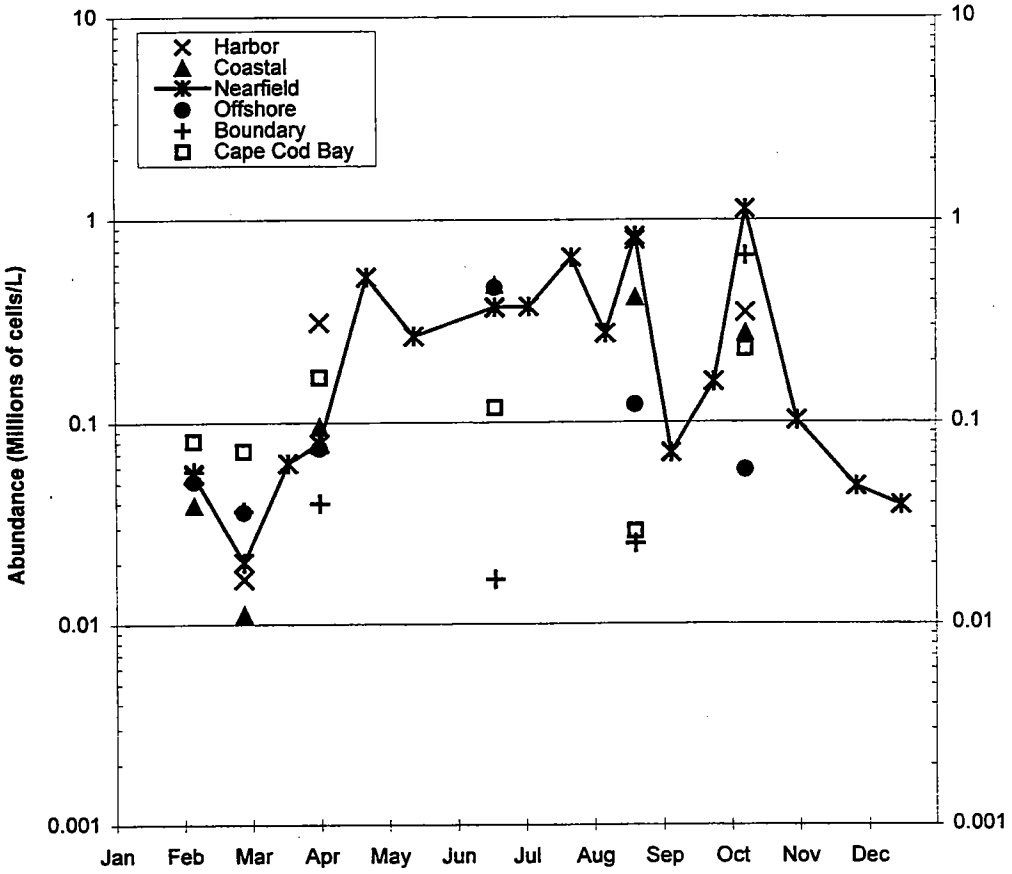

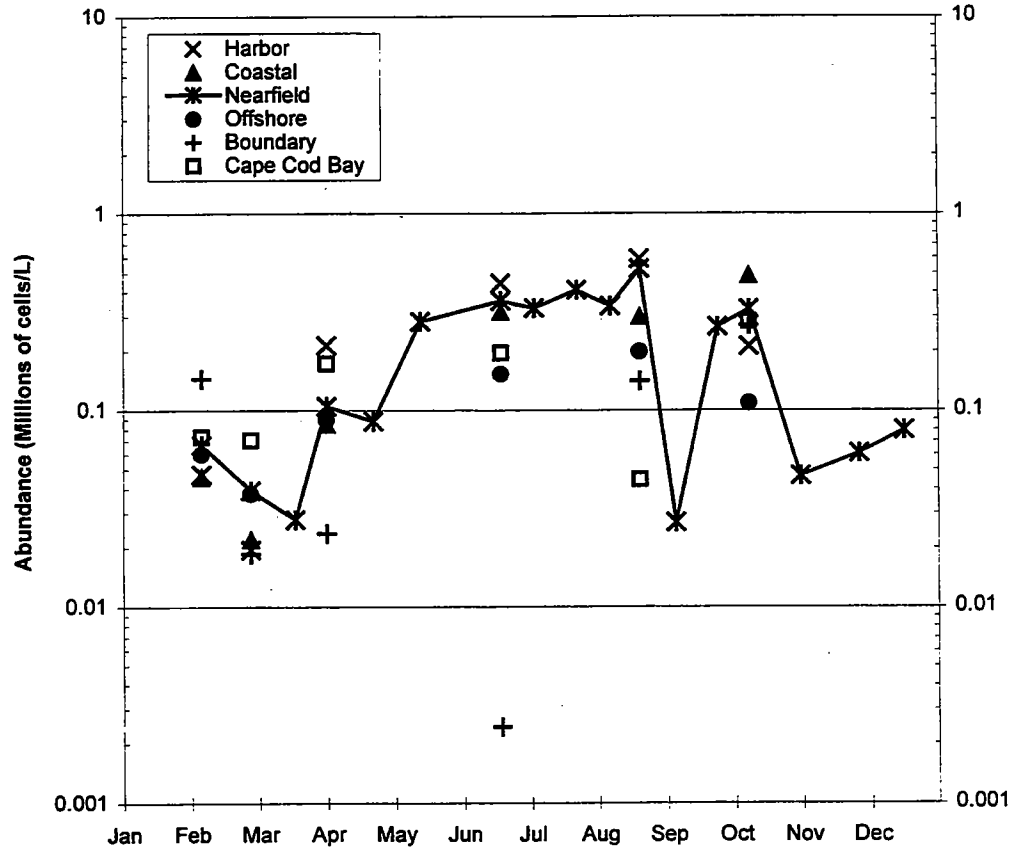

FIGURE 8-9
1995 Regional Abundances for Cryptophytes
Top: Surface Data, Bottom: Chlorophyll a Maximum Data

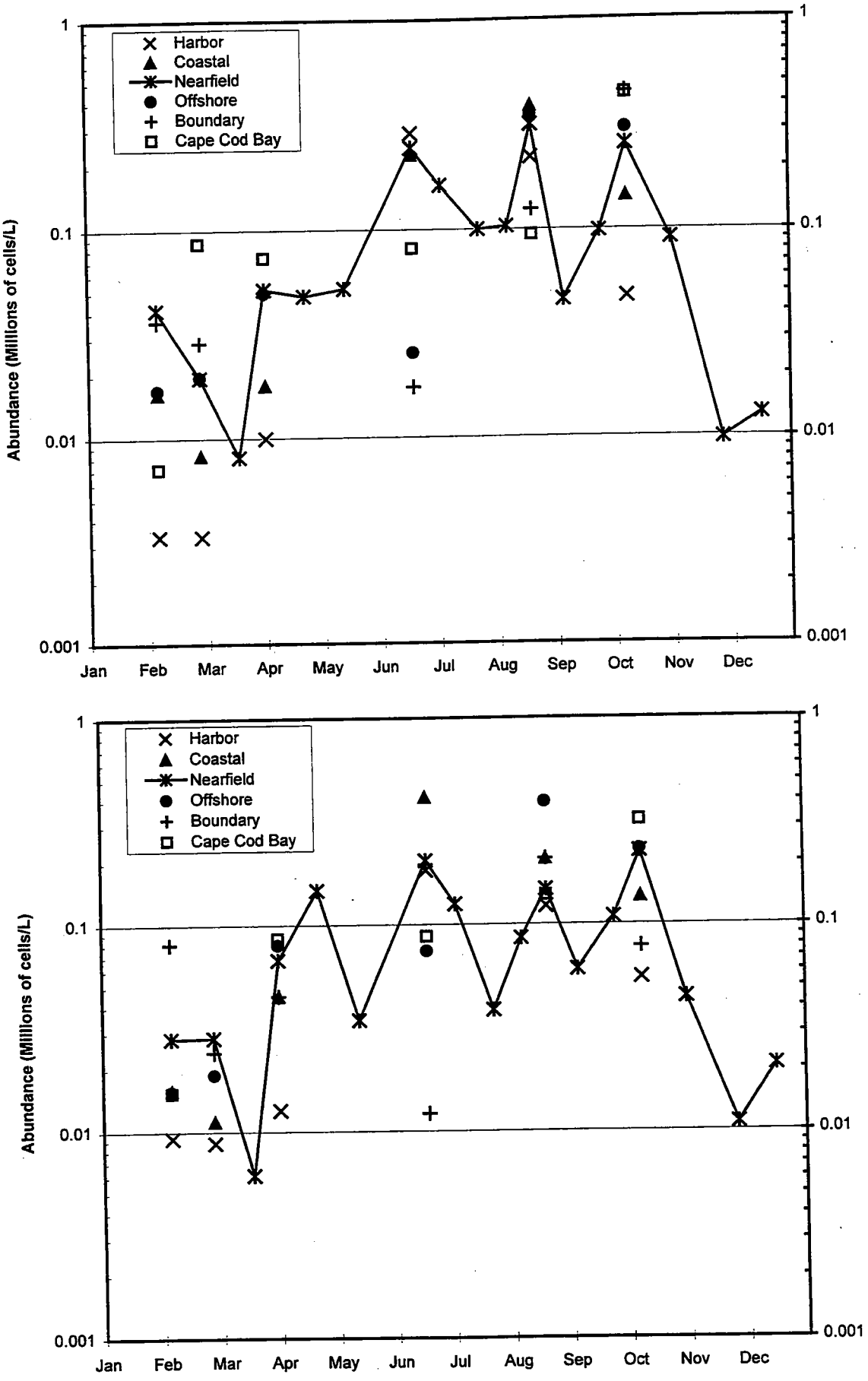

FIGURE 8-10
1995 Regional Abundances for Dinoflagellates
Top: Surface Data, Bottom: Chlorophyll a Maximum Data

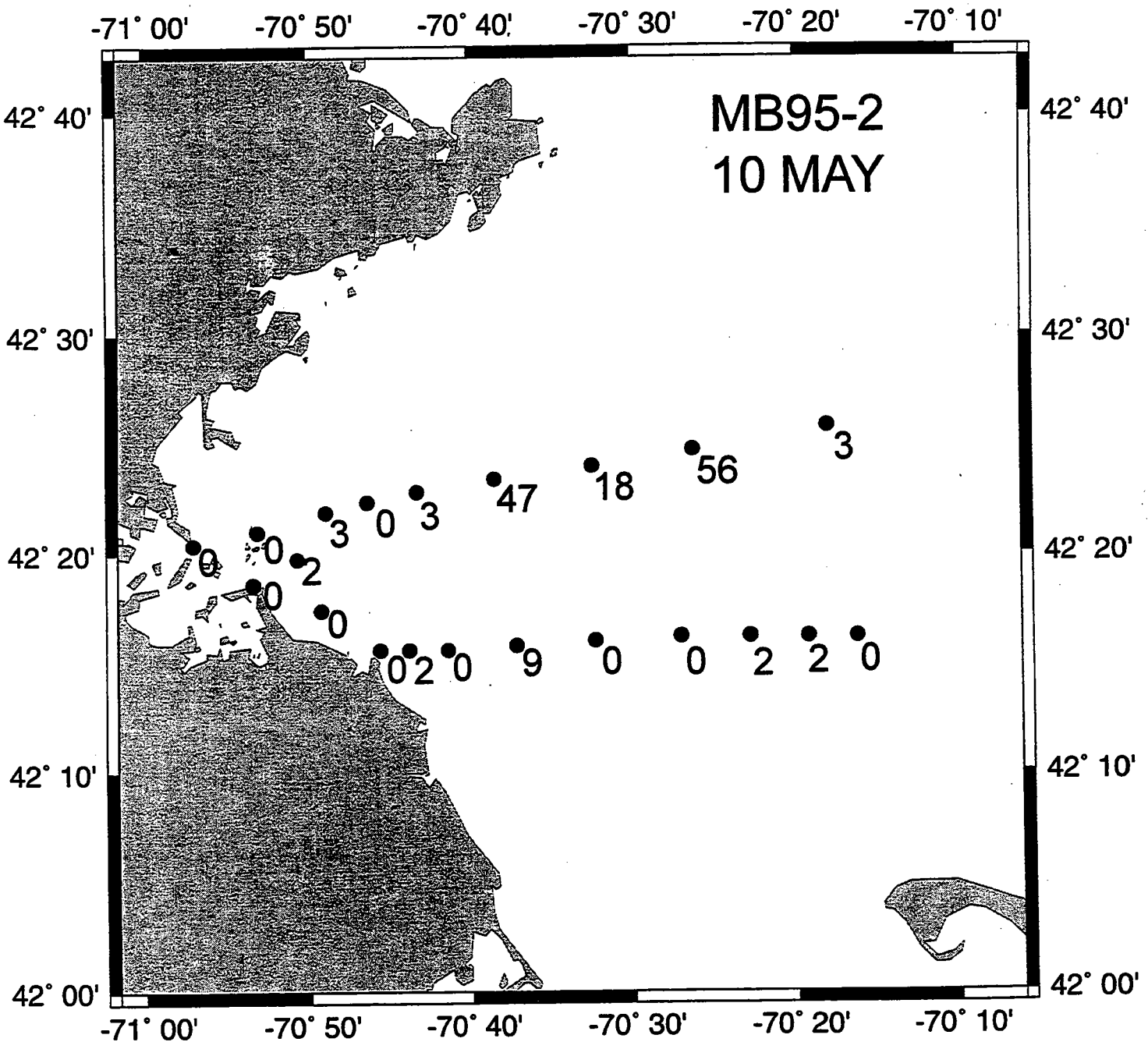

Figure 8-11. Surface cell concentration (cells liter^{-1}) of the toxic dinoflagellate *Alexandrium* sp. along two transects in Massachusetts Bay on May 10, 1995. An antibody-based detection method with a fluorescent microscope was used for the observations where the estimates ranged from non-detectable to about 50 cells per liter^{-1}. These relatively low abundances were the highest recorded in 1995 and were not enough to cause outbreaks in shellfish toxicity along the shore.

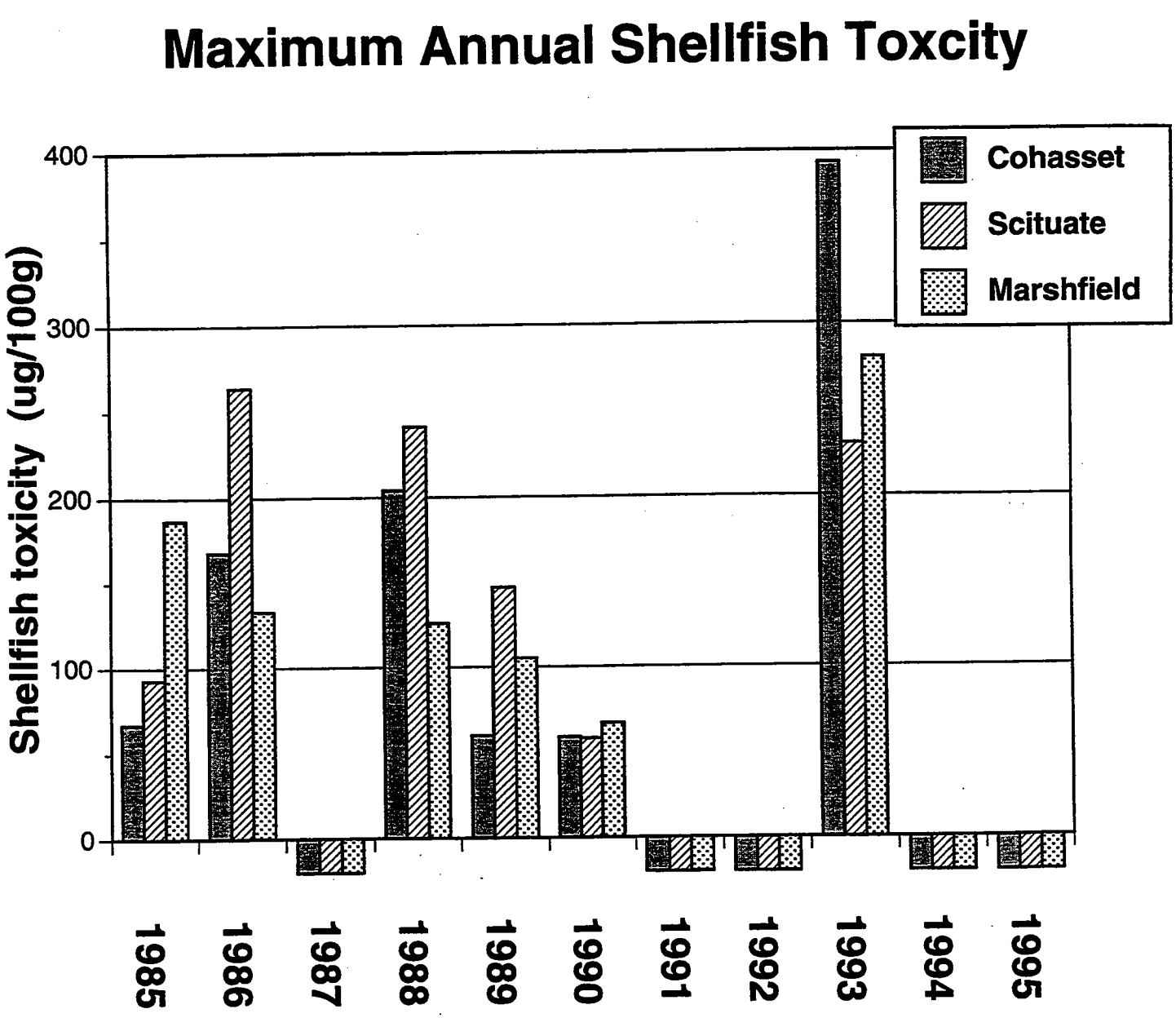

Figure 8-12. Bar graph of the maximum recorded shellfish toxicity at three primary shellfish monitoring stations along the "South Shore" in Massachusetts Bay for the years 1985-1995. The mouse bioassay measurements from the indicator species, mussels (*Mytilus edulis*), range from non-detectable in some years (i.e. bars shown below zero) to greater than several hundred µg toxin/100g of the shellfish tissue. Data supplied by David Whitaker of the Massachusetts Division of Marine Fisheries.

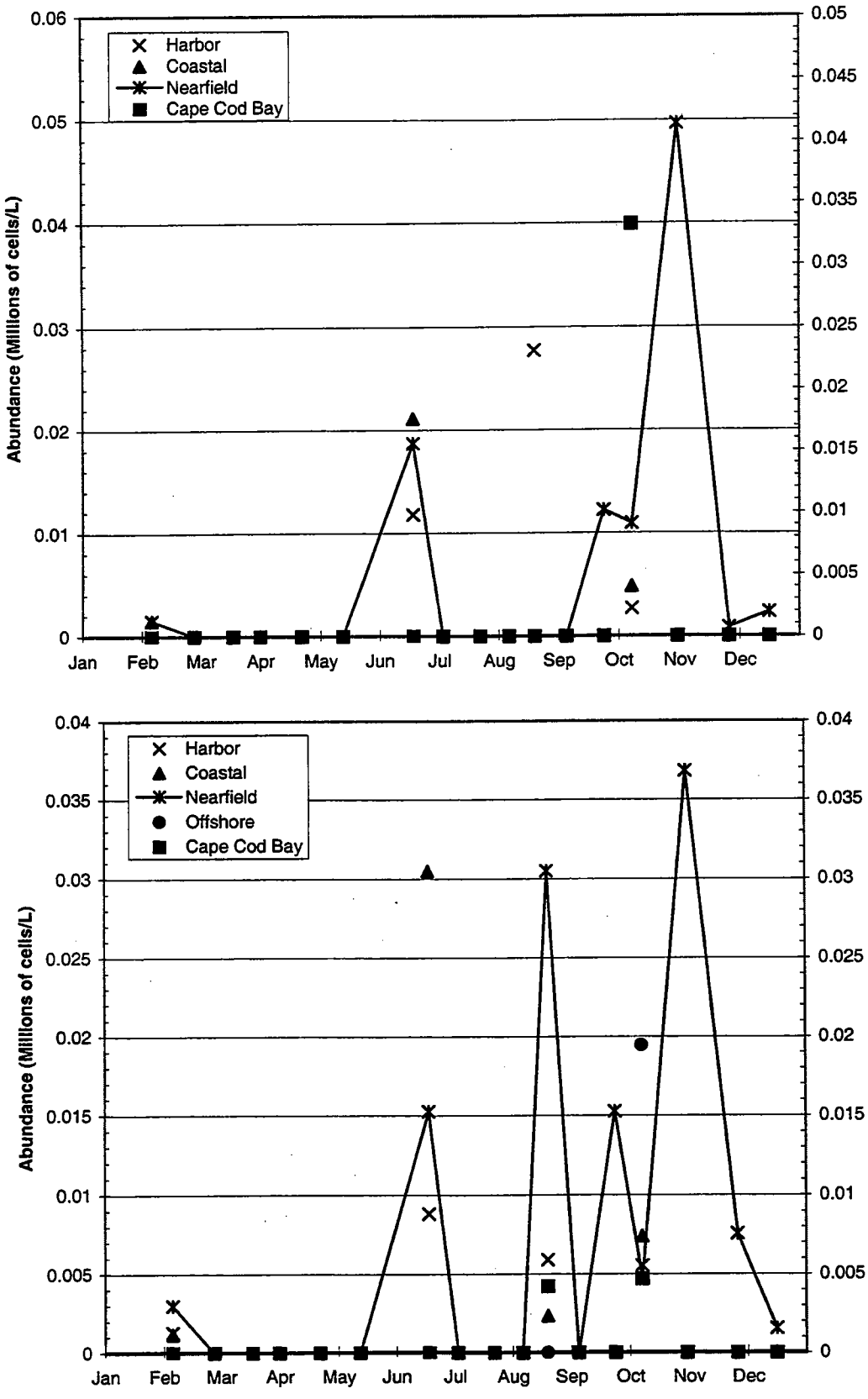

FIGURE 8-13

1995 Regional Abundance of *Pseudo-nitzschia*
Top: Surface Data, Bottom: Chlorophyll a Maximum Data

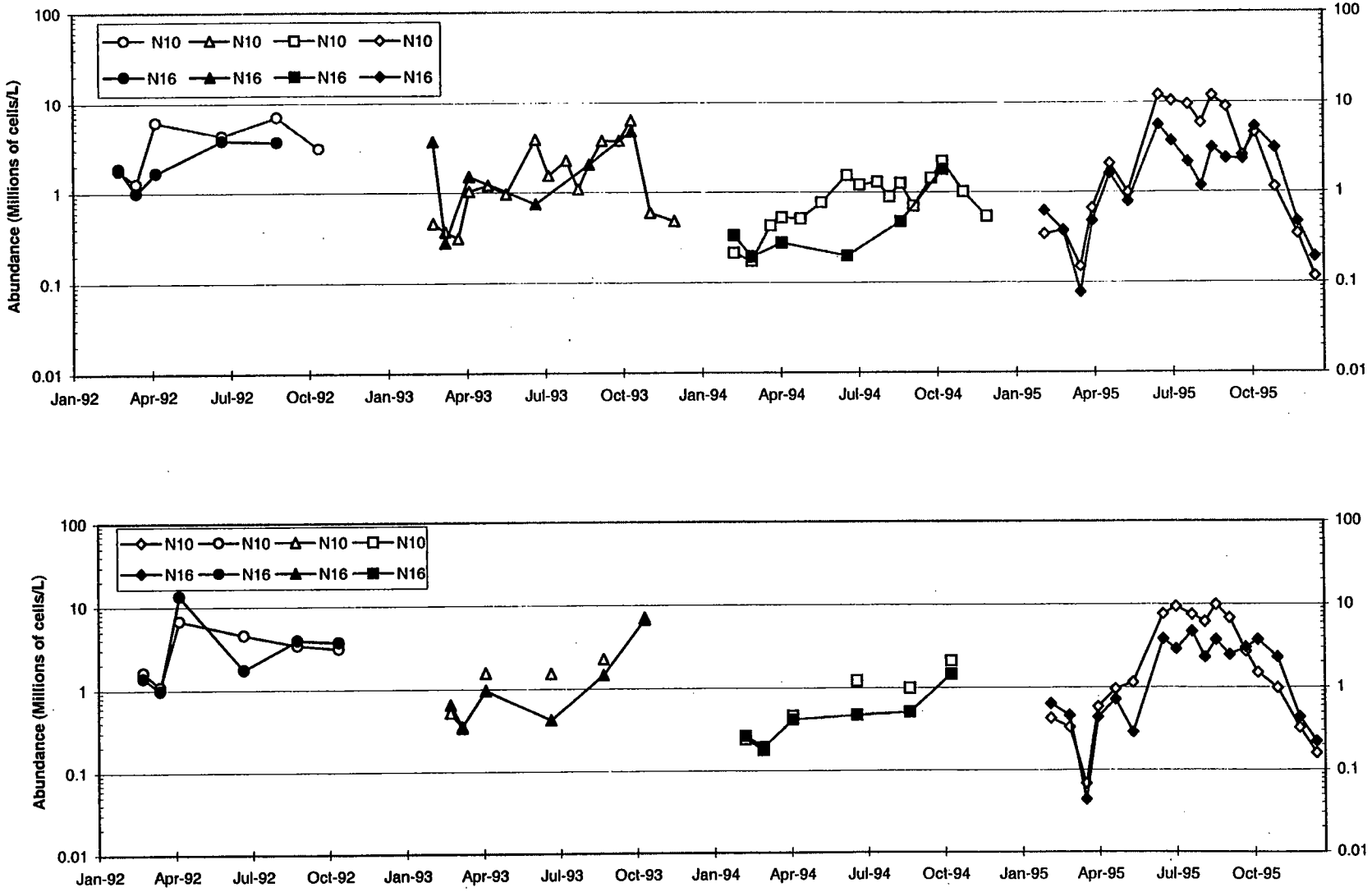

FIGURE 8-14
1992 -1995 Total Phytoplankton Abundance in Nearfield Stations N10 and N16
Top: Surface Data, Bottom: Chlorophyll a Maximum Data

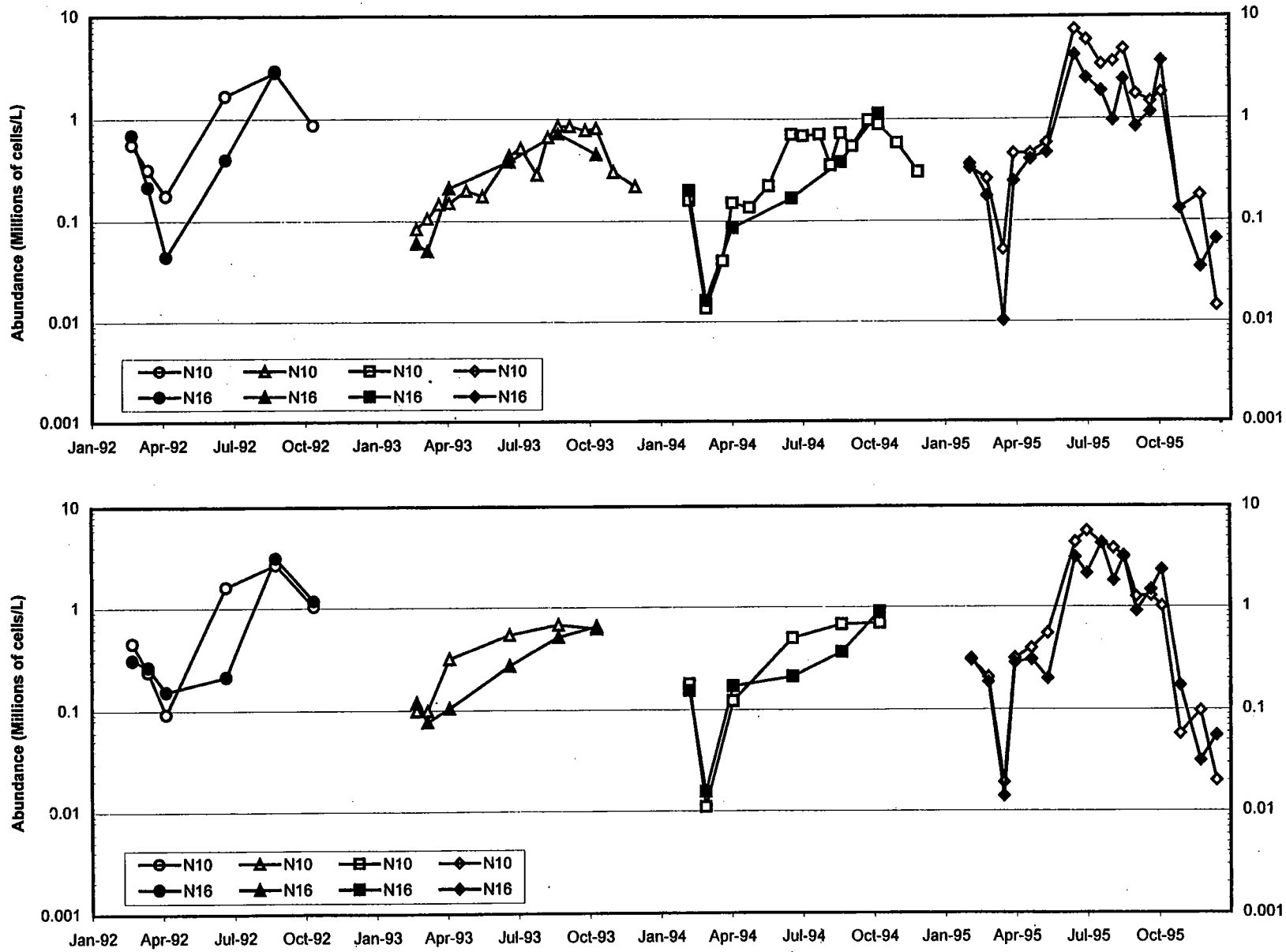

FIGURE 8-15

1992-1995 Seasonal Nearfield Pattern for Microflagellates in Nearfield Stations N10 and N16

Top: Surface Data, Bottom: Chlorophyll a Maximum Data

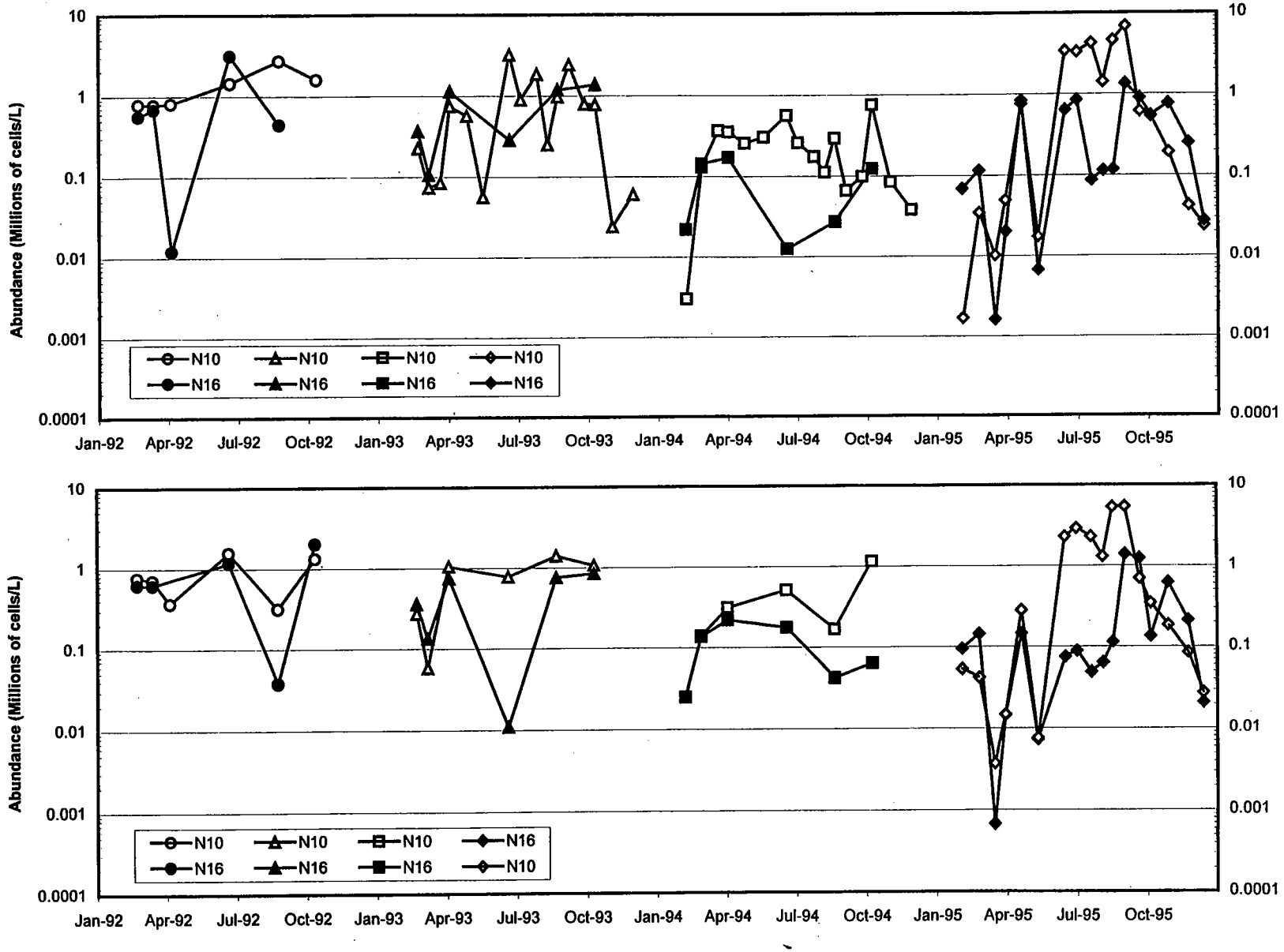

FIGURE 8-16

1992-1995 Seasonal Nearfield Pattern for Centric Diatoms in Nearfield Stations N10 and N16
Top: Surface Data, Bottom: Chlorophyll a Maximum Data

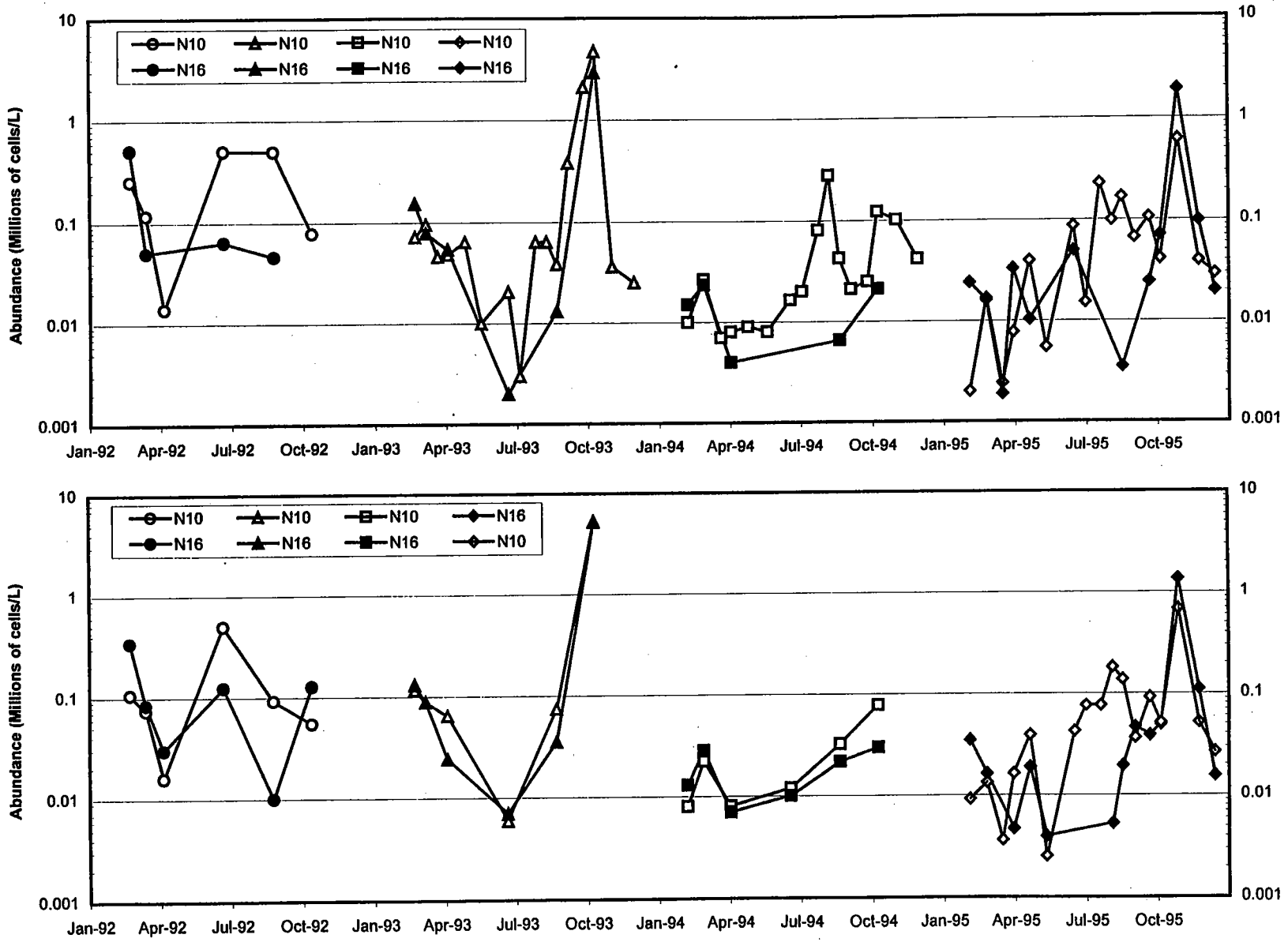

FIGURE 8-17

1992-1995 Seasonal Nearfield Pattern for Pennate Diatoms in Nearfield Stations N10 and N16

Top: Surface Data, Bottom: Chlorophyll a Maximum Data

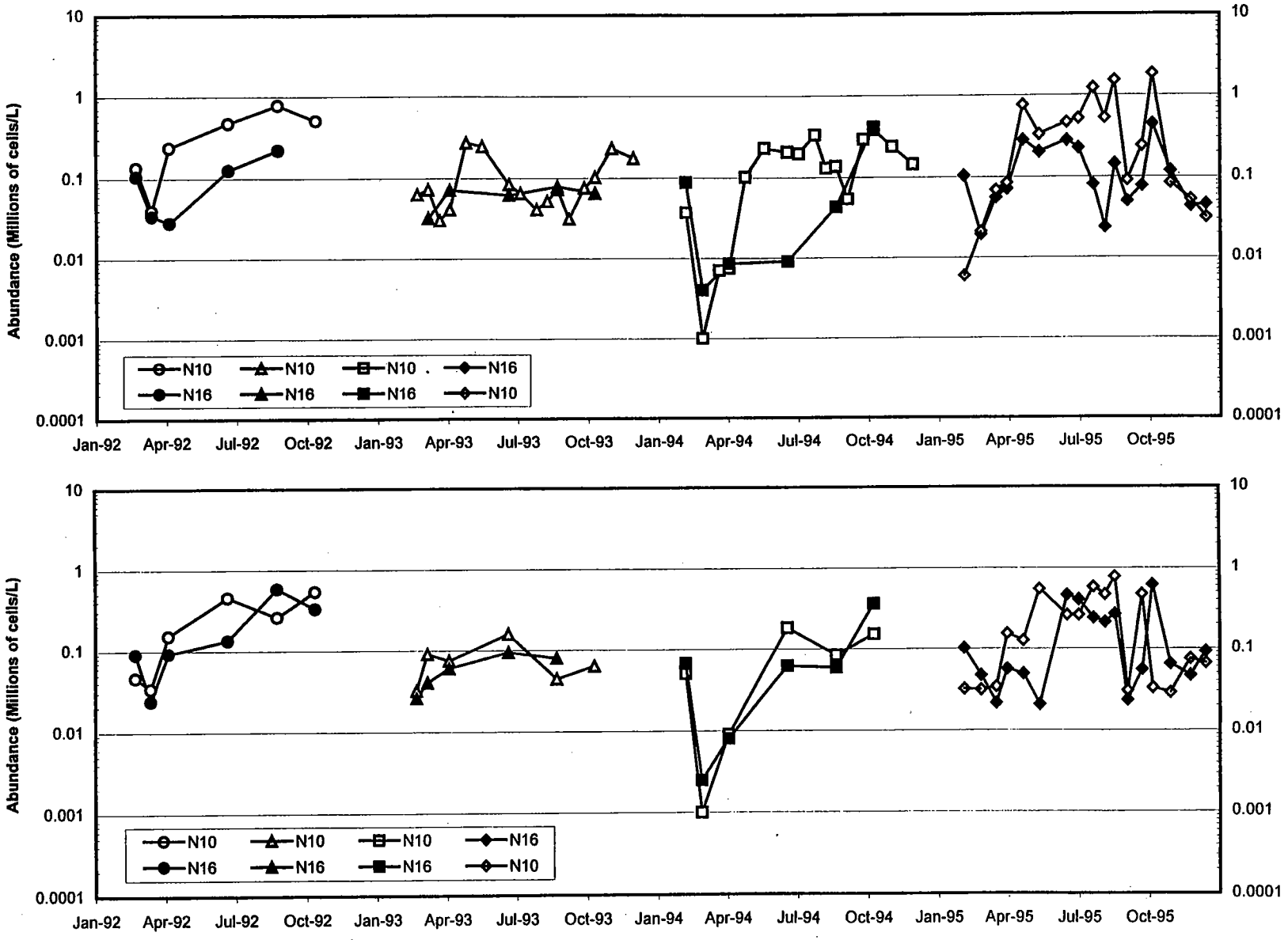

FIGURE 8-18

1992-1995 Seasonal Nearfield Pattern for Cryptophytes in Nearfield Stations N10 and N16

Top: Surface Data, Bottom: Chlorophyll a Maximum Data

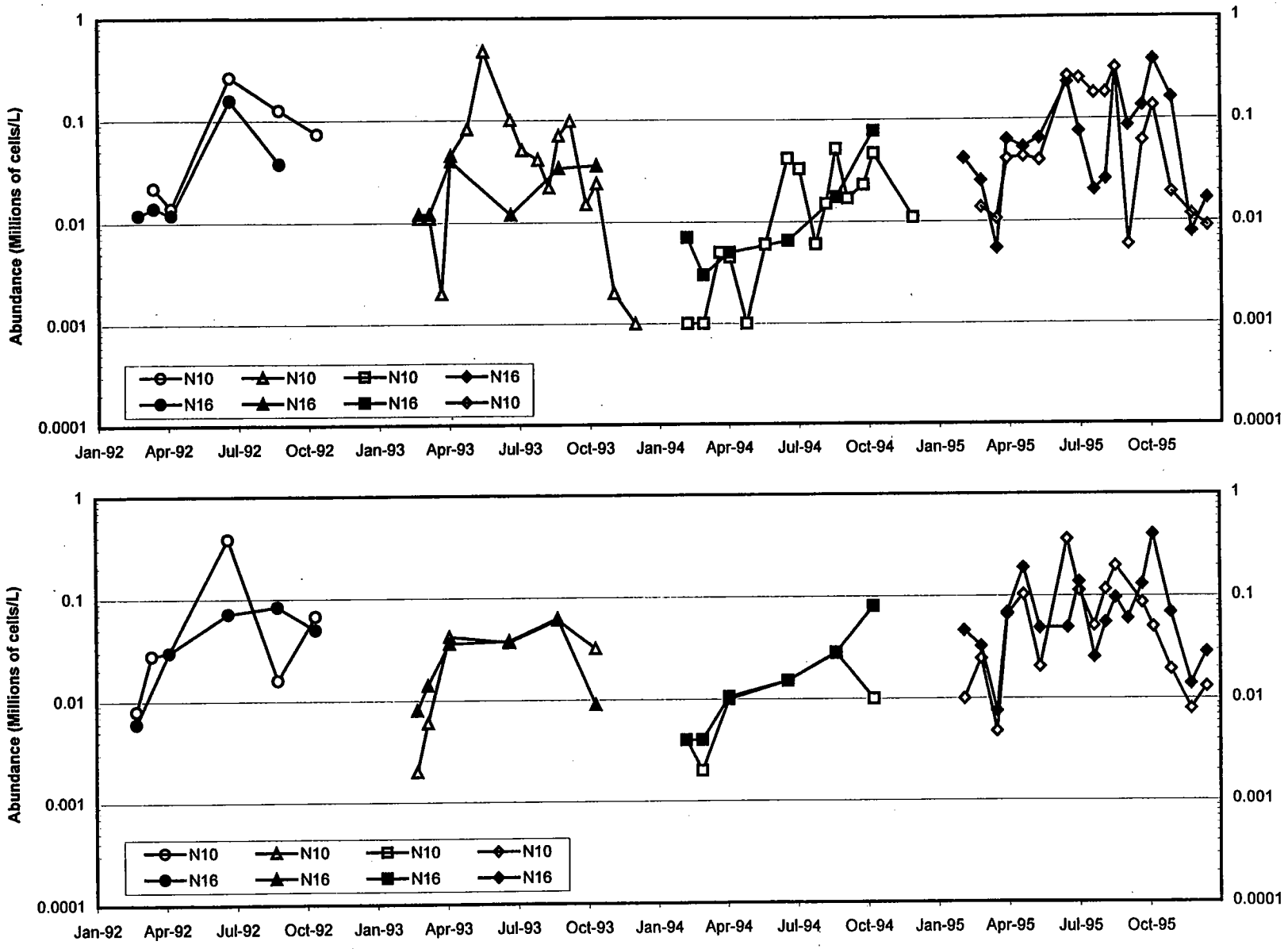

FIGURE 8-19

1992-1995 Seasonal Nearfield Pattern for Dinoflagellates in Nearfield Stations N10 and N16

Top: Surface Data, Bottom: Chlorophyll a Maximum Data

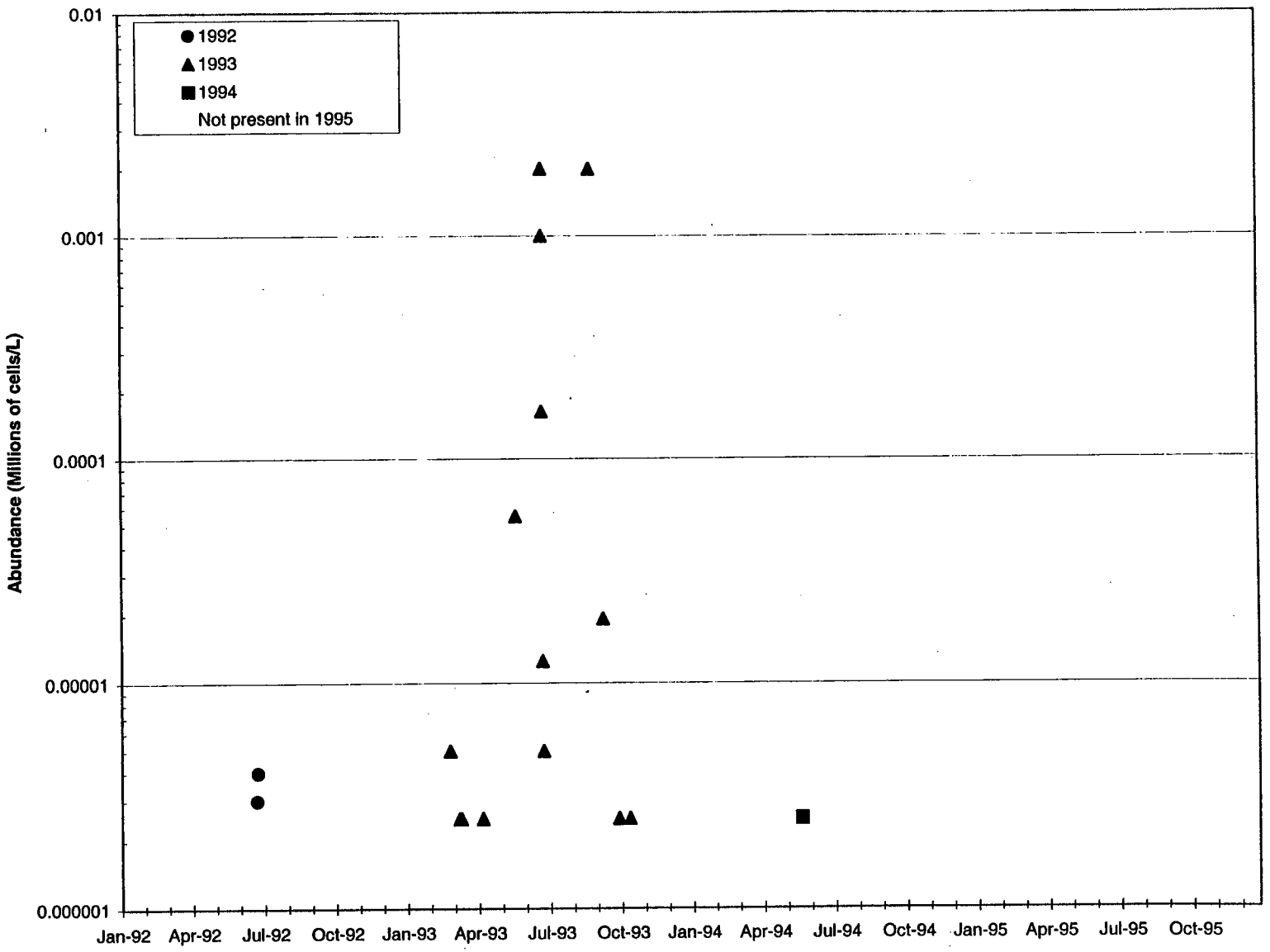

FIGURE 8-20

1992- 1995 Occurrence of *Alexandrium tamarense*

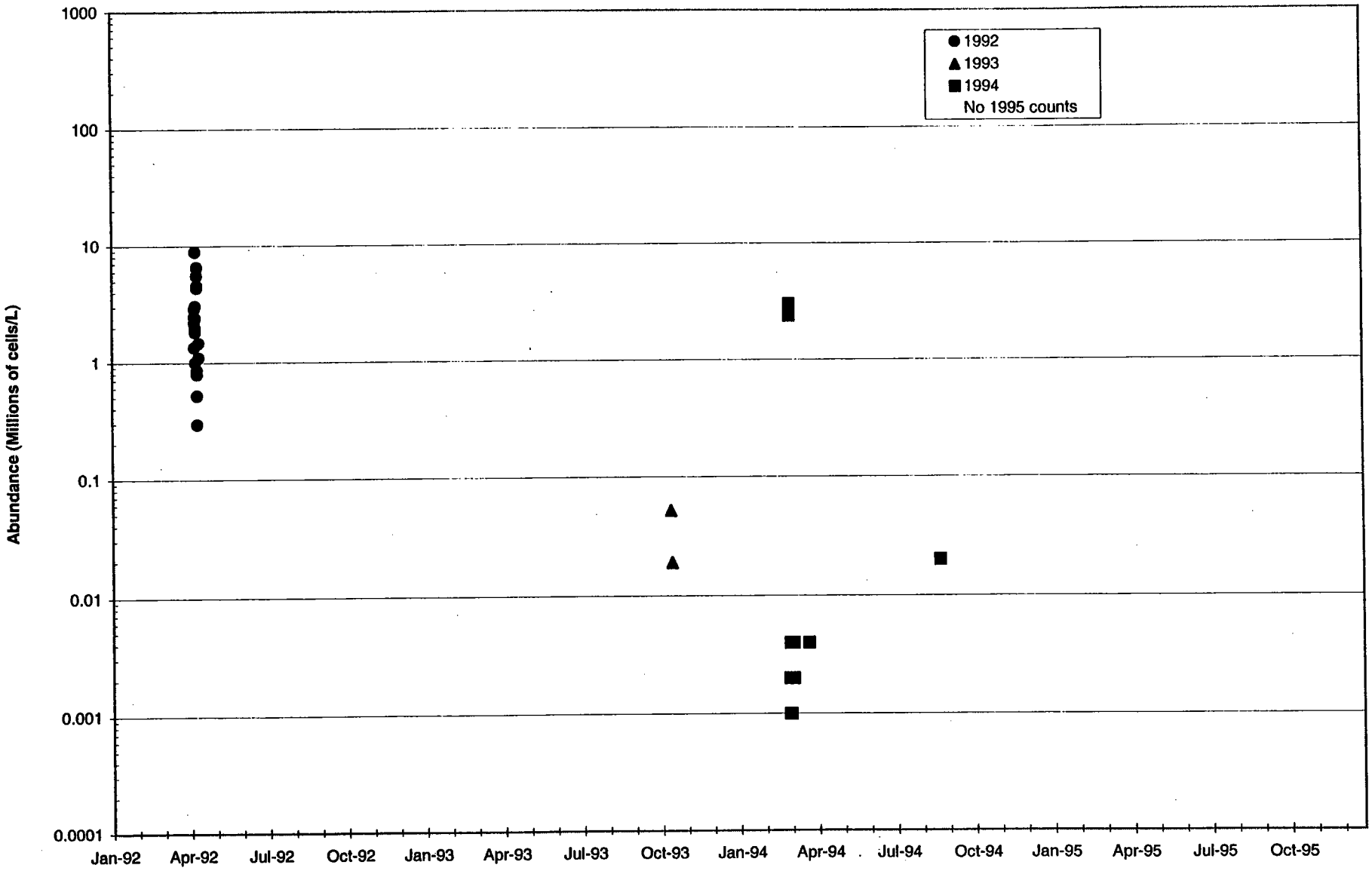

FIGURE 8-21

1992- 1995 Occurrenc[illegible] *Phaeocystis pouchetii*

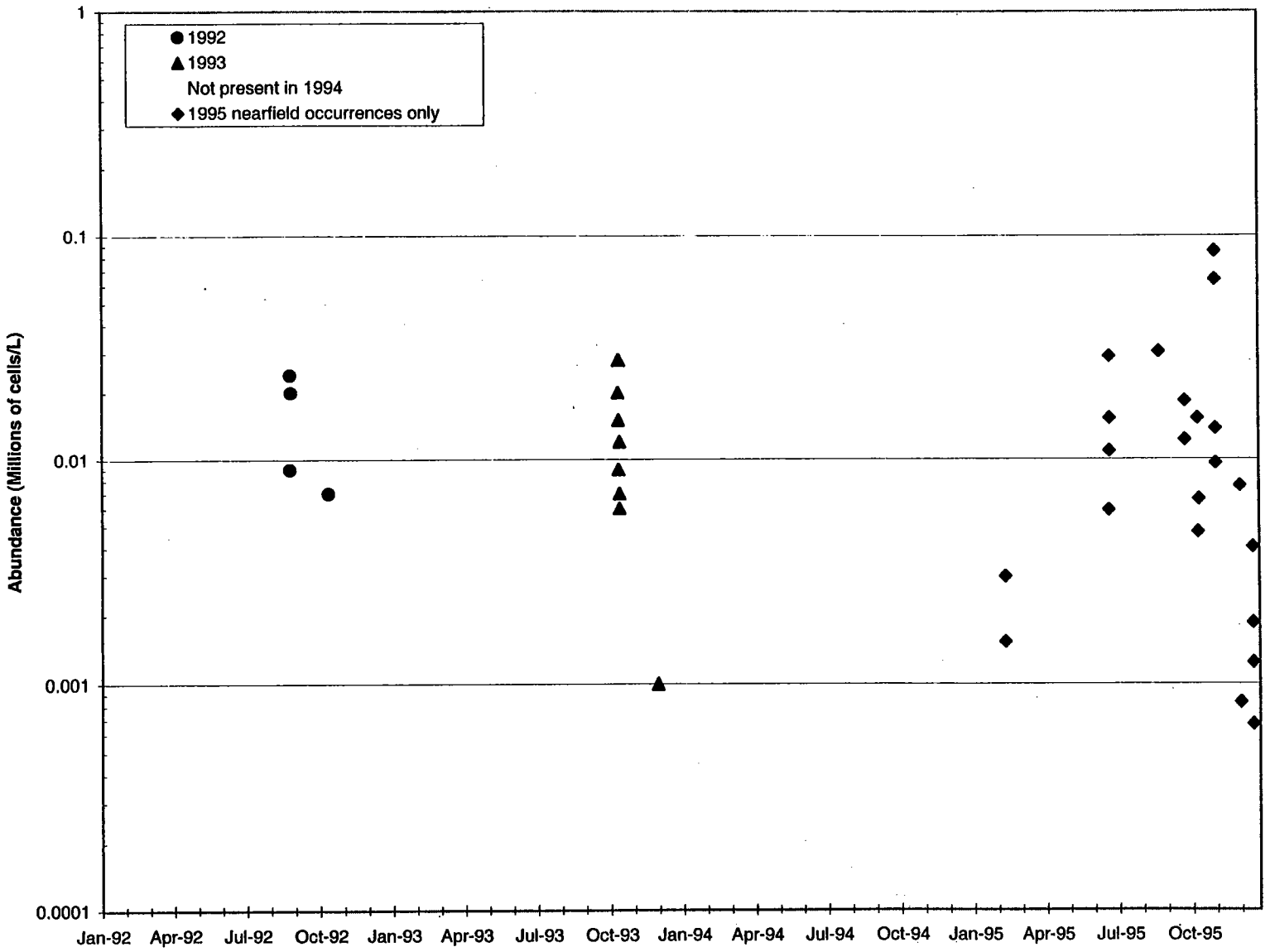

FIGURE 8-22

1992- 1995 Occurrence of *Pseudo-nitzschia pungens*

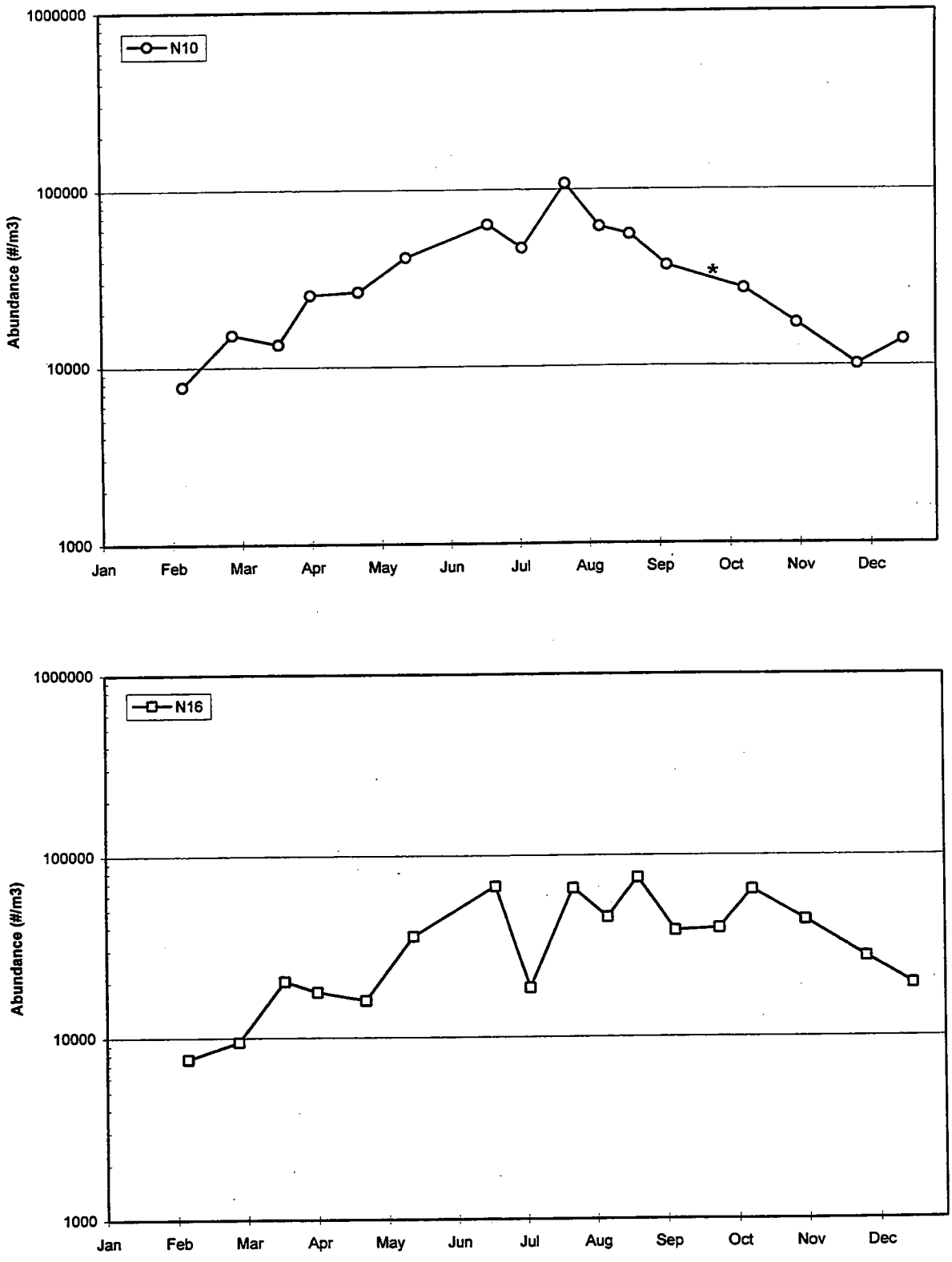

* No data for W9513

FIGURE 8-23
1995 Total Zooplankton
Nearfield Stations
Top: N10, Bottom: N16

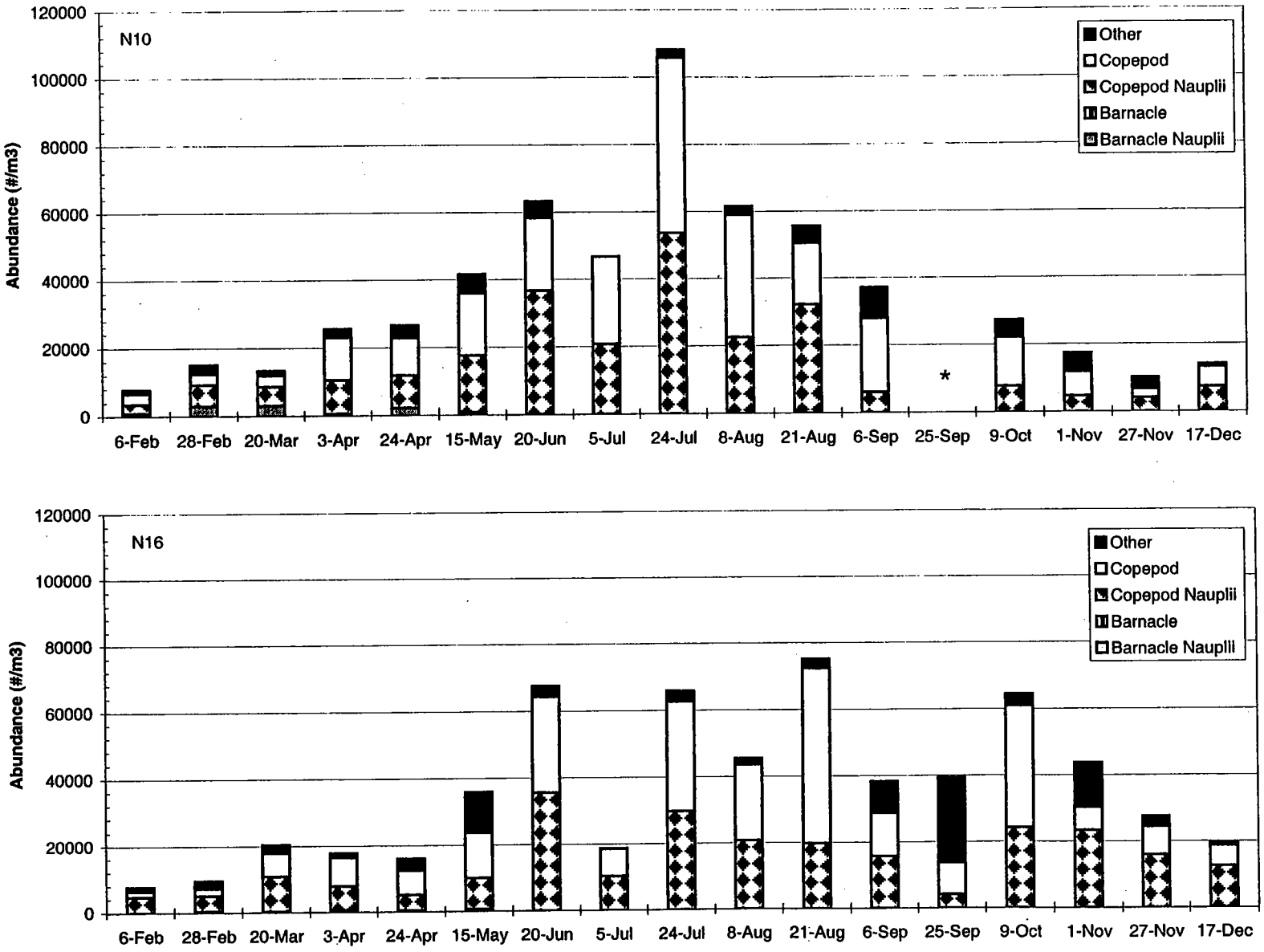

* No data for September 25

FIGURE 8-24
1995 Total Zooplankton Abundance by Group
Surface Data
Top: N10, Bottom: N16

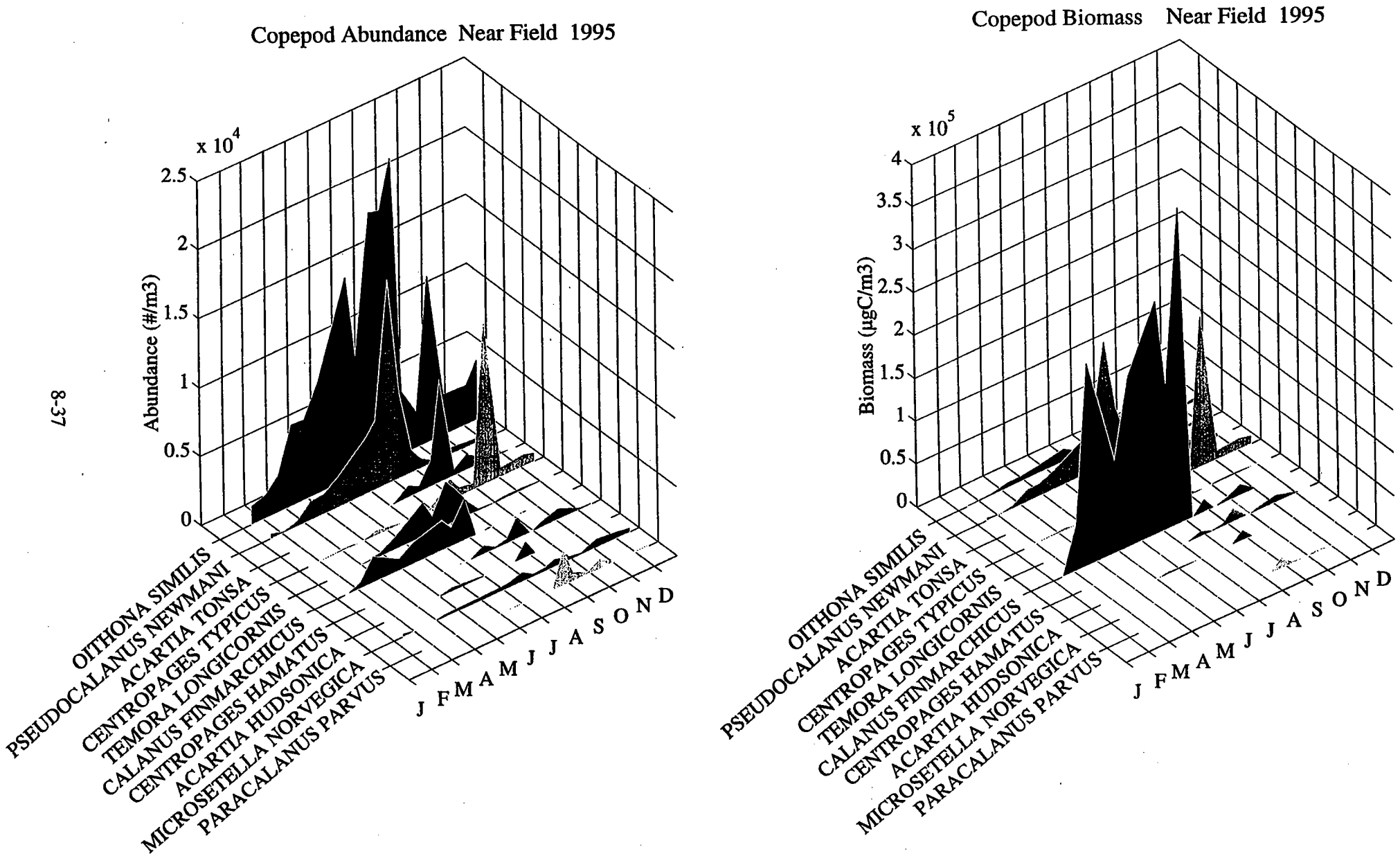

FIGURE 8-25
1995 Seasonal Abundance and Biomass of Dominant Copepod Species in Nearfield

FIGURE 8-26
1995 Nearshore Zooplankton Assemblages (Note maxima at top for each plot)

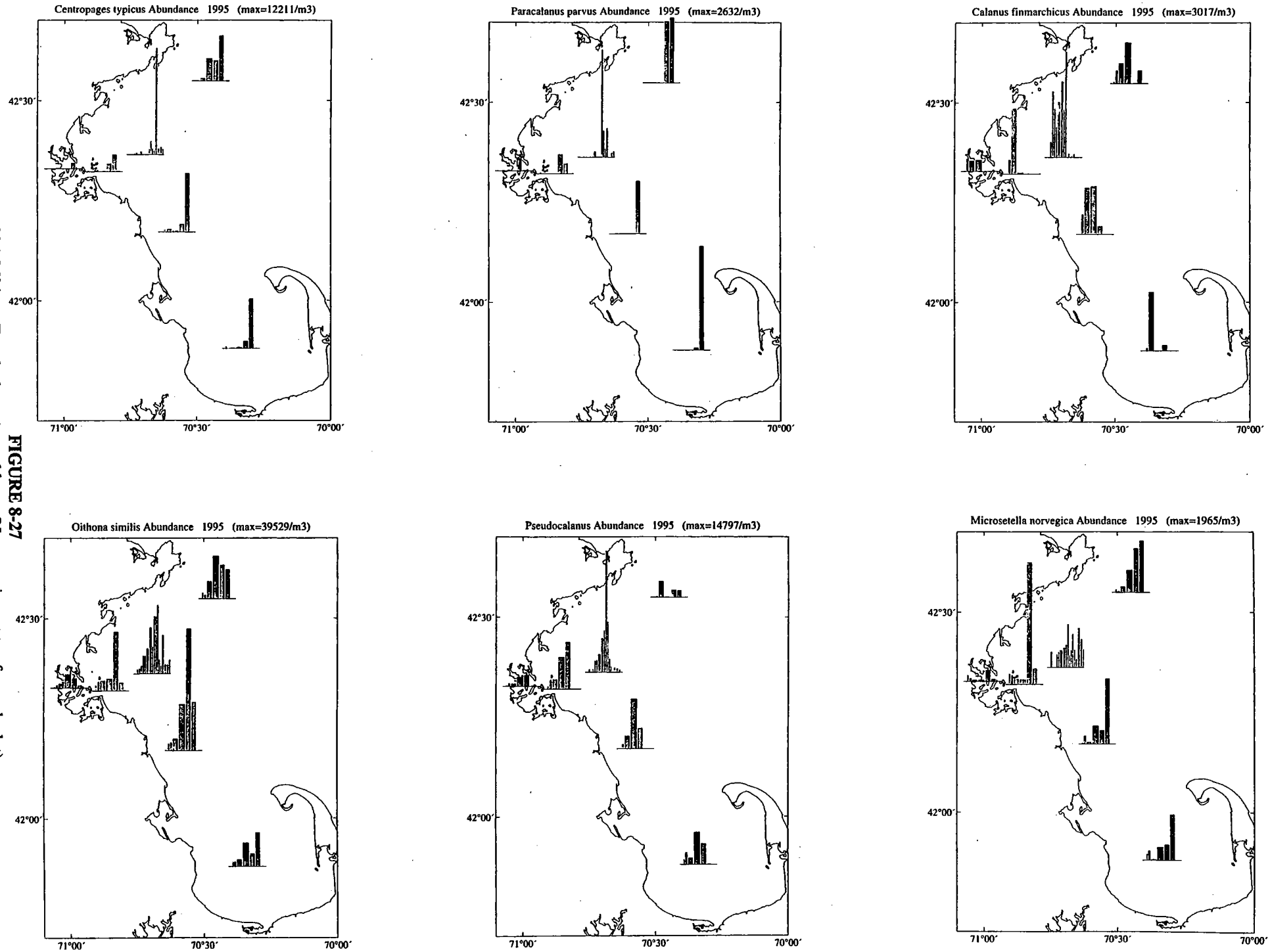

FIGURE 8-27
1995 Offshore Zooplankton Assemblages (Note maxima at top for each plot)

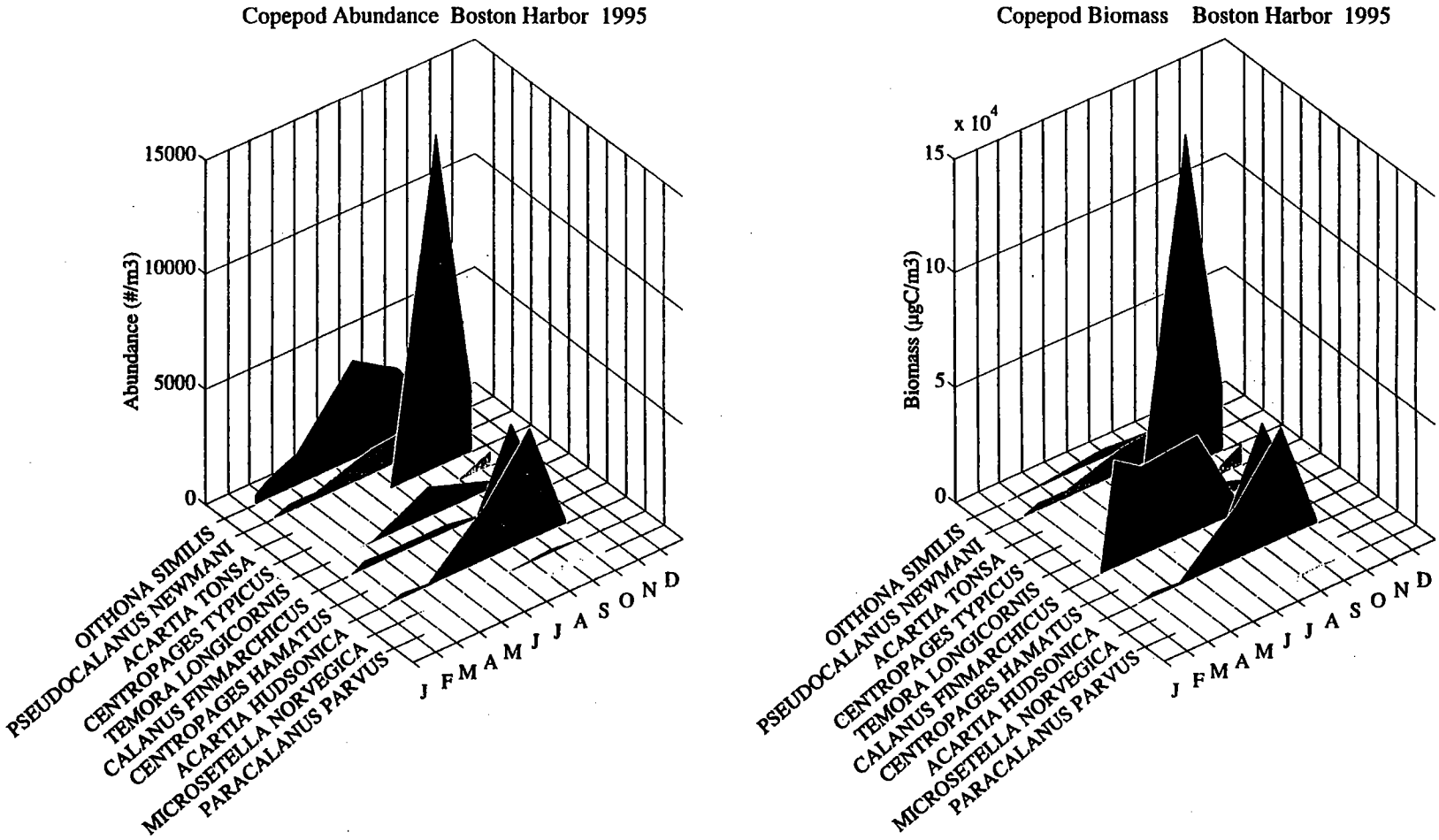

FIGURE 8-28
1995 Seasonal Abundance and Biomass of Dominant Copepod Species
at Boston Harbor Stations

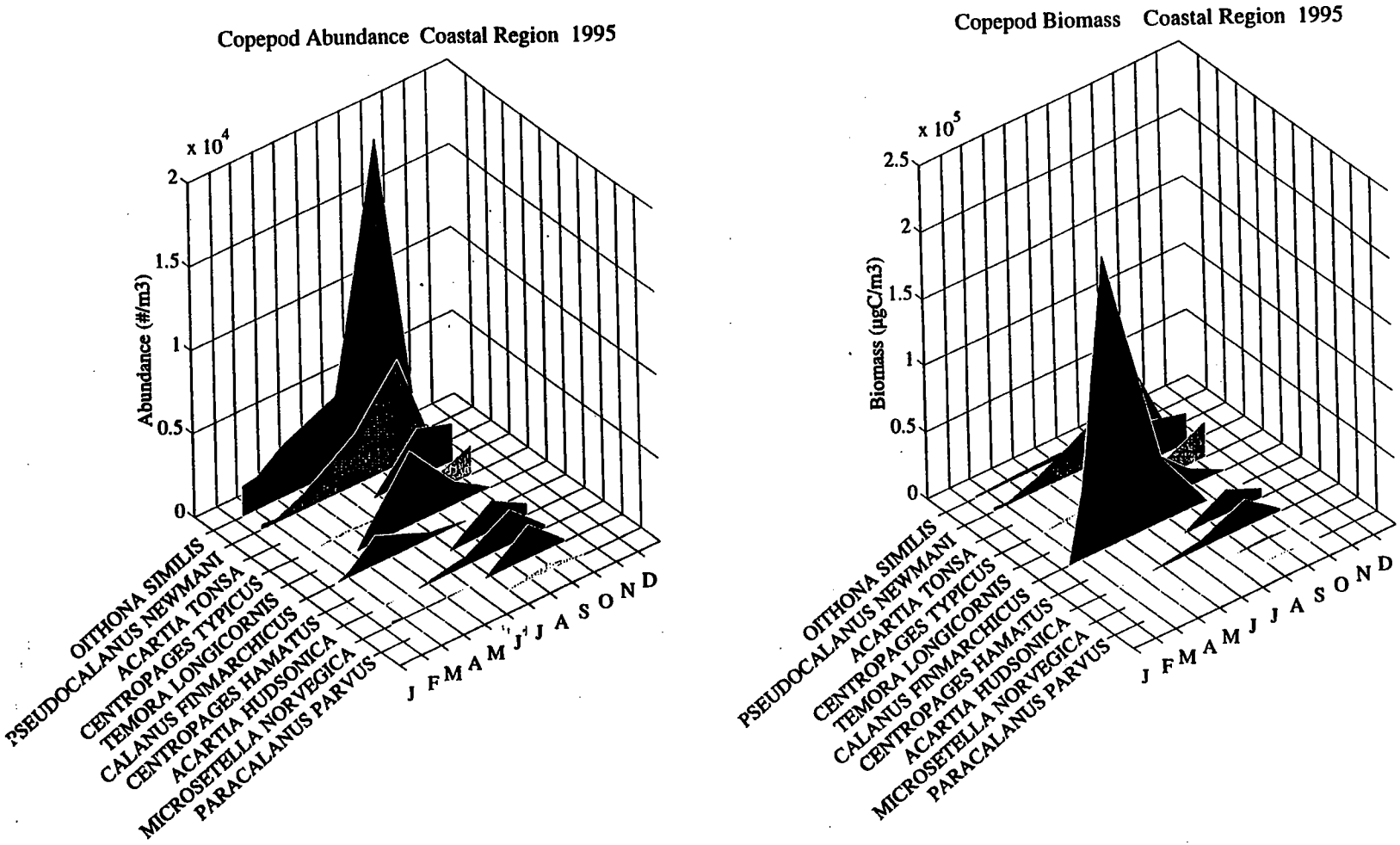

FIGURE 8-29
1995 Seasonal Abundance and Biomass of Dominant Copepod Species
at Coastal Stations

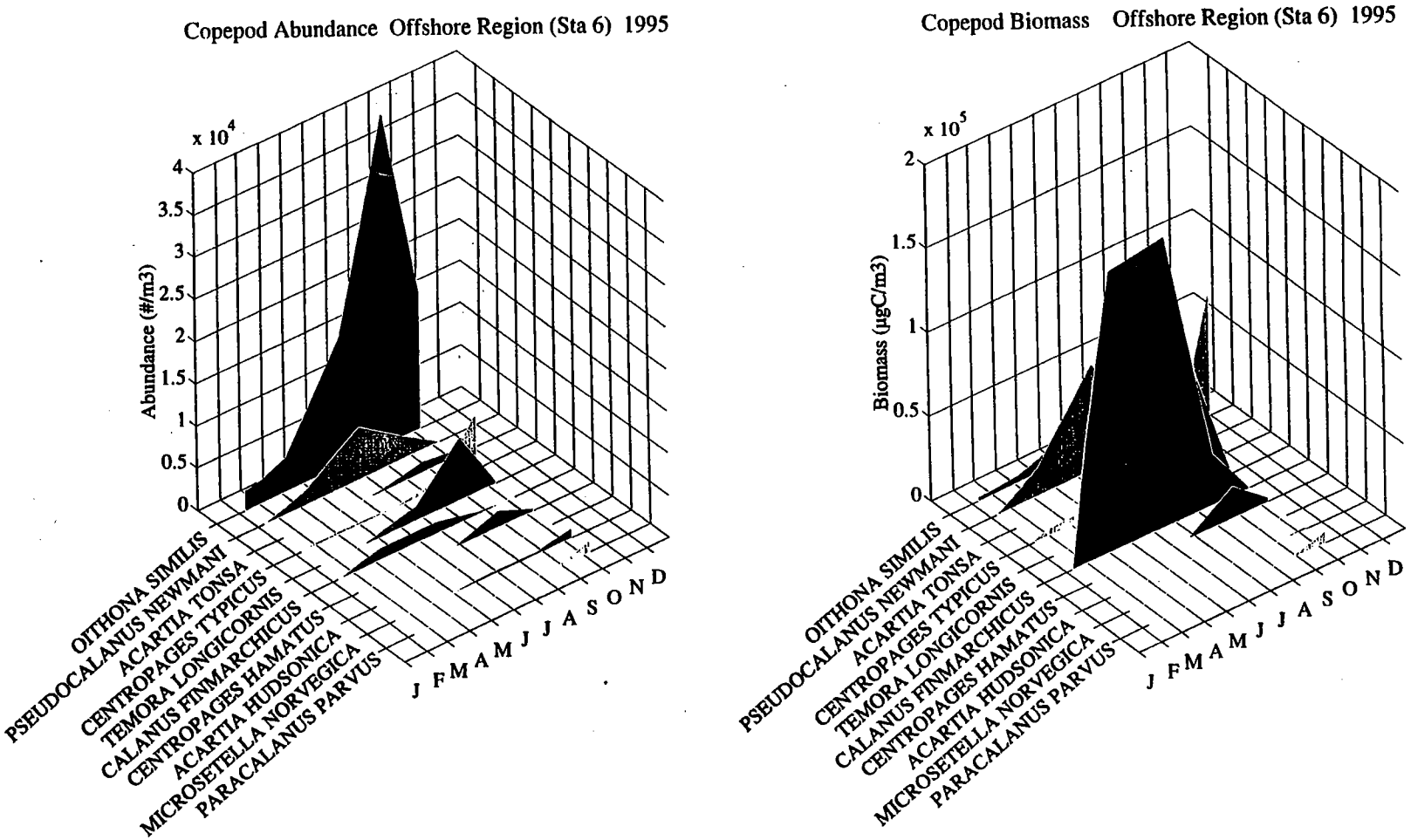

FIGURE 8-30
1995 Seasonal Abundance and Biomass of Dominant Copepod Species
at Offshore Stations

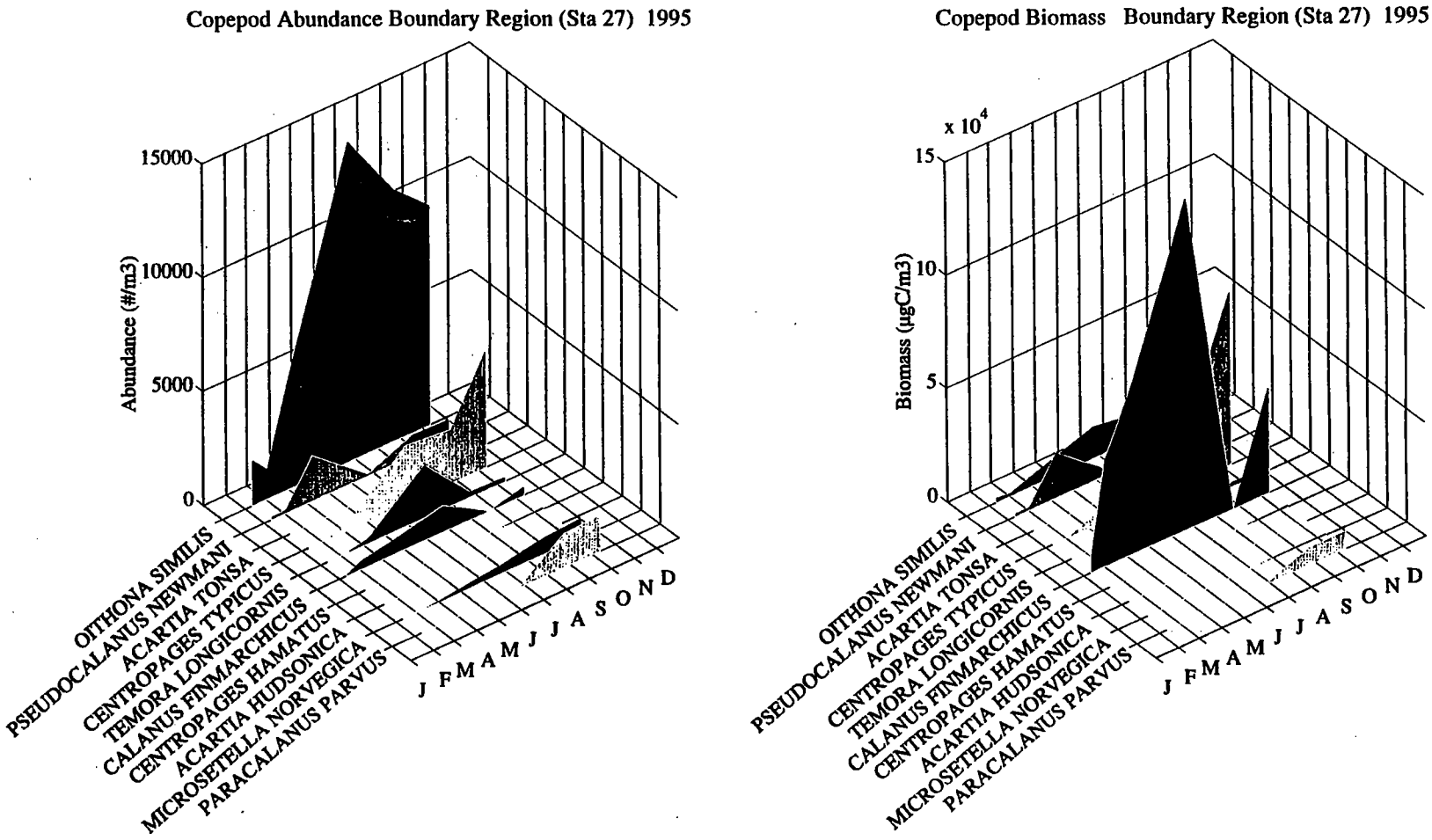

FIGURE 8-31
1995 Seasonal Abundance and Biomass of Dominant Copepod Species
at Boundary Stations

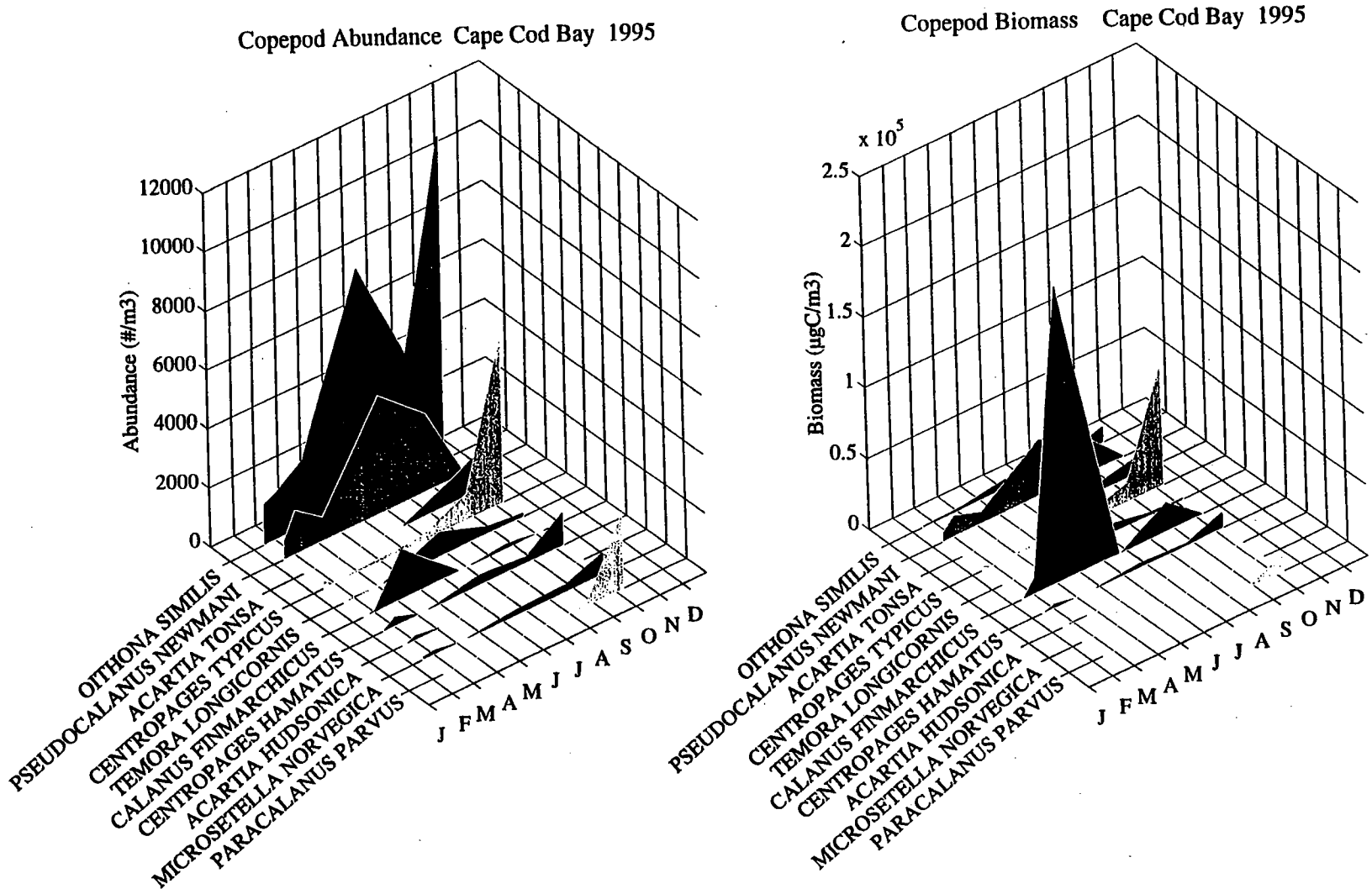

FIGURE 8-32
1995 Seasonal Abundance and Biomass of Dominant Copepod Species
at Cape Code Bay Stations

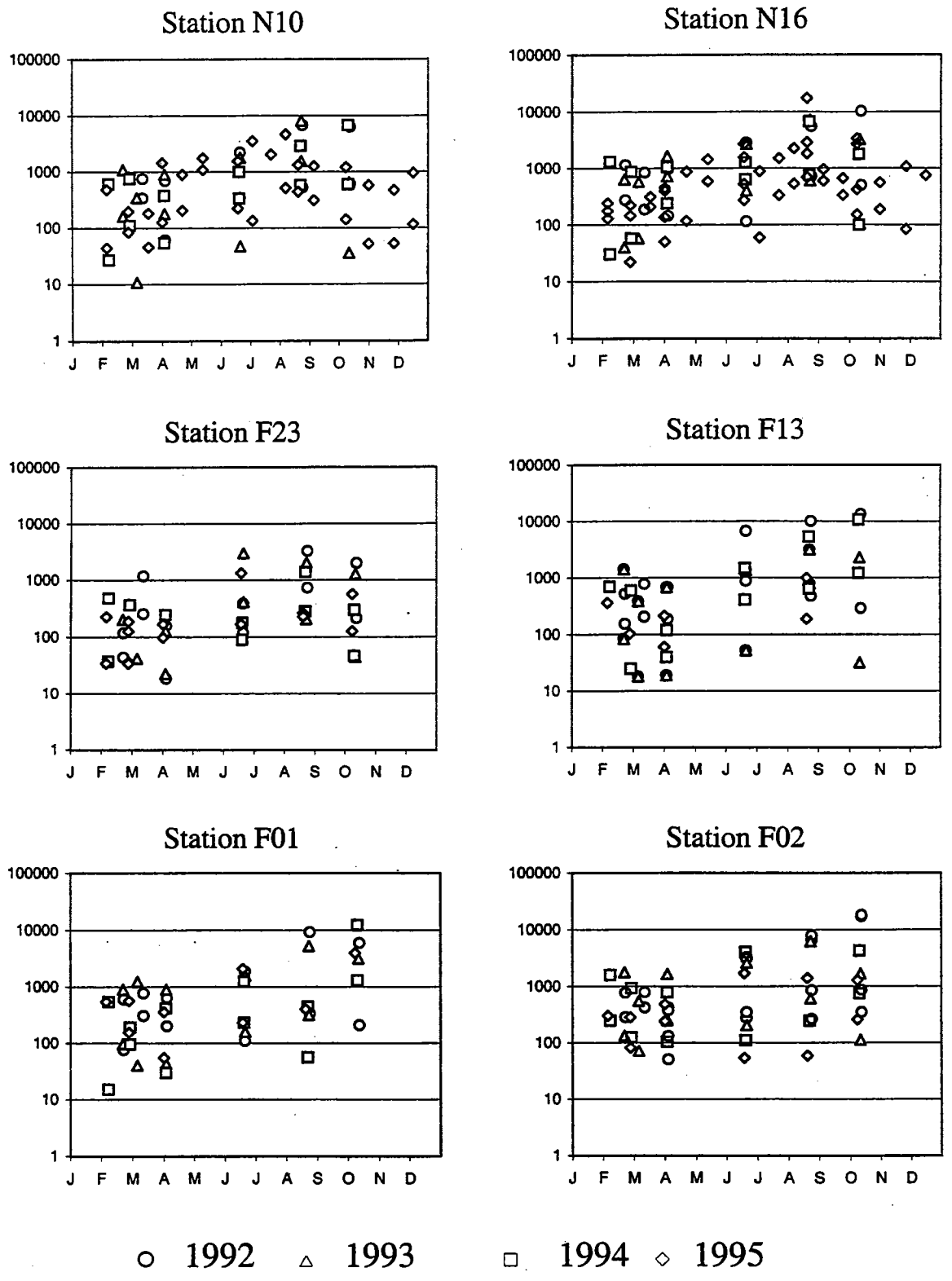

FIGURE 8-33

Interannual Distribution of *Oithona similis* adults by Region

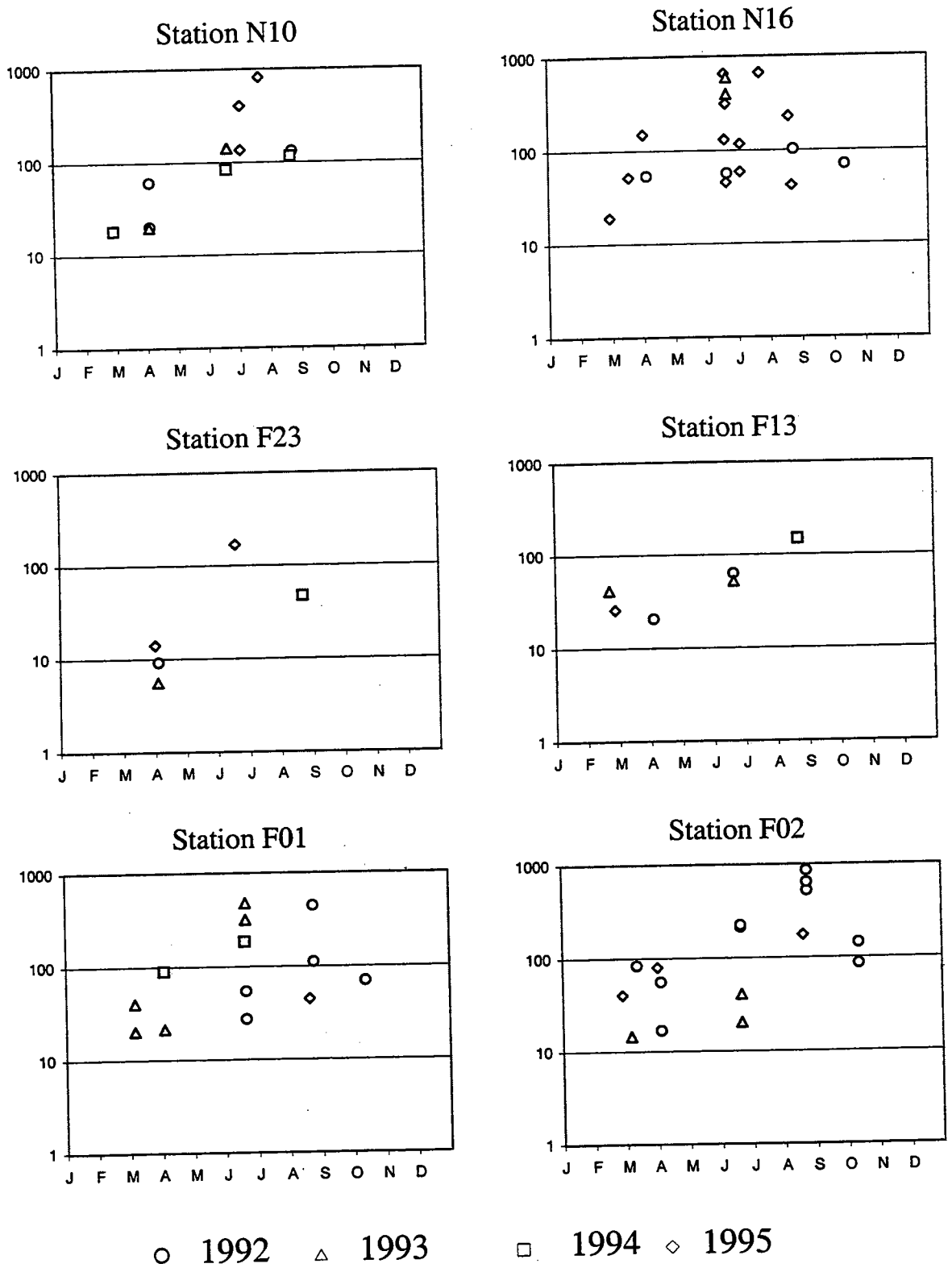

FIGURE 8-34

Interannual Distribution of *Calanus finmarchicus* adults by Region

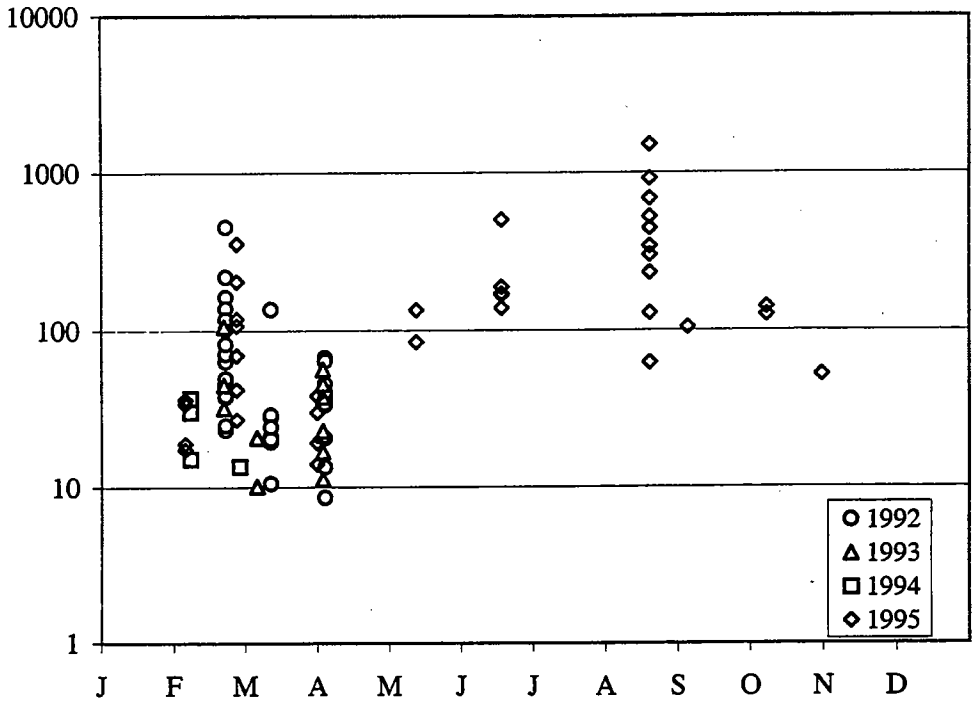

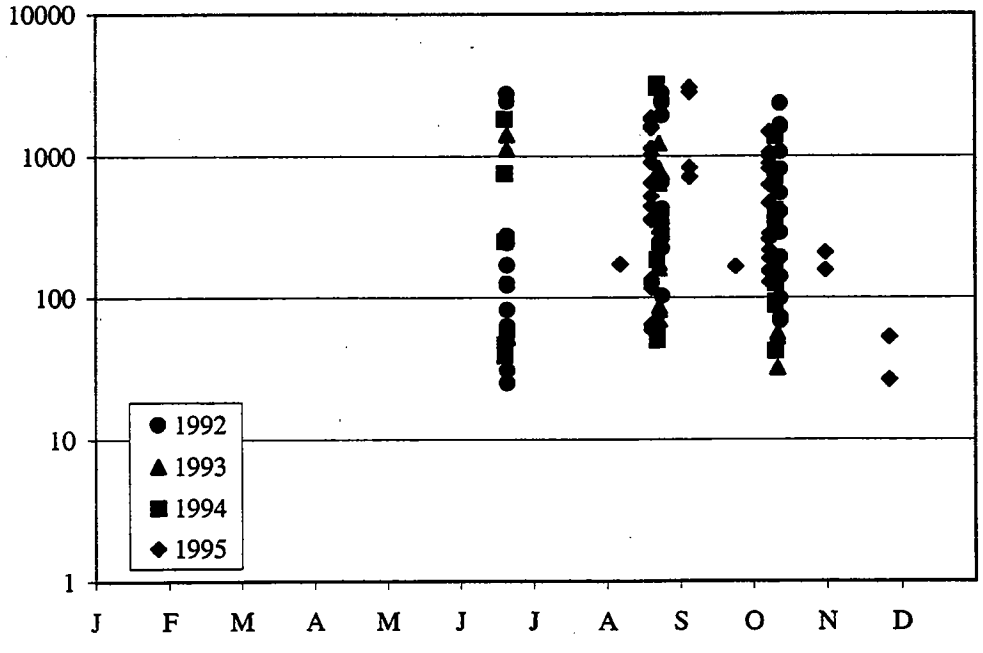

FIGURE 8-35

Seasonal Distribution of (a) *Acartia hudsonica* adults and (b) *Acartia tonsa* adults

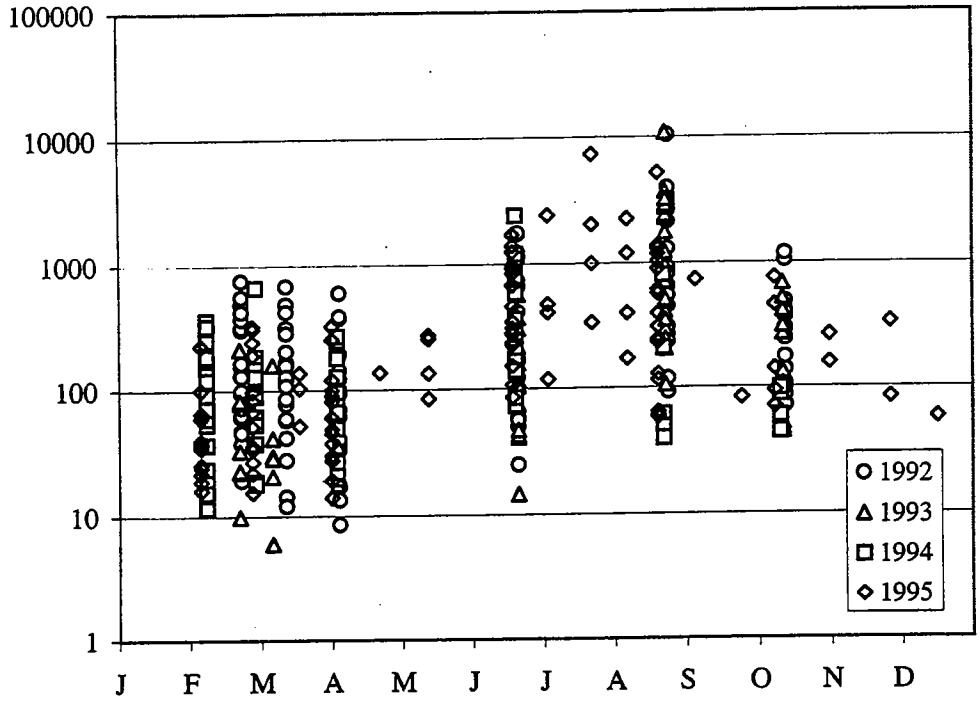

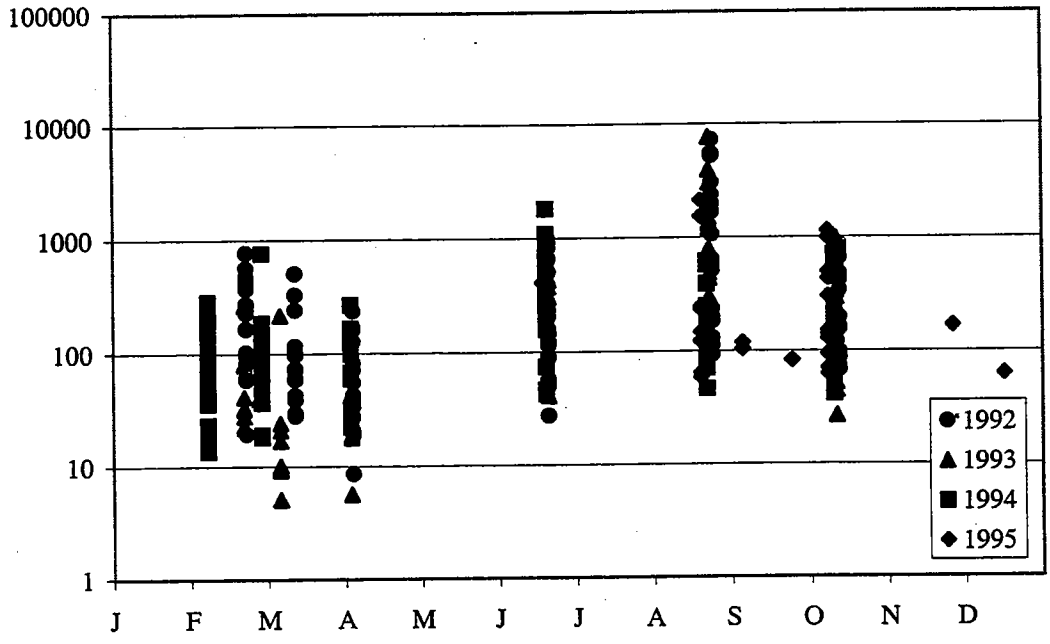

FIGURE 8-36

Seasonal Distribution of (a) *Pseudocalanus newmani* adults *and* (b) *Paracalanus parvus* adults

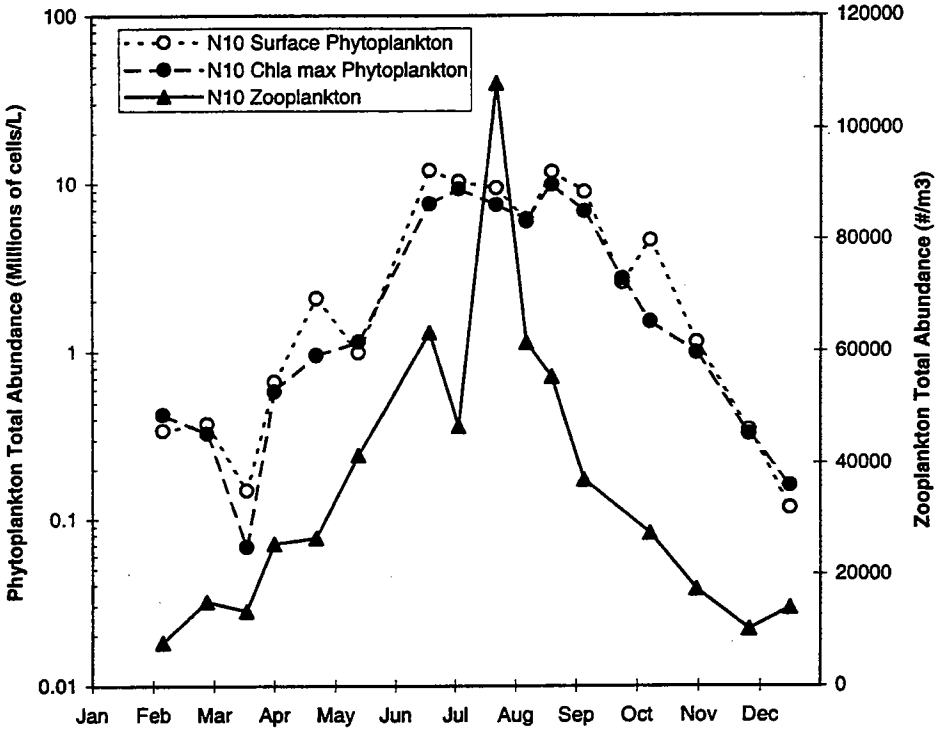

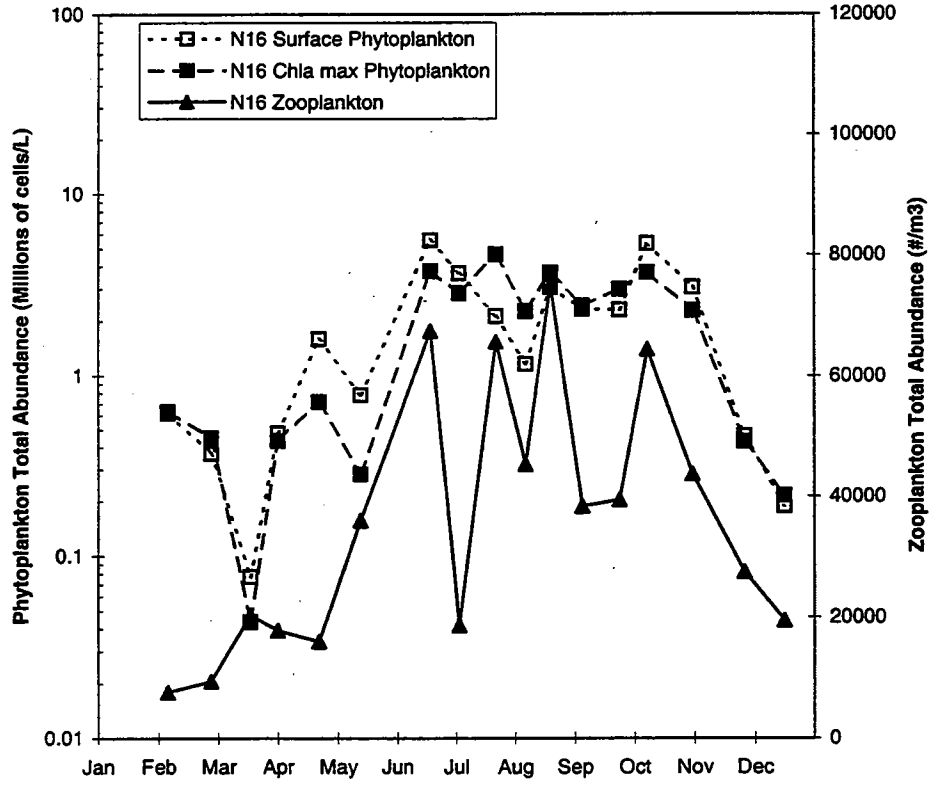

FIGURE 8-37
1995 Phytoplankton and Zooplankton Annual Cycles for Nearfield Stations N10 and N16

9.0 DISCUSSION

In this section, the results from the 1995 HOM monitoring activities are first summarized, then discussed with respect to oxygen and carbon cycling. Potential approaches for modeling of primary production which offer predictive capabilities are then discussed. The section concludes with suggestions for potential modifications of the water column monitoring program. These modifications would focus sampling efforts on the critical periods of activity and ensure data requirements for evaluating the potential effects of the outfall relocation are met.

9.1 Overview of 1995 Monitoring Results

The results presented in the preceding sections of this report are summarized in Table 9-1. For each area of the water column monitoring program, significant events in terms of the structure and biotic activity in the nearfield are identified, facilitating integration of the various monitoring results.

Water column stratification (shaded period in Table 9-1) began in early June and lasted until the onset of the fall turnover in early October (indicated symbolically as "T" in the table). Throughout the year, there was evidence of mixing (M) and upwelling (U) events, and well as water mass intrusions from the Gulf of Maine (GOM). These latter events were typically accompanied by reductions in surface water salinity (F).

Nutrient concentration trends are symbolized by up and down arrows. Upwelling was observed to increase nutrient concentration and biological rates in the surface water. Seasonal peaks in chlorophyll biomass are indicated, as are annual maxima and minima for dissolved oxygen. Evidence of bottom water ventilation suggested by the DO record is depicted as a mixing event (M).

The intensity of seasonal peaks in primary productivity and chlorophyll-specific production are also depicted, as are the dynamics of respiration in the surface (S) mid-depth (M) and bottom water (B). Finally, seasonal trends in plankton abundance are shown, indicating the contribution of centric and pennate diatoms in seasonal bloom events.

9.2 Oxygen Balance of Massachusetts Bay and Stellwagen Basin Bottom Waters

Given the data presented in earlier sections it is possible to construct oxygen (Section 9.2) and carbon (Section 9.3) balances for regions within the bays. These balances provide one type of framework for data integration which will be refined as work continues. However, at present they indicate some basic principles as to the functioning of Massachusetts Bay and Stellwagen Basin.

The objectives of the oxygen balance is to determine the role of *in situ* respiration in the observed oxygen depletion of bottom waters during the interval of stratification. The balance requires: (1) that the bottom water remains relatively "in place" during the interval of stratification (approximately 140 days) or that horizontal advection comprises biogeochemically similar water masses, (2) the volume of water below the pycnocline, (3) the rate of water column respiration below the pycnocline, (4) the rate of sediment respiration, and (5) the time course of oxygen decline below the pycnocline.

For the first requirement, it appears that during stratification the movement of bottom water through the nearfield is relatively slow, and not vertically mixed (Geyer *et al.*, 1992). Relative to the second, the volume of water below the pycnocline can be estimated from CTD hydrocasts and water depths on the monitoring surveys (Figures 3-14, 3-15, 3-16, 3-17). With respect to the third requirement, the rates of water column respiration (Figures 7-34 and 7-35) are relatively well known for Massachusetts Bay (17 surveys) and Stellwagen Basin (6 surveys and five sediment oxygen demand surveys). One major weakness within the bottom water respiration dataset is the lack of information on the potential vertical distribution of water column respiration within the hypolimnion. Since only near bottom samples are collected, we have to assume that they are representative of rates throughout the hypolimnion.

Assumptions must also be made for the fourth requirement, as sediment respiration rates are also limited in areal coverage. It is an overestimate to assign the rates from the depositional sediments (Figure 7-45) to the whole nearfield region because only about 30% of the benthos is represented by depositional sediments (Knebel, 1993). However, it is likely that the rates in the non-depositional sediments are significantly higher than previously assumed during the stratified period (Giblin *et al.*, 1995). Given the relatively non-turbulent nature of the bottom waters, it is highly likely that deposition of particulate carbon from spring bloom and summer production during stratification is relatively uniform. Since most of the summer's sediment respiration is almost certainly dominated by recent deposition, the rates of oxygen consumption may be relatively uniform (two-fold range) throughout the nearfield. The deposition of marine detritus within the nearfield sediments is apparent from video sampling of the benthos (Hilbig *et al.*, 1997). However, direct measurements of oxygen uptake during the stratified interval in non-depositional areas is difficult to measure, requiring elaborate *in-situ* methodologies.

Finally, measurements of bottom water oxygen concentrations are conducted as part of the hydrocasts. Improvements in the water column program to gain more Winkler measurements of bottom water oxygen levels is currently increasing the accuracy of these measurements. Oxygen declines during the stratified interval result from consumption during respiration in sediments and bottom waters and from the restriction of ventilation by the density barrier. The rates of potential hypolimnion respiration can be estimated from the rate of decline of the bottom water oxygen pool (Figure 6-3, 6-7). Care must be taken in this approach to sample consistently within the same layer of the bottom waters. This is especially true within Stellwagen Basin where there appears to be a relatively steep oxygen gradient between the

pycnocline and bottom (Figure 9-1). The steepness of the oxygen gradient illustrates the potential importance of sediment oxygen uptake to total oxygen uptake within the hypolimnion.

The oxygen budget of the nearfield and Stellwagen Basin for the stratified interval of 1995 (Table 9-2), is a clear indication that *in situ* respiration was sufficient to account for the observed rates of oxygen depletion. This suggests that ventilation of bottom waters during the stratified period of 1995 was small. The generally linear decline in bottom water oxygen levels also suggests that short-term mixing events may not have caused major ventilation. However, the observed mid-July anomaly in oxygen levels in the nearfield illustrated the potential effects that larger events might impose. Anomalies were also observed in previous years (Section 6.3) which may well have had effect on DO. More frequent or larger mixing events during the stratified period would thus appear to mitigate annual DO minima as suggested by data from 1992 and 1993.

The apparent balance between oxygen decline and measured respiration rates in 1995 suggests that organic matter inputs to the sediments and bottom waters (which drive *in situ* respiration) are the ultimate cause of bottom water oxygen deficits. These findings, when coupled with the indications that respiration is controlled by the quality and quantity of available organic matter and *in situ* temperature (Section 7), suggest that additional inputs of labile organic matter may further affect the bottom water oxygen deficit.

While respiration appears to determine the rate of bottom water oxygen decline, the magnitude of depression is controlled by the oxygen field at the initiation of stratification, the duration of stratification, and the degree to which ventilation occurs. Significant effects from increased substrate availability may not be apparent in DO measurements alone due to the variable mediation from physical factors. However, increases in measured respiration rates will permit assessments of potential effects using either measured or assumed parameters for physical mediation.

9.3 Carbon Balance of Massachusetts Bay: Nearfield

A preliminary carbon balance can be constructed based upon the carbon remineralization rates measured as water column and sediment respiration and measured rates of photosynthesis (Section 7). The carbon balance is based on the observations from recent data that carbon fixation and mineralization within Massachusetts Bay appear to be dominated by *in situ* processes and that organic matter import from inshore is either a small fraction of the carbon balance or is balanced by export from the nearfield. The functional area of the balance is likely on the order of several days horizontal advection. Under the present pre-discharge conditions, the functional region spans to the north of the nearfield to within the nearfield grid). Tailoring the carbon balance to post-discharge conditions will require an evaluation of the extent to which horizontal carbon transport may increase due to increased photosynthesis within the nearfield region. The primary goal of constructing a carbon balance for the nearfield is to evaluate

changes in carbon cycling under stratified and unstratified conditions. In addition, constructing even simple balances yields insight into key processes and can indicate program data-gaps.

The basic outline of the carbon balance for Massachusetts Bay (which is still evolving for Stellwagen Basin) focuses on the inputs of phytoplankton carbon to the surface euphotic layer and its subsequent decomposition within the mixed layer and bottom water (during stratification) and within the sediments (Figure 9-2). Since the vertical transport of organic matter from the photic zone to the bottom appears to vary with stratification (Section 7.2.1), the locus of carbon mineralization may shift with the degree of physical mixing. Therefore, separate carbon balances were constructed for the fall-winter-spring mixed period and the summer stratified interval. Since phytoplankton do not remain within the water column for extended periods (week) due to grazing or senescence, and since horizontal transport within the mixed layer is relatively rapid (days to weeks), the balances assume that carbon fixed during either the mixed or stratified periods leaves the water column before the next interval. "Leaving" the water column can be through horizontal advection (exported) from the region or by heterotrophic (and dark autotrophic) consumption or deposition to sediments within the balance region.

Since the rate of carbon fixation varies with the amount of incident light as well as the phytoplankton abundance and physiological state, the integrated measured rates and the maximum potential daily light production represent the end-members for actual photosynthetic input of organic matter (Section 7.1). Therefore, we have listed the range of total production within each interval based upon the measured versus potential rate. Carbon mineralization within the water column and sediments is based upon the measured respiration rates (Sections 7.2, 7.3) assuming an RQ of 1.

During the unstratified period, most of the organic matter production can be accounted for by *in situ* mineralization, 78%-96% (Figure 9-3). Water column respiration within surface waters was slightly higher than at the bottom, combining to account for almost 90% of the total carbon mineralized. The fate of the residual production (9-62 g m^{-2}) is uncertain. It is available for export (outwelling) or for deposition and storage within the sediments. Given the vertical transport of POC during mixing, it is likely that some of this organic matter (particularly spring bloom) may be deposited to the sediment effecting later respiration rates. Overall, the carbon balance indicates a system in relative equilibrium.

In contrast, the stratified interval (Figure 9-4), indicates a non-uniform water column that is not in equilibrium. During stratification, surface waters are the dominant site of remineralization. While water column respiration accounts for the majority of the carbon input (54%-59%) and most of the total system respiration (84%), it appears that produced organic matter is being "lost" from the system. The amount of estimated export increases two to three fold during this interval. It is unlikely that a significant amount of this "missing" carbon is entering the sediments, since it would likely result in a large increase in respiration given the temperature of the bottom waters. Clearly, the "missing" carbon has either been

horizontally advected from the region or has been remineralized at sites not measured by the present sampling program.

While the potential for remineralization at other locations within the nearfield cannot be ruled out, the amount of carbon to be accounted for is more than the total amount remineralized in the bottom waters and sediments during this interval. It is possible that during stratification, the horizontal transport of organic particles within the mixed layer is higher than during the unstratified period. It is also possible that rates of primary production during stratification (but not during unstratified periods) are significant overestimates. A direct examination of these issues is required in order to ascertain the fate of photosynthetic production within the nearfield region. With the current understanding, at present it appears that during the mixed period, the observed carbon remineralization was in balance with local carbon fixation. In contrast, the observed imbalance during stratification, the nearfield region suggests that organic matter is being lost through horizontal advective processes.

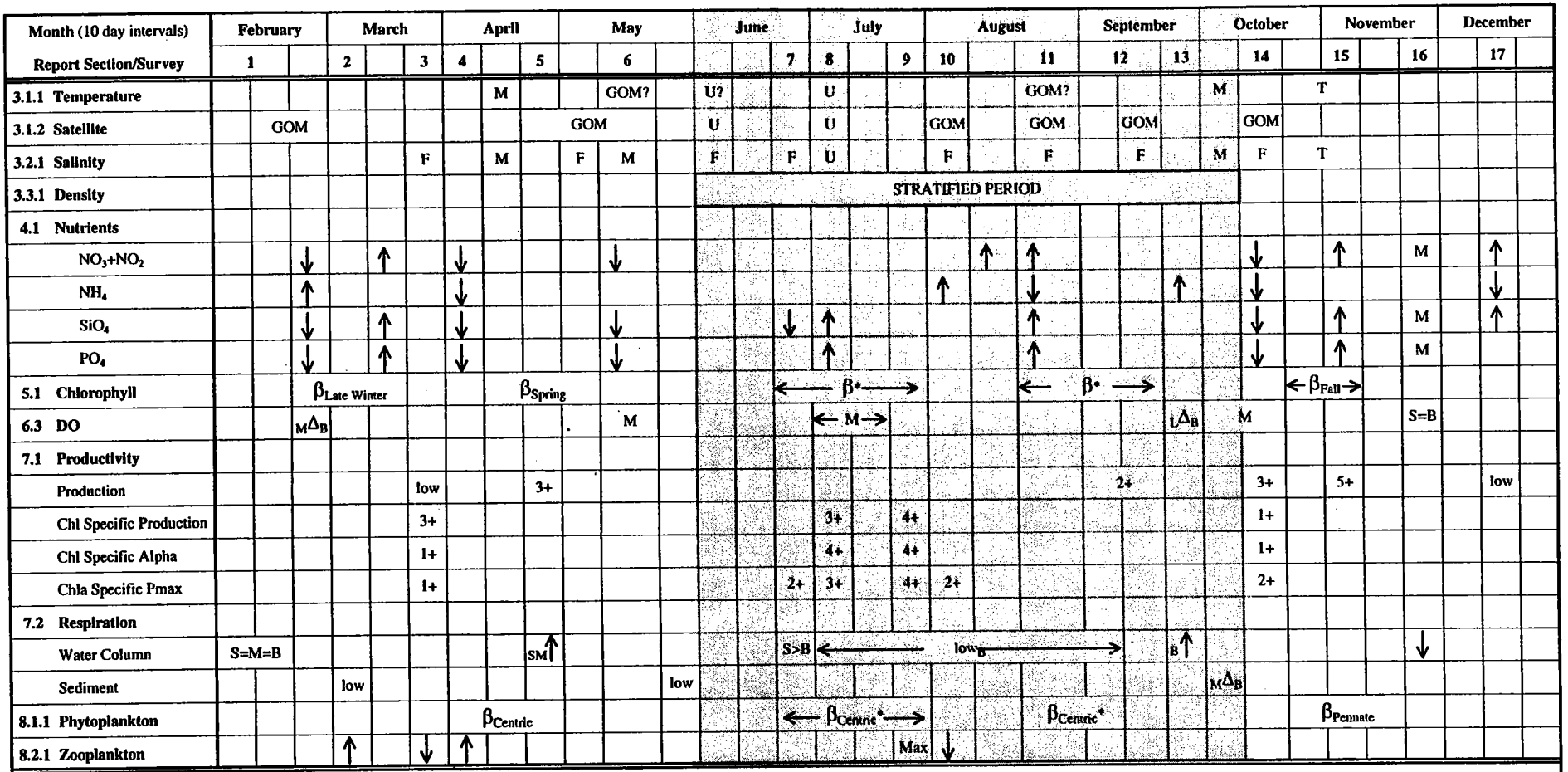

TABLE 9-1
Overview of 1995 Nearfield Water Column

TABLE 9-2

Contribution of Water column and Sediment Respiration to Bottom water Oxygen Decline in the Nearfield and Stellwagen Basin, 1995

Source of O_2 Uptake	Rate (mg/L/d)	% Observed Decline
Nearfield: D.O. Depletion	-0.027	100
Watercolumn Respiration[1]	-0.0164	61
Sediment Respiration	-0.0211	78[2]
Total Respiration	-0.0375	139[2]
Stellwagen Basin: D.O. Depletion	-0.017	100
Watercolumn Respiration[1]	-0.0109	73
Sediment Respiration	-0.0043	29
Total Respiration	-0.0152	101

[1] Assumes pycnocline depth of 20 m
[2] Maximum estimate assuming 100% depositional sediments

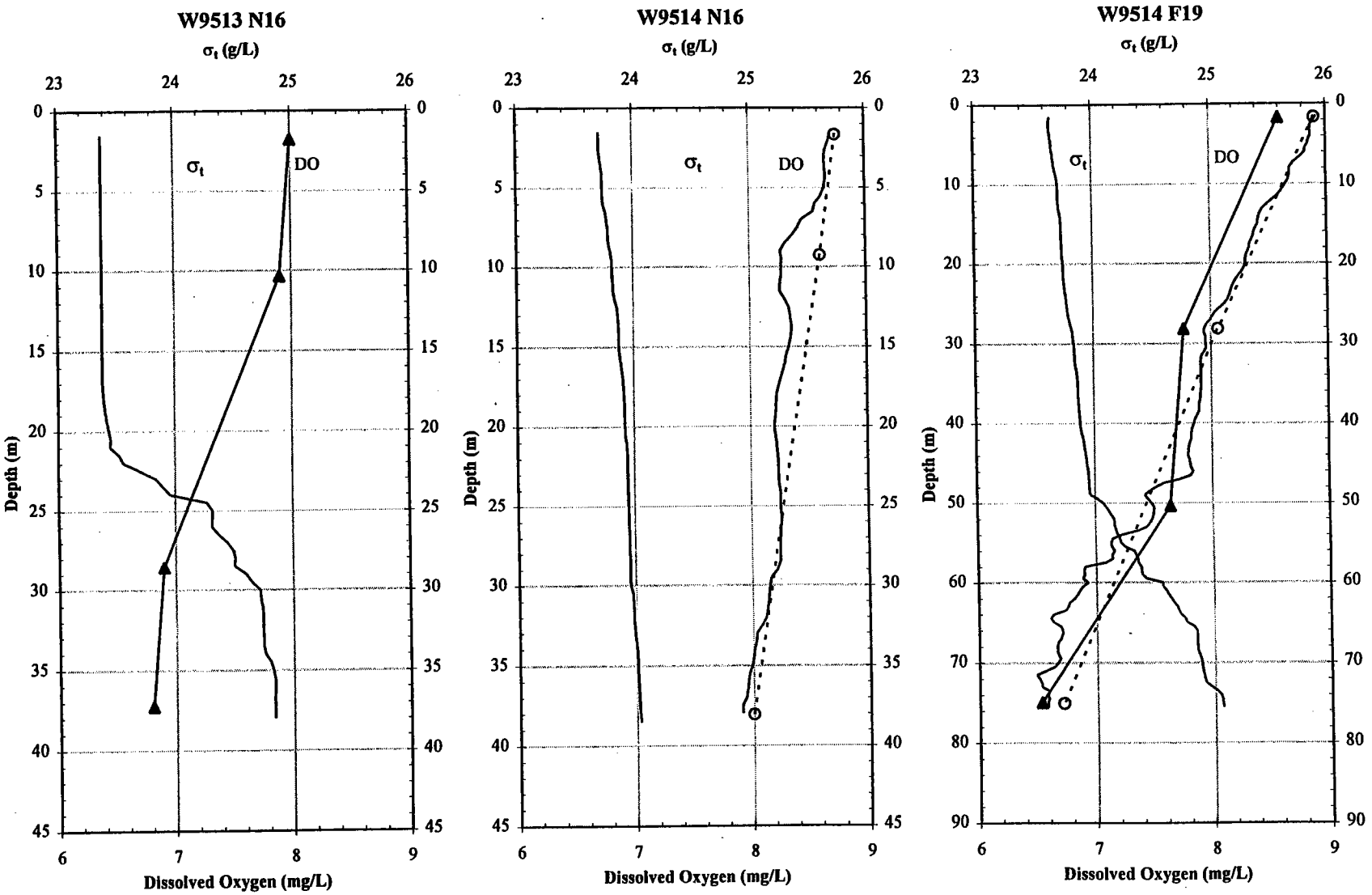

FIGURE 9-1

Distribution of Water Column Oxygen Relative to the Density Gradient in the Nearfield (N16) and Stellwagen Basin (F19)

Open symbols = WHOI data; Closed symbols = E3I data

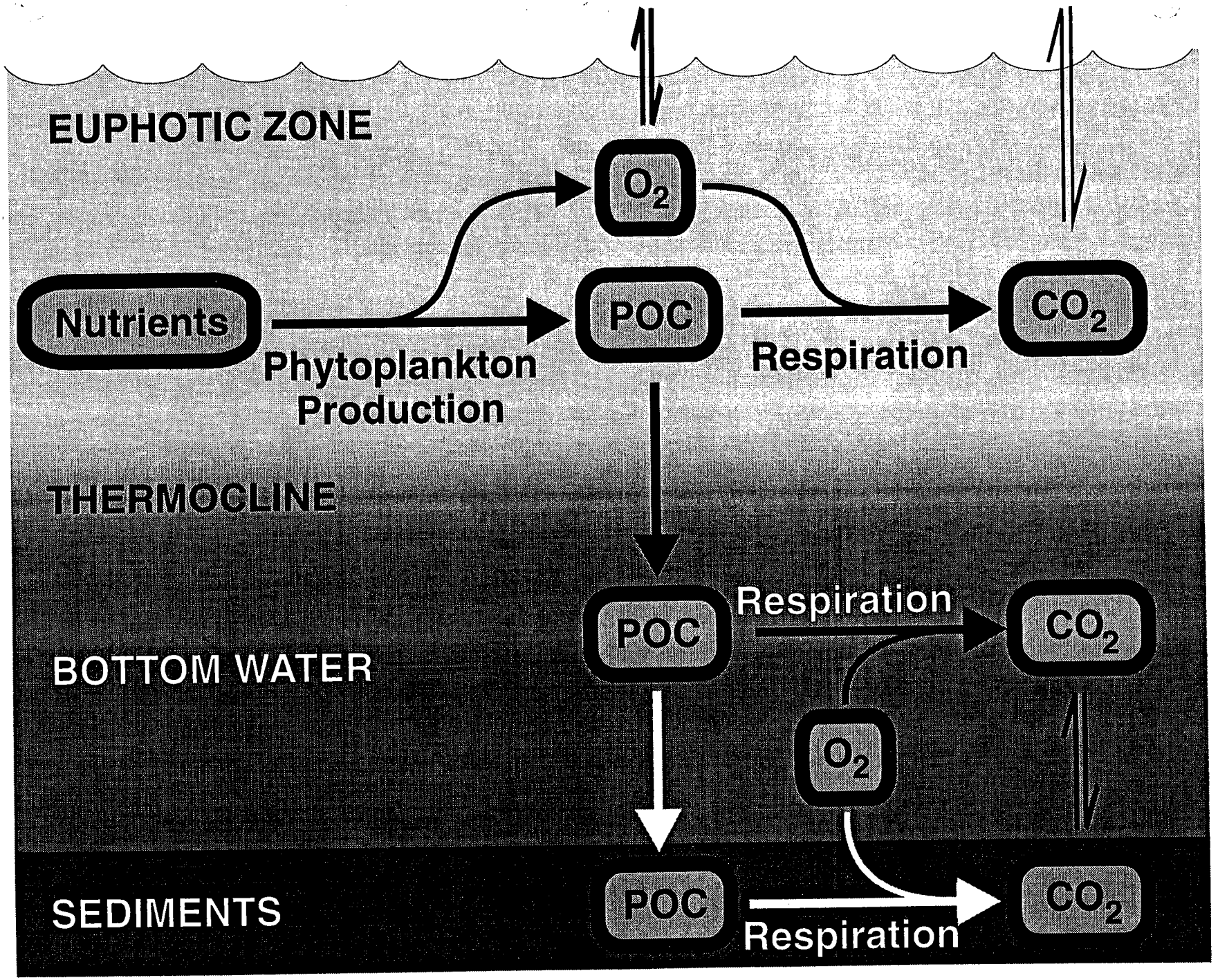
EUPHOTIC ZONE
O_2
Nutrients
POC
CO_2
Phytoplankton Production
Respiration
THERMOCLINE
POC
Respiration
CO_2
BOTTOM WATER
O_2
SEDIMENTS
POC
Respiration
CO_2

FIGURE 9-2

Carbon Balance, Nearfield: Unstratified

Values shown are mean (standard error)

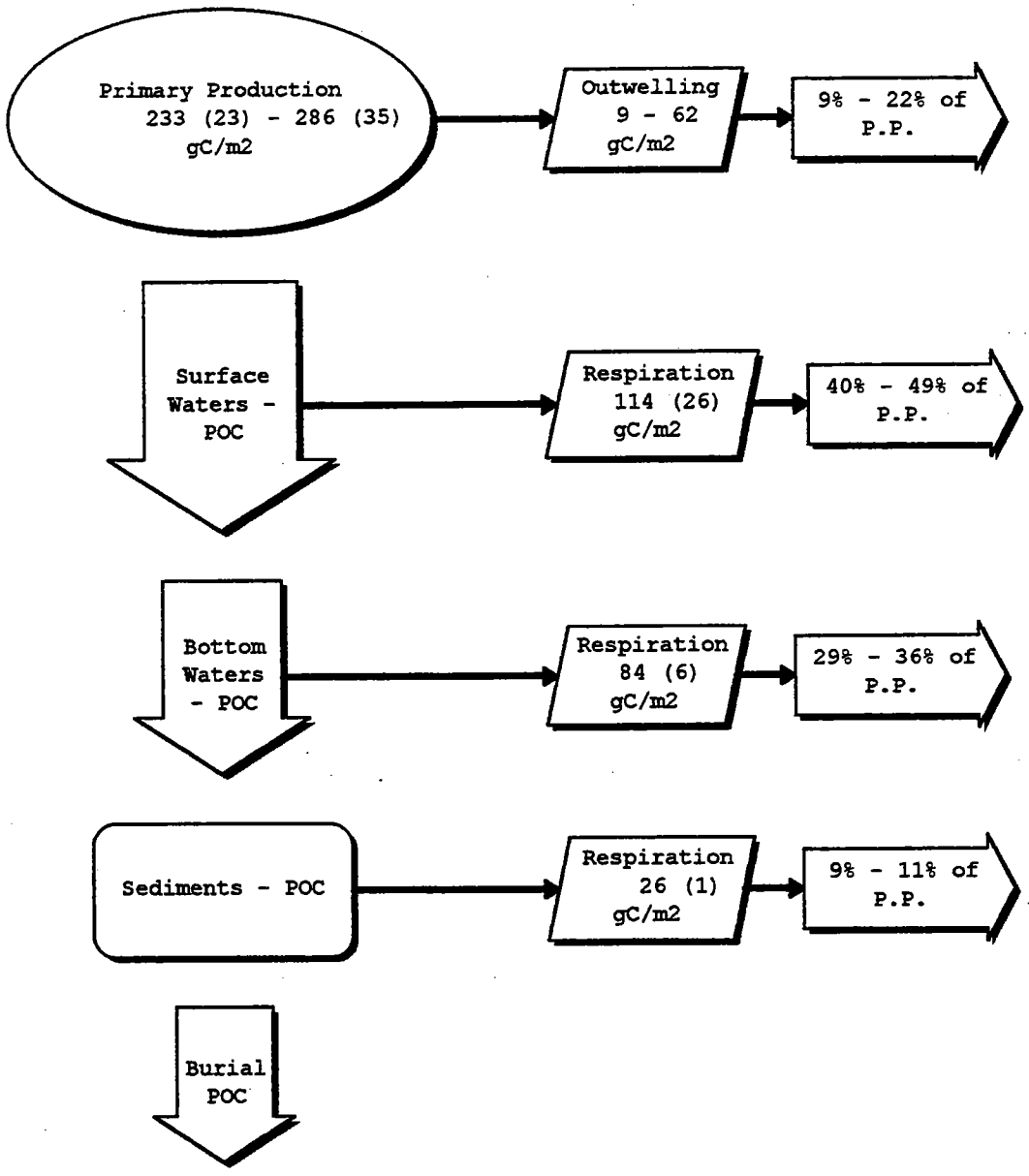

b. howes | B. Howes | 10/25/1996 | 13:44 | c:\all3\mwra_mix.acl

page 1 of 1

FIGURE 9-3

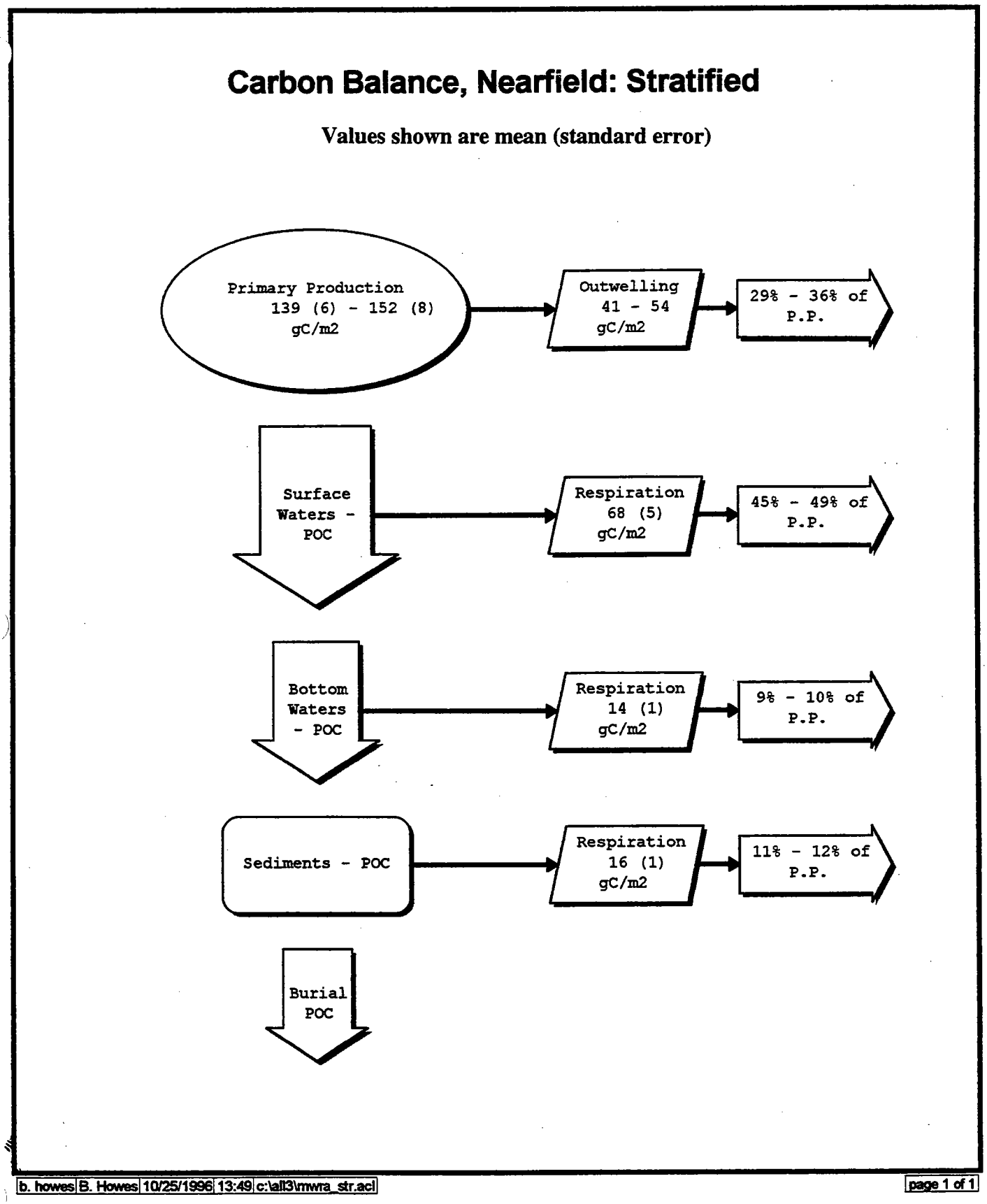
Carbon Balance, Nearfield: Stratified
Values shown are mean (standard error)
Primary Production
139 (6) - 152 (8)
gC/m2
Outwelling
41 - 54
gC/m2
29% - 36% of
P.P.
Surface
Waters -
POC
Respiration
68 (5)
gC/m2
45% - 49% of
P.P.
Bottom
Waters
- POC
Respiration
14 (1)
gC/m2
9% - 10% of
P.P.
Sediments - POC
Respiration
16 (1)
gC/m2
11% - 12% of
P.P.
Burial
POC
b. howes B. Howes 10/25/1996 13:49 c:\all3\mwra_str.acl
page 1 of 1

FIGURE 9-4

10.0 REFERENCES

Anderson, D.M. and B.A. Keafer. 1992. Paralytic shellfish poisoning on Georges Bank: *In situ* growth or advection of established dinoflagellate populations. **In:** J. Wiggen et al. (eds.), Gulf of Maine Workshop Report.

Anderson, D.M. and B.A. Keafer. 1995. Toxic red tides in Massachusetts and Cape Cod Bays. Final report to the Massachusetts Water Resources Authority, January 31, 1995.

Arfi, R; Champalbert, G; Patriti, G. 1981. Plankton systems and urban pollution: an aspect of zooplankton populations. Mar. Biol., vol. 6, no. 2-3, pp. 133-141.

Bates, S.S. 1997. Personal communication with S. Cibik, March 5, 1997. Also, see: http://www.maritimes.dfo.ca/science/mesd/he/science/toxins/index.html

Bowen, J., K. Hickey, B. Zavistoski, T. Loder, B. Howes, C. Taylor, E. Butler, and S. Cibik. 1997. Draft Combined Work/Quality Assurance Project Plan for water quality monitoring: 1995-1997. Prepared for the Massachusetts Water Resources Authority, Boston, MA, under Contract S186. 73pp.

Brown, J. and C.S. Yentsch. 1995. Monthly synoptic overview letter reports. Prepared by Bigelow Laboratory for Ocean Sciences for the Massachusetts Water Reources Authority, Boston, MA. Also see http://narwhal.gso.uri.edu/cwatch1.html

Champalbert, G, and G. Patriti. 1982. Impact of pollution on zooplankton communities in the distribution zone of the urban emission of Marseille. Hydrobiologia., 89, 17-27.

Cleveland, J.S., M.J. Perry, D.A. Kiefer and M.C. Talbot. 1989. Maximal quantum yield of photosynthesis in the northwestern Sargasso Sea. J. Mar. Res. 47, 869-886.

Durbin, E. G., A. G. Durbin,, T. J. Smayda, and P. G. Verity. 1983. Food limitation of production by adult *Acartia tonsa* in Narragansett Bay, Rhode Island, Limnol. Oceanogr., 28 (6), 1199-1213.

Durbin, E. G., A. G. Durbin,, and R. G. Campbell. 1992. Body size and egg production in the marine copepod *Acartia hudsonica* during a winter-spring diatom bloom in Narragansett Bay, Limnol. Oceanogr.,37(2), 342-360.

Durbin, E. G., and A. G. Durbin. 1992. Effects of temperature and food abundance on grazing and short-term weight change in the marine copepod *Acartia hudsonica*, Limnol. Oceanogr., 37(2), 361-378.

Franks, P.J.S. and D.M. Anderson. 1992. Alongshore transport of a toxic phytoplankton bloom in a buoyancy current: *Alexandrium tamarense* in the Gulf of Maine. Mar. Biol. 112:153-164.

Fulton, R S. 1984. Effects of chaetognath predation and nutrient enrichment on enclosed estuarine copepod communities. OECOLOGIA., vol. 62, no. 1, pp. 97-101.

Geyer, W.R., G.B. Gardner, W.S. Brown, J. Irish, B. Butman, T.C. Loder, and R.P. Signell. 1992. Final report: physical oceanographic investigation of Massachusetts and Cape Cod Bays. August 1, 1992. 497 pp.

Giblin, A., C. Hopkinson, J. Tucker, B. Nowicki, and J. Kelly. 1995. Metabolism, nutrient cycling, and denitrification in Boston Harbor and Massachusetts Bay sediments in 1994. #95-13.

Hunt, C.D. and M. Steinhauer. 1994 . MWRA nutrient indicator workshop, held on January 20, 1994. Proceedings prepared for the Massachusetts Water Resources Authority.

Hydroqual and Normandeau. 1995. A water quality model for Massachusetts and Cape Cod Bays: calibration of the Bays Eutrophication Model (BEM). MWRA Enviro. Quality Dept. Tech. Rpt. Series No. 95-8. Massachusetts Water Resources Authority, Boston, MA 402 pp.

Kelly, J. 1993. Nutrients and Massachusetts Bay: an update of eutrophication issues. MWRA Technical; Report 93-17. 119 pp.

Kelly, J.R. and P.H. Doering. 1995. Nutrient issues update 1995: metabolism in Boston Harbor, Massachusetts and Cape Cod Bays, MA (USA) during 1992-1994. MWRA Technical Report 95-19. 38 pp.

Kelly, J.R and J. Turner. 1995. Water column monitoring in Massachusetts and Cape Cod Bays: annual report for 1994. MWRA Technical Report 95-17. 163 pp.

Knebel, H.J. 1993. Sedimentary environments within a glaciated estuarine-inner shelf system: Boston Harbor and Massachusetts Bay. Marine Geology 110:7-30

Lohrenz, S.E., G.L. Fahnenstiel and D.G. Redalje. 1994. Spatial and temporal variations of photosynthetic parameters in relation to environmental conditions in coastal waters of the Northern Gulf of Mexico. Estuaries. 17, 779-795.

Murray, P.M., S.J. Cibik, K.B. Lemieux, R.A. Zavistoski, B.L. Howes, C.D. Taylor, D.M. Anderson, C.S. Davis, and T.L. Loder. 1997a. Draft 1995 semi-annual water column monitoring report, February - July, 1995.

Murray, P.M., S.J. Cibik, K.B. Lemieux, R.A. Zavistoski, B.L. Howes, C.D. Taylor, D.M. Anderson, C.S. Davis, and T.L. Loder. 1997b. Draft 1995 semi-annual water column monitoring report, August - December, 1995.

NRCC. 1996. Personal communication between Kathy Vreeland of the Northeast Regional Climate Data Center, Ithaca, NY., and S. Cibik October 6, 1996. Also, see: http://met-www.cit.cornell.edu/

Oudot, C., R. Gerard, and P. Morin. 1988. Precise shipboard determination of dissolved oxygen (Winkler procedure) for productivity studies with a commercial system. Limnology and Oceanography 33:146-150.d

Paffenhofer G, and D. Stearns. 1988. Why is *Acartia tonsa* restricted to nearshore environments?. Mar. Ecol. Prog. Ser. 42:33-38.

Peterson, W. T. and D. C. Bellatoni. 1987. Relationship between water-column stratification, phytoplankton cell size and copepod fecundity in Long Island Sound and off central Chile. S. Afr. J. Mar. Sci., 5, 411-421.

Proni, J., J. Stamates, and J. Craynock. 1996. Massachusetts Bay water column particulate study (DW 13940107-01-0). Prepared for the Massachusetts Water Reources Authority, Boston, MA., May 1996.

Scofield, O., B.B. Prezelin, R.C. Smith, P.M. Stegmann, N.B. Nelson, M.R. Lewis and K.S. Baker. 1991. Variability in spectral and nonspectral measurements of photosynthetic light utilization efficiencies. Mar. Ecol. Prog. Ser. 78, 253-271.

Sullivan, BK; Banzon, PV 1990. Food limitation and benthic regulation of populations of the copepod *Acartia hudsonica* Pinhey in nutrient-limited and nutrient-enriched systems. Limnol. Oceanogr., 35, no. 7, pp. 1618-1631.

Taylor, C.T. and B.L. Howes. 1994. Effect of sampling frequency on measurements of seasonal primary production and oxygen status in nearshore coastal ecosystems. Mar. Ecol. Prog. Ser. 108:193-203.

Theodorou, A J, Ballay, D, Asano, T, Bhamidimarri, R, Chin, KK, Dahlberg, AG, Grabow, WOK, Ohgaki, S, Zotter, K, Milburn, A, Izod, EJ, Nagle, PT (eds). 1994. The ecological state of the Elefsis Bay prior to the operation of the Athens sea outfall. Water Quality International '94. part 10: Water Quality Monitoring; Lake Management., 1994, pp. 161-171, Water Sci. Technol., 30, no. 10.

Toner, RC. 1981. Interrelationships between biological, chemical and physical variables in Mount Hope Bay, Massachusetts. Estuar. Coast. Shelf Sci., vol. 12, no. 6, pp. 701-712

Townsend, D.W., L.M. Cammen, J.P. Christensen, S.G. Ackelson, M.D. Keller, E.M. Haugen, S. Corwin, W.K. Bellows, J.F. Brown. 1991. Seasonality of oceanographic conditions in Massachusetts Bay. 114 pp. Bigelow Laboratory for Ocean Sciences Technical Report No. 83, October 1991. West Boothbay Harbor, ME 04575. MWRA Technical Report MS-1.

Turner, J.T. 1994. Planktonic copepods of Boston Harbor, Massachusetts Bay, and Cape Cod Bay, 1992. Hydrobiologia, 292/293: 405-413

USGS. 1996a. Personal communication between F. Hotchkiss, USGS Woods Hole, MA., and S. Cibik, October 1, 1996. See: http://woodshole.er.usgs.gov/~fhotchki/plotindex.html

USGS. 1996b. Personal communication between T. Shepard, USGS Marlborough, MA., and S. Cibik, September 25, 1996.

APPENDIX A

Methods

Production Analyses by ^{14}C - Field Procedures.

From each of the 5 productivity depths at each productivity station, samples were obtained by filtration through 300 mm Nitex screen (to remove zooplankton) from the Niskin bottles into opaque 1 gal polyethylene bottles. Under subdued green light, sub-samples were transferred by siphon into individual 75 ml acid cleaned polycarbonate bottles. Each bottle was flushed with approximately 250 ml of sample. A total of 16 bottles (14 light bottles, 2 dark bottles) were filled for each depth and incubated in a light and temperature controlled incubator. Light bottles from each depth are incubated at 14 light intensities (250 W tungsten-halogen lamps attenuated with Rosco neutral density filters) and all bottles incubated within 2° C of the *in situ* temperature at each depth for 4-6 hr (actual time was recorded). Single bottles of sample collected from each depth was assayed for background (time-zero) activity.

The 75 ml samples were incubated with 5-10 μCi ^{14}C-bicarbonate (higher activity during winter and spring season) and biological activity terminated by filtration of the entire contents of the bottles through 2.5 cm diameter Whatman GF/F glass fiber filters and immediate contact of the filters with 0.2 ml of a 20% aqueous solution of acetic acid contained in pre-prepared 20 ml glass scintillation vials (vials immediately recapped). For specific activity determination 0.1 ml aliquots of sample were placed in pre-prepared 20 ml scintillation vials containing 0.2 ml of benzethonium hydroxide (approximately 1.0 M solution in methanol; Sigma Chemical Company) to covalently sequester the ^{14}C inorganic carbon (vials immediately recapped). Specific activity was determined from the measured activity and measurements of DIC.

Samples for DIC analysis were collected from the Niskin bottles into 300 ml BOD bottles, following collection procedures used for oxygen analyses. Within 6 hr. of BOD sample collection, duplicate 10 ml samples were injected into 20 ml crimp-sealed serum bottles containing 0.5 ml of a 2N aqueous solution of sulfuric acid for subsequent I.R. analysis (Beckman IR-315 infrared analyzer) of the gaseous phase (5 - 150 ml samples) at the W.H.O.I. laboratory.

During summer months 1995 some of the ^{14}C incubations (W9508-W9513) were incubated on shore in the MWRA laboratory at Deer Island. Samples were collected in opaque bottles and maintained at *in situ* temperature until transport to the lab. The ^{14}C incubations were begun approximately 2 - 3 hr from sample collection and should compare favorably with samples that are incubated aboard the ship.

Production Analyses by ^{14}C - Laboratory Procedures.

Sample processing. Upon arrival to the W.H.O.I. laboratory scintillation cocktail (10 ml Scintiverse II) were added to the scintillation vials containing the specific activity samples and analyzed using a Packard Tricarb 4000 liquid scintillation counter which possesses automated routines for quench correction. Vials containing acidified filters were opened and placed in a

ventilator in the hood for overnight to allow the filters to dry and excess ^{14}C carbon dioxide dissipate. The vials containing the filters were analyzed by scintillation spectroscopy as described above.

Calculation of Primary production. Volume specific primary production was calculated using equations similar to that of Strickland and Parsons (1972) as follows:

$$P(i) = \frac{1.05(DPM(i)-DPM(blk))}{V_s A_{sp} T}$$

$$P(d) = \frac{1.05(DPM(d)-DPM(blk))}{V_s A_{sp} T}$$

$$A_{sp} = \frac{DPM(sa)-DPM(back)}{V_{sa} DIC}$$

where:

P(i) = primary production rate at light intensity i, ($\mu gC\ l^{-1}h^{-1}$ or $mgC\ m^{-3}h^{-1}$)
P(d) = dark production, ($\mu gC\ l^{-1}h^{-1}$ or $mgC\ m^{-3}h^{-1}$)
A_{sp} = specific activity (DPM/μgC)
DPM(i) = dpm in sample incubated at light intensity i
DPM(blk) = dpm in zero time blank (sample filtered immediately after addition of tracer)
DPM(d) = dpm in dark incubated sample
DPM(back) = background dpm in vial containing only scintillation cocktail
V_s = volume of incubated sample (l)
T = incubation time (h)
V_{sa} = volume counted of specific activity sample (ml)
DIC = concentration of dissolved inorganic carbon (μg/ml)

P-I curves. For each of the 5 depths for each photosynthesis station a P-I curve was obtained from the data P(I) = P(i)-P(d) vs. the irradiance (I, $\mu E\ m^{-2}s^{-1}$) that the incubating sample is exposed. The P-I curves were fit via one of two possible models, depending upon whether or not significant photoinhibition occurs. In cases where photoinhibition is evident the model of Platt et al. (1980) was fit (SAAM II, 1994) to obtain the theoretical maximum production, and terms for light-dependent rise in production and degree of photoinhibition:

$$P(I) = P_{sb}"(1 - e^{-a})e^{-b}$$

$$P\max" = P_{sb}"[\alpha"/(\alpha" + \beta")][\beta"/(\alpha" + \beta")]^{\beta"/}$$ (Lohrenz et al., 1994)

where:

P(I) = primary production at irradiance I, corrected for dark fixation (P(i)-P(d))
P_{sb}"= theoretical maximum production without photoinhibition
a = α"I/Psb", and α"is the initial slope the light-dependent rise in production

b = β"I/Psb", and β"is a term relaying the degree of photoinhibition
P_{max}"= light saturated maximum production

If it is not possible to converge upon a solution the model of Webb et al. (1974) was similarly fit to obtain the maximum production and the term for light-dependent rise in production:

$$P(I) = P_{max}"\left(1 - e^{-a'}\right)$$

where:

P(I) = primary production at irradiance I corrected for dark fixation (P(i)-P(d))
P_{max}"= light saturated maximum production
a' = α"I/Pmax", and α"is the initial slope the light-dependent rise in production

Nearly all P-I curves obtained did not show evidence of photoinhibition and were fit according to the Webb model.

Light vs. depth profiles. To obtain a numerical representation of the light field throughout the water column bin averaged CTD light profiles (0.5 m intervals) was fit (SAAM II, 1994) to an empirical sum of exponentials equation of the form:

$$I_Z = A_1 e^{-a_1 Z} + A_2 e^{-a_2 Z}$$

which is an expansion of the standard irradiance vs. depth equation:

$$I_Z = I_0 e^{-kZ}$$

where:

I_Z = light irradiance at depth Z
I_0 = incident irradiance (Z=0)
k = extinction coefficient
A_1, A_2 = factors relating to incident irradiance ($I_0 = A_1+A_2$)
a_1, a_2 = coefficients relating to the extinction coefficient ($k = a_1+a_2$)

The expanded equation was used as pigment absorption and other factors usually resulted in significant deviation from the idealized standard irradiance vs. depth equation. The best fit profiles were used to compute percent light attenuation for each of the sampling depths.

Daily incident light field. During normal CTD hydrocasts the incident light field was routinely measured via a deck light sensor at high temporal resolution. The average incident light intensity was determined for each of the CTD casts to provide, over the course of the photoperiod (12 hr period centered upon solar noon), a reasonably well resolved irradiance time series consisting of 12-17 data points. A 48 point time series (every 15 min.) of incident was obtained from these data by linear interpolation.

Calculation of daily primary production. Given the best fit parameters (Pmax", α", β") of the P-I curves obtained for each of the 5 sampling depths, percent *in situ* light attenuation at each depth determined from the sum of exponential fits of the *in situ* light field, and the photoperiod incident light (I_0) time series it was possible to compute daily volumetric production for each depth. To do this at a given depth, hourly production was determined for the *in situ* light intensity computed for each 15 min. interval of the photoperiod, using the appropriate P-I parameters and *in situ* irradiance computed from the percent attenuation and incident irradiance. Daily production ($\mu gC\ l^{-1}d^{-1}$) was obtained by integration of the determined activity throughout the 12 hr photoperiod. An advantage of this approach is that seasonal changes in photoperiod length are automatically incorporated into the integral computation. For example, during winter months computed early morning and late afternoon production contributes minimally to whole day production, whereas during summer months the relative contribution during these hours is more significant. The investigator does not have to decide which factor to employ when converting hourly production to daily production. The primary assumption for the approach is that the P-I relationship obtained at the time of sample procurement (towards the middle of the photoperiod) is representative of the majority of production occurring during the photoperiod.

Calculation of daily areal production. Areal production ($mgC\ m^{-2}d^{-1}$) was obtained by trapezoidal integration of daily volumetric production vs. depth from the sea surface down to the 0.5% light level. The P-I factors from the uppermost sampling depth (approximately 1.2 - 2.7 m, depending upon weather state) were used to compute the contribution of the portion of the water column between the sea surface interface and uppermost sampling depth to areal production (rather than to assume that the activity in the uppermost sample is representative of that section of the water column, which is not always the case).

Calculation of chlorophyll-specific parameters. Chlorophyll-specific measures of the various parameters were determined by dividing by the appropriate chlorophyll term obtained from independent measurements:

$$\alpha = \frac{\alpha"}{[chla]}$$

$$P\max = \frac{P\max"}{[chla]}$$

where:

α = chlorophyll-a-specific initial slope of light-dependent production $[(gC(gchla)^{-1}h^{-1}(\mu Em^{-2}s^{-1})^{-1}]$

Pmax = light saturated chlorophyll-specific production $[gC(gchla)^{-1}h^{-1}]$

APPENDIX B

W9501 Station F23

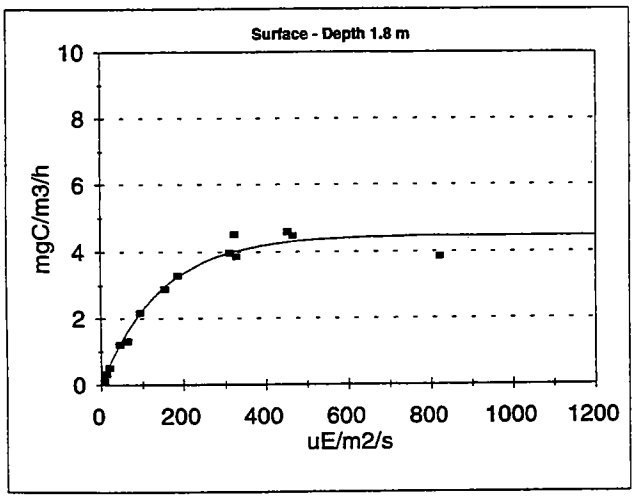

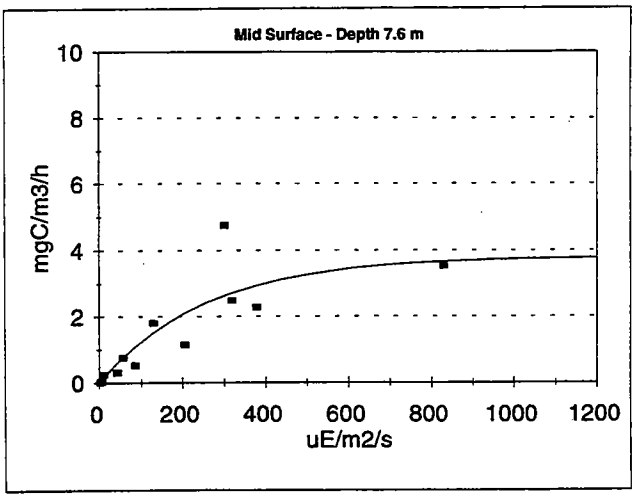

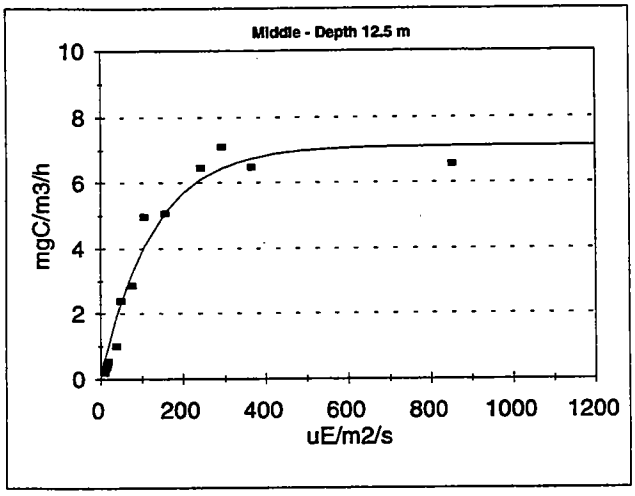

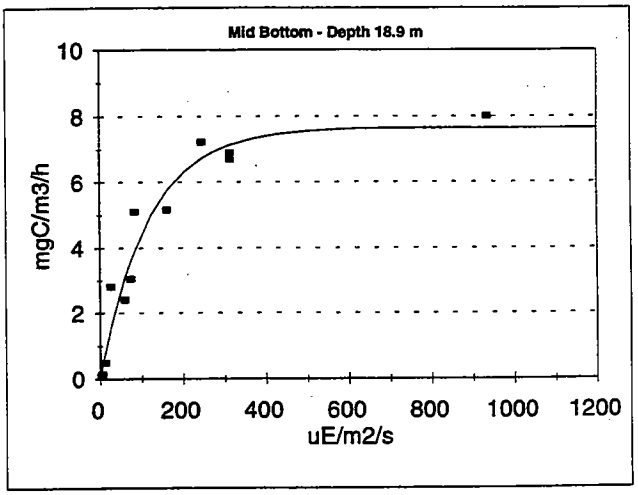

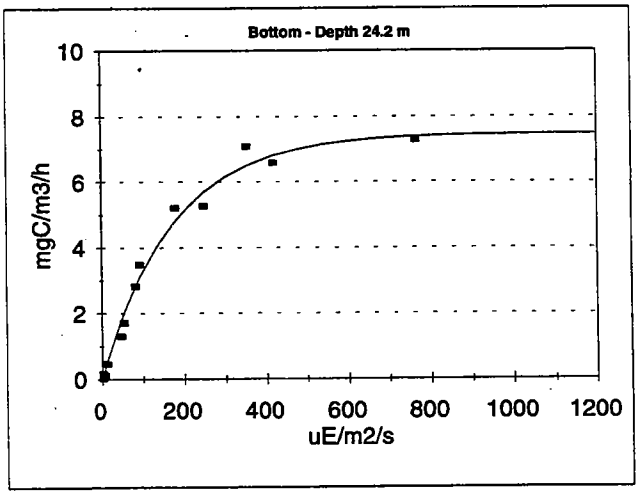

W9501 Station N04

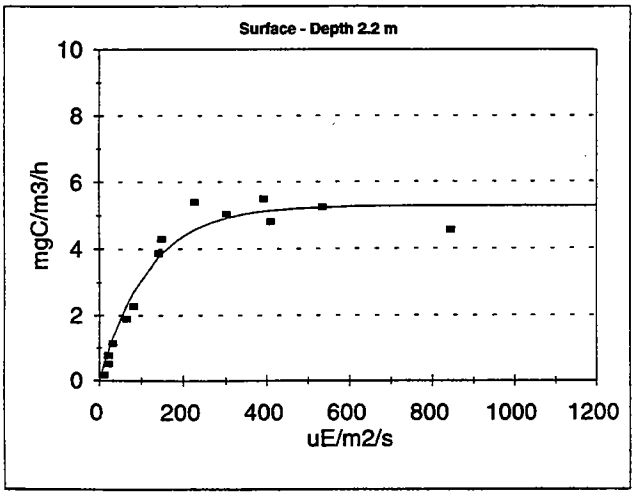

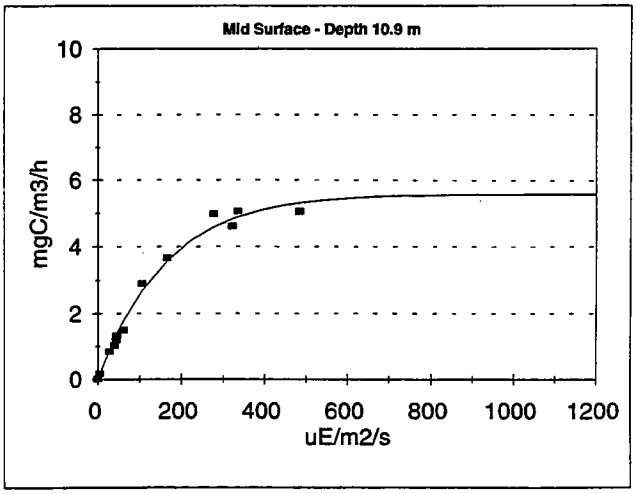

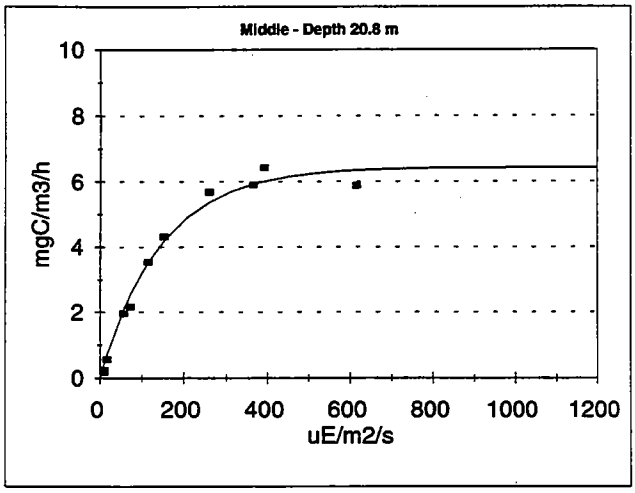

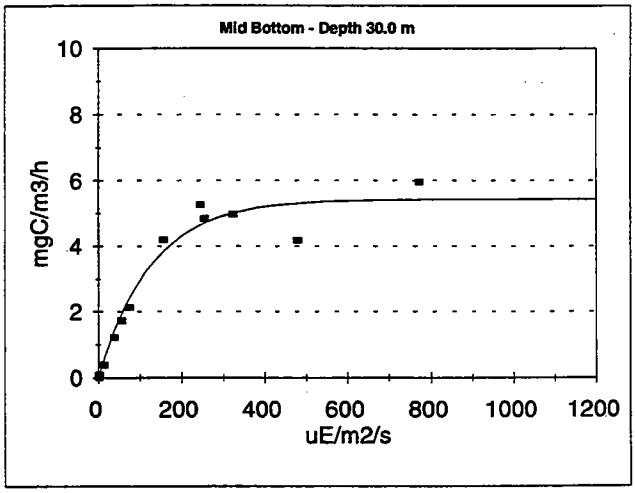

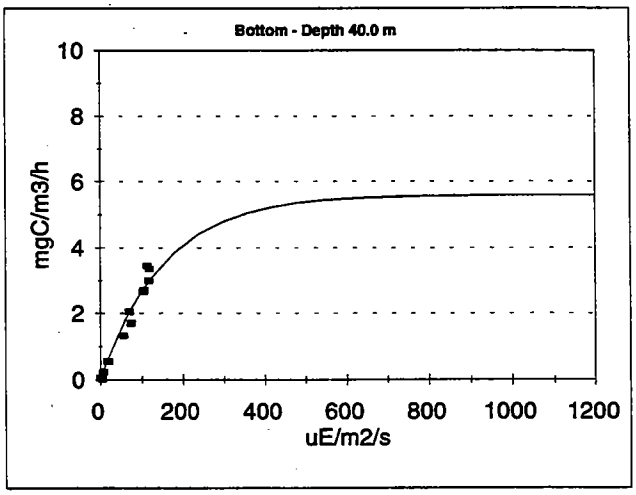

W9501 Station N07

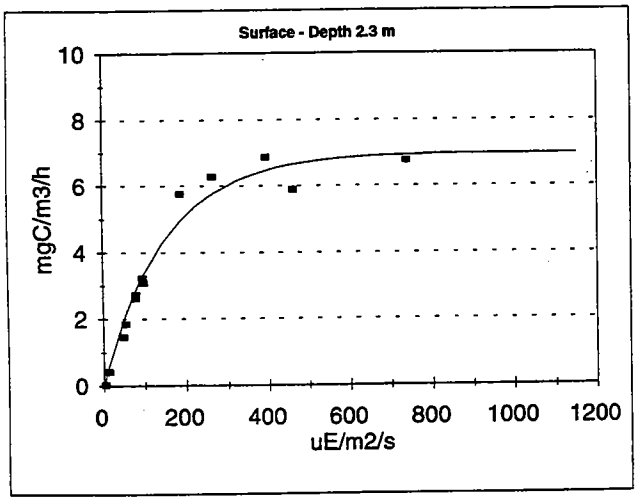

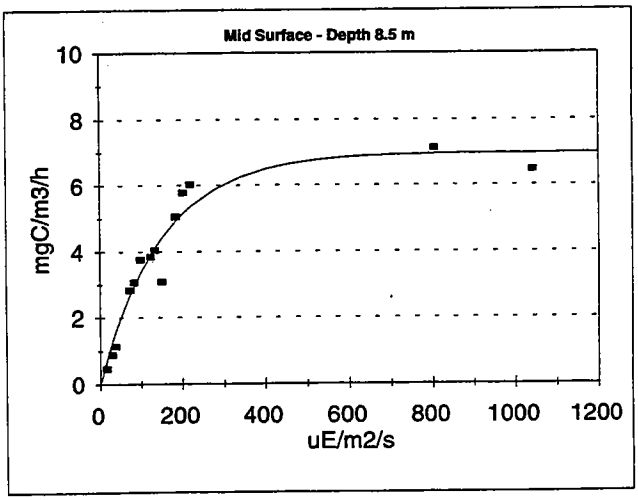

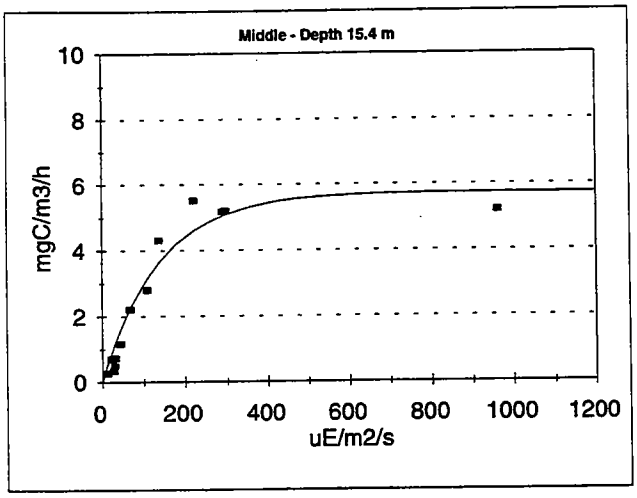

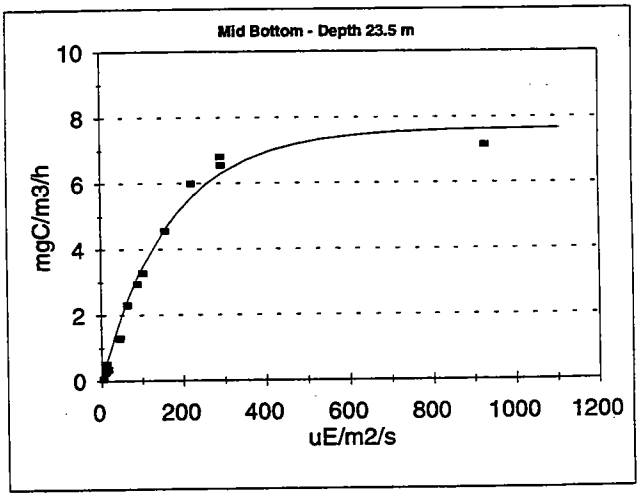

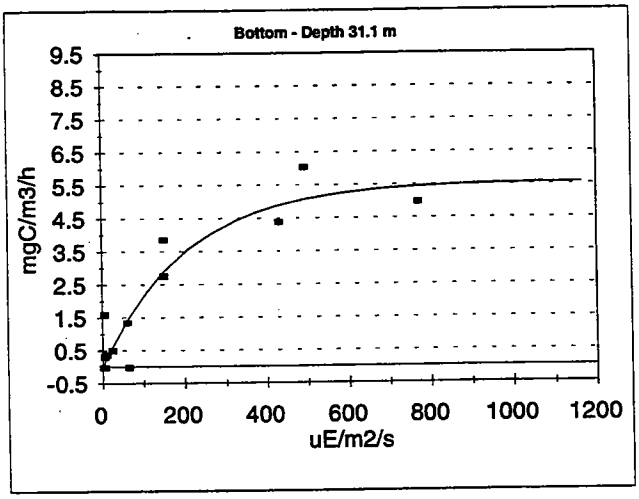

W9501 Station N16

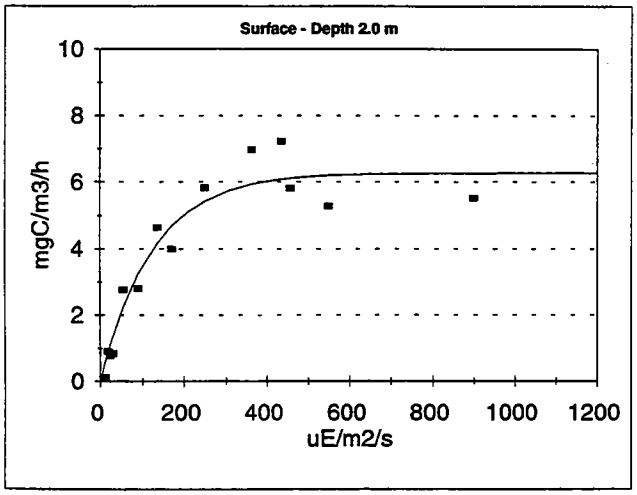

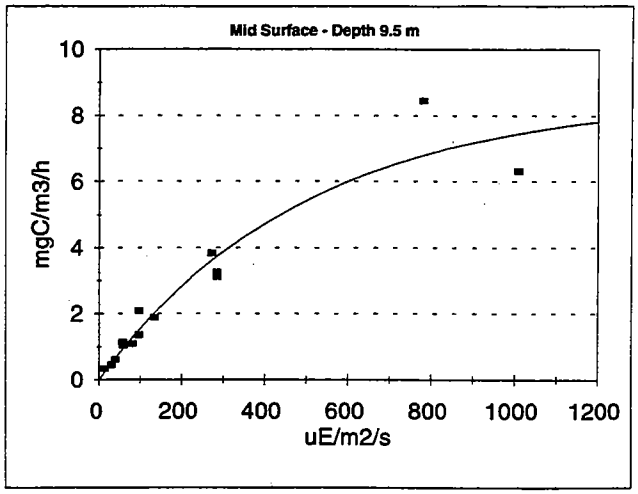

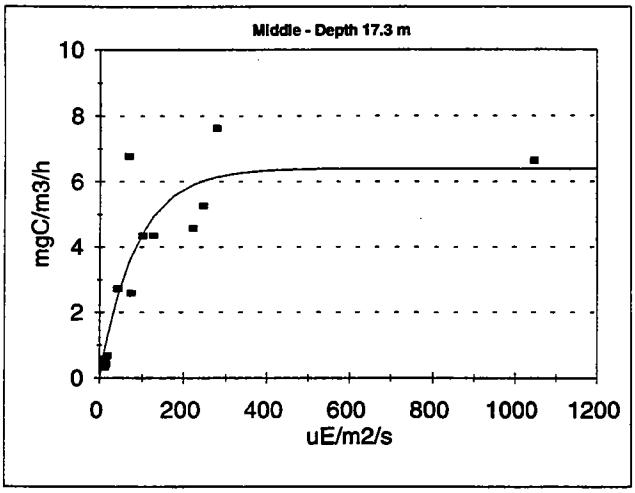

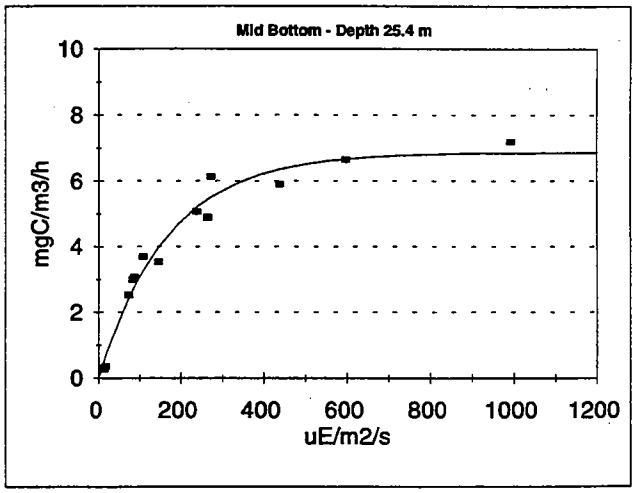

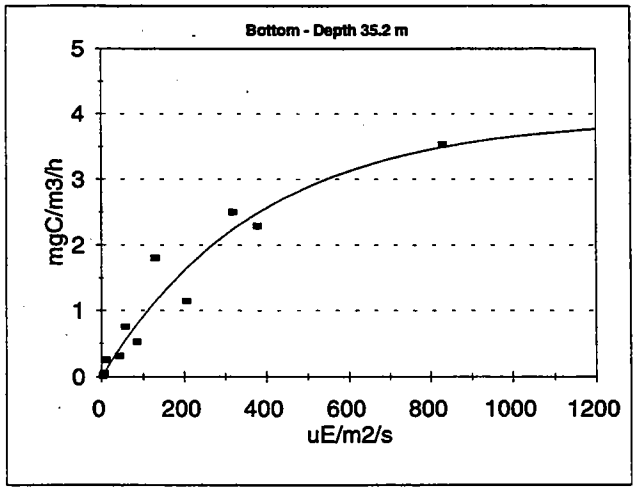

W9502 Station F23

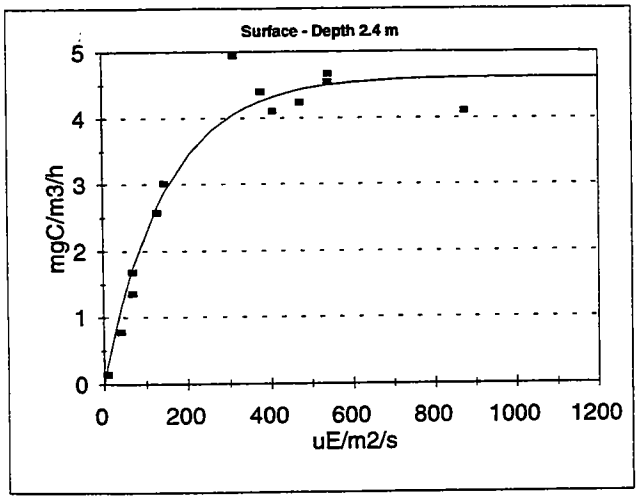

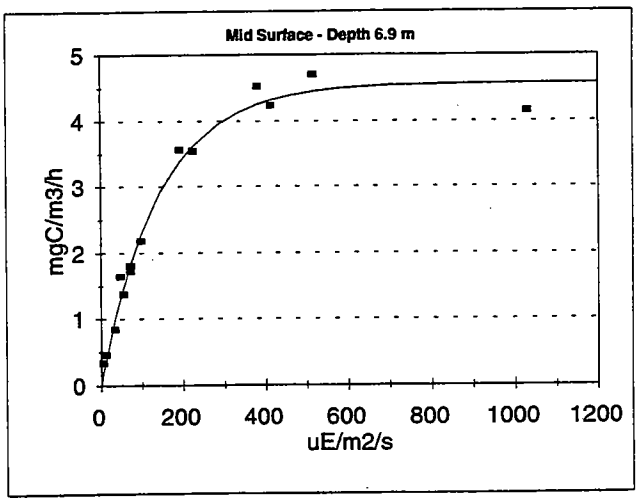

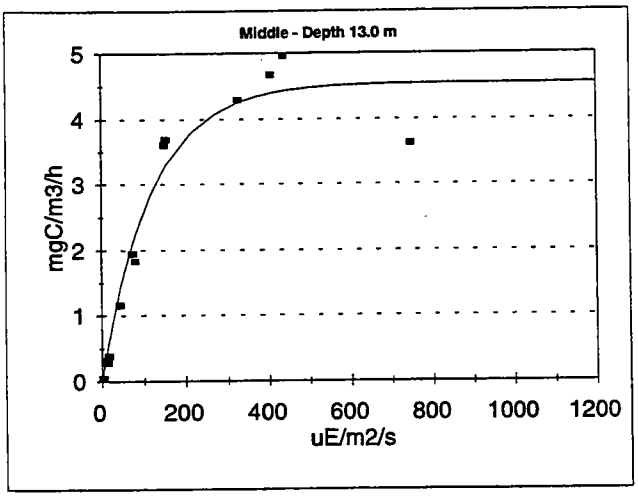

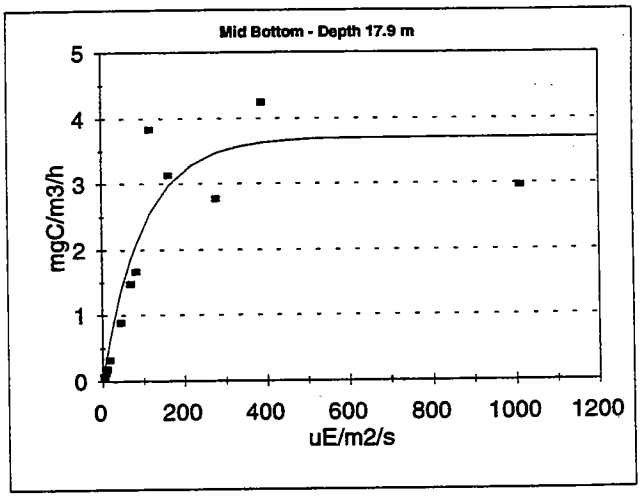

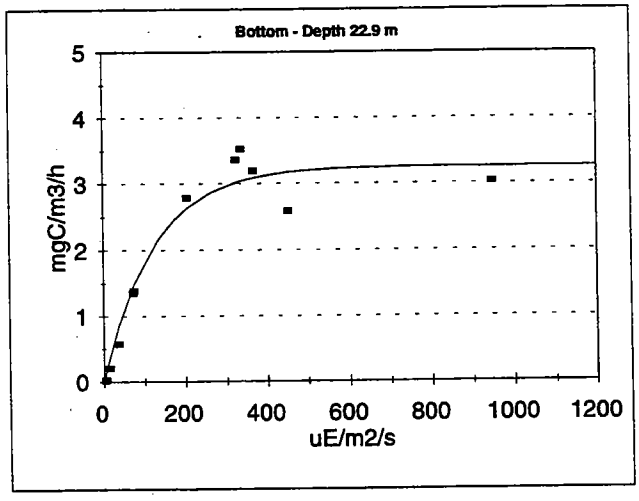

W9502 Station N04

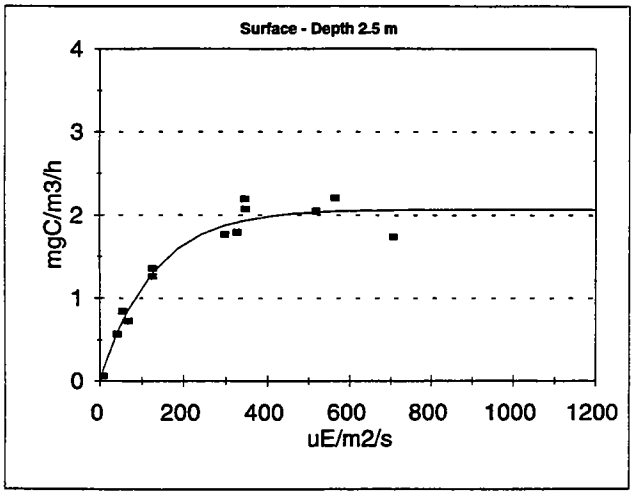

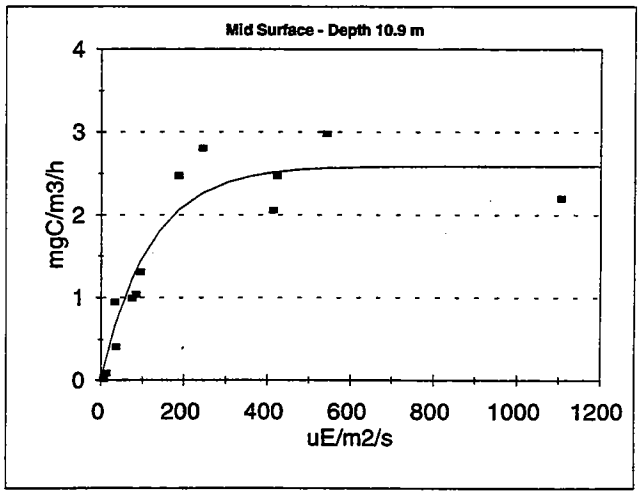

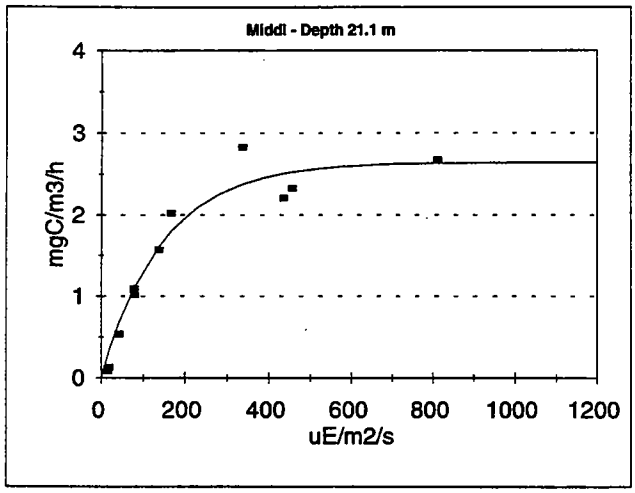

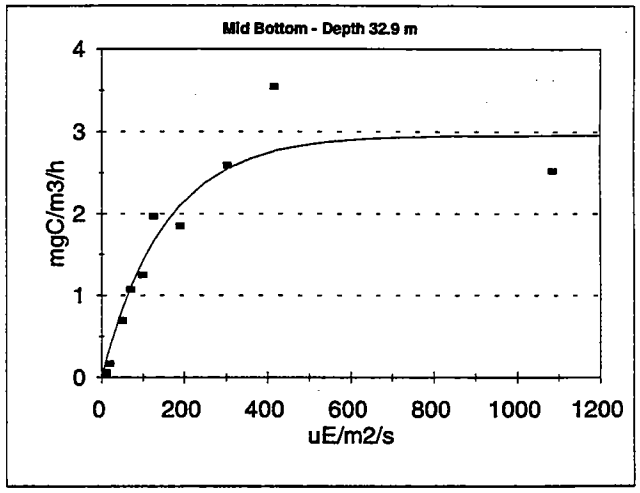

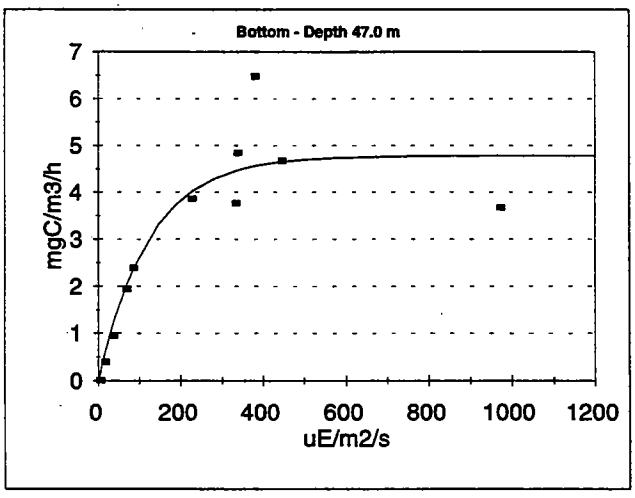

W9502 Station N07

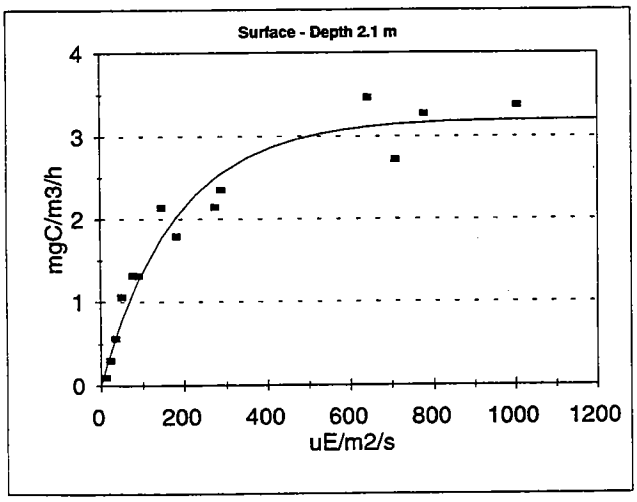

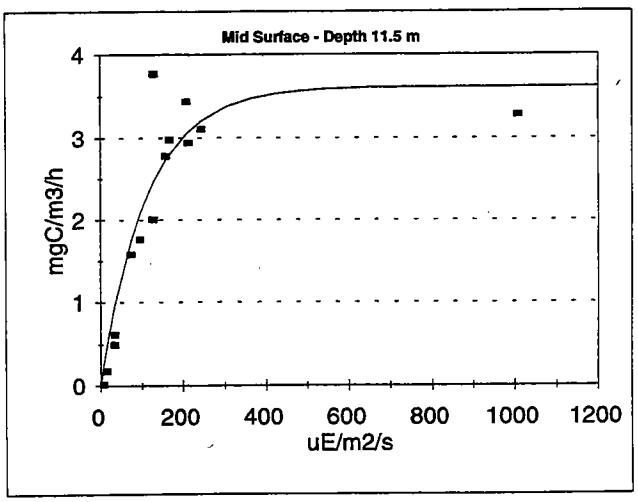

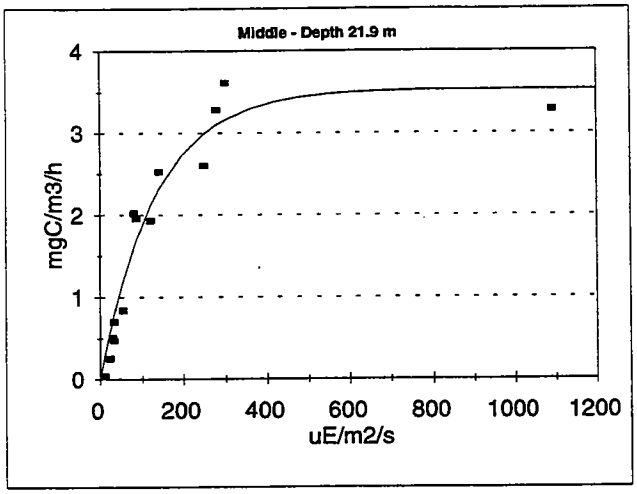

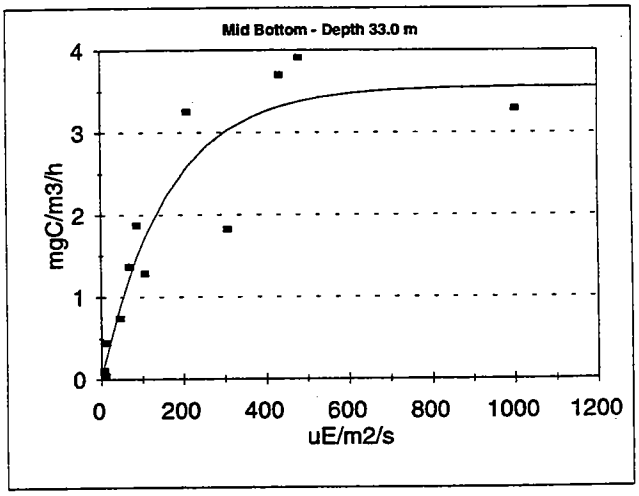

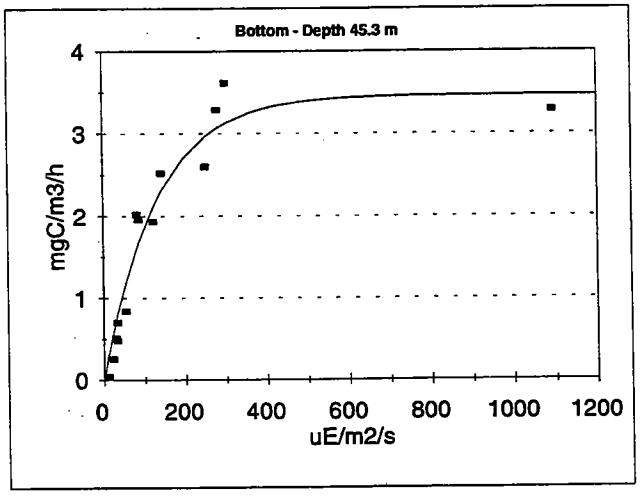

W9502 Station N16

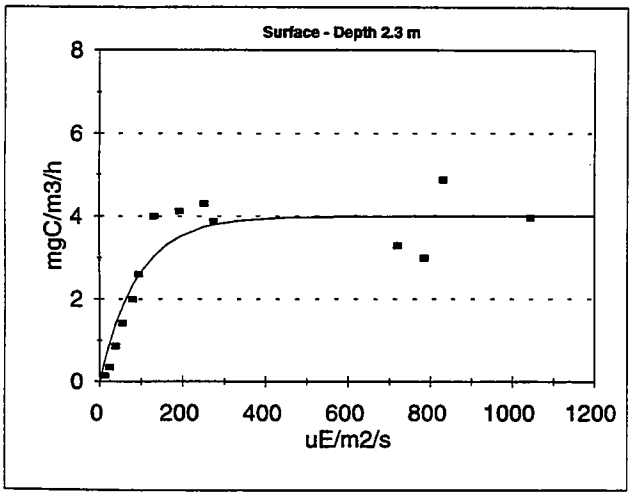

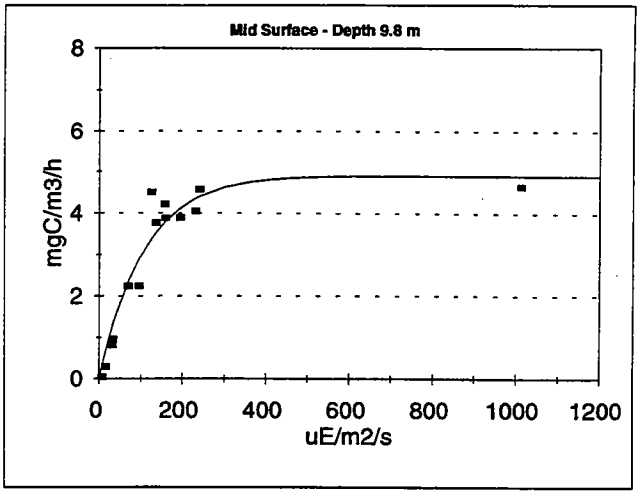

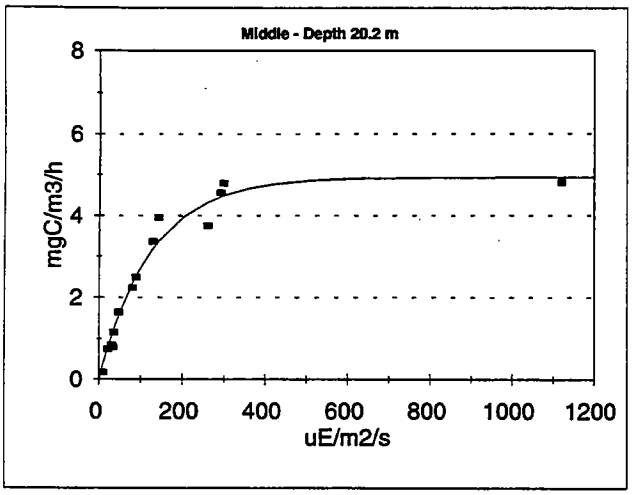

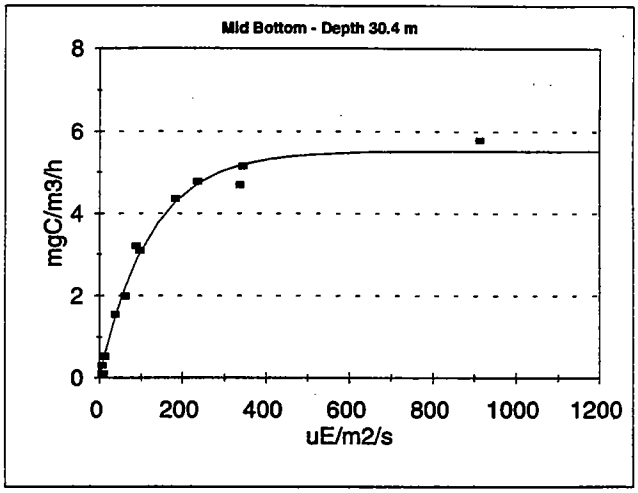

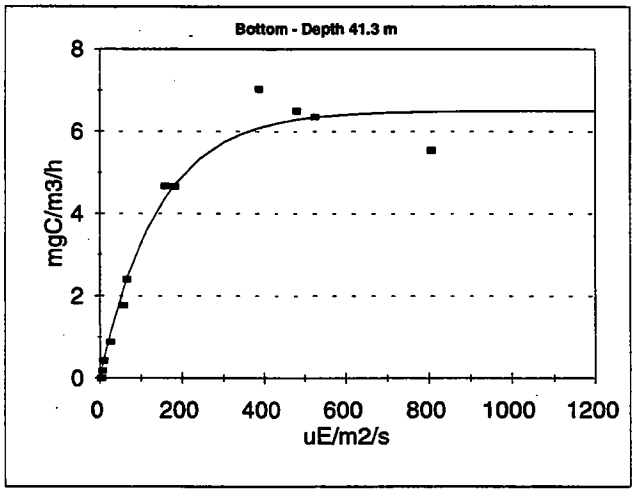

W9503 Station N04

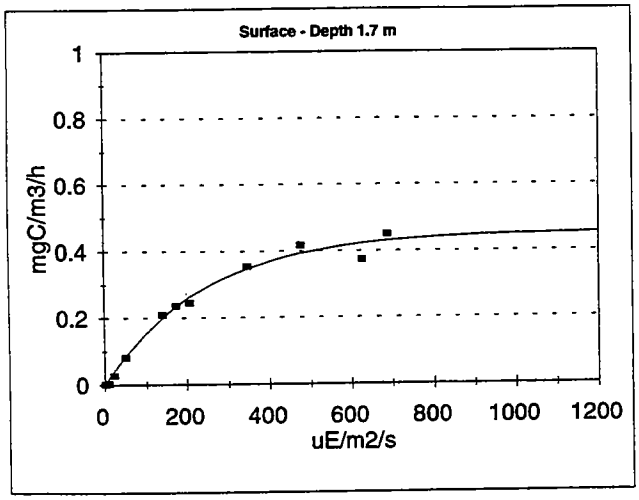

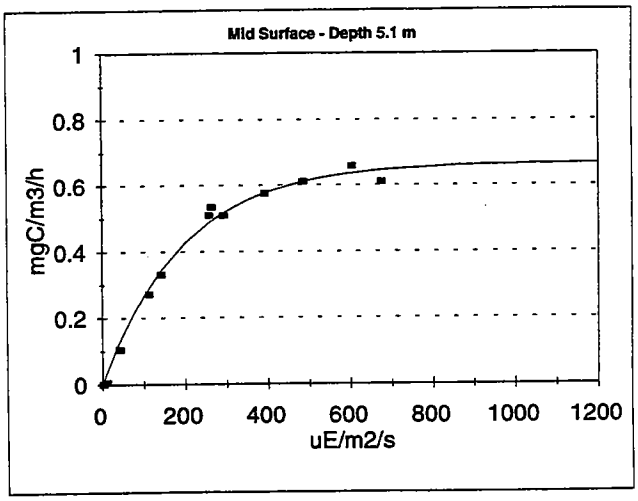

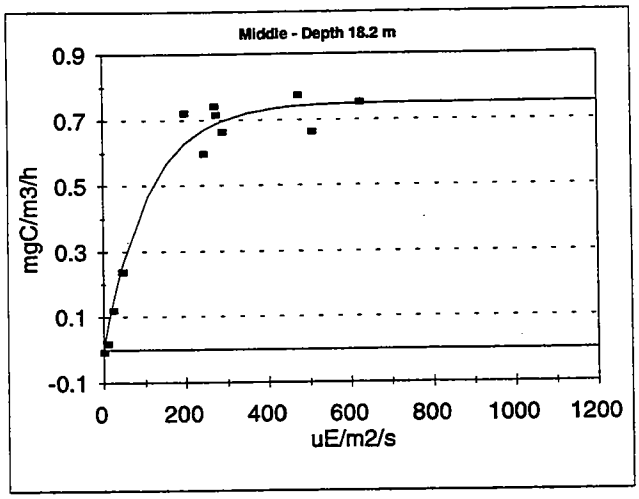

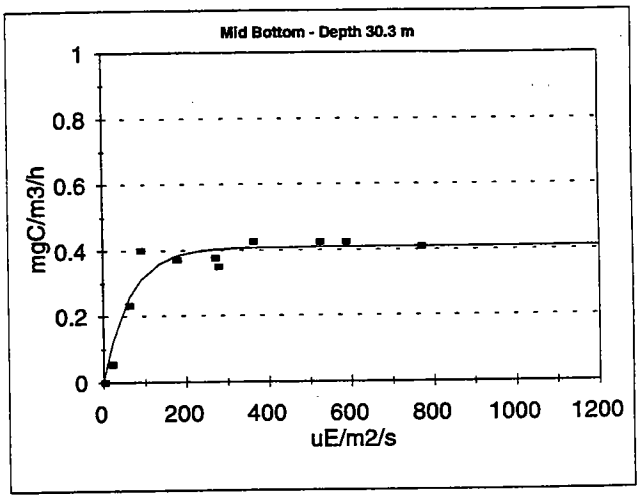

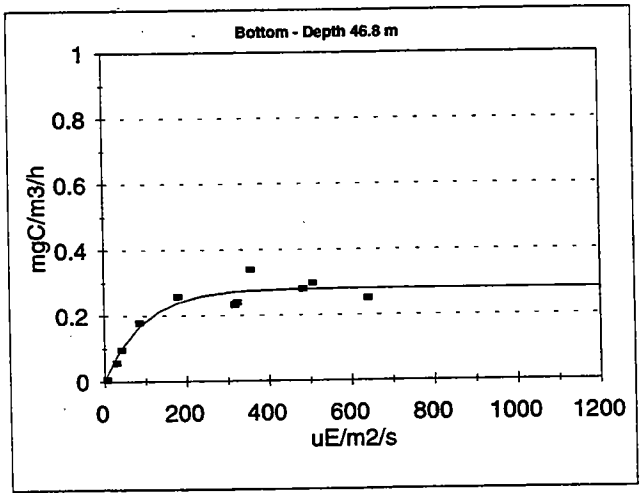

W9503 Station N16

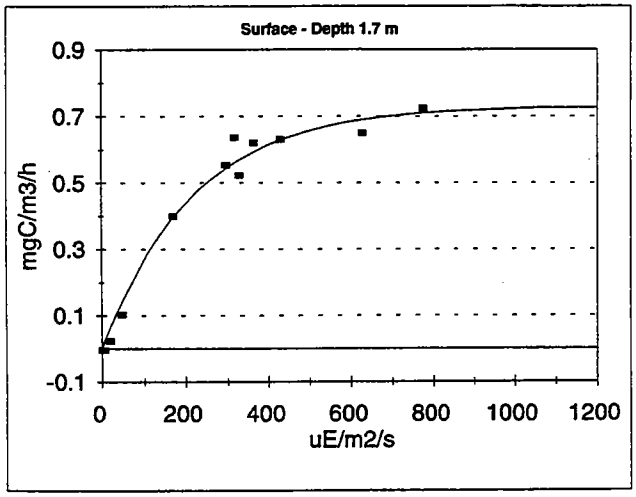

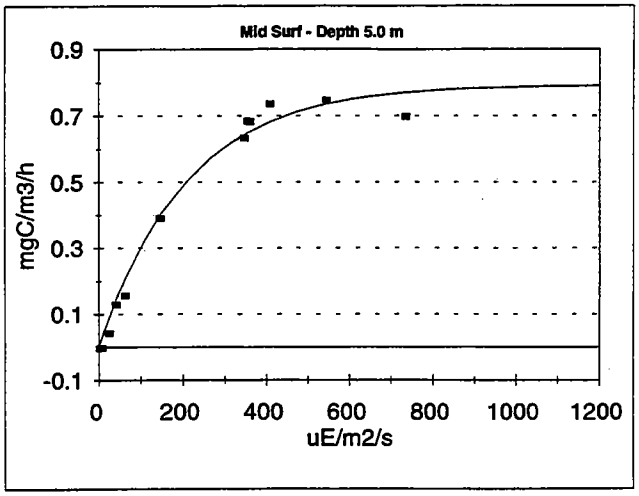

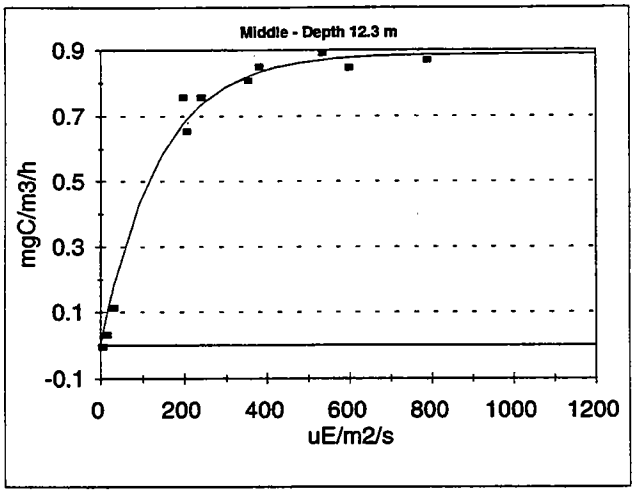

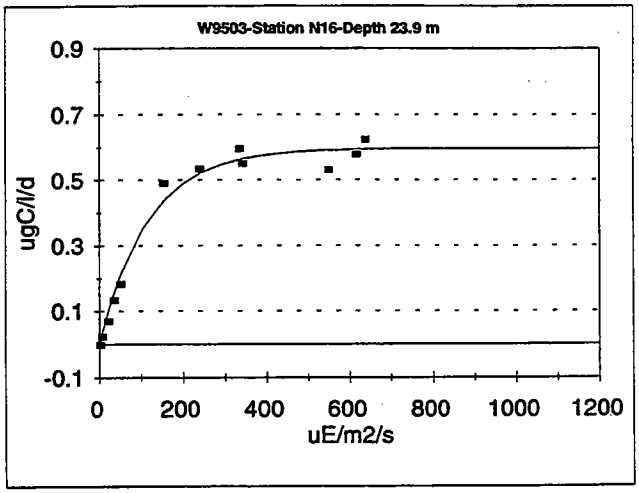

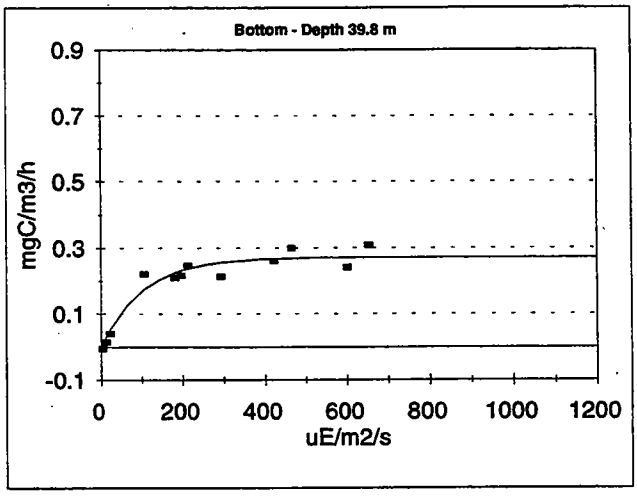

W9504 Station F23

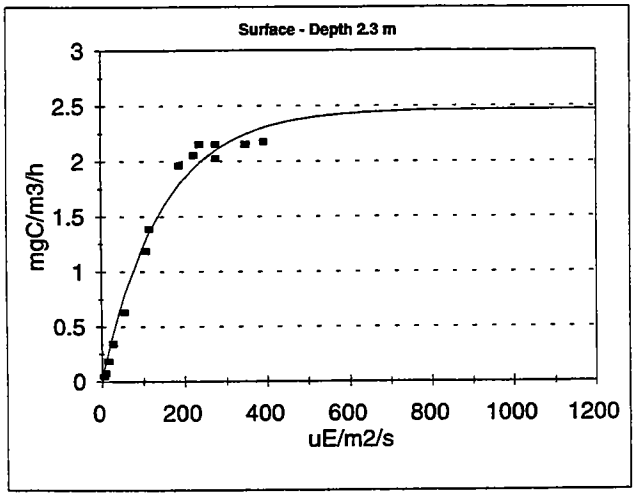

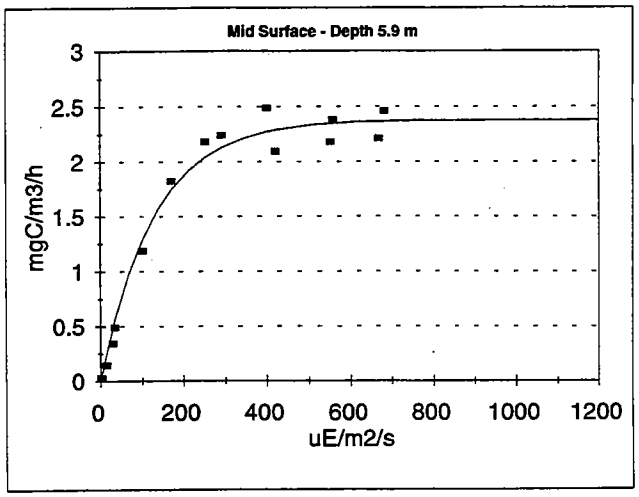

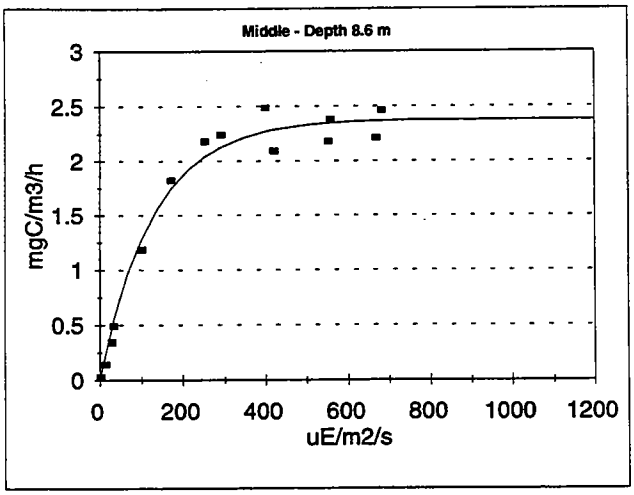

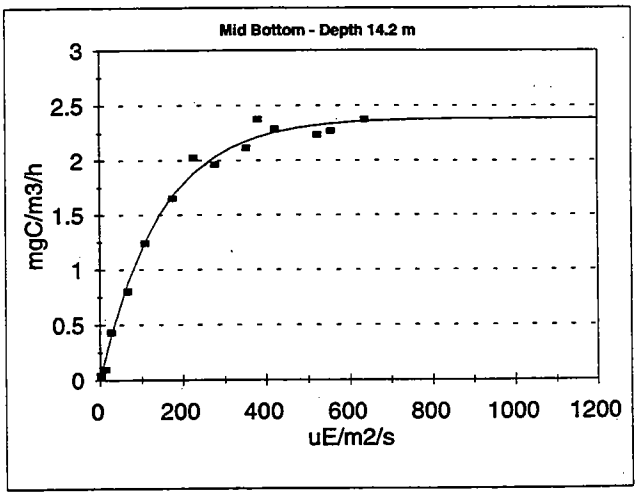

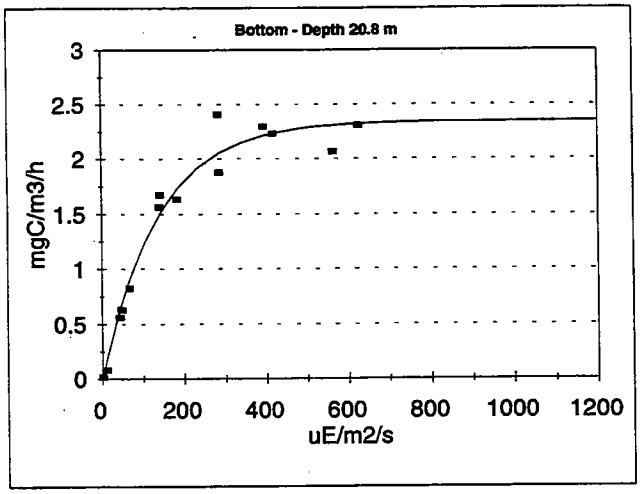

W9504 Station N04

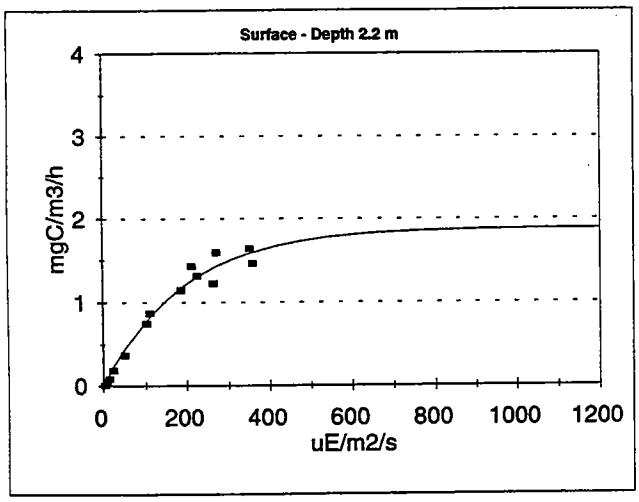

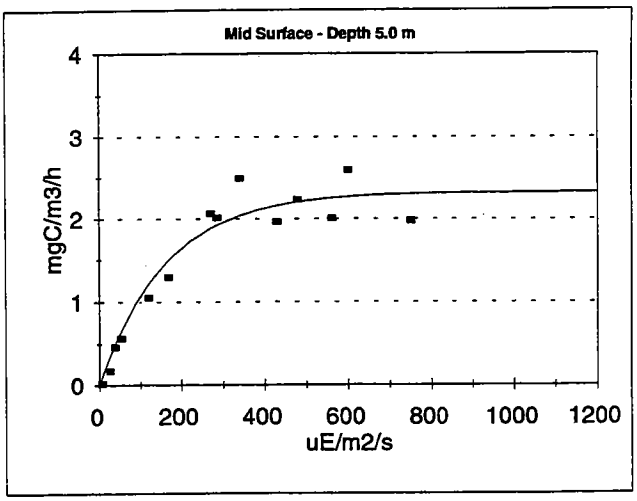

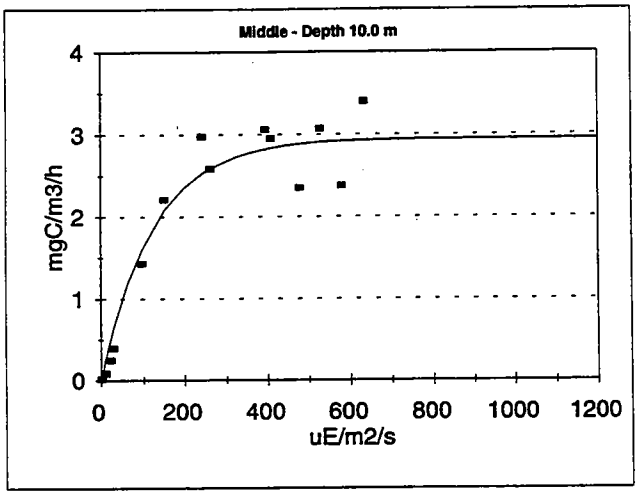

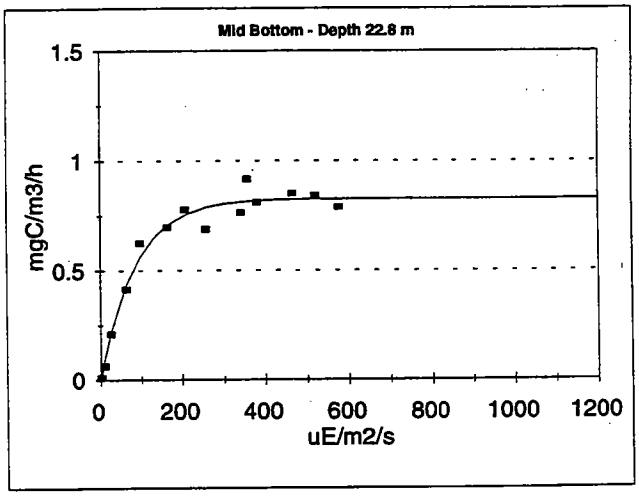

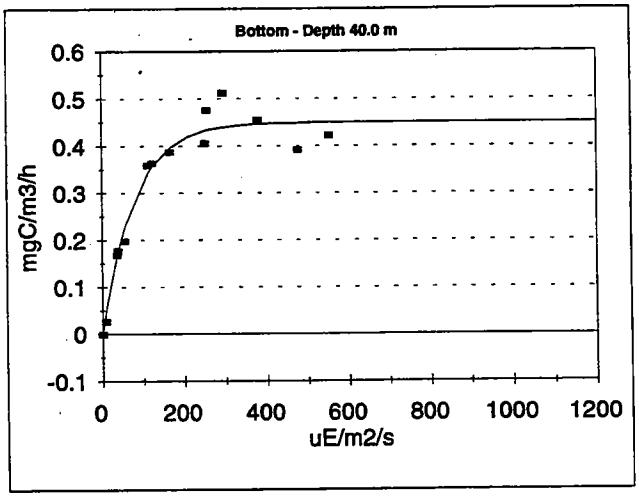

W9504 Station N07

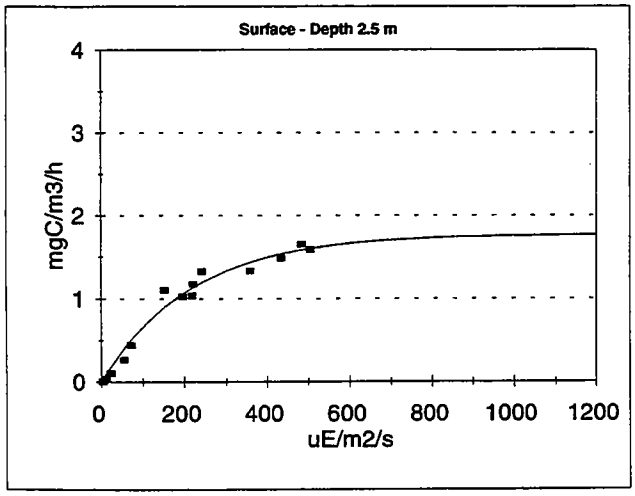

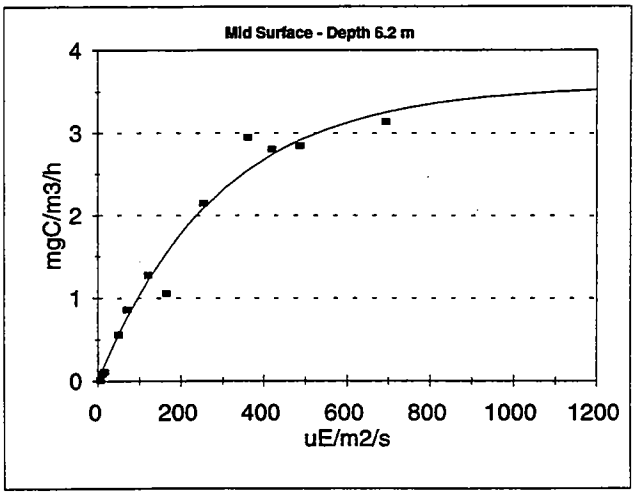

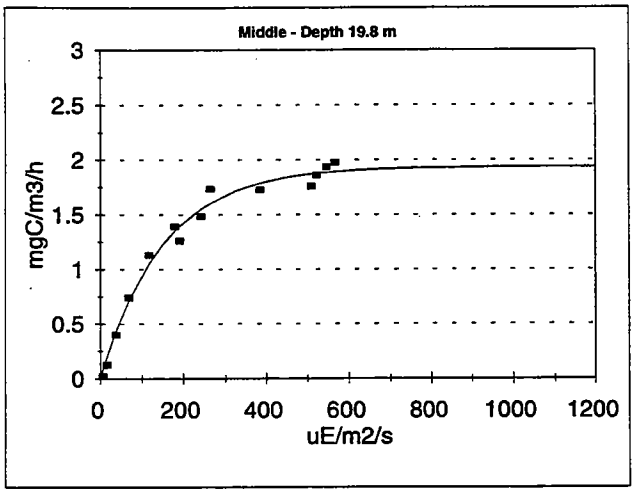

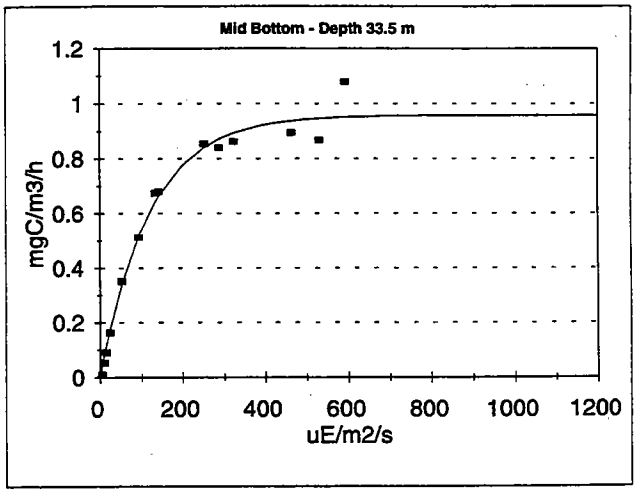

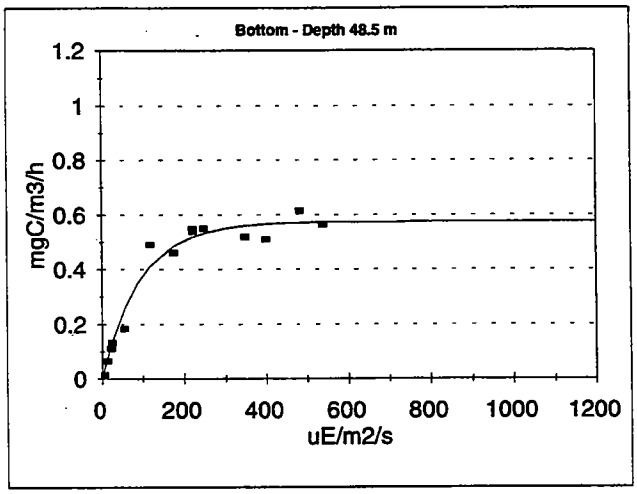

W9504 Station N16

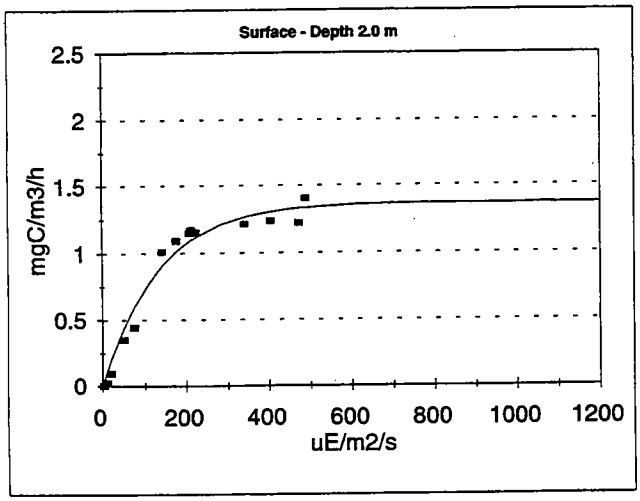

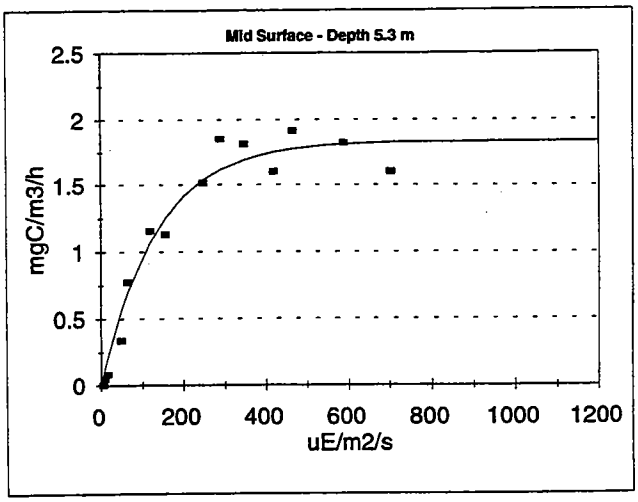

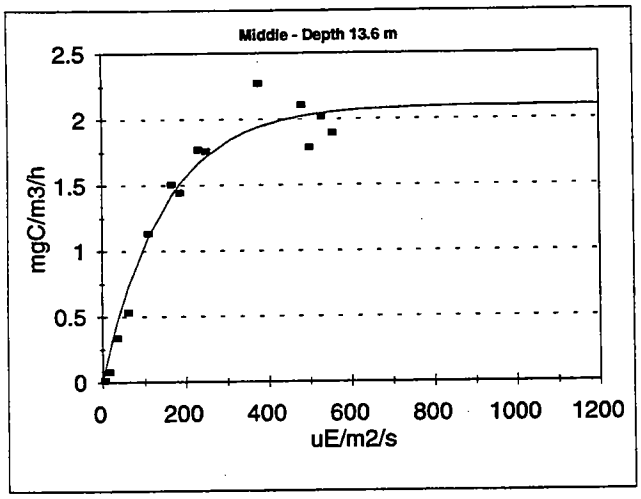

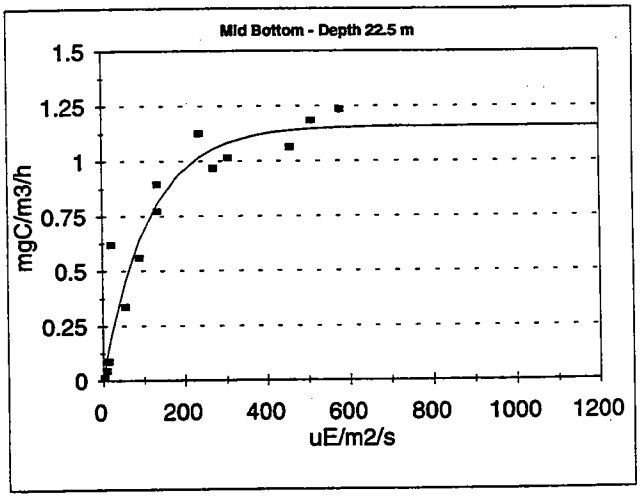

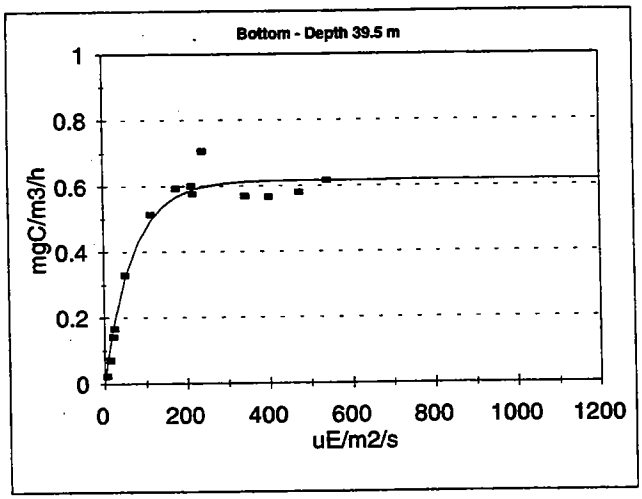

W9505 Station N04

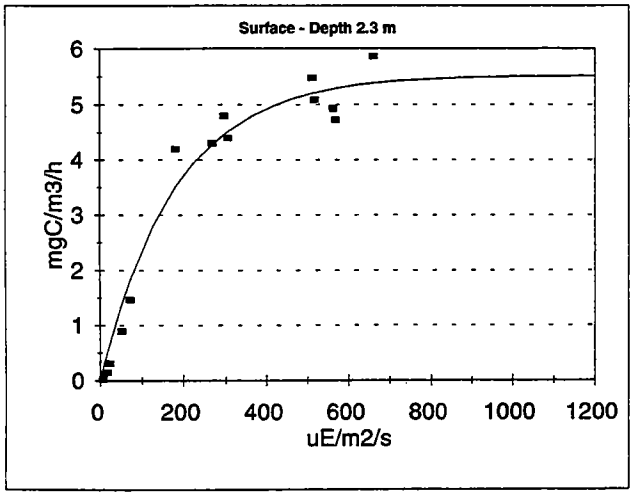

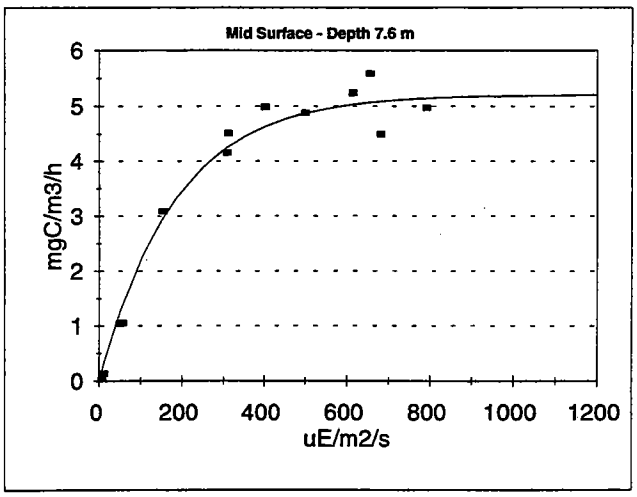

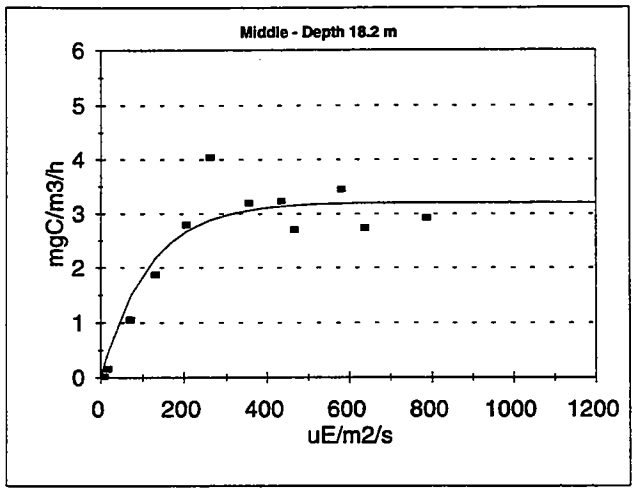

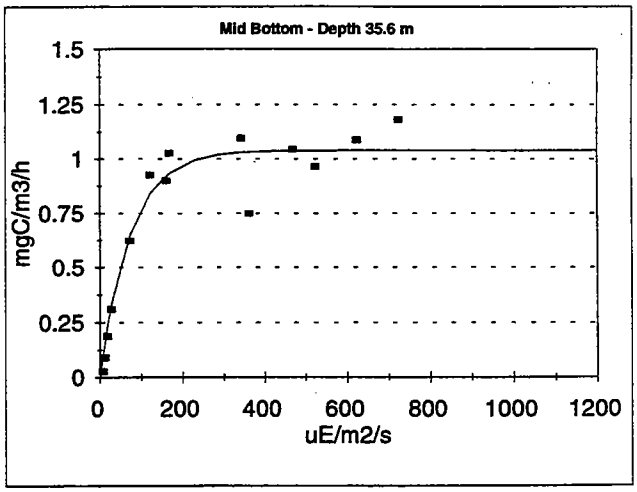

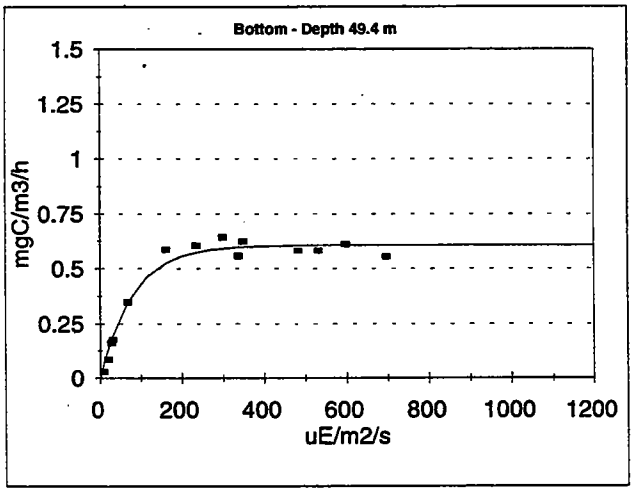

W9505 Station N16

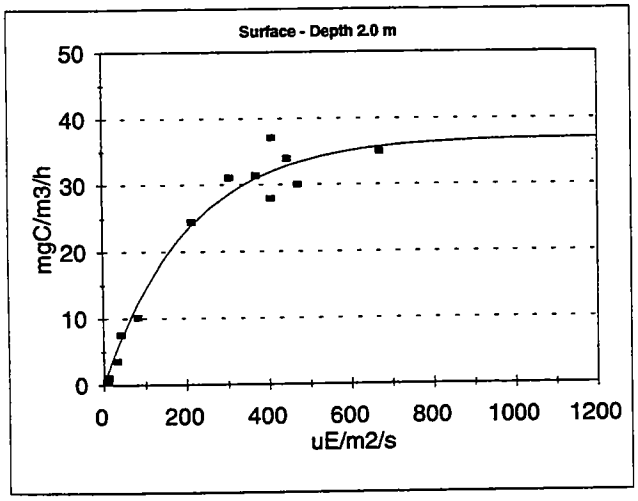

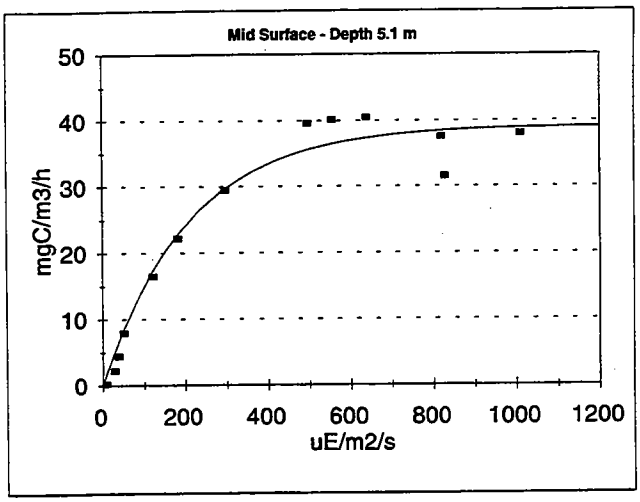

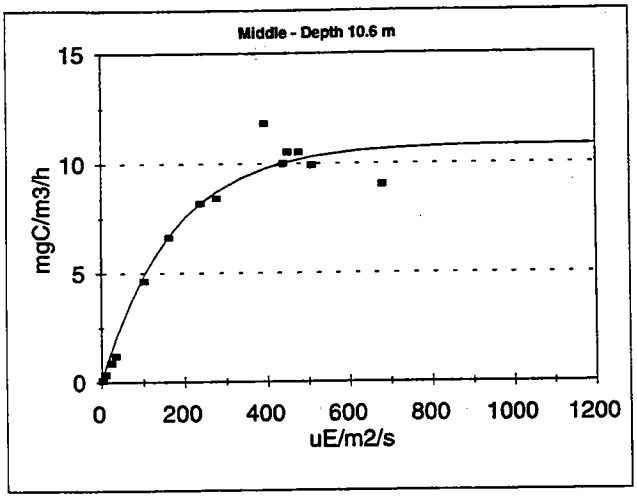

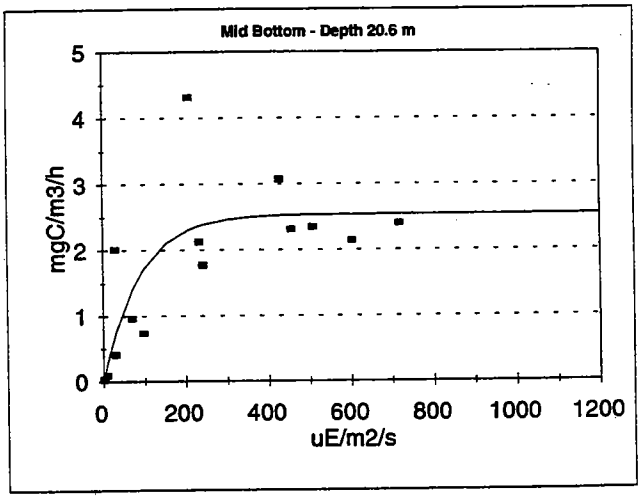

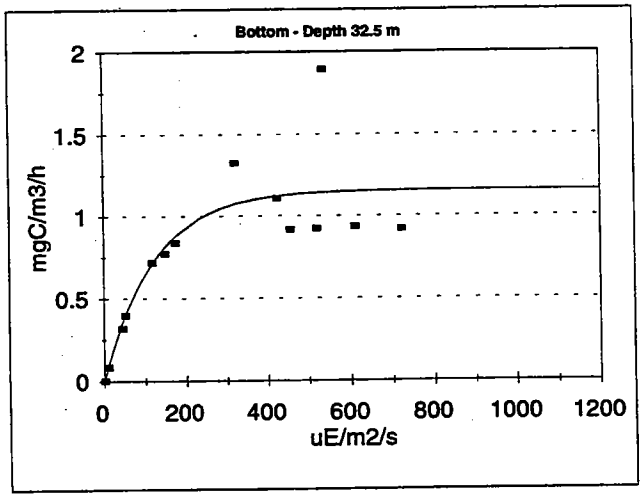

W9506 Station N04

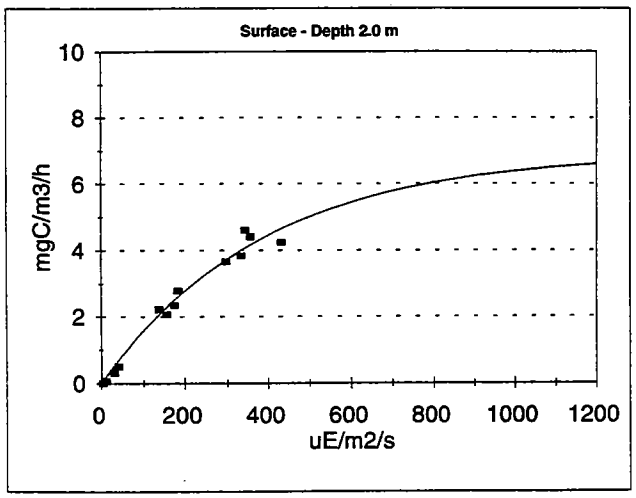

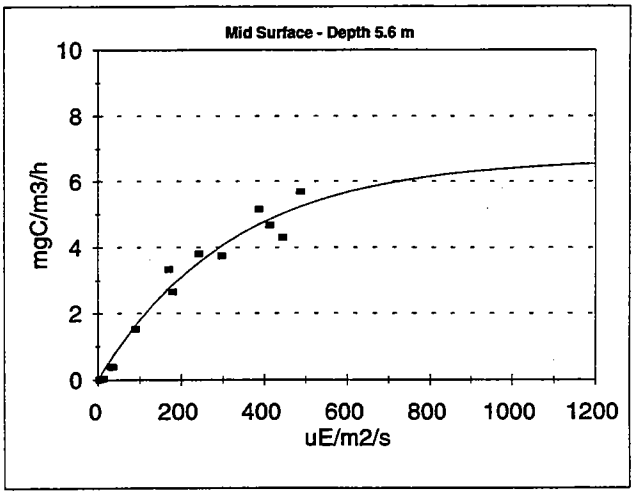

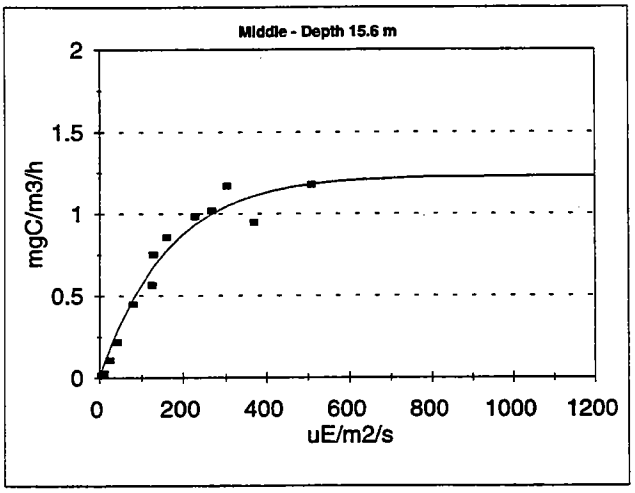

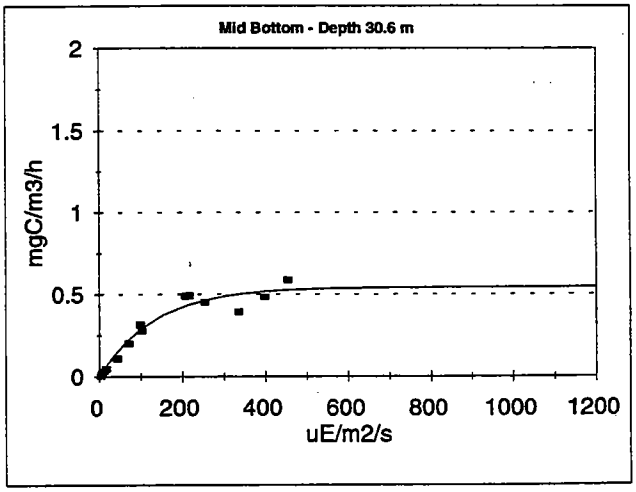

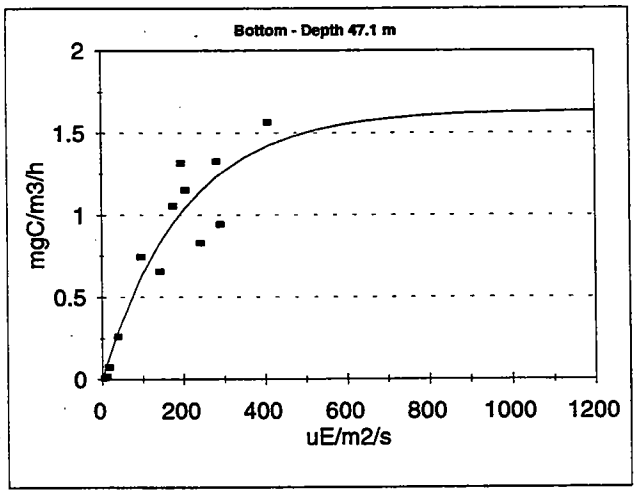

W9506 Station N16

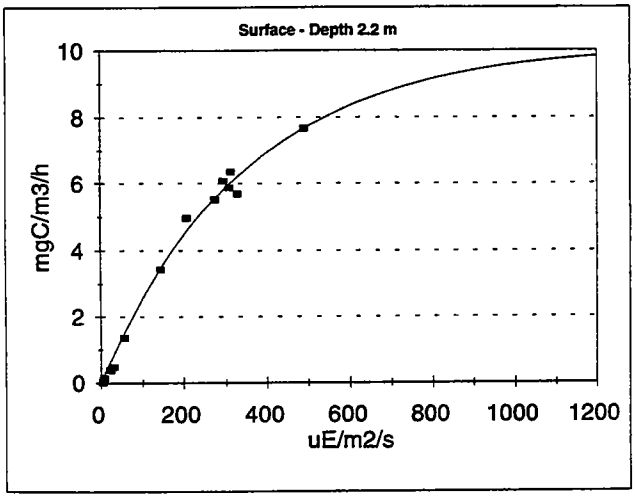

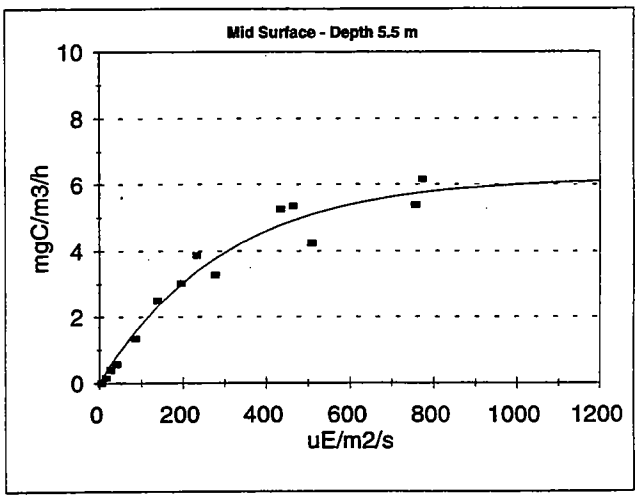

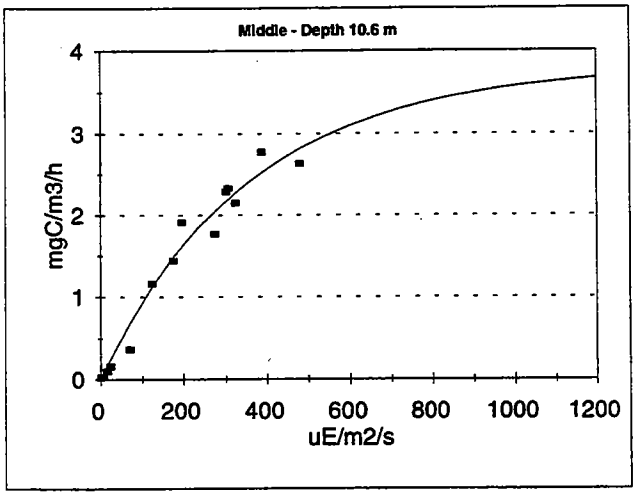

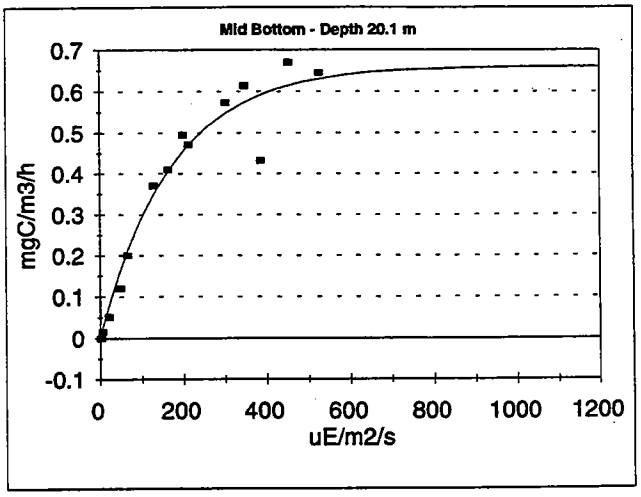

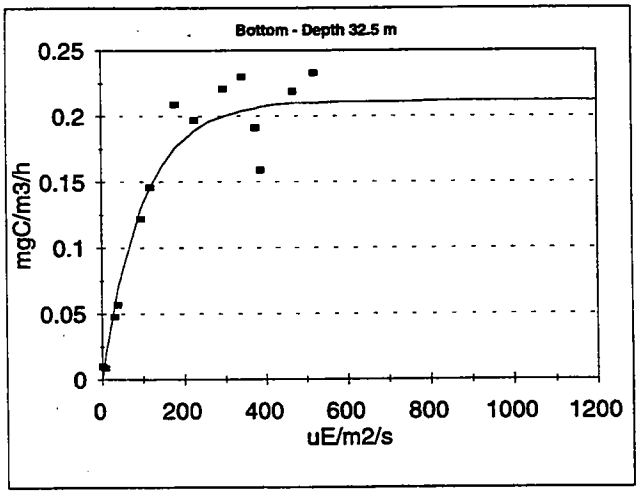

W9507 Station F23

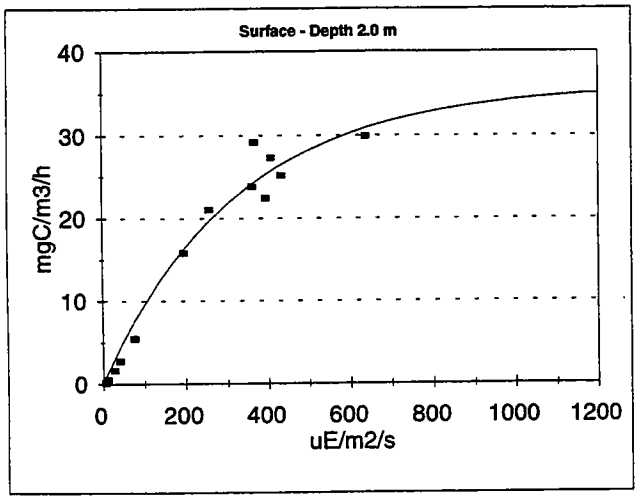

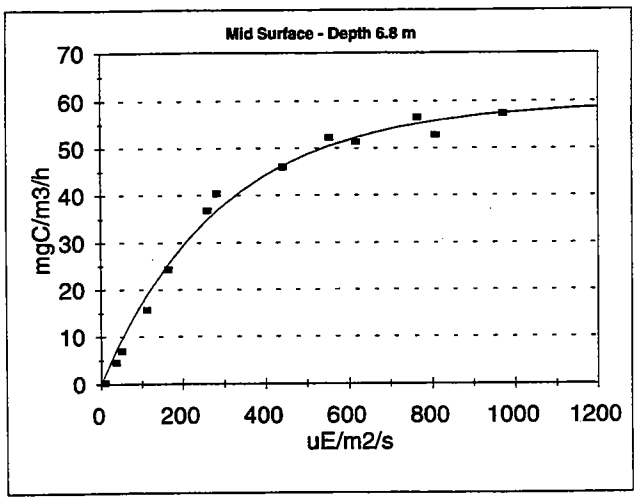

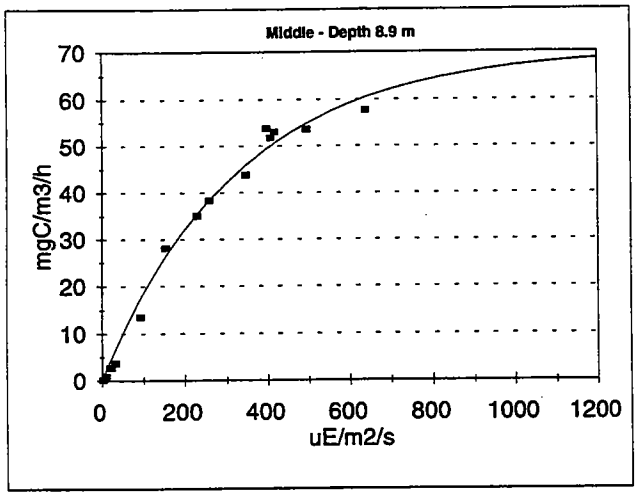

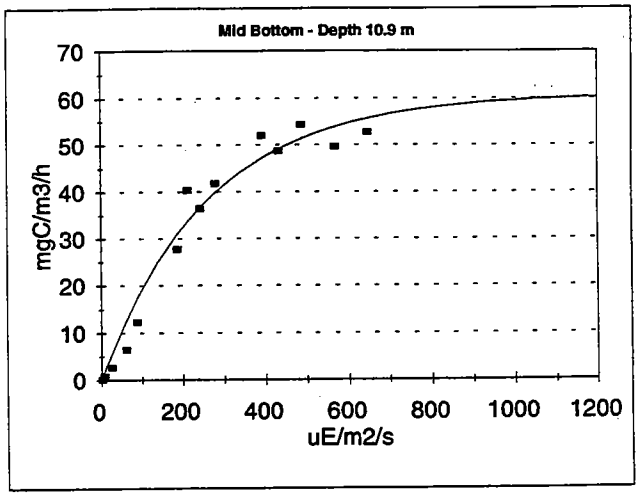

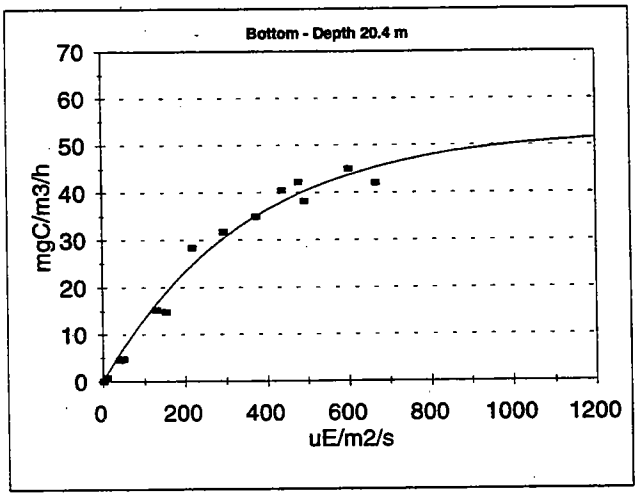

W9507 Station N04

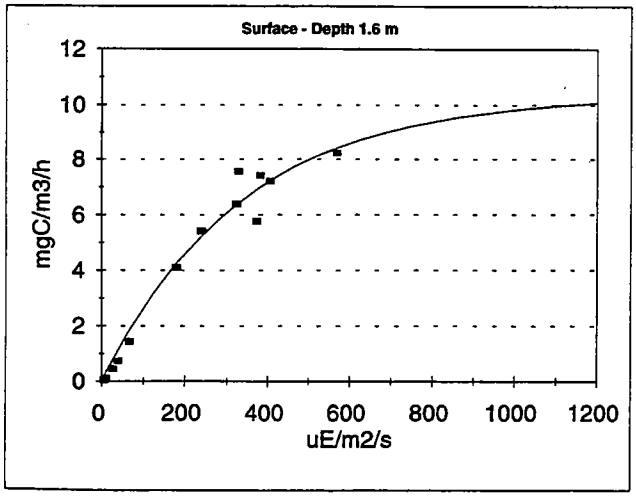

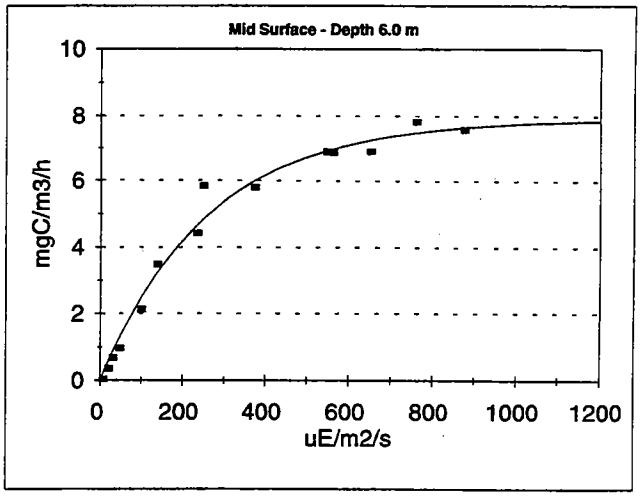

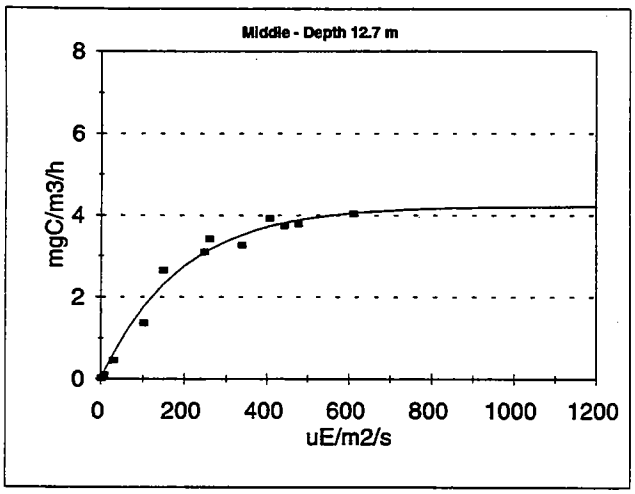

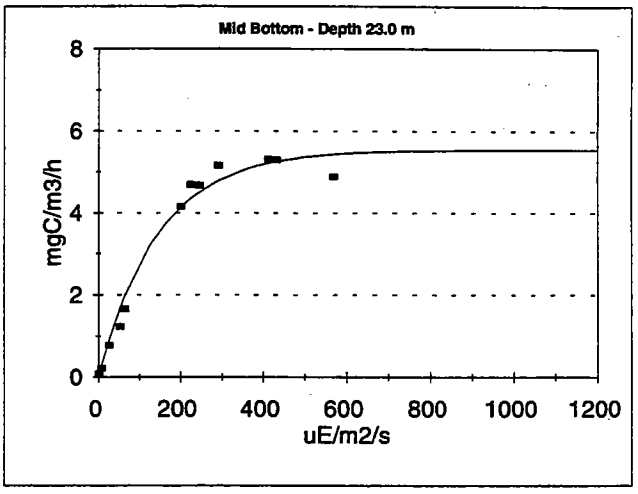

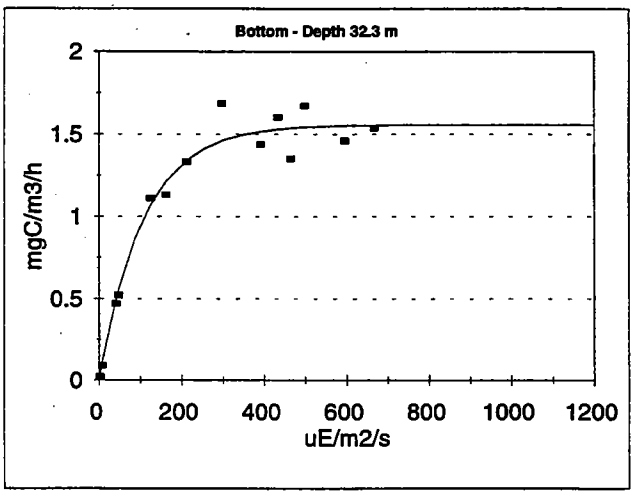

W9507 Station N07

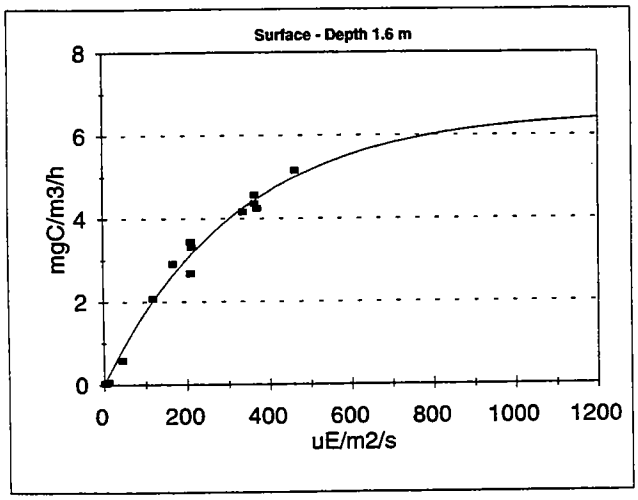

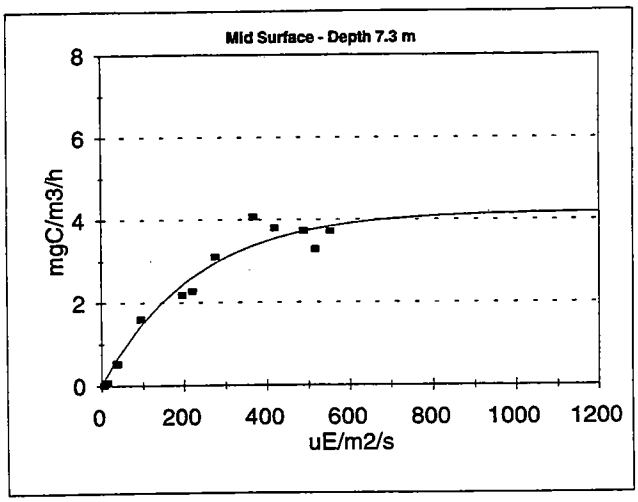

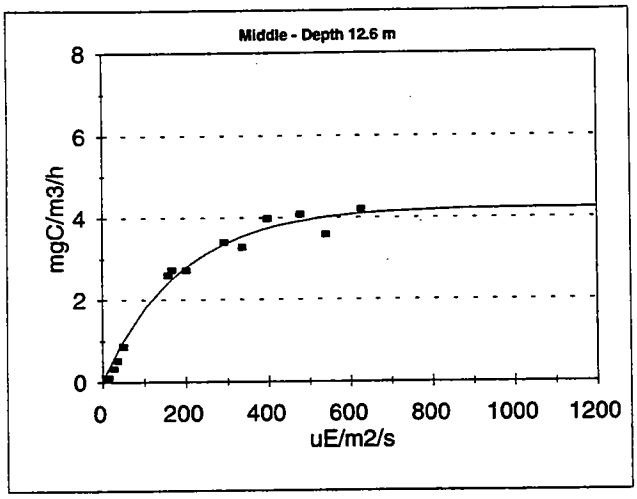

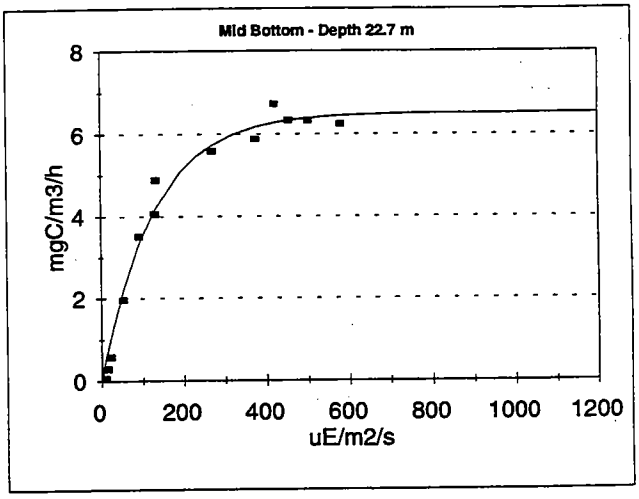

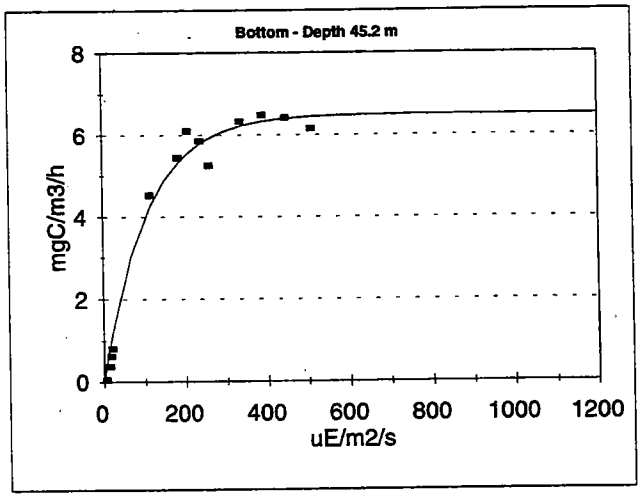

W9507 Station N16

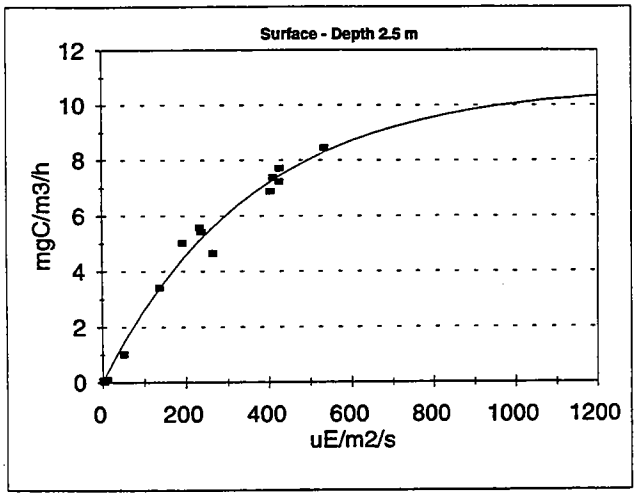

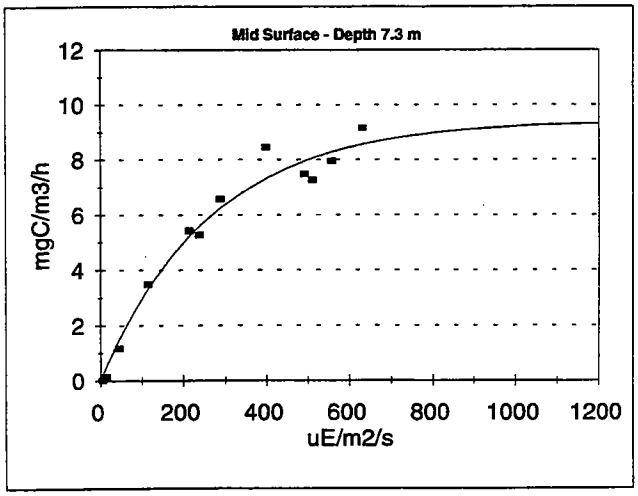

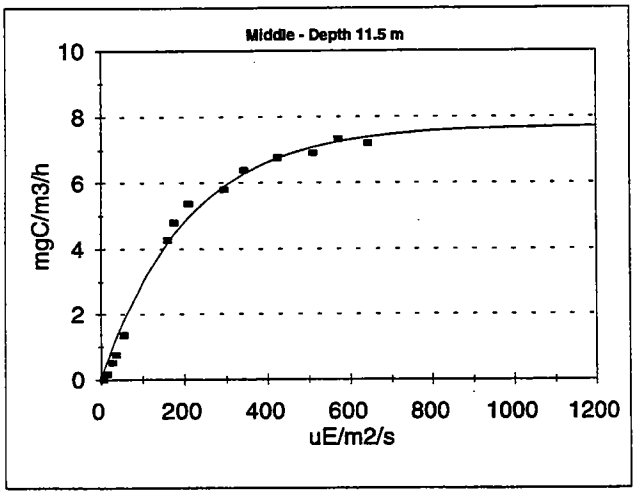

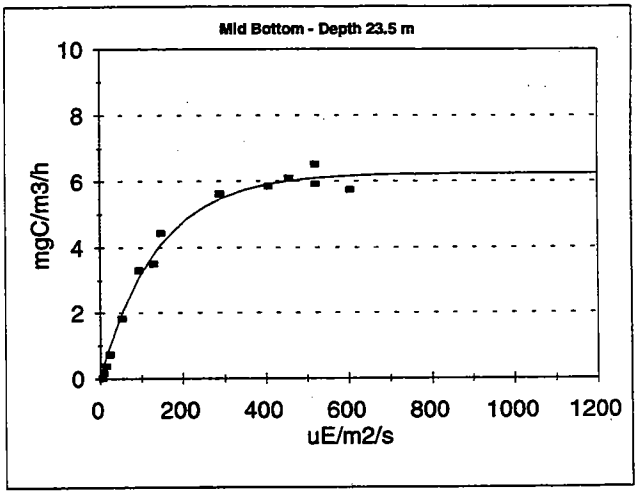

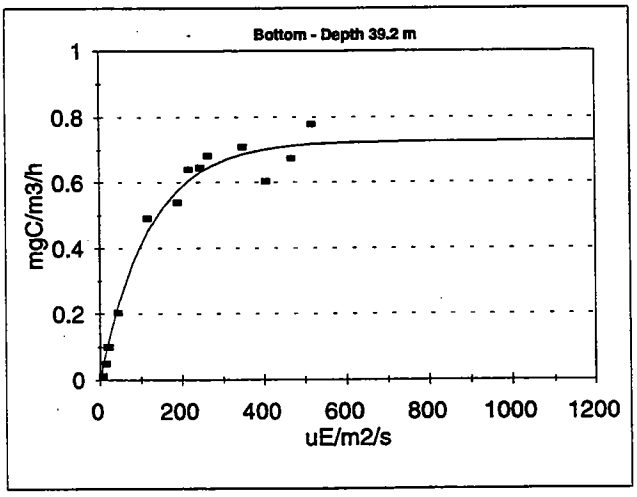

W9508 Station N04

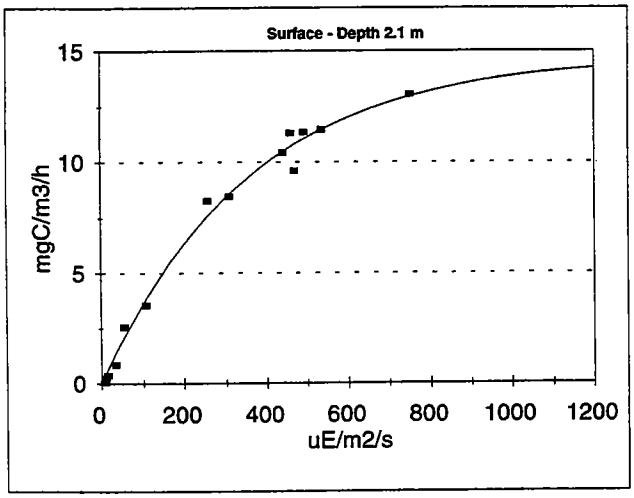

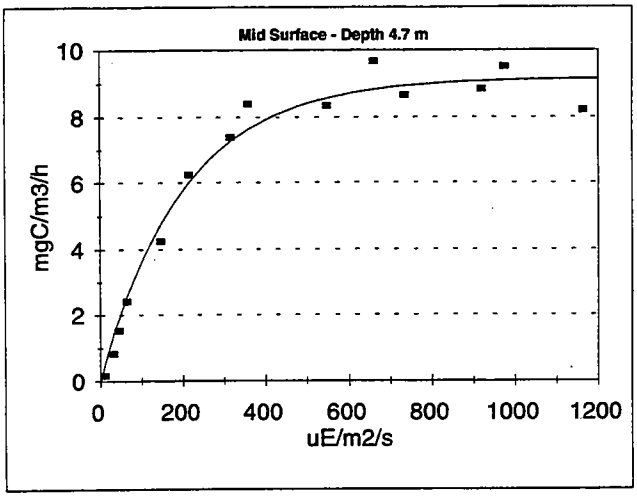

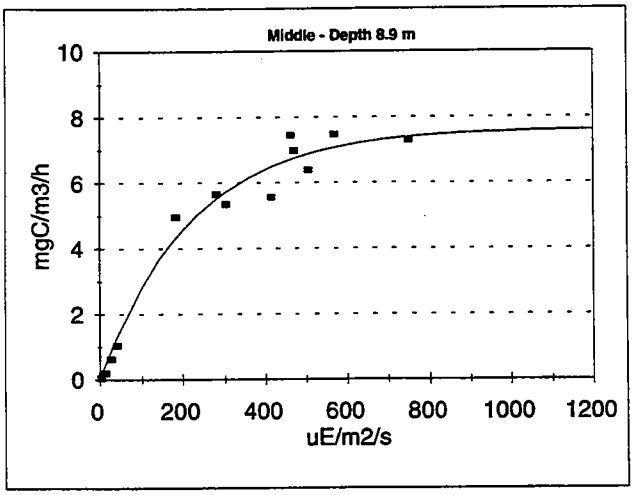

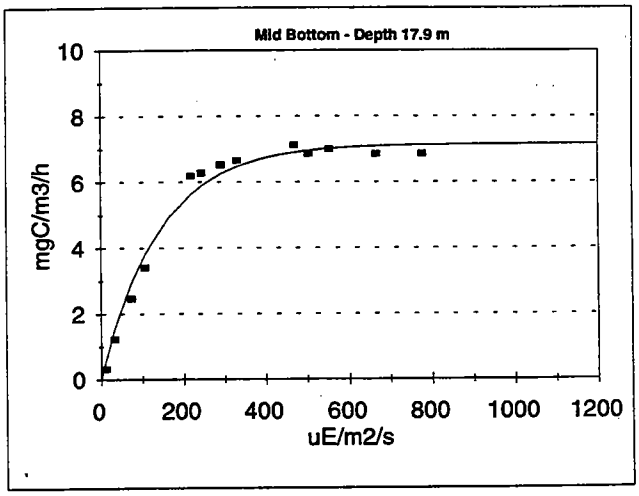

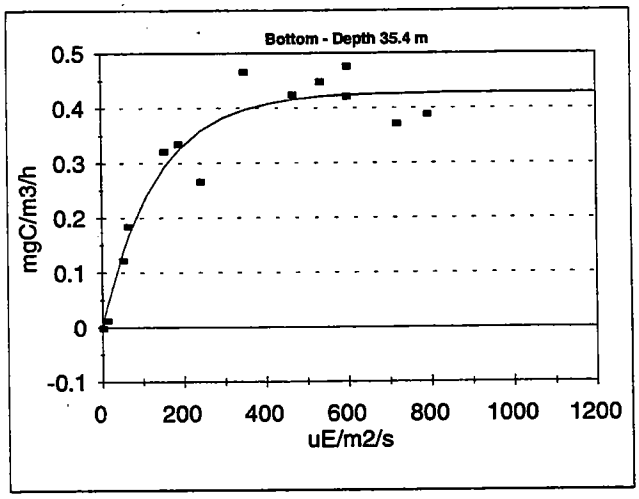

W9508 Station N16

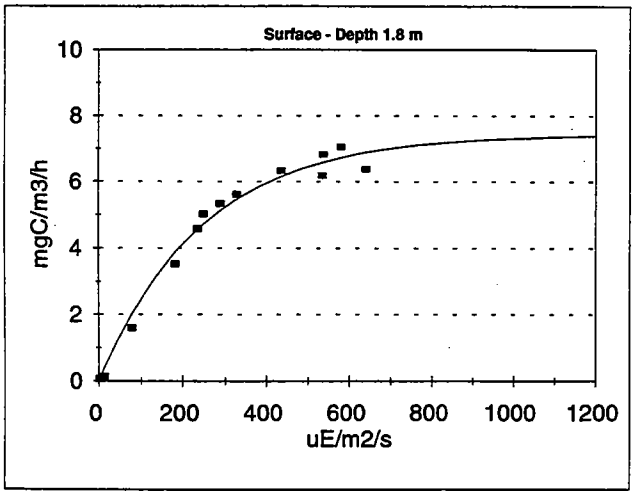

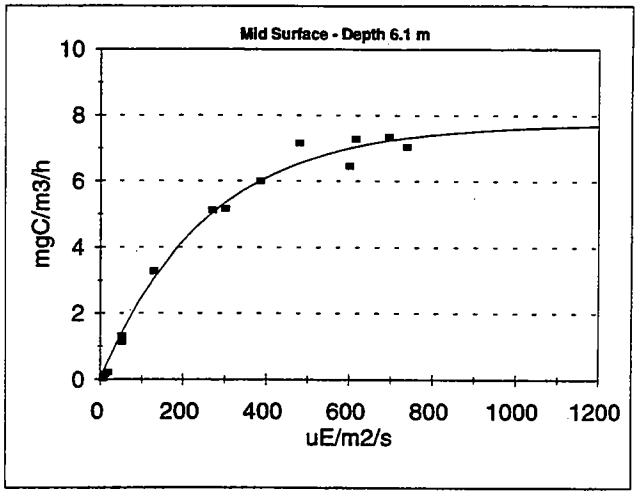

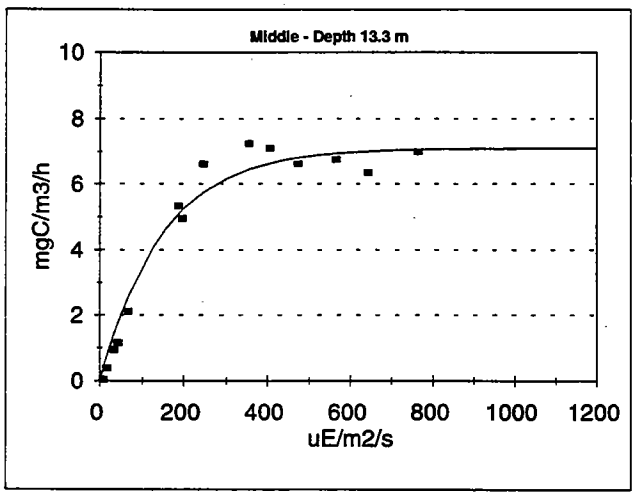

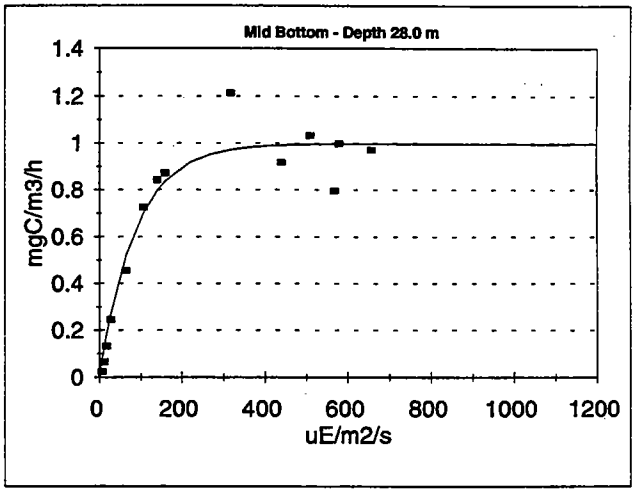

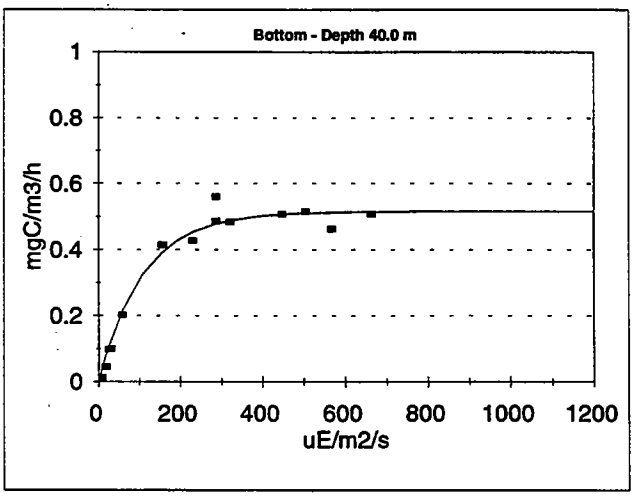

W9509 Station N04

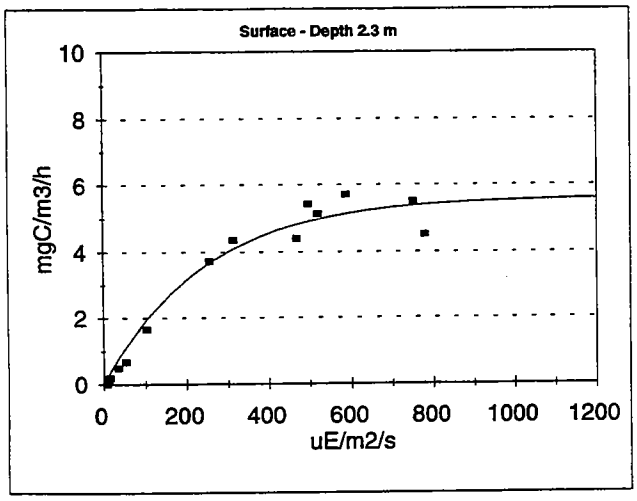

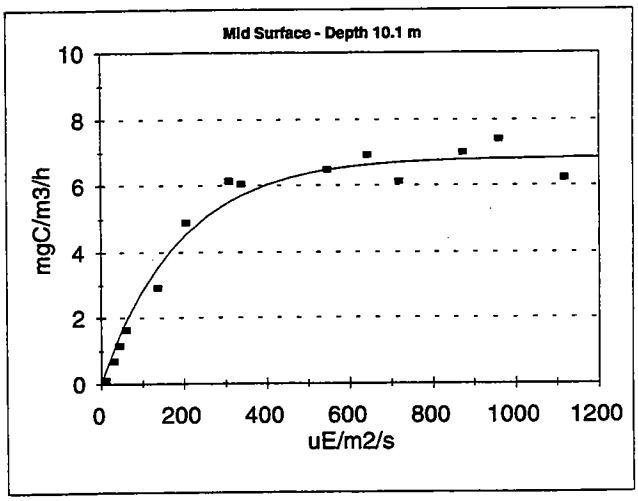

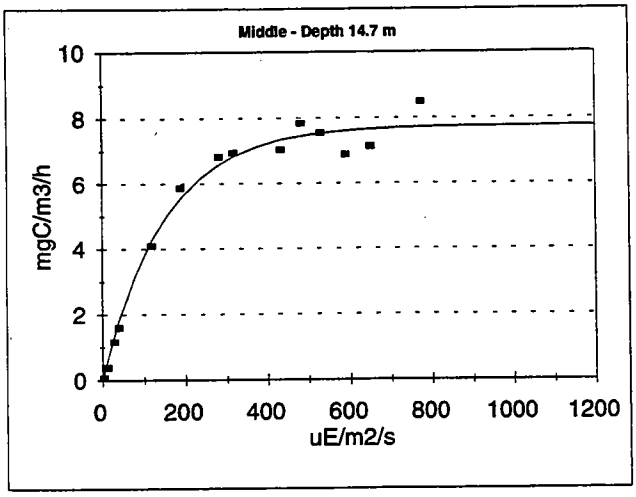

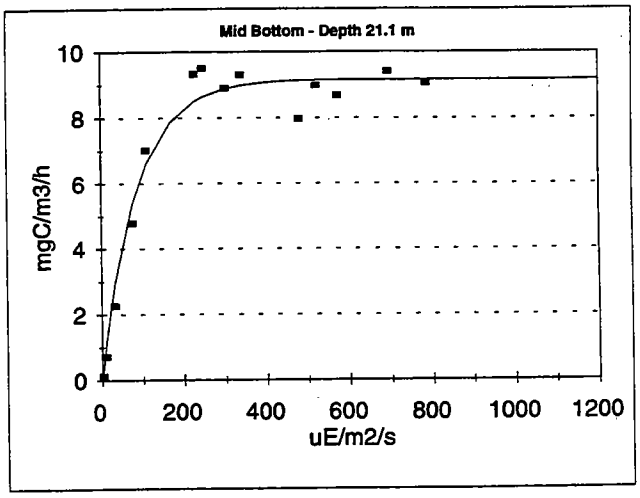

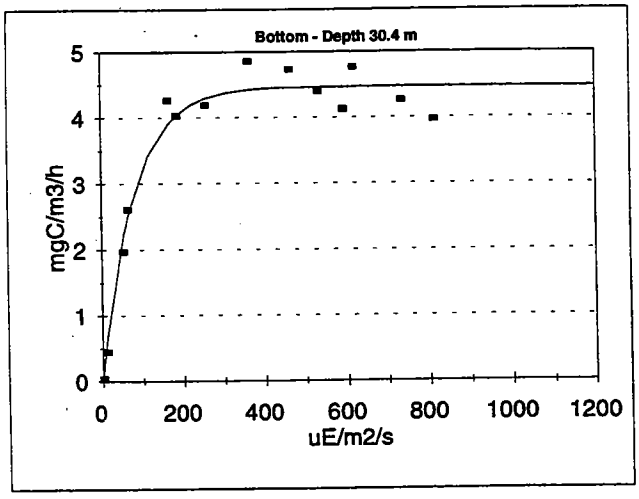

W9509 Station N16

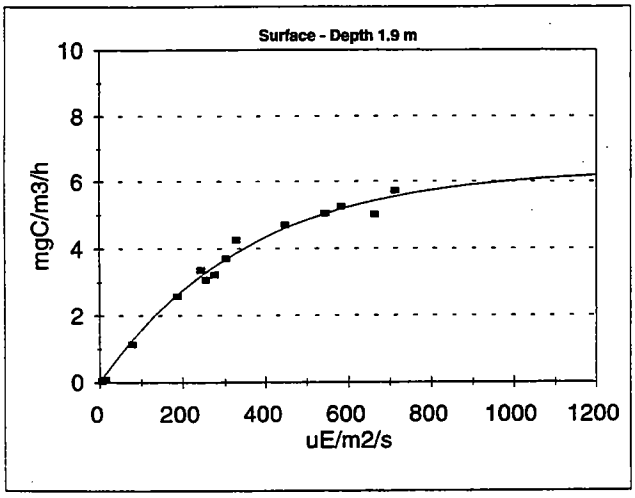

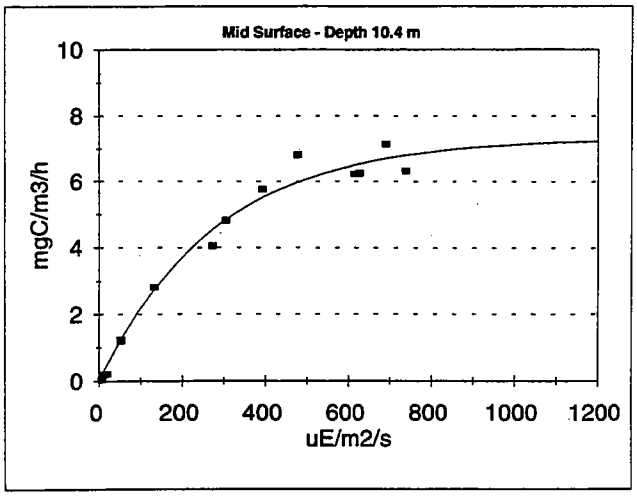

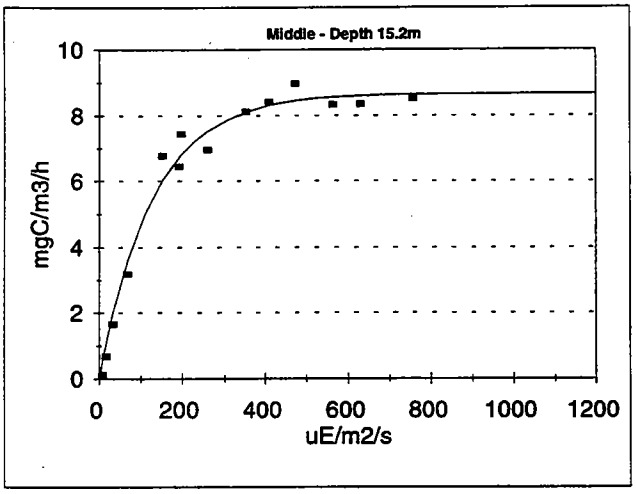

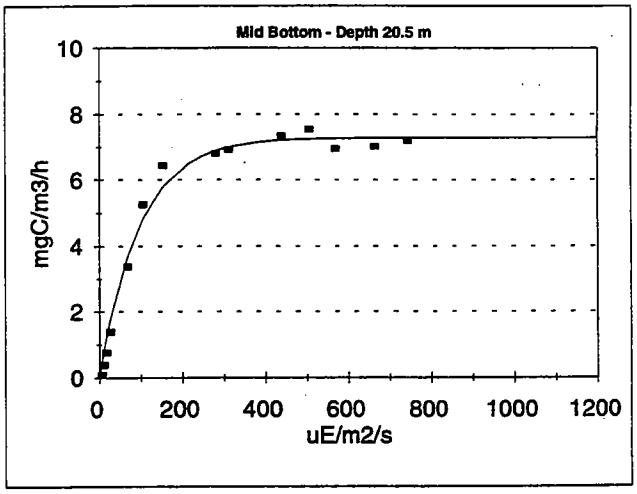

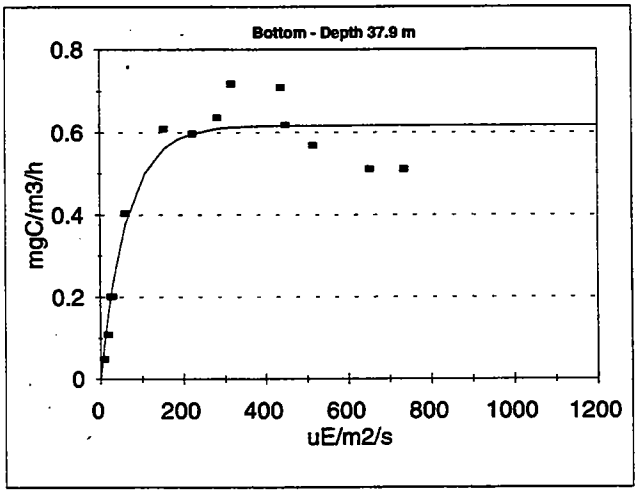

W9510 Station N04

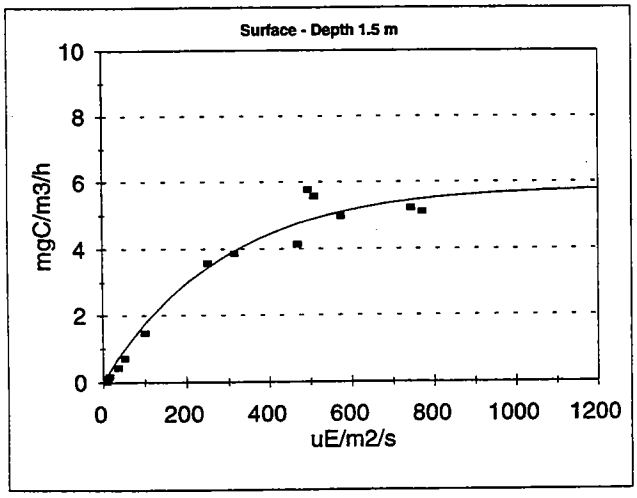

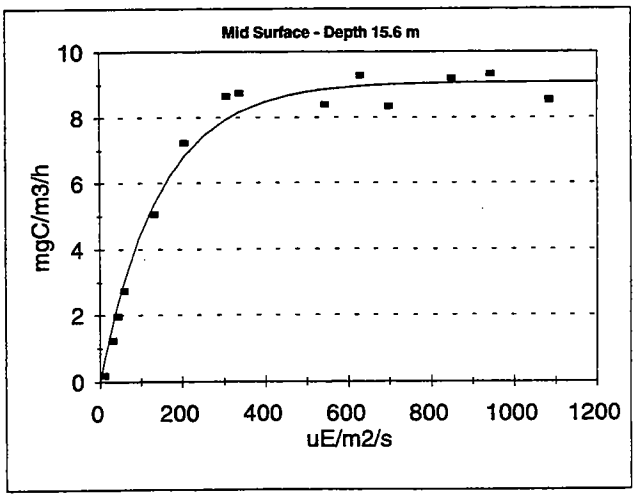

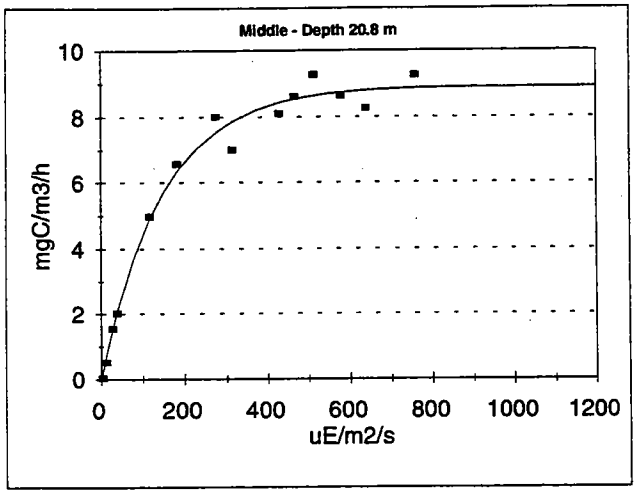

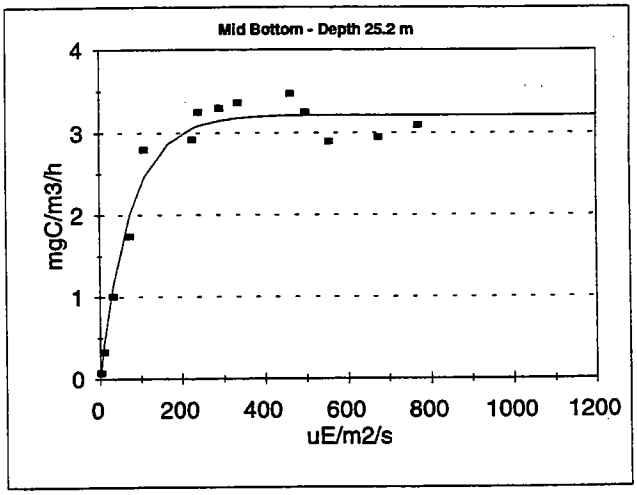

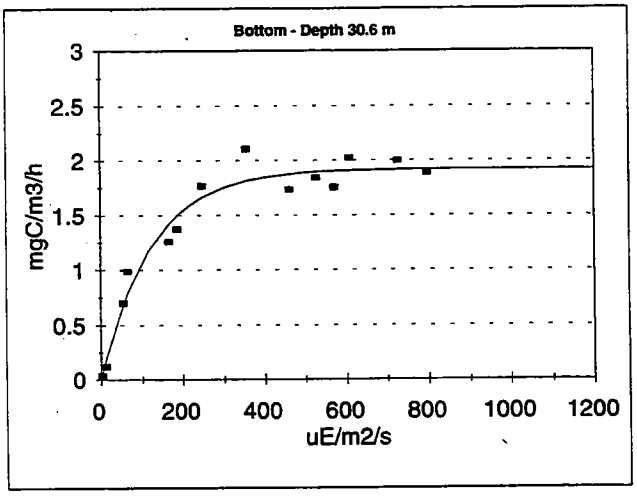

W9510 Station N16

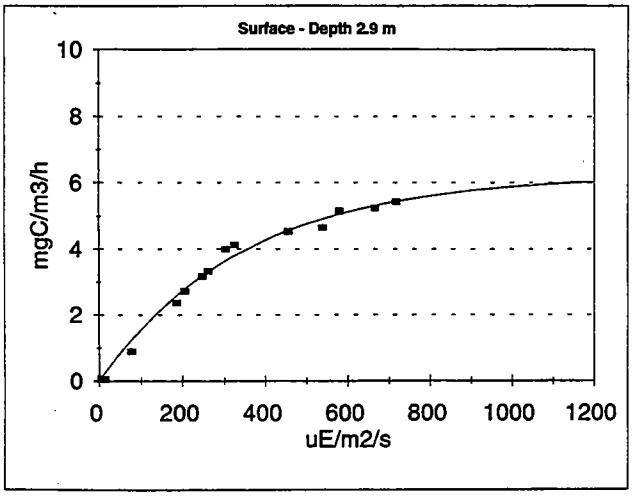

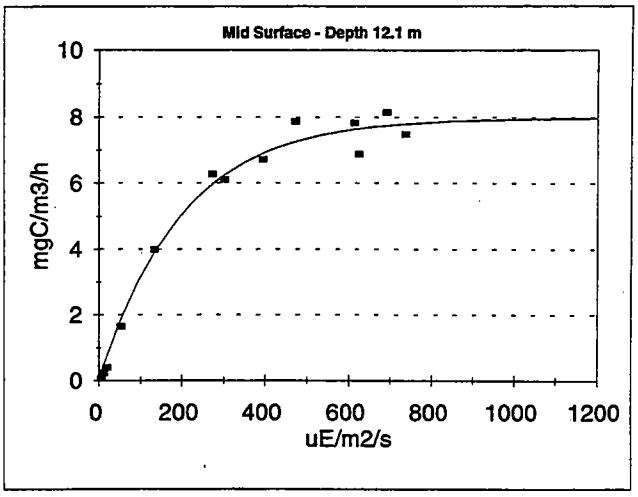

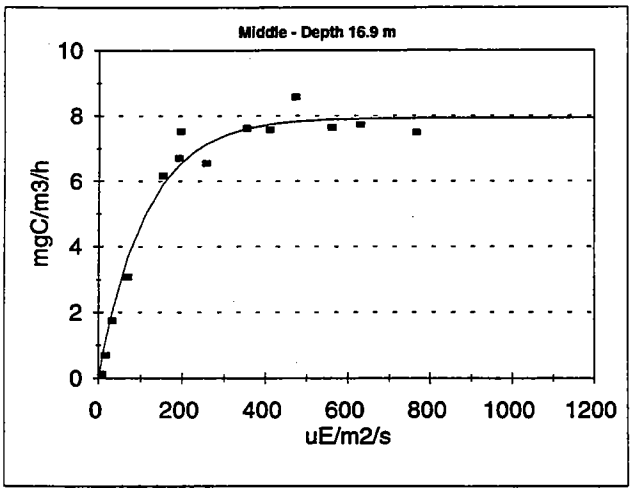

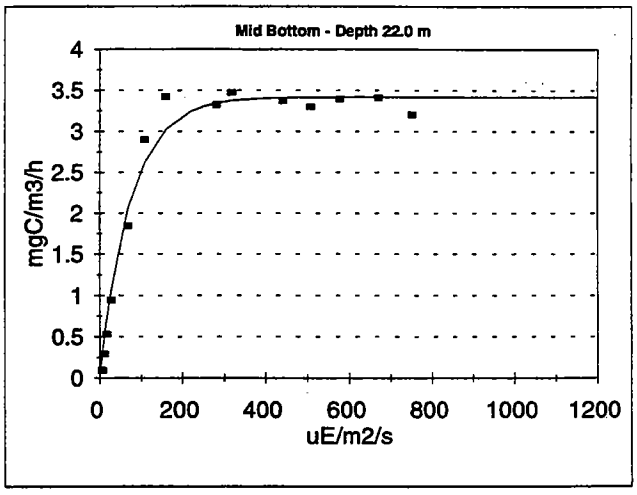

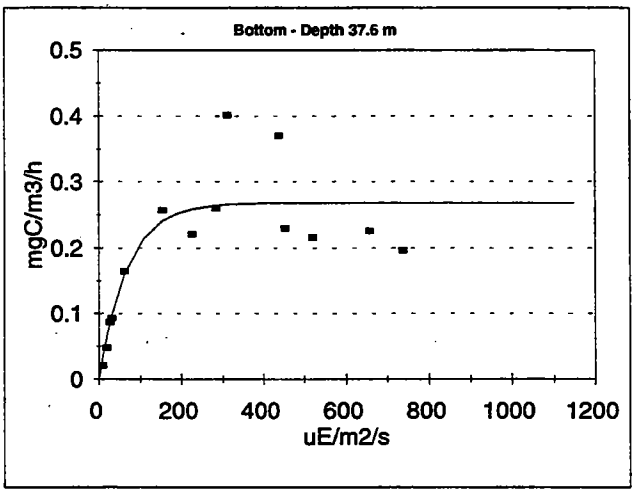

W9511 Station F23

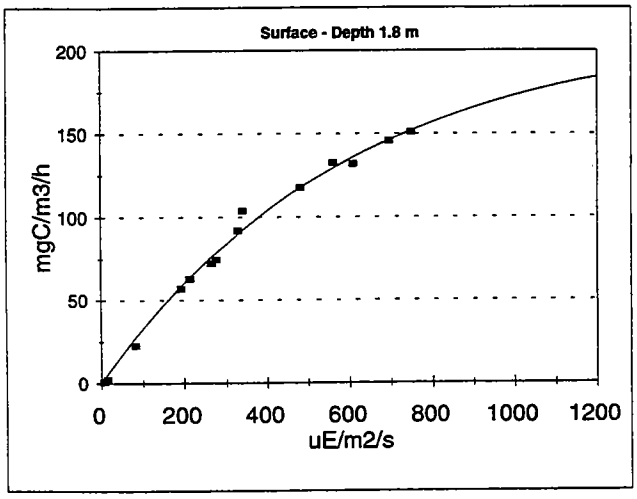

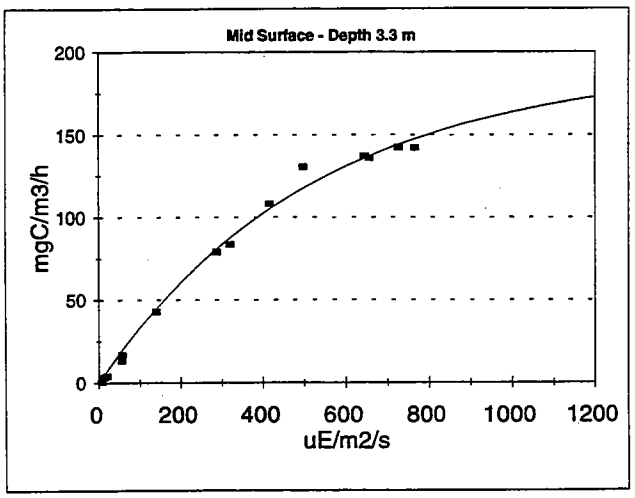

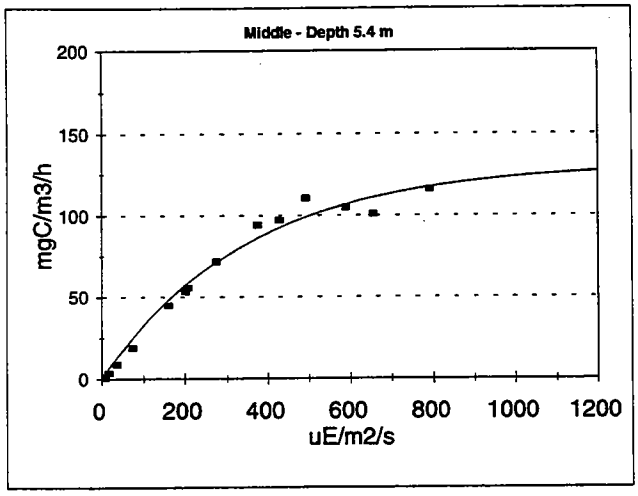

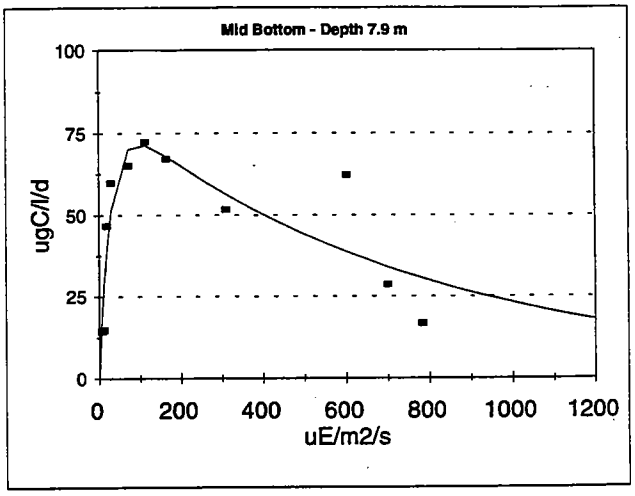

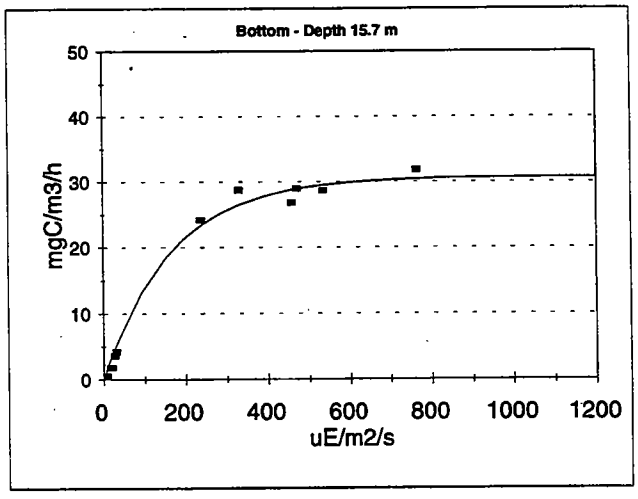

W9511 Station N04

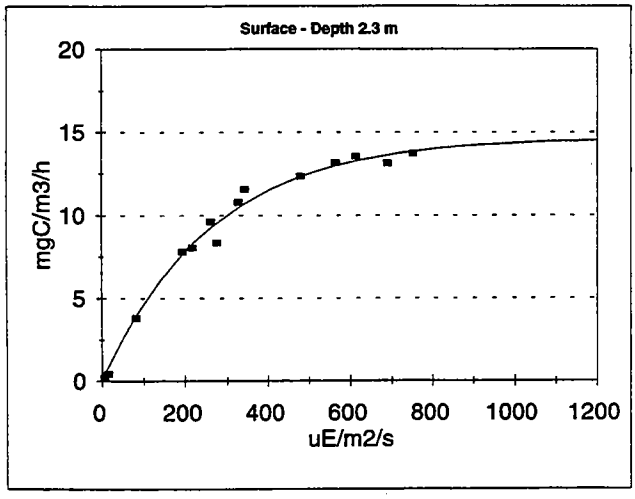

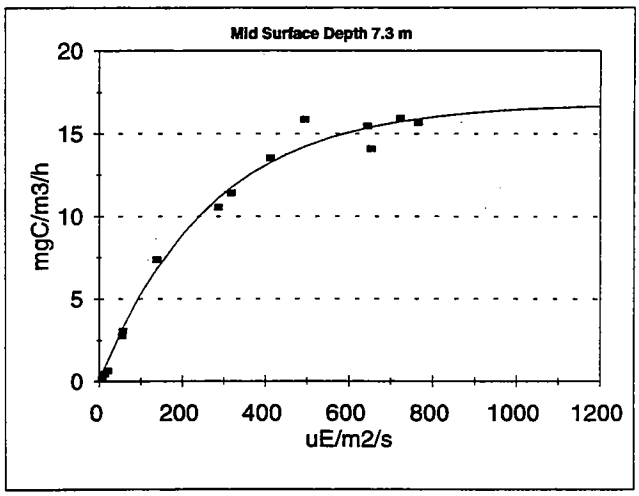

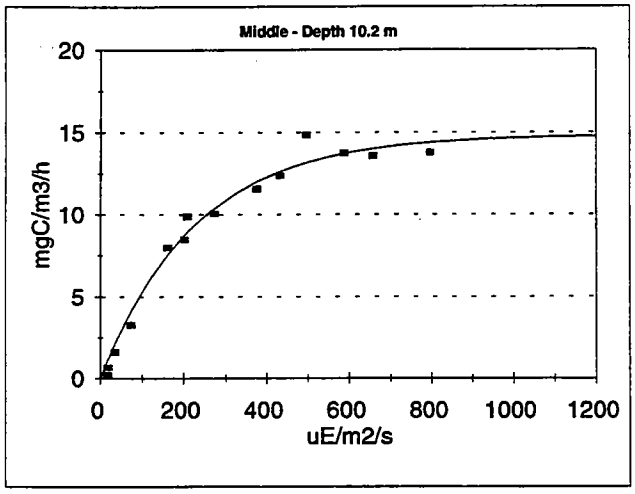

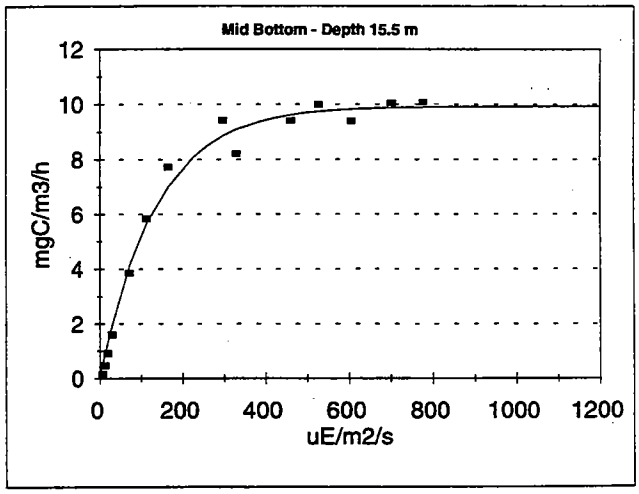

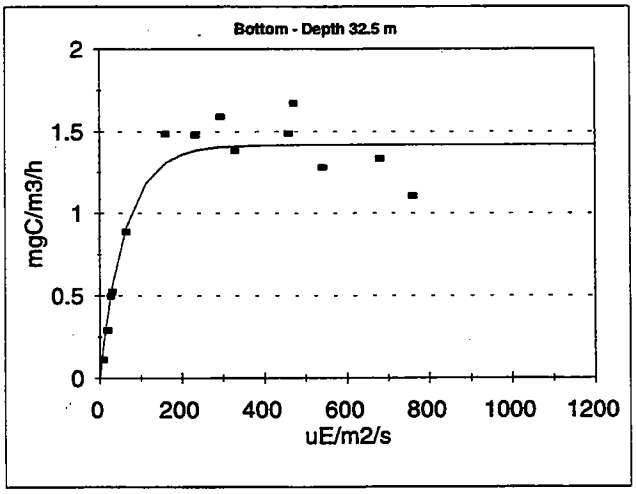

W9511 Station N07

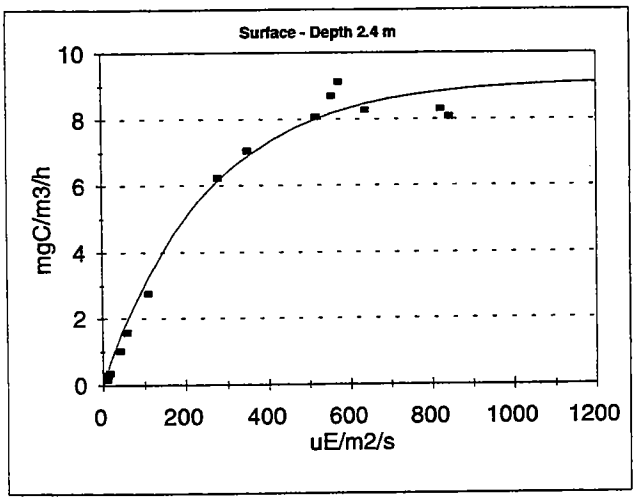

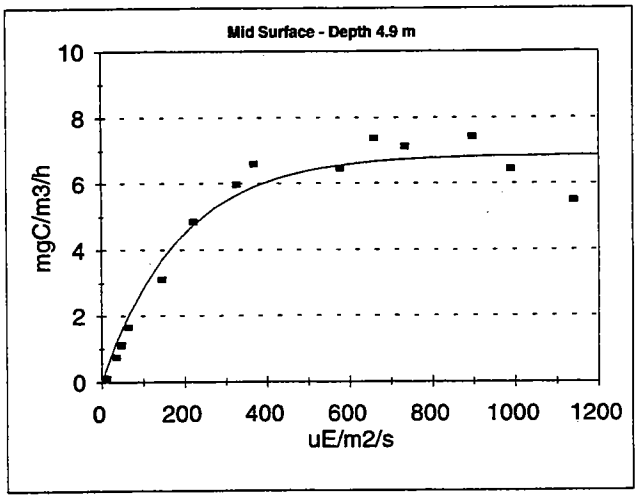

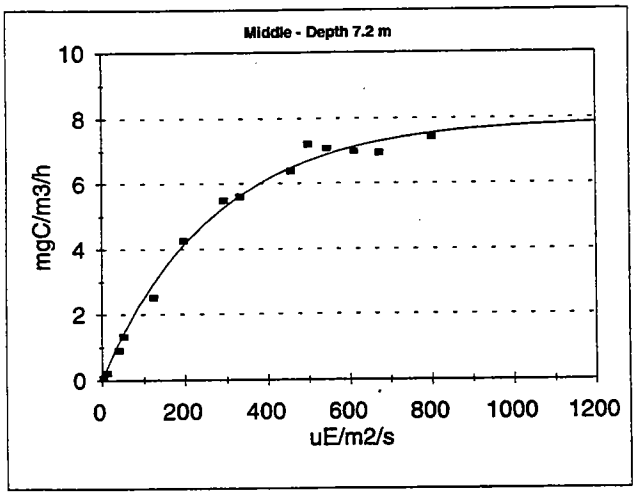

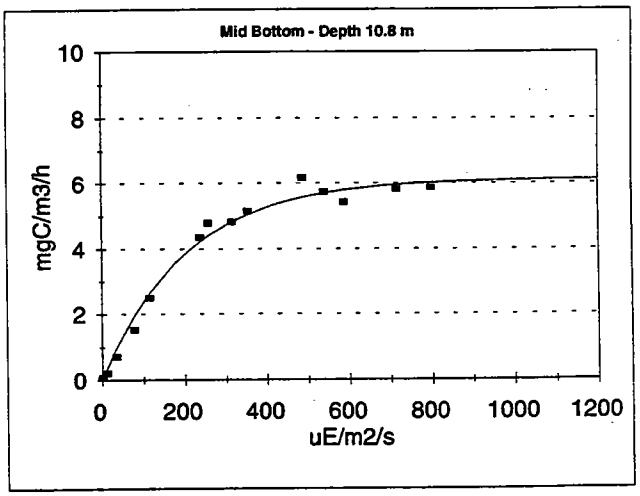

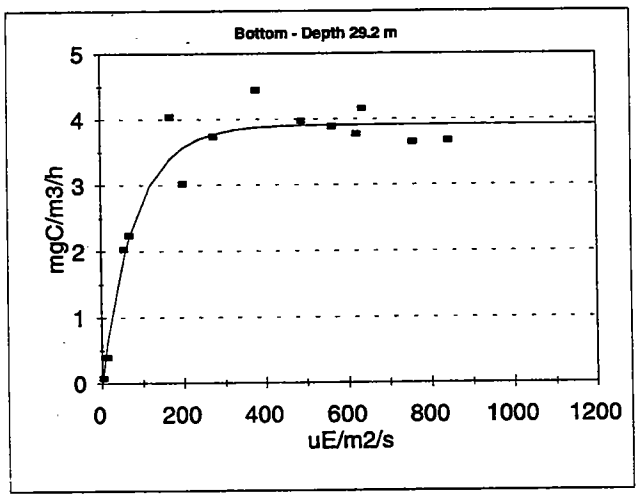

W9511 Station N16

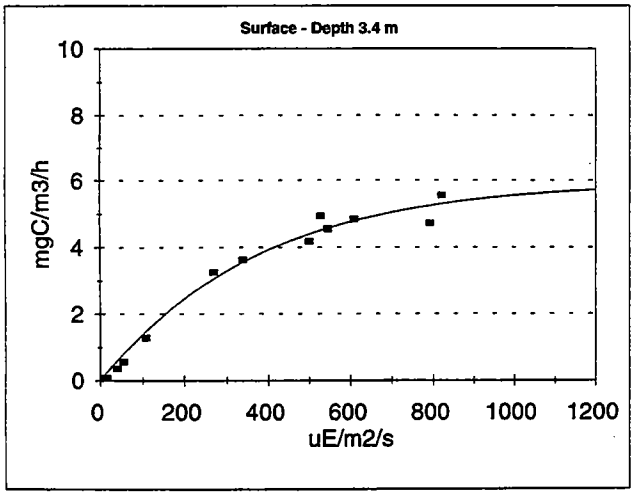

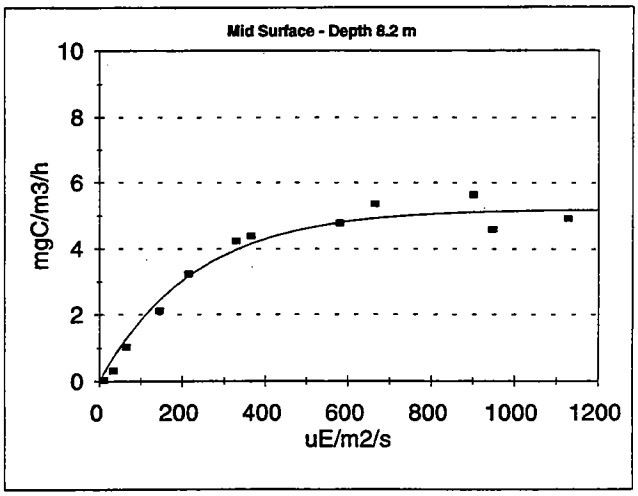

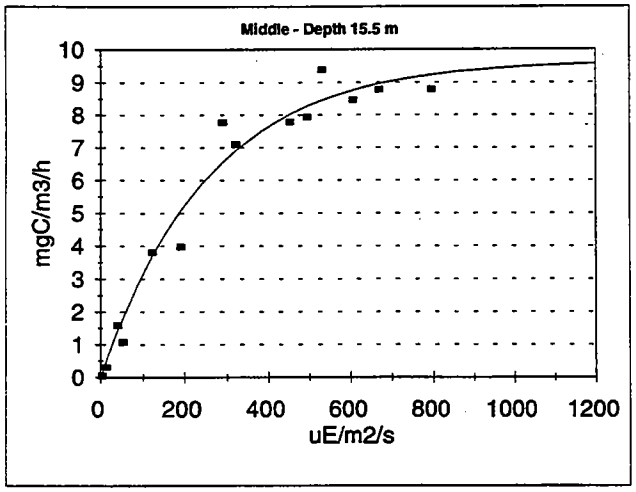

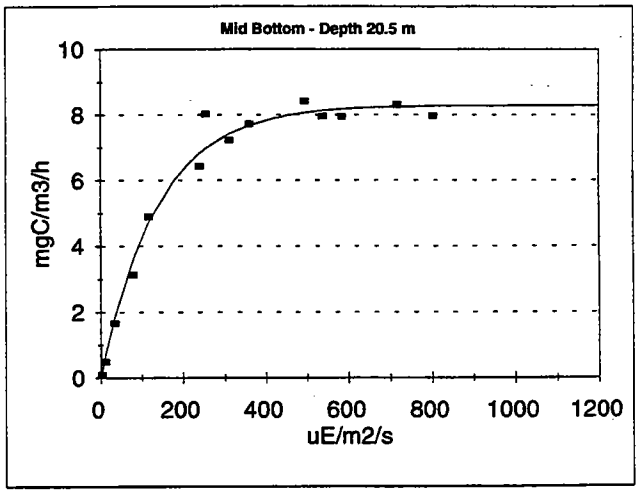

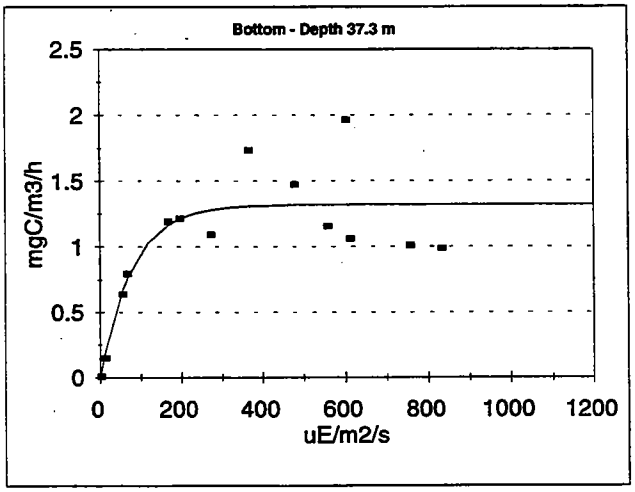

W9512 Station N04

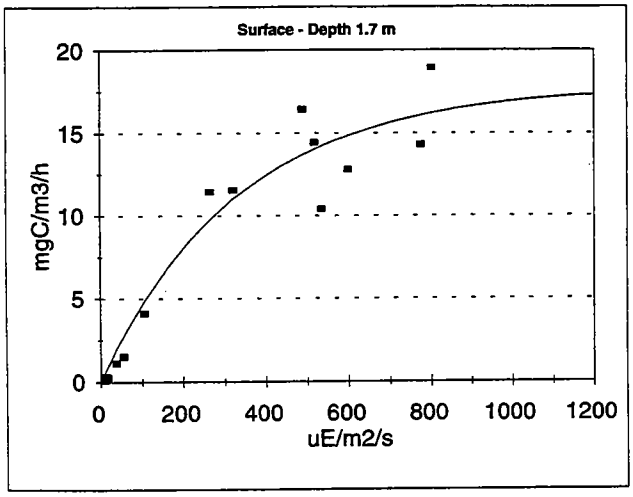

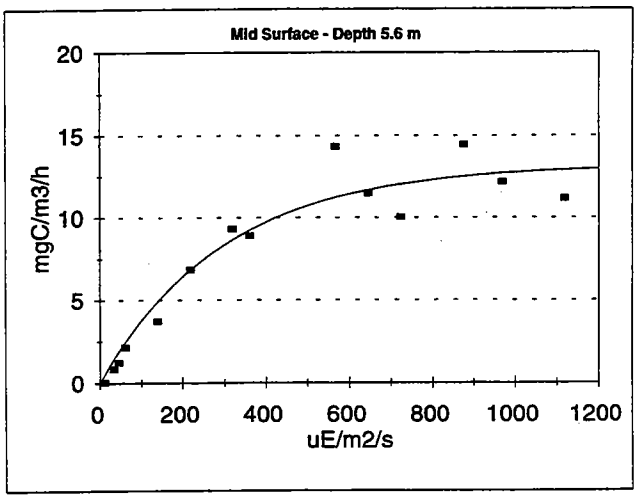

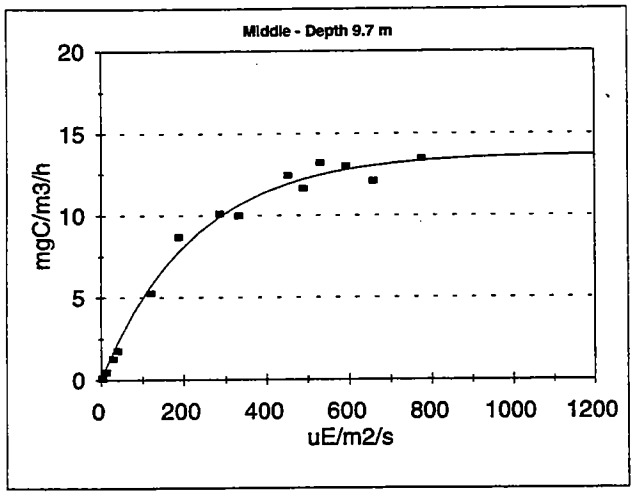

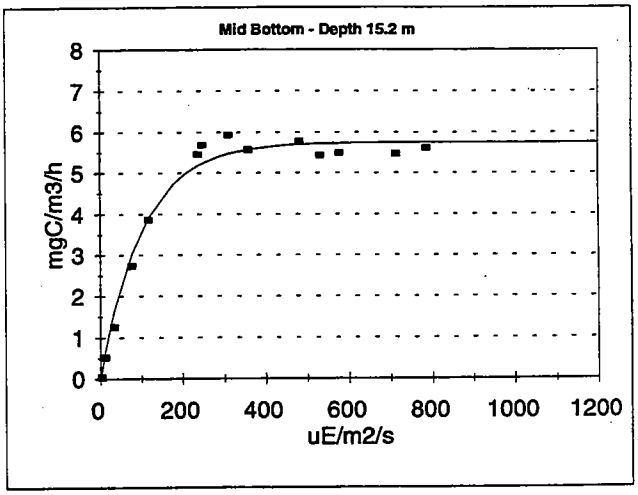

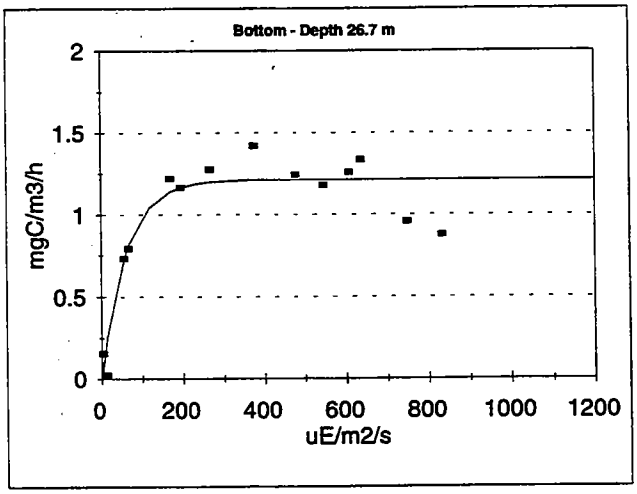

W9512 Station N16

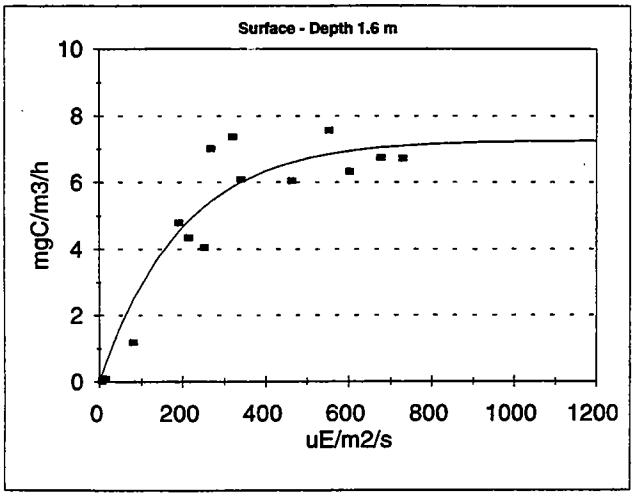

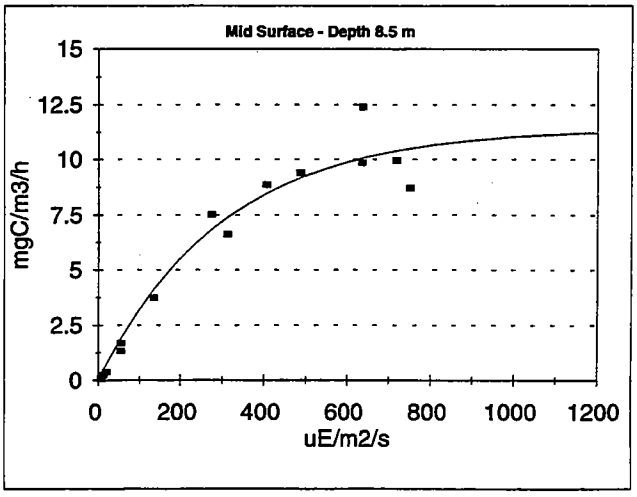

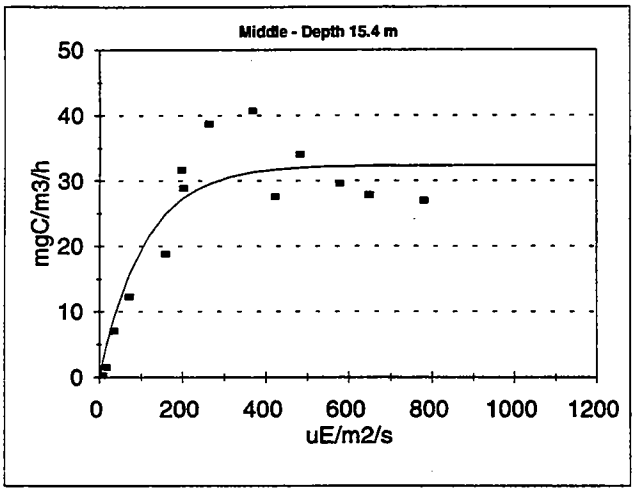

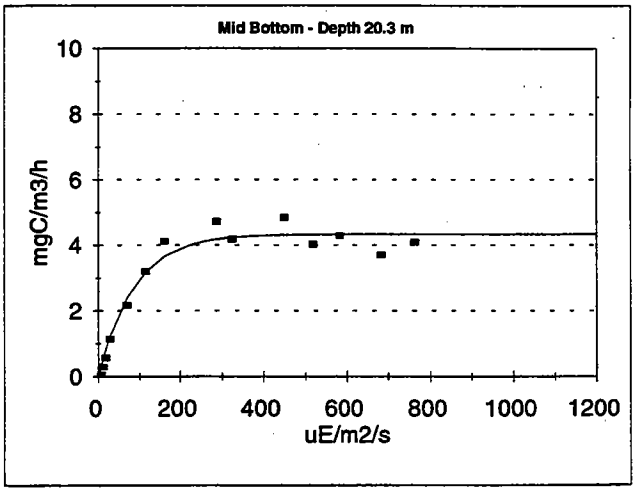

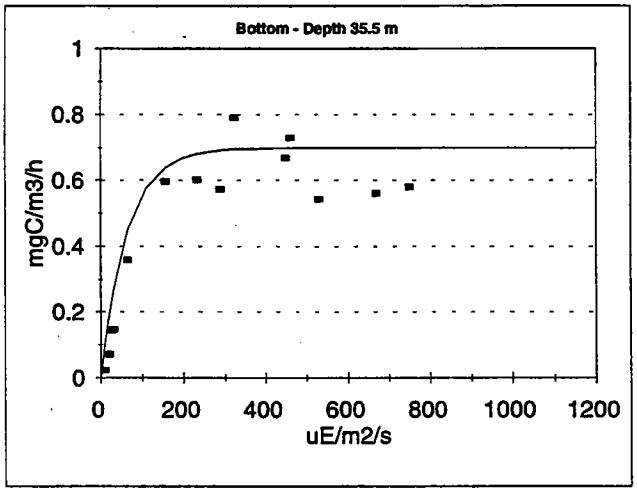

W9513 - Station N04

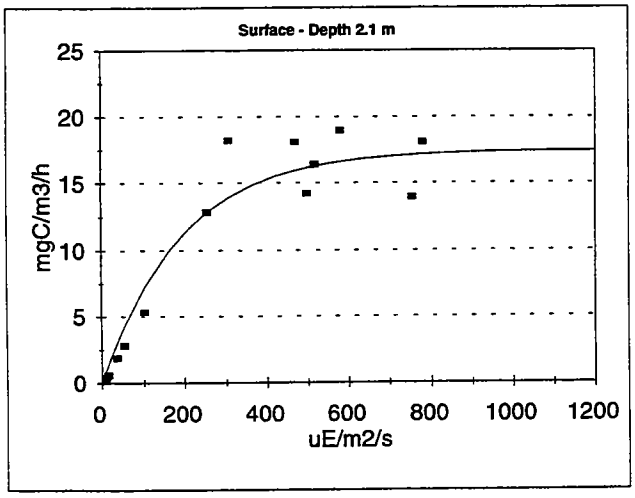

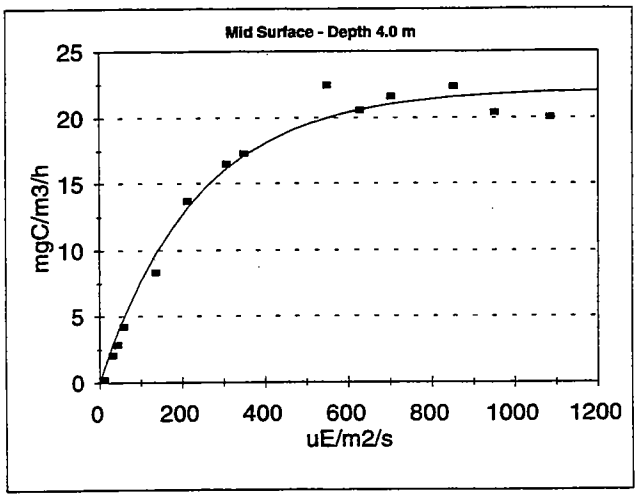

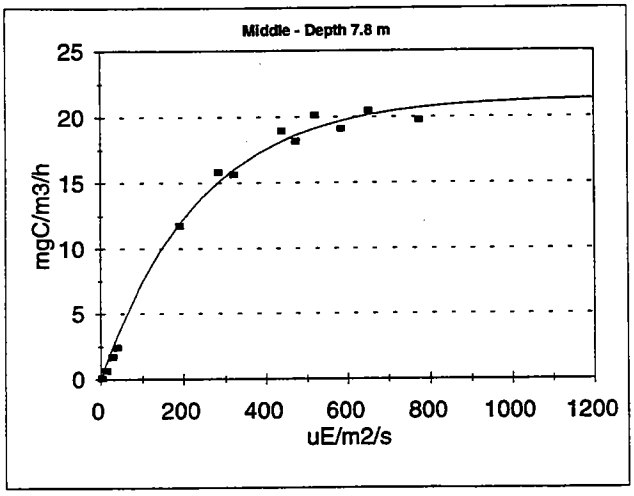

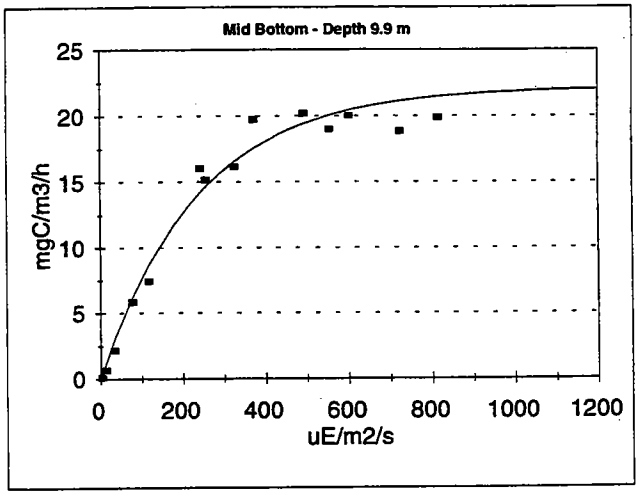

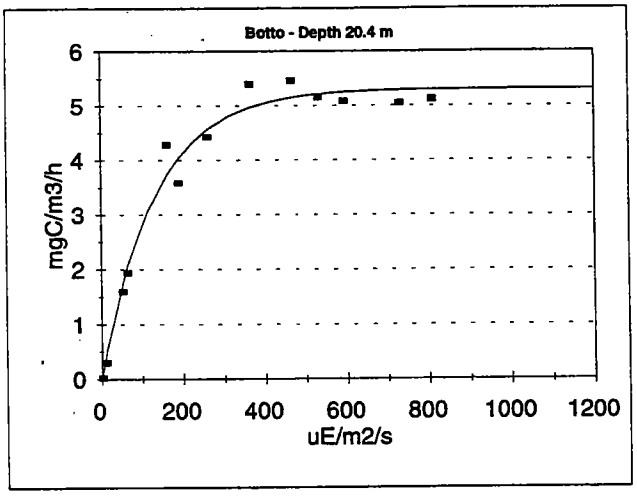

W9513 Station N16

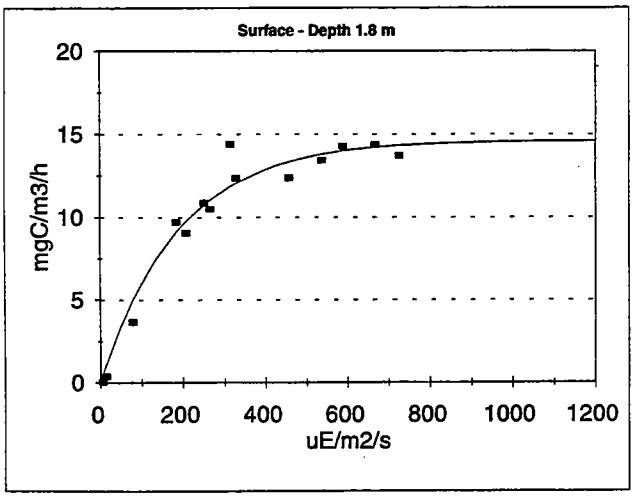

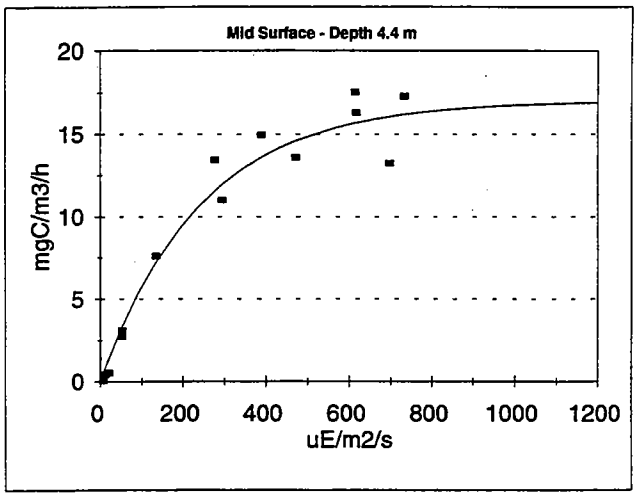

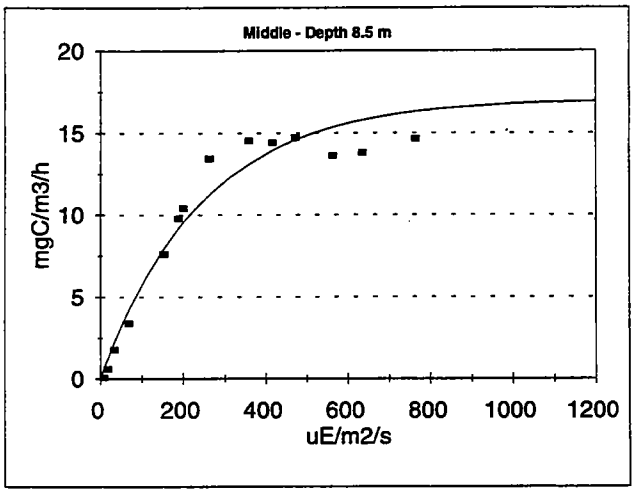

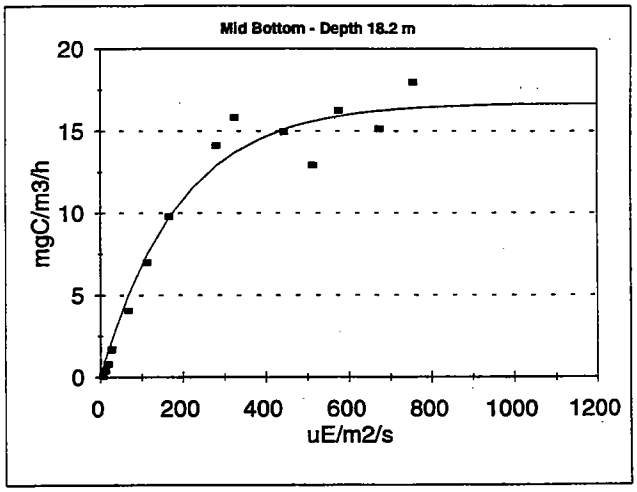

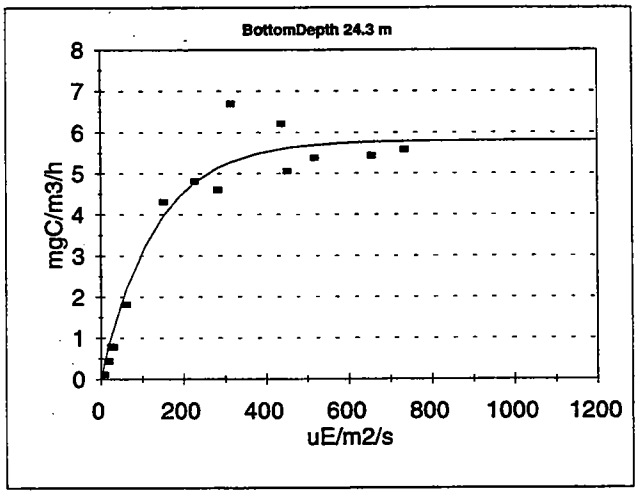

W9514 Station F23

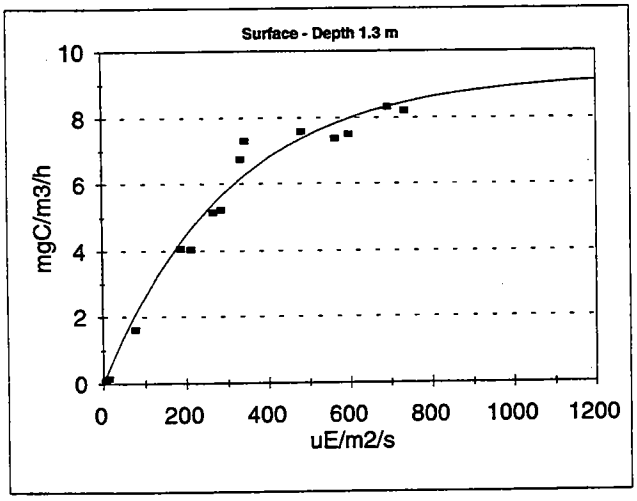

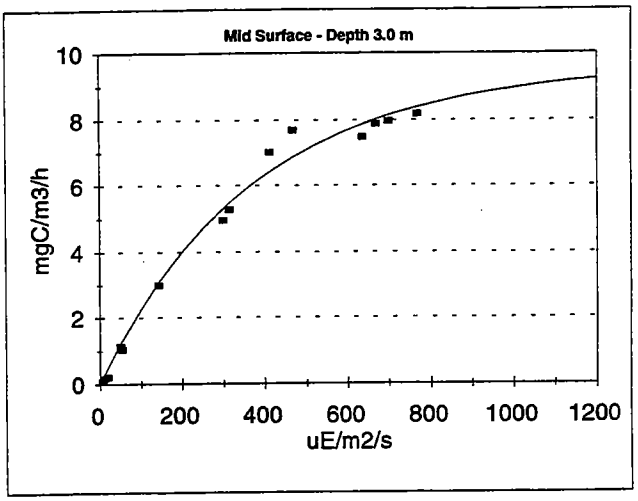

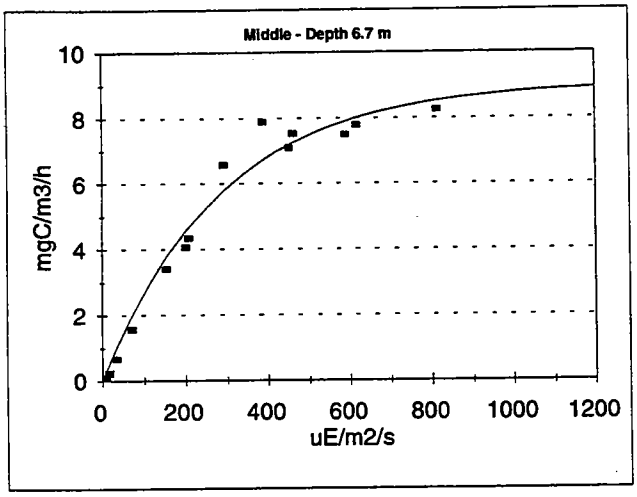

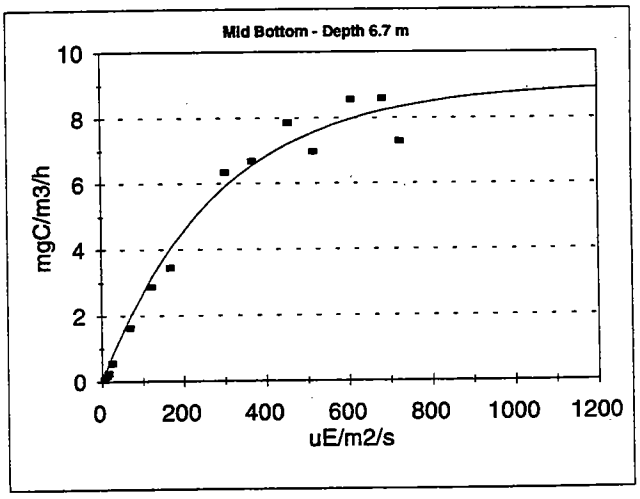

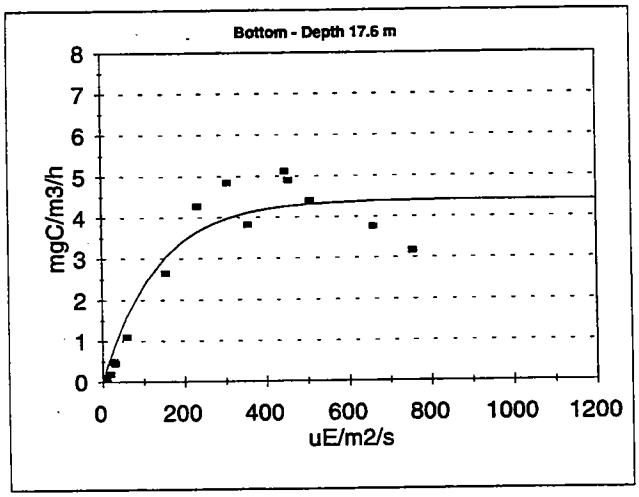

W9514 Station N04

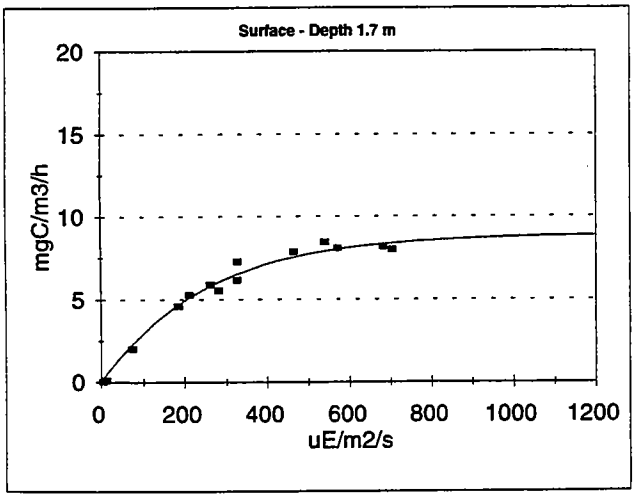

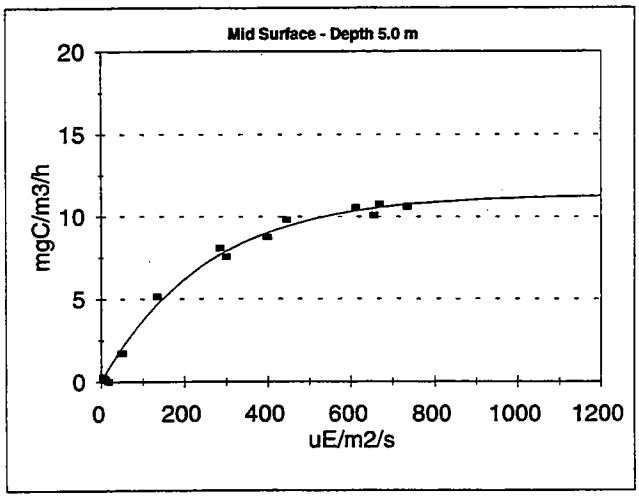

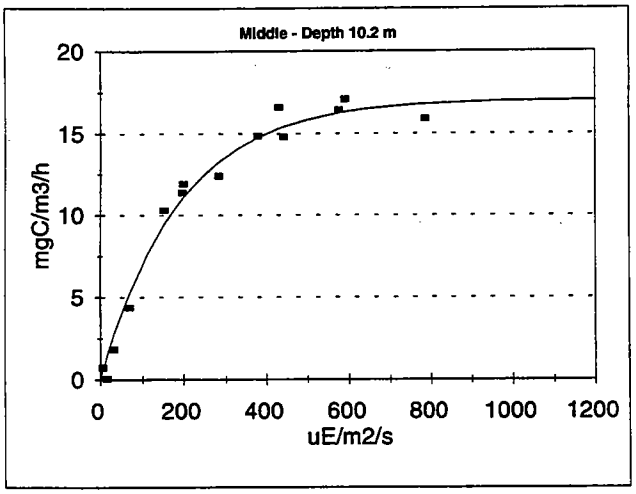

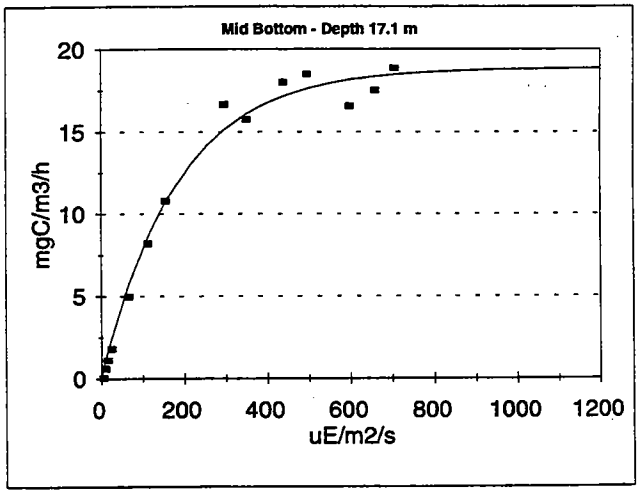

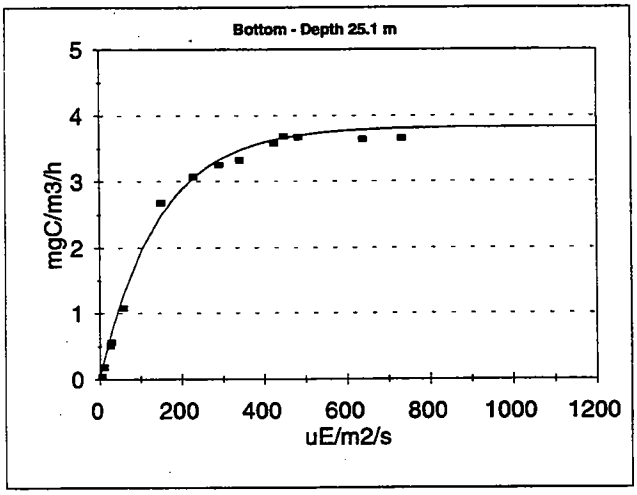

W9514 Station N07

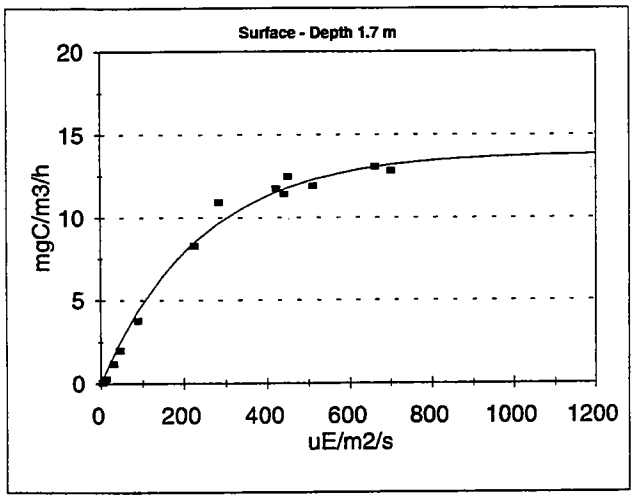

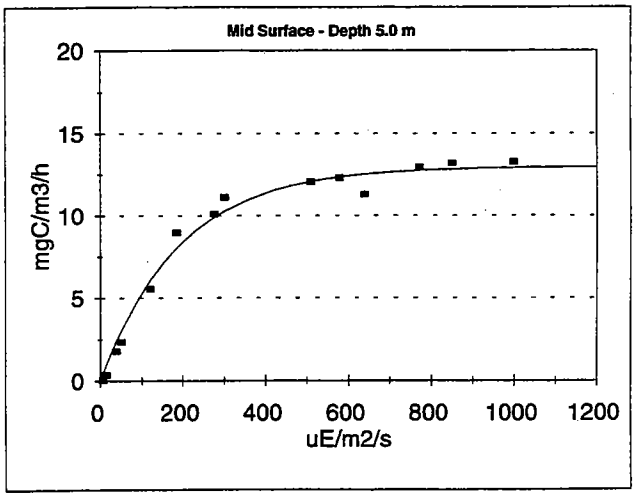

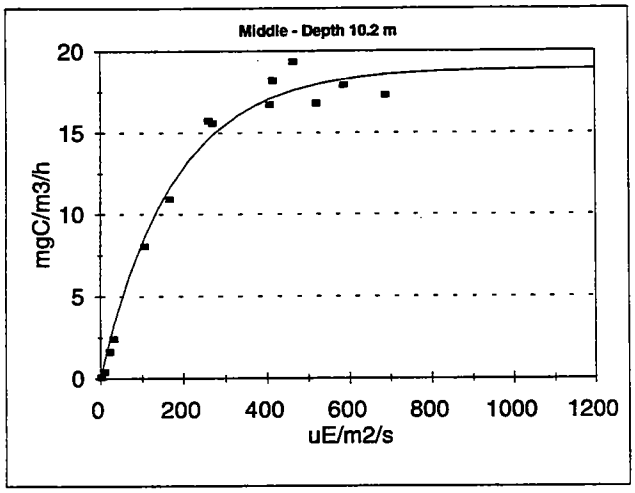

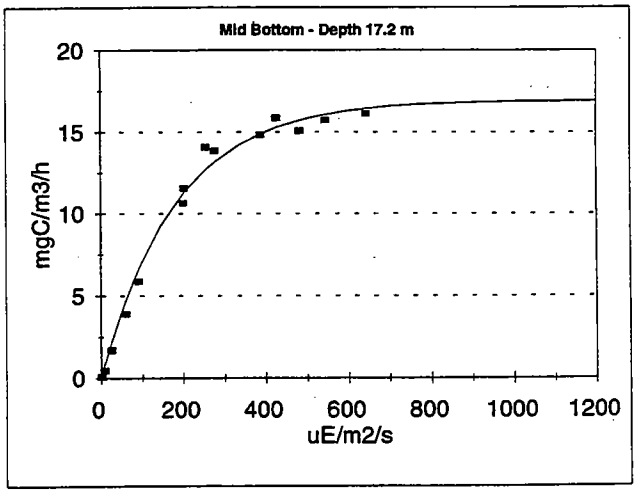

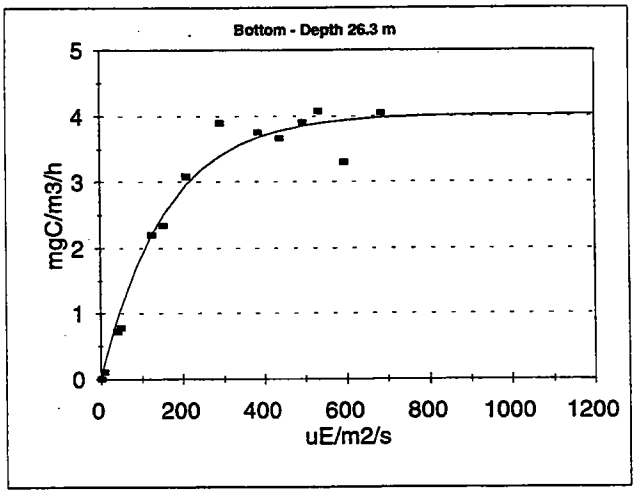

W9514 Station N16

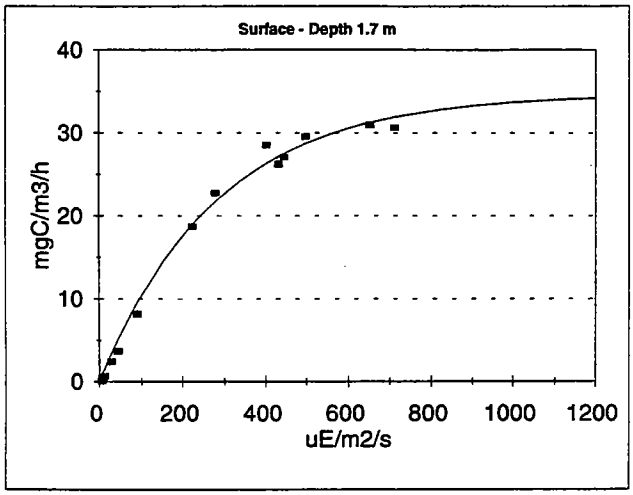

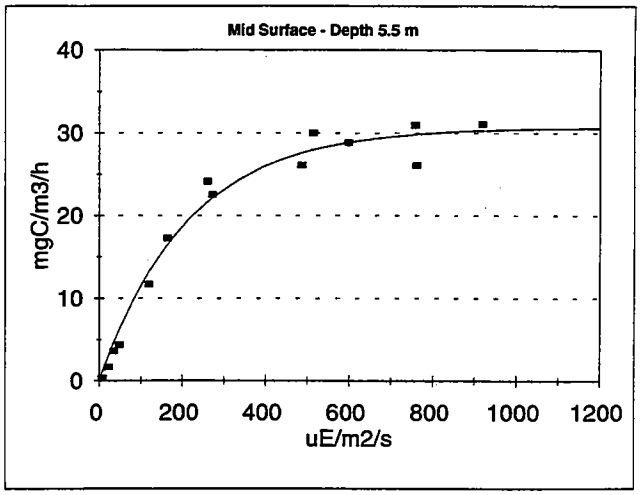

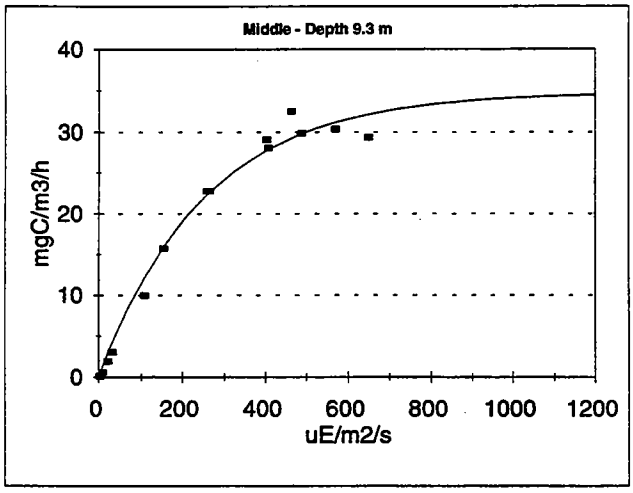

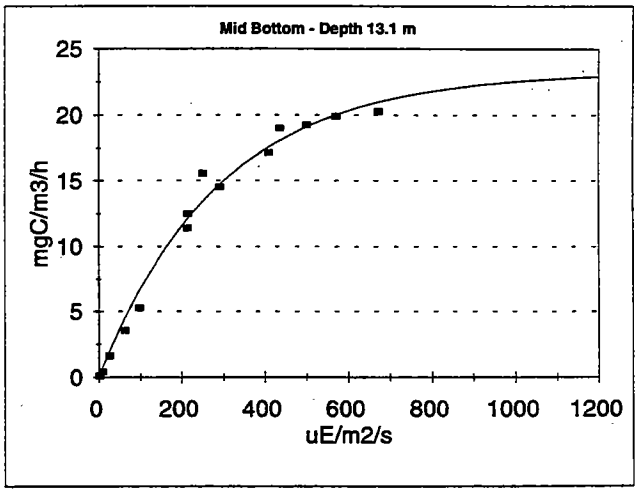

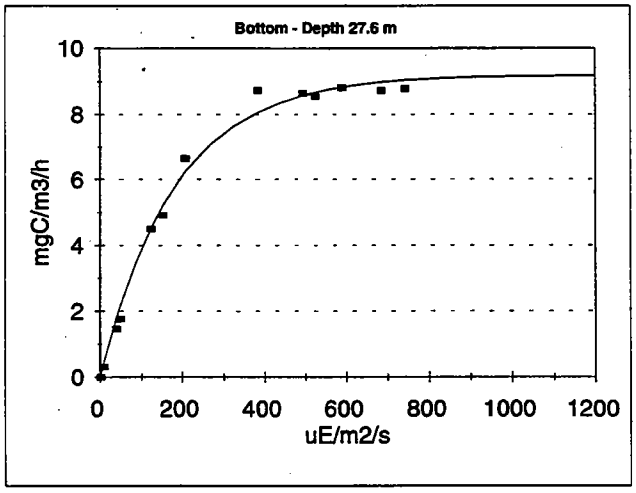

W9515 Station N04

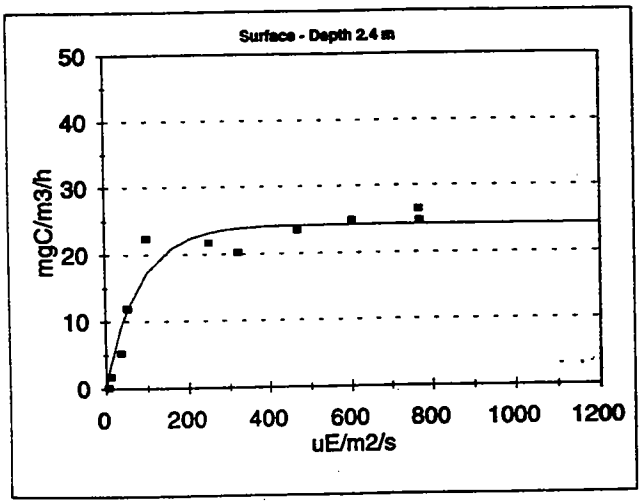

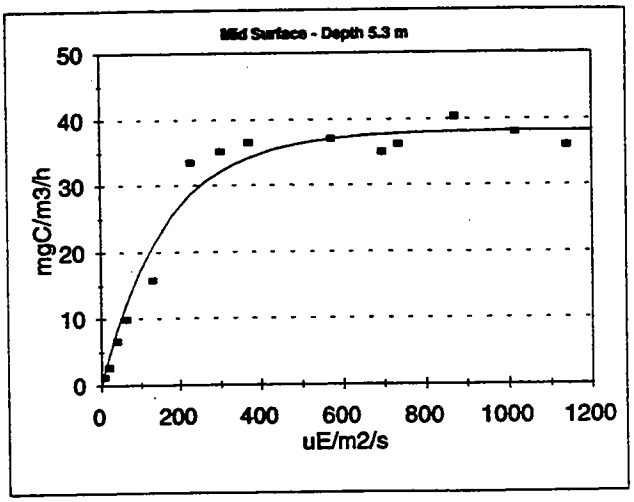

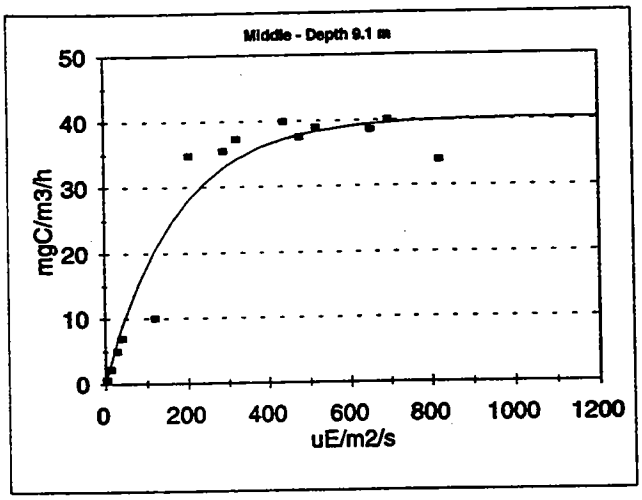

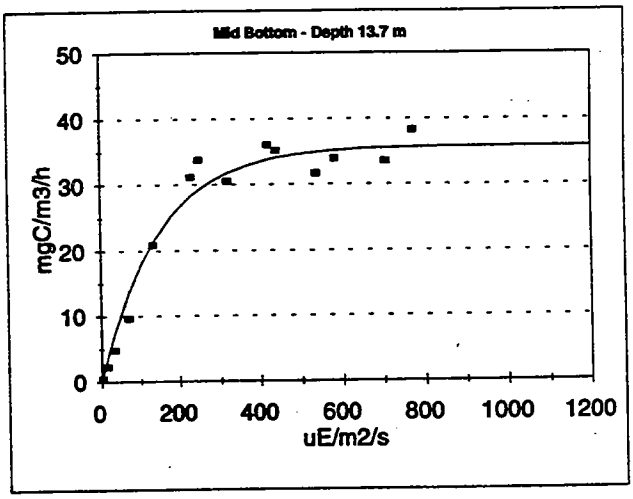

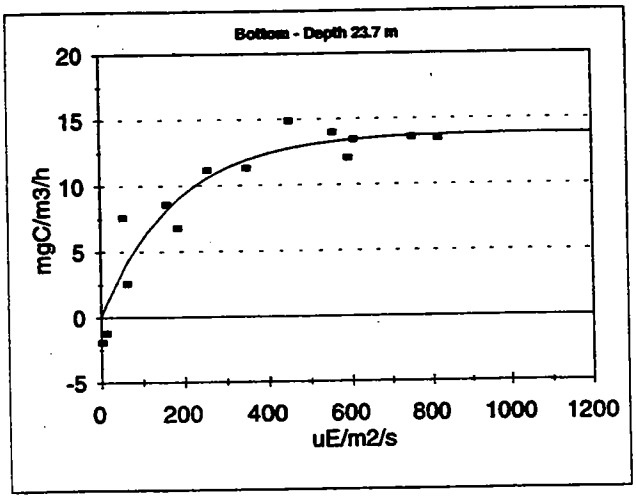

W9515 Station N16

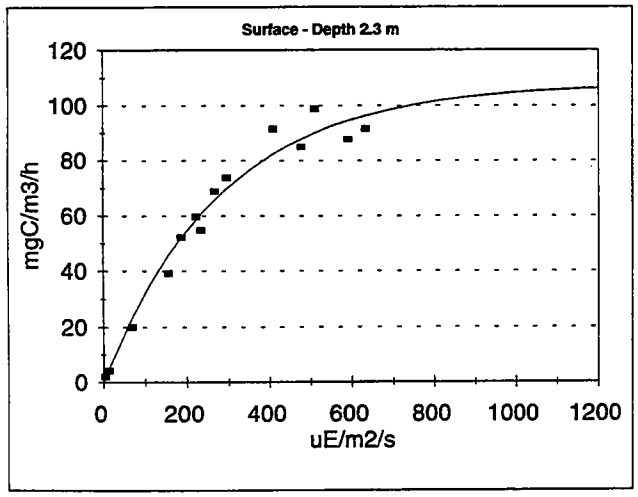

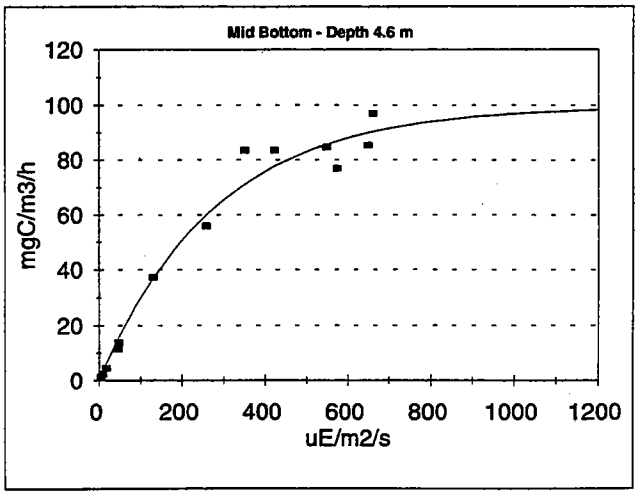

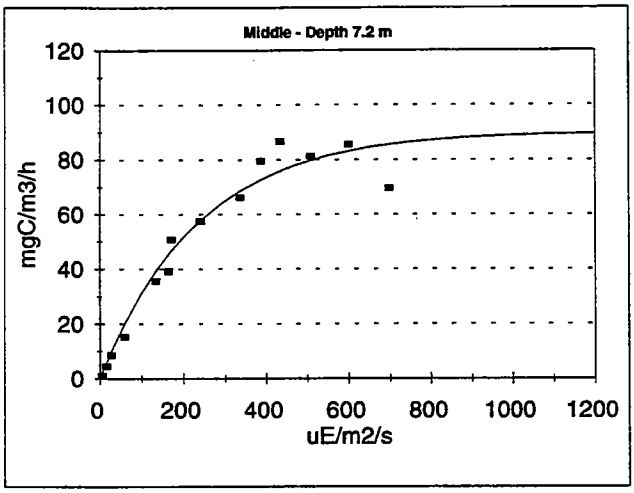

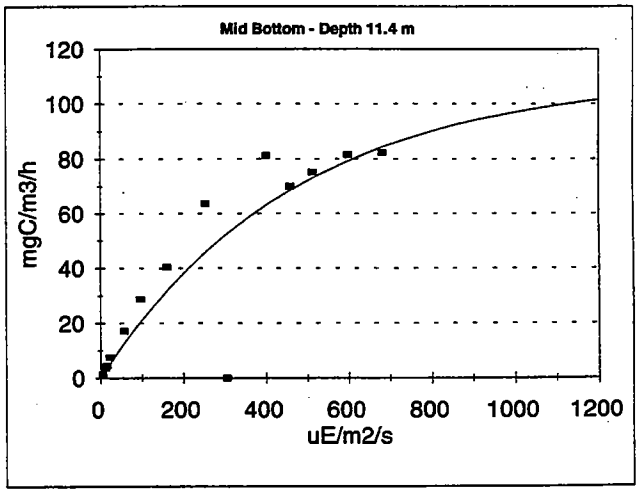

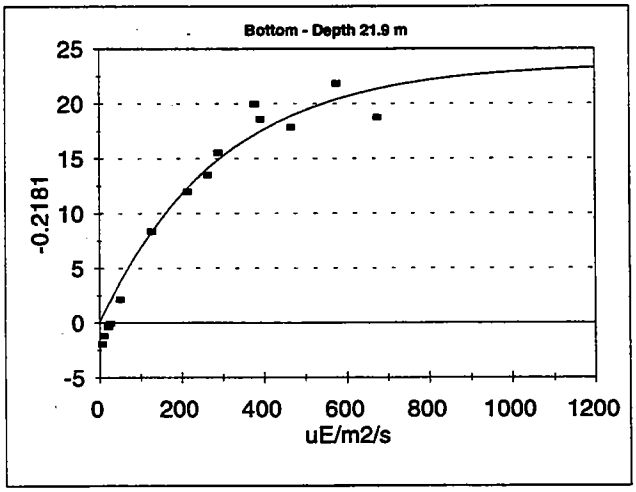

W9516 Station N04

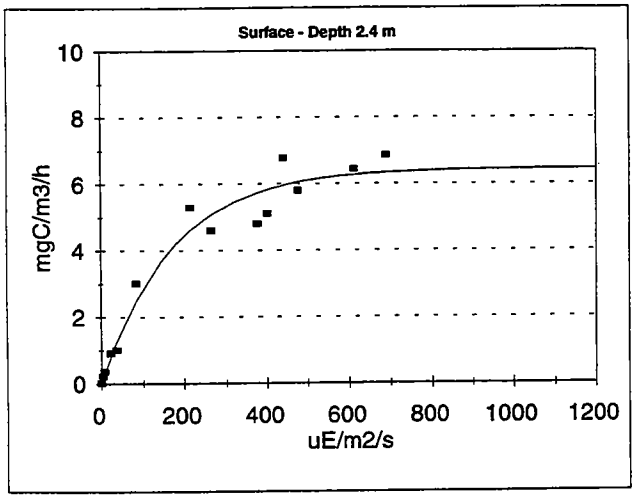

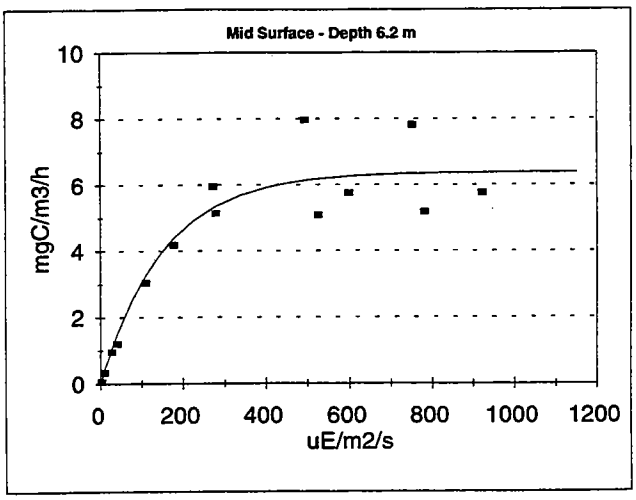

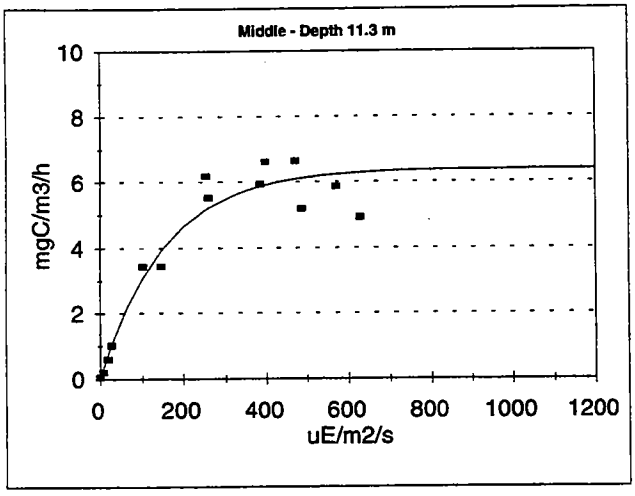

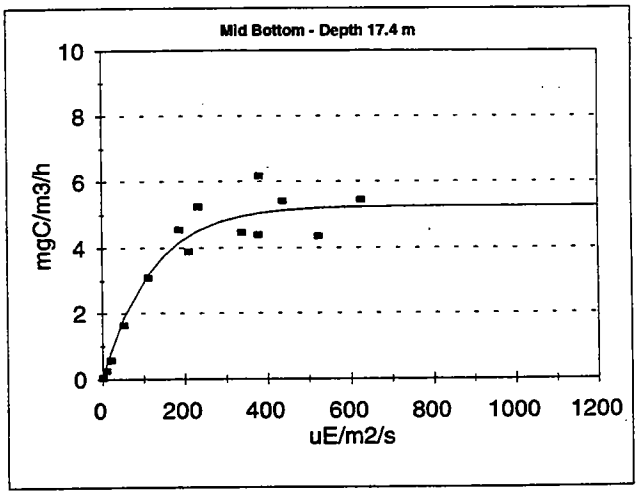

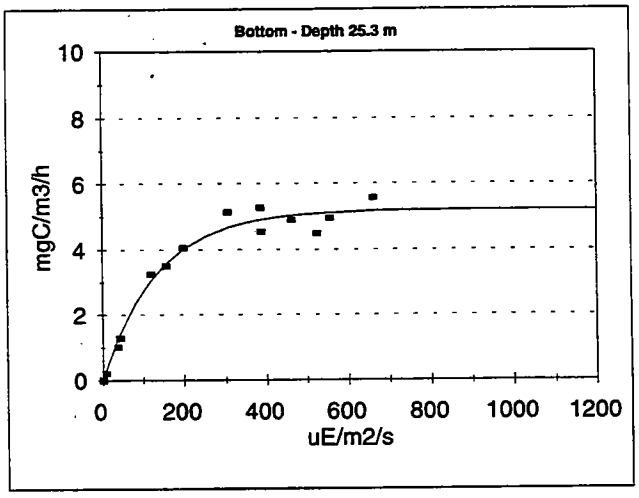

W9516 Station N16

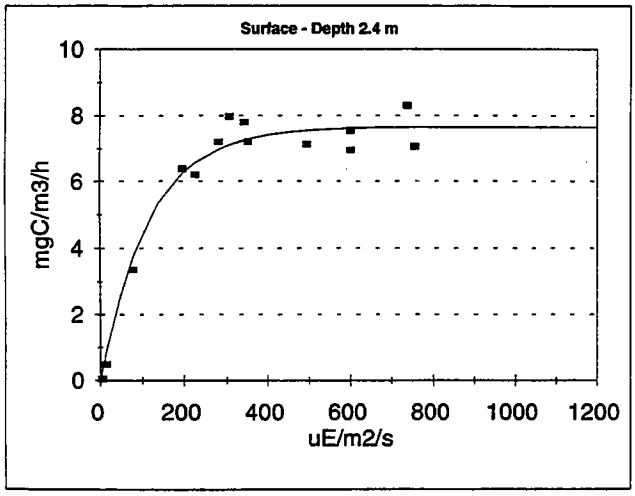

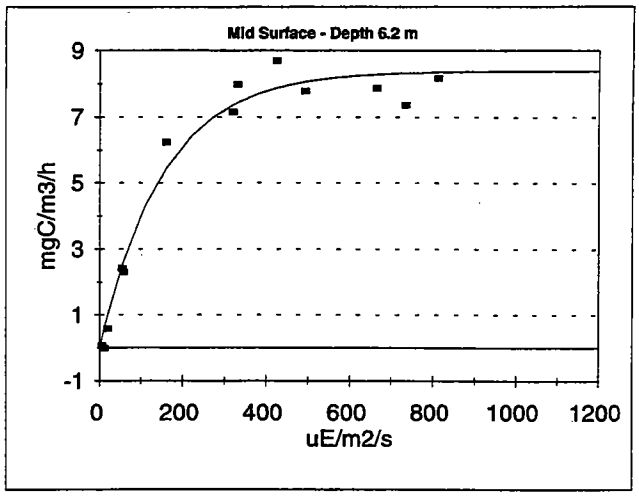

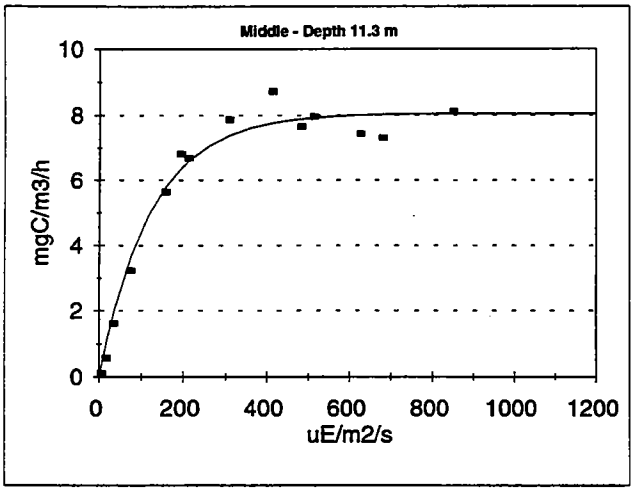

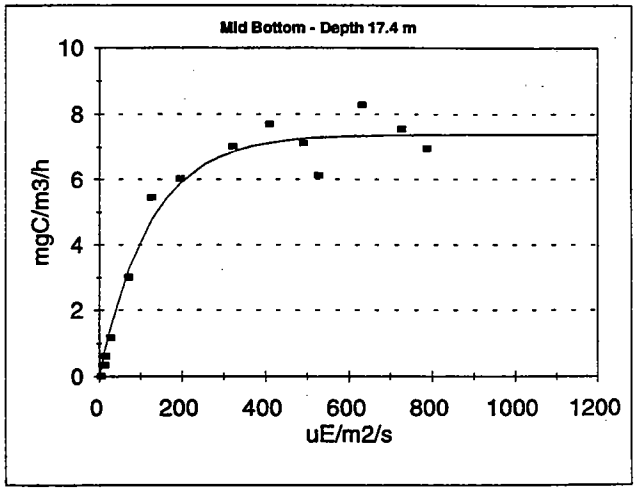

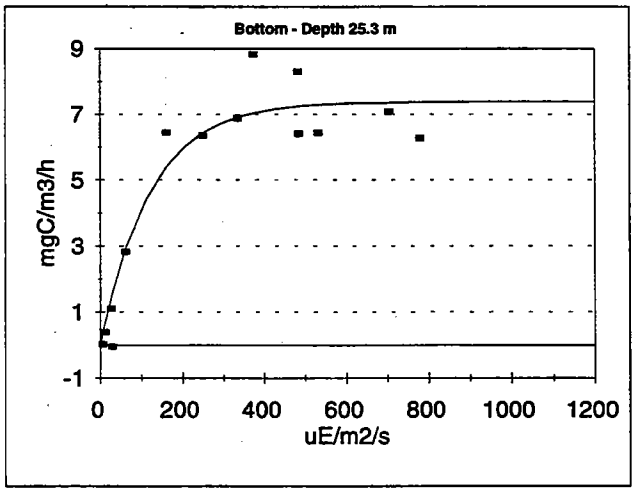

W9517 Station N04

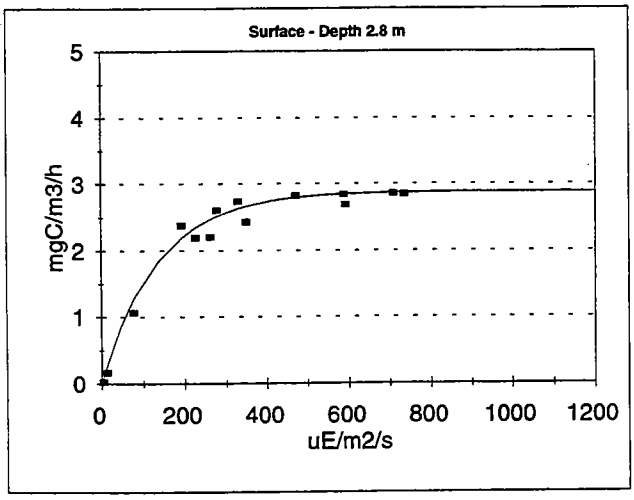

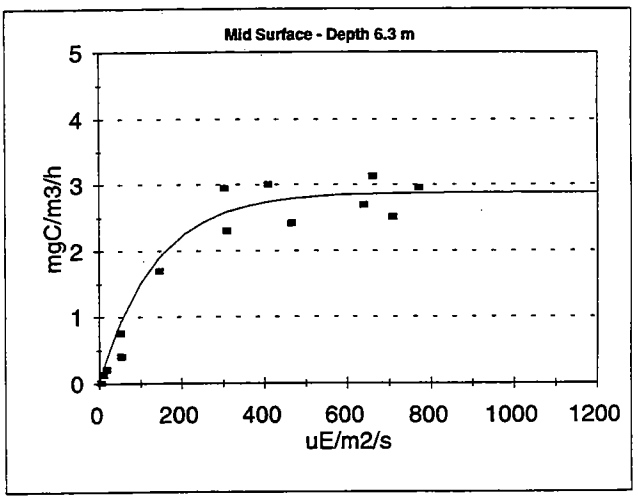

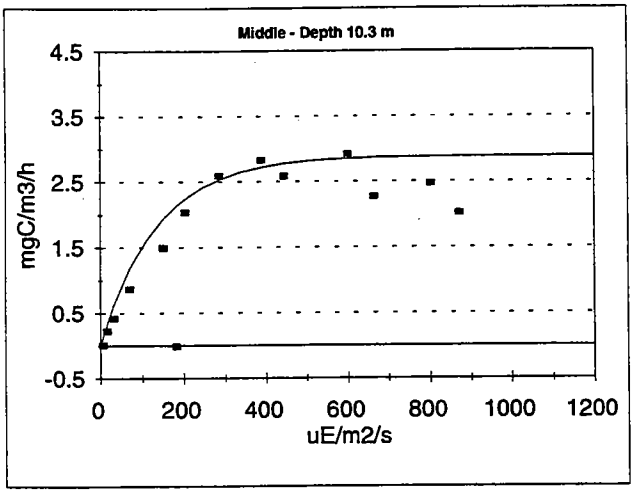

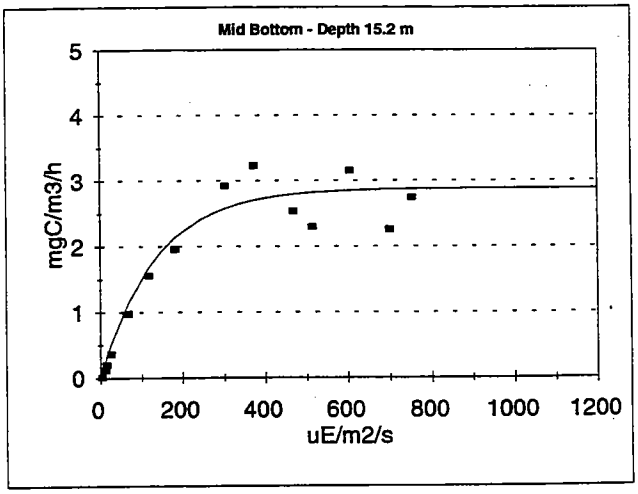

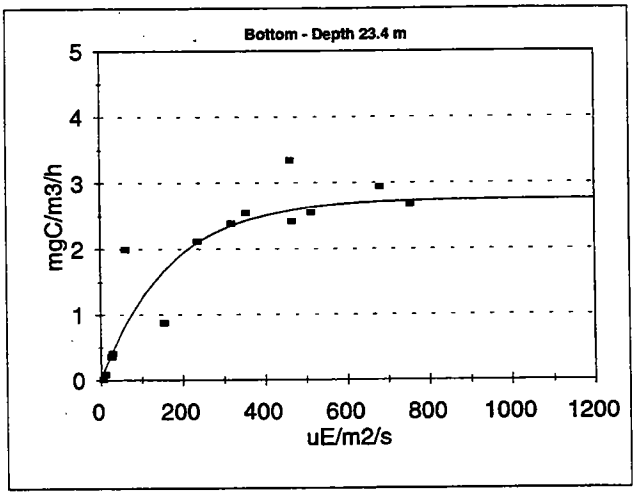

W9517 Station N16

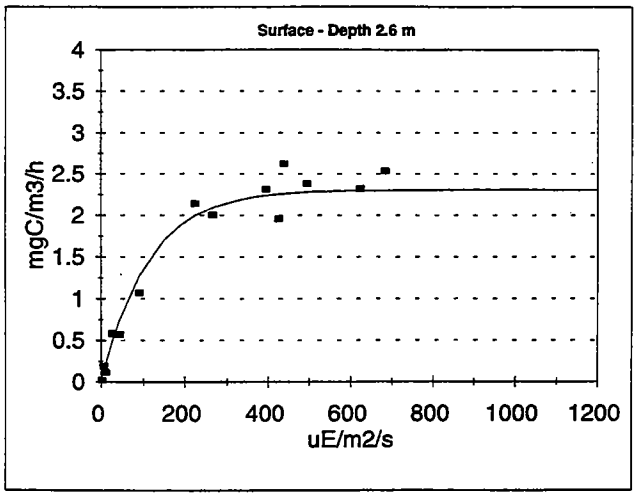

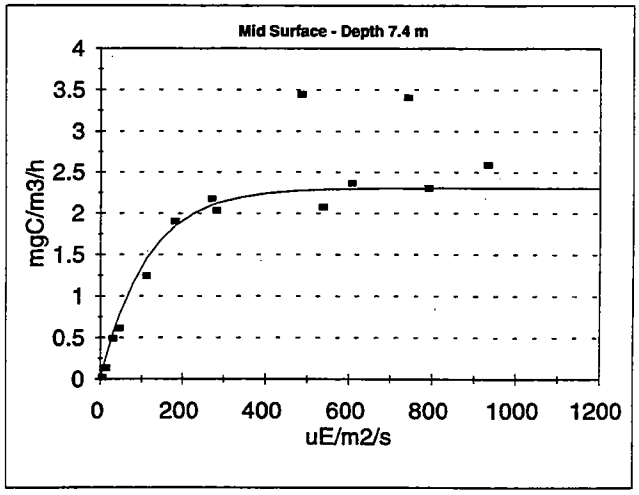

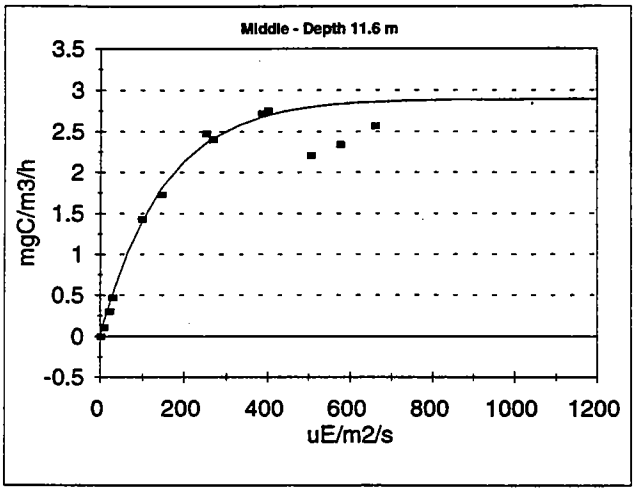

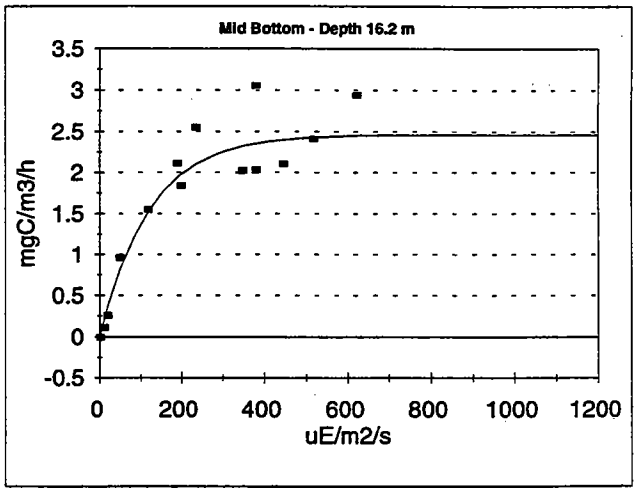

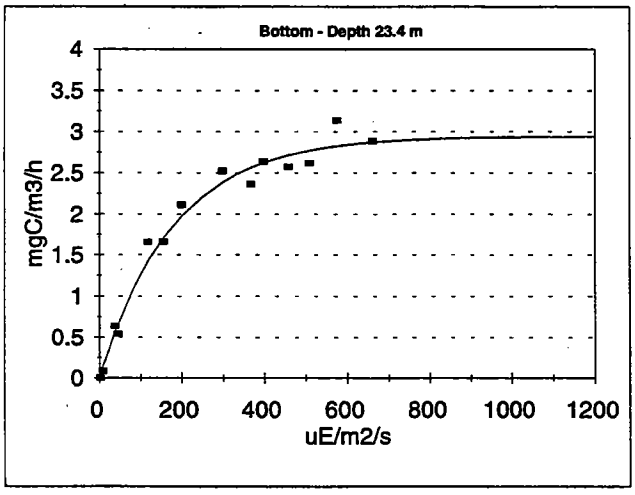

APPENDIX C

Event: W9501

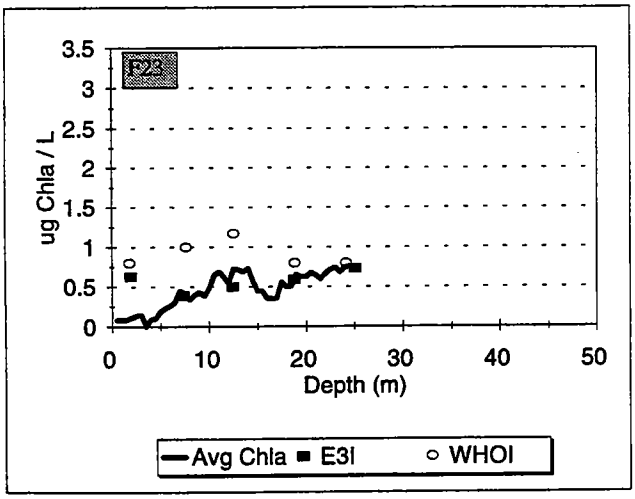
F23
ug Chla / L
Depth (m)
Avg Chla
E3I
WHOI

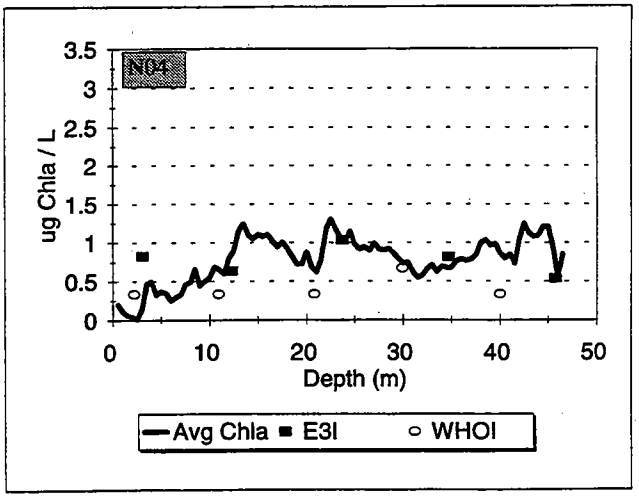
N04
ug Chla / L
Depth (m)
Avg Chla
E3I
WHOI

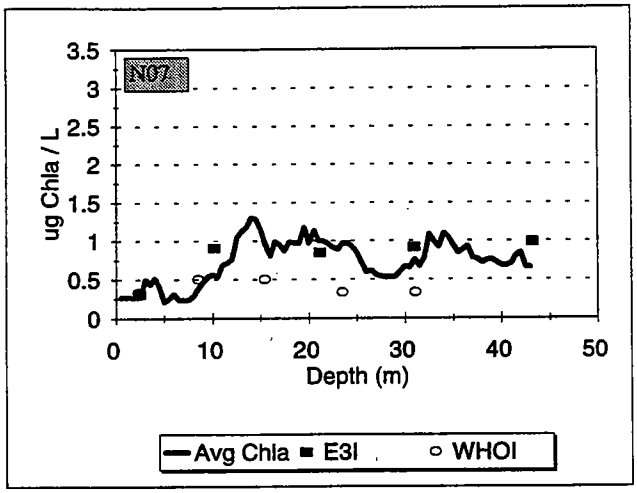
N07
ug Chla / L
Depth (m)
Avg Chla
E3I
WHOI

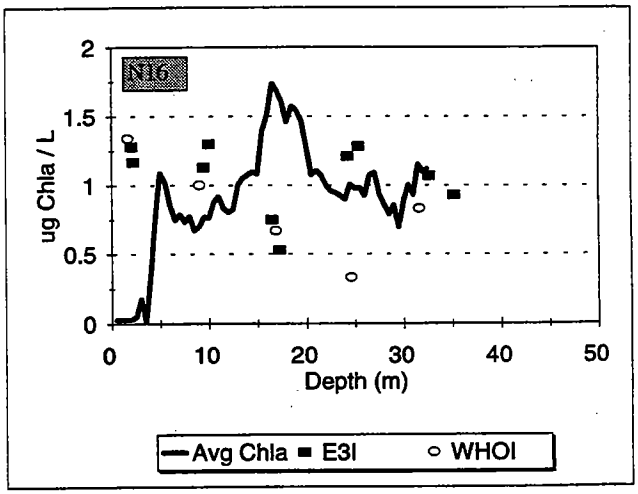
N16
ug Chla / L
Depth (m)
Avg Chla
E3I
WHOI

Event: W9502

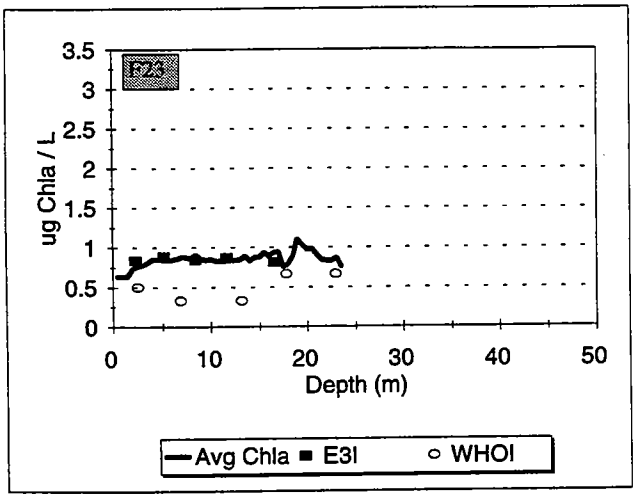
F24
ug Chla / L
Depth (m)
Avg Chla
E3I
WHOI

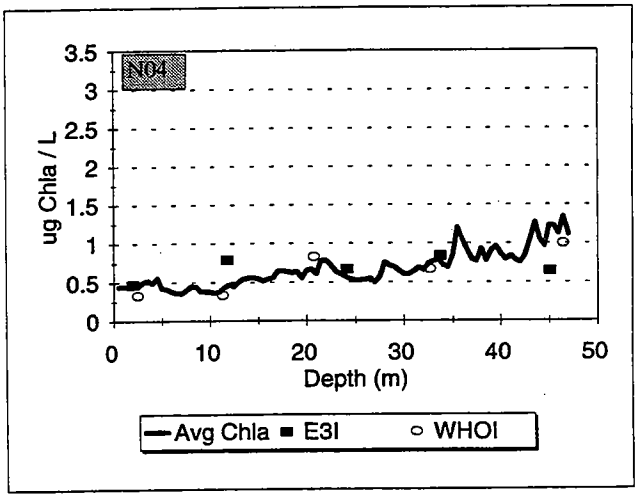
N04
ug Chla / L
Depth (m)
Avg Chla
E3I
WHOI

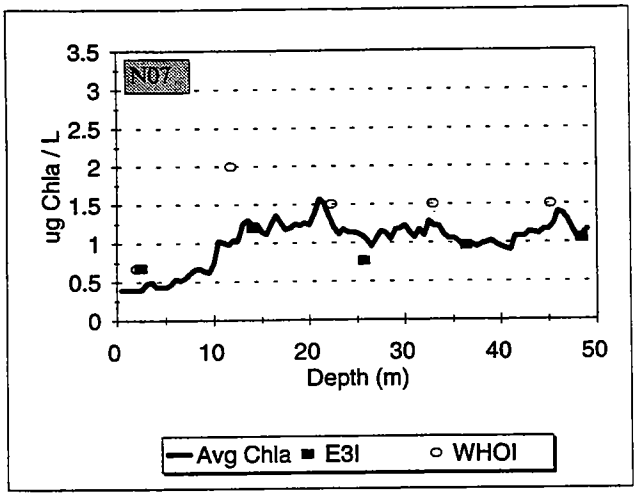
N07
ug Chla / L
Depth (m)
Avg Chla
E3I
WHOI

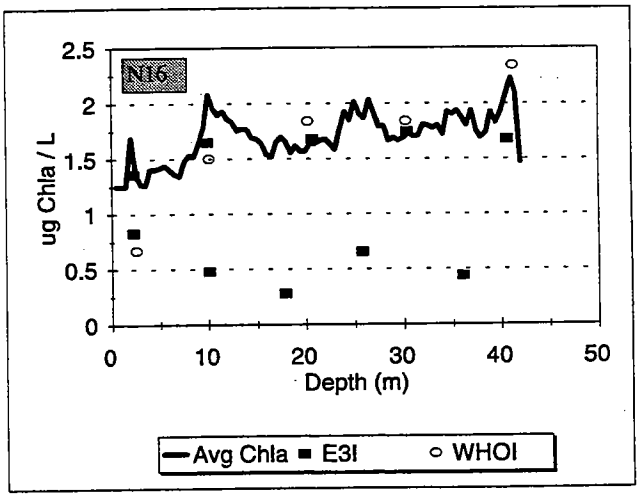
N16
ug Chla / L
Depth (m)
Avg Chla
E3I
WHOI

Event: W9503

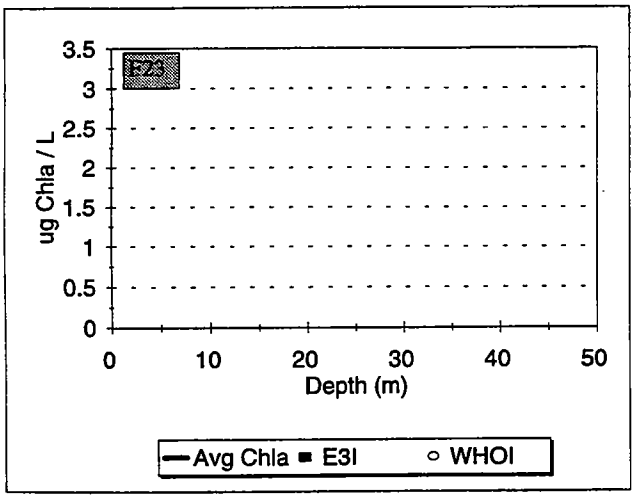
E23
ug Chla / L
3.5
3
2.5
2
1.5
1
0.5
0
0 10 20 30 40 50
Depth (m)
Avg Chla E3I WHOI

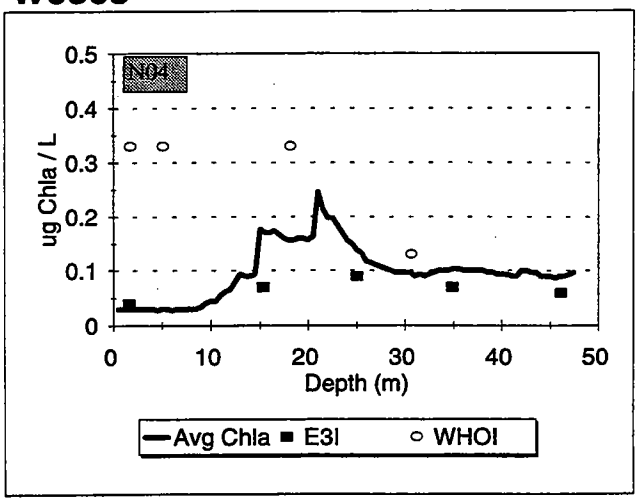
N04
ug Chla / L
0.5
0.4
0.3
0.2
0.1
0
0 10 20 30 40 50
Depth (m)
Avg Chla E3I WHOI

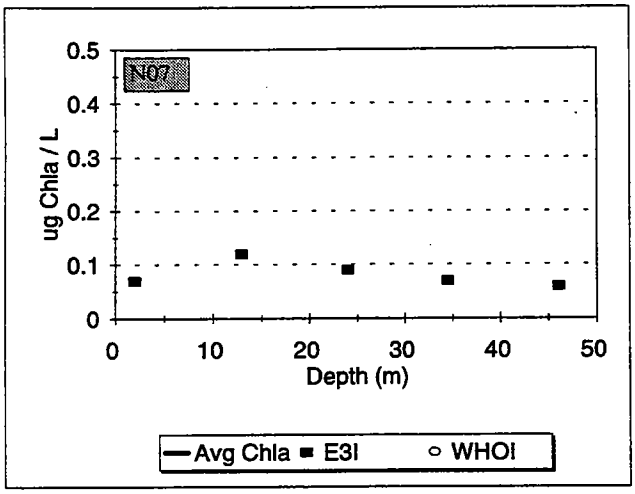
N07
ug Chla / L
0.5
0.4
0.3
0.2
0.1
0
0 10 20 30 40 50
Depth (m)
Avg Chla E3I WHOI

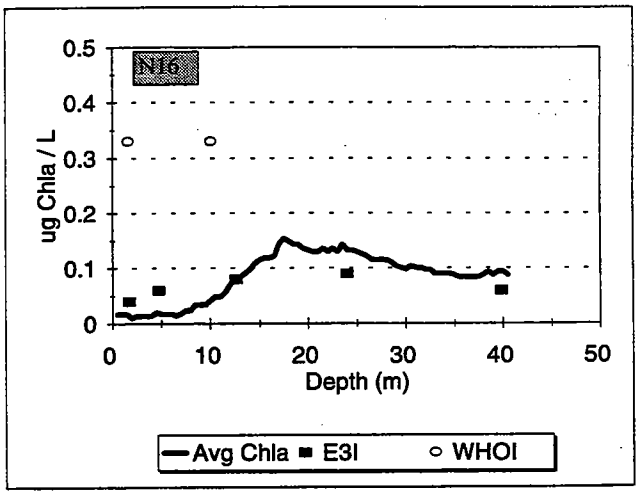
N16
ug Chla / L
0.5
0.4
0.3
0.2
0.1
0
0 10 20 30 40 50
Depth (m)
Avg Chla E3I WHOI

Event: W9504

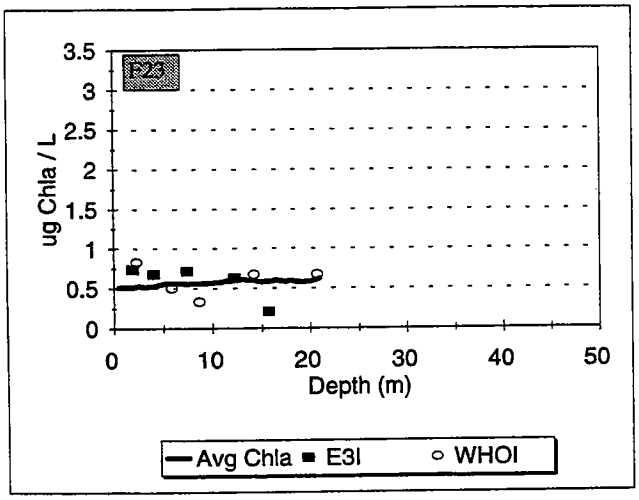

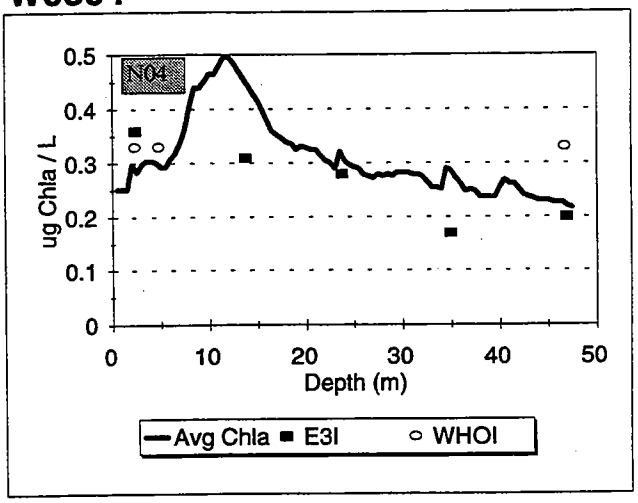

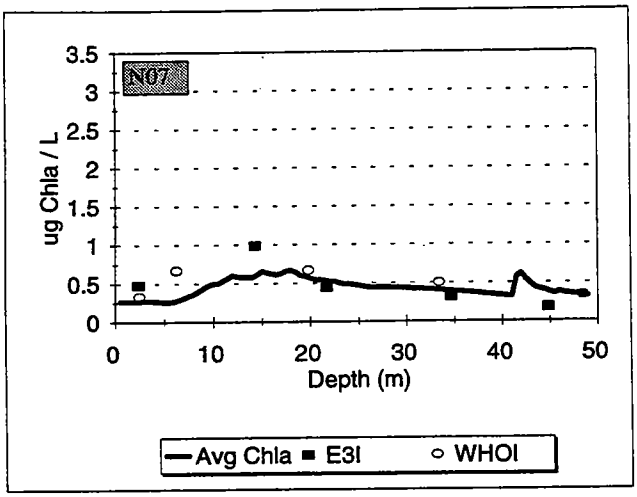

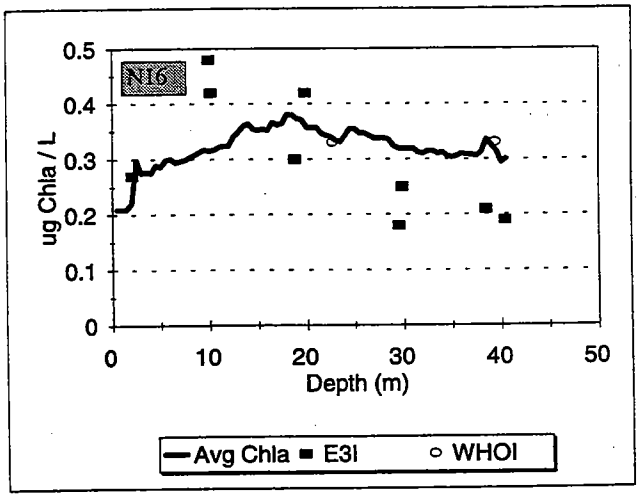

4

Event: W9505

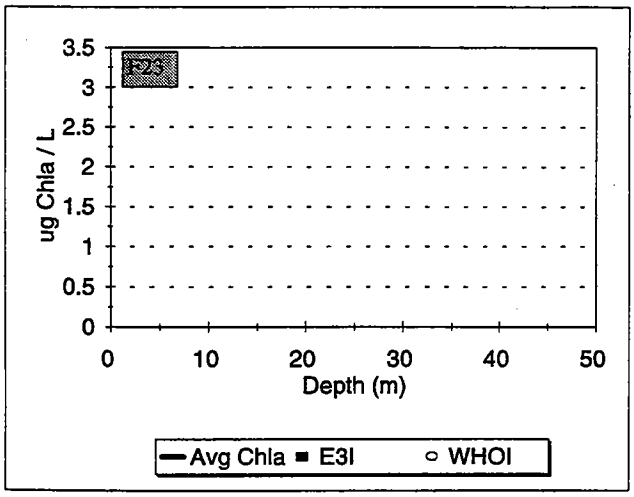
P25
ug Chla / L
Depth (m)
Avg Chla
E3I
WHOI

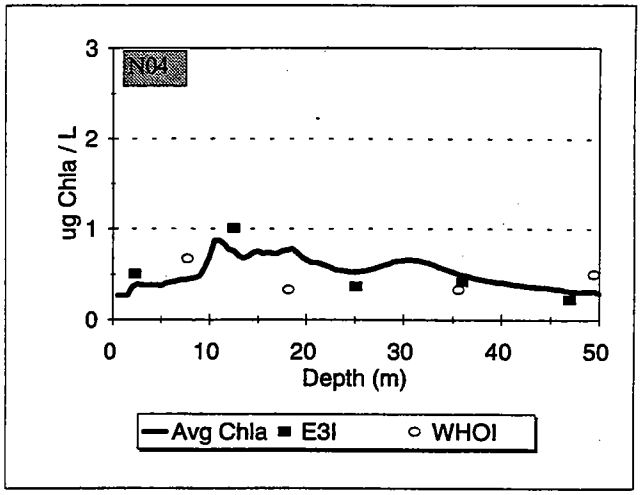
N04
ug Chla / L
Depth (m)
Avg Chla
E3I
WHOI

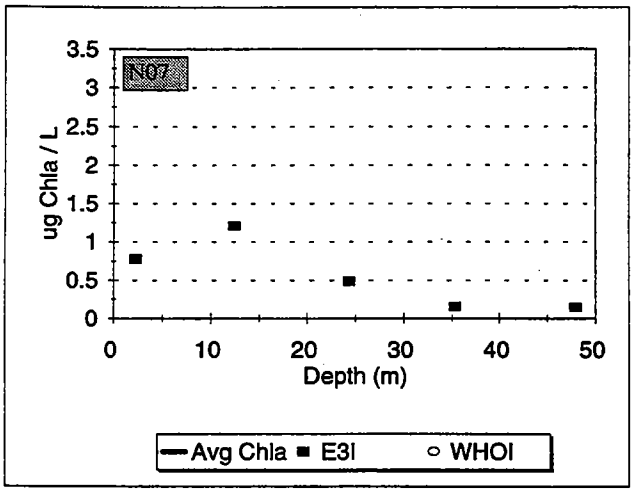
N07
ug Chla / L
Depth (m)
Avg Chla
E3I
WHOI

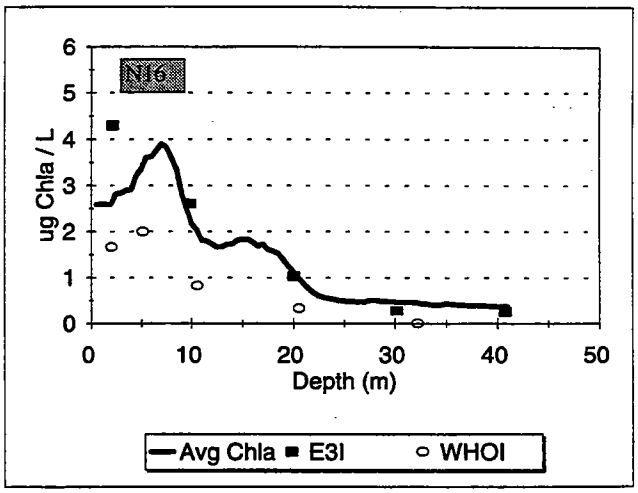
N16
ug Chla / L
Depth (m)
Avg Chla
E3I
WHOI

Event: W9506

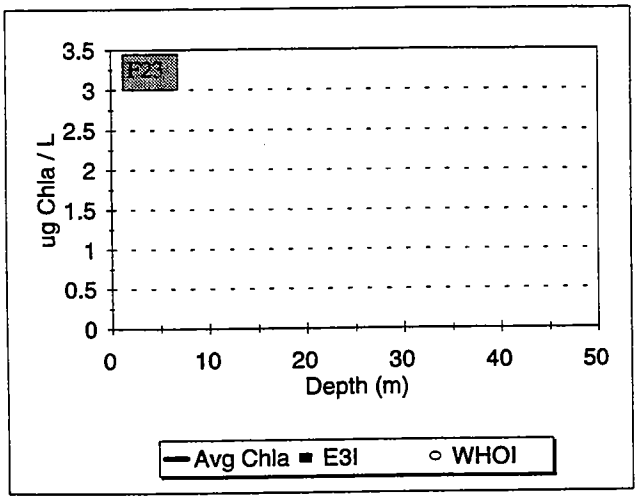
P23
ug Chla / L
Depth (m)
Avg Chla
E3I
WHOI

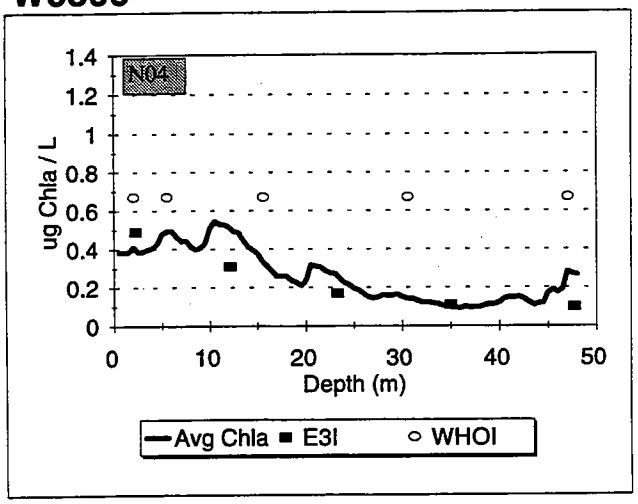
N04
ug Chla / L
Depth (m)
Avg Chla
E3I
WHOI

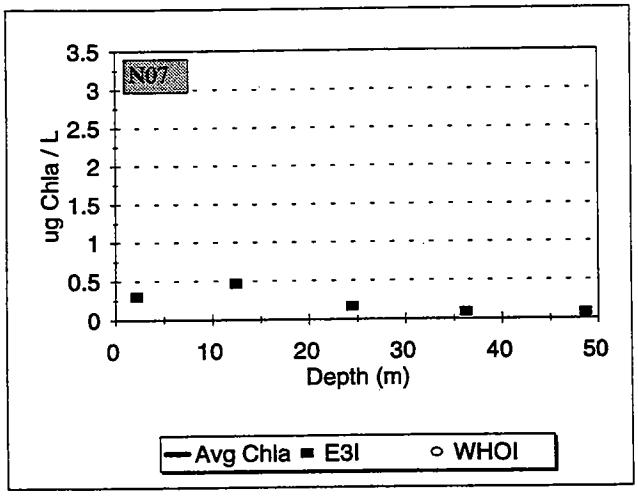
N07
ug Chla / L
Depth (m)
Avg Chla
E3I
WHOI

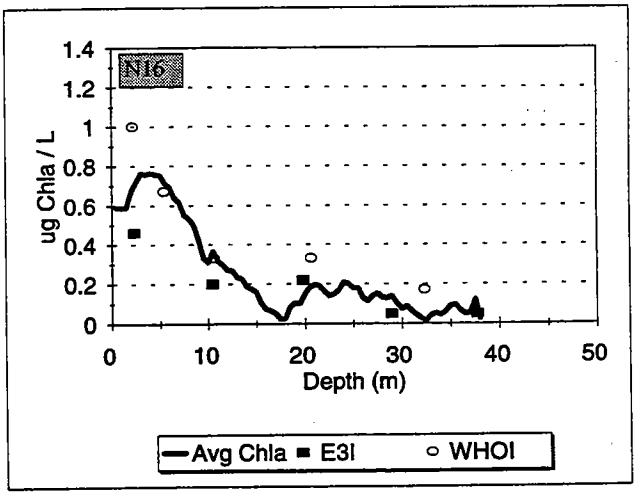
N16
ug Chla / L
Depth (m)
Avg Chla
E3I
WHOI

Event: W9507

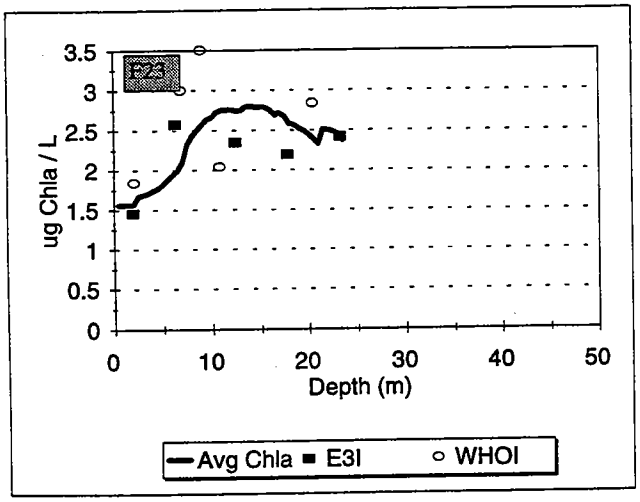
E23
ug Chla / L
Depth (m)
Avg Chla
E3I
WHOI

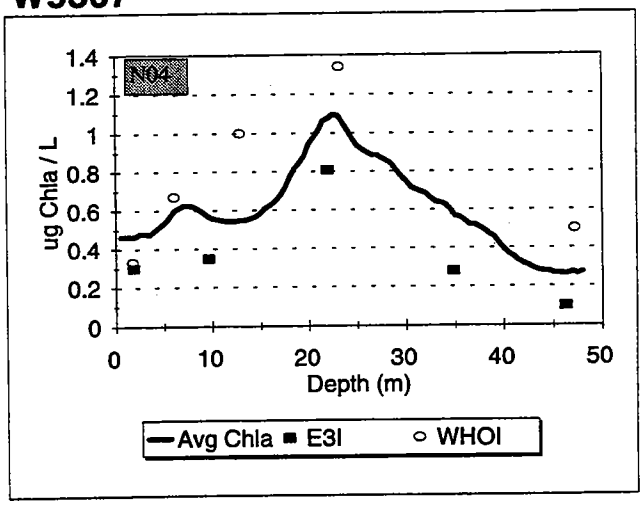
N04
ug Chla / L
Depth (m)
Avg Chla
E3I
WHOI

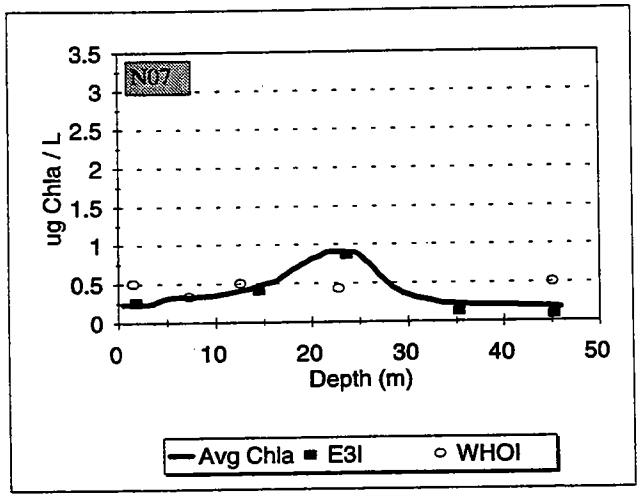
N07
ug Chla / L
Depth (m)
Avg Chla
E3I
WHOI

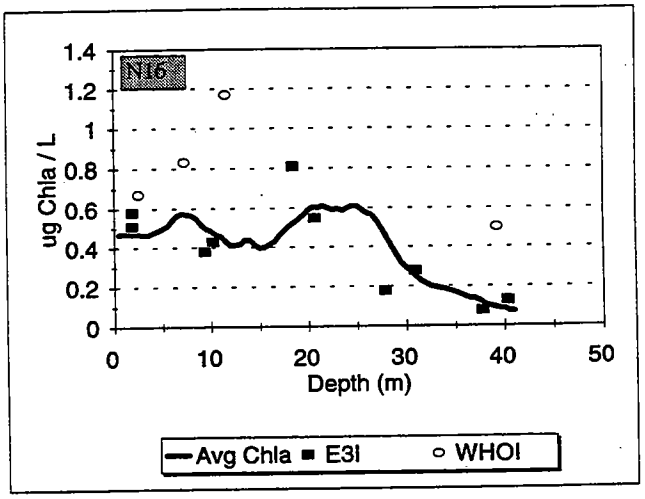
N16
ug Chla / L
Depth (m)
Avg Chla
E3I
WHOI

Event: W9508

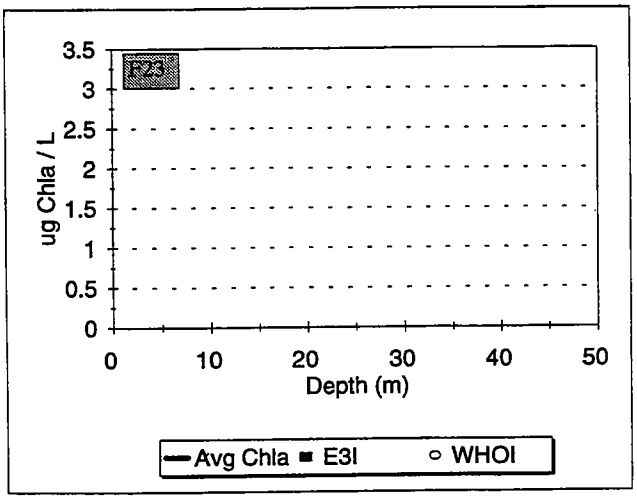
F23
ug Chla / L
Depth (m)
Avg Chla
E3I
WHOI

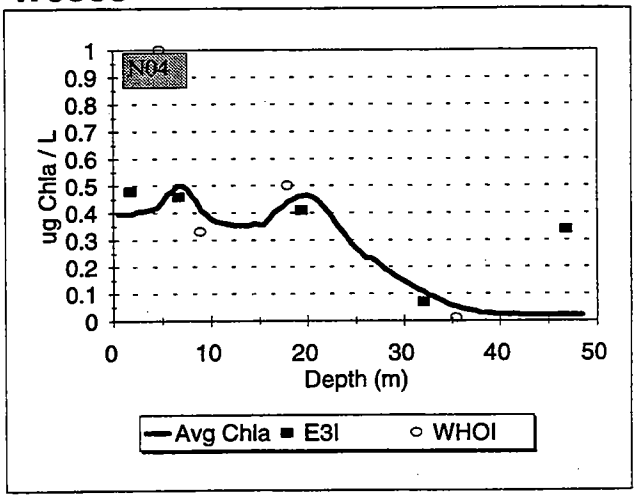
N04
ug Chla / L
Depth (m)
Avg Chla
E3I
WHOI

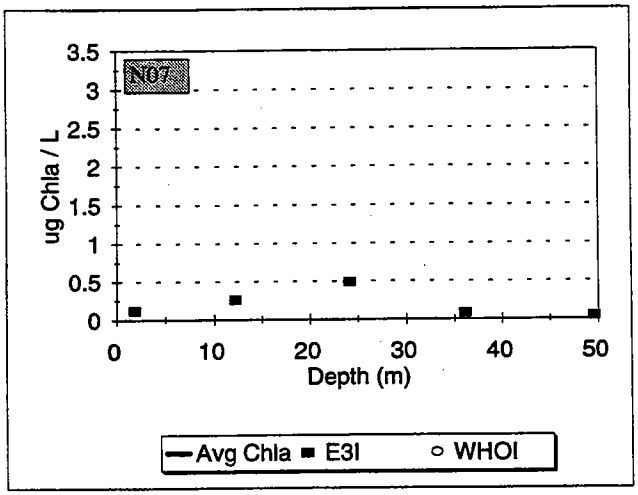
N07
ug Chla / L
Depth (m)
Avg Chla
E3I
WHOI

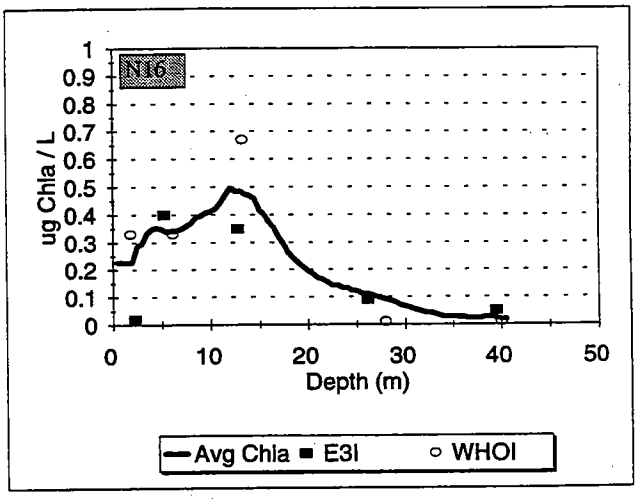
N16
ug Chla / L
Depth (m)
Avg Chla
E3I
WHOI

Event: W9509

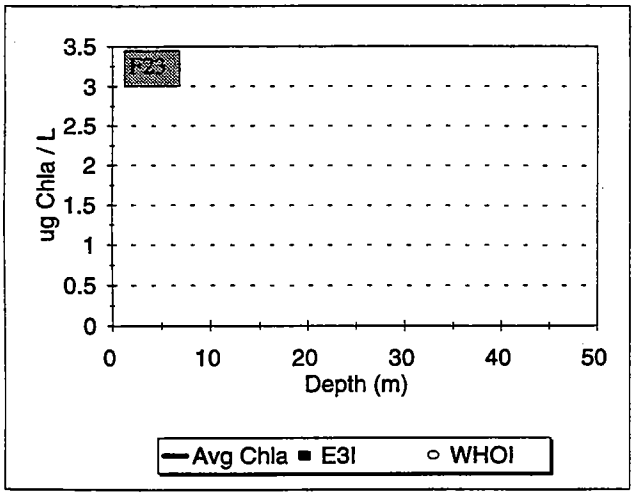
F23
ug Chla / L
Depth (m)
Avg Chla
E3I
WHOI

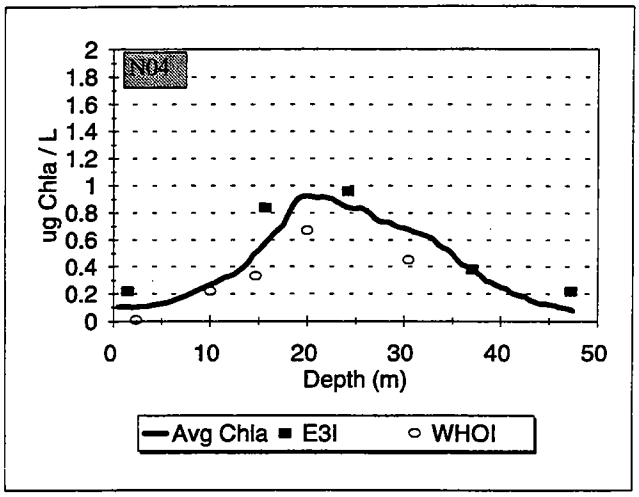
N04
ug Chla / L
Depth (m)
Avg Chla
E3I
WHOI

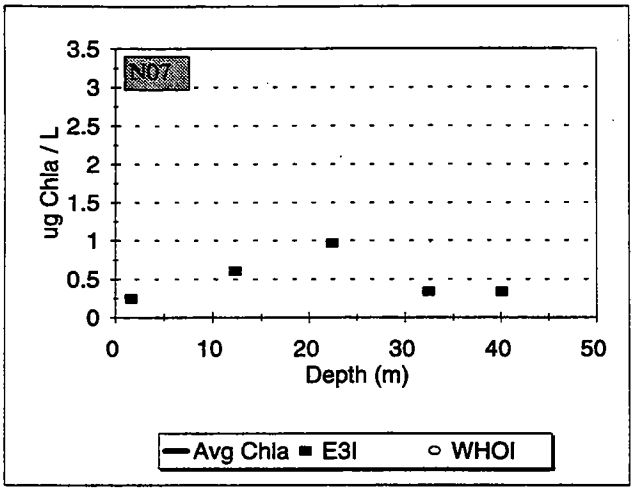
N07
ug Chla / L
Depth (m)
Avg Chla
E3I
WHOI

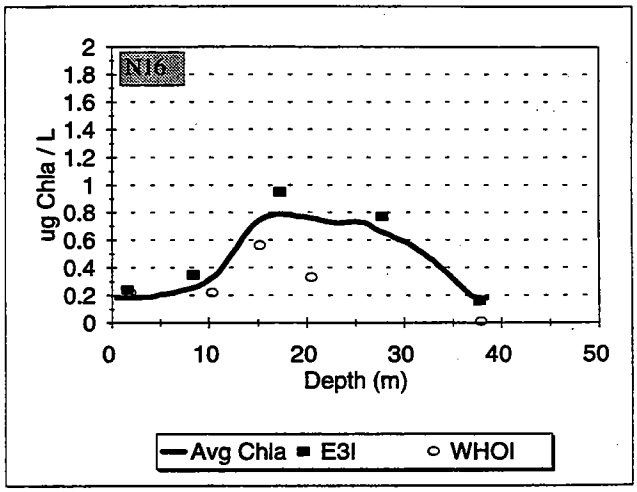
N16
ug Chla / L
Depth (m)
Avg Chla
E3I
WHOI

Event: W9510

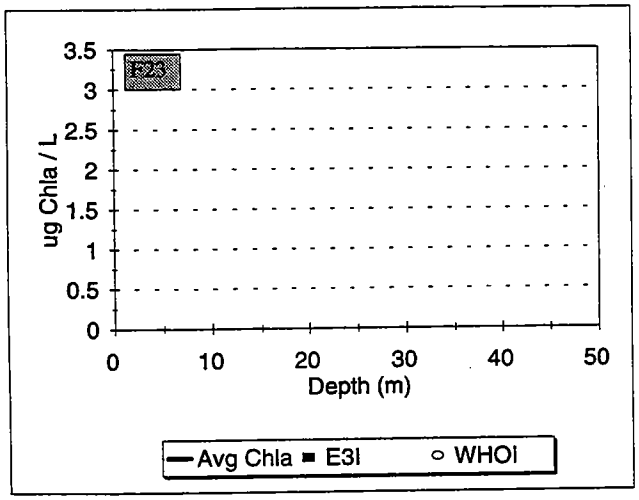
F23
ug Chla / L
Depth (m)
Avg Chla
E3I
WHOI

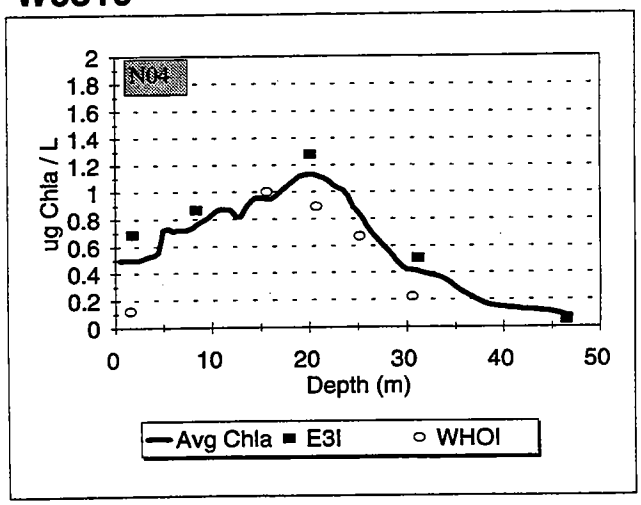
N04
ug Chla / L
Depth (m)
Avg Chla
E3I
WHOI

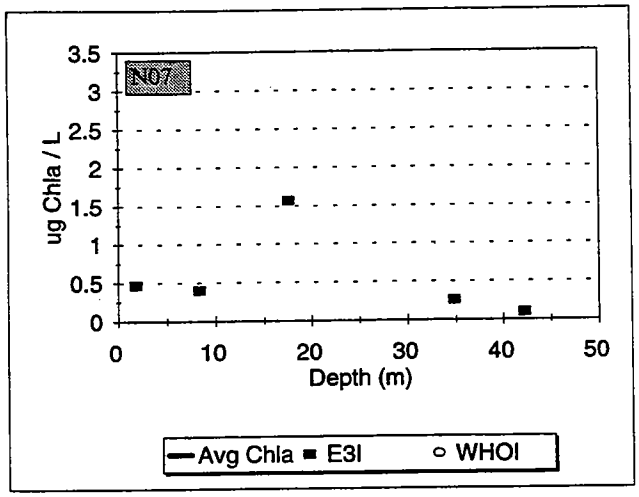
N07
ug Chla / L
Depth (m)
Avg Chla
E3I
WHOI

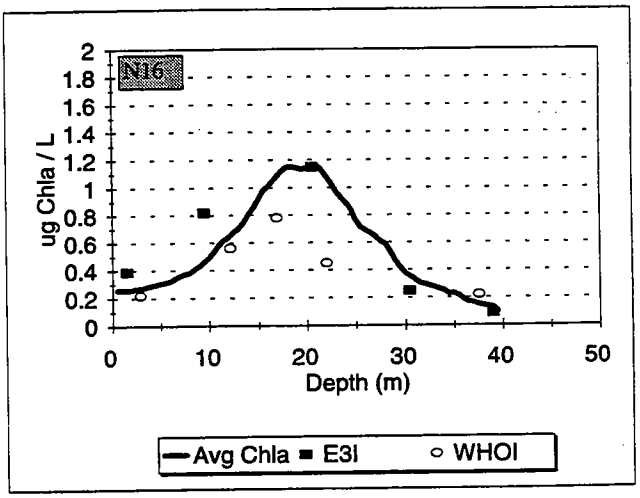
N16
ug Chla / L
Depth (m)
Avg Chla
E3I
WHOI

Event: W9511

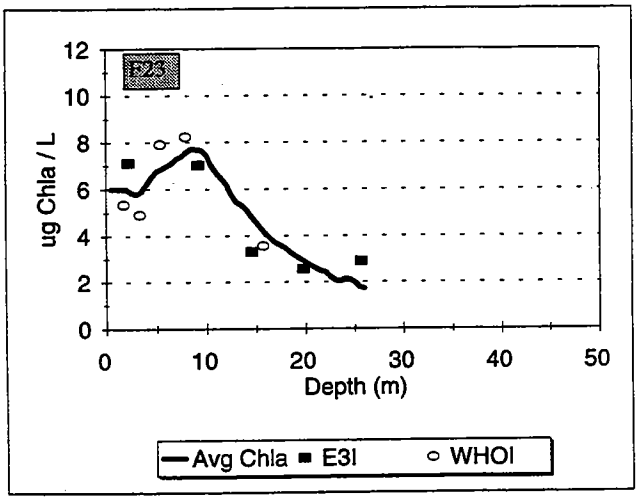
F25
ug Chla / L
Depth (m)
Avg Chla
E3I
WHOI

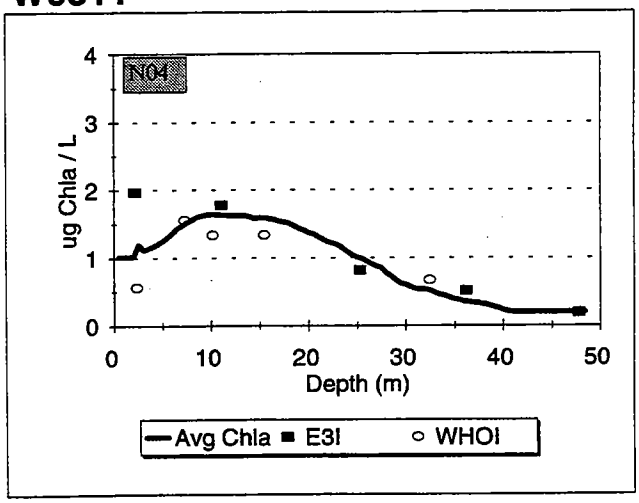
N04
ug Chla / L
Depth (m)
Avg Chla
E3I
WHOI

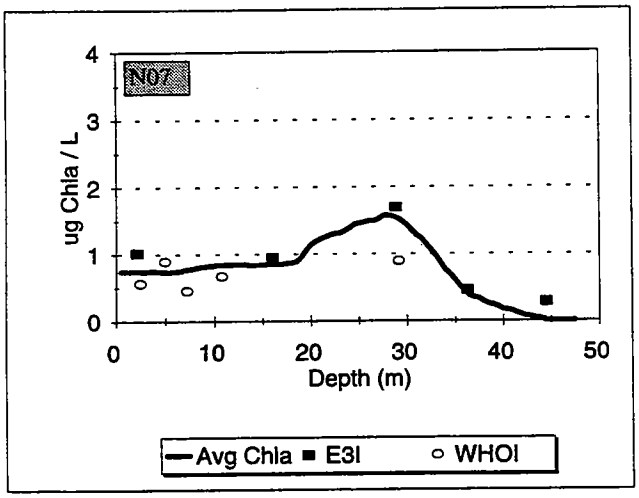
N07
ug Chla / L
Depth (m)
Avg Chla
E3I
WHOI

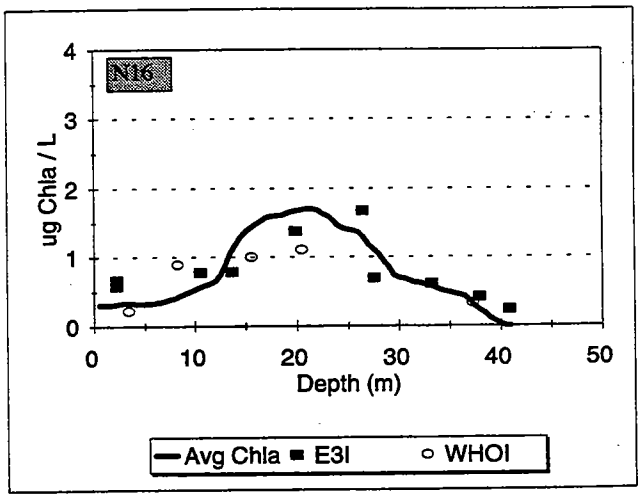
N16
ug Chla / L
Depth (m)
Avg Chla
E3I
WHOI

Event: W9512

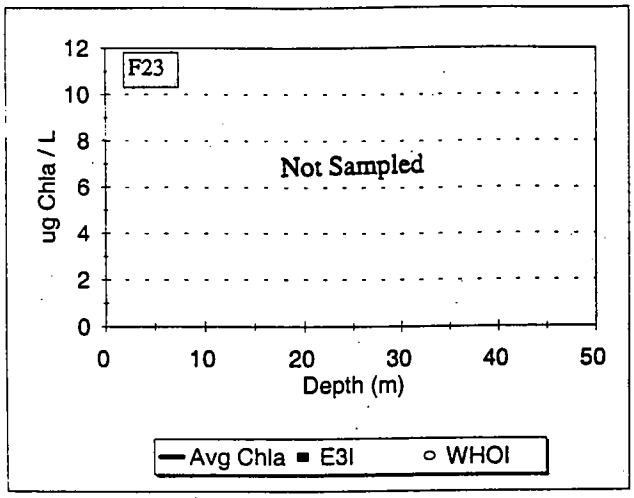
F23
Not Sampled
ug Chla / L
Depth (m)
Avg Chla
E3I
WHOI

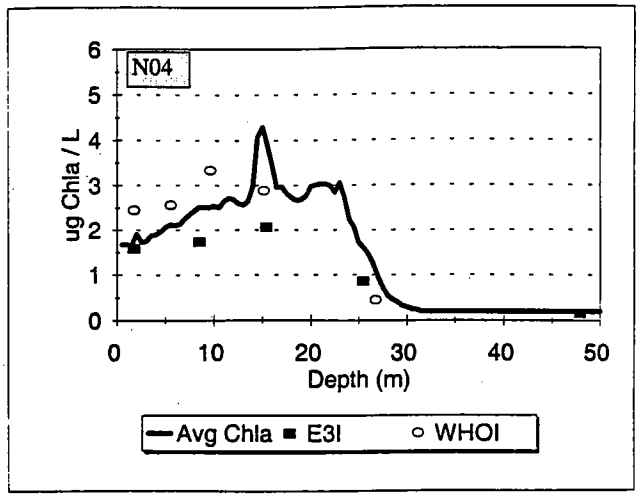
N04
ug Chla / L
Depth (m)
Avg Chla
E3I
WHOI

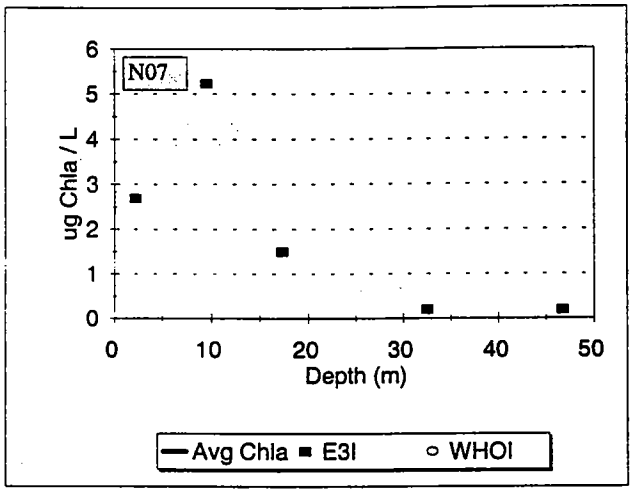
N07
ug Chla / L
Depth (m)
Avg Chla
E3I
WHOI

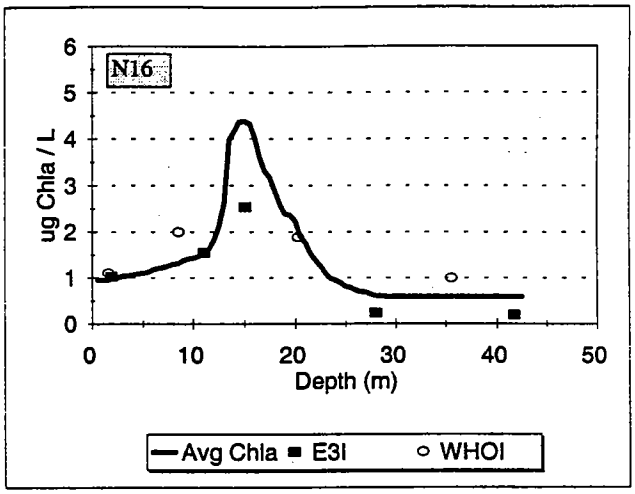
N16
ug Chla / L
Depth (m)
Avg Chla
E3I
WHOI

Event: W9513

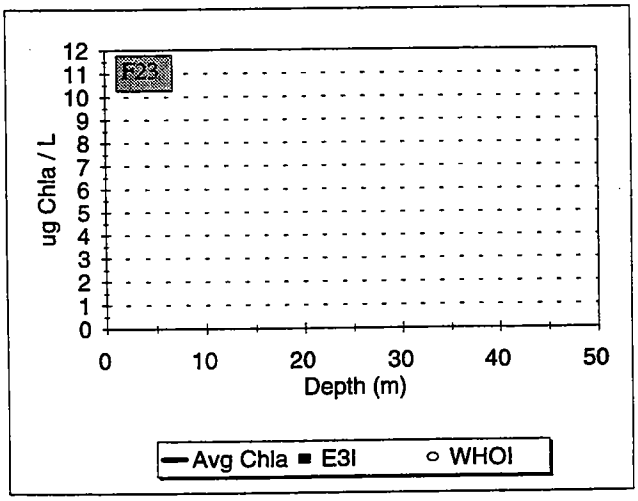
F23
ug Chla / L
Depth (m)
Avg Chla
E3I
WHOI

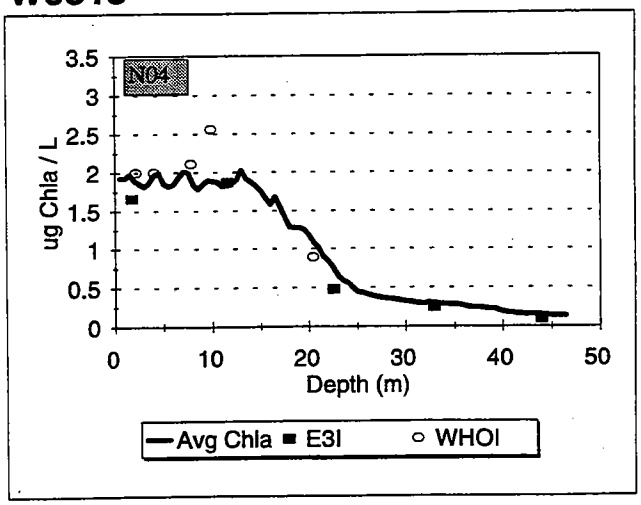
N04
ug Chla / L
Depth (m)
Avg Chla
E3I
WHOI

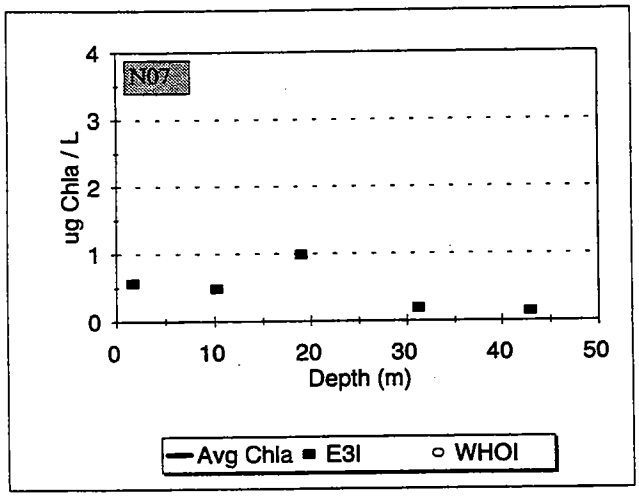
N07
ug Chla / L
Depth (m)
Avg Chla
E3I
WHOI

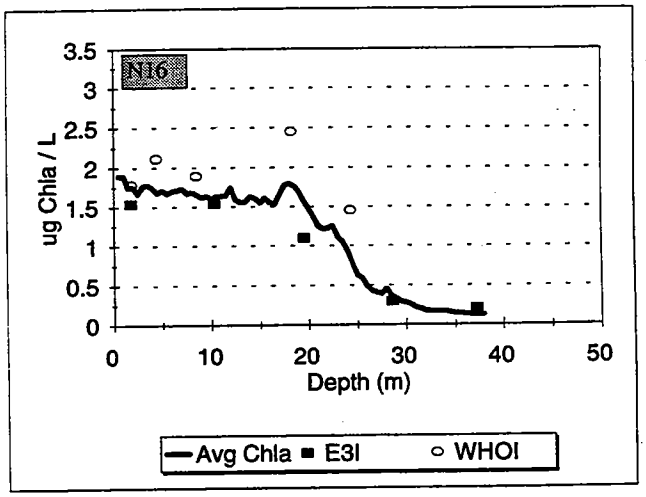
N16
ug Chla / L
Depth (m)
Avg Chla
E3I
WHOI

Event: W9514

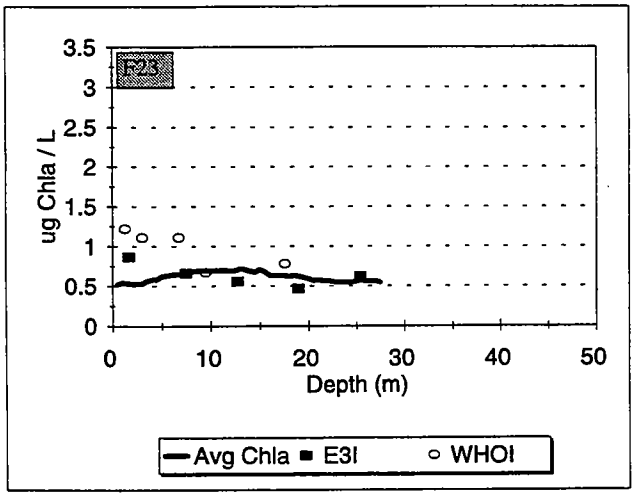
F23
ug Chla / L
Depth (m)
Avg Chla
E3I
WHOI

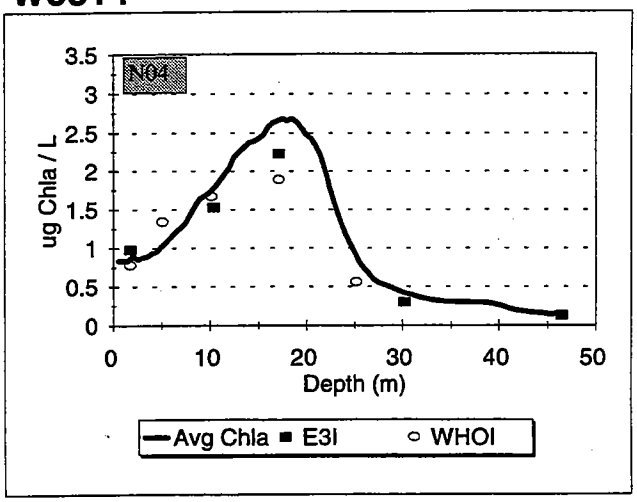
N04
ug Chla / L
Depth (m)
Avg Chla
E3I
WHOI

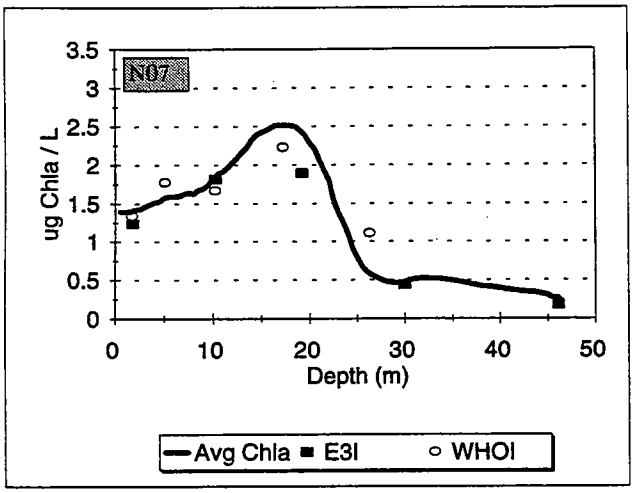
N07
ug Chla / L
Depth (m)
Avg Chla
E3I
WHOI

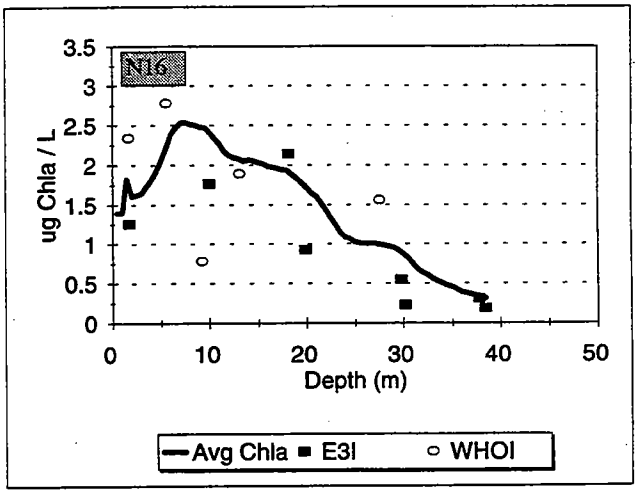
N16
ug Chla / L
Depth (m)
Avg Chla
E3I
WHOI

Event: W9515

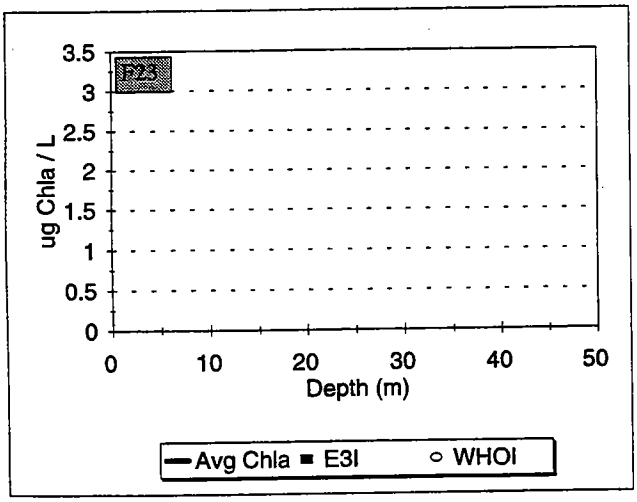
P23
ug Chla / L
Depth (m)
Avg Chla
E3I
WHOI

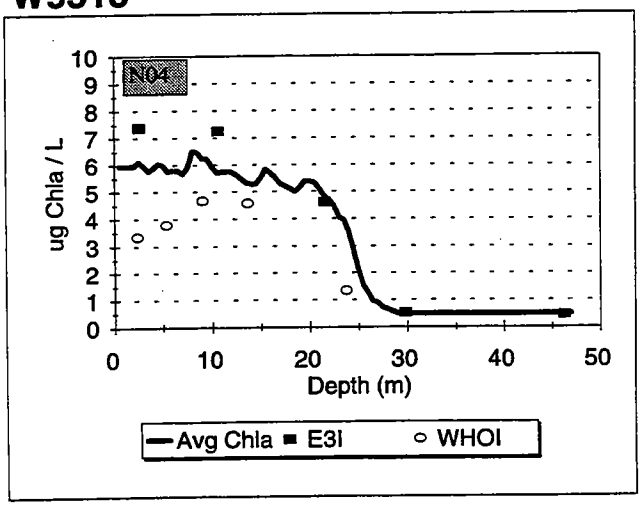
N04
ug Chla / L
Depth (m)
Avg Chla
E3I
WHOI

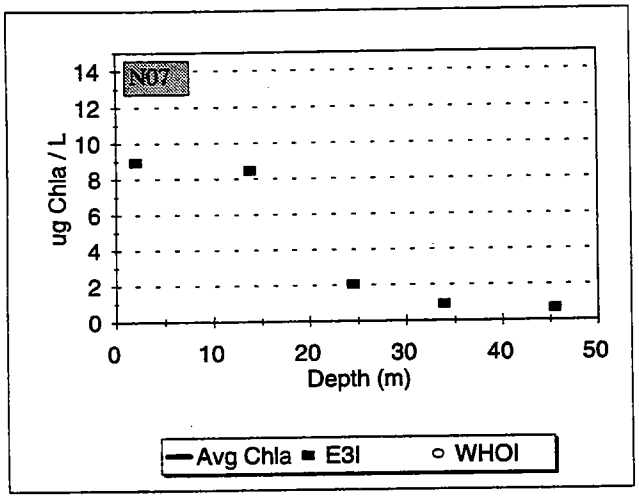
N07
ug Chla / L
Depth (m)
Avg Chla
E3I
WHOI

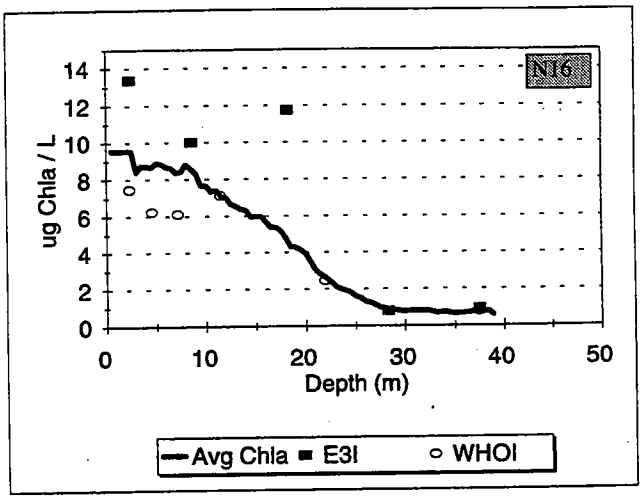
N16
ug Chla / L
Depth (m)
Avg Chla
E3I
WHOI

Event: W9516

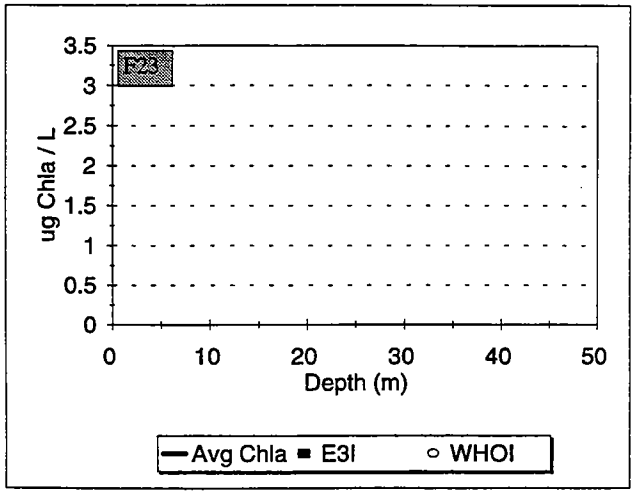
F23
ug Chla / L
Depth (m)
Avg Chla
E3I
WHOI

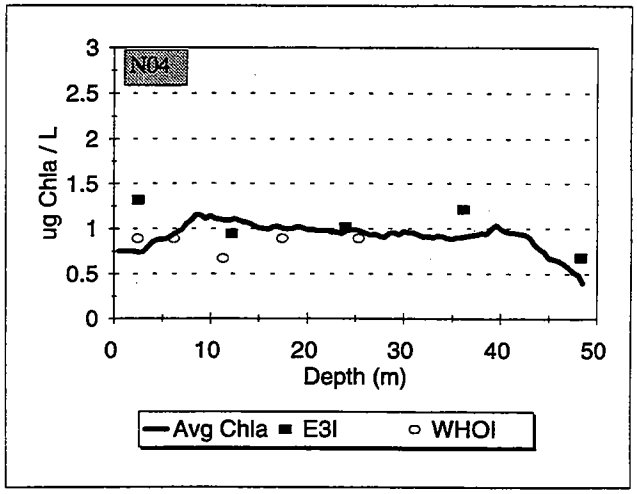
N04
ug Chla / L
Depth (m)
Avg Chla
E3I
WHOI

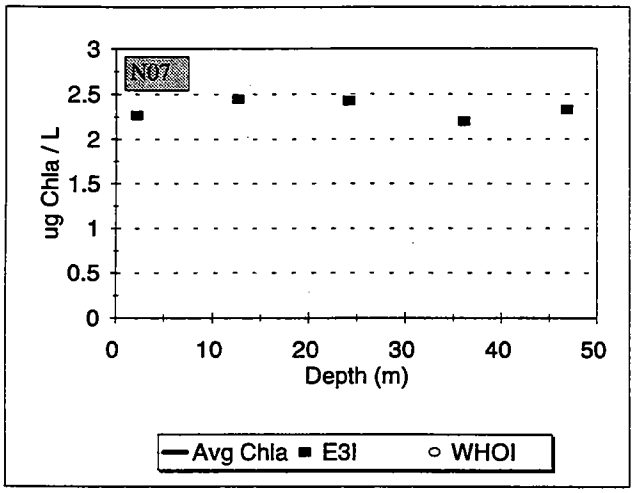
N07
ug Chla / L
Depth (m)
Avg Chla
E3I
WHOI

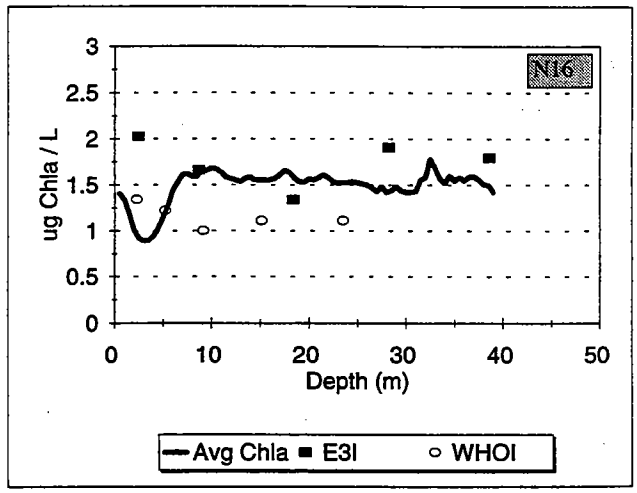
N16
ug Chla / L
Depth (m)
Avg Chla
E3I
WHOI

Event: W9517

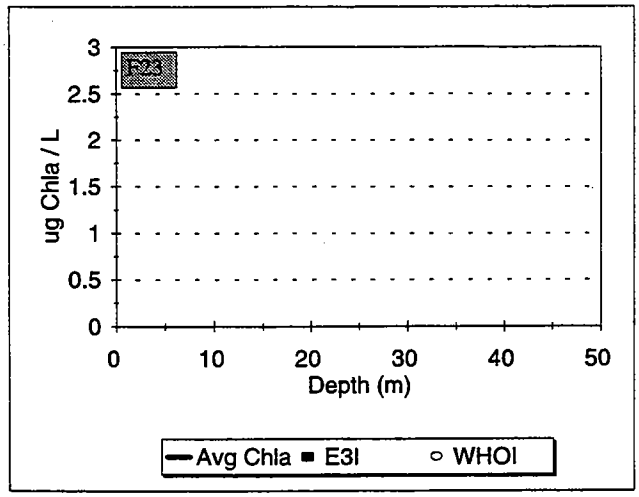
F23
ug Chla / L
3
2.5
2
1.5
1
0.5
0
0
10
20
30
40
50
Depth (m)
Avg Chla
E3I
WHOI

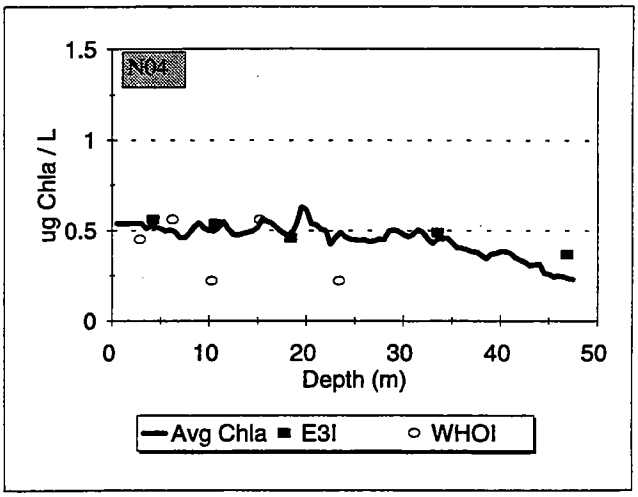
N04
ug Chla / L
1.5
1
0.5
0
0
10
20
30
40
50
Depth (m)
Avg Chla
E3I
WHOI

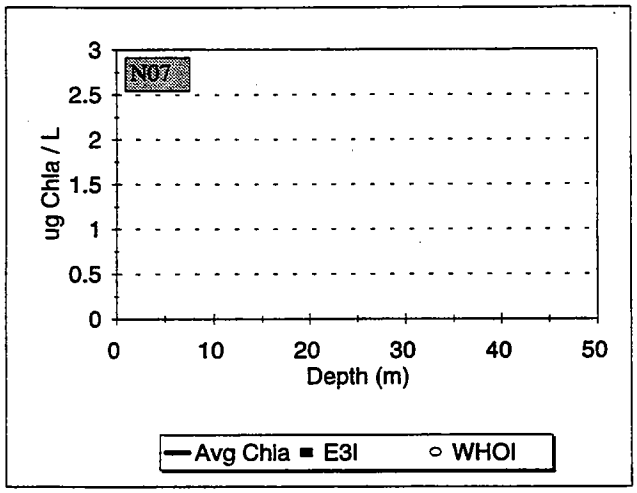
N07
ug Chla / L
3
2.5
2
1.5
1
0.5
0
0
10
20
30
40
50
Depth (m)
Avg Chla
E3I
WHOI

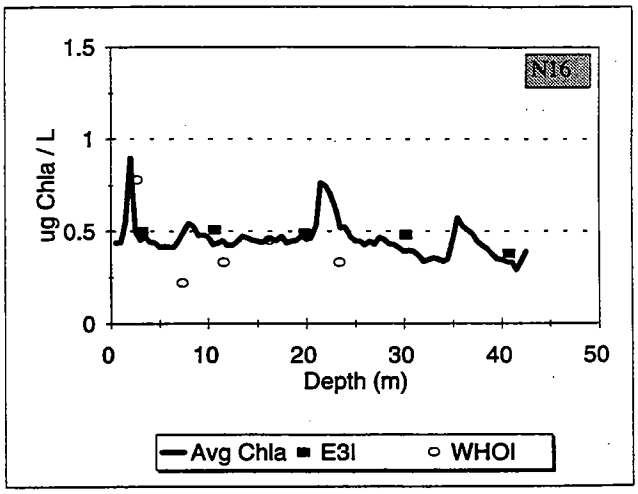
N16
ug Chla / L
1.5
1
0.5
0
0
10
20
30
40
50
Depth (m)
Avg Chla
E3I
WHOI

APPENDIX D

W9501

F23

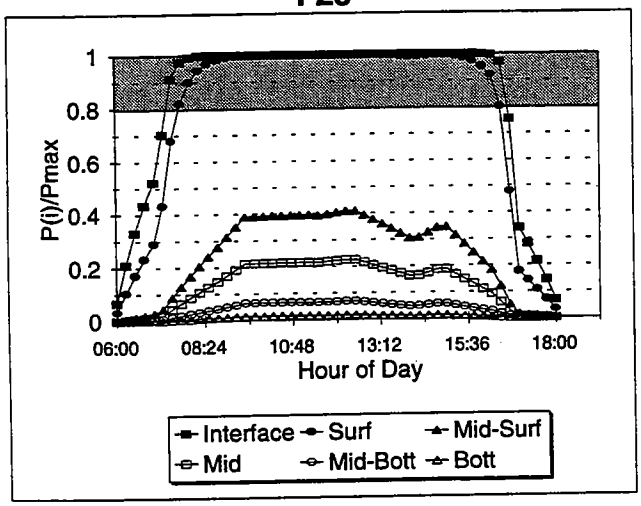

N04

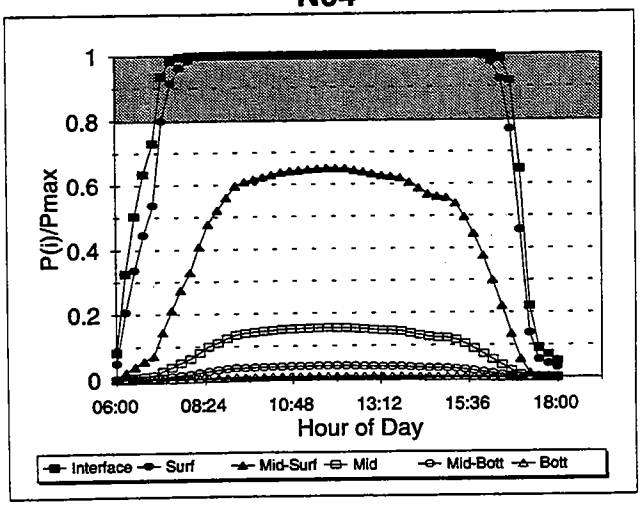

N07

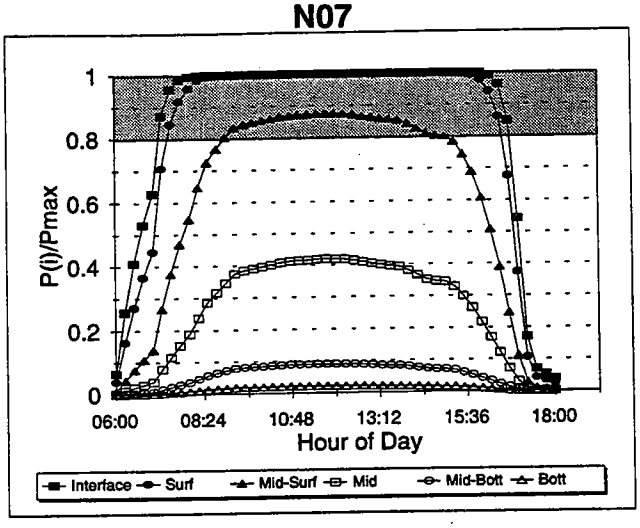

N16

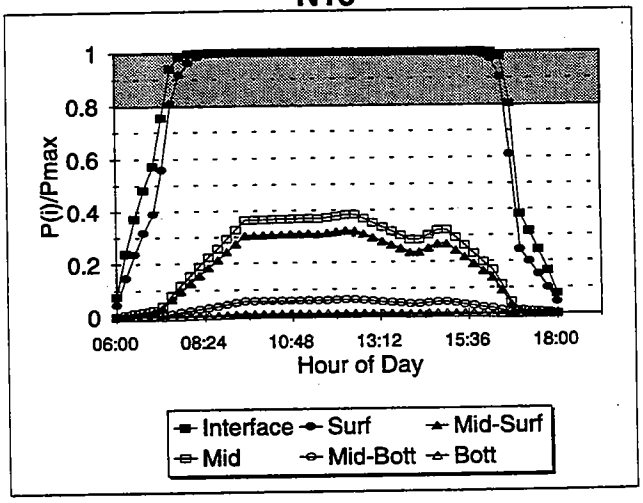

W9502

F23

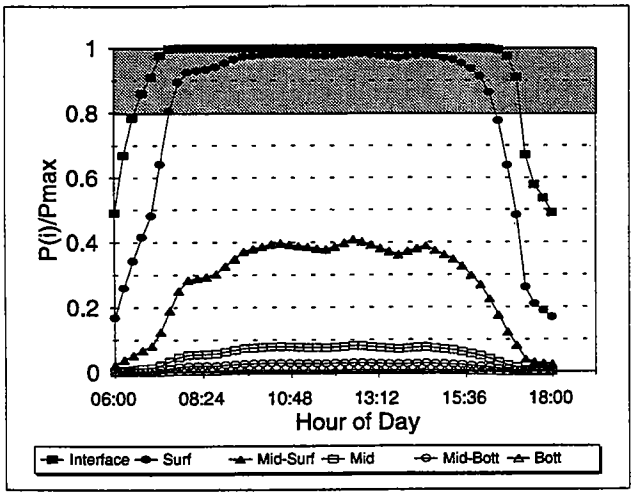

N04

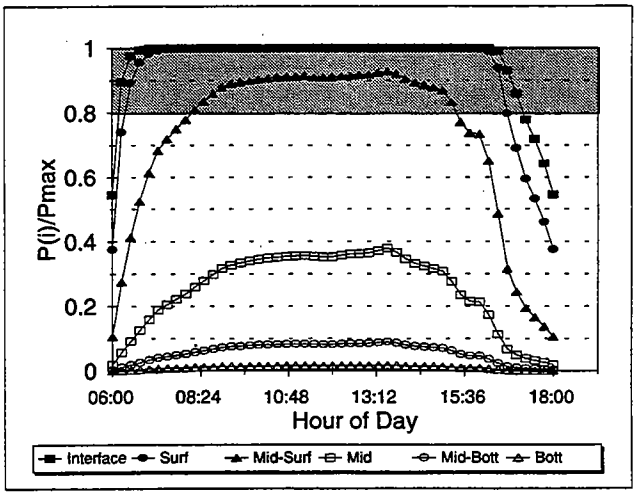

N07

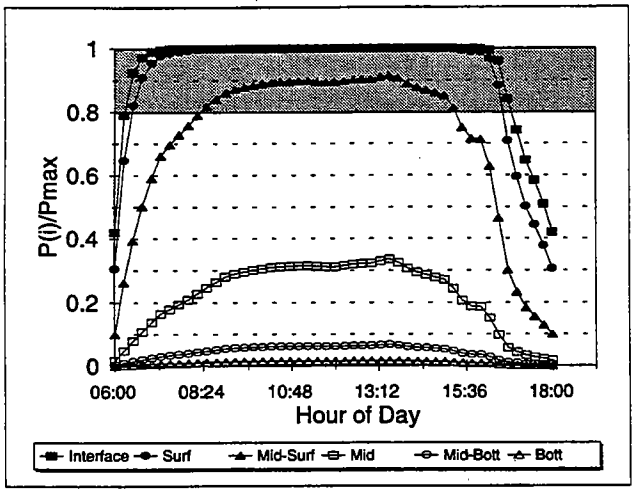

N16

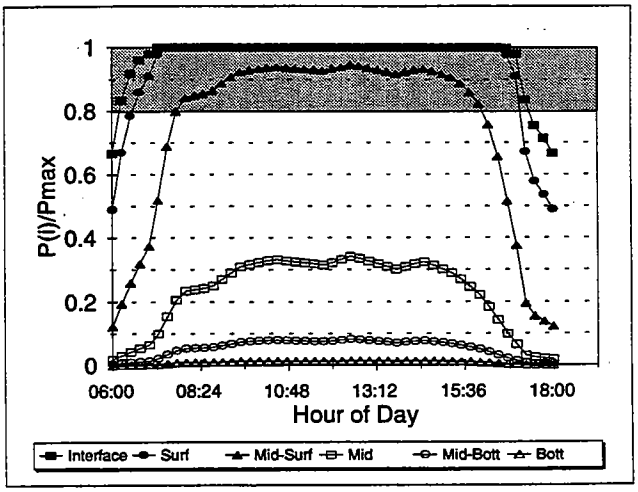

W9503

N04

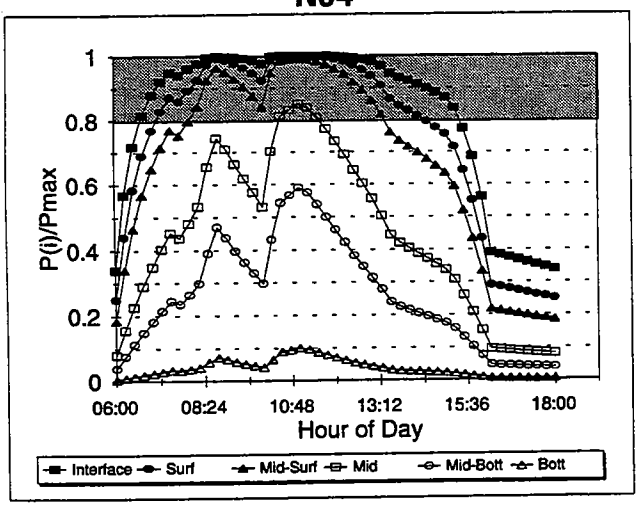

N16

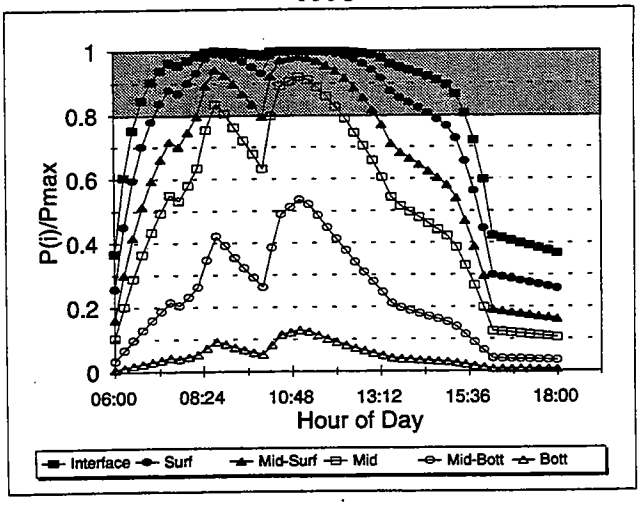

W9504

F23

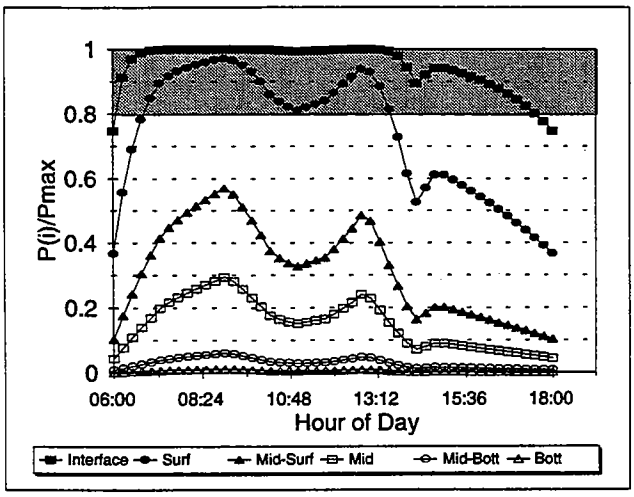

N04

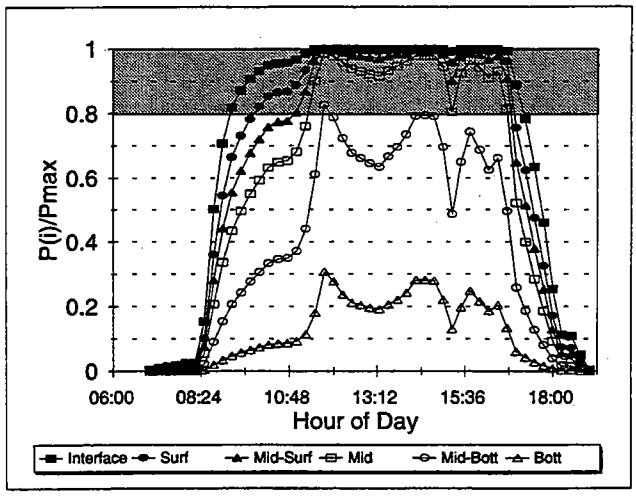

N07

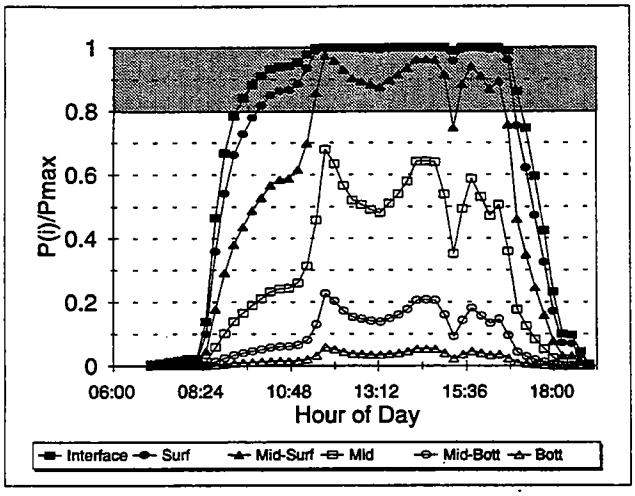

N16

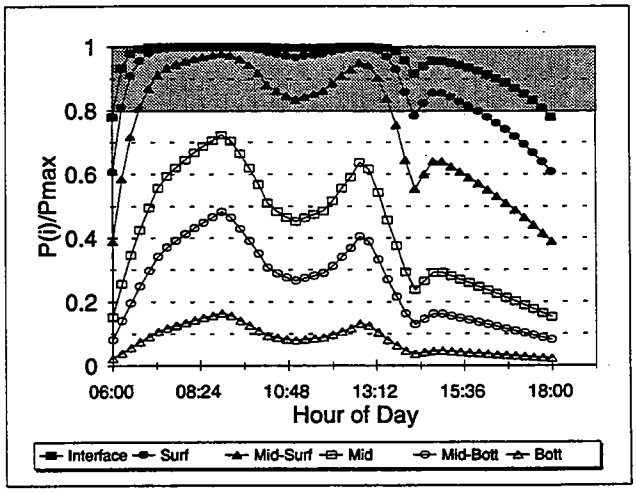

Figure 7-32
Calculation figure in App x D

W9505

N16

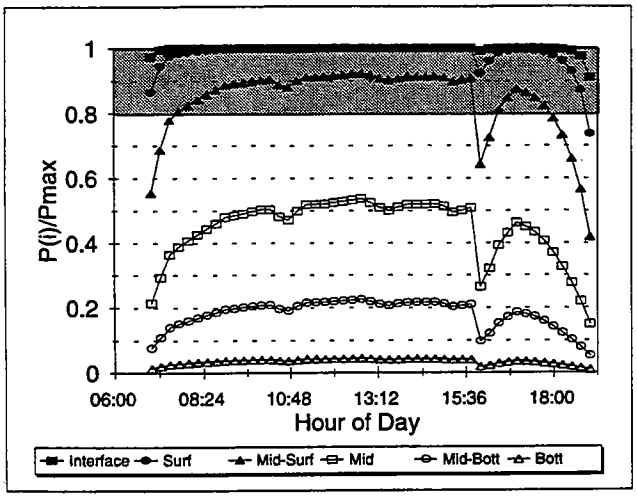

N04

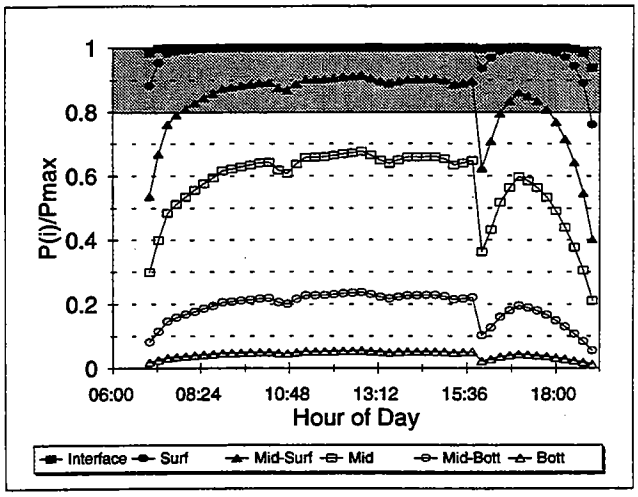

W9506

N16

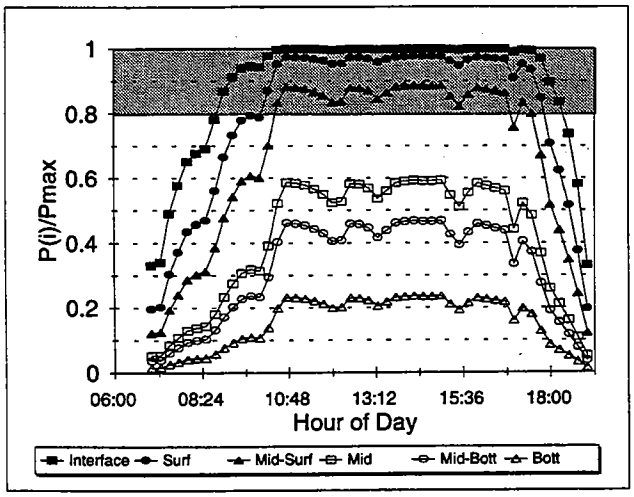

N04

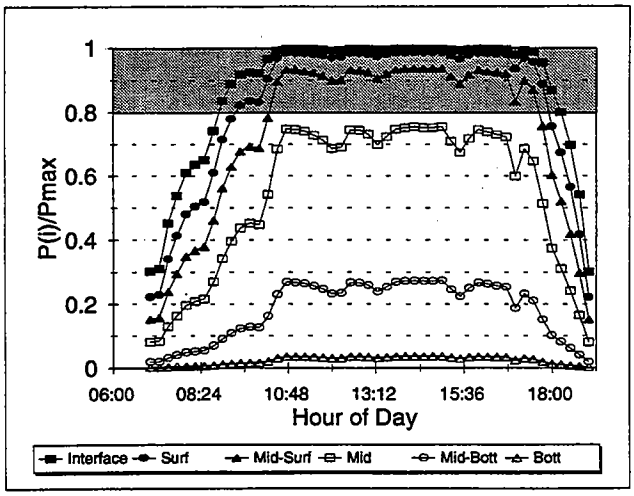

W9507

F23

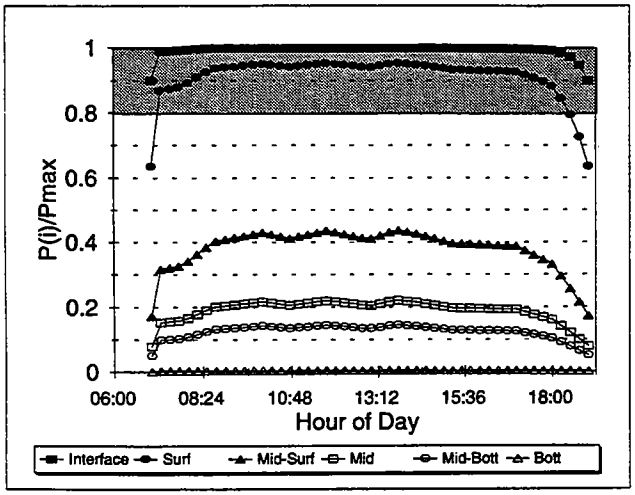

N04

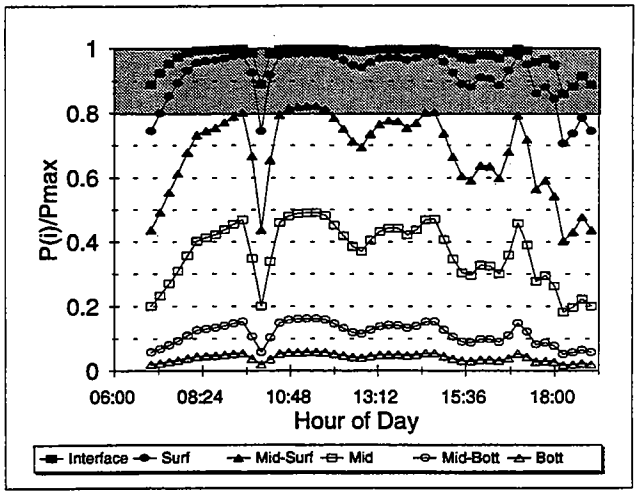

N07

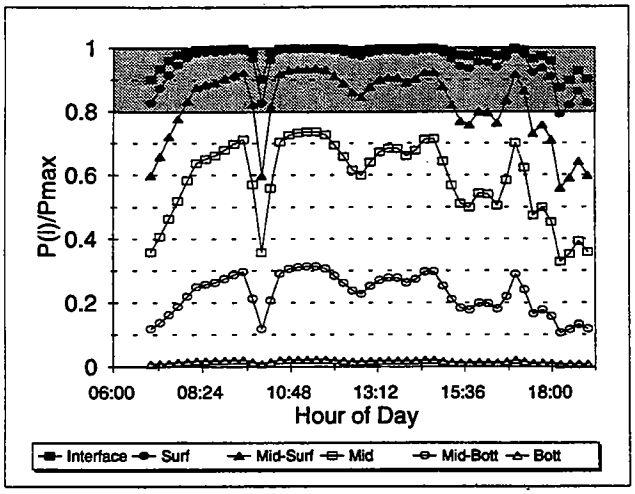

N16

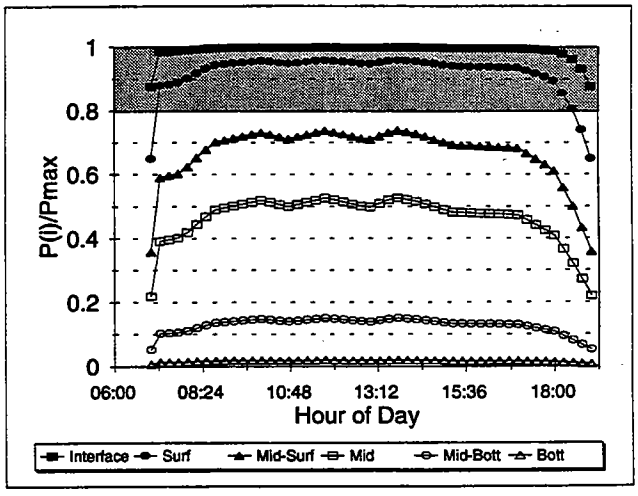

W9508

N04

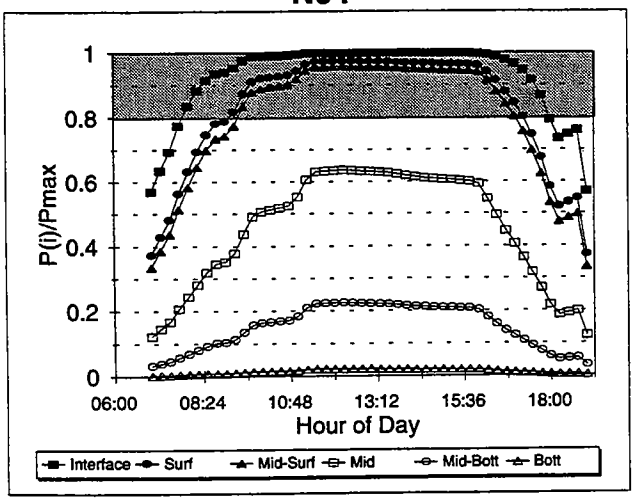

N16

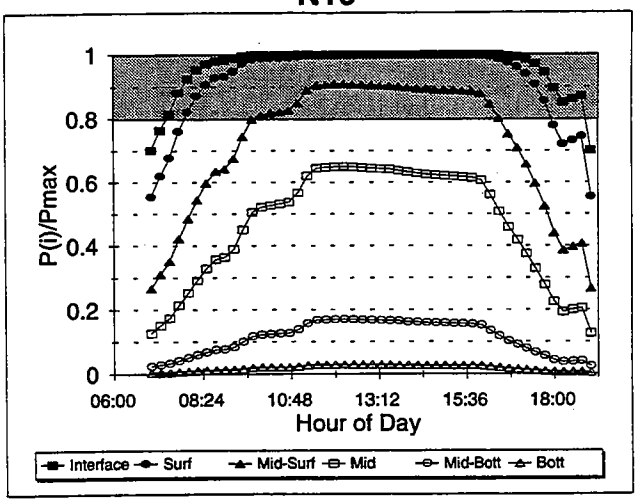

W9509

N04

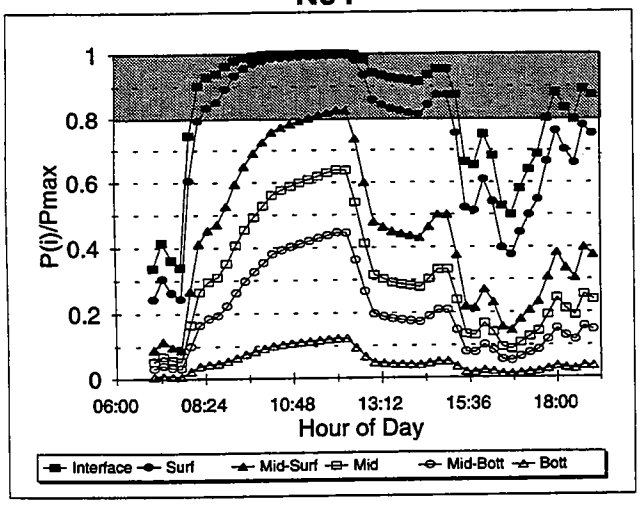

N16

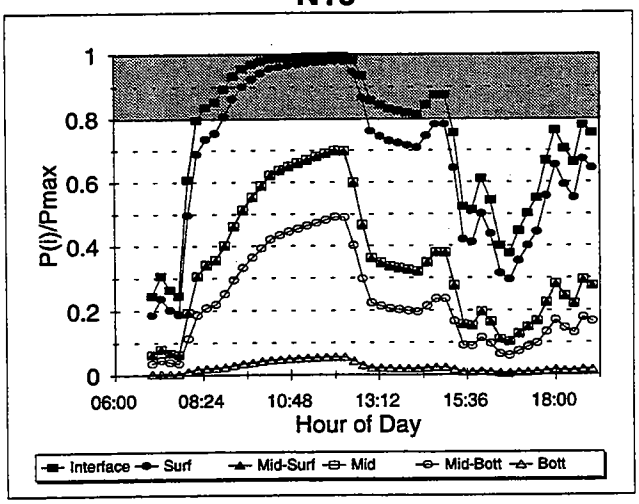

W9510

N04

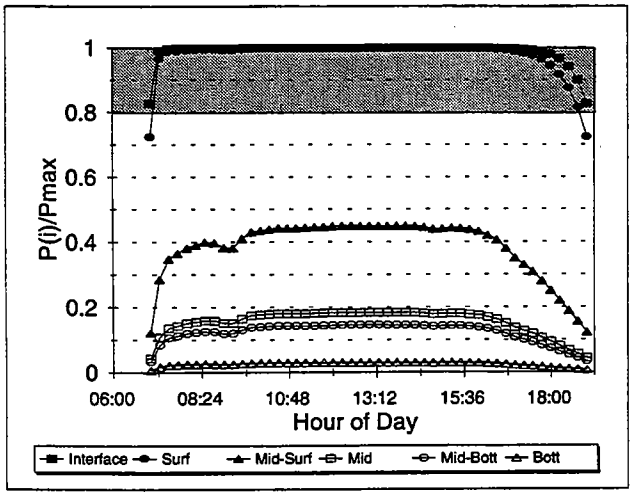

N16

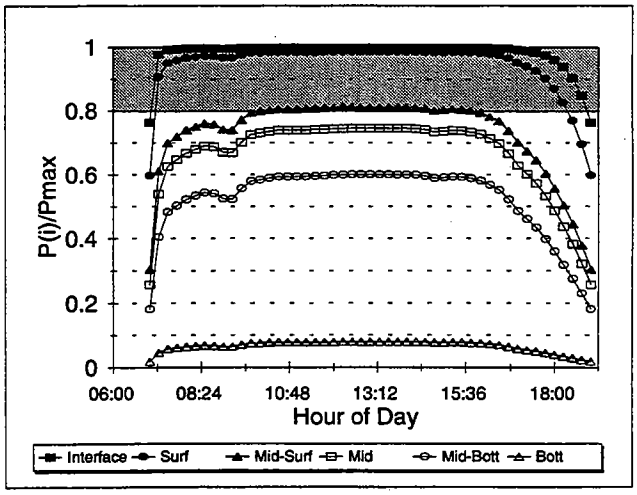

W9511

F23

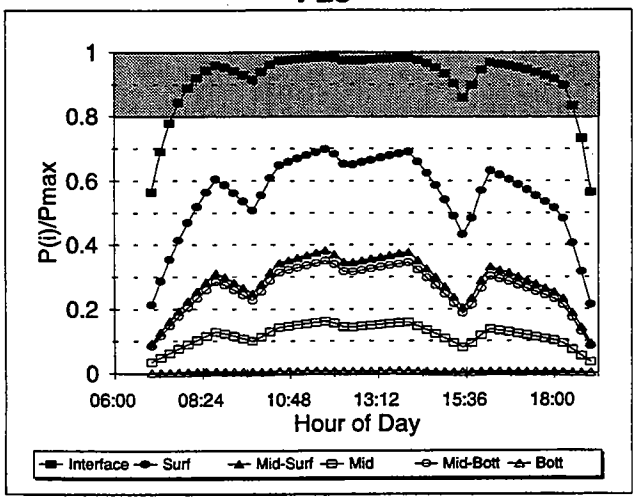

N04

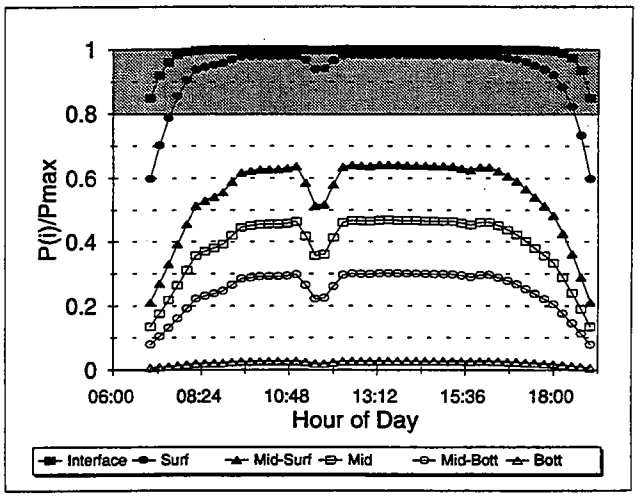

N07

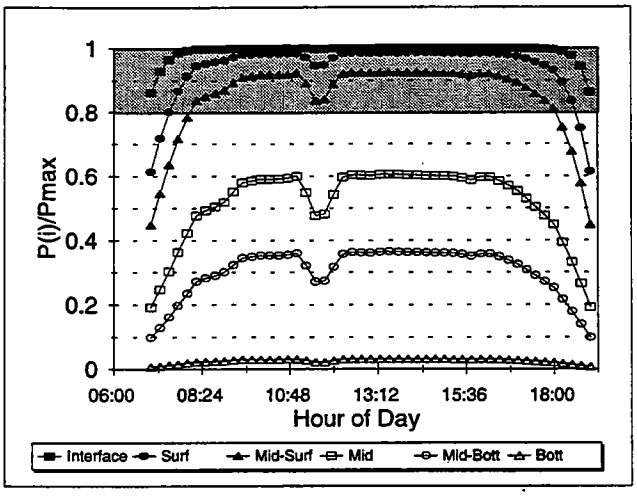

N16

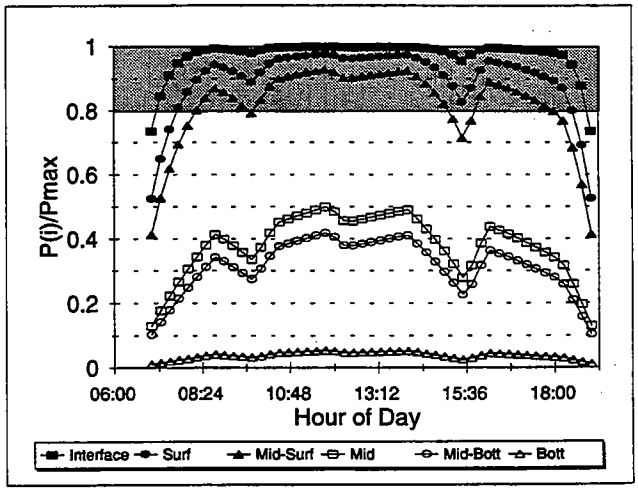

W9512

N04

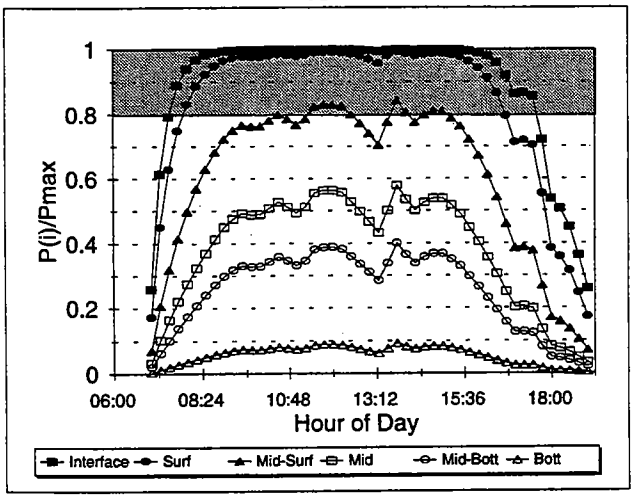

N16

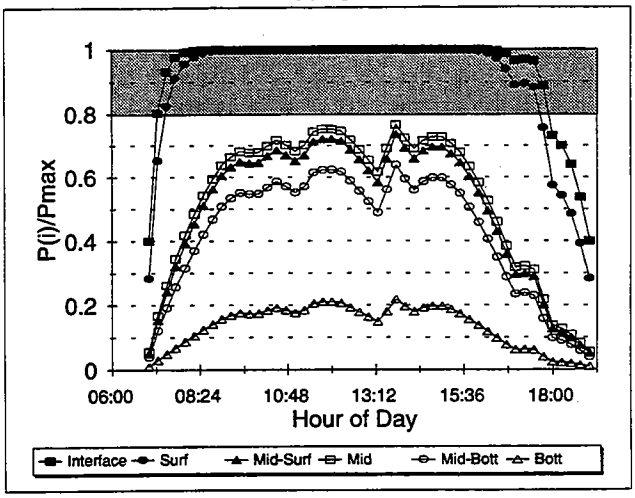

W9513

N04

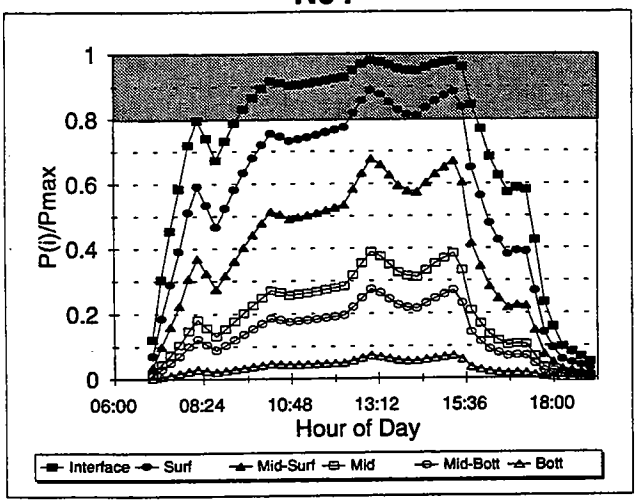

N16

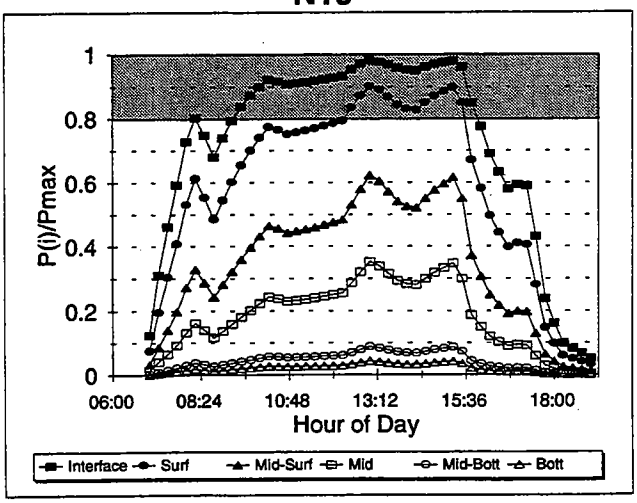

W9514

F23

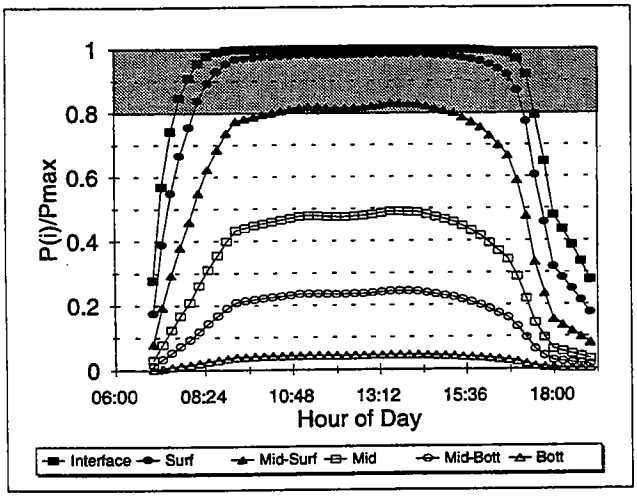

N04

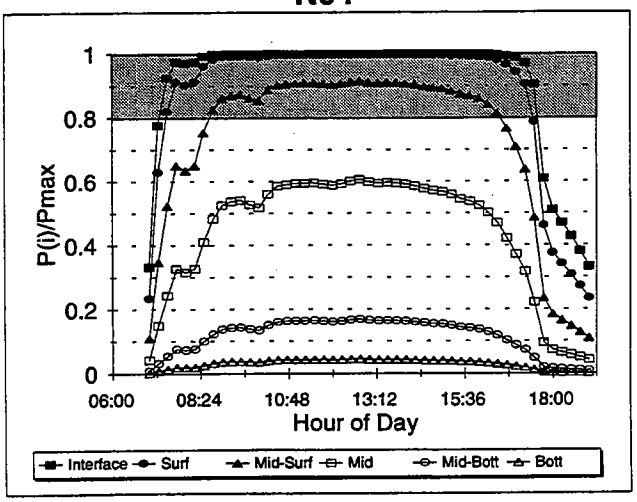

N07

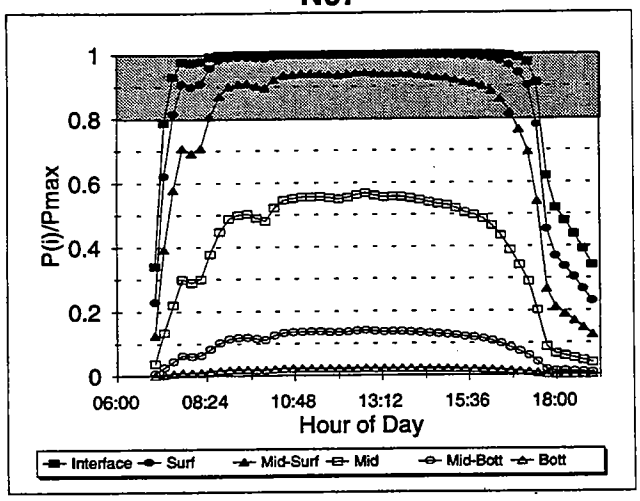

N16

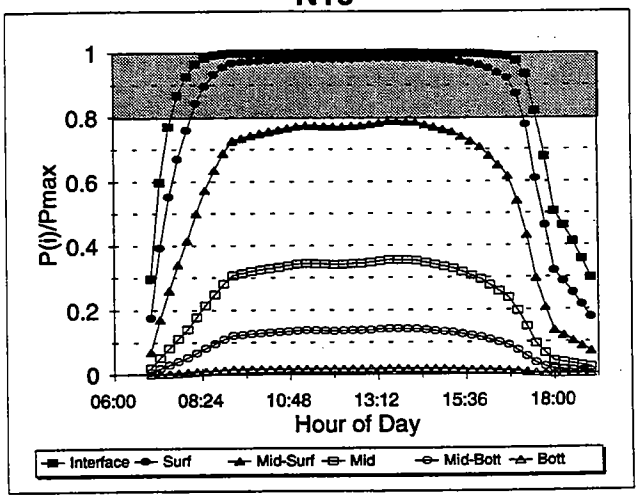

W9515

N04

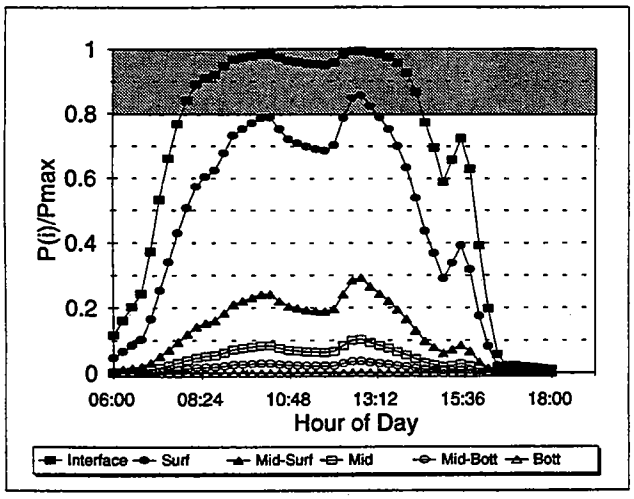

N16

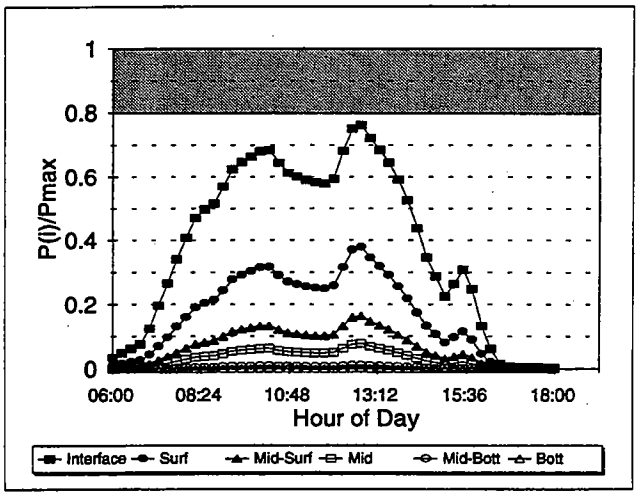

W9516

N04

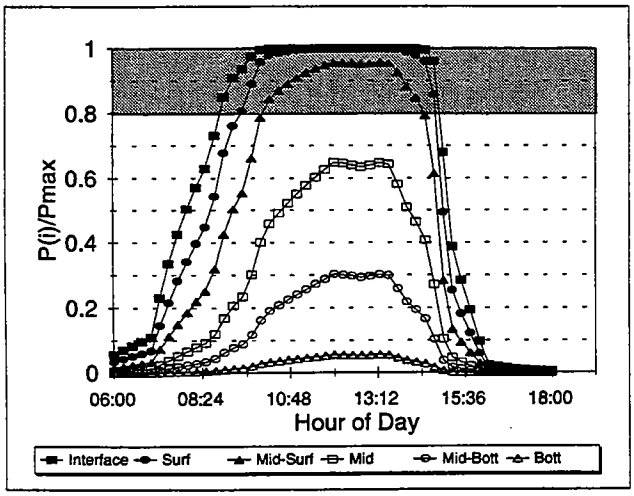

N16

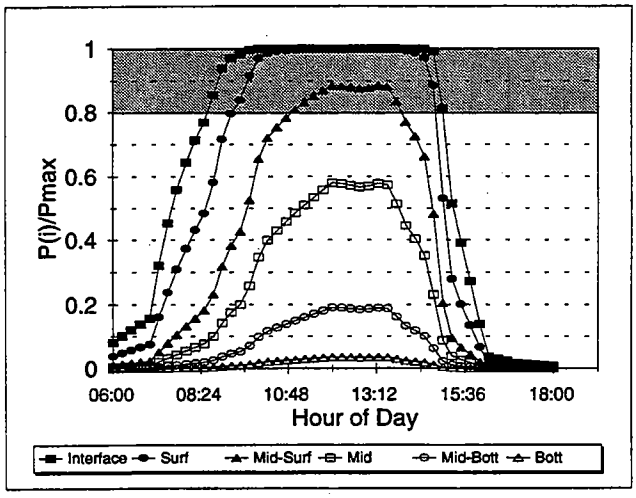

W9517

N04

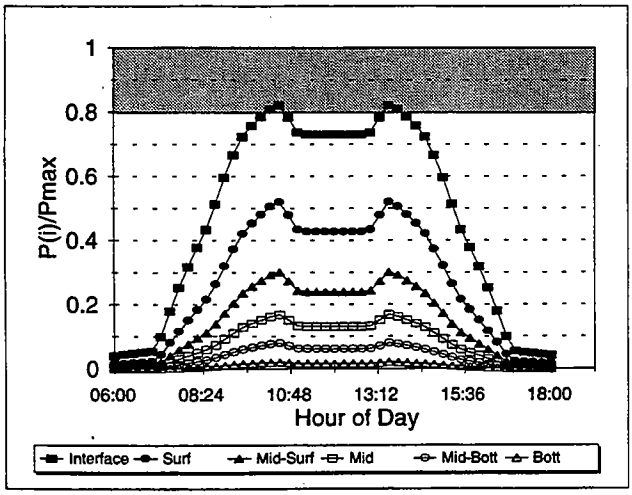

N16

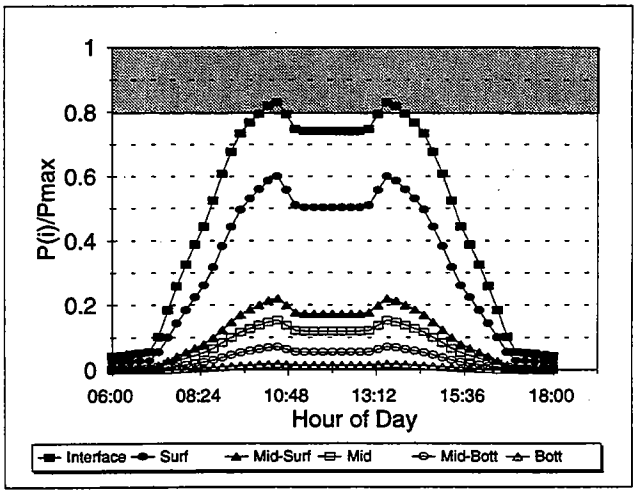

Massachusetts Water Resources Authority
Charlestown Navy Yard
100 First Avenue
Boston, MA 02129
(617) 242-6000
http://www.mwra.state.ma.us